Self-organisation of liquid crystal diphenyl acetylenes.

James Brailey-Partridge

PhD

University of York

Chemistry

February 2021

Abstract

The diphenyl acetylene unit has been incorporated into a series of oligomers, chiral dimers and ultimately supermolecular *Janus* liquid crystals. In this way a family of *Janus* liquid crystals featuring incompatible cyanobiphenyl and perfluoroalkyl mesogenic units have been synthesised and characterised. The dominant mesophase organisation of these materials is smectic A due to microphase segregation of the perfluoroalkyl and cyanobiphenyl units. A dendritic structure derived from either pentaerythritol or 1,1,1-tris(hydroxymethyl)ethane has been used to incorporate branching on either side of the diphenyl acetylene core, and in this way the relative volumes of the two faces of the *Janus* materials have been altered. When the mismatch in volume between the two faces is increased the molecular shape becomes tapered and the curvature is expressed into the mesophase structure for example by the formation of columnar mesophases.

A family of chiral dimers featuring either ester or ether linkages between a terminal chiral chain – (S)-2-methylbutyl or 1-methylheptyl – and the diphenyl acetylene unit are reported. The ether linkage increases the polarizability of the diphenyl acetylene core and thus strength of the intermolecular interactions, therefore favouring the formation of smectic A or smectic C* phases. Contrastingly the ester linkage favours the formation of chiral nematic phases and these dimers provide a greater helical twisting power when incorporated as chiral dopants into a nematic host, E7.

Compounds containing the diphenyl acetylene unit can undergo cyclotrimerisation reactions to provide hexaphenyl benzene materials providing a rapid increase in molecular complexity in a single step. The reaction of mixtures of symmetrical diphenyl acetylenes to provide *Janus* hexaphenyl benzene liquid crystals has been investigated.

List of Contents

List of Tables

List of Figures

List of Schemes

List of Equations

Abbreviations and nomenclature

APCI – atmospheric pressure chemical ionisation

Ar – aromatic

BP – blue phase

Bu – butyl

CB – cyanobiphenyl

CED – cohesive energy density

Col_h – hexagonal columnar phase

Col_r – rectangular columnar phase

Cr – crystal

Cu – cubic

d – doublet (NMR spectra)

DCC – N,N-dicyclohexylcarbodiimide

DCM – dichloromethane

DMAP – 4-dimethylaminopyridine

DSC – differential scanning calorimetry

EDAC – 1-ethyl-3-(3-dimethylaminopropyl)carbodiimide

ESI – electrospray ionisation

Et – ethyl

g – glass

HAB – hexa-aryl benzene

HTP – helical twisting power

Iso – isotropic liquid

J – coupling constant (NMR spectra), Hz

LC – liquid crystal

m – multiplet (NMR spectra)

MALDI – matrix assisted laser desorption ionisation

Me – methyl

MS – mass spectrometry

N – nematic phase

N* – chiral nematic phase

N_D – discotic nematic phase

NMR – nuclear magnetic resonance

OCB – alkoxy cyanobiphenyl

PE – pentaerythritol

Ph – phenyl

POM – polarised optical microscopy

ppm – parts per million

q – quartet (NMR spectra)

R_F – perfluorinated chain

R_H – alkyl chain

s – singlet (NMR spectra)

SmA – smectic A phase

SmB – smectic B phase

SmC – smectic C phase

SmC* – chiral smectic C phase

SmC_A* – antiferroelectric chiral smectic C phase

SmE – smectic E phase

SmX – unidentified smectic phase

SWAXS – small and wide-angle X-ray scattering

T – temperature

t – triplet (NMR spectra)

TGB – twist grain boundary phase

TFA – trifluoroacetic acid

THF – tetrahydrofuran

TLC – thin layer chromatography

TMS – trimethyl silyl

TOF – time of flight mass spectrometery

X – unidentified phase

Acknowledgements

Firstly, I would like to thank the supervisors for my project Dr Isabel Saez and Dr Stephen Cowling. I am very grateful for their help and support throughout the course of the research project and in constructing this thesis. In addition, I would like to thank the other members of the E214 lab in York including Dr Richard Mandle for his advice and guidance both with synthetic chemistry and liquid crystal characterisation.

I would like to thank Dr Graeme McAllister, Karl Heaton, Heather Fish, Dr Adrian Whitwood and Dr Scott Hicks for providing elemental analysis, mass spectrometry, NMR, single crystal X-ray diffraction and HPLC services respectively.

Finally, I would like to acknowledge the support provided by my family and friends both in York and beyond for helping me through this project. Especially Rachel whose never-ending patience and support has been essential.

Authors Declaration

I declare that this thesis is a presentation of original work and I am the sole author. This work has not previously been presented for an award at this, or any other, University. All sources are acknowledged as References.

Chapter 1. Introduction

1.1 Introduction to liquid crystals

A liquid crystal phase is a state of matter in which the molecules adopt a degree of organisation, less than that of a crystalline lattice but more ordered than that of an isotropic liquid. This is achieved by molecules possessing long range orientational order, and either short range or no positional order. The properties of a material in a liquid crystal phase can therefore reflect both those of a crystal, and of a liquid.

The first distinction to be made regarding liquid crystalline materials and phases is to demark the organisation as being either thermotropic (temperature induced) or lyotropic (induced by the concentration of molecules in a solvent). As the work detailed in this project regards thermotropic materials this case will be discussed first and in more detail. To a first approximation thermotropic liquid crystals can be simplified as being the result of a sequential loss of order starting from a crystalline lattice (Figure 1). The crystalline lattice is heated above the melting point (transition 1) and gains liquid like properties such as flow, while losing the long range positional order of a crystal giving rise to a smectic phase e.g. (smectic A, smectic C). The term smectic is used to denote liquid crystal phases in which the molecules self-organise into parallel stratified layers. Within this layered structure there are many possible organisations depending upon the degree and direction of any tilting of the molecules. Shortly, in the smectic C phase the molecules tilt along the director n in order to more efficiently pack themselves and avoid empty or void spaces. Upon further heating this tilted organisation may be lost while the molecules remain within the smectic layered structure giving a smectic A mesophase structure (transition 2). Further heating leads to additional loss of order within the mesophase resulting in the molecules no longer being stratified into layers, instead only having a general alignment along the director, n, i.e. a nematic phase (transition 3). Further heating of this nematic phase overcomes the intermolecular forces stabilising this general organisation thus giving an isotropic liquid with no positional order.
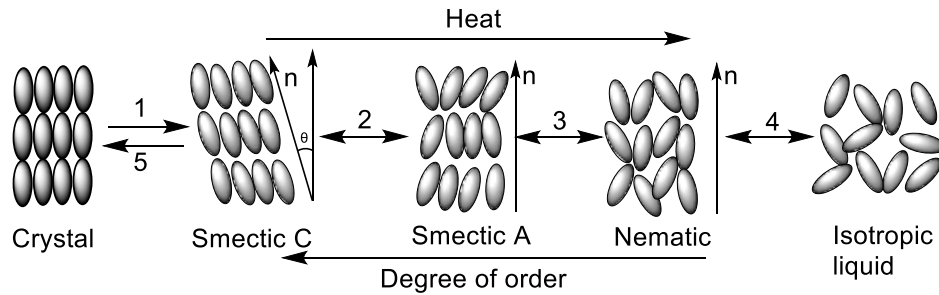
Figure 1. Liquid crystallinity can be likened to a gradual loss of order from a crystalline lattice, the transitions 2-4 are reversible, however melting from a crystal often shows hysteresis.

The second class of liquid crystals – lyotropics are formed depending upon the relative concentrations of the liquid crystal compound and a solvent. Lyotropic materials are a class of amphiphile having hydrophobic and hydrophilic sections within the molecule. The nature of the interactions between the solvent and two regimes of the material differ with examples including surfactants, and biological membranes. This organisation can be expressed simply by the concept of 'like with like' for example exposing a polar, hydrophilic head group of the lyotropic material to a polar solvent, while burying a non-polar, hydrophobic alkyl chain within a cluster of hydrophobic chains. This can also be inverted in the presence of a hydrophobic solvent where the hydrophilic headgroup is buried within a core and hydrophobic chains are exposed.

While the materials discussed within this work are not being studied for lyotropic behaviour, there exist significant similarities between lyotropic mesophases and the thermotropic behavior of amphiphiles. In the lyotropic case the hydrophilic head group swells as it becomes hydrated and hence the effective shape of the surfactant changes. This gives rise to a change in the curvature and packing leading to changes in phase structure (Figure 2, top). This illustrates the role of the overall molecular shape as an extension of the 'like with like' concept. For lyotropic materials once a critical concentration of material is reached the intermolecular interactions of the solvent and dissociated lyotropic materials will become unfavourable leading to self-assembly which allows for example, hydrophobic chains to be buried in the core of a micelle. Likewise, for thermotropic liquid crystals the structure of the liquid crystal phase formed depends upon the shape of the individual molecules.

Lyotropic amphiphiles are often discussed in terms of a 'head' and 'tail'. In lyotropic materials, the hydrophilic head group can swell as it becomes hydrated and hence the

effective shape of the surfactant changes. This gives rise to a change in the curvature and packing leading to changes in phase structure. If the volume of the head and tail groups are close to equal then lamellar structures are favourable resulting in lamellar organisations (Figure 2, bottom).[1] Increasing the volume of one section of the molecule leads to intramolecular curvature. Forming lamellar structures from wedged or tapered shapes may leave void spaces.[2] In order to avoid void volume tapered molecules instead self-assemble into columns, or spheres depending upon the degree of curvature as shown below (Figure 2, bottom).
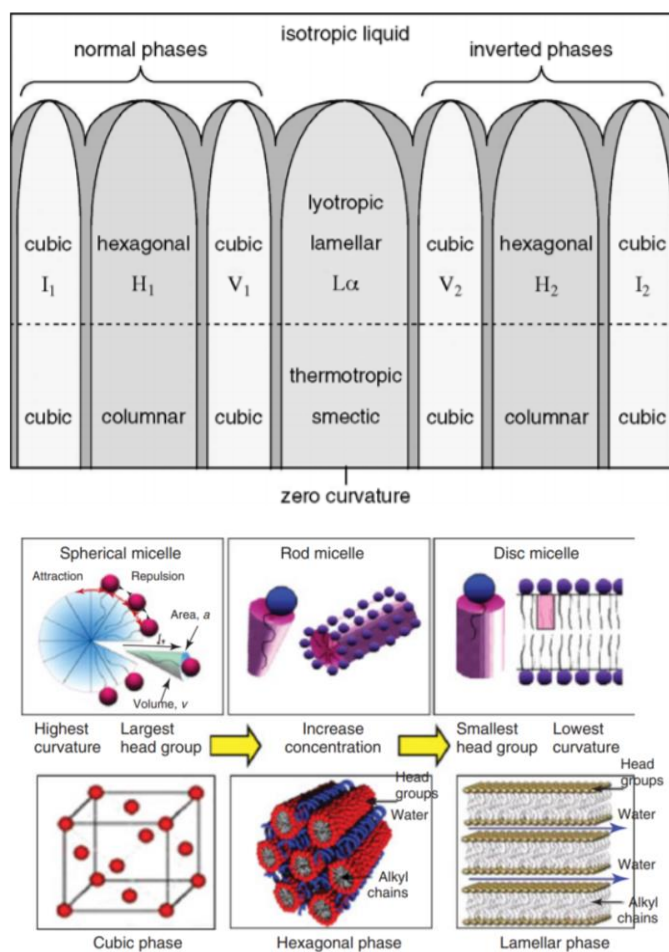
Figure 2. Lyotropic liquid crystal phases which emerge as a result of curvature (top, image reproduced from reference 2). Arrangement of molecules in the lyotropic phases (bottom, image reproduced from reference 1).

1.2 Liquid crystal mesophases

A brief discussion of liquid crystal mesophases will be given below as an introduction to the work presented in this thesis. The origin or absence of liquid crystalline behaviour can be thought of as depending upon the general molecular shape of the molecule. The units of a compound responsible for driving the organisation into a

liquid crystalline phase are referred to as mesogenic units or simply as mesogen(s). Due to the constant motion of the molecules constituting a liquid crystal the shape of the molecules can be simplified to an averaged topology such as those shown in Figure 3. These shapes can be classified as either calamitic (rod-like) or discotic (disc-like). By treating molecules as these simplified shapes a general discussion of the factors driving the self-organisation into a mesophase can be made. However, these abstractions must not mask specific structural factors, for example the presence of chirality. Chiral information from a chiral moiety in a liquid crystalline molecule or dopant can be translated into the mesophase structures of some phases such as the chiral nematic (N*) or chiral smectic C (SmC*) phases.

As shown in Figure 1, the structure of liquid crystalline phases can be viewed as a sequential loss of order from a crystalline lattice to an isotropic liquid. In this overview the liquid crystal mesophases will be introduced as the reverse, a progressive increase in the degree of liquid crystalline organisation beginning with the nematic phase.

1.2.1 Structure of the nematic phase

In the nematic phase the molecules exhibit long range orientational order but no positional order. The average orientation of the molecules in the phase lies along an axis referred to as the director which is denoted by the symbol n. In the nematic phase there are as many molecules oriented 'head-up' as there are 'head-down' (Figure 3). In general terms the nematic phase may be either comprised of 'rod-like' or 'disc-like' molecules, although other molecular structure exhibiting nematic phases are known. Firstly, the nematic phase comprising of calamitic materials will be discussed as it is of most relevance and most widely used in applications. In this mesophase structure the molecules are free to rotate around their long axis and though slightly restrained rotate around their short axis i.e. end over end. The extent to which the molecules align with the director is called the order parameter and is denoted by the letter 'S'. The order parameter of the mesophase is defined by Equation 1.

$$S = \frac{1}{2} \langle 3Cos^2 \emptyset - 1 \rangle$$

Equation 1. The order parameter of the nematic mesophase.

The symbol θ refers to the angle between an individual molecule and the director and the triangular brackets denote that this is averaged over a large quantity of molecules.

Typical order parameters of calamitic nematic mesophases lie between $S = 0.4$ and $S = 0.7$. S = 1 would represent perfect alignment between the long axis of each molecule and the director, while $S = 0$ defines an isotropic liquid.
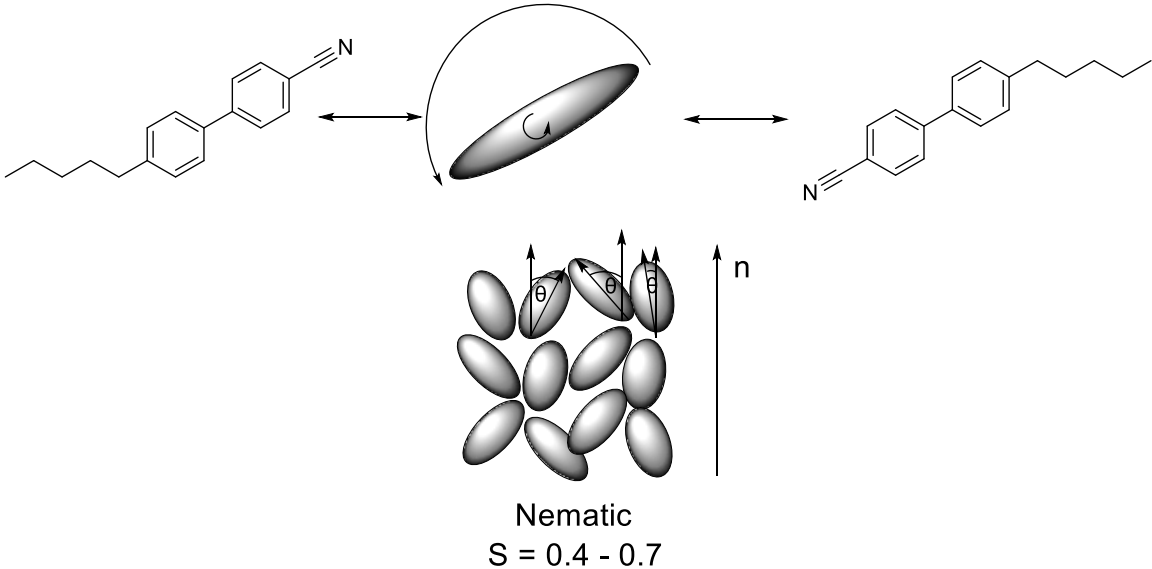
Nematic
S = 0.4 - 0.7

Figure 3. Calamitic material approximated to a rod-like cartoon. Head-to-tail structural detail is lost in the nematic phase and just the degree of orientational order is relevant.

The discotic nematic (N_D) phase is far less common than that of calamitic materials however it has been used in devices, for example optical films used to increase viewing angles in display devices. The discotic nematic mesophase resembles the calamitic nematic phase, however in this case the molecules orient the faces of their disk-like shapes along the director. This is achieved *via* orientational order whereby the faces are aligned similarly to the arrangement of coins upon a surface with the director perpendicular to the faces of the molecules (Figure 4).[3]

Schematic representation of the N_D phase

Coins in analogy to the N_D phase
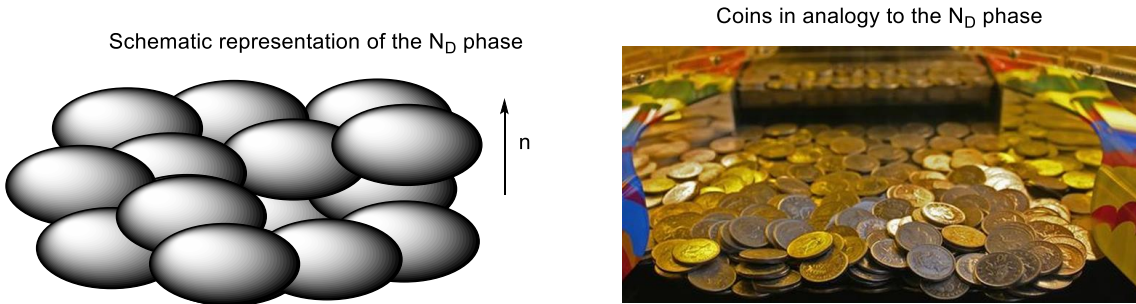
Figure 4. Structure of the nematic discotic (N_D) mesophase.

1.2.2 Structure of the smectic phases

Smectic phases are by definition characterised by the packing of molecules into repeated layer structures. Within these layered structures the molecules may have

short range order as in the SmA and SmC phases, short range order and local hexagonal packing as found in the SmB, SmI and SmF phases, long ranged order and hexagonal packing found in B, G and H phases or long range orthorhombic packing in E, J and K phases. For the sake of brevity the focus will be upon smectic A and smectic C phases.

1.2.2.1 Structure of the smectic A phase

Smectic A mesophases comprise of weakly defined layers where the molecules are arranged along a director perpendicular to the layer plane. Molecules can be arranged to give monolayered (SmA$_1$), bilayered (A$_2$), interdigitated (A$_d$) or ribbon-like (SmÃ) structures (Figure 5). In a similar manner to the nematic phase the molecules within these layers are not perfectly aligned along the director. Molecules in the smectic A phase undergo rapid rotation around the long axis and the organisation between the layers remains relatively diffuse. The layers in the Smectic A phase are defined as a sinusoidal density wave of masses.

Organisation of the molecules into interdigitated semi-bilayers (Smectic A$_d$) is largely driven by pairing of individual molecules due to favourable intermolecular interactions. This may be required to account for a mismatch of volumes across the molecule, to allow for interactions between polar terminal groups i.e. cyanobiphenyl, or due to self-segregation of units such as perfluoroalkyl. The layer spacing in interdigitated phases is often around 1.4 times the molecular length. Alternatively, the molecules can organise into an expanded bilayer giving layer spacings equal to twice the molecular length (SmA$_2$). To form this mesophase structure some intermolecular interactions must be available only when sections of the molecules are arranged with this repeating order. For example, minimising the costs of incompatible chemical moieties or shapes. Ribbon phases (SmÃ) are formed when the molecular lengths of a

dimer and its constituent monomers cannot be efficiently packed within space without rearrangement of the layers to provide the ribbon-like structure.

Smectic A$_1$

Molecules may be arranged pointing up or down

Diffuse layers, no periodicity

Layer spacing = Molecular length (*d*)

Smectic A$_d$

Semi-bilayer forms due to favourable associations

Layer spacing = < Twice molecular length (~1.4 *d*)

Smectic Ã

Overall equal facings between layers

ribbon-like structure from antiparrallel arragement within layers

Smectic A$_2$

Layer spacing = Twice molecular length (2 x *d*)

Second layer points opposite therefore overall equal facings

Molecules within layers face the same direction

Figure 5. Various mesophase structures within the smectic A phase.

The tilted smectic C phase is formed when the molecular axis is tilted away from the layer normal. This serves to increase intermolecular interactions either by providing greater overlap of polar and apolar regions within the cores[4], or due to the packing of molecules with zigzag molecular shapes giving a structure which resembles stacked chairs.[5]

The tilting of molecules within the layers that occurs at the transition from a smectic A to smectic C phase is a second-order transition. The majority of molecules in one domain will tilt in one general direction. The angle of tilting in the smectic C phase is temperature dependent, and at lower temperatures the tilt angle increases introducing more order and greater interaction between molecules. The smectic C mesophase structures are formed similarly to the smectic A analogues shown above,

with the exception of the Smectic C$_A$ phase shown below (Figure 6), and that the tilted structure of the smectic C mesophase allows for chiral smectic C phases (1.2.4.2).
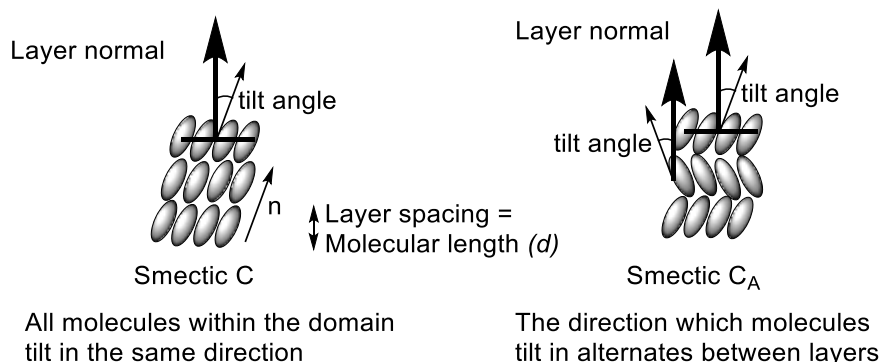
Figure 6. Cartoon representations of the smectic C (left) and alternating smectic C$_A$ (right) mesophase structures. In chiral materials these give rise to ferroelectric and antiferroelectric behaviours respectively.

1.2.3 Structure of columnar mesophases

Columnar liquid crystal phases are formed by stacking individual molecules into supramolecular columns which are often represented *via* thin disks due to the structures of molecules which commonly possess these phases (hexa-substituted benzenes, triphenylenes etc.) (Figure 7).[6] Typically these are formed due to strong π-π interactions between these aromatic cores which favour alignment of these faces in close proximity of around 4 Å. These columnar materials often require aliphatic chains to introduce disorder and disrupt packing so as to suppress crystallisation so that a liquid crystalline phase is observed. Once the constituent molecules have formed into the supramolecular columns these must pack themselves efficiently and do so by forming a two-dimensional lattice. Due to the liquid-like nature of the liquid crystal phase the columns can often move amongst each other and have only short range order within themselves[7] giving a 'disordered' columnar phase. Alternatively, the structure may be more discrete giving an 'ordered' columnar phase. The two-dimensional lattice structure can be defined, with hexagonal or rectangular as the main classes.[8,9] The symmetry of these lattices can be described by space groups with

a hexagonal columnar phase (Col$_h$) belonging to the space group P6/mmm, while multiple space groups are possible in rectangular lattices (P2$_1$/a, P2/a, C2/m).

RO OR   R = Alkyl chain
RO OR
RO OR
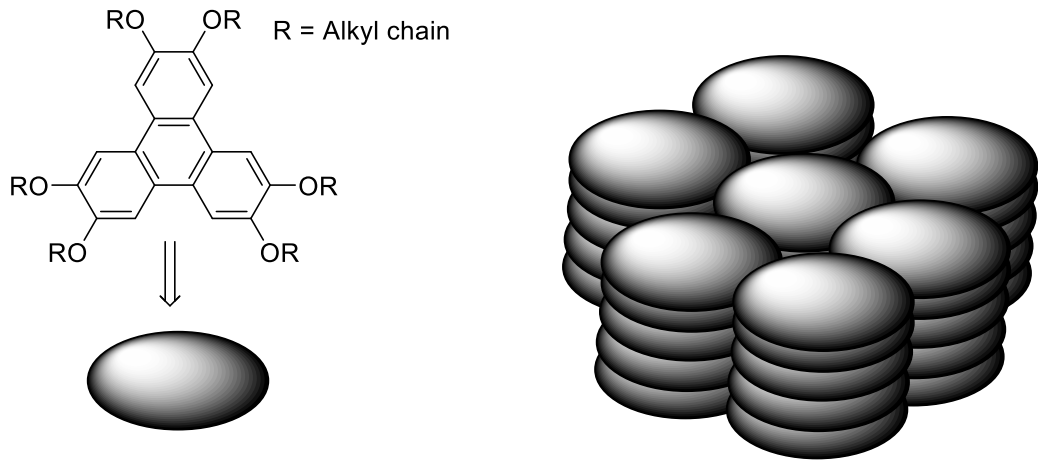
Figure 7. Columnar liquid crystals formed from discotic compounds.

The defined lattice structures allow X-ray diffraction studies to identify which columnar phase is formed due to the diffraction peaks observed. The space group of the lattice is responsible for the relationship between diffraction peaks. In a hexagonal lattice the two primary peaks observed in the X-ray diffraction pattern are described by the Miller indices (hk) = (10) and (11), (Figure 8). These peaks are described by equation 2 shown below. The diffraction peaks and lattice parameter are described by equation 3 where d is the diffraction peak, h and k the Miller indices and a the lattice parameter. This results in a characteristic pattern whereby peaks are expected in a ratio of 1:1/√3:1/√4:1/√7:1/√9 and further.
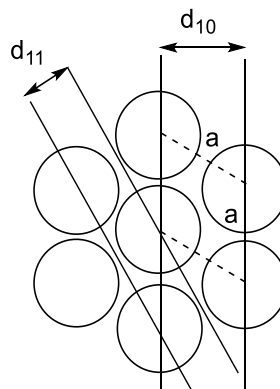
Figure 8. A hexagonal columnar lattice has two primary reflections (10) and (11) as shown.

$$d_{11} = \frac{d_{10}}{2\cos 30°} = \frac{d_{10}}{\sqrt{3}}$$

Equation 2. For a hexagonal lattice (P6/mmm) the d spacings measured via X-ray diffraction for the (10) and (11) reflections are referred to as (d$_{11}$ and d$_{10}$).

$$\frac{1}{d_{hk}^2} = \frac{4}{3} \frac{h^2 + k^2 + hk}{a^2}$$

Equation 3. Diffraction peaks from a hexagonal lattice (P6/mmm) are related to the Miller indices (h, k) and lattice parameter (a).

The rectangular columnar mesophase (Col$_r$) can have one of three different mesophase structures due to tilting of the constituent molecules with respect to the columns and as such the cross sections through the columns appears eliptical. As previously stated the space groups for the rectangular lattices are P2$_1$/a, P2/a and C2/m, shown in Figure 9. Due to a breakdown of symmetry in the rectangular columnar liquid crystals the (10) peak of a hexagonal columnar mesophase is split into a (20) and (11) reflection in the rectangular columnar phase. The *d* spacings are related to the Miller indices (hk) and lattice parameters *a* and *b* by equation 4.

rectangular (P2$_1$/a)   rectangular (P2/a)   rectangular (C2/m)
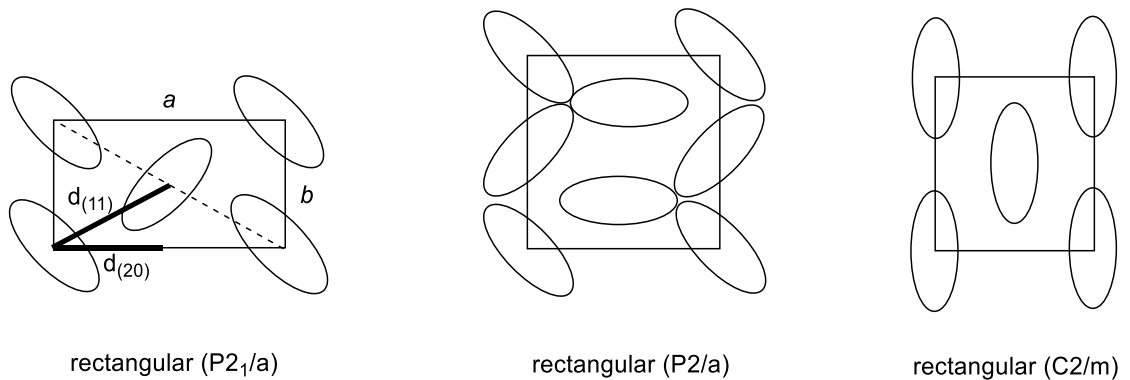
Figure 9. The three space groups of rectangular lattices.

$$\frac{1}{d_{hk}^2} = \frac{h^2}{a^2} + \frac{k^2}{b^2}$$

Equation 4. The expected diffractions from a rectangular columnar mesophase are related to the lattice parameters (hk) and lattice parameters a and b.

Indexing a columnar rectangular mesophase by assigning each peak to a reflection and then determining the lattice parameters can be achieved using equation 4. However, the conditions required for a reflection to be observed is complex and thus this can prove challenging and require many peaks to be present in the diffraction pattern.

1.2.4 Chiral liquid crystal phases

The introduction of chirality into a liquid crystal material enables the formation of various chiral mesophases.

1.2.4.1 Chiral nematic phase

Incorporating a chiral centre into a nematic phase material or alternatively doping an achiral nematic host with a chiral dopant results in the formation of macroscopic helical twisting within the bulk material. Within this structure the director precesses within the helix with a full rotation of 360° giving an interval called the pitch (Figure 10). The molecular chirality of a material is propagated into macromolecular optical activity in the chiral nematic phase by this helical twist.
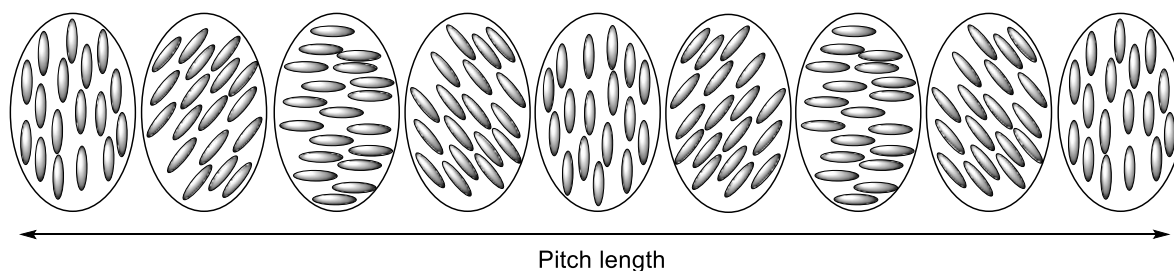
Pitch length

Figure 10. Representation of the chiral nematic helix via imaginary slices.

When the pitch of the chiral nematic phase is within the visible wavelengths of light it selectively reflects light, thus giving a coloured appearance. The pitch changes with temperature so at high temperatures the pitch is short and blue wavelengths are reflected but at low temperatures the pitch becomes longer and a shift to the red occurs.[10]

1.2.4.2 Chiral Smectic C

In addition to the chiral nematic phases, chirality can be expressed into the tilted structure of the smectic C phase. These phase structures provide useful electronic properties being either ferroelectric (SmC*)[11] or antiferroelectric (SmC*$_A$) (Figure 6).[12] This comes about due to restricted rotation within the tilted layers, meaning that polarisation within the molecules is preserved into the layered structures. The antiferroelectric smectic C phase (smectic C*$_A$) describes a mesophase structure where the averaged tilt angle (i.e. tilt director) alternates between layers of single molecules.

1.2.4.3 Blue phases

In addition to minimizing energy by aligning calamitic molecules in parallel as seen in the nematic and smectic phases, the introduction of a chiral helix introduces another factor to be minimised by the packing arrangement. In the chiral nematic phase the helical twist occurs in just one axis however this energy may be further minimised *via* introducing twisting along all axes perpendicular to the helix.[13] So long as the average

orientation of molecules along the original helix is unchanged the structure can be transferred to three dimensions and is referred to as a double twist (Figure 11).
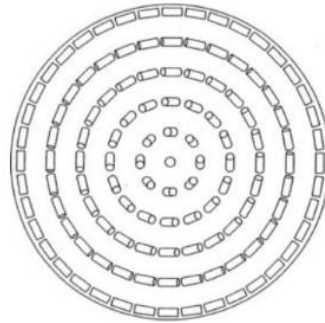
Figure 11. A schematic of a double twist cylinder showing the director twisting radially away from the centre (Reproduced from reference 13).

When this is generalised across the bulk, the effect is decreased to the point of eventually being trivial. Therefore, there is a set of competing effects between the stabilisation afforded by the double twist structure within a small distance of the origin, and the formation of disclinations, where neighbouring molecules of independent double twist cylinders are no longer parallel. Should the stabilisation induced by the double twist structure outweigh the costs of these disclinations the structure is stable and a blue phase is formed. There are multiple arrangements with which these double twist cylinders can be packed giving BPI, BPII and BPIII (Figure 12).[14,15] Blue phases occur above the chiral nematic phase and typically exist over very narrow temperature ranges.
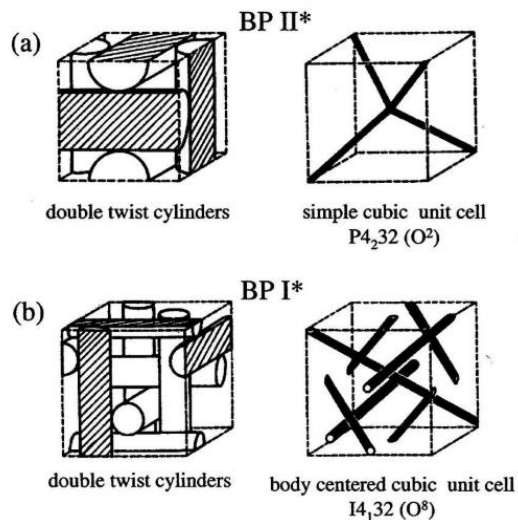
Figure 12. Structure of BPI and BPII reproduced from reference 14.

1.2.4.4 Twist grain boundary phase

Another example of a frustrated phase is the twist grain boundary or TGB phase which results from a material having a tendency to both form a smectic layered structure (i.e. smectic A behaviour), and exhibit a helical precession of the director found in many chiral mesophases. The TGB phase comprises of blocks of molecules in smectic A like structures which want to twist with respect to each other forming a helix. This cannot occur continuously and as a result the twisting is stabilised by a lattice of screw dislocations. (Figure 13).[16] TGB phases are observed for some systems at the transition between the chiral nematic and the smectic A phase. As with the blue phases it is usually only observed in systems with short pitch lengths and occurs over very narrow temperature ranges. TGB phases occur more frequently in asymmetric dimesogenic structures where each mesogenic core has a tendency to form smectic phases with differing periodicities.[17]
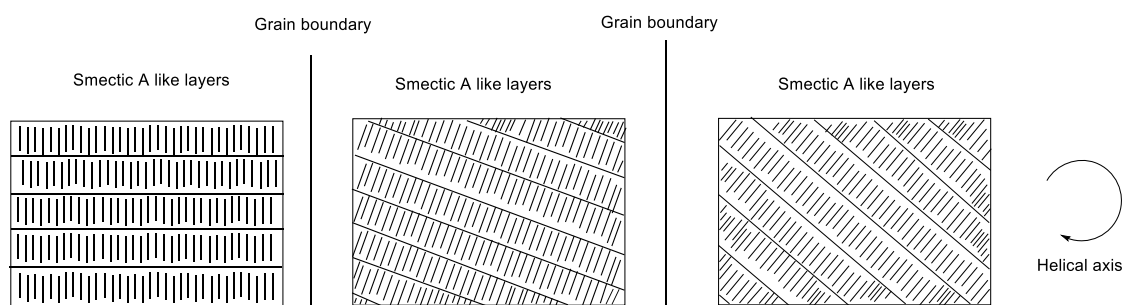
Figure 13. Mesophase structure of the TGB phase.

1.3 Mesogens and mesogenic units

As thermotropic liquid crystals are a vast area of research with many materials being known it is helpful to refer to several classifications to help understand their behaviour. Most simply this can be a classification as either low molar mass or high molar mass liquid crystals, although these categories can be subdivided (Figure 14). While there are clear differences in the behaviour of single calamitic mesogens and polymeric materials there exist many intermediate classes of liquid crystalline materials for which their behaviour shows similarities to both types of structures.
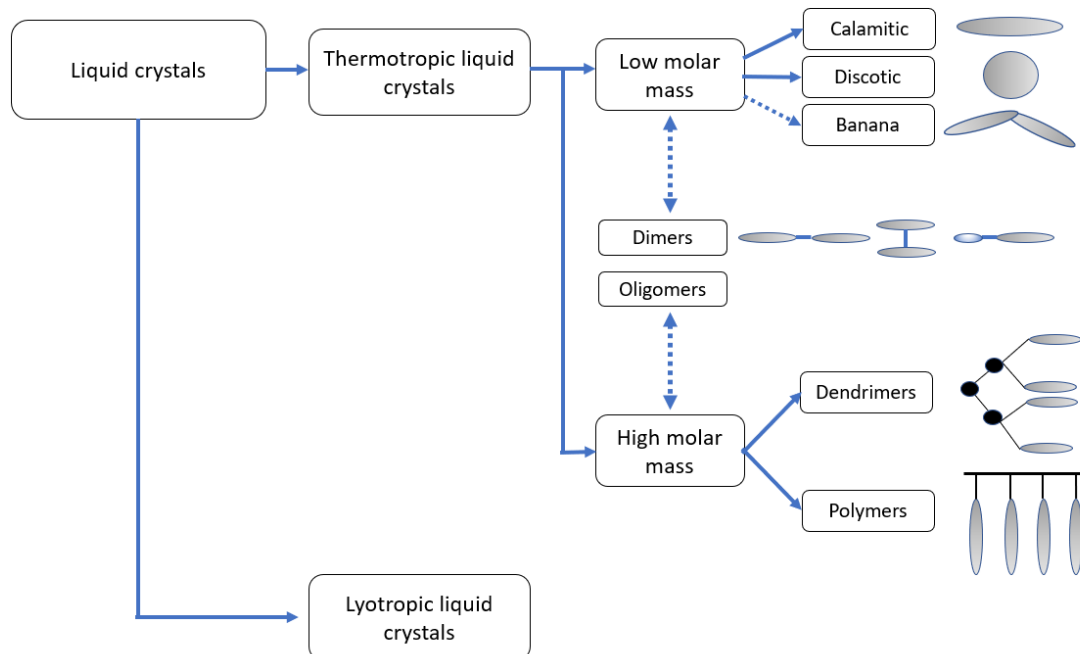
Figure 14. Categorisation of liquid crystalline materials.

1.3.1 Low molar mass liquid crystals

The first thermotropic liquid crystal material to be discovered was cholesteryl benzoate **1** in 1888 (Figure 15) by Friedrich Reinitzer who observed two 'melting points', the first giving a cloudy liquid before transitioning again to a clear liquid.[18] This behaviour is reliant on the presence of a mesogen, the term used to describe a section of a material which stabilises the formation of a liquid crystal mesophase (meso, from the Greek mésos meaning middle). To function as an effective mesogen two key factors are required, firstly anisotropy of shape and secondly some degree of rigidity. The combination of these two factors leads to a molecule exhibiting different intermolecular interactions with neighbouring molecules depending upon the orientation between themselves (see Figure 16). When one orientation is more favourable i.e. maximises the positive interactions between neighbours this promotes orientational order between neighbours within the liquid, thus providing liquid crystallinity. Secondly the mesophase structure is dependent upon the optimised packing of molecules within the bulk material so as to exclude void space.[19] Increasing the temperature of the system breaks down these interactions and so the liquid crystalline organisation is lost.

Cr 145.5 N* 178.5 Iso °C
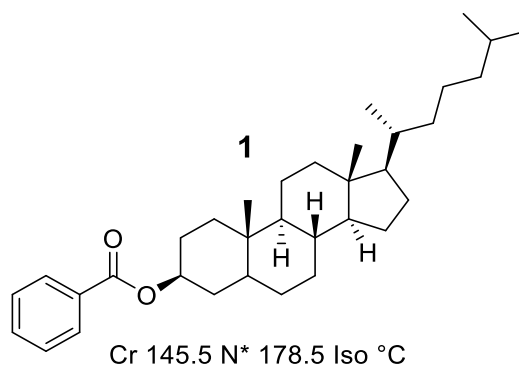
Figure 15. The structure of cholesteryl benzoate 1.

The most common route to achieve this anisotropy of shape is to design calamitic or rod-like materials such as cholesteryl benzoate shown above. The high aspect ratio (ratio of molecular length to breadth) of these materials provides anisotropy and so the strengths of intermolecular interactions differ depending upon orientation (Figure 16). Rigidity, such as that provided by fused or bonded ring systems is required to maintain the elongated anisotropic shape. While most materials in this project are best described in terms of calamitic mesogens the organisation of some materials may be considered discotic or disk-like. Discotic materials can also possess anisotropy *via* one shortened axis. In this case the interactions can be maximised by stacking-up of these discs.
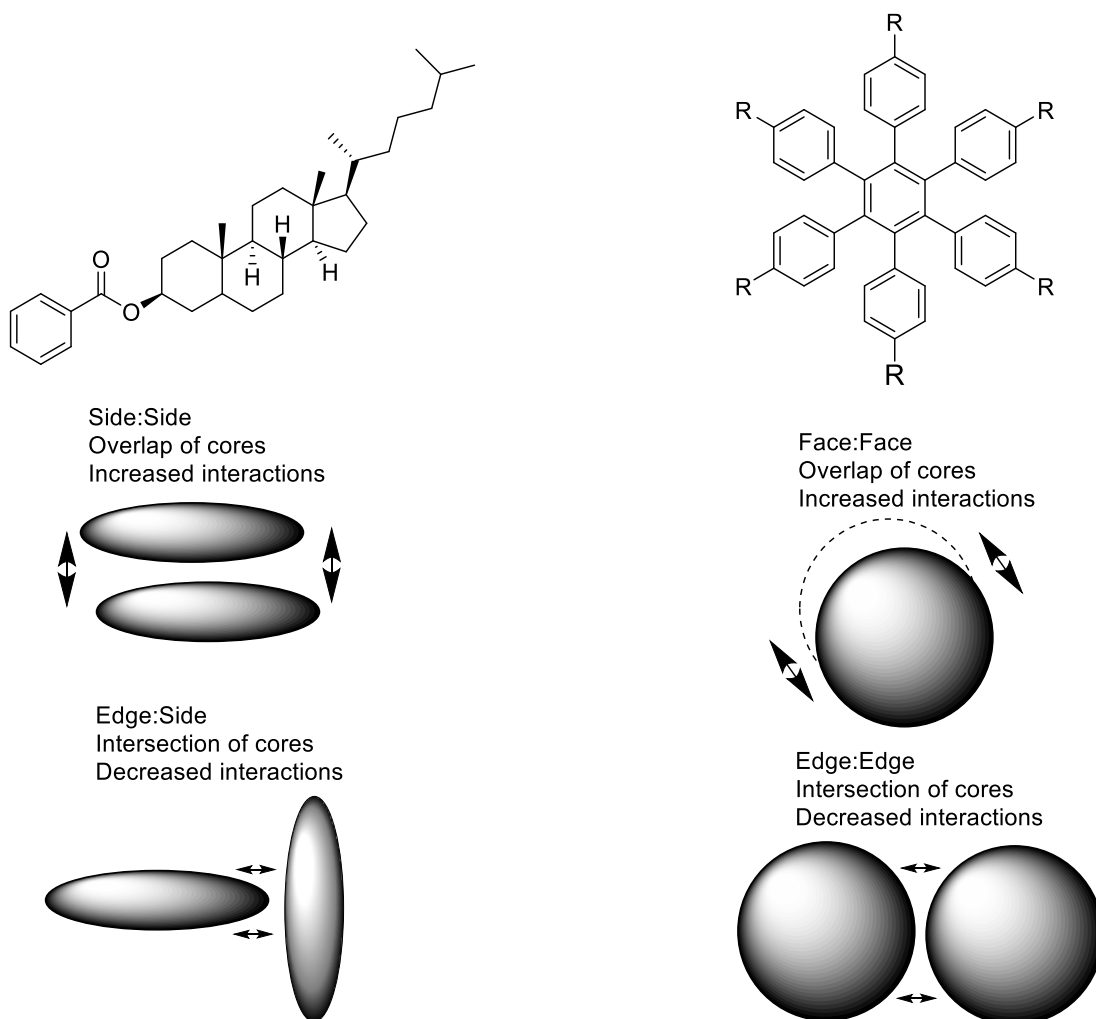
Figure 16. Examples of a rod-like or calamitic liquid crystal (left), and a disc-like or discotic liquid crystal (right). Interactions between neighbouring molecules can either be maximised (middle) or reduced (bottom) by a change in orientation.

As the requirements for liquid crystallinity or mesogenic behaviour are non-specific several calamitic mesogenic units are common in the literature such as linked rings (phenyl esters, azobenzenes and Schiff's bases)[20] or bonded rings such as biphenyls and cyanobiphenyls (Figure 17).[21,22] Extending the length of the cores either by multiple linking groups **2** or extended bonded rings such as terphenyl compound **3** rapidly increases the transition temperatures of the liquid crystal.

Phenyl esters

Biphenyls

Azobenzenes

Cyanobiphenyls

2

Cr 165.9 N 369.0 Iso °C[20]

Extended linked cores

3

SmB 216 SmA 229 Iso °C[21]

Extended fused cores
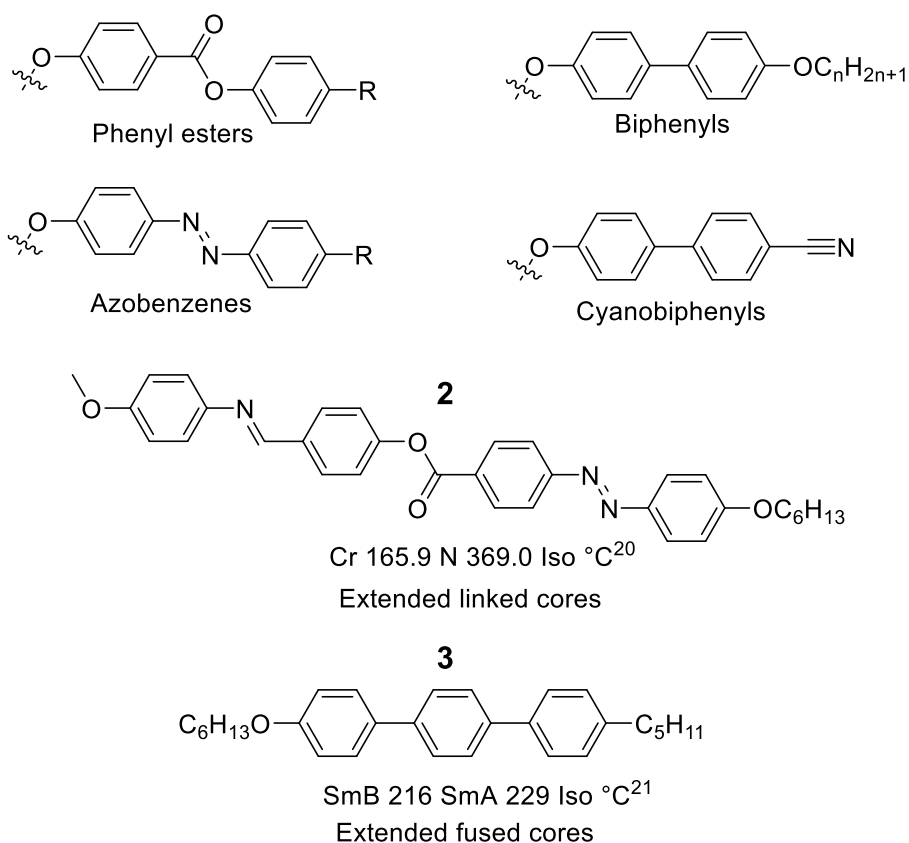
Figure 17. Examples of calamitic mesogenic units.[20,21]

Most commonly these mesogenic cores require a terminal alkyl chain to further increase the molecular length and thus the aspect ratio to ensure the stability of mesophases. Furthermore, terminal alkyl chains help to introduce flexibility around the mesogenic unit, disrupting its packing and thus reducing the melting point of the material. One further aspect related to both terminal alkyl chains, and alkyl chains linking mesogenic units is a tendency to show odd-even effects (See Figure 19). As an exception to the terminal chains featured in many mesogenic cores the cyanobiphenyl mesogen lacks this feature, however, remains an extremely commonly used mesogen. The cyanobiphenyl unit is indeed the most commonly used mesogenic unit in this work, and so will be discussed further.

The high polarity of the cyano- functional group forms a permanent dipole parallel to the long axis of the molecule. This is further enhanced by mesomeric effects due to the polarisable nature of electrons within the biphenyl ring system, and +M effect of the ether linkage giving a strong dipole of 4.2 D. This dipole provides stabilisation to an anti-parallel arrangement between two cyanobiphenyl molecules which effectively increases the aspect ratio of the mesogen further (Figure 18).[23] Evidence of this is

commonly seen in X-ray diffraction experiments, especially of smectic cyanobiphenyl compounds whereby the layer spacing observed relates to around 1.4 times the molecular length. This antiparallel arrangement provides a degree of local anisotropy giving liquid crystalline organisation. However, the antiparallel 'pairing' is time dependent between multiple states and so does not readily crystallise. This quadrupolar interaction increases the anisotropy of interactions shown in Figure 16, however provides conflict when calamitic mesogens stray from a rod-like shape for example by linking together multiple mesogens (See Figure 30).

Cyanobiphenyl

Quadrupolar interaction
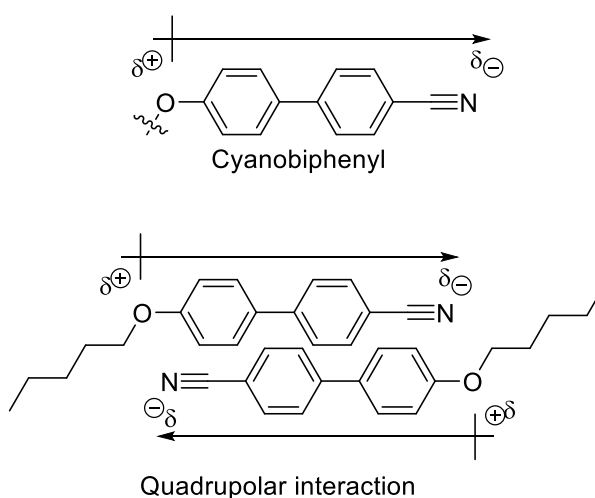
Figure 18. The cyanobiphenyl mesogen for which strong dipoles can lead to antiparrallel arrangements.

The 'odd-even' effect can be seen in simple single mesogens as shown here *via* the n-alkylcyanobiphenyls (Figure 19).[24] For short terminal chain lengths, the materials mesomorphism is entirely monotropic and as such the first point of the effect is shown with the butyl chain. It is clear that the clearing point increases sharply upon the extension of the alkyl chain from n = 4 to n = 5, before decreasing again in the case of n = 6. This trend continues as the length of the terminal alkyl chain increases further.
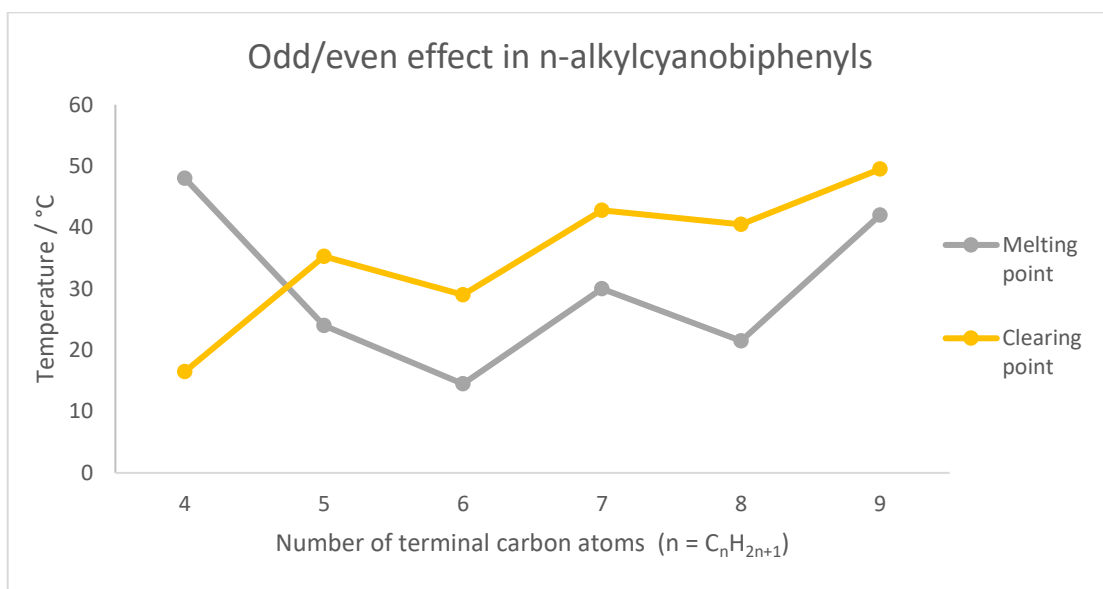
Figure 19. Graph showing the odd-even effect in simple n-alkylcyanobiphenyls.

This repeating odd-even pattern is termed the odd-even effect and is due to the changing conformation of the alkyl chain.[25] While the alkyl chain is in constant motion and rotation, the free energy of each carbon-carbon bond is minimised in the antiperiplanar conformation, where the chain is fully extended or 'all trans'. As the associated energy is lower, the fully extended state is more heavily populated, and so the addition of a methylene unit to the chain will change the angle of the terminal methyl unit relative to the mesogenic core (Figure 20). When n = 5 the clearing point is higher as the terminal methyl unit is 'in line' with the core, however when n = 6 this terminal methyl unit is 'off axis'. This change to the projection of the terminal methyl unit disrupts the local packing of the molecules and is thus expressed strongly in the transition temperatures as shown in Figure 19.
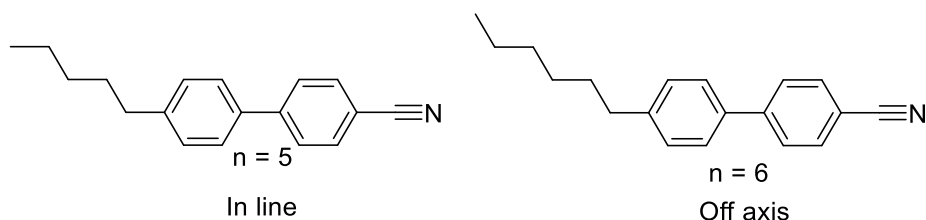
Figure 20. Lengthening the alkyl chain from n = 5 to n = 6 changes the angle of the terminal methyl unit relative to the core, this disrupts local packing and lowers transition temperatures.

This effect is largest when short alkyl units are used and are diluted as the length of the alkyl chain is increased. Longer chains possess more carbon-carbon bonds and thus

entropy dictates the fully extended 'all trans' conformation is less likely to occur. Therefore, the flexibility of the chain increases due to synperiplanar and gauche conformations (Figure 21). This in turn reduces the magnitude of the odd-even effect on the transition temperatures.
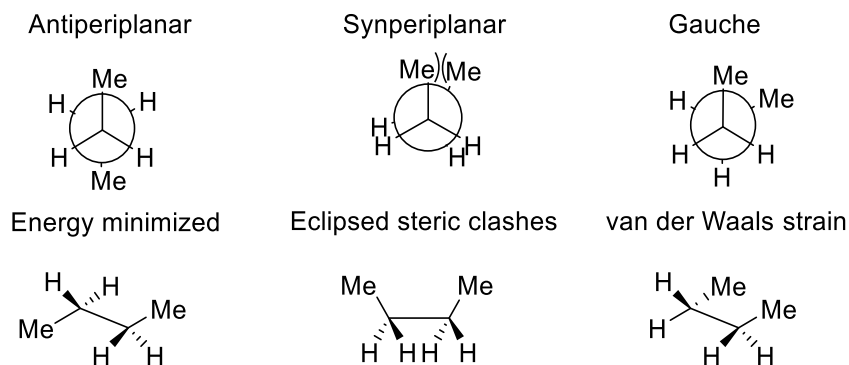
Figure 21. Alkane stereochemistry favours the antiperiplanar and gauche conformations around each carbon-carbon bond to avoid eclipsing interactions as shown in the synperiplanar projection.

Other relevant alterations to the structures of low molar mass liquid crystals include chirality discussed in chapter 6 and the use of short perfluoroalkyl to increase the order of the mesophase.[26] This is described in more detail as microphase segregation and the fluorophobic effect (see section 1.5.2).

1.3.2 High molar mass liquid crystals

High molar mass liquid crystals comprise of three sub-divisions: polymeric materials, dendrimers and supermolecular liquid crystals. The trends observed in polymeric materials can be applied to materials closer to those at the blurred lines between high and low molecular weight materials.

1.3.2.1 Liquid crystal polymers

Macromolecular structures such as polymers can show self-organisation and mesomorphic behaviour. While a review of polymeric liquid crystals is beyond the scope of this thesis, brief aspects will be highlighted as they apply to structure-property relationships. Polymerisation methods include addition and condensation polymerisations[27] and recent work frequently uses living polymerisation techniques such as RAFT.[28,29] Mesogenic units containing polymerisable groups can be polymerised to produce either main chain[30] (Figure 22) or side chain[27] (Figure 23) polymers. In the case of main-chain liquid crystal polymers aromatic cores such as p-phenyl or p-biphenyl may be linked *via* ester or amide linkages by condensation

polymerisation. The properties of main chain liquid crystal polymers can be controlled by increasing the proportion of biphenyl or terphenyl units to stiffen the backbone and so increase transition temperatures. Alternatively, by introducing kinked moieties which break the linearity of the polymer, or by incorporating lateral alkyl chains to reduce the intermolecular interactions of the polymer chains, the stiffness and thus transition temperatures of the polymer can be reduced.
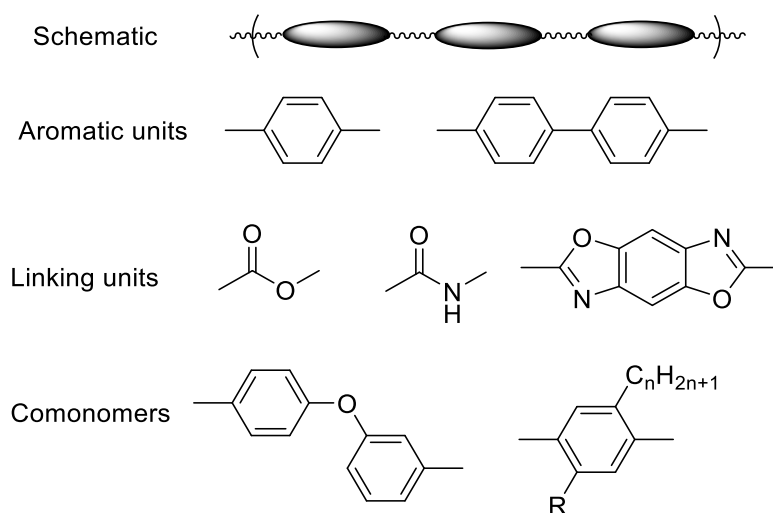
Figure 22. Schematic of a main-chain liquid crystal polymer. Aromatic cores may be linked via units such as esters or amides to form a mesomorphic material, control of the properties is enabled via kinks in the chain or laterally substituted units.

Side-chain liquid crystal polymers have mesogenic units attached as pendant groups on a polymer backbone. These mesogenic units are attached to the polymeric backbone via a flexible aliphatic spacer. Properties of the polymer may be controlled by varying the type of polymer backbone, the mesogenic pendant group and the spacer length (Figure 23).
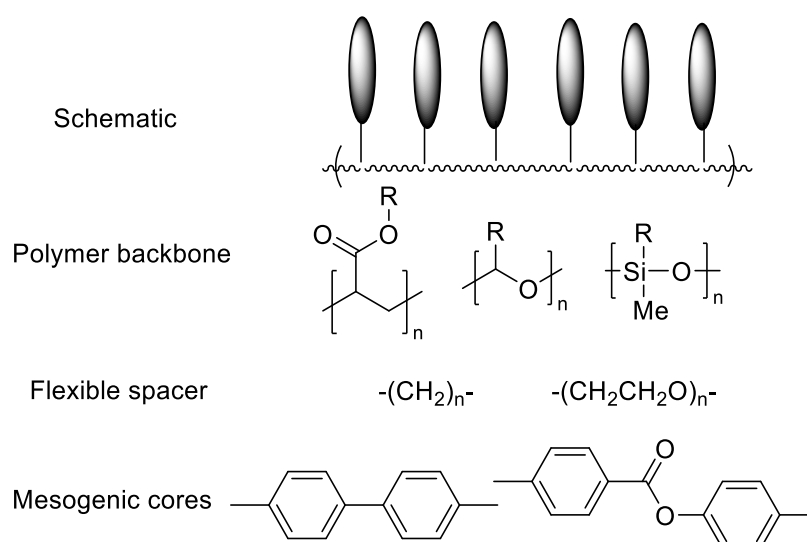
Figure 23. Schematic of a side-chain liquid crystal polymer. The Polymerisable backbone features flexible spacers such as methylene, or oxyethylene chains leading to mesogenic cores featuring aromatic ring units.

Due to the nature of the polymerisation reactions used to provide main-chain or side-chain polymers each gives a product with polydisperse molecular weight. Polydispersity has the effect of broadening the phase transitions of these materials. While polymeric systems and dendrimers are both supermolecular, dendrimers are monodisperse, and therefore there exists a trade off with the ease of synthesis of liquid crystal polymers compared with the challenging synthesis of liquid crystal dendrimers. There are however different methods by which to control polydispersity with some polymerisation techniques such as living polymerisation giving very low polydispersity or nearly monodisperse samples. Examples of this include work by Pugh and Schrock.[31] In these cases the transitions tend to be sharper and by having more easily controlled structures, the properties of the material desired can be more accurately refined.

1.3.2.2 Mesogenic units of polymers and dendrimers

Calamitic mesogens may be attached to the polymer backbone either in an end-on or side-on manner (Figure 24). This method of attachment is key to the self-organisation of side-chain liquid crystal polymers and dendrimers.[32] Side-on attachment is strongly nematogenic, inducing disorder and disrupting the formation of smectic layers. End-on attachment has a strong tendency to favour the formation of layers and thus smectic mesophases are possible, although nematic mesophases are also commonly

observed as a result of a more disordered mesophase or weaker mesogenic units. End-on mesogens in the form of cyanobiphenyls are solely used in this project though others may be used in wider work as shown in Figure 17. Commonly used side-on mesogens include various phenyl esters. These attachment types may be combined within a single molecule to provide a *Janus* material[32] (see 1.5.3) or combined polymer.[33]
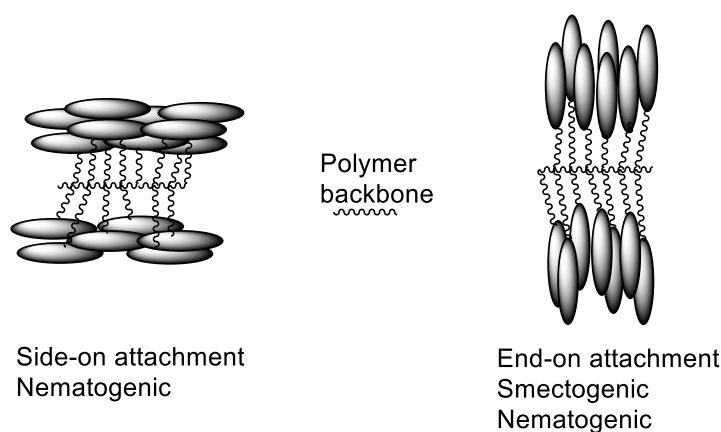
Figure 24. End-on and side-on attachment of mesogens in polymeric systems.

1.3.2.3 Spacer length

The role of the spacer in side-chain liquid crystals is to increase the flexibility and freedom of orientation experienced by the mesogens. This increases the amount of disorder present and reduces the crystallinity of the polymer, while also being able to decouple the motions of the backbone and mesogenic units.[34] Decoupling of the motions of the mesogenic group and main chain allows the mesogenic groups the freedom to move and ultimately achieve the orientational order required for a liquid crystal phase as described above. The behaviour associated with the spacer is also vital in other high molecular weight liquid crystal systems such as liquid crystal dendrimers and the dendritic supermolecular liquid crystals described in this thesis. Side-chain liquid crystal polymers may possess a mesophase without the use of a spacer giving

direct-linkage-type materials (Figure 25) though these tend to have narrower mesophase ranges.[35]

$$R = C_nH_{2n+1},$$
$$n = 2, 4, 6, 8, 12, 16$$
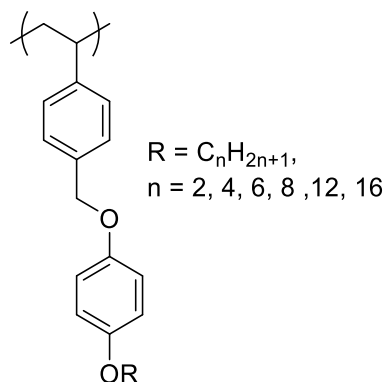
Figure 25. A Side-chain polymer with no flexible spacer for which liquid crystal behaviour is observed for chain lengths (n = 12, 16). In this case flexibility is introduced via the flexible benzyl alcohol unit.

The vast majority of side-chain liquid crystal polymers feature aliphatic spacers with general trends observed whereby increasing the spacer length will reduce the glass transition temperature of the polymer, though the behaviour of the clearing point is less well defined. Longer spacer lengths are far more effective at decoupling the mesogenic core and polymer backbone with eleven atoms typically being seen as sufficient to provide effective decoupling and mobility. Changing the length of a spacer may introduce an odd-even effect and changes the relationship between the backbone and mesogenic unit, therefore for direct comparison of materials equal spacer lengths are desired.

1.3.2.4 Dendrimers

Dendrimers offer an interesting counterpart to polymeric systems. The word dendron comes from the Greek word for tree and relates to a class of highly branched macromolecules. These materials can be imagined as being highly symmetrical around a point of origin at the core of the dendrimer, from which a branching point splits into multiple arms in analogy to the formation of branches in a tree (Figure 26). Dendrimers are described in terms of their generation, that is, the number of branching units encountered between the core and periphery of the dendrimer. After several generations the structure of dendrimers is expected to be roughly spherical and highly three dimensional.[36,37] The properties of dendrimers are largely dominated by the behaviour of the functionality at the periphery. The structures of dendrimers are

highly monodisperse when compared to polymeric systems and this has understandable appeal in terms of exhibiting highly tunable and precise properties.
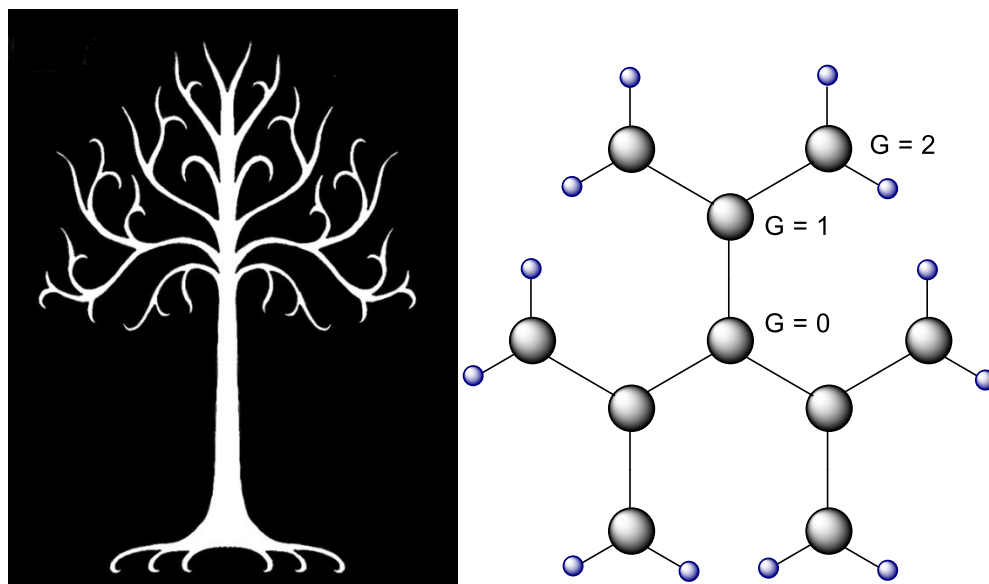
Figure 26. Tree and schematic image of a dendrimer showing the branching structure and generations.

The synthesis of dendrimers may be either convergent or divergent (Figure 27). In a convergent synthesis the peripheral groups are used as the building blocks, sequentially combining these blocks to form each generation of the dendrimer before finally joining multiple dendrons to form the core of the dendrimer in the final step.[38] This is beneficial as the number of reactions required in each step is limited by the branching multiplicity, however the final reaction between dendrons tends to be low yielding due to the huge steric bulk of each dendron, which is required to be in close proximity to react. The alternative is to follow a divergent approach whereby the core of the dendrimer is extended according to the branching multiplicity, then the process is repeated until the desired generation is reached.[39] While this successfully avoids challenging reactions at the core of the dendrimer by instead reacting at the exposed periphery, this approach requires high numbers of successful reactions to occur in the same step which can itself reduce the yield or lead to incomplete substitution, invalidating the monodisperse nature.
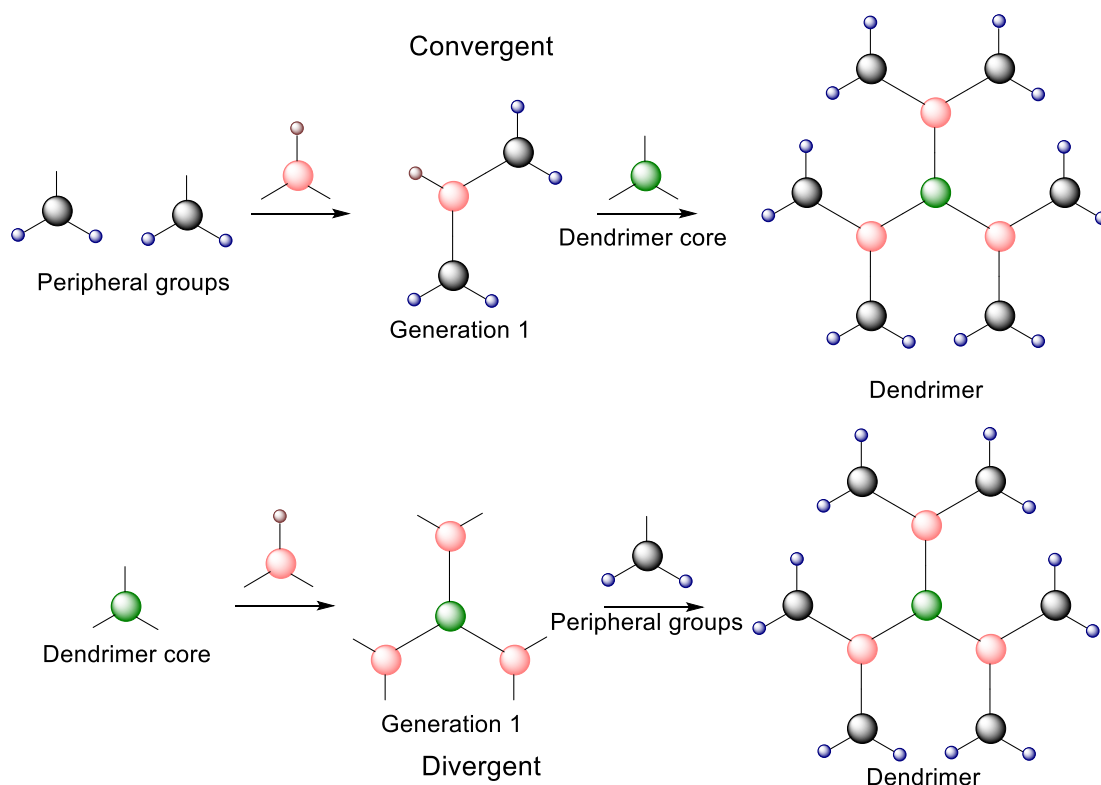
Figure 27. Convergent and divergent approaches to the synthesis of dendrimers.

The liquid crystal properties of dendrimers featuring different types of mesogenic units (Figure 28) is closely related to that of polymers with the same key features of spacer length, class of mesogen and attachment. The structure property of several liquid crystal dendrimers are described in section 1.5.3 *Janus* liquid crystals.
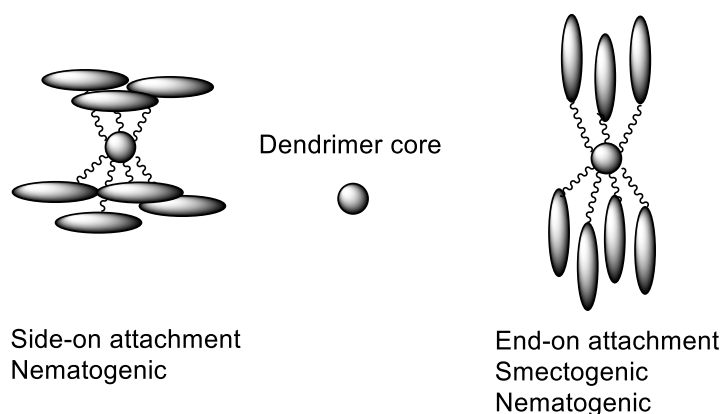
Figure 28. End-on and side-on attachment of mesogens in dendritic systems.

As a class of macromolecule the study of liquid crystal dendrimers occupies a middle ground between liquid crystal polymers and oligomers. In this way dendrimers can be considered as one example of a class referred to as supermolecular liquid crystals.

1.4 Liquid crystal dimers and oligomers

Dimers and oligomers comprise either two or more mesogenic units and bridge the gap between low molecular weight and high molecular weight liquid crystals (polymers and dendrimers). This is represented by Figure 29 showing the degree of discretion when it comes to classifying these materials.
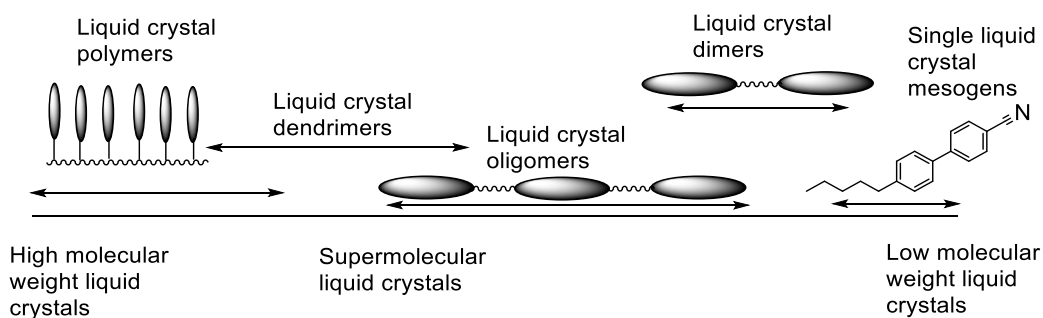
Figure 29. Descriptions such as supermolecular liquid crystal are not discrete and many types of structure can provide liquid crystalline behaviour.

Firstly, liquid crystal dimers consist of two typically low molecular weight mesogenic units tethered together by a spacer. This still offers a wide array of molecular arrangements with some example topographies shown in Figure 30 including T-shaped[40] and H-shaped[41] dimers. In addition, more complexity can be introduced as the dimer may either be symmetrical or unsymmetrical.
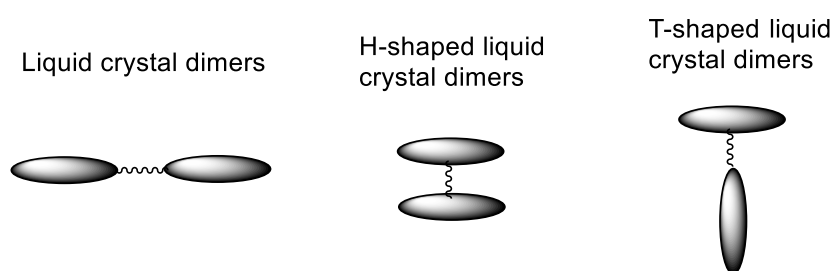
Figure 30. Many molecular arrangements and thus shapes are possible for liquid crystal dimers.

Similarly, to the behaviour of supermolecular liquid crystals, the length and parity of the spacer or linking group between mesogenic units in dimers is important. Liquid crystal dimers in particular have a strong tendency to show large odd-even effects similar to these shown in Figure 19 for alkyl cyanobiphenyls. Often the amplitude of the odd/even effect is greater in dimeric liquid crystals. This is because in the case of the dimers the mesogenic units are either parallel to each other or arranged at an angle to each other (Figure 31). Therefore, higher transition temperatures are

common for cyanobiphenyl dimers such as **5** with even parity spacers often giving a nematic phase and a linear structure. Contrastingly odd spacer parities as found in **6** give bent molecular structures and novel twist-bend nematic phases have been observed. In order to access the N_{TB} phase a material must be of a bent molecular shape, for example, as a dimer or other oligomer with an odd-membered spacer (due to the 'all trans' conformation).[42]
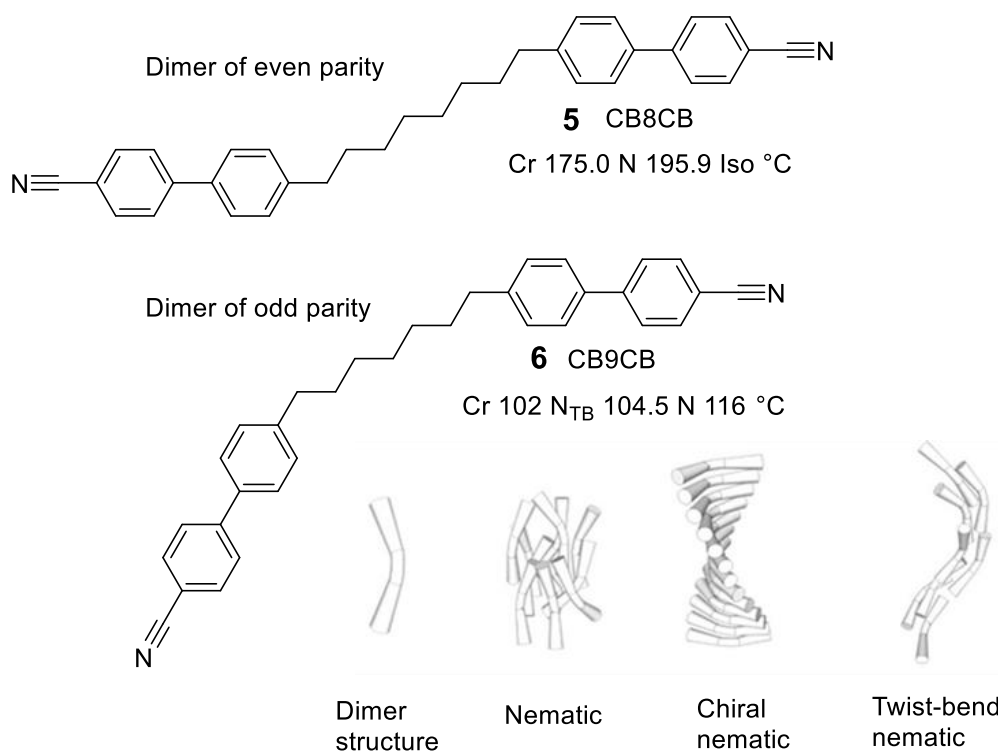
Figure 31. Odd-even effect in dimers can have large implications on the transition temperatures, or allow the formation of exotic phases (cartoon representation of a bent-dimer, and its organisation in the nematic, chiral nematic and twist-bend nematic reproduced from reference 42).

Aside from the parity of the spacer in liquid crystal oligomers, longer spacers allow for greater flexibility to the point of decoupling the motion of the two mesogenic units as described for polymeric materials. With very short spacers (n = 2, 3) the cores cannot effectively separate and the behaviour is instead analagous to a material with a single extended core.

Finally the point of attachment of the spacer is also key to the mesophase organisation. In the case of T-shaped oligomers the side-on attachment with respect to one of the cores induces a strong tendency to nematic phases while linear dimers can give nematic or smectic phases. The properties of H-shaped dimers can vary more

widely with some materials behaving similarly to the linear analogues and others behaving like side-on dimers.[43]

Similarly, oligomers can take several forms either being linear molecules where each mesogenic unit is linked by a series of spacers, or branched molecules referred to as multipedes. A final class of molecular organisation are disc-rod oligomers with a simplified example structure shown in Figure 32.

Linear liquid crystal oligomers

Liquid crystal mulitpedes

Disc-rod liquid crystal oligomers
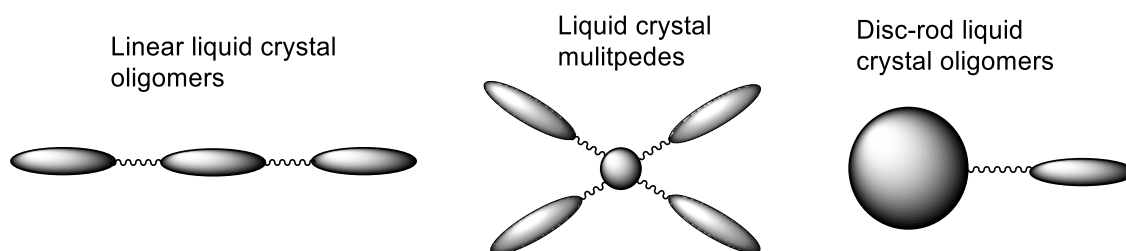
Figure 32. Structures of various classes of liquid crystal oligomers.

In the case of disc-rod oligomers these materials can behave as shape amphiphiles and can be considered as a class of *Janus* material. These materials may help bridge the behaviour of discotic and calamitic materials in pursuit of the theoretically predicted biaxial nematic (N_b) phase as seen in lyotropic liquid crystals. Mixtures of calamitic and discotic liquid crystals phase separate into two separate phases. It is suggested that by linking mesogenic units together the phase seperation could be avoided providing the N_b phase. Often attaching calamitic mesogens such as cyanobiphenyl to discotic materials such as **7** results in microsegregated mesophase structures giving calamitic behaviour **8** (Figure 33).[44]

7 R = Br   Cr 82 Col$_h$ °C

8 R =
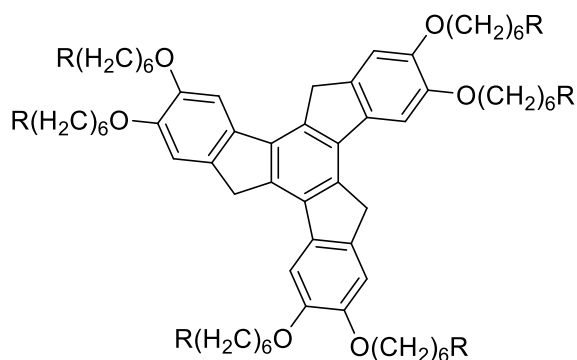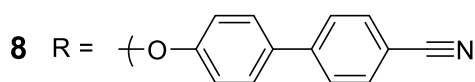
Cr 181 (177 N) Iso °C

Figure 33. An example material investigated as a disk-rod liquid crystal.

Liquid crystal multipedes represent an alternative method of linking several mesogenic units, by being branched at the core rather than being attached in a linear fashion. These multipedes can feature dendritic structures of low generation and some can be considered as examples of supermolecular liquid crystals. Treating these materials as a supermolecular liquid crystal, the core, spacers and mesogens all play a role in the mesophase type and structure (section 1.5). A common moiety used to introduce branching into liquid crystalline materials is pentaerythritol (Figure 34).[45]
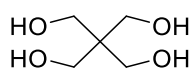
Figure 34. Pentaerythritol used as a tetrahedral branching unit from one quaternary carbon.

Pentaerythritol features the simplest imaginable branching point, that of a quarternary carbon. Each arm leading from this unit can be substituted with a mesogen as desired with many spacers used reflecting the synthetic route that was chosen. Due to the tetrahedral geometry of the quarternary carbon, symmetrical materials often pack easily into smectic mesophases by forming cylindrical pairs and not extending fully into a three-dimensional structure although this is dependent upon the relative volumes of the chains (Figure 35).[46] In general highly branched structures tend to suppress crystallisation giving glassy materials.

Flexibility of the tetrahedral centre allows two main conformations

Tetrahedral structure with 3:1 distribution
of mesogens, allowing seperation

Lamellar structure with even distribution
of mesogens on each face
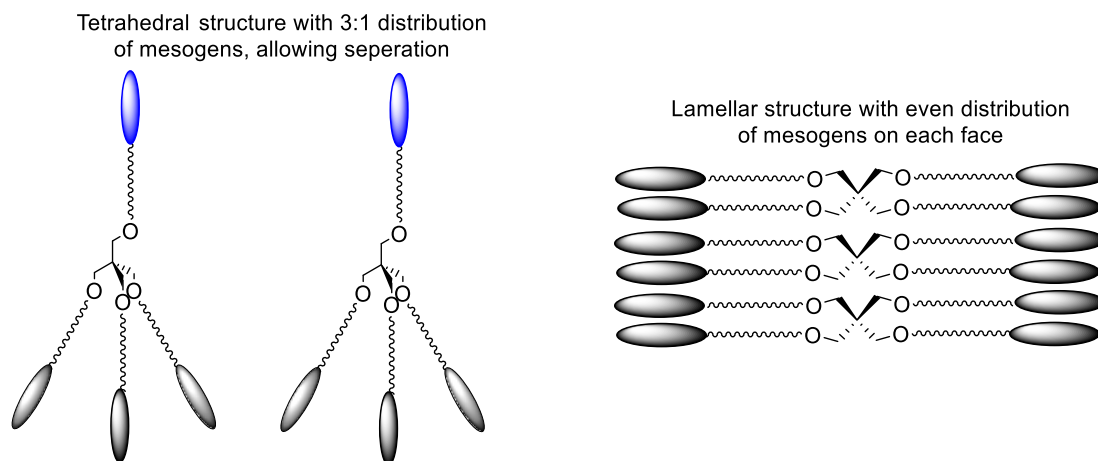
Figure 35. Three dimensional structures of pentaerythritol derived branching units.

1.5 Supermolecular liquid crystals

The most appealing aspect of the supermolecular liquid crystals is the ability to mirror the thermal properties of both polymeric and low-molecular-weight liquid crystals. In addition, supermolecular liquid crystals provide a route to combine multiple self-organising segments which may enrich phase behaviour, or allow the incorporation of functional moieties such as the fullerene unit in compound **9** (Figure 36).[47,48] Compared to polymeric liquid crystals, the monodispersity of supermolecular liquid crystals due to the use of discrete structures provides a more precisely controlled shape and overall architecture to the liquid crystal material, which is translated into the mesophase. The incorporation of functional segments will be discussed in detail later (1.5.3.6) however provides routes to several applications including photosensitive and sensing technologies.[49]
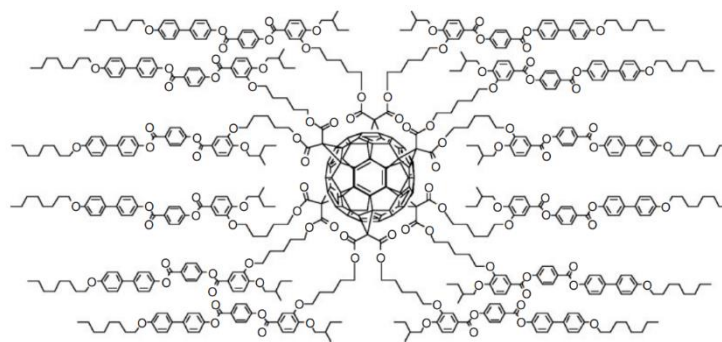
9

g 47 N* 103 °C Iso

Figure 36. A functional liquid crystal bearing a large, isotropic fullerene core may be coated with mesogenic units to provide a liquid-crystalline material (Figure reproduced from reference 48).

The overall shape of the supermolecular liquid crystal is expressed in the mesophase organisation *via* the overall curvature. With anisotropic supermolecules, differences in polarity, shape or rigidity can lead to phase segregation giving lamellar, columnar or cubic phases with similarity to lyotropic systems.[50]

1.5.1 Effect of the core on supermolecular liquid crystals

The interplay between the spacer length and core are important to the mesomorphic properties of supermolecular liquid crystal. This behaviour closely mirrors that of side-chain liquid crystal polymers. However, the core of a supermolecular liquid crystal may be chosen to provide a greater impact. With short spacers the mesogenic units are not decoupled from the core and so the entirety of the molecule is reflected in the mesophase. With longer spacers however, the motions of the mesogenic units are essentially decoupled from the core and so the mesophase often resembles that of the free low-molar-mass liquid crystal mesogen. The effectiveness of longer spacers is particularly impressive in the case of functional liquid crystals where large, isotropic units such as fullerene or polyhedral silsesquioxane may be incorporated into the supermolecule without suppressing liquid crystallinity.[51]

In the case of isotropic cores such as fullerene, multiple mesogenic units may be required to induce mesomorphism. This is often achieved by introducing branching into the supermolecule. This may be in the form of dendrimers or dendritic units or alternatively, smaller dimers or oligomers. Typically branching introduces a high degree of disorder which is often manifested by the suppression of crystallisation, and thus a widening of the mesophase range. This is typified by the glassy core-pendant

liquid crystals such as **10** (Figure 37) which feature multiply substituted, space-excluding cores linked to well-established mesogenic units such as cyanobiphenyl by short flexible spacers *i.e*. ethylene-pentylene.[52]

10

g 64 N 131 Iso °C
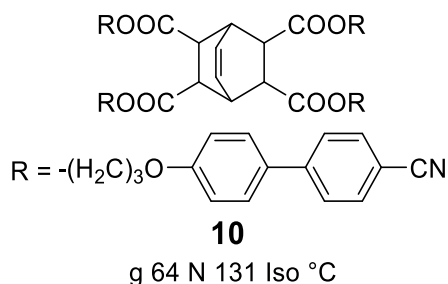
Figure 37. An example glassy liquid crystal showing a glass transition at 64 °C.

The number of mesogens or more specifically the density of mesogens around the supermolecular core plays a large part in controlling the self-organisation of the material. This is achieved *via* altering the overall molecular shape such as the largely spherical – isotropic structure assumed for high generation dendrimers, or semi 'rod-like' structures formed with fewer mesogenic units. With high numbers of mesogens it is no surprise that the mesogenic units are less free to move and self-organise, as there is less volume available for them to do so thus generating spherical or discotic organisations. With lower number of mesogens the packing of the system is typically optimised by organisation into rod-like shapes and thus the number of mesogens can control the molecular shape.

The examples provided above showing the effective incorporation of isotropic cores into liquid-crystalline phases, risks downplaying the possible effects of the core. The core itself may induce microphase segregation or provide interesting topology – that is the location of attachment or branching of mesogens with respect to the core. In the case of topology the discrete control over molecular structure enabled in supermolecular liquid crystals provides an advantage to polymeric systems. Changing the topology of the supermolecules core can result in different mesophases being expressed. This may easily be imagined in the case of cores which already possess a clear shape such as rods or discs where the shape may be preserved following the addition of mesogens. However, this idea can be extended further using the example of spherical fullerene cores, several investigations into the effects of topology by the synthesis of various substituted regioisomers has been carried out. A series of

bisadducts of [60]Fullerene dendrimers in either equatorial, or one of the two possible trans isomers as shown below (Figure 38).[53]

Compound number	Transition	Temperature /°C
12	Cr – SmA	44
	SmA – Iso	153
13	g – SmA	60
	SmA – X	167
	X – Iso	170
14	g – SmA	61
	SmA – Iso	169
15	Cr – SmA	42
	SmA – Iso	166
16	g – SmA	52
	SmA – Iso	161
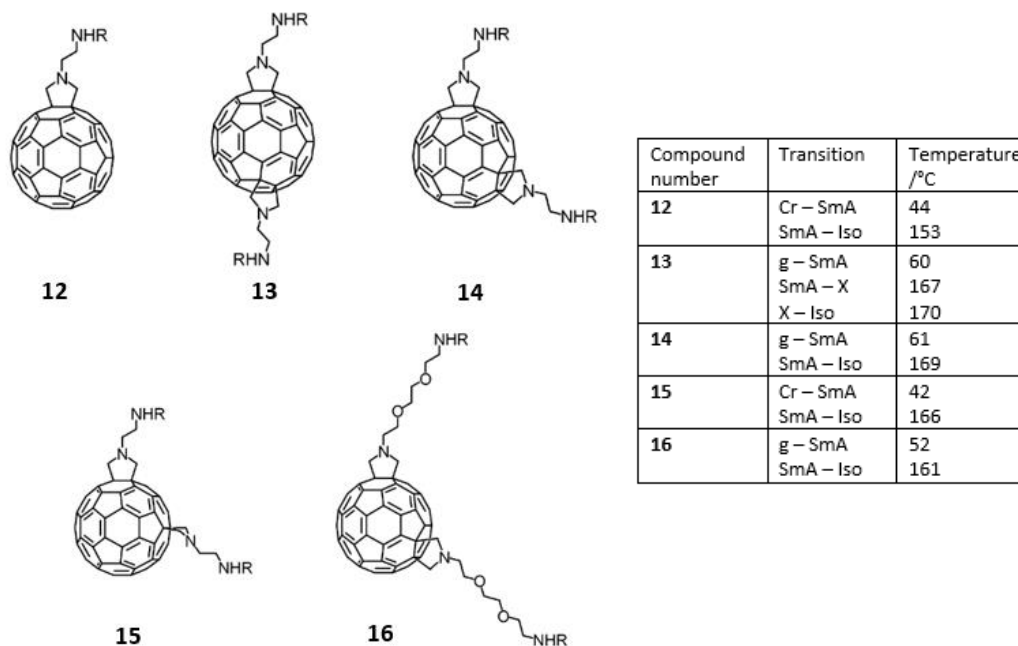
Figure 38. Functional supermolecular liquid crystals using a fullerene core. Varying the topology via regioisomers may introduce new phases or be expressed in the melting points.[53]

As expected, the differing substitution patterns were reflected in the liquid crystal properties. The two possible trans-isomers **13** and **14** had very similar glass transitions and temperature ranges of their liquid crystal phases, however compound **13** had an additional phase over a small temperature range which was not identified. The equatorial regioisomer **15** had a significantly lower melting point and slightly lower clearing point. It is worth noting the long spacer between the cyanobiphenyl bearing dendrimers and cores as there was an inverse relationship between spacer length and mesophase stability as shown by **16** and **14**. In all cases the liquid-crystalline phases cleared at temperatures lower than the parent carboxylic acid dendron. Further interesting examples of the effect of the topology around the core include penta-adduct 'shuttlecock' materials featuring substitution around one hemisphere of the fullerene which provides materials with columnar phases (Figure 39).[54] Many other examples were developed by Deschenaux and Felder-Flesch.[55,56,57]
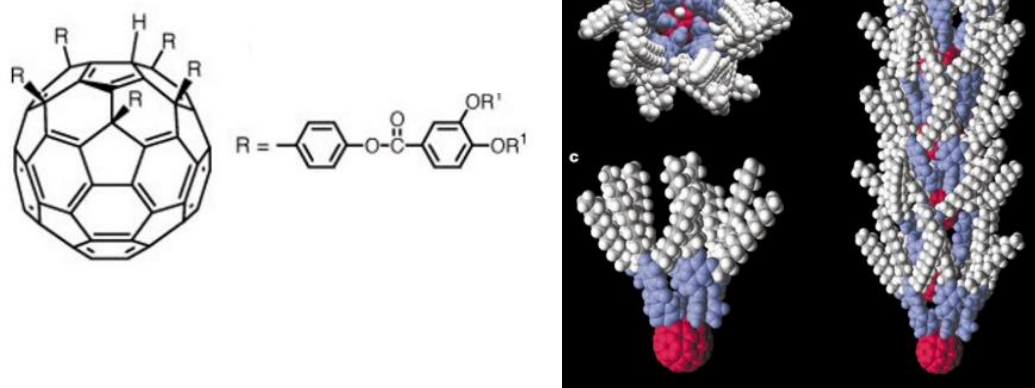
Figure 39. 'Shuttlecock' like materials which self-organise into columnar phases made from regioselectively substituted fullerenes (Figure reproduced from reference 54).

As mentioned previously the core may be used to introduce microphase segregation, a phenomenon discussed in more detail in the following section 1.5.2 One example of this has been shown in materials featuring polyhedral silsesquioxanes cores with simple alkyl chains providing lamellar phases (Figure 40).[58] The silsesquioxane cores are well-defined, rigid structures which therefore facilitate the study of the spatial distribution of mesogens. Liquid-crystalline materials within this broad category have been reviewed recently by Saez[59], with further reviews of star-shaped liquid crystals by Lehman.[60] One other aspect in the design of supermolecular liquid crystals is the presence of one or more chiral centres in the molecule. Chiral centres in either the core or mesogenic units leads to the formation of chiral liquid crystal mesophases (See 1.2.4), although no systematic studies have been performed regarding the interplay between core and end unit chirality.[61] Nevertheless in most materials another analogy to polymeric systems can be drawn as the type of mesogen (i.e. end-on; smectogenic

or side-on; nematogenic) will provide most of the stabilisation to the liquid crystalline phase and thus play a key role in the self-organisation.
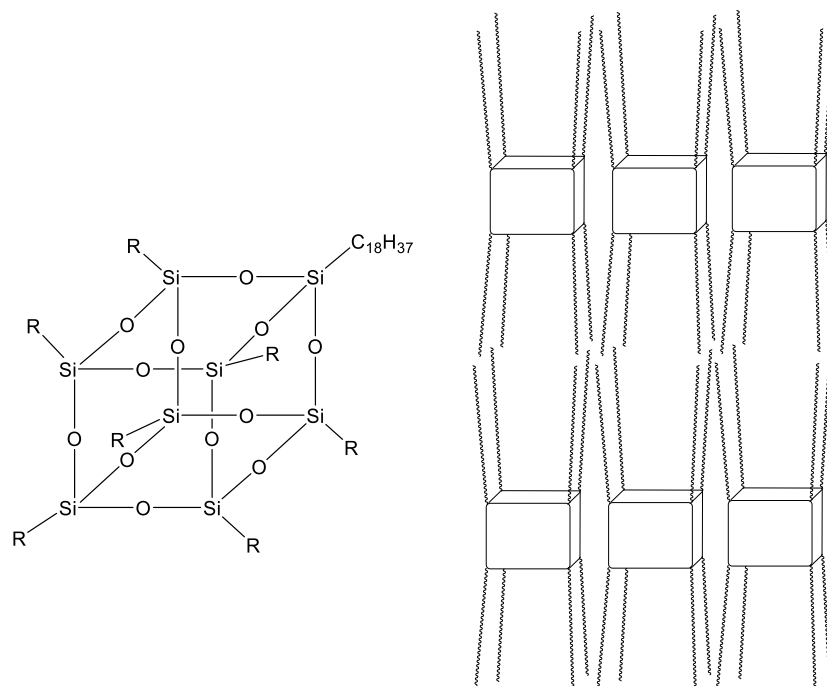
Figure 40. Polyhedral silsesquioxanes bearing long alkyl chains possess lamellar mesophases due to microphase segregation.

1.5.2 Microphase segregation and the fluorophobic effect

Amphiphilic materials offer one route to control the self-organisation of liquid crystalline materials, either in lyotropic materials or thermotropic materials *via* the lyotropic/thermotropic analogy. This can be demonstrated with differences of polarity such as lyotropic materials shown in Figure 2, hydrocarbon-fluorocarbon *Janus* materials (see figure 44) or size/shape amphiphiles (Figure 40). These materials use incompatibility between the two regimes of the molecule to enable microphase segregation – that is the division into two or more distinct nano-sized spaces. To enable this microphase segregation to be spontaneous the Gibbs free energy for segregation must be negative, or to be viewed the other way the free energy associated with mixing the components must be positive (Equation 5).[62]

$$\Delta G_{mix} = \Delta H_{mix} - T\Delta S_{mix}$$

Equation 5. Equation for the Gibbs free energy of the mixing of two fractions.

The term ΔH_{mix} can be evaluated based upon the cohesive energy density of the components of the mixture. To form a mixture the system must become less ordered

than its segregated components, and so the entropy of the system will increase, and therefore ΔS_{mix} is positive. For microsegregation to occur the magnitude of the favourable intermolecular interactions that are lost (ΔH_{mix}) must be more positive than the entropic gain of the mixed system ($-T\Delta S_{mix}$) is negative. This can be achieved in two ways, making ΔH_{mix} larger or ΔS_{mix} smaller. That is microphase segregation can either be driven by enthalpic contributions such as in polar/apolar, or hydrocarbon/fluorocarbon systems, or entropic effects such as the rigid core/flexible chains of discotic materials. A third system may be formed upon the basis of excluded volume, that is components which are otherwise unable to pack and fill space effectively such as shown by polyhedral silsesquioxanes (Figure 40).[63]

Of these categories of microphase segregation, it is manipulation of ΔH_{mix} which is of most relevance to this report. This is achieved in systems where the cohesive energy density of the two fractions are very different. This is easily understood for polar systems where interactions such as hydrogen bonding will vastly increase the cohesive energy of one component of the mixture. An alternative route may be achieved *via* introducing perfluorinated chains which have very low cohesive energy density due to their non-polarisable nature reducing their Van der Waals interactions.[64] This is possibly confusing at first sight as a singular C-F bond itself is highly polarised however along a perfluorinated chain these many dipoles are cancelled out due to the overall symmetry of the chain.

A second factor enabling microphase segregation in perfluorinated chains is their relative size, with a perfluorinated chain being roughly one and a half times larger than the hydrocarbon analogue. Due to the larger size of the perfluorinated chain its ease of packing – and thus intermolecular interactions – that contributes to the cohesive energy density are reduced. Additionally, the bulk of the fluorine atoms induces helical conformations along perfluoroalkyl chains by favouring rotation of roughly 13° around each carbon-carbon bond. This is accompanied by an increase in chain stiffness as the flexibility around each bond is reduced due to the larger steric bulk of the constituents. These two factors further discourage mixing of sufficiently long perfluoroalkyl and hydrocarbon chains. Overall, this effect resembles the hydrophobic effect whereby the hydrophobic components are buried to avoid disrupting the intermolecular interactions of water. In this case the perfluorinated chains are segregated to allow for

the hydrocarbon chains to interact more freely, thus this behaviour is termed the fluorophobic effect.[65]

It is this behaviour which contributes to the previously recognised smectogenic nature of perfluorinated chains, as an antiparallel smectic mesophase structure allows for segregation of the perfluorinated units into discrete layers. An additional case of interest is that of tapered molecules whereby a perfluorinated periphery and hydrocarbon or polar apex may pack into a columnar liquid crystal.[66] Mixtures of multiple amphiphiles each featuring different numbers of perfluorinated chains and thus taper angles, can be used to provide the full curvature related phase sequence from SmA – Cubic bicontinuous – Hexagonal columnar – Cubic micellar. This demonstrates that in systems of mixed and freely miscible amphiphiles it is the average curvature which determines the overall mesophase structure.

1.5.3 *Janus* liquid crystals.

With the factors controlling the self-assembly of supermolecular liquid crystals laid out, more specific examples in the context of *Janus* liquid crystals will now be explored. The anisotropy and self-organisation of *Janus* structures lend themselves to liquid-crystalline phases.

1.5.3.1 Mesogenic units

As described above the mesogenic units incorporated into supermolecular liquid crystal will generally reflect the mesophases observed in the low molecular weight liquid crystal analogue. While the mesogen's ability to induce a mesophase is normally maintained in *Janus* supermolecular liquid crystals, the combination of multiple mesogens complicates the phase behaviour and so may disrupt certain mesophases. This was demonstrated initially with *Janus* liquid crystals featuring both terminal and lateral attachment of mesogens, in which case the smectic phase induced by the terminally attached mesogens was disrupted by the incorporation of laterally attached mesogens (Figure 41).[32]
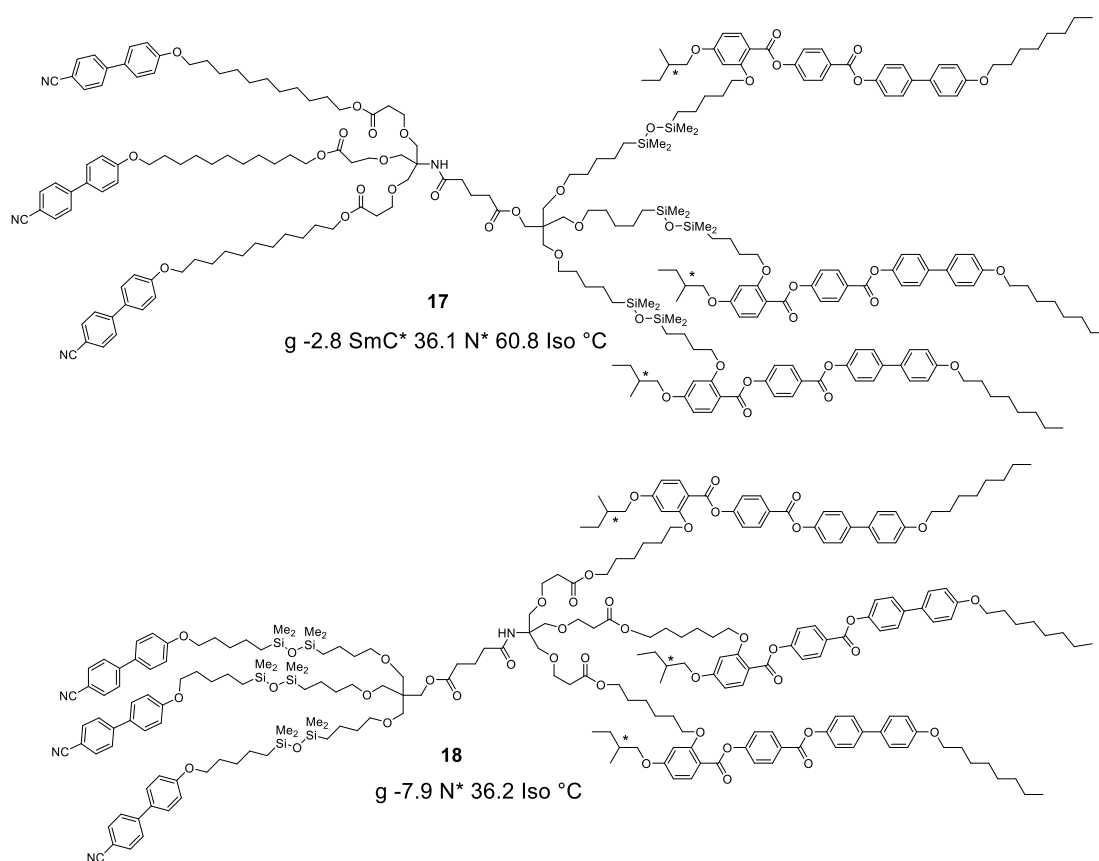
Figure 41. Janus liquid crystals featuring both terminally and laterally substituted mesogens.

Deschenaux reported a *Janus* liquid crystal dendrimer featuring a Percec-style dendritic segment opposite a dendritic unit substituted with cyanobiphenyl benzoate mesogens. This material exhibited a rectangular columnar (Col_r) phase and Smectic A phase upon heating (Figure 42).[67] The lower temperature rectangular columnar mesophase appeared to show interdigitation of the cyanobiphenyl groups as expected. A similar mesophase structure was observed in the smectic A phase, where the d/L ratio found by X-ray diffraction of 1.16 suggests a bilayer with heavy interdigitation so as to promote the intermolecular interactions of the cyanobiphenyl dipoles. Both of these mesophase structures are highly reliant on a flexible alkyl unit linking the two lobes of the *Janus* material.
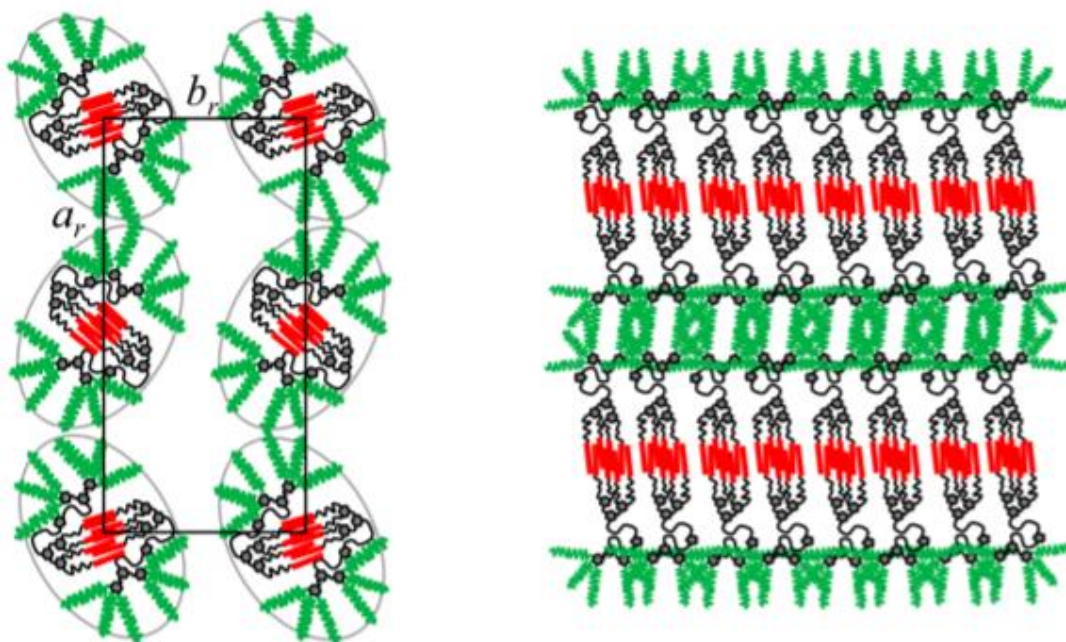
Figure 42. Janus liquid crystal dendrimer featuring cyanobiphenyl units (red) and a Percec-style dendrimer (green), cyanobiphenyl interdigitation is preserved in the Col_r (left), Smectic A (right) phases. Reproduced from reference 67.

Unique phase behaviour may also be generated by a *Janus* liquid crystal structure. Yoshizawa has reported a family of materials, synthesised as part of a series of compounds with a range of one to three cyanobiphenyl mesogens opposite of a perfluorinated chain (Figure 43). The series shows the effect of increasing the interfacial curvature of the overall molecule with compound **19** featuring an even ratio of perfluorinated to cyanobiphenyl mesogens exhibiting a smectic C phase, and compound **20** giving columnar and smectic A phases, while finally compound **21** exhibited cubic and smectic A phases.[68]

19

Cr 110.3 SmC 140.2 Iso °C

20

Cr 62.2 Col 134.2 SmA 170.6 Iso °C

21

Cr 83.2 Cub 141.1 SmA 154.9 Iso °C
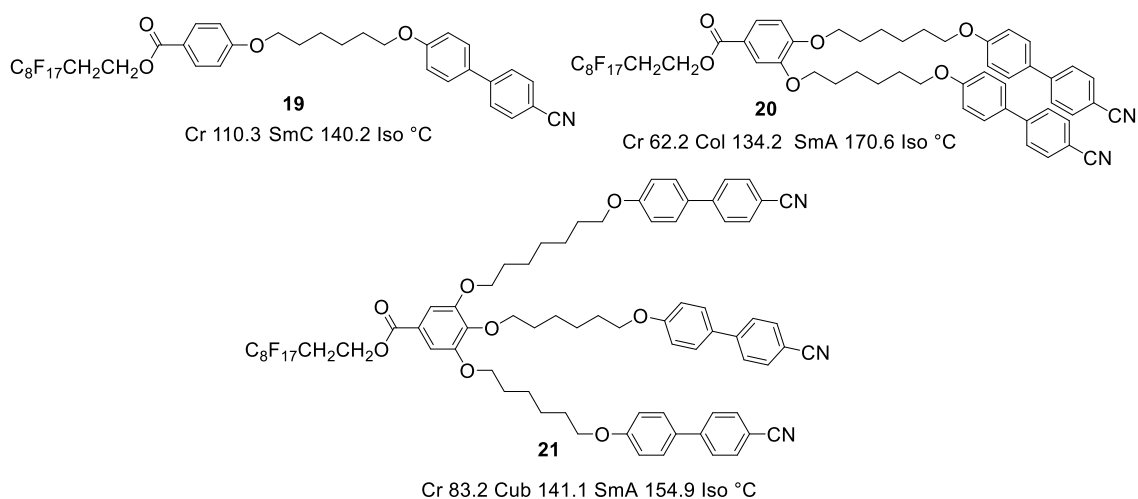
Figure 43. A series of amphiphiles bearing a perfluorinated chain and 1-3 cyanobiphenyl mesogens.

The formation of a cubic phase from cyanobiphenyl mesogens is rare thus showing the potential to gain new mesophases *via* the incorporation of mesogens into a *Janus* liquid crystal structure. In this example the cubic phase is formed due to the competition between the desired segregation of the immiscible fluorinated and aliphatic spacers and the steric effects of the highly tapered shape. This highlights the importance of shape in the behaviour of *Janus* liquid crystals, as well as that of microphase segregation of immiscible regions.

1.5.3.2 Size/Shape

The relative incompatibility of the two faces of the *Janus* liquid crystal will clearly differ with the combination of mesogens, and their sizes. The example in Figure 44 demonstrates how the ratio of mesogenic units in a *Janus* liquid crystal offers control over the overall shape of molecule and may affect the incompatibility of the two halves. The smectic A phase of **20** with a 1:2 ratio of perfluorinated to cyanobiphenyl units has a longer layer spacing than that of the compound **21** with a 1:3 ratio, as the increased steric constraints force the perfluorinated chains to intercalate with the aliphatic spacer units (Figure 44).[68]
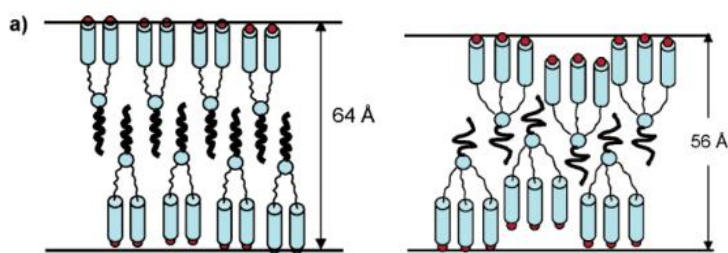
*Figure 44. The proposed structure of the smectic phases of compounds **20** and **21** as determined by X-ray diffraction, showing the forced intercalation of perfluorinated and aliphatic regions. Reproduced from reference 68.*

As the faces of a *Janus* structure become less compatible, the level of self-segregation will increase, typically increasing the stability of the liquid-crystalline phases and inducing more ordered phases.[69] The size of each incompatible mesogen must pass a threshold to enable self-segregation, and also affects the overall shape and curvature of the molecule.

1.5.3.3 Wedge shaped molecules

Strongly wedge-shaped molecules can form columnar or cubic liquid crystal phases (Figure 45). This is more likely if the apex and peripheral groups show a tendency for microphase segregation.[70–71]
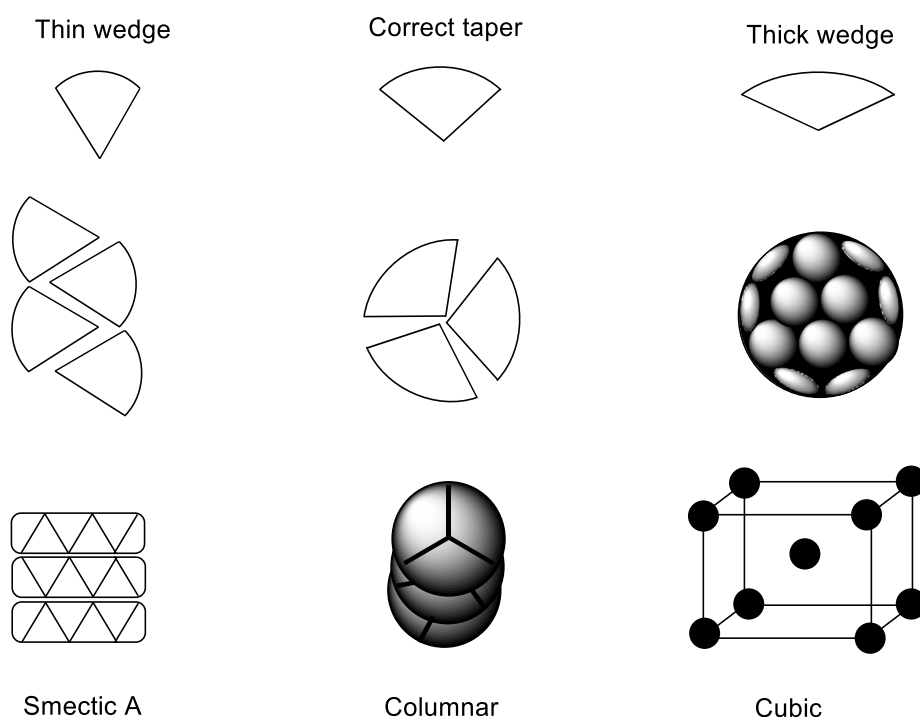
Figure 45. Schematic representation of columnar mesophase forming from wedge-shaped molecules.

This microphase segregation can be achieved by utilising either polar and non-polar groups or of particular importance to the work in this thesis, using perfluorinated chains to enable the fluorophobic effect. In addition to the segregation of the core and periphery, the correct tapered shape is required to enable the formation of discs which can be thought of as resembling slices from a pie (Figure 46).[72] This requires a fine balance as thin tapering will likely result in the formation of a smectic phase where antiparallel packing can space-fill effectively.[73] However thick wedges may not be able to pack into the desired columns and instead form micellar-like cubic structures.[74,75] This behaviour is closely related to that of lyotropic materials and is shown well in the

family of cyanobiphenyl:perfluoroalkyl compounds produced by Yoshizawa (Figure 44). Even in the absence of the fluorophobic effect wedge shaped dendritic compounds still show a sequential progression between smectic to columnar and finally cubic liquid crystal mesophases.[76]

$(3,4,5PBp-(3,5PBP))^{n-1}12G_n-X$

n = 1
X = CO$_2$CH$_3$, Lam$_{(k,bilayer)}$ (25 °C): a = 45.5 Å
X = CH$_2$OH, Lam$_{(k,bilayer)}$ (25 °C): a = 43.8 Å

n = 1
X = CH$_2$OH, Φ$_{r-s}$ (42 °C): a = 45.1 Å, b = 31.2 Å,
D$_a$ = 45.1 Å, D$_b$ = 31.2, μ = 6, α' = 60.0 °

n = 2
X = CO$_2$CH$_3$, Φ$_{r-c}$ (20 °C): a = 105.6 Å, b = 87.6 Å,
D$_a$ = 60.9 Å, D$_b$ = 87.6 Å, μ = 7, α' = 48.6 °

n = 2
X = CH$_2$OH, Tet (40 °C): a = b = 206.1 Å; c=107.4 Å,
D = 66.2 Å, μ = 53, α' = 6.8 °

n = 3
X = CO$_2$CH$_y$ Cub (X)

n = 3
X = CH$_2$OH, Tet (30 °C): a = b = 234.0 Å; c=132.4 Å,
D = 77.3 Å, μ = 39, α' = 9.1 °

$(3,4PBp-(3,5)^{n-1})12G_n-X$

n = 1
X = CO$_2$CH$_3$, Lam$_{(k,bilayer)}$ (30 °C): a = 49.9 Å
X = CH$_2$OH, Lam$_{(k,bilayer)}$ (30 °C): a = 48.3 Å

n = 2
X = CO$_2$CH$_3$, Lam$_{(k, bilayer)}$ (25 °C): a = 52.8 Å

n = 2
X = CH$_2$OH, Φ$_h$ (65 °C): a = 67.5 Å,
D = 67.5 Å, μ = 8, α' = 43.2 °

n = 2
X = CH$_2$OH, QLC (73 °C): a =77.8 Å
D = 50.3 Å, μ = 30 , α' = 12.1 °

n = 3
X = CO$_2$CH$_3$, Φ$_h$ (55 °C): a = 73.1 Å,
D = 73.1 Å, μ = 5, α' = 78.0 °

n = 3
X = CH$_2$OH, Cub(65 °C): a = 142.3 Å,
D = 88.3 Å, μ = 75, α' = 4.8 °

$(4PBp-3,4PBp-(3,5PBp)^{n-1})12G_n-X$

n = 1
X = CO$_2$CH$_3$, Φ$_h$ (170 °C): a = 49.7 Å,
D = 49.7 Å, μ = 6, α' = 58.0 °

n = 1
X = CO$_2$CH$_3$, Φ$_{r-c}$ (35 °C): a = 124.1 Å, b = 87.4 Å,
D$_a$ = 71.6 Å, D$_b$ = 87.4 Å, μ =16, α' = 22.7 °
X = CH$_2$OH, Φ$_{r-c}$ (180 °C): a = 191.6 Å, b = 179.7 Å,
D$_a$ = 110.6 Å, D$_b$ = 180 Å, μ = 52, α = 7.0 °

n = 2
X = CO$_2$CH$_3$, Φ$_{r-c}$ (135 °C): a = 163.2 Å, b = 149.2 Å,
D$_a$ = 94.2 Å, D$_b$ = 149.2 Å, μ = 17, α' = 21.5 °
X = CH$_2$OH, Φ$_{r-c}$ (180 °C): a = 194.1 Å, b = 84.3 Å,
D$_a$ = 112.1 Å, D$_b$ = 84.3 Å, μ = 11, α' = 31.5 °

n = 2
X = CO$_2$CH$_3$, Cub (185 °C): a = 275.9 Å,
D = 171.2 Å, μ = 770

R = n-C$_{12}$H$_{25}$

Figure 46. Wedge shaped dendrons reported by Percec, Figure reproduced from reference 72.

The addition of solvent can provide an alternative method to change the size of one or more domains and thus curvature of the structure.[77] Molecules bearing polar and apolar domains will swell each domain selectively when in contact with polar or apolar solvents. Perfluorinated chains can be swollen similarly with perfluorinated solvents.

1.5.3.4 Janus Dendrimers

Janus dendrimers allow good control over the morphology of the products with the possibility for rational design. Percec has reported comprehensive libraries of dendrimers based on pentaerythritol cores and benzyl ether or benzyl ester peripheries.[78] These may be modified to yield *Janus* materials with the typical complex conformation and morphologies. These self-assembled structures have been studied extensively to develop an understanding of structure-property relationships. The microphase segregation available in *Janus* dendrimers has been demonstrated by the co-assembly or self-sorting of dyes based upon the composition of the giant vesicles used (Figure 47).[79]
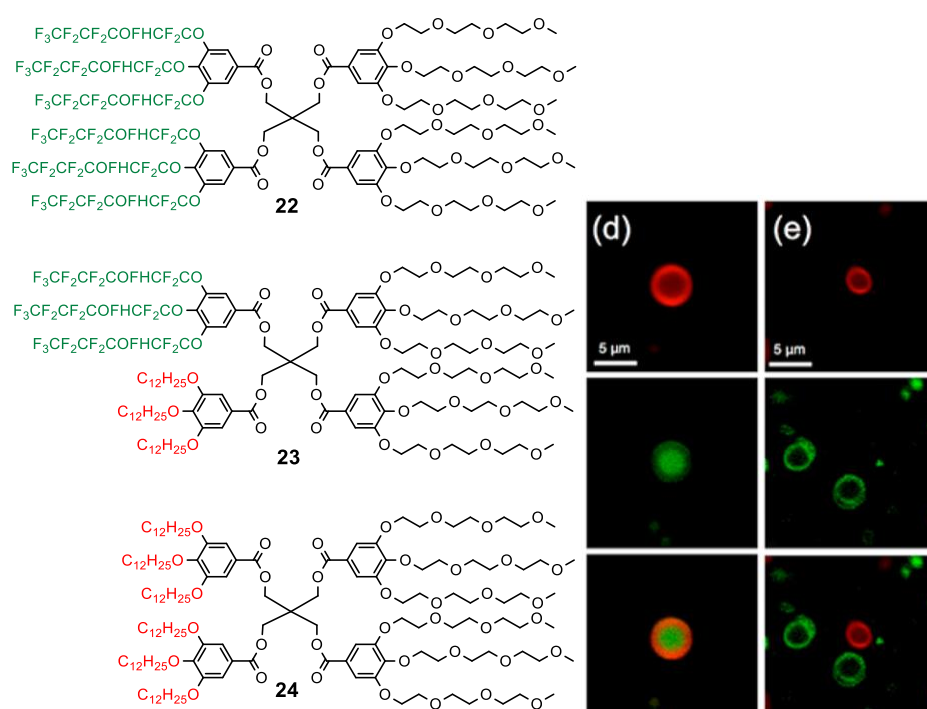
Figure 47. Examples of Janus dendrimers of polyethylene glycol and fluorinated, hydrophobic or mixed chains. Mixtures of these form dendrimersomes as shown by segregation of dyes. (Reproduced from reference 79).

Hydrophobic and fluorinated chains were attached to either pentaerythritol or tris(hydroxymethyl)aminomethane (not shown) cores bearing hydrophilic ethylene glycol chains. This gave the desired hydrophobic, fluorinated and mixed *Janus* dendrimers. One of the polyethylene glycol chains of **22** or **24** can be substituted for a red or green fluorescent dye. Depending on the composition of the mixtures the vesicles may separate when containing 0% of mixed **23** (Figure 47 (e)) or self-assemble if mixed **22** is present (Figure 8 (d)). In both sets of images (d) and (e) the proportion

of **22** and **24** are equal. Potential applications for this self-assembly include the co-assembly of hydrophobic dendrimers with bacterial and human cells, while fluorinated dendrimers may offer slow release drug delivery technology.

Materials with a dendritic hydrophilic core and Percec type hydrophobic dendron have been reported by Bury *et al.* as amphiphilic block codendrimers (Figure 48).[80] Following a systematic study, some details of the structure:property relationship were found such as the role of the hydrophilic hydrogen bonding core in stabilising the mesophase. By changing the volume of this lobe the mesophase could be modified, and likewise by changing the generation of the Percec type dendron used as the exterior, the mesophase could be incrementally changed from columnar to cubic. Related *Janus* dendrimers featuring polyethylene glycol (PEG) chains have recently been used to tune wettability of hybrid dendrimer:gold nanoparticle materials.[81]
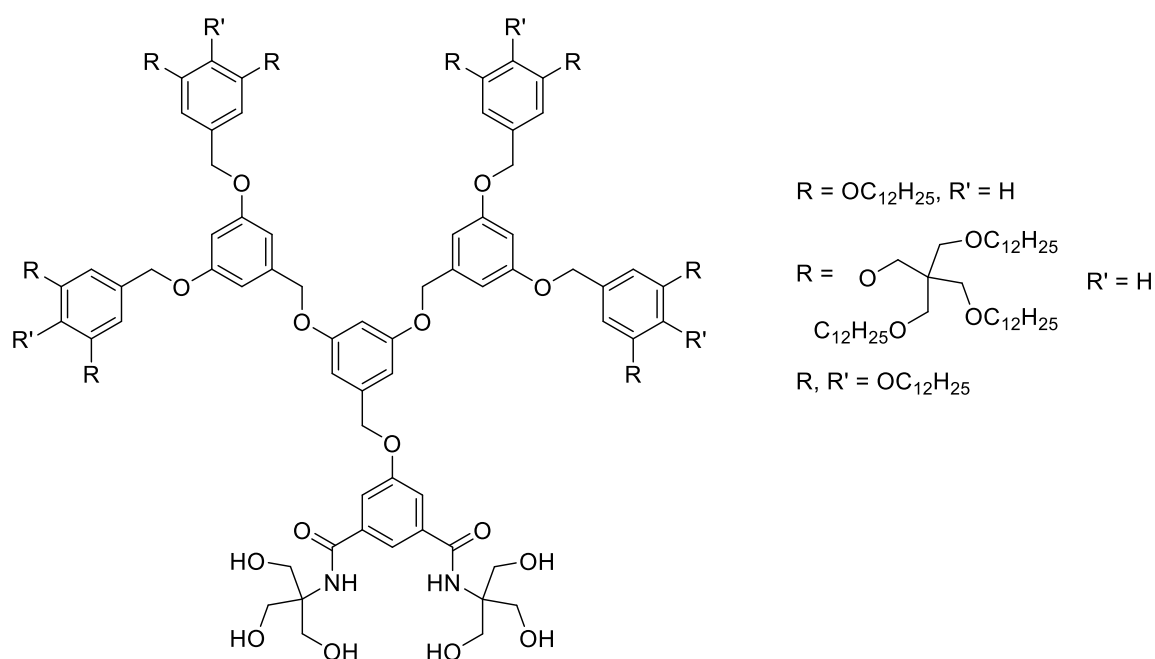
Figure 48. Janus materials featuring a hydrophilic core and hydrophobic Percec-style dendron.

Janus dendrimers have been studied for use in drug delivery either using compartmentalisation *via* micelles or dendrimersomes or by covalent bonding of the drug to a dendrimer suitable for targeting or enhanced solubility.[77] Of these two categories only the formation of dendrimersomes and micelles is of relevance in this review. The work in this field was pioneered by Fréchet and Gillies.[82]

These materials have similar thicknesses to biological membranes and may be useful in cell-like assemblies or synthetic biology. Many more examples of using *Janus* dendrimer structures for drug delivery and potential combination therapies are provided in a review, however little is said about the mechanisms controlling the mesophase.[83]

1.5.3.6 Functional materials

One possible architecture for *Janus* materials is provided by the hexaaryl benzenes. Hexaaryl benzene (HAB) derivatives are also of interest in several fields of research with a comprehensive review being performed by Kumar.[84] These materials are propeller shaped due to steric clashes between the aryl rings which suppresses aggregation and crystallinity, which otherwise cause issues with similar polyaryl materials. HAB derivatives may be modified for use in OLED or chemical switches while the unaltered hexaphenyl benzene structure has moderately good emissive properties. Interestingly aggregation of HAB materials in poor solvents appears to reduce the rotation available to the peripheral units, thus increasing the π-conjugation and increasing luminescence.

Attaching mesogenic units to the periphery to generate HAB derivatives often induces columnar phases. These units are often chosen to continue the conjugated system. However, alkyl chains have also been shown to grant columnar liquid crystalline phases while different polar systems can have several different effects and applications.[85] Of most relevance to this project are HAB derivatives with one alkyl and perfluorinated chain per peripheral ring (Figure 49).[86] These materials were synthesised from diphenylacetylene precursors, which themselves show self-assembly into pure domains of perfluorinated, alkyl and aromatic units.
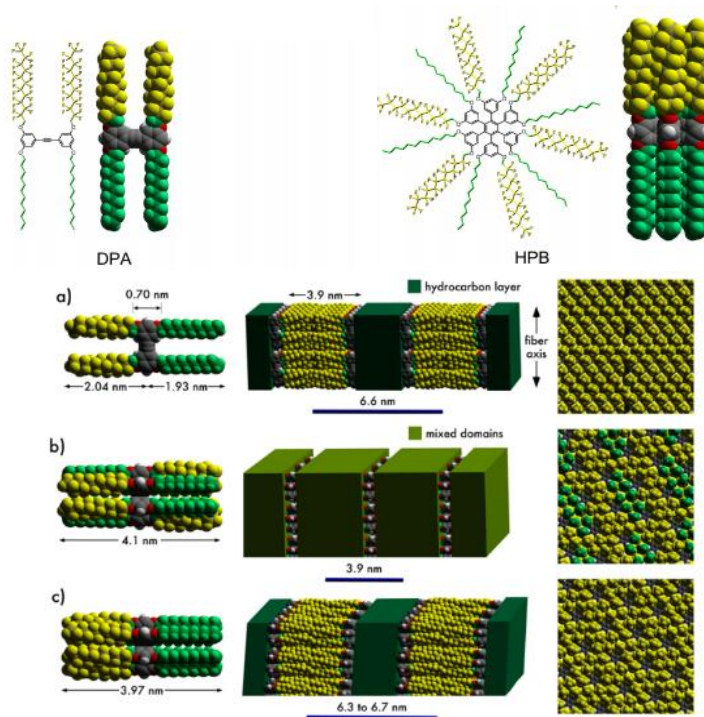
Figure 49. The self-assembly of an amphiphilic diphenylacetylene and hexaarylbenzene featuring alkyl and perfluorinated chains a) shows the self-assembly of the diphenylacetylene, b) the hexaarylbenzene, and c) the hexaarylbenzene doped with 1% of the diphenylacetlyne which induces the separation of the chains. Reproduced from reference 86.

Once the diphenylacetylene has undergone reaction to give the HAB derivative the perfluorinated and alkyl chains are instead trapped in a mixed domain in a lamellar structure. Addition of 1% of the diphenylacetylene is enough to restore separation of the perfluorinated and alkyl chains above 90 °C, while at lower temperatures the perfluorinated chains are again mixed with the alkyl domains.

Contrary to the appeal of HAB as a non-aggregating material, another reason for the interest in these compounds is the potential for oxidation to hexabenzocoronene (HBC) derivatives. These materials have uninterrupted π-stacks which may be useful as organic-based electronics, or photovoltaic devices where they may stabilise the formation of holes.[87]

In addition *Janus* liquid crystal dendrimers have been studied by Serrano for use in charge transport (Figure 50).[88] This is achieved by having highly conductive regions at the core of a columnar liquid crystal, where these conductive regions are microsegregated away from the rest of the molecule, and other supermolecular columns. This is an appealing avenue for advancement within the field of organic electronics and highlights the multidisciplinary nature of liquid crystal research.
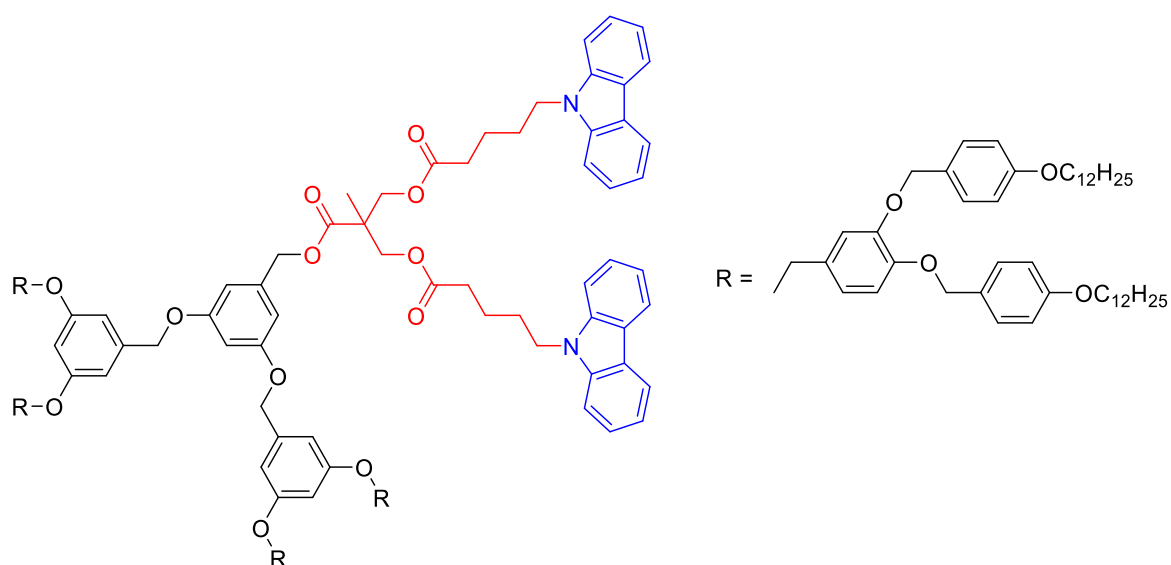
Figure 50. Functional Janus Liquid crystal dendrimer using a Percec-style dendron to stabilise functional carbazole units (blue) which have good electron transfer properties.

1.6 Characterisation of liquid crystal phases

The most common techniques used to characterise liquid crystalline mesophases and behaviour are polarised optical microscopy (POM), differential scanning calorimetry (DSC) and small/wide angle X-ray diffraction (SWAXS). These techniques are summarised below.

1.6.1 Polarised Optical microscopy

Polarised optical microscopy is a key technique in the characterisation of liquid crystal mesophases. Liquid crystals are anisotropic and as a result they exhibit two refractive indexes which are associated with the ordinary and extraordinary rays, n_0 and n_e respectively (Figure 51). These materials exhibit birefringence as described by equation 6. This is brought about by interactions of light with the polarisable cloud of electrons from the aromatic cores common in liquid crystals.
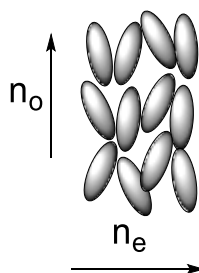
Figure 51. The refractive index differs depending on direction of the lights propagation, this phenomenon is called birefringence.

$$\Delta n = n_e - n_o$$

Equation 6. Birefringence Δn is given by the difference between the ordinary and extraordinary rays.

This birefringence allows for liquid crystalline materials to be viewed under polarised optical microscopy (Figure 52). Polarised optical microscopy uses a microscope with crossed polarisers – i.e. a polariser between the light source and the sample, and an analyser between the sample and the eye piece – to observe the birefringent textures arising from the arrangement of molecules on a glass slide. Each liquid crystalline phase exhibits its own characteristic texture based upon the defects arising within the phase.[89]
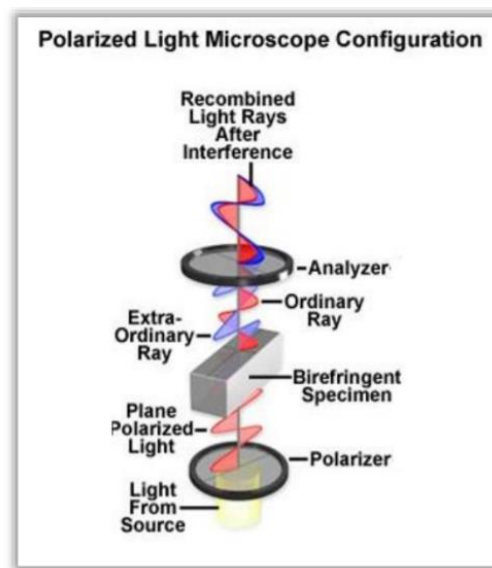
Figure 52. Cartoon representation of polarised optical microscopy equipment. Reproduced from reference 89.

1.6.1.1 Nematic phase

The nematic phase exhibits a distinctive texture on the microscope called a schlieren texture. This arises from a rapid change in the orientation of the molecules around point defects (singularities). Defect lines occur between the point singularities when the local director field is parallel to either the polariser or analyser and two distinctive defects are observed;[90] either 2-brush or 4-brush defects. These 2- and 4-brush defects can be classified as $S = \frac{1}{2}$ or $S = 1$ defects according to equation 7.

$$S = \frac{\text{number of brushes}}{4}$$

Equation 7. Brushes within the Schlieren texture are denoted by the letter S according to equation 7.

The S_1 or $S_{1/2}$ defects are classed as either + or − as shown in (Figure 53, left). The nature of the defect can be discerned as + or − by rotating the polariser and analyzer of the microscope together. The brushes either rotate in the same direction (+) or in the opposite (-) direction to the polariser and analyser. An example of the nematic texture showing 2- and 4-brush defects within the schlieren is shown below (Figure 53, right).
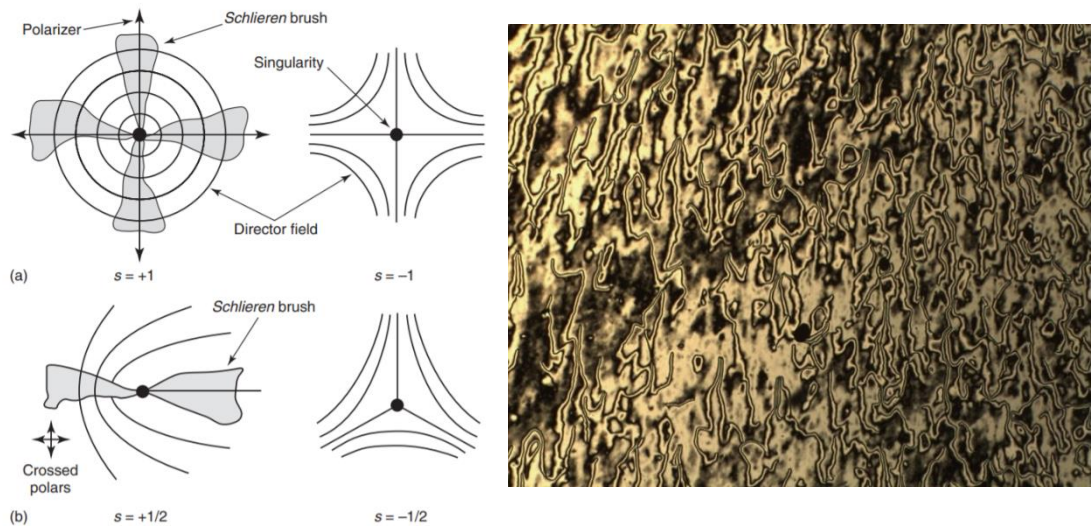
Figure 53. Point defects within the nematic mesophase resulting in 2-brush and 4-brush defects (left), and example within the schlieren texture (right). Diagram reproduced from reference 90.

Alternatively, the marble nematic texture can be observed; this texture is often observed upon melting a crystalline material into the nematic as the long molecular axis remain aligned and as such large areas with uniform director orientation can form. This texture is typically highly uniform with slight changes in colour due to variations in birefringence brought about by changes in the director or sample thickness.

1.6.1.2 Smectic A phase

The characteristic texture of the smectic A phase is the formation of a focal-conic defect. The layers within a smectic phase bend or wrap around point defects. The result of this bending is a three-dimensional structure referred to as a *Dupin cyclide* which shows two lines of optical discontinuity (Figure 54) referred to as the ellipse and the hyperbola. In three dimensions this gives rise to the focal conic structure. The structure of the focal conic can be difficult to visualise but a 2D image based on *Dupin cyclides* showing the two defect lines and a 3D image showing the focal conic structure are shown in figure 54.
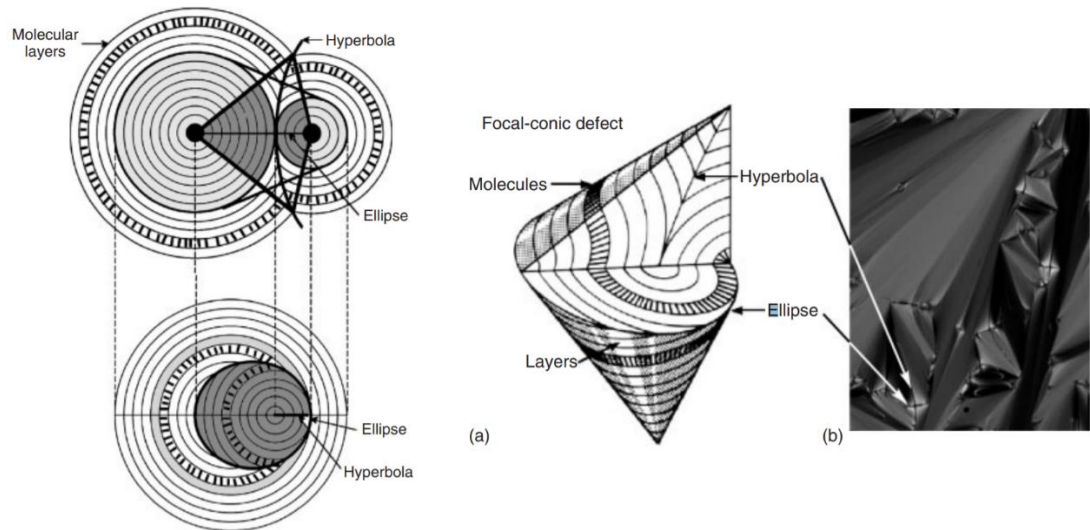
Figure 54. 2D and 3D representations of the focal-conic defect found in smectic phases. Reproduced from reference 90.

Typically, the focal conic texture has a fan-like texture and the ellipse and hyperbola appear as crossed defect lines with these fans. The smectic A texture also exhibits a homeotropic region which results from the molecules being arranged perpendicular to the plane of the slide and so no birefringent texture is observed in these domains i.e. it is optically extinct (Figure 55).
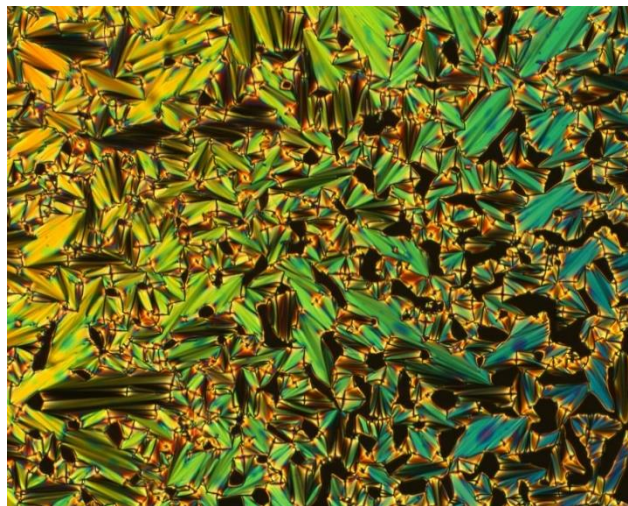
Figure 55. Photomicrograph of the smectic A mesophase showing the fan-like domains and focal-conic pair ellipse and hyperbolae defects along with small areas of homeotropic alignment.

1.6.1.3 Smectic C phase

The smectic C phase also exhibits a focal-conic defect texture, although the fan-like domains appear patchy or crumpled as a result of tilt domains occurring within the local domains. Upon transition from the smectic A phase the molecules within the

homeotropic domains tilt and as a result a schlieren texture is observed (Figure 56). In the smectic C phase only 4-brush defects are observed which distinguishes it from the nematic phase.
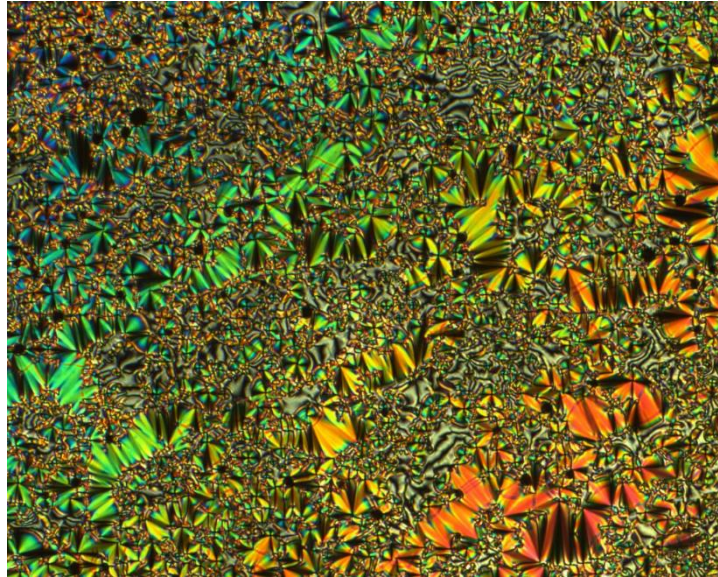
Figure 56. Photomicrograph showing the smectic C$_A$ phase featuring 2- and 4-brush defects in the schlieren.

1.6.1.4 Columnar phases

Columnar mesophases comprise of hexagonal columnar or rectangular columnar lattices. There are different textures that can be observed for the columnar phase. The first example is the pseudo homeotropic domain that grows dendritically as a result of the local symmetry within the packing arrangement. When two of these homeotropic domains merge spine defects form as a result of a rapid reorientation at the boundary of the domains. When there is homogeneous alignment of the columns such that the direction of the column is parallel to the surface of the slide, disc-like domains with dark brushes occur. This requires the director to be parallel to both the polariser and analyser with the director field either being continuous across neighbouring domains or discontinuous (Figure 57).
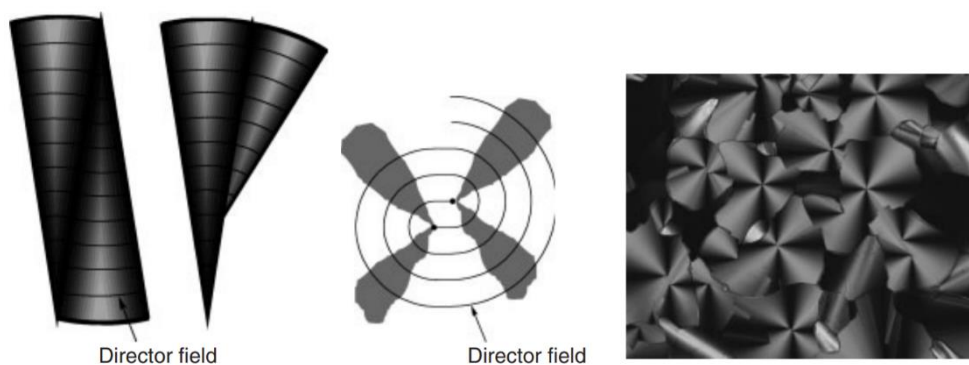
Figure 57. Formation of characteristic defects in the hexagonal columnar phase. Reproduced from reference 90.

Contrastingly for the rectangular columnar phase, the same defects may form however as the unit cell in the rectangular columnar mesophase tends to be elongated the domains appear patchy or broken, which is similar to the smectic A to smectic C transition (Figure 58). This is caused by the domain containing several different orientations of the unit cell. Due to difficulties in distinguishing rectangular and hexagonal columnar mesophases typically X-ray diffraction is used to provide an unequivocal assignment along with the unit cell parameters.
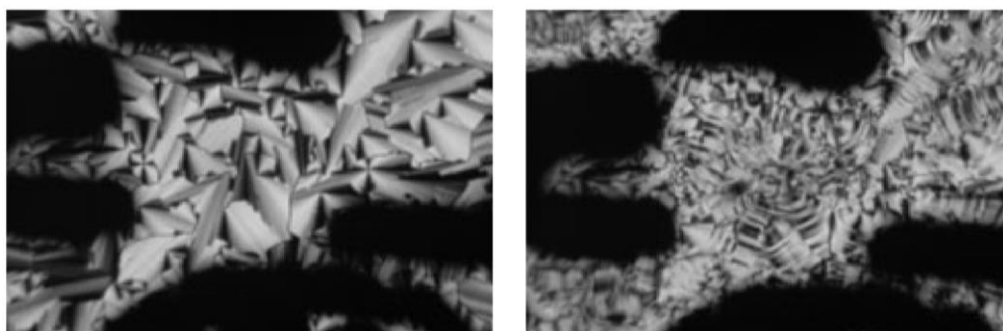
Figure 58. The rectangular columnar phase (right) can be seen as a patchy or broken version of the hexagonal columnar phase (left) in analogy to smectic C and smectic A phases respectively. Reproduced from reference 90.

1.6.1.5 Chiral nematic phase

The chiral nematic phase exhibits three classical textures, the Grandjean planar, fingerprint and pseudo-focal conic textures.[91] In the planar texture the helical axis is normal to the surfaces of the cell or slide (Figure 59) and the texture is coloured as a result of the pitch of the chiral nematic mesophase. Defects in the texture may be seen as "oily streaks" which occur between the regions in which the helices are aligned. The fingerprint texture arises from the pitch lying in the plane of the glass substrate. The

orientation of the pitch around defects forms dislocations which give rise to a texture resembling a fingerprint.

Planar	Fingerprint
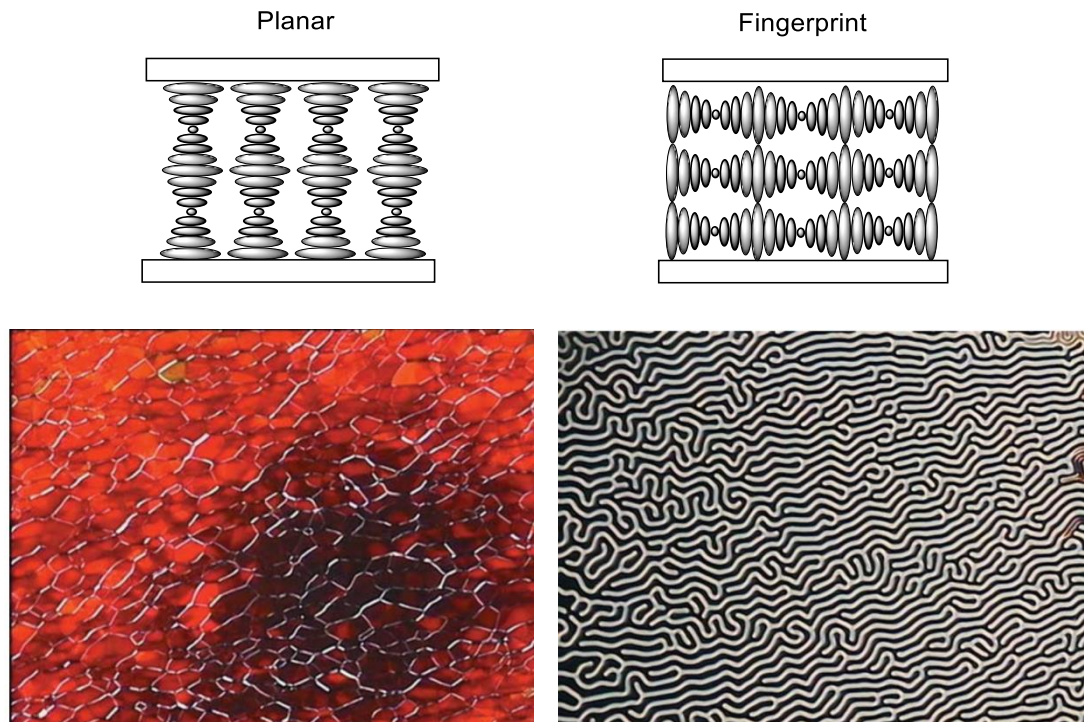
Figure 59. Alignment of the helical axis in the planar and fingerprint textures respectively. Reproduced from reference 93.

The final texture seen for the chiral nematic phase is the pseudo-focal conic or fan-like texture which can closely resemble the focal-conic texture of the smectic A phase. It arises in short pitch chiral nematics where the periodic order gives rise to a quasi-layered structure. In this case the helical axis is not aligned with either the optical axis or surface of the material and varies across the sample. The pseudo-focal conic texture can be distinguished from the focal-conic texture by shearing the material, often forming the planar oily streaks texture.

1.6.1.6 Blue phases.

There are three blue phases which can be identified *via* optical microscopy and diffraction studies. All three phases have cubic symmetry with BPI having a body-centered cubic structure and BPII having a simple cubic structure.[92] Both BPI and BPII show platelet structures *via* polarised optical microscopy. BPIII is the highest temperature phase and is observed as an amorphous dark blue fog by POM. There are multiple theories to explain the appearance of this texture including the double twist cylinders described above.[93]

Examples of the platelet textures of BPI and BPII observed *via* POM are shown in photomicrographs below (Figure 60). These platelet textures arise due to Bragg reflections from different Miller planes of the cubic lattices giving a range of colours. In BPII the platelets appear to be smooth however in BPI the platelets gain a rippled appearance as a result of the change in the cubic lattice structure from BPII.
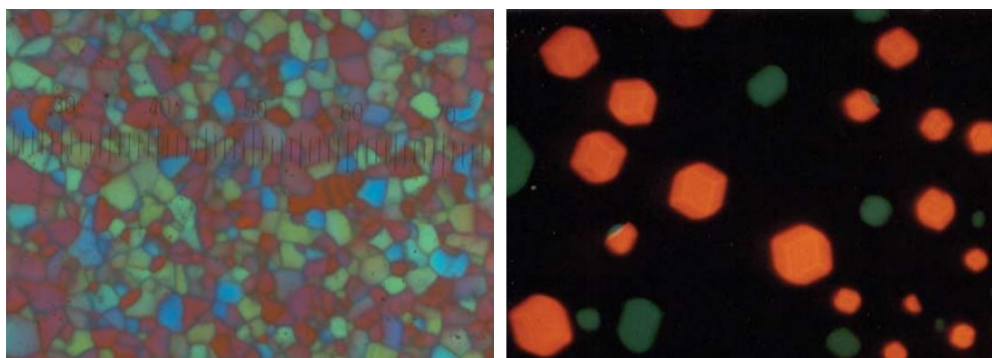
Figure 60. Photomicrographs of the platelet textures of BPI (left) and BPII (right). Reproduced from reference 93.

1.6.1.7 Twist grain boundary (TGB) phase

The TGB phase can be difficult to detect by microscopy and there are many textures possible depending upon the temperature range of the phase, anchoring conditions, and whether the phase is reached from the N* or SmA phase. One texture referred to as the filament texture can be observed upon transition from a homeotropic smectic A phase to the TGB phase (Figure 61). In this case the helical axis of the phase is perpendicular to the optical axis and as such the formation of the helical structure is seen as a rapid growth of filaments where the molecules were previously aligned homeotropically and become tilted to show birefringence.
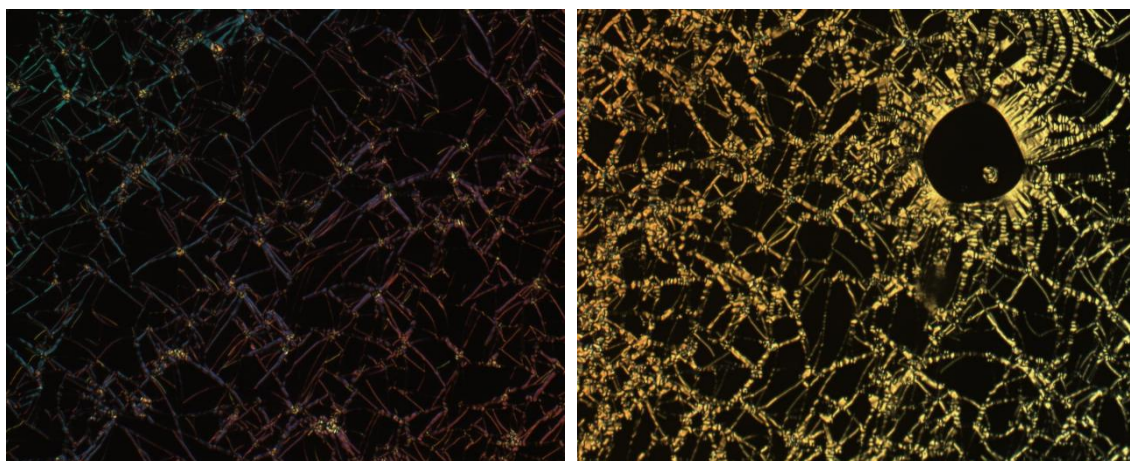
Figure 61. Photomicrographs of the TGB phase showing the growth of the filament texture from a homeotropic smectic A phase.

1.6.2 Differential Scanning Calorimetry

Upon going through a phase change such as ice melting into water, the sample must first take in an amount of energy – in this case the enthalpy of fusion – before the temperature may change. In differential scanning calorimetry a pair of identical furnaces are used where one furnace contains the sample to be analysed and the other furnace contains a reference material (Figure 62). The furnaces are controlled such that the temperatures of both are always equal, and as such when the sample undergoes a phase transition, such as the melting of ice more energy is required to change the temperature of the sample furnace than that of the reference. The amount of energy required for the transition to occur is directly proportional to the enthalpy of the transition. This can be calibrated against known transitions such as the melting of indium and as such be used to find the enthalpy change of unknown transitions.
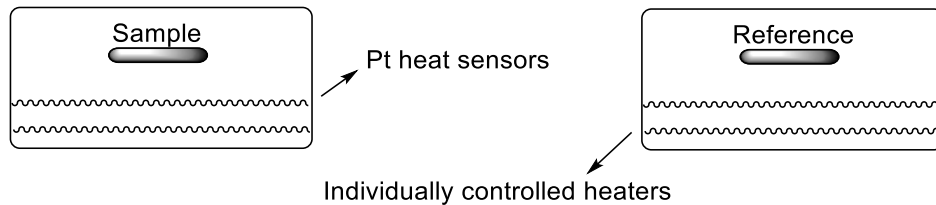
Figure 62. Schematic representation of DSC equipment.

With the enthalpy of the transition known, the entropy is related to the Gibbs Free Energy by equation 8a. The first and second derivatives are also shown.

$$G = H - TS \ (8a)$$

$$\left(\frac{\mathrm{d}G}{\mathrm{d}T}\right)_P = -S \ (8b)$$

$$\left(\frac{\mathrm{d}^2 G}{\mathrm{d}T^2}\right)_P = -\frac{C_P}{T} \ (8c)$$

Equation 8. Equations for the Gibbs Free Energy (a) and its first (b) and second derivatives (c).

If at the phase transition $\left(\frac{\mathrm{d}G}{\mathrm{d}T}\right)$ is discontinuous the transition is described as first order and the enthalpy change at the transition is referred to as the latent heat of the transition. This is the most common form of phase transition including melting or most liquid crystal to liquid crystal transitions (Figure 63). However, a second class of transition is possible where there is no change in entropy or enthalpy and as such $\left(\frac{\mathrm{d}G}{\mathrm{d}T}\right)$

is continuous. These transitions are described as second order and instead a discontinuity is seen in the second derivative i.e. the heat capacity. Commonly this is seen for glass transitions.
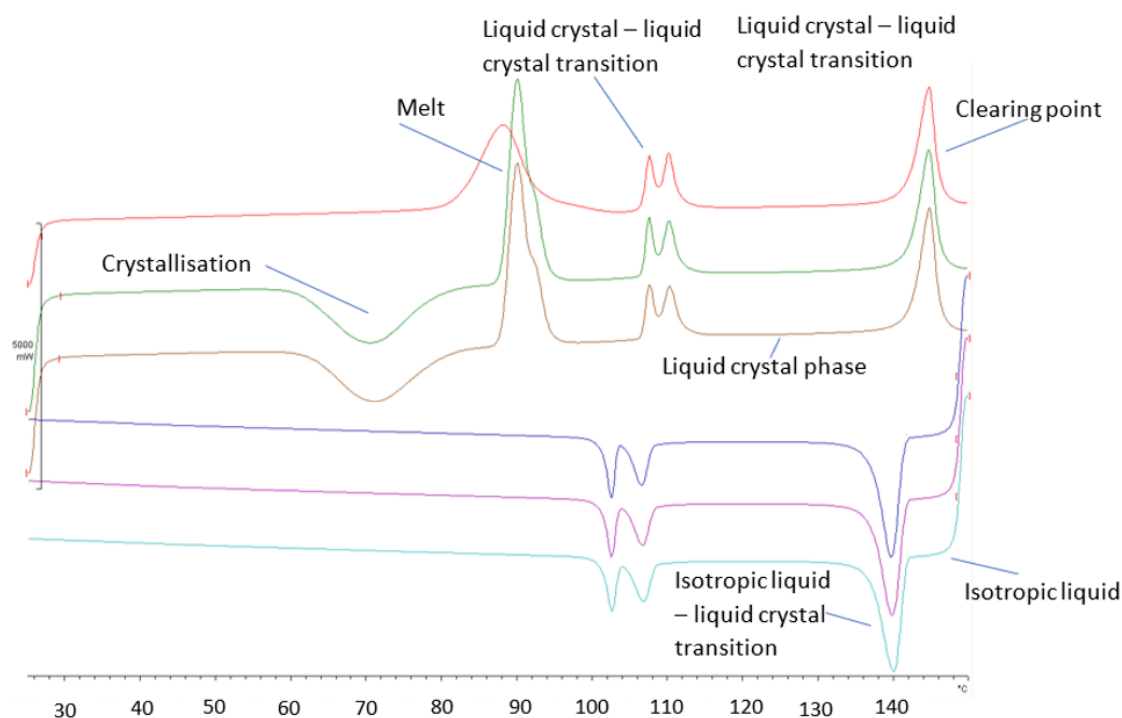
*Figure 63. Indicative DSC trace of compound **133** showing key features (See chapter 6).*

1.6.2.1 DSC Experiments

Commonly aluminium pans are used to hold the samples and as such an empty pan is used as the reference in the second furnace. To avoid artifacts, good contact is required between both the heating device and pan, and pan and sample. This can make the first heating cycle irreproducible as the crystalline solids being analyzed may not be in optimal contact with the pan. A second consideration in DSC experiments is the size of the sample being analysed, larger samples will take longer to fully melt resulting in some thermal lag or poor resolution. Meanwhile small samples will provide smaller peaks, but give better resolution and accuracy as the transitions are quicker. The final consideration is the heating rate, with 10 °C per minute being the most commonly used. Increasing the heating rate will increase the width of the transition peaks, and as such decrease the resolution making it more difficult to pick apart close transitions. By decreasing the heating rate individual transitions may be separated, however this results in slower transitions which spread the enthalpy change over a wider range and so are less easily detected. Typically, DSC transitions are reported

using the enthalpy change and onset of the transition as the peak is variable with the heating rate.

To achieve this, the enthalpy is calculated from the integral under the peak associated with the phase transition. This is complicated slightly as there are often pre-transitional organisational changes in the mesophase structure which can result in changes to the heat capacity and thus diminish the magnitude of the first order transition. The magnitude of the enthalpy of various mesophase-mesophase transitions are known and empirically predicted ranges can be given (Table 1). This is most interesting when converted to the entropy of a transition to show the degree of order within a phase which can be used to help identify unknown phases.[94]

Table 1. Example enthalpy and entropy changes of mesophase transitions. Ranges from selected examples taken from reference 94.

Transition	Enthalpy / kJ mol^{-1}	Entropy / J K^{-1} mol^{-1}	Order of transition
SmC to SmA	0.1-0.2	0.1-2.3	1st/2nd
SmB to SmA	1.2-3.2	3-14	1st
SmA to N	0.4-3.2	1-10	1st
SmA to Iso	3-30	9-30	1st
N to Iso	0.5-2	2-5	1st

1.6.3 X-Ray Diffraction

In the context of this thesis X-ray diffraction has been used as a tool to gain insight into the organisation of the liquid crystal phases in more detail than simply the type of phase and transition temperatures.

1.6.3.1 X-ray diffraction experiments

Liquid crystalline phases are characterised by a periodic distribution of electron density due to the self-organisation of the constituent molecules. X-rays are scattered by the electrons within the constituent molecules and under certain conditions given by Bragg's law (Equation 9) constructive interference of the incident X-rays will occur. The term θ represents the angle of incidence, n is any integer, λ is the wavelength of

the X-rays used and d is the separation between lattice planes within the periodic structure.

$$n\lambda = 2d \sin\theta$$

Equation 9. Bragg's law which describes the conditions for constructive interference.

X-ray diffraction experiments from liquid crystal samples can be performed in one of two manners. Firstly, sequentially moving a point detector to measure each diffraction angle from a sample allows the measurement of a quantitative data set.[95] Secondly using a two-dimensional area detector allows a semi-quantitative data set to be collected over a wide range of diffraction angles in a single experiment (Figure 64). This second option is sufficient to report on the structure of the phase and is therefore more common and is the type of experiment used in this report. In the example shown in Figure 64 the diffraction pattern is typical of an unaligned Smectic A phase.
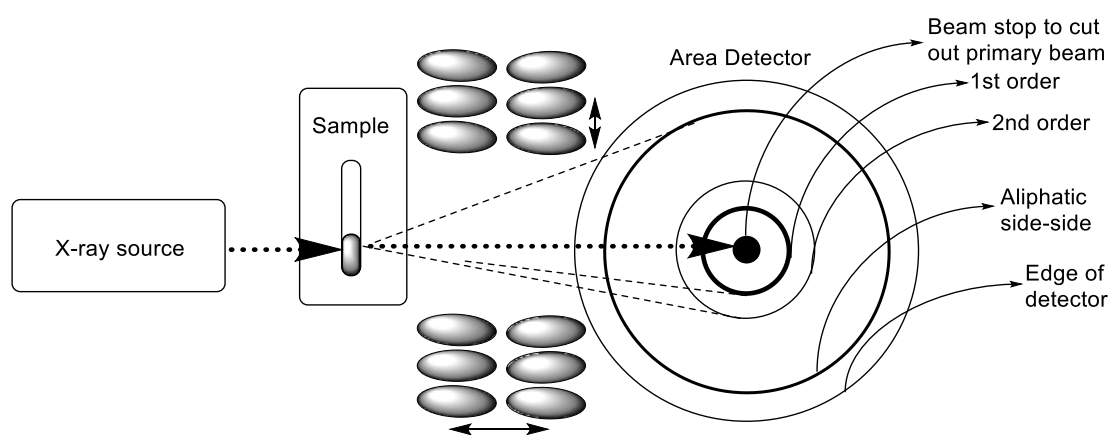
Figure 64. Schematic diagram of an X-ray diffraction experiment using an area detector able to simultaneously collect a wide range of diffraction angles.

1.6.3.2 Diffraction patterns

The output from X-ray diffraction experiments are diffraction patterns which consist of two regions. Centrally the small angle region contains information due to diffractions correlating with longer distance relationships between molecules such as layer spacings. The information contained in the outer region (wide angle) diffractions are characteristic of short distance such as side-side liquid like interactions of aliphatic chains. The majority of the phases reported in this project are nematic or smectic A and so typically the small angle will consist of a ring for an unaligned sample

corresponding to the average molecular length. For an aligned sample the vertical section above and below the center of the beam corresponds to the axis along the director and so again diffraction corresponding to the average molecular length is seen. In the wide angle of an unaligned sample a characteristic diffuse ring corresponding to the 4.5 Å side to side molecular interactions is seen. For aligned samples these are seen mirrored horizontally as the interactions are perpendicular to the director. In this way the diffraction patterns of nematic and smectic A phases are similar, with the differences being much sharper peaks observed for smectic A compounds and a higher chance to see secondary reflections. The diffraction patterns of columnar mesophases are more complicated and are described in section 1.2.3.

1.7 References

1   J. N. Israelachvili, *Surfactants in Solution (eds K.L. Mittal and P. Bothorel), Plenum Press,* New York, 1984.

2   F. Dumoulin, D. Lafont, T. L. Huynh, P. Boullanger, G. Mackenzie, J. J. West and J. W. Goodby, *Chem. Eur. J.*, 2007, **13**, 5585–5600.

3   A. N. Cammidge and H. Gopee, in Handbook of Liquid Crystals, eds. J. W. Goodby, P. J. Collings, T. Kato, C. Tschierske, H. F. Gleeson, P. Raynes, Wiley-VCH Verlag GmbH & Co. KGaA, 2nd., 2014, Vol. 3, Ch 10, pp. 1.

4   J. W. Goodby in Handbook of Liquid Crystals, eds. J. W. Goodby, P. J. Collings, T. Kato, C. Tschierske, H. F. Gleeson, P. Raynes, Wiley-VCH Verlag GmbH & Co. KGaA, 2nd., 2014, Vol. 4, Ch 1, pp. 1.

5   A. Wulf, *Phys. Rev. A*, 1975, **11**, 365–375.

6   a) S. Kumar, *Chem. Soc. Rev.*, 2006, 35, 1139-1241 b) T. Wohrle, I. Wurzback, J. Kirres, A. Kostidou, N. Kapernaum, J. Litterscheidt, J. C. Haenle, P. Staffeld, A. Baro, F. Giesselmann and S. Laschat, *Chem. Rev.* 2016, 116, 3, 729-739 c) T. Yasuda, Y. Kamikawa, M. Yoshio and T. Kato, *Chem. Commun.*, 2009, 83-109

7   H. Detert, M. Lehmann and H. Meier, *Materials.*, 2010, **3**, 3218–3330.

8   S. Chandrasekhar, P. S. K. Prasad, D. S. S. Rao, V. S. K. Balagurusamy, *PINSA.*, 2002, 68, 175-191

9   S. Laschat, A. Baro, N. Steinke, F. Giesselmann, C. Hägele, G. Scalia, R. Judele, E. Kapatsina, S. Sauer, A. Schreivogel and M. Tosoni, *Angew. Chem.Int. Ed.*, 2007, **46**, 4832–4887.

10   I. Dierking, *Symmetry.*, 2014, **6**, 444–472.

11   S. T. Lagerwall in Handbook of Liquid Crystals, eds. J. W. Goodby, P. J. Collings, T. Kato, C. Tschierske, H. F. Gleeson, P. Raynes, Wiley-VCH Verlag GmbH & Co. KGaA, 2nd., 2014, Vol 4, Ch 5, pp 1.

12   H. Takezoe and M. Cepi in Handbook of Liquid Crystals, eds. J. W. Goodby, P. J. Collings, T. Kato, C. Tschierske, H. F. Gleeson, P. Raynes, Wiley-VCH Verlag GmbH & Co. KGaA, 2nd., 2014, Vol 4, Ch 6, pp 1.

13   P. J. Collings in Handbook of Liquid Crystals, eds. J. W. Goodby, P. J. Collings, T. Kato, C. Tschierske, H. F. Gleeson, P. Raynes, Wiley-VCH Verlag GmbH & Co. KGaA, 2nd., 2014, Vol 3, Ch 18, pp 1.

14   B. Dubois-Violette, E. Pansu, *Mol. Cryst. Liq. Cryst.,* 1988, **165**, 151-182.

15   T. Paul and J. Saha, *Sci. Rep.,* 2020, **10**, 1–11.

16   H. S. Kitzerow in Chirality in Liquid Crystals, eds H. S. Kitzerow, C. Bahr, Springer Verlag: New York, NY, USA, 2001, Ch 10. pp 296.

17   A. Yoshizawa, *Liq. Cryst.*, 2017, **44**, 1877–1893.

18   M. Mitov, *Chem. Phys. Chem.,* 2014, **15**, 1245–1250.

19   J. W. Goodby, R. J. Mandle, E. J. Davis, T. Zhong and S. J. Cowling, *Liq. Cryst.*, 2015, **42**, 593–622.

20   N. H. S. Ahmed, G. R. Saad, H. A. Ahmed and M. Hagar, *RSC Adv.*, 2020, **10**, 9643–9656.

21   G. W. Gray, M. Hird and K. J. Toyne, *Mol. Cryst. Liq. Cryst.*, 1991, **206**, 187.

22   J. W. Goodby, E. J. Davis, R. J. Mandle and S. J. Cowling, in Handbook of Liquid Crystals, eds. J. W. Goodby, P. J. Collings, T. Kato, C. Tschierske, H. F. Gleeson, P. Raynes, Wiley-VCH Verlag GmbH & Co. KGaA, 2nd., 2014, Vol 1, Ch 8, pp 1

23   G. W. Gray, *Molecular Structure and Properties of Liquid Crystals. Academic Press, New York, 1962*

24   J. Jan, R. Dąbrowski, T. Lech and G. Czechowski, *J. Chem. Eng. Data*, 2001, **46**, 110–112.

25   A. D. Pink, *J. Chem. Phys.,* 1975, **63**, 2533

26   M. E. Neubert, S. S. Keast, C. C. Law, M. C. Lohman and J. C. Bhatt, *Liq. Cryst.*, 2005, **32**, 781–795.

27   S. Ujiie and T. Kato, in Handbook of Liquid Crystals, eds. J. W. Goodby, P. J. Collings, T. Kato, C. Tschierske, H. F. Gleeson, P. Raynes, Wiley-VCH Verlag GmbH & Co. KGaA, 2nd., 2014, Vol 7, Ch 11, pp 1.

28   V. Percec, Q. Xiao, G. Lligadas and M. J. Monteiro, *Polymer.*, 2020, **211**, 123252.

29   X. Zhang, S. Boissé, C. Bui, P. A. Albouy, A. Brûlet, M. H. Li, J. Rieger and B. Charleux, *Soft Matter*, 2012, **8**, 1130–1141.

30   A. Greiner and H. Schmidt, in Handbook of Liquid Crystals, eds. J. W. Goodby, P. J. Collings, T. Kato, C. Tschierske, H. F. Gleeson, P. Raynes, Wiley-VCH Verlag GmbH & Co. KGaA, 2nd., 2014, Vol 7, Ch 8, pp 1.

31   C. Pugh and R. R. Schrock, *Macromolecules*, 1992, **25**, 6593–6604.

32   I. M. Saez and J. W. Goodby, *Chem. Eur. J.*, 2003, **9**, 4869–4877.

33   M. Wang, W. W. Bao, W. Y. Chang, X. M. Chen, B. P. Lin, H. Yang and E. Q. Chen, *Macromolecules*, 2019, **52**, 5791–5800.

34   H. R. Finkelmann, H., M. Happ, M. Portugall, *Makromol. Chem.,* 1978, **179**, 2541.

35   J. F. Zheng, Z. Q. Yu, X. Liu, X. F. Chen, S. Yang and E. Q. Chen, *J. Polym. Sci. Part A Polym. Chem.*, 2012, 50, 5023–5031.

36   S. Hernández-Ainsa, M. Marcos and J. L. Serrano, Jose Luis in Handbook of Liquid Crystals, , eds. J. W. Goodby, P. J. Collings, T. Kato, C. Tschierske, H. F. Gleeson, P. Raynes, Wiley-VCH Verlag GmbH & Co. KGaA, 2nd., 2014, Vol 7, Ch 7, pp 1.

37   B. Donnio and D. Guillon, *Adv. Polym. Sci.*, 2006, **201**, 45–155.

38   J. W. Lee, B. K. Kim, H. J. Kim, S. C. Han, W. S. Shin and S. H. Jin, *Macromolecules*, 2006, **39**, 2418–2422.

39   L. Gehringer, D. Guillon and B. Donnio, *Macromolecules*, 2003, **36**, 5593–5601.

40   J. W. Lee, X. L. Piao, Y. K. Yun, J. Il Jin, Y. S. Kang and W. C. Zin, *Liq. Cryst.*, 1999, **26**, 1671–1685.

41   S. Huh and J. Jin, *Liq. Cryst.*, 1998, 25, 285-293

42   R. J. Mandle, *Soft Matter*, 2016, **12**, 7883–7901.

43   Y. K. Kim, R. Breckon, S. Chakraborty, M. Gao, S. N. Sprunt, J. T. Gleeson, R. J. Twieg, A. Jákli and O. D. Lavrentovich, *Liq. Cryst.*, 2014, **41**, 1345–1355.

44   I. Bala and S. K. Pal, *Liq. Cryst.*, 2016, **43**, 963–971.

45   (a) P. Van de Witte and J. Lub, *Liq. Cryst.*, 1999, **26**, 1039. (b) T. Pfeuffer, D. Hanft and P. Strohriegl, *Liq. Cryst.*, 2002, **29**, 1555 c) R. Eidenschink, F.-H. Kreuzer and W. H. De Jeu, *Liq. Cryst.*, 1990, **8**, 879 (d) L. M. Wilson, *Liq. Cryst.*, 1994, 16, 6, 1005.

46   D. Yao, B. Zhang, Y. Li and W. Xiao, Tetrahedron letters, 2004, 45, 8953.

47   I. M. Saez, J. W. Goodby, in Liquid Crystalline Functional Assemblies and Their Supramolecular Structures, eds T. Kato, Springer, Berlin, Heidelberg, 2008, Structure and Bonding Vol 128, pp. 1.

48   S. Campidelli, T. Brandmüller, A. Hirsch, I. M. Saez, J. W. Goodby and R. Deschenaux, *Chem. Commun.*, 2006, 4282–4284.

49   X. Zhang, C. H. Hsu, X. Ren, Y. Gu, B. Song, H. J. Sun, S. Yang, E. Chen, Y. Tu, X. Li, X. Yang, Y. Li and X. Zhu, *Angew. Chemie - Int. Ed.*, 2015, **54**, 114–117.

50   C. Tschierske in Handbook of Liquid Crystals, eds. J. W. Goodby, P. J. Collings, T. Kato, C. Tschierske, H. F. Gleeson, P. Raynes, Wiley-VCH Verlag GmbH & Co. KGaA, 2nd., 2014, Vol 5, Ch 1, pp 1.

51   T. Kato, J. Uchida, T. Ichikawa and T. Sakamoto, *Angew. Chem. Int. Ed.*, 2018, 57, 4355–4371.

52   H. M. P. Chen, J. J. Ou and S. H. Chen, in Nanoscience with Liquid Crystals; Ed, Q. Li, Springer International Publishing: Cham, Switzerland, 2014, Ch 6, pp 179.

53   S. Campidelli, E. Vázquez, D. Milic, J. Lenoble, C. A. Castellanos, G. Sarova, D. M. Guldi, R. Deschenaux and M. Prato, *J. Org. Chem.*, 2006, **71**, 7603–7610.

54   M. Sawamura, K. Kawai, Y. Matsuo, K. Kanie, T. Kato and E. Nakamura, *Nature*, 2002, **419**, 702–705.

55   P. Pieper, V. Russo, B. Heinrich, B. Donnio and R. Deschenaux, *J. Org. Chem.*, 2018, **83**, 3208–3219.

56   S. Campidelli, J. Lenoble, J. Barberá, F. Paolucci, M. Marcaccio, D. Paolucci and R. Deschenaux, *Macromolecules*, 2005, **38**, 7915–7925.

57   a) H. Mamlouk, B. Heinrich, C. Bourgogne, B. Donnio, D. Guillon and D. Felder-Flesch, *J. Mater. Chem.*, 2007, 17, 2199 b) D. Guillon, B. Donnio, C. Bourgogne, L. Rupnicki and D. Felder-Flesch, *J. Mater. Chem.*, 2006, 16, 304-309

58   E. L. Heeley, D. J. Hughes, Y. El Aziz, I. Williamson, P. G. Taylor and A. R. Bassindale, *Phys. Chem. Chem. Phys.*, 2013, **15**, 5518–5529.

59   I. M. Saez in Handbook of Liquid Crystals, eds. J. W. Goodby, P. J. Collings, T. Kato, C. Tschierske, H. F. Gleeson, P. Raynes, Wiley-VCH Verlag GmbH & Co. KGaA, 2nd., 2014, Vol 7, Ch 6, pp 1.

60   M. Lehmann in Handbook of Liquid Crystals, eds. J. W. Goodby, P. J. Collings, T. Kato, C. Tschierske, H. F. Gleeson, P. Raynes, Wiley-VCH Verlag GmbH & Co. KGaA, 2nd., 2014, Vol 5, Ch 5, pp 1.

61   a) I. M. Saez and J. W. Goodby, *J. Mater. Chem.*, 2011, 11, 2845 b) S. Campidelli, C. Eng, I. M. Saez, J. W. Goodby and R. Deschenaux, *Chem. Commun.*, 2003, 1520

62   C. Tschierske, *Isr. J. Chem.*, 2012, **52**, 935–959.

63   C. Tschierske, *Angew. Chem. - Int. Ed.*, 2013, **52**, 8828–8878.

64   C. Tschieske in Topics in Current Chemistry, 2012, vol 318, pp 1.

65   D. F. Eaton and B. E. Smart, *J. Am. Chem. Soc.*, 1990, **112**, 2821–2823.

66   I. Bury, B. Heinrich, C. Bourgogne, G. H. Mehl, D. Guillon and B. Donnio, *New J. Chem.*, 2012, **36**, 452–468.

67   S. Guerra, T. L. A. Nguyen, J. Furrer, J. F. Nierengarten, J. Barberá and R. Deschenaux, *Macromolecules*, 2016, **49**, 3222–3231.

68   A. Yamaguchi, Y. Maeda, H. Yokoyama and A. Yoshizawa, *Chem. Mater.*, 2006, 18, 5704.

69   S. N. Chvalun, M. A. Shcherbina, I. V. Bykova, J. Blackwell and V. Percec, *Polymer Science Series A.,* 2002, **49**, 158

70   L. de Campo, M. J. Moghaddam, T. Varslot, N. Kirby, R. Mittelbach, T. Sawkins and S. T. Hyde., *Chem. Mater.,* 2015, **27**, 3, 857-866

71   a) V. Percec, D. Schlueter and G. Ungar, *Macromolecules*, 1997, **30**, 645–648. b) G. Johansson, V. Percec, G. Ungar and K. Smith, *Chem. Mater.*, 1997, **9**, 164–175.

72   B. M. Rosen, C. J. Wilson, D. A. Wilson, M. Peterca, M. R. Imam and V. Percec, *Chem. Rev.,* 2009, 6275–6540.

73   V. Percec, D. Schlueter, Y. K. Kwon, J. Blackwell, M. Möller and P. J. Slangen, *Macromolecules*, 1995, **28**, 8807–8818.

74   G. Ungar, V. Percec, M. N. Holerca, G. Johansson and J. A. Heck, *Chem. Eur. J.*, 2000, **6**, 1258–1266.

75   N. Y. Kostina, A. M. Wagner, T. Haraszti, K. Rahimi, Q. Xiao, M. L. Klein, V. Percec and C. Rodriguez-Emmenegger, *Soft Matter*, 2021, **17**, 254.

76   B. M. Rosen, D. A. Wilson, C. J. Wilson, M. Peterca, B. C. Won, C. Huang, L. R. Lipski, X. Zeng, G. Ungar, P. A. Heiney and V. Percec, *J. Am. Chem. Soc.*, 2009, **131**, 17500–17521.

77   J. Pan, M. Wen, D. Yin, B. Jiang, D. He and L. Guo, *Tetrahedron*, 2012, 68, 14, 2943.

78   H.-J. Sun, S. Zhang and V. Percec, *Chem. Soc. Rev.* 2015, **3900**, 3900–3923.

79   Q. Xiao, J. D. Rubien, Z. Wang, E. H. Reed, D. A. Hammer, D. Sahoo, P. A. Heiney, S. S. Yadavalli, M. Goulian, S. E. Wilner, T. Baumgart, S. A. Vinogradov, M. L. Klein and V. Percec, *J. Am. Chem. Soc.,* 2016, **138**, 38, 12655.

80   I. Bury, B. Heinrich, C. Bourgogne, D. Guillon and B. Donnio, *Chem. Eur. J.*, 2006, **12**, 8396–8413.

81   K. C. Elbert, D. Jishkariani, Y. Wu, J. D. Lee, B. Donnio and C. B. Murray, *Chem. Mater.*, 2017, **29**, 8737–8746.

82   a) E. R. Gillies, E. Dy, J. M. Fréchet and F. C. Szoka, *Mol. Pharm.*, 2005, 2, 2, 129 b) C. C. Lee, E. R. Gillies, M. E. Fox, S. J . Guillaudeu, J. M. Fréchet, E. Dy and F. C. Szoka*, Proc. Natl. Acad. Sci. USA.*, 2006, 103, 45, 16649.

83   D. R. Sikwal, R. S. Kalhapure and T. Govender, *Eur. J. Pharm. Sci.*, 2017, 97, 113.

84   V. Vij, V. Bhalla and M. Kumar, *Chem. Rev.*, 2016, **116**, 9565–9627.

85   T. Yasuda, K. Tanabe, T. Tsuji, K. K. Coti, I. Aprahamian, J. F. Stoddart and T. Kato, *Chem Commun*., 2010, 46, 1224.

86   M. M. Elmahdy, C. G. Clark, H. J. Butt, K. Müllen and G. Floudas, *J. Phys. Chem. B*, 2012, **116**, 13812–13820.

87   J. Wu, M. D. Watson and K. Müllen, *Angew. Chem. Int. Ed*., 2003, 42, 5329.

88   V. Iguarbe, J. Barberá and J. L. Serrano, *Liq. Cryst.*, 2020, **47**, 301–308.

89   Polarised light microscopy, Microscopy, MicroscopyU. Introduction to Polarised Light Microscopy. Polarised Light Configuration. www.microscopyu.com/articles/polarised/polarisedintro.html, (accessed 24 March 2020).

90   S. J. Cowling in Handbook of Liquid Crystals, eds. J. W. Goodby, P. J. Collings, T. Kato, C. Tschierske, H. F. Gleeson, P. Raynes, Wiley-VCH Verlag GmbH & Co. KGaA, 2nd., 2014, Vol 1, Ch 9, pp 1.

91   I. F. Castles and S. M. Morris, in Handbook of Liquid Crystals, eds. J. W. Goodby, P. J. Collings, T. Kato, C. Tschierske, H. F. Gleeson, P. Raynes, Wiley-VCH Verlag GmbH & Co. KGaA, 2nd., 2014, Vol 3, Ch 15, pp 1.

92   I. Nishiyama and A. Yoshizawa, in Handbook of Liquid Crystals, eds. J. W. Goodby, P. J. Collings, T. Kato, C. Tschierske, H. F. Gleeson, P. Raynes, Wiley-VCH Verlag GmbH & Co. KGaA, 2nd., 2014, Vol 3, Ch 17, pp 1.

93   I. Dierking, *Texture of Liquid Crystals*, Wiley-VCH Verlag GmbH & Co. KGaA, Weinheim, 2008.

94   W. E. Acree and J. S. Chickos, *J. Phys. Chem. Ref. Data*, 2006, **35**, 1051–1330.

95   N. Agra-Kooijman and S. Kumar in Handbook of Liquid Crystals, eds. J. W. Goodby, P. J. Collings, T. Kato, C. Tschierske, H. F. Gleeson, P. Raynes, Wiley-VCH Verlag GmbH & Co. KGaA, 2nd., 2014, Vol 1, Ch 10, pp 1.

Experimental reagents and techniques

Starting materials reagents and solvents.

All starting materials and reagents were commercially available unless otherwise stated, and used without further purification. Solvents were obtained from Sigma-Aldrich, Fisher or VWR. Dry 1,4-Dioxane was obtained via distillation from CaH_2 onto molecular sieves. Other dried solvents were either obtained from Sigma-Aldrich or dried over alumina columns (DCM, THF). Low-sulfur toluene was produced by washing with sulfuric acid. Co_2CO_8 was purchased from Sigma-Aldrich and stored cold in a glove box prior to use.

Thin layer chromatography and column chromatography.

Reaction progress was monitored by thin layer chromatography using appropriate solvent systems. TLC plates were purchased from Merck (Kieselgel 60 F-254) – Silica coated aluminium TLC plates – and visualised either by UV light at wavelengths of 254 nm and 365 nm or by use of potassium permanganate staining solutions. For column chromatography, flash grade silica from Sigma-Aldrich (40 – 63 μm particle size) was used. Yields are given for spectroscopically homogenous material.

Nuclear Magnetic Resonance

A JEOL ECS spectrometer was used to record NMR spectra operating at either 400 MHz (^{1}H), 100.5 MHz (^{13}C{^{1}H}) or 376 MHz (^{19}F) with solutions in either deuterated chloroform or deuterated DMSO. NMR spectra were referenced to residual protic solvent within the solution at 7.26 (^{1}H) and 77.16 (^{13}C{^{1}H}) for $CDCl_3$, or 2.50 (^{1}H) for DMSO-d_6. The chemical shifts are quoted in ppm δ to two decimal places. *J* coupling constants have been rounded to the nearest 0.5 Hz for the sake of consistency, the following abbreviations used to represent the multiplicity of the peaks observed.

s – singlet	d – doublet	t – triplet	q – quartet
m – multiplet	dd – doublet of doublets		aq – apparent quartet

Mass spectrometry

Mass spectrometry was performed by the University of York mass spectrometry service and Karl Heaton is thanked for providing spectra and guidance. ESI-MS and APCI-MS were recorded on a Bruker compact time of flight mass spectrometer. MALDI-MS was recorded on a Bruker Solarix FT-ICR MS.

Polarised optical microscopy

Polarised optical microscopy (POM) was performed using a Zeiss Axioskop 40Pol microscope using a Mettler FP82HT hotstage which was controlled by a Mettler FP90 central processor. Photomicrographs were recorded *via* an InfinityX-21 MP digital camera mounted atop the microscope.

Differential Scanning Calorimetry

Differential scanning calorimetry was performed on a Mettler DSC822 using an autosampler and operating using Mettler Star software under an atmosphere of dry nitrogen. Samples were constrained within a 20 μL Aluminium pan. An indium standard was used to calibrate the equipment (Onset = 156.55 ± 0.2 °C, ΔH = 28.45 ± 0.40 J g^{-1}).

High performance liquid chromatography

High performance liquid chromatography (HPLC) was performed by the University of York chromatography service and Scott Hicks is thanked for providing chromatograms and guidance. An Agilent 1100 system was used utilising a Waters Spherisorb S3 CN 2.0 x 150 mm column at 35.0 °C with a flow rate of 0.2 mL min^{-1} and a variable UV-vis detector operating between 190 to 400 nm.

X-ray diffraction

X-ray diffraction experiments were performed using a Bruker D8 Discover with a temperature controlled bored graphite rod furnace using two 1T magnets perpendicular to the incident beam for alignment which was custom built at the University of York. The radiation source was copper Kα (λ = 0.154056 nm) from a 1 μS microfocus source. Diffraction patterns were recorded using a 2048x2048 pixel Bruker Vantec 500 area detector at variable distances between 121 and 300 mm from the sample contained in 0.9 mm I.D capillary tubes. Diffraction patterns were evaluated using the DIFFRAC.SUITE software package.

Elemental analysis

Elemental analyses were performed using a CE-440 elemental analyser from Exeter Analytical Inc using a Sartorius SE2 analytical balance. Vanadium pentoxide was used as a combustion aid for samples containing perfluorinated chains or high molecular weights (>1000 Da).

Chapter 2. Aims

Previous work has focused on the synthesis and characterisation of *Janus* liquid crystals featuring a flexible core to separate the two opposing faces and more recently several *Janus* perfluoroalkyl:cyanobiphenyl diphenyl acetylene compounds have been shown to possess complex phase behaviour due to microphase segregation. This thesis focuses on the synthesis and characterisation of liquid crystalline materials featuring the diphenyl acetylene moiety as the supporting core of supermolecular materials (Figure 65). The diphenyl acetylene unit can be assembled using the Sonogashira coupling reaction in a convergent synthesis. This strategy will be used to synthesise a range of dimeric, trimeric and supermolecular liquid crystals, which feature structural factors such as chirality, or chemically incompatible units. The aim is to allow for multiple factors which drive self-organisation of these materials to be placed in competition with each other. To enable these competing factors to be studied, the diphenyl acetylene moiety has been chosen as a rigid unit which will support microphase segregation between the two faces of a *Janus* structure. In addition, the diphenyl acetylene moiety allows for further reactivity by cyclotrimerisation reactions to provide substituted hexaphenyl benzenes. This allows for a rapid increase in molecular complexity in a single synthetic step.
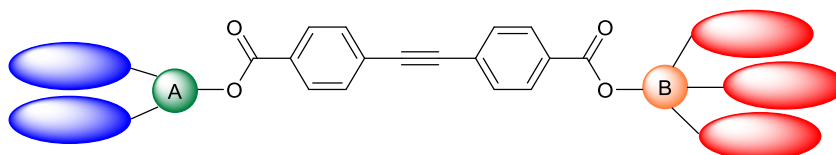
Figure 65. Schematic structure of a supermolecular Janus diphenyl acetylene.

Figure 65 shows two branching units represented by the letters A and B. The aim of the dendritic branching structure is to allow the incorporation of one, two or three mesogenic units on either side of the diphenyl acetylene core. 1,1,1-Tris(hydroxymethyl)ethane and pentaerythritol were selected as the branching units A and B respectively, see Figure 66. Increasing the number of mesogenic units increases the potential number of intermolecular interactions to stabilise a mesophase. More importantly, increasing the number of mesogenic units changes the molecular shape, and therefore the effect of the intermolecular interactions may be modulated. By producing a range of cyanobiphenyl and perfluoroalkyl substituted *Janus* diphenyl acetylenes with different numbers of mesogenic units, the volume of

each face and therefore overall molecular shape of the *Janus* supermolecule can be varied. The molecular shape is expressed into the mesophase type, and mesophase structure along with the intermolecular interactions of the self-organising units chosen.
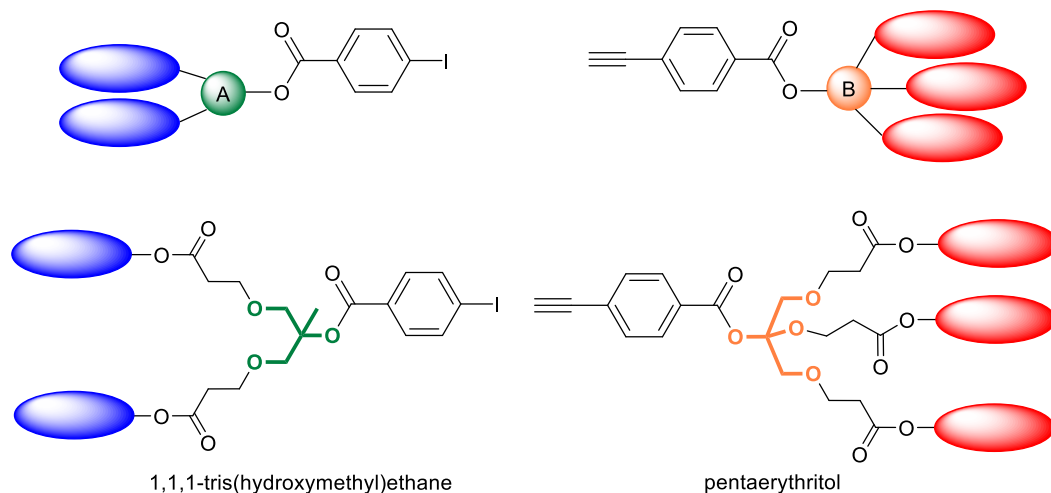
Figure 66. The structure of the two dendritic branching units used in this work, 1,1,1-tris(hydroxymethyl)ethane and pentaerythritol

These dendritic branching units have branching multiplicities of G = 2 and 3 respectively and have been selected due to their tetrahedral shape and increased flexibility when compared to aromatic branching units. By using a convergent synthesis, iodo-aryl and ethynyl-aryl derivatives of 1,1,1-tris(hydroxymethyl)ethane and pentaerythritol may be coupled in the final synthetic step. Examples of structures of the intermediates are shown in Figure 67. This convergent approach is more efficient than using a divergent approach and allows for the liquid crystal properties

of the mesogenic intermediates to be studied. This in turn allows the self-organisation of the *Janus* diphenyl acetylene compounds and their intermediates to be compared.
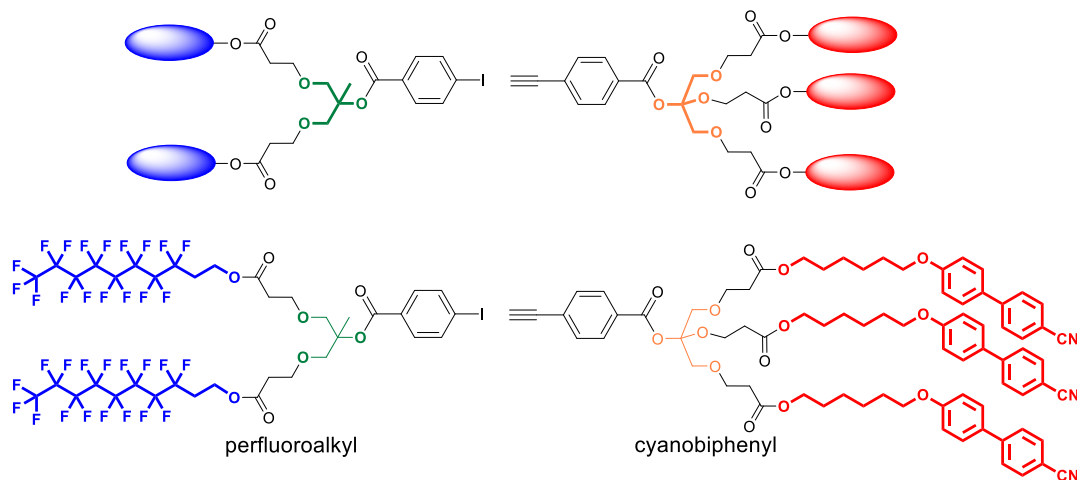
Figure 67. The two self-organising units used in this thesis, perfluoroalkyl chains and cyanobiphenyl mesogens.

The mesogenic units shown in blue and red have been chosen as perfluoroalkyl and cyanobiphenyl respectively. Perfluorinated chains of eight or more carbon atoms are known to exhibit self-organising effects via microphase segregation driven by the fluorophobic effect. 1H,1H,2H,2H-Perfluorodecanol will be used as the perfluorinated unit due to ease of use in synthesis and ready availability. Examples of the perfluoroalkyl and cyanobiphenyl building blocks are given in Figure 67. The cyanobiphenyl unit is commonly used in low molecular weight liquid crystals and its behaviour is well understood. A spacer is required between the cyanobiphenyl mesogen and branching unit to allow decoupling of the motions of the cyanobiphenyl and remainder of the molecule. Therefore, a hexyl spacer is used between the pentaerythritol derived branching unit and cyanobiphenyl units. Due to the different intermolecular interactions of the two self-organising units chosen the effects of both units will be expressed upon the mesophase type and mesophase structure. By changing the overall molecular shape using the dendritic branching units, the self-organising effects (microphase segregation, quadrupolar interactions) will be placed into competition.

A family of chiral dimers featuring the diphenyl acetylene core will be synthesised to investigate the impact of chirality upon the self-organisation. The chiral groups (S)-2-methylbutyl and (S)-1-methylheptyl have been chosen due to their tendency to give

chiral phases with short helical pitches in other liquid crystalline systems. Both units will be incorporated into the structure from chiral alcohols (S)-2-methyl butanol and (S)-1-methylheptanol. The liquid crystal properties of the chiral dimers produced will be studied, alongside their ability to impart chirality into an achiral nematic host. The helical twisting power of the diphenyl acetylene liquid crystal dimers will be measured.

In addition to changing the chiral chain, the nature of the linking group X which links the chiral unit to the diphenyl acetylene core (see Figure 68) will be varied. By changing the electronic properties of the linking group, X between ether and ester moieties, the electronic effects on the diphenyl acetylene unit will be changed. Ether groups are more flexible than ester groups, and provide a +M mesomeric effect. The +M mesomeric effect will provide a dipole in a push-pull effect when opposite the ester (-M) used on the other side of the diphenyl acetylene unit. This will increase the strength of the intermolecular interactions between the diphenyl acetylene unit and other mesogenic units. Alternatively, both sides of the diphenyl acetylene may be linked by ester units. This will reduce the flexibility of the chiral unit and reduce the strength of the intermolecular interactions shared by the diphenyl acetylene. In addition to the effect of the chiral structure on liquid crystal phase behaviour, the helical twisting power of each compound will be investigated to assess their dopant properties in an achiral nematic host, E7.
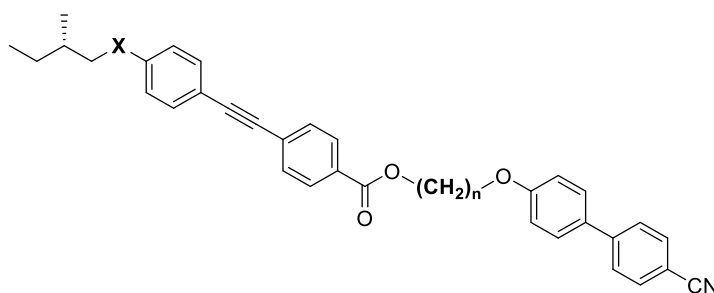
Figure 68. The generic structure of the chiral dimers reported in this thesis bearing an (S)-2-methylbutyl chiral unit, the letter X represents an ether or ester linking unit.

The final structural factor to be changed for the chiral dimers produced is the length of the alkyl spacer linking the diphenyl acetylene core and cyanobiphenyl unit. When a hexyl spacer is used, as with the *Janus* diphenyl acetylenes the motions of the cyanobiphenyl and diphenyl acetylene units are not decoupled. Alternatively, the length of the spacer may be extended (decyl, undecyl) which will allow for more freedom in the motion of the cyanobiphenyl unit increasing the stability of the

mesophase. By investigating spacers with both odd and even parity the tendency for an odd-even effect between the spacer length and mesophase stability may be detected.

Because the diphenyl acetylene unit is featured in the materials discussed in this thesis, they are candidates to undergo cyclotrimerisation reactions. The cyclotrimerisation of the diphenyl acetylene materials prepared will be investigated to yield hexaphenyl benzene materials as a tool to increase molecular complexity. In this way the molecular complexity of the diphenyl acetylene may be rapidly increased in one synthetic step giving a hexaphenyl benzene compound (Figure 69a). Cobalt-catalysed cyclotrimerisation reaction of the diphenyl acetylene core will be investigated as a route to hexaphenyl benzene compounds. Cyclotrimerisation of an asymmetrical diphenyl acetylene provides a mixture of isomers with 1,3,5 and 1,2,4-substitution patterns (Figure 69b). This may be used to investigate the effect of chirality upon hexaphenyl benzenes which have an intrinsic propeller shape.
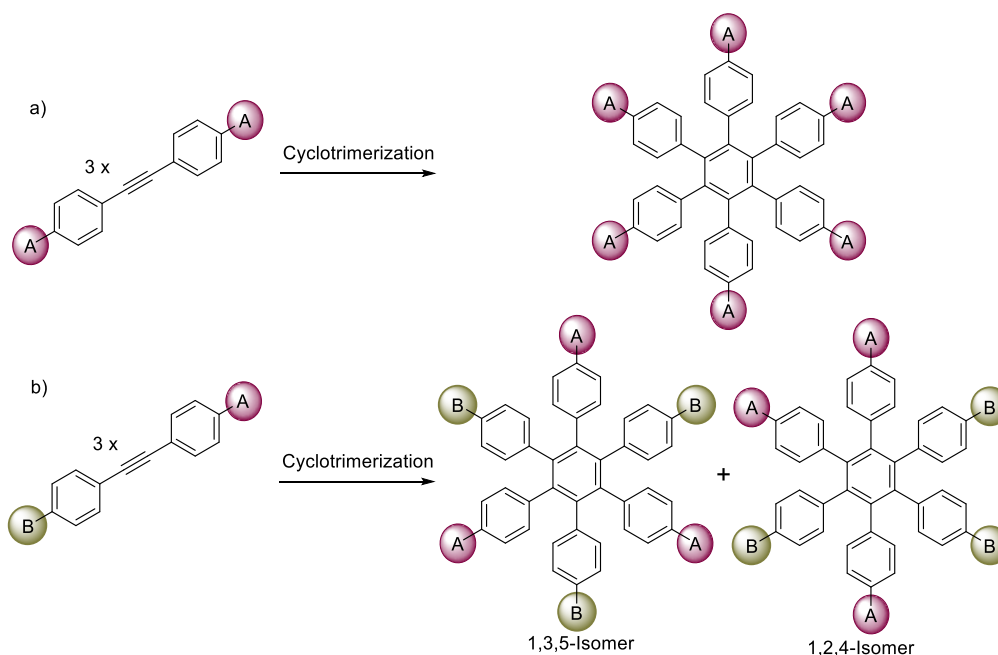
Figure 69. Cyclotrimerisation reactions of the diphenyl acetylene unit are to be investigated.

In particular, cotrimerisation reactions featuring two different diphenyl acetylene reactants in different ratios will be investigated as a method to rapidly increase the molecular complexity while retaining controlled regiochemistry. Due to the controlled regiochemistry of the cotrimerisation reaction the products from these reactions may be considered *Janus* hexaphenyl benzenes. Methods to exert control over the

outcome of the cotrimerisation reaction and therefore the incorporation of chiral units into hexaphenyl benzene materials will be investigated. The impact of chirality upon the self-organisation of the hexaphenyl benzenes will be investigated, as will the nature of these materials as chiral dopants.
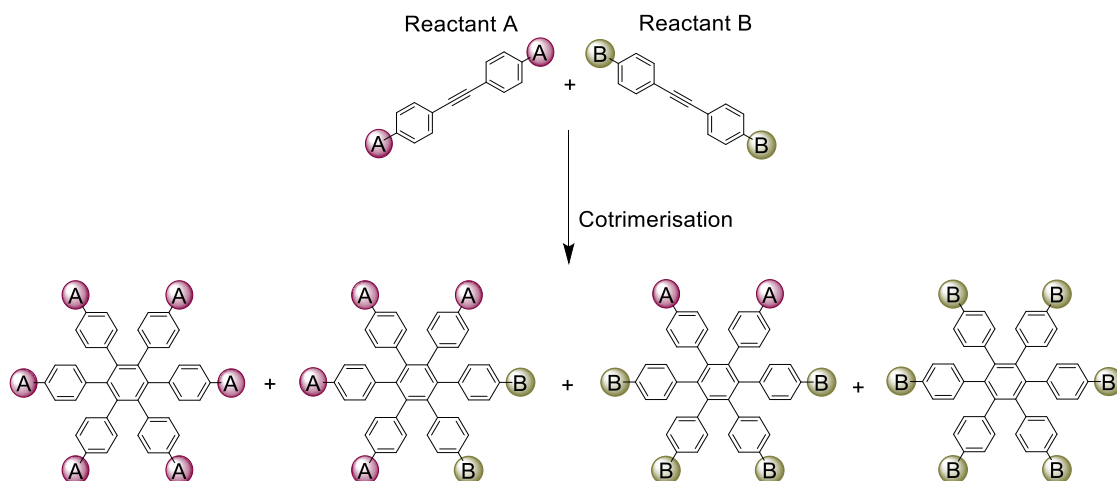
Figure 70. Potential outcomes of a cotrimerisation reaction of diphenyl acetylenes A and B.

In each investigation the liquid crystal behaviour of the materials produced will be investigated using polarised optical microscopy (POM) and differential scanning calorimetry (DSC). This will allow the type of mesophase formed by each compound to be identified from the characteristic textures. DSC will allow for the enthalpy and entropy of the phase transitions to be measured, and the degree of order within the mesophase to be known. In the case of the supermolecular *Janus* diphenyl acetylene materials the mesophase structure will be investigated using X-ray diffraction. This will allow further probing of the self-organisation of these materials to investigate different mesophase structures within the same type of liquid crystalline phase.

Chapter 3. Phenyl acetylene and iodo-aryl derivatives

In order to synthesise the desired family of *Janus* diphenyl acetylene compounds a convergent approach was utilized, combining iodo-aryl and phenyl acetylene moieties which are described in this chapter. A synthetic strategy was devised using a Sonogashira coupling of the relevant iodo-aryl and phenylacetylene partners. These iodo-aryl and phenylacetylene units may either be linear in nature or dendritic with a branching multiplicity of two or three.

The work presented in this chapter details the synthesis of intermediate units which were selected due to the ease of synthetic protocols required, and to maximise reaction yields. Due to this the family of compounds produced is not comprehensive, however as some of the intermediates prepared included mesogenic units – either partially fluorinated alkyl chains or cyanobiphenyls – several of these materials exhibited liquid crystalline behaviour. Examination of the liquid crystalline behaviour of these intermediate materials allowed an understanding of how the behaviour changed upon formation of more complex *Janus* systems. Specifically, the odd-even effect, and the role of branching was examined.

3.1 Synthesis

The initial starting material for all of these syntheses was 4-iodobenzoic acid **25** which was either used as the desired iodo-aryl compound, or transformed through a three step protocol into the alkynyl analogue 4-ethynylbenzoic acid **28** (Scheme 1.). To incorporate the ethynyl functionality a Fischer esterification[1] was used to protect the carboxylic acid as a methyl ester *via* refluxing **25** in methanol in the presence of catalytic sulfuric acid, which provided the desired product **26** in quantitative yield. Compound **26** underwent a Sonogashira coupling with trimethyl silyl acetylene to convert the iodo-aryl functionality to TMS protected acetylene **27** in good yield. Finally, both the trimethyl silyl and methyl ester protecting groups were cleaved simultaneously *via* base hydrolysis with sodium hydroxide in ethanol to give 4-ethynyl benzoic acid **28** with 90% yield.
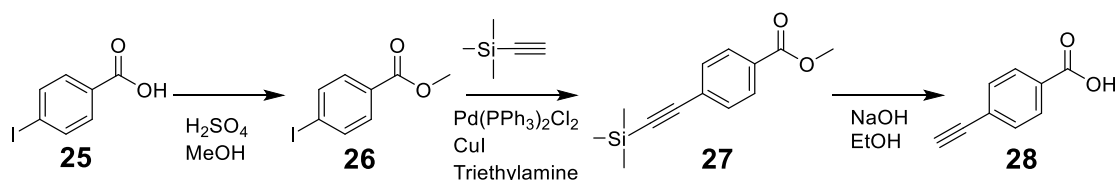
Scheme 1. Three step synthesis of 4-ethynyl benzoic acid from 4-iodobenzoic acid starting materials.

The two carboxylic acids (**25** and **28**) were used as the starting point to synthesise the desired mesogenic faces to be used as coupling partners in the synthesis of *Janus* diphenyl acetylene compounds. The first compounds to be introduced are the linear compounds, and then branched intermediates containing either two or three mesogenic units will be discussed.

3.1.1 Linear phenyl acetylene compounds

The carboxylic acid precursors were esterified using one of several mesogenic alcohols (see schemes 2 and 3) such as cyanobiphenyls **32**i-v[2] or commercially available 1H,1H,2H,2H-perfluorodecan-1-ol. The synthesis of intermediates **33**i, **33**iv, and **33**v by Steglich esterification was reported previously.[3,4] The mechanism of this reaction is shown in Figure 71. Subsequent synthesis of intermediates **33**ii and **33**iii followed this methodology, however, EDC.HCl (N-3-dimethylaminopropyl-N'-ethyl -carbodiimide hydrochloride) was used as the coupling agent rather than DCC (N,N'-Dicyclohexylcarbodiimide).

The Steglich esterification uses a stoichiometric ratio of DCC or EDC.HCl to the carboxylic acid and alcohol coupling partners. DCC and EDC.HCl serve as coupling agents to activate the carboxylic acid by providing a better leaving group. While the activated carboxylic acid can react with an alcohol directly this is relatively slow compared to reaction with DMAP (4-Dimethylaminopyridine). The catalytic behaviour of DMAP is achieved by reacting quickly with the activated O-acylisourea which produces a highly reactive species which can readily react with alcohols to give the desired ester. In the absence of DMAP the O-acylisourea intermediates react slowly and as such are prone to rearrangements which form inactive byproducts. Following

the addition of DMAP to the O-acylisourea the reaction intermediates can no longer undergo such rearrangements.
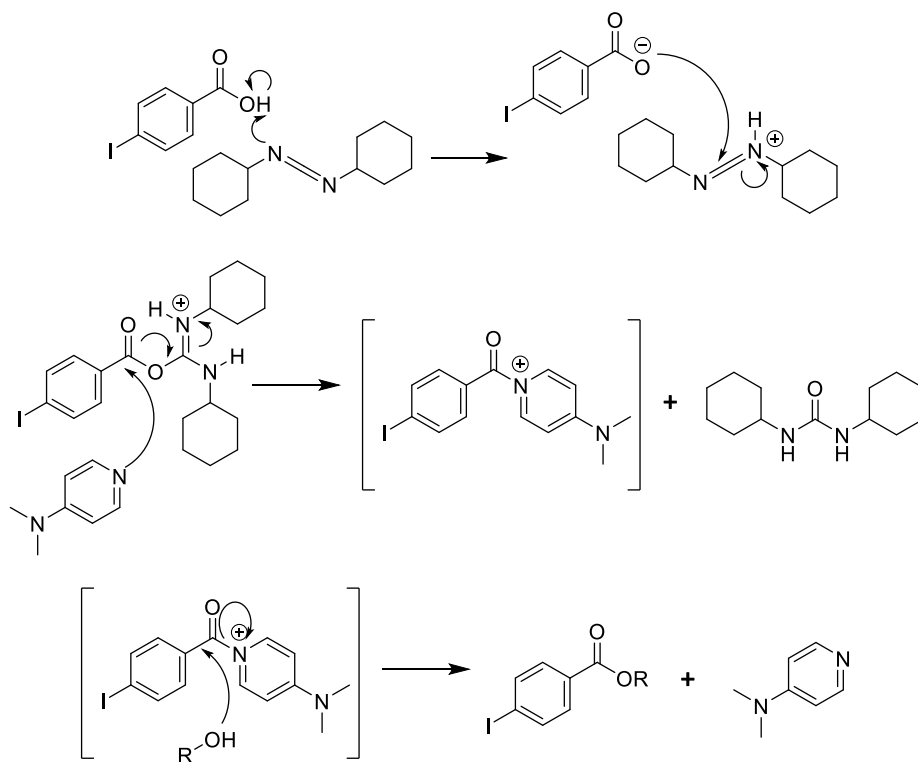
Figure 71. Mechanism of the Steglich esterification reaction. The carboxylic acid is activated by a carbodiimide coupling agent then the nucleophilic catalyst DMAP intercepts the activated acid and further increases reactivity, prior to nucleophilic attack via the alcohol.

EDC.HCl was largely preferred over DCC as the coupling agent in this project due to the ease of separation of reaction byproducts. Additionally, due to the formal charge of EDC.HCl separation of excess coupling agent is trivial by column chromatography and so an excess of the coupling agent may be used to decrease reaction times.[5] In contrast DCC and in particular the main byproduct of its use, dicyclohexylurea (DCU), have the potential to coelute with the desired product during column chromatography. DCC is non-polar and as such elutes quickly during column chromatography, as do non-polar esterification products such as perfluoroalkyl compound **30**. DCU is considerably more polar and so may coelute with more polar reaction products such as cyanobiphenyl compound **29** (Scheme 2).

In addition, dimethylaminopyridinium tosylate (DPTS) was occasionally used in place of DMAP as the nucleophilic catalyst (Scheme 3). DPTS has been reported to have increased activity compared to DMAP and therefore provides a greater conversion into

the desired product.[6,7] The use of DPTS in this project originated from a desire to increase the yield of esterification reactions of dendritic di- and tri- acids for which multiple reactive sites each require conversion to the desired ester (see Scheme 8). Reactions at multiple sites are typically more challenging and provide reduced yields compared to reactions in which only a single reactive site is present. A final modification was again taken from the synthesis of dendritic materials *via* Steglich esterification where it is common to use a greater amount of the catalytic DMAP then required as a true catalyst. Compared to catalytic loadings of DMAP (typically 5% or lower), loadings reaching substoichiometric or stoichiometric ratios may decrease reaction times and increase yields[8], this modification was adopted for some linear materials such as **37** (see Scheme 4).

*Scheme 2. Esterification of 4-iodo benzoic acid **25** to provide the simple linear iodo-aryl coupling partners desired for the project.*

*Scheme 3. Esterification of 4-ethynyl benzoic acid **28** to provide the simple linear ethynyl-aryl coupling partners desired for the project.*

These intermediate compounds have the advantage of being able to be prepared using standard esterification reactions. Their structure is uncomplicated meaning that liquid crystalline behaviour can be directly related to structure and intermolecular interactions. However, their simple structure does not allow understanding of the role of branching to be considered as is the case for the dendritic target compounds.

The same mesogenic alcohol **32**ᵢ was used in the synthesis of both linear and dendritic materials. However, the presence of a branching unit in the dendritic materials effectively increases the length of the aliphatic spacer between the mesogenic unit and diphenyl acetylene core. The role of the branching unit as an extension of the spacer cannot be ignored as this complicates comparisons between linear and branched materials as both variables – the presence of branching and effective increase in spacer length must be accounted for. To investigate the role of branching compounds **37** and **40** incorporate a methyl-branched spacer and only a single mesogenic unit (Scheme 4, 5). Synthetically this was achieved using a phase transfer catalyst as demonstrated with pentaerythritol by Dupuy.[9,10] This approach utilised the Michael addition of an alcohol, in this case 2,2-dimethylpropane-1,3-diol to tert-butyl acrylate to provide a statistical mixture of the mono- and di-substituted products which may then be purified *via* column chromatography to afford **34** (Scheme 4, 5). As the mono-substituted product was desired a slightly substoichiometric ratio of 0.85 equivalents of tert-butyl acrylate to 1 equivalent of 2,2-dimethylpropane-1,3-diol was utilised. This limited the ratio of di-substituted products obtained from the reaction mixture, and the dimethylpropane-1,3-diol starting material was easily separable by column chromatography. The successful isolation of the desired product was proven by the integration of ^{1}H NMR spectra, and by ESI-ms.

Compound **34** was esterified with aryl acids **25** or **28** using a Steglich esterification yielding compound **35** and **38** respectively (Scheme 4, 5). The tert-butyl protecting group was cleaved *via* the addition of trifluoroacetic acid (TFA) in dry dichloromethane (DCM). Dry solvent is required in this step to prevent the undesired hydrolysis of the aryl ester. Upon the reaction reaching completion the solvent and excess TFA were removed via vacuum distillation, residual TFA was removed as an azeotrope with toluene *in vacuo* to afford the carboxylic acids **36** and **39** which were used without further purification. In the final step an esterification was performed to provide the

cyanobiphenyl derivative **37** (Scheme 4), or partially fluorinated iodo-aryl compound **40** (Scheme 5).
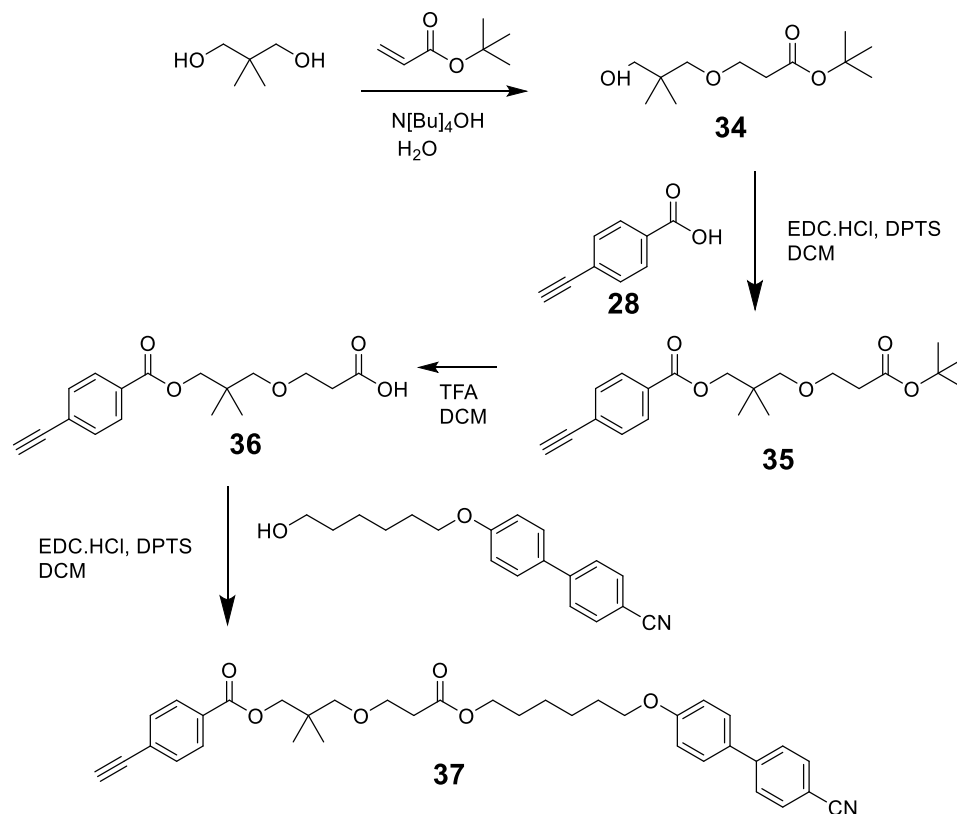
*Scheme 4. The synthesis of Compound **37** featuring a single mesogenic unit and a branched unit analogous to the branching point of the pentaerythritol or 1,1,1,-tris(hydroxymethyl)ethane.*
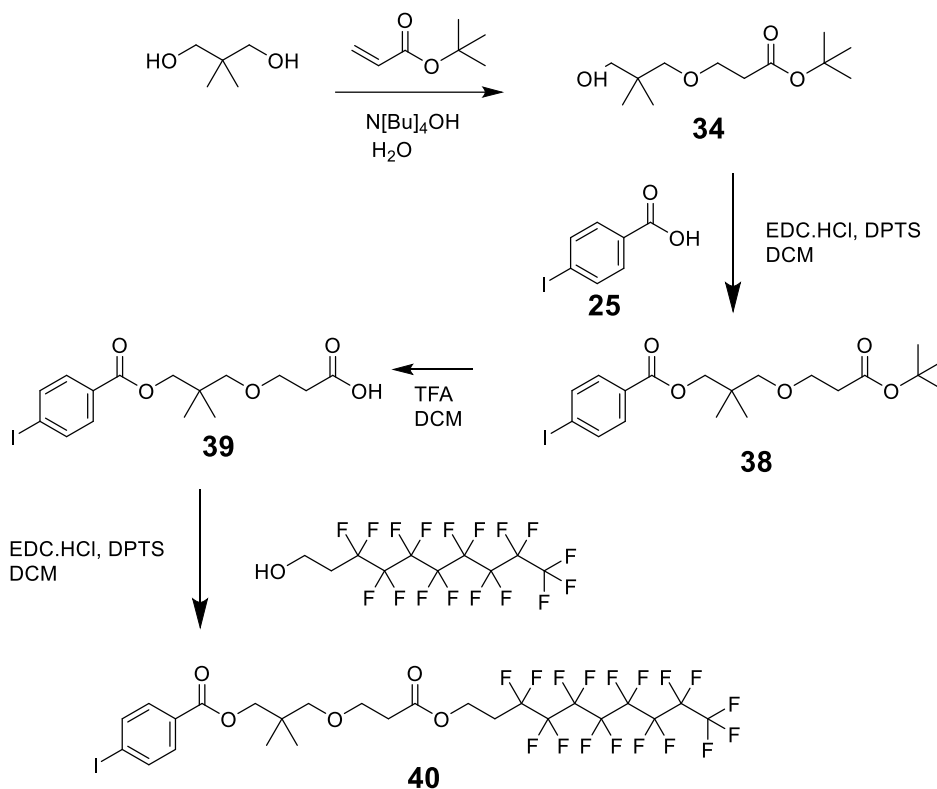
*Scheme 5. The synthesis of compound **40** featuring a single mesogenic unit and a branched unit analogous to the branching point of the pentaerythritol or 1,1,1,-tris(hydroxymethyl)ethane.*

3.1.2 Branched phenyl acetylene compounds

Several materials were produced with branching multiplicity G = 2 or 3. This was achieved by incorporating 1,1,1,-tris(hydroxymethyl)ethane or pentaerythritol (Schemes 6 – 7 and 8 – 9 respectively). Although the structure is more complex, the synthetic methodology is similar to that presented in schemes 4 and 5. For the target compounds derived from tris(hydroxymethyl)ethane a stoichiometry of 2.36 equivalents of tert-butyl acrylate to 1 equivalent of tris(hydroxymethyl)ethane were used to synthesise **34** using phase transfer catalysis. In this case the di-substituted product featuring a singly unprotected alcohol was desired and so a slightly greater ratio of acrylate was used. Unfortunately, neither the tri-substituted or mono-substituted byproducts were of use in the project and thus were not isolated. The increased ratio of acrylate was intended to skew the ratio of byproducts towards the di- and tri-substituted compounds, as the tri-substituted byproduct was marginally easier to separate from the desired product than the mono-substituted byproduct, which was found to coelute with the final fractions of the desired product **41**. In this way the reaction produced a mixture of compounds but separation of the target

compound **41** was achieved with 25% yield increasing the complexity of the intermediates and providing synthons for the dendritic target compounds.

For the following esterification step, initial attempts to provide branched ester **42** were low yielding due to the relatively sterically hindered primary alcohol of the hydroxymethyl group. Although a primary alcohol, the nucleophile is alpha to the quaternary carbon of the branching unit, increasing the reaction times required and seeming to decrease the yield. Due to the long reaction times larger quantities of DMAP rather than catalytic amounts were used which led to increases in yield from 37% to 60%. Deprotection of the tert-butyl ester was carried out using TFA in dry DCM. The excess TFA was removed as an azeotrope with toluene *in vacuo* to give the diacid **43**. The diacid was used as prepared without further purification. This did not appear to have a negative effect upon the next reaction as the desired products could be isolated in acceptable yields. The cyanobiphenyl substituted final compounds **44** and **48**, were isolated in 63 and 67% yields for the ethynyl- and iodo- products respectively (Schemes 6, 7). Considering two reactions are required to provide the desired product, each single reaction can be considered to occur with 80 or 82% yield. In the case of the perfluorinated products **45** and **49**, the desired ethynyl- and iodo-products were obtained in 84 and 89% yields respectively, which corresponds to a greater than 90% yield per reactive site. The nature of the nucleophilic alcohols differs between the cyanobiphenyl and perfluoroalkyl mesogenic units due to the strongly electron withdrawing perfluoroalkyl chain showing a -I effect, contrasted with the +I effect of the alkyl chains. As the greater yield was obtained for the poorer perfluoroalkyl nucleophile it is clear that the limiting factor in the synthesis of the cyanobiphenyl substituted final compounds was the purification from excess starting material, rather than reactivity.
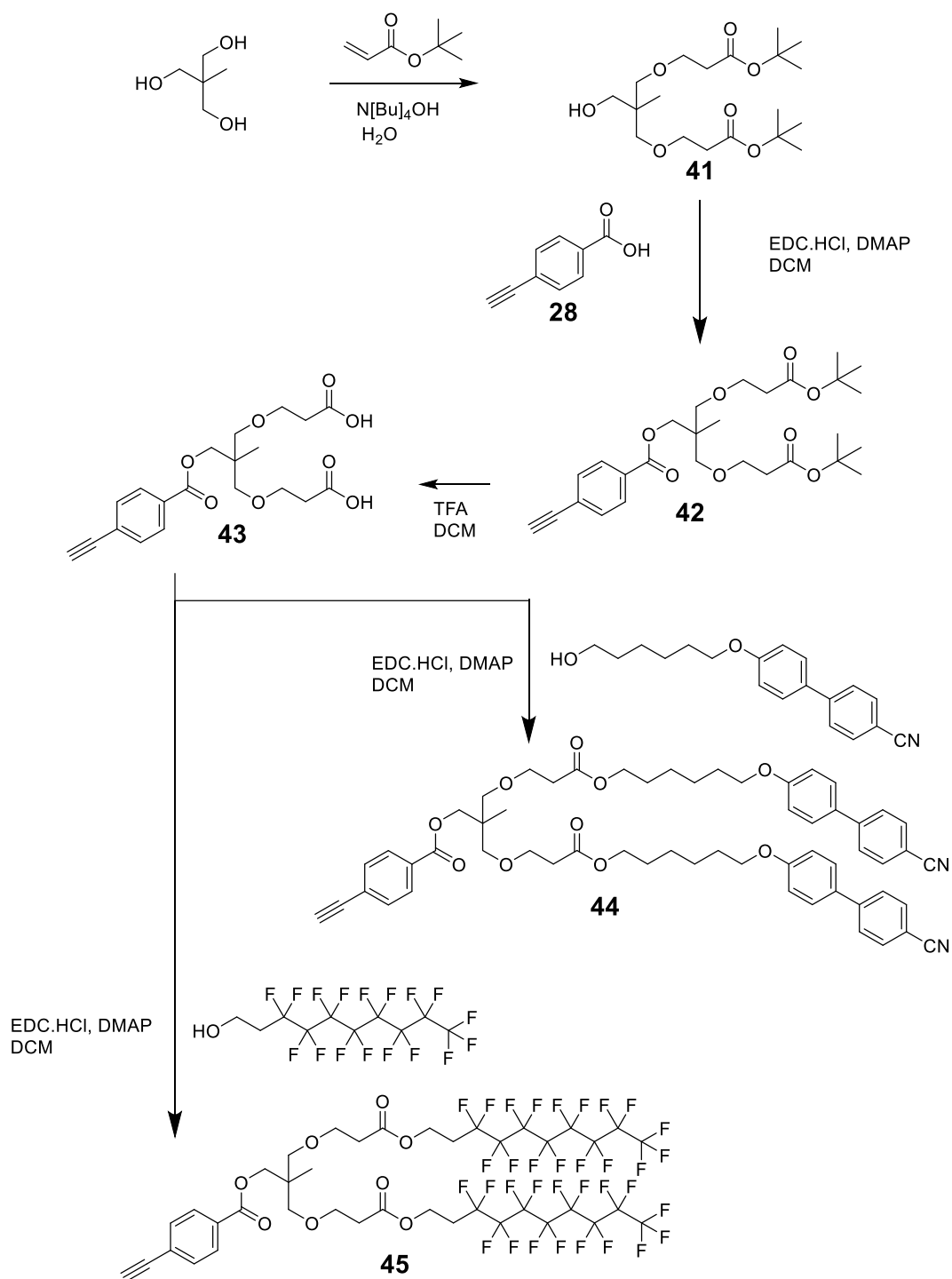
*Scheme 6. The synthesis of ethynyl intermediates incorporating cyanobiphenyl (**44**) or perfluoroalkyl (**45**) units with branching multiplicity G = 2, derived from 1,1,1,-tris(hydroxymethyl)ethane.*
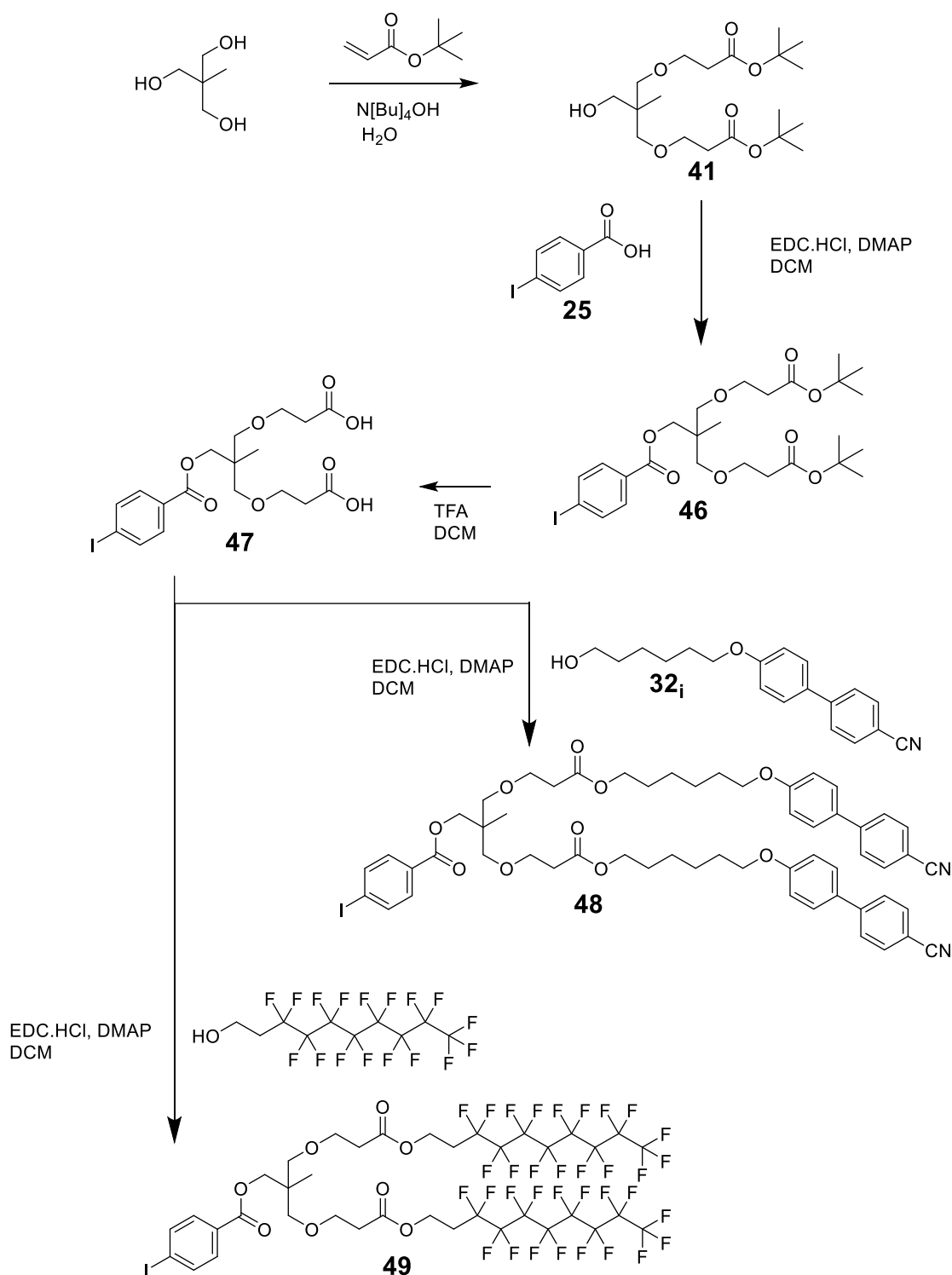
*Scheme 7. The synthesis of ethynyl intermediates incorporating cyanobiphenyl (**48**) or perfluoroalkyl (**49**) units with branching multiplicity G = 2, derived from 1,1,1,-tris(hydroxymethyl)ethane.*

A similar reaction protocol was repeated for the pentaerythritol branching unit to afford dendritic units (G = 3) with three mesogenic arms as reported by Ma[11] (Schemes 8 – 9). For completeness these compounds have been included to provide a wider study of structure-property relationships to be carried out. The synthetic methodology

used was similar to that described for the tris(hydroxymethyl) ethane derived compounds. The reaction stoichiometry used in these reactions was the same as found in Ma's thesis.
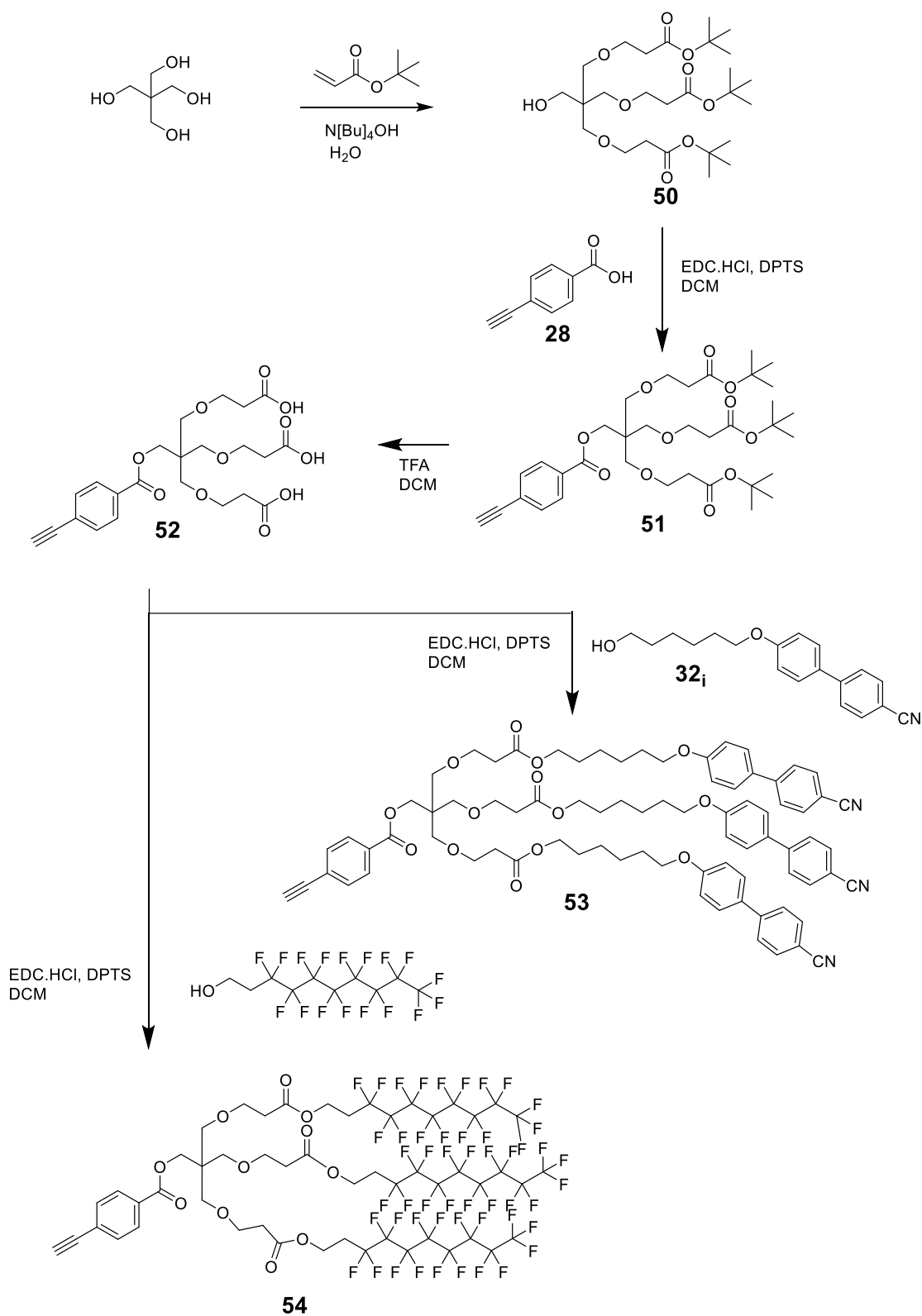
Scheme 8. The synthesis of ethynyl intermediates incorporating cyanobiphenyl (**53**) or perfluoroalkyl (**54**) units with branching multiplicity G = 3, derived from pentaerythritol.
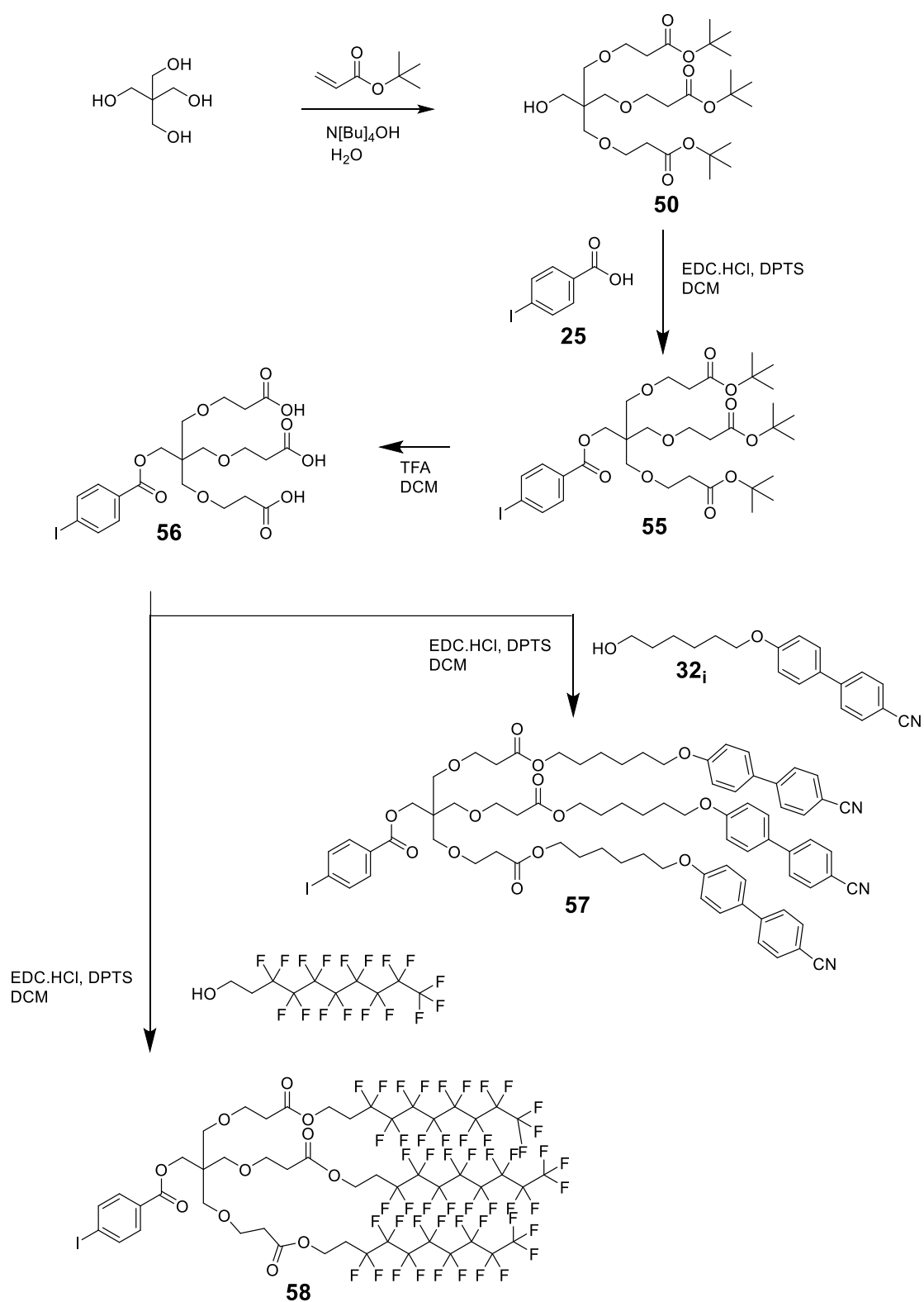
*Scheme 9. The synthesis of ethynyl intermediates incorporating cyanobiphenyl (**57**) or perfluoroalkyl (**58**) units with branching multiplicity G = 3, derived from pentaerythritol.*

In summary, the synthesis of intermediates has given access to esters derived from iodobenzoic acid and ethynylbenzoic acid bearing one, two or three pendant groups. These groups are comprised of fluorinated chains or cyanobiphenyl units. A summary of the compounds produced this way is given in Tables 2 – 4, with the compounds broken down into families from which comparisons can be drawn.

Table 2. Linear cyanobiphenyl compounds featuring iodo-aryl or ethynyl-aryl units.
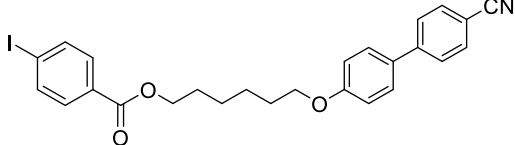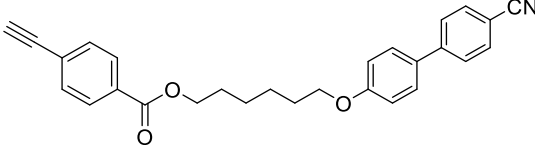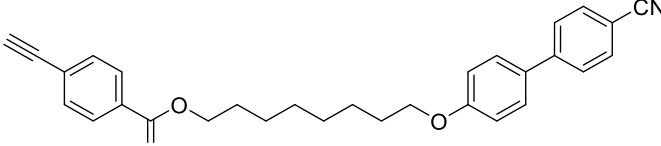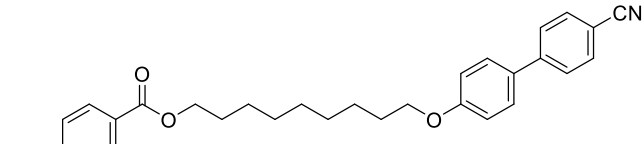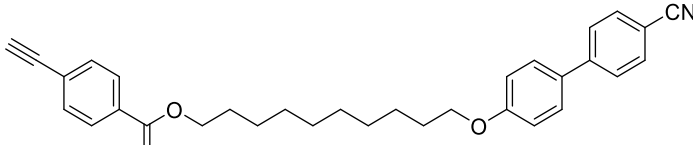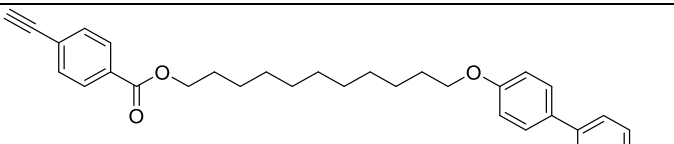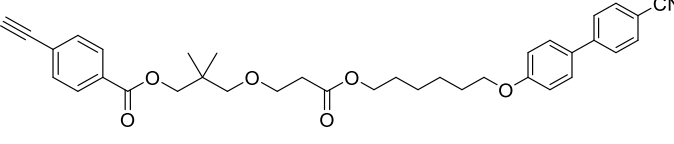
Compound number	Chemical structure	Transition temperatures/°C
29		Cr 107.4 Iso °C
33ᵢ		Cr 112.2 Iso °C
33ᵢᵢ		Cr 94.7 (N 77.3) Iso °C
33ᵢᵢᵢ		Cr 119.8 (N 111.1) Iso °C
33ᵢᵥ		Cr 86.2 (N 80.6) Iso °C
33ᵥ		Cr 115.5 (N 100.1) Iso °C
37		Cr 64.0 Iso °C

Table 3. Branched cyanobiphenyl compounds featuring iodo- or ethynyl-aryl units. Transition was broad.*
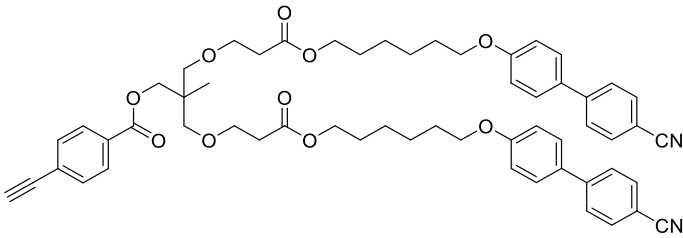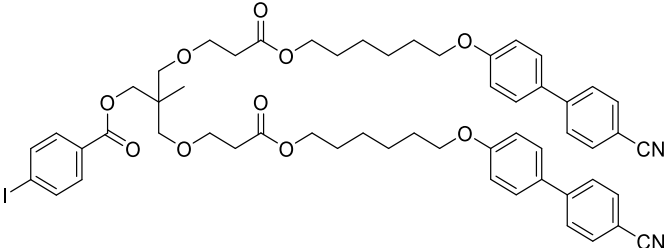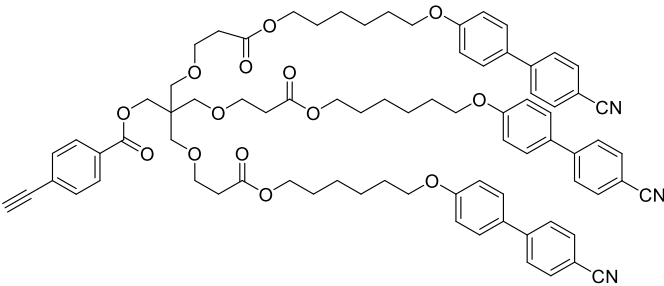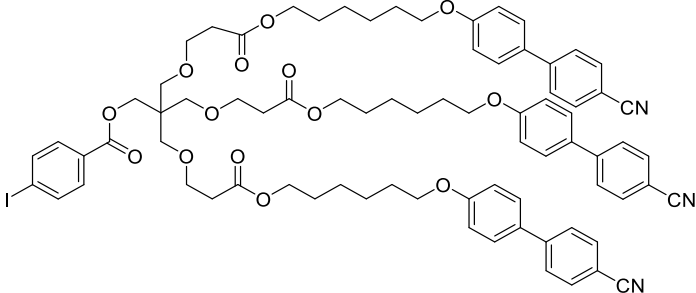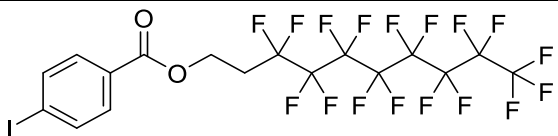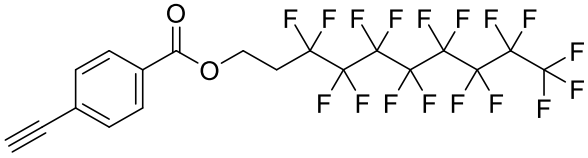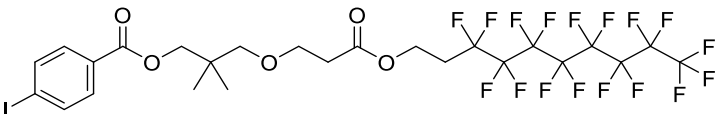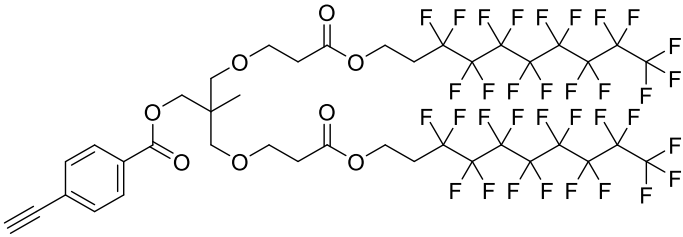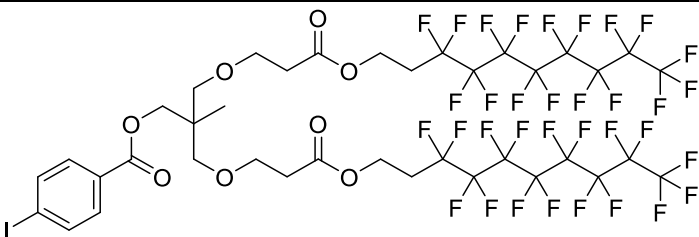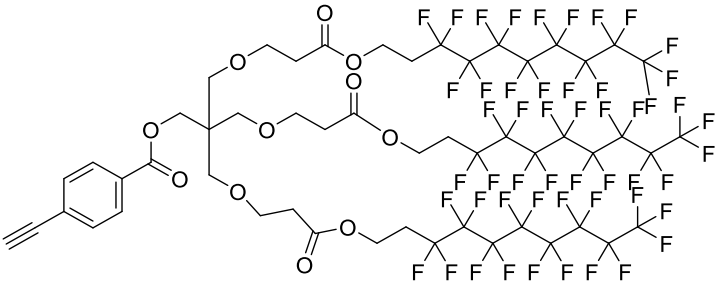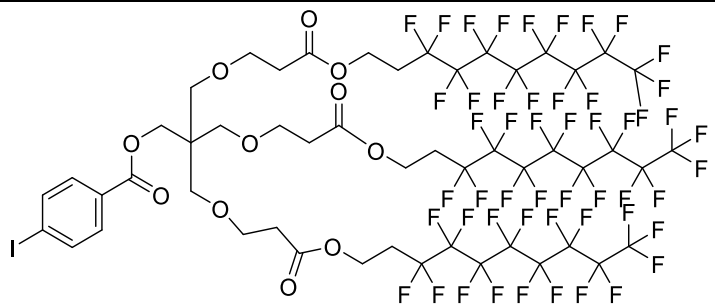
Compound number	Chemical structure	Transition temperatures /°C
44		g -13.6 N 13.9 Iso °C
48		g -11.4 N 9.1 Iso °C
53		g 2.0 SmA 46.4* N 43.9 Iso °C
57		g 1.7 SmA 33.7 N 37.1 Iso °C

Table 4. Linear and branched perfluoroalkyl compounds with iodo- or ethynyl-aryl units.

Compound number	Chemical structure	Transition temperatures /°C
30		Cr 77.2 Iso °C
31		Cr 78.5 Iso °C
40		Cr 58.9 Iso °C
45		Cr 64.1 Iso °C
49		Cr 62.6 Iso °C
54		Cr 31.5 SmA 49.2 Iso °C
58		Cr 37.4 SmA 49.1 Iso °C

3.2 Liquid crystal properties

The intermediates incorporating cyanobiphenyl units were investigated for their liquid crystalline properties. Transition temperatures and phase types were determined by polarised optical microscopy (POM) and the enthalpies and entropies of transitions determined by differential scanning calorimetry (DSC). For completeness previously reported intermediates which were resynthesised are included in Tables 5 – 7 below and are noted with the signs † or $.

3.2.1 Ethynyl-aryl and iodo-aryl linear cyanobiphenyl compounds

The first materials to be discussed are the linear cyanobiphenyl compounds shown in Table 3. Transition temperatures, enthalpies and entropies of transitions are summarised in Table 5 below.

Table 5. Transition temperatures, enthalpies and entropies of transition of linear phenyl acetylene compounds. † = reported previously[3,4].

Compound number	Transition	T /°C	ΔH / kJ mol^{-1}	ΔS / J K^{-1} mol^{-1}
29	Cr – Iso	107.4	55.2	145
33$_i$†	Cr – Iso	112.2	59.2	154
33$_{ii}$	Cr – Iso	94.7	22.2	63
	(N – Iso)	77.3	0.4	1
33$_{iii}$	Cr – Iso	119.8	27.3	70
	(N – Iso)	111.1	0.9	2
33$_{iv}$†	Cr – Iso	86.2	38.1	106
	(N – Iso)	80.6	2.3	7
33$_v$†	Cr – Iso	115.5	56.6	146
	(N – Iso)	100.1	-	-
37	Cr – Iso	64.0	-	-

Examination of the transition temperature data across the series shows that both compounds with hexamethylene spacers **29** and **33$_i$** were non-liquid crystalline. The extended compound with the dimethyl branching unit, compound **37** was also not liquid crystalline and DSC was not performed. Previously published results reported that the C$_{12}$ ethynyl- cyanobiphenyl compound was also non-liquid crystalline.[12,13] All

of the intermediate chain lengths of compounds **33ii** – **33v** exhibited monotropic nematic phases. Photomicrographs of the nematic phases of compounds **33ii** and **33iii** are shown in Figure 72. The monotropic nematic to isotropic transition of **33v** was not observed by DSC and so no thermodynamic data could be obtained.
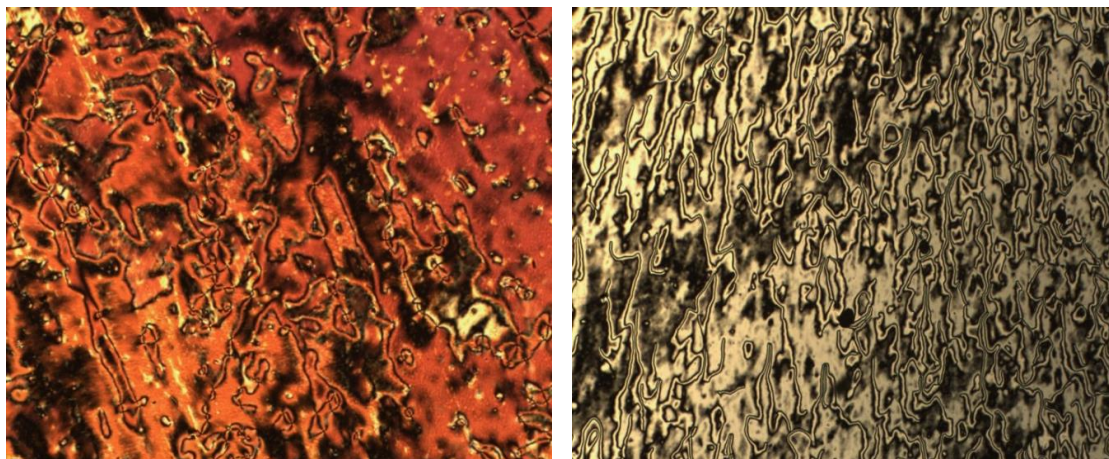
*Figure 72. Photomicrographs (x100 magnification) of the nematic phase of **33ii** (left, 70.1 °C) and **33iii** (right, 95.2 °C).*

There is a pronounced odd-even effect (Figure 73) which is observed in classical low molecular weight liquid crystals such as cyanobiphenyls[14], and have also been observed in dimers[15] (Chapter 6) and trimers. In this series the parity of the spacer is dominating the transition temperatures. With the atoms of the phenyl ester and biphenyl ether linkages being included, the odd-alkyl chain lengths will provide an even number of atoms linking the aromatic units and vice versa. While the trend is observed over just four chain lengths the same trend is maintained in the chiral diphenyl acetylene compounds discussed in chapter 6. This effect is explained by virtue of changing the parity of the spacer which affects the overall conformation of the molecule, with the end groups either projecting down in the same orientation to give a linear shape (**33iii**, **33v** above, odd) or forming a curved shape (**33i**, **33ii**, **33iv**, even) as shown in Figure 31 of the introduction. The linear shape allows for good overlap and efficient packing of the molecules which will lead to stronger intermolecular interactions. The bent shaped molecules cannot pack together as efficiently and so weaker intermolecular interactions occur.
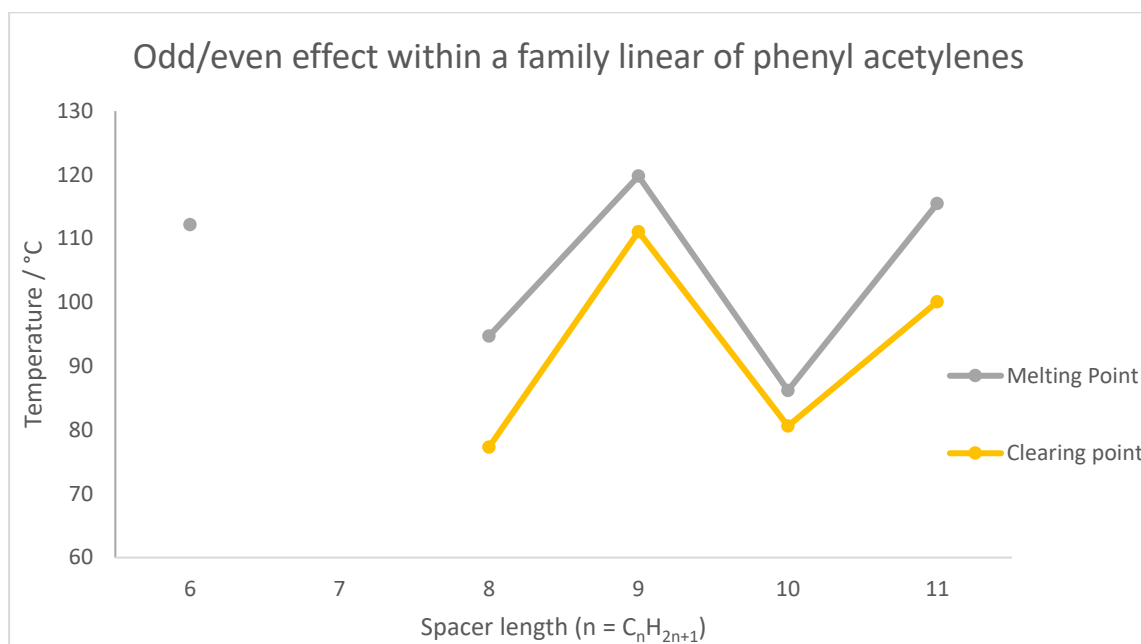
Figure 73. Odd/even effect observed for phenyl acetylene compounds 33ᵢ – 33ᵥ. Compound 33ᵢ n = 6, 33ᵢᵢ n = 8 , 33ᵢᵢᵢ n = 9, 33ᵢᵥ n = 10, 33v n = 11.

As well as the odd-even effect, the transition temperatures reveal an optimum alkyl spacer length of C_9 corresponding to a total of 12 atoms in the spacer. Similarly, the clearing point of **33**$_{iv}$ with a C_{10} spacer is greater than **33**$_{ii}$ with a C_8 spacer showing that increasing the spacer length provided a positive effect. The total length of the spacer is one of the factors contributing to the lack of liquid crystallinity shown by compound **37** and the previously reported C_{12} analogue for which the melting point was not reported. Increasing the spacer lengths increases the conformational freedom of the end group, the increased flexibility brought about by the longer C_{12} spacer introduces more disorder into the packing and so suppresses the potential for a mesophase. In addition to the spacer length, lateral substitutions such as the methyl units featured in the branching unit analogue of **37** disrupt efficient packing within the mesophase. This decreases the intermolecular interactions possible, and so inhibits liquid crystalline behaviour.

The nature of the mesophase in each case remains that of a monotropic nematic phase. The phenyl acetylene, or indeed iodophenyl unit, is not expected to greatly stabilise the mesophase or behave as a potential dimesogen as is suggested for the extended core of the diphenyl acetylene compounds. In the case of these materials multiple chain lengths of the iodo-aryl compounds were not required for use as

intermediates and so were not produced in order to study the effect of varying the end group. One iodo-aryl material was produced for which a slight reduction in the transition temperatures was observed compared to **33i**. To allow for a brief discussion of the role of the end group, comparisons to a family of liquid crystal styrene compounds can be made (Figure 74). These materials feature an ether linkage to an alkyl spacer and cyanobiphenyl mesogen and are comparable to the family of compounds reported in this chapter.[16] The odd-even effect is inverted with regards to the alkyl chain length due to the ether linkage containing one less atom than the ester and hence the parity of the alkyl spacer is effectively inverted.
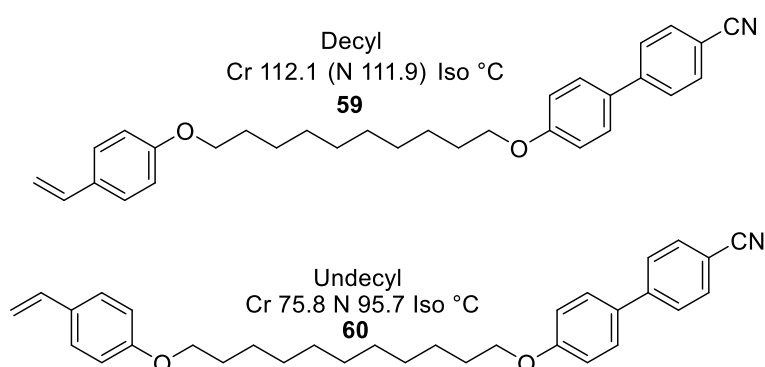
Figure 74. Styrene compounds reported by McKeown incorporating an ether linked spacer.[16]

The mesophase properties of the styrene compounds are similar to those of the ethynyl compounds reported here i.e. largely dominated by monotropic nematic behaviour. Comparison between the two families is complicated due to the inverted nature of the odd-even effect. Comparing ethynyl compounds **33iii** and **33v** with the decyl styrene compound **59** above shows very similar transition temperatures, as the total number of atoms in the spacers are very similar. In the ethynyl compounds the decyl spacer **33iv** provides a higher clearing point than octyl **33ii** while the opposite is seen in the styrenes. This is possibly due to the increased flexibility of the ether linkage being favourable with shorter spacer lengths. Separating the effect of the linking unit and end group beyond this is not possible, without the introduction of additional examples.

Also included in the report by McKeown was an investigation of various aryl substitutions including styrene (i.e. vinyl), chloro-, bromo-, and cyano. These end groups were tethered to the cyanobiphenyl unit via an undecyl spacer and the majority

of these compounds showed monotropic mesomorphism with the vinyl compound being the only compound to show enantiotropic behaviour.

While the cyano-substituted compound had the highest melting point due to the push-pull mesomeric effect on the aryl ring, this high transition temperature masked any liquid crystalline behaviour. To compare the effects of the iodo- and ethynyl- end groups used in this work the mesomeric effects of the aryl substituents may be compared, alongside the packing considerations. The work by McKeown reveals the bromo-aryl compound showed a melting point 20 °C higher than the chloro-aryl. There are two approaches to explain this behaviour, firstly the electronic effects including polarisability of the halogen and secondly the size of the halogen atom. The Hammett equation uses quantified constants for different aromatic substituents to indicate how strongly electron donating they are when positioned para- to a benzoic acid. The substituent constants show that increasing the size of the halogen atom increases the electron donating effect (chloro < bromo < iodo). This is due to the increased polarisability of the halogen, though this effect is mediated by reduced overlap between carbon and halogen orbitals. The Hammett constants suggest that increasing the size of halogen to iodo- as used in this work would further increase the melting point. This effect is expected to dominate the effect observed when increasing the size of the halogen atom in terms of packing into a liquid crystal mesophase.

3.2.1 Branched ethynyl-aryl and iodo-aryl cyanobiphenyl compounds

The second family of compounds to be discussed are the branched cyanobiphenyl compounds derived from 1,1,1-tris(hydroxymethyl) ethane and pentaerythritol as shown in Table 4. The transition temperatures, enthalpies and entropies of transition are presented in Table 6. The dendritic branched compounds produced for this work have been put into context alongside those reported previously, which have been used for the synthesis of the desired *Janus* materials reported in this project.

Table 6. Transition temperatures, enthalpies and entropies of transition of branched ethynyl-aryl and iodo-aryl cyanobiphenyl compounds. $ = reported by Ma.[11]

Compound number	Transition	T /°C	ΔH / kJ mol^{-1}	ΔS / J K^{-1} mol^{-1}
44	g – N	-13.6	-	-
	N – Iso	13.9	0.8	3
48	g – N	-11.4	-	-
	N – Iso	9.1	0.9	3
53$^\$$	g – SmA	2.0	-	-
	SmA – N	* Broad	-	-
	N – Iso	43.9	6.7	21
57$^\$$	g – SmA	1.7	-	-
	SmA – N	33.7	0.7	2
	N – Iso	37.1	0.4	1

Within the family of branched cyanobiphenyl compounds, all exhibited liquid crystalline mesophases. The cyanobiphenyl compounds based on the 1,1,1-tris(hydroxymethyl) ethane linkage exhibited enantiotropic nematic phases for both the iodo and ethynyl compounds **44** and **48**. The clearing points of these compounds were below room temperature and neither compound crystallised but instead formed a glass. In the case of the compounds derived from pentaerythritol **53** and **57** it was possible to observe both SmA and nematic phases.

The cyanobiphenyl compounds detailed above provide an insight into the competing effects that an increase in the number of mesogens (with the concomitant increasing of branching multiplicity) has on the mesomorphic behaviour of these dendritic materials. The competing effects at play are interrelated, increasing both the disorder and number of mesogens when the branching multiplicity is increased. In contrast with the perfluorinated compounds discussed below that require three mesogenic arms to provide a liquid crystal mesophase, the cyanobiphenyl equivalents with two or three mesogenic arms are all liquid crystalline. The phase behaviour of **53** and **57** was reported by Ma whereby the phase behaviour of **53** showed a broad transition between the nematic and the smectic A phase around 44 °C. DSC revealed multiple

maxima within a small temperature range (46.4, 47.2 and 48.4 °C) during the cooling cycle for this compound. The peaks could not be fully resolved but the complex behaviour is linked to a larger value for the enthalpy and thus entropy of the transition.

The introduction of branching *via* the 2,2,2-tris(hydroxymethyl) ethane unit resulted in a sharp drop in the melting point relative to the linear materials presented in Table 6. The introduction of a lateral methyl group will have a detrimental impact as discussed for compound **37**, however this is likely to be minimal compared to the introduction of a second cyanobiphenyl unit. The quaternary carbon is the simplest branching unit and possesses tetrahedral geometry. Many oligomers featuring this core such as pentaerythritol derivatives have previously been reported.[17,18] The tetrahedral geometry allows for the two cyanobiphenyls of **44** and **48** to project in the same plane. However, the remaining arms will not contribute to the mesophase stability. In comparison the compounds with three cyanobiphenyl units **53** and **57** can project a three-dimensional cone, or alternatively have one cyanobiphenyl raised away from the others to offset the difference in volumes (Figure 75).

Branching multiplicity g = 3   Branching multiplicity g = 2
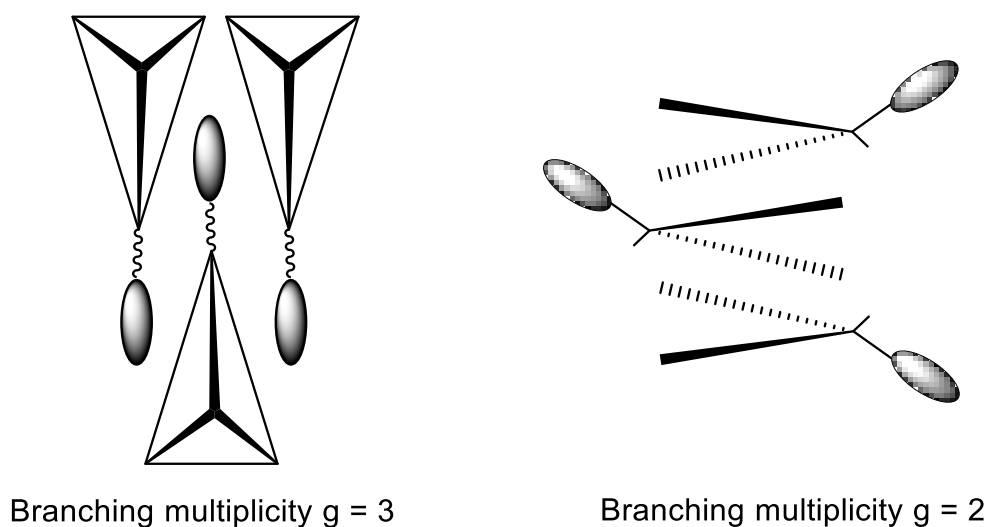
Figure 75. Example of the three- dimensional structures of pentaerythritol and 1,1,1-tris(hydroxymethyl) ethane.

3.2.3 Iodo-aryl and ethynyl-aryl perfluoroalkyl compounds

Finally, the iodo-aryl and ethynyl-aryl materials featuring perfluorinated chains shown in Table 5 are to be discussed. The transition temperatures, enthalpies and entropies of transition are presented in Table 7.

Table 7. Transition temperatures, enthalpies and entropies of transition of ethynyl-aryl and iodo-aryl perfluoroalkyl compounds. $ = reported by Ma.[11]

Compound number	Transition	T /°C	ΔH / kJ mol⁻¹	ΔS / J K⁻¹ mol⁻¹
30	Cr – Iso	77.2	-	-
31	Cr – Iso	78.5	-	-
45	Cr – Iso	64.1	44.0	1301
49	Cr – Iso	62.6	41.4	123
54$	Cr – SmA	31.5	11.0	36
	SmA – Iso	49.2	5.1	16
58$	Cr – SmA	37.4	12.5	40
	SmA – Iso	49.1	4.7	15
40	Cr - Iso	58.9	-	-

While the pentaerythritol derived compounds **54** and **58** containing three perfluorinated self-organising units exhibited a Smectic A mesophase, reducing the branching multiplicity and thus number of perfluorinated chains to two (**45** and **49**) suppressed any liquid crystallinity.

The melting point of the branched perfluoroalkyl containing compounds with G = 2 (**45** and **49**) were considerably higher than that of the more heavily branched compounds with G = 3 (**54** and **58**). Therefore, the lack of liquid crystallinity for **45** and **49** is unsurprising as fewer perfluoroalkyl self-organising units are present to stabilize the mesophase and the melting point is greater, for example **49** crystallised at 62.6 °C, more than 13 °C above the clearing point of **58**.

In each of the cyanobiphenyl branched compounds shown in Table 6, perfluoroalkyl compounds shown in Table 7 and diphenyl acetylene materials discussed in Chapter 5 there is a consistent and large decrease in the materials transition temperatures upon introducing branching. In the cyanobiphenyl compound (Table 6) and diphenyl acetylenes (Chapter 5) increasing the branching multiplicity from 2 to 3 was typically well tolerated and often increased the transition temperatures. In contrast, the perfluorinated materials shown in Table 7 appear to have a smaller initial decrease

due to branching, however introducing a third chain decreases the melting point further. This likely reflects the difference in the intermolecular interactions between the perfluoroalkyl and alkyl units.

Comparison between the crystalline packing which result in the changes in melting point and the mesophase structure are to be treated with care. The presence of liquid crystalline behaviour for some of the branched compounds featuring perfluorinated chains is an example of the fluorophobic effect. Here the entropic cost of the more organised liquid crystalline state is lower than the free energy associated with an increase in favourable hydrocarbon-hydrocarbon interactions associated with the microphase segregation of the perfluorinated chains. However, the mesomorphism of **54** and **58** must relate to the molecular shape in a way that **45** and **49** cannot (Figure 75). Considering the tetrahedral shape **54** and **58** can be considered to project as a pyramid with the point relating to the smaller aryl unit.[19] This can pack in an antiparallel arrangement to give a layered smectic structure. In comparison **45** and **49** possess two fluorinated chains which will lie in one plane, with a smaller alkyl unit projecting above or below it.

3.3 Experimental

Compounds **53**, **54**, **57** and **58**[11] were synthesised following procedures which have been described previously. The characterisation data (^{1}H NMR spectra, mass spectrometry) of these compounds were in agreement with those reported previously.
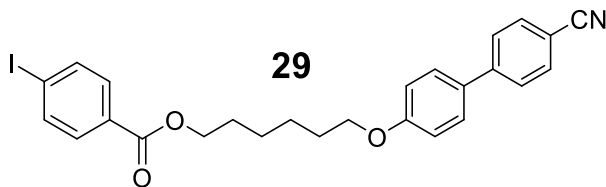
4-Iodobenzoic acid (0.51 g, 1.79 mmol), 4'-((6-hydroxyhexyl)oxy)-4-cyanobiphenyl (0.60 g, 2.03 mmol), EDC.HCl (0.41 g, 2.65 mmol) and DMAP (0.03 g, 1.39 mmol) were dissolved in DCM (30 mL) and the reaction mixture was stirred at room temperature for 18 hrs. The solvent was removed *in vacuo* and the crude product was purified by column chromatography (10:1 DCM:EtOAc as eluent) to give the target compound **29** as a white powdery solid (0.84 g, 1.60 mmol, 89% yield).

^{1}H NMR (400 MHz, CDCl$_3$) δ 7.78 (d, *J* = 8.5 Hz, 2H, Ar*H*), 7.73 (d, *J* = 8.5 Hz, 2H, Ar*H*), 7.69 (d, *J* = 8.5 Hz, 2H, Ar*H*), 7.64 (d, *J* = 8.5 Hz, 2H, Ar*H*), 7.52 (d, *J* = 8.5 Hz, 2H, Ar*H*), 6.98 (d, *J* = 8.5 Hz, 2H, Ar*H*), 4.33 (t, *J* = 6.5 Hz, 2H, COOC*H$_2$*), 4.02 (t, *J* = 6.5 Hz, 2H, OC*H$_2$*), 1.88 – 1.78 (m, 4H, OCH$_2$C*H$_2$*), 1.63 – 1.47 (m, 4H, OCH$_2$CH$_2$C*H$_2$*).

APCI-MS: m/z = 526.1 [M+H]$^+$

30
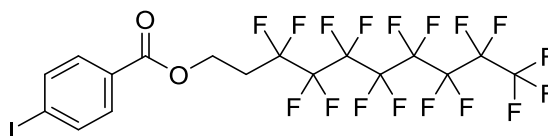
4-Iodobenzoic acid (0.25 g, 1.00 mmol), 1H,1H,2H,2H-perfluorodecanol (0.50 g, 1.08 mmol), DCC (0.22 g, 1.07 mmol) and DMAP (0.04 g, 0.33 mmol) were charged to a dry flask and purged with nitrogen and dry DCM (15 mL) was added. The reaction mixture was stirred at room temperature for 2 days and then filtered through a pad of celite. The solvent was removed *in vacuo* and the crude product was purified by column chromatography (10:3 hexane:diethyl ether as eluent) to give the target compound **30** as a white crystalline solid (0.62 g, 0.89 mmol, 89% yield).

^{1}H NMR (400 MHz, CDCl$_3$) δ 7.82 (d, *J* = 8.5 Hz, 2H, Ar*H*), 7.74 (d, *J* = 8.5 Hz, 2H, Ar*H*), 4.62 (t, *J* = 6.5 Hz, 2H, COOC*H$_2$*), 2.56 (tt, *J* = 18.5, 6.5 Hz, 2H, CF$_2$C*H$_2$*).

APCI-MS: m/z = 694.9 [M+H]

31
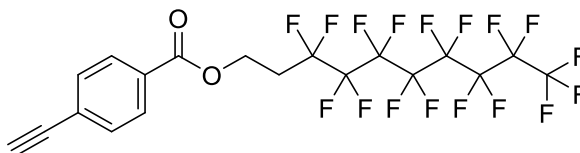
4-Ethynylbenzoic acid (0.21 g, 1.44 mmol), 1H,1H,2H,2H-perfluorodecanol (0.51 g, 1.10 mmol), EDC.HCl (0.32 g, 1.67 mmol) and DPTS (0.13 g, 0.43 mmol) were charged to a dry flask and purged with nitrogen and dry DCM (25 mL) was added. The reaction mixture was stirred at room temperature for 2 days and then filtered through a pad of celite. The solvent was removed *in vacuo* and the crude product was purified by column chromatography (10:3 hexane:diethyl ether as eluent) to give the target compound **31** as a white crystalline solid (0.51 g, 0.86 mmol, 78% yield).

^{1}H NMR (400 MHz, CDCl$_3$) δ 7.95 (d, *J* = 8.5 Hz, 2H, Ar*H*), 7.66 (d, *J* = 8.5 Hz, 2H, Ar*H*), 4.59 (t, *J* = 7.0 Hz, 2H, COOC*H$_2$*), 3.23 (s, 1H, CC*H*), 2.55 (tt, *J* = 18.5, 6.5 Hz, 2H, CF$_2$C*H$_2$*).

APCI-MS: m/z = 593.0 [M+H]$^+$

32ii
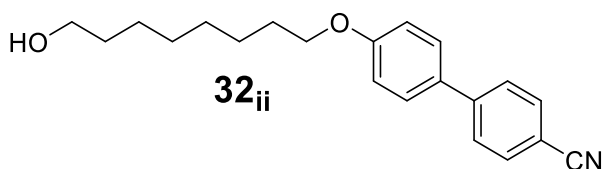
8-Bromo-1-nonanol (1.00 g, 4.78 mmol), 4'-hydroxy-4-cyanobiphenyl (1.10 g, 5.64 mmol) and potassium carbonate (1.40 g, 10.13 mmol) were mixed together in acetone (30 mL),and the reaction mixture was heated to reflux for 18 hrs. The solvent was removed *in vacuo* and the crude mixture redissolved in DCM (200 mL), washed with deionised water (2 x 100 mL), brine (100 mL) and dried over magnesium sulfate. The solvent was removed *in vacuo* and the crude product was purified by column chromatography (DCM:EtOAc as eluent) to give the target compound **32ii** as a white powdery solid (1.54 g, 4.57 mmol, 81% yield).

^{1}H NMR (400 MHz, CDCl$_3$) δ 7.69 (d, *J* = 7.5 Hz, 2H, Ar*H*), 7.61 (d, *J* = 7.5 Hz, 2H, Ar*H*), 7.52 (m, *J* = 7.5 Hz, 6H, Ar*H,* Ar*H*), 6.99 (d, *J* = 7.5 Hz, 2H, Ar*H*), 4.01 (t, *J* = 6.5 Hz, 2H, OC*H$_2$*), 3.69 (t, *J* = 6.5 Hz, 2H, HOC*H$_2$*), 1.88 − 1.73 (m, 2H, OCH$_2$C*H$_2$*), 1.54 − 1.31 (m, 10H, CH$_2$C*H$_2$*). OH proton not observed.

32iii
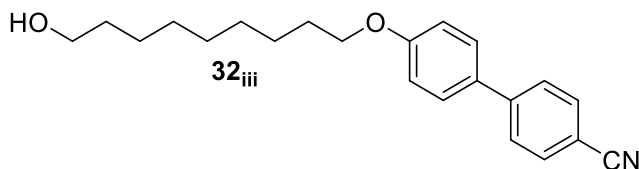
9-Bromo-1-nonanol (5.00 g, 23.91 mmol), 4'-hydroxy-4-cyanobiphenyl (4.30 g, 22.03 mmol) and potassium carbonate (4.70 g, 34.00 mmol) were mixed together in acetone (80 mL), the reaction mixture was heated to reflux for 18 hrs. The solvent was removed *in vacuo* and the crude mixture redissolved in DCM (200 mL), washed with deionised water (2 x 100 mL), brine (100 mL) and dried over magnesium sulfate. The solvent was removed *in vacuo* and the crude product was purified by column chromatography (DCM:EtOAc as eluent) to give the target compound **32iii** as a white powdery solid (6.01 g, 18.55 mmol, 84% yield).

^{1}H NMR (400 MHz, CDCl$_3$) δ 7.68 (d, *J* = 7.5 Hz, 2H, Ar*H*), 7.62 (d, *J* = 7.5 Hz, 2H, Ar*H*), 7.53 (m, *J* = 7.5 Hz, 6H, Ar*H,* Ar*H*), 6.98 (d, *J* = 7.5 Hz, 2H, Ar*H*), 4.00 (t, *J* = 6.5 Hz, 2H, OC*H$_2$*), 3.68 (t, *J* = 6.5 Hz, 2H, HOC*H$_2$*), 1.90 − 1.75 (m, 2H, OCH$_2$C*H$_2$*), 1.57 − 1.34 (m, 12H, CH$_2$C*H$_2$*). OH proton not observed.

33$_i$
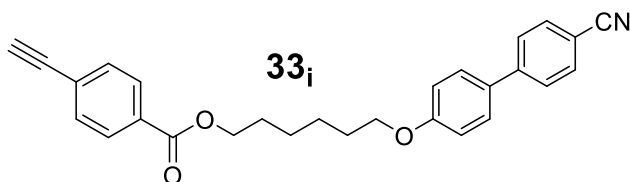
4-Ethynylbenzoic acid (0.15 g, 1.03 mmol), 4'-((6-hydroxyhexyl)oxy)-4-cyanobiphenyl (0.33 g, 1.18 mmol), EDC.HCl (0.22 g, 1.42 mmol) and DMAP (0.02 g, 0.17 mmol) were dissolved in DCM (20 mL) and the reaction mixture was stirred at room temperature for 18 hrs. The reaction mixture was then filtered through a short pad of silica, the solvent removed *in vacuo* and the product was purified by column chromatography (10:1 DCM:EtOAc as eluent) to give the target compound **33$_i$** as a powdery white solid (0.29 g, 0.69 mmol, 67% yield).

^{1}H NMR (400 MHz, CDCl$_3$) δ 7.99 (d, J = 8.54 Hz, 2H, ArH), 7.69 (d, J = 8.5 Hz, 2H, ArH), 7.64 (d, J = 8.5 Hz, 2H, ArH), 7.53 (d, J = 6.0 Hz, 2H, ArH), 7.51 (d, J = 8.5 Hz, 2H, ArH), 6.98 (d, J = 8.5 Hz, 2H, ArH), 4.34 (t, J = 6.5 Hz, 2H, COOCH_2), 4.02 (t, J = 6.5 Hz, 2H, OCH_2), 3.22 (s, 1H, CCH), 1.99 − 1.73 (m, 4H, OCH$_2$CH_2), 1.68 − 1.43 (m, 4H, OCH$_2$CH$_2$CH_2).

APCI-MS: m/z = 424.2 [M+H]$^+$

33$_{ii}$
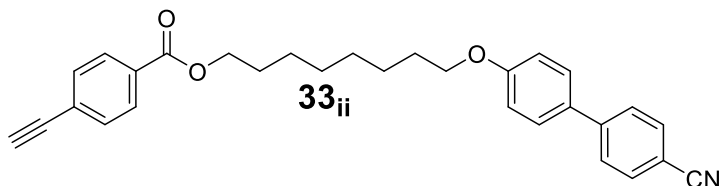
4-Ethynyl benzoic acid (0.23 g, 1.58 mmol), **32$_{ii}$** (0.50 g, 1.48 mmol), EDC.HCl (0.45 g, 2.36 mmol) and DPTS (0.10 g, 0.82 mmol) were dissolved in DCM (20 mL), and the reaction mixture was stirred at room temperature for 18 hours. The solvent was removed *in vacuo* and the crude product was purified by column chromatography (DCM as eluent) to give the target compound **33$_{ii}$** as a white solid (0.51 g, 1.17 mmol, 74% yield).

^{1}H NMR (400 MHz, CDCl$_3$) δ 7.99 (d, J = 7.5 Hz, 2H, ArH), 7.69 (d, J = 7.5 Hz, 2H, ArH), 7.63 (d, J = 7.5 Hz, 2H, ArH), 7.58 − 7.49 (m, 4H, ArH, ArH), 6.98 (d, J = 7.5 Hz, 2H, ArH), 4.32 (t, J = 6.5 Hz, 2H, COOCH_2), 4.00 (t, J = 6.5 Hz, 2H, OCH_2), 3.22 (s, 1H, CCH), 1.86 − 1.73 (m, 2H, OCH$_2$CH_2), 1.53 − 1.36 (m, 8H, CH$_2$CH_2).

APCI-MS: m/z = 425.2 [M+H]$^+$

33ᵢᵢᵢ
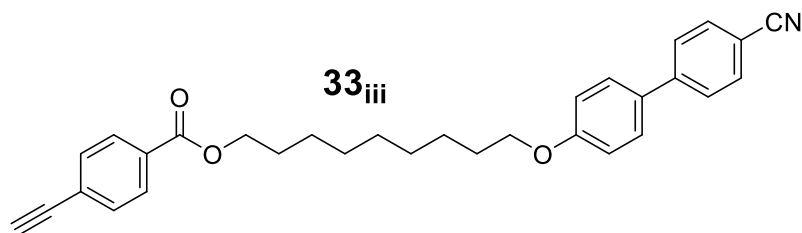
4-Ethynyl benzoic acid (0.90 g, 6.16 mmol), **32ᵢᵢᵢ** (2.00 g, 5.93 mmol), EDC.HCl (1.2 g, 6.26 mmol) and DPTS (0.40 g,3.28 mmol) were dissolved in DCM (60 mL), and the reaction mixture was stirred at room temperature for 18 hours. The solvent was removed *in vacuo* and the crude product was purified by column chromatography (DCM as eluent) to give the target compound **33ᵢᵢᵢ** as a white solid (2.17 g, 4.81 mmol, 78% yield).

^{1}H NMR (400 MHz, CDCl$_3$) δ 7.99 (d, J = 7.5 Hz, 2H, ArH), 7.69 (d, J = 7.5 Hz, 2H, ArH), 7.63 (d, J = 7.5 Hz, 2H, ArH), 7.59 – 7.49 (m, 4H, ArH), 6.99 (d, J = 7.5 Hz, 2H, ArH), 4.32 (t, J = 6.5 Hz, 2H, COOCH_2), 4.00 (t, J = 6.5 Hz, 2H, OCH_2), 3.22 (s, 1H, CCH), 1.86 – 1.71 (m, 4H), 1.51 – 1.32 (m, 10H).

34
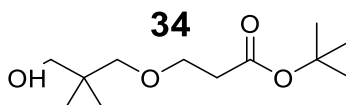
2,2-Dimethyl-1,3-propanediol (5.0 g, 48.0 mmol), tetra-n-butyl ammonium hydroxide (40% in H$_2$O, 12 mL) and tert-butyl acrylate (6 mL, 5.25 g, 41.0 mmol) were stirred together at room temperature for 72 hours. The mixture was diluted with water (50 mL) and then extracted with ethyl acetate (3 x 100 mL). The extracts were combined and the solvent removed *in vacuo*. The crude product was purified by column chromatography (10:2 hexane:EtOAc as eluent) to give the target compound **34** as a colourless oil (3.51 g, 15.13 mmol, 37% yield).

^{1}H NMR (400 MHz, CDCl$_3$) δ 3.64 (d, J = 6.0, 2H, CH_2OH), 3.39 (t, J = 6.5, 2H, OCH_2CH$_2$), 3.28 (s, 2H, CCH_2O*)*, 2.45 (t, J = 6.5, Hz, 2H, CH_2COO), 1.42 (s, 9H, C(CH$_3$)$_3$), 0.99 (s, 6H, C(CH$_3$)$_2$).

ESI-MS: m/z = 253.17 [M+Na]$^+$

35
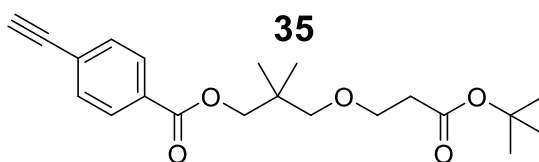
4-Ethynylbenzoic acid (0.31 g, 2.12 mmol), compound **34** (0.50 g, 2.15 mmol) EDC.HCl (0.6 g, 3.13 mmol) and DPTS (0.04 g, 0.33 mmol) were dissolved in DCM (30 mL) and the mixture was stirred at room temperature for 48 hours. The solvent was removed *in vacuo* and the crude product was purified by column chromatography (DCM as eluent) to give the target compound **35** as a colourless oil (0.59 g, 1.94 mmol, 60% yield).

^{1}H NMR (400 MHz, CDCl$_3$) δ 7.98 (d, *J* = 8.5 Hz, 2H, Ar*H*), 7.54 (d, *J* = 8.5 Hz, 2H, Ar*H*), 4.11 (s, 2H, COOC*H$_2$*), 3.65 (d, *J* = 6.5 Hz, 2H, OC*H$_2$*CH$_2$), 3.27 (s, 2H, CC*H$_2$*O), 3.22 (s, 1H, CC*H*), 2.44 (t, *J* = 6.5 Hz, 2H, C*H$_2$*COO), 1.42 (s, 9H, C(CH$_3$)$_3$), 0.99 (s, 6H, C(C*H$_3$*)$_2$).

36
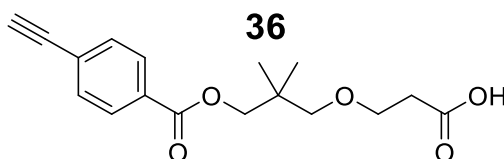
Compound **35** (0.55 g, 1.30 mmol) was dissolved in dry DCM (10 mL) and TFA (0.1 mL, 1.44 mmol) was added. The mixture was stirred at room temperature for 18 hours then the solvent was removed *in vacuo*. Toluene (20 mL) was added and then removed *in vacuo* to give the target compound **36** as an oil which was used without further purification (0.55 g, 1.81 mmol).

^{1}H NMR (400 MHz, CDCl$_3$) δ 7.95 (d, *J* = 8.5 Hz, 2H, Ar*H*), 7.56 (d, *J* = 8.5 Hz, 2H, Ar*H*), 4.16 (s, 2H, COOC*H$_2$*), 3.68 (d, *J* = 6.5 Hz, 2H, OC*H$_2$*CH$_2$), 3.28 (s, 2H, CC*H$_2$*O), 3.21 (s, 1H, CC*H*), 2.47 (t, *J* = 6.5 Hz, 2H, C*H$_2$*COOH), 0.99 (s, 6H, C(CH$_3$)$_2$). Acid proton not observed.

37
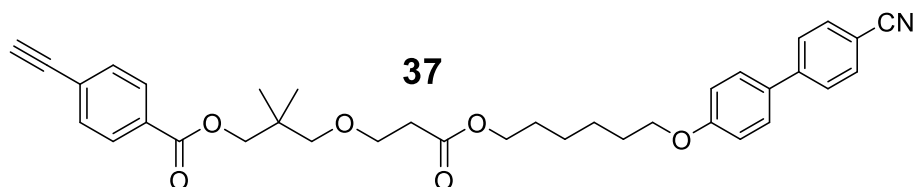
Compound **36** (0.55 g, 1.81 mmol), 4'-((6-hydroxyhexyl)oxy)-4-cyanobiphenyl (0.64 g, 2.17 mmol), EDC.HCl (0.65 g, 3.14 mmol) and DPTS (0.1 g, 0.82 mmol) were dissolved in DCM (30 mL) and the mixture was stirred at room temperature for 48 hours. The solvent removed *in vacuo* and the crude product was purified by column chromatography (DCM as eluent) to give the target compound **37** as an off-white white powdery solid (0.53 g, 0.91 mmol, 50% yield)

^{1}H NMR (400 MHz, CDCl$_3$) δ 7.97 (d, *J* = 8.5 Hz, 2H, Ar*H*), 7.67 (d, *J* = 8.5 Hz, 2H, Ar*H*), 7.62 (d, *J* = 8.5 Hz, 2H, Ar*H*), 7.57 – 7.47 (m, 4H, Ar*H*), 6.96 (d, *J* = 8.5 Hz, 2H, Ar*H*), 4.11 (t, *J* = *6.5* Hz, 2H, COOC*H$_2$*), 4.09 (s, 2H, COOC*H$_2$*), 3.98 (t, *J* = 6.5 Hz, 2H, C*H$_2$*OAr), 3.68 (t, *J* = 6.5 Hz, 2H, OC*H$_2$*CH$_2$), 3.27 (s, 2H, CC*H$_2$*O), 3.21 (s, 1H, CC*H*), 2.53 (t, *J* = 6.0 Hz, 2H, C*H$_2$*COO), 1.85 – 1.73 (m, 8H, OCH$_2$C*H$_2$* and OCH$_2$CH$_2$C*H$_2$*), 0.98 (s, 6H, C(C*H$_3$*)$_2$).

38
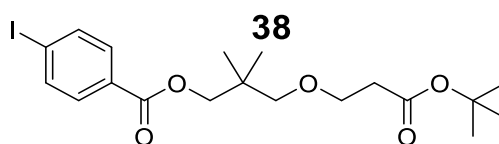
4-Iodobenzoic acid (0.55 g, 2.22 mmol), compound **34** (0.55 g, 2.36 mmol) EDC.HCl (0.6 g, 3.13 mmol) and DPTS (0.04 g, 0.33 mmol) were dissolved in dichloromethane (30 mL), the reaction mixture was stirred at room temperature for 48 hours. The solvent was removed *in vacuo* and the crude product was purified by column chromatography (DCM as eluent) to give the target compound **38** as a colourless oil (0.61 g, 1.32 mmol, 60% yield).

^{1}H NMR (400 MHz, CDCl$_3$) δ 7.79 (d, *J* = 8.5 Hz, 2H, Ar*H*), 7.73 (d, *J* = 8.5 Hz, 2H, Ar*H*), 4.22 (s, 2H, COOC*H$_2$*), 3.38 (t, *J* = 6.5 Hz, 2H, OC*H$_2$*CH$_2$), 3.30 (s, 2H, CC*H$_2$*O), 2.40 (t, *J* = 6.0, Hz, 2H, C*H$_2$*COO), 1.43 (s, 9H, C(CH$_3$)$_3$), 0.99 (s, 6H, C(CH$_3$)$_2$).

39
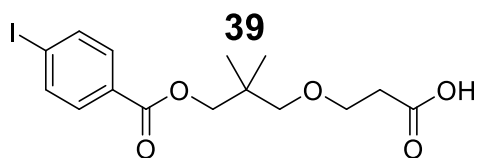
Compound **38** (0.60 g, 1.30 mmol) was dissolved in dry DCM (10 mL) and TFA (0.1 mL, 1.44 mmol) was added. The mixture was stirred at room temperature for 18 hours then the solvent was removed *in vacuo*, toluene (20 mL) was added and then removed *in vacuo* to give the target compound **39** as a colourless oil which was used without further purification (0.6 g, 1.48 mmol).

^{1}H NMR (400 MHz, CDCl$_3$) δ 7.80 – 7.67 (m,4H, ArH), 4.20 (s, 2H, COOCH_2), 3.35 (t, J = 6.5 Hz, 2H, OCH_2CH$_2$), 3.28 (s, 2H, CCH_2O), 2.52 (t, J = 6.0, Hz, 2H, CH_2COOH), 0.99 (s, 6H, C(CH$_3$)$_2$). Acid proton not observed.

40
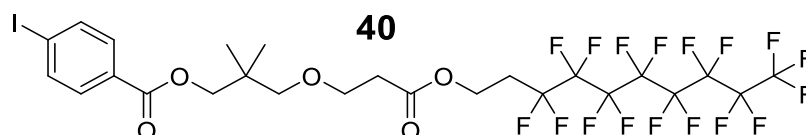
Compound **39** (0.6 g, 1.48 mmol), 1H,1H,2H,2H-perfluorodecanol (0.81 g, 1.75 mmol), EDC.HCl (0.45 g, 2.36 mmol) and DMAP (0.1 g, 0.82 mmol) were dissolved in DCM (30 mL) and the mixture was stirred at room temperature for 48 hours. The solvent was removed *in vacuo* and the crude product was purified by column chromatography (DCM as eluent) to give the target compound **40** as a waxy white solid (0.56 g, 0.66 mmol, 45% yield)

^{1}H NMR (400 MHz, CDCl$_3$) δ 7.79 (d, J = 8.5 Hz, 2H, ArH), 7.72 (d, J = 8.5 Hz, 2H, ArH), 4.36 (t, J = 6.5 Hz, 2H, OCH_2CH$_2$CF$_2$), 4.11 (s, 2H, COOCH_2), 3.38 (t, J = 6.5 Hz, 2H, OCH_2CH$_2$), 3.26(s, 2H, CCH_2O), 2.55 (t, J = 6.0, Hz, 2H, CH_2COO), 2.44 (tt, J = 18.5, 6.5 Hz, 2H, CH_2CF$_2$), 0.97 (s, 6H, C(CH$_3$)$_2$).

41
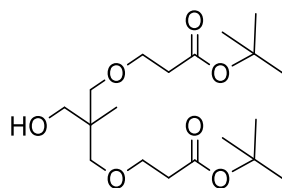
1,1,1-Tris(hydroxymethyl)ethane (5.99 g, 49.85 mmol) was dissolved in tetra-n-butyl ammonium hydroxide (40% in H_2O, 15 mL) and the mixture purged with nitrogen. The mixture was cooled in an ice bath and then tert-butyl acrylate (17.25 mL, 15.09 g, 117.73 mmol) was added by syringe. The reaction mixture was warmed to room temperature and stirred for 72 hours forming a white precipitate. The mixture was diluted with water (50 mL) and then extracted with ethyl acetate (3 x 100 mL). The extracts were combined and the solvent removed *in vacuo*. The product was purified by column chromatography in two batches. (gradient elution hexane:EtOAc, 95:5 to 75:25) to give the target compound **41** as a colourless oil (4.59 g, 12.19 mmol, 25% yield).

^{1}H NMR (400 MHz, CDCl$_3$) δ 3.62 (t, *J* = 6.0 Hz, 4H, OC*H$_2$*CH$_2$), 3.48 (s, 2H, HOC*H$_2$*), 3.36 (apparent quartet, *J* = 9.0 Hz, 4H, CC*H$_2$*O), 2.44 (t, *J* = 6.0 Hz, 4H, C*H$_2$*COO), 1.43 (s, 18H, C(C*H$_3$)$_3$* and C(C*H$_3$)$_3$*), 0.81 (s, 3H, CC*H$_3$*). OH proton not observed.

^{13}C{^{1}H} NMR (101 MHz, CDCl$_3$) δ 171.2, 80.7, 75.3, 68.8, 67.3, 40.7, 36.3, 28.2, 17.5.

ESI-MS: m/z = 399.2 [M+Na]$^+$

42
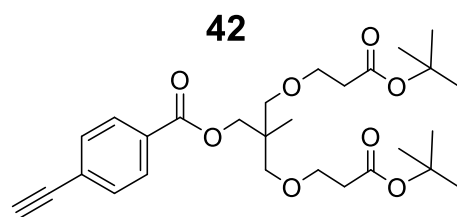
4-Ethynylbenzoic acid (0.56 g, 3.85 mmol), compound **41** (1.02g, 2.71 mmol), EDC.HCl (0.59 g, 3.81 mmol) and DMAP (0.42 g, 3.44 mmol) were dissolved in THF (40 mL) and the reaction mixture was stirred at room temperature for 18 hours. The solvent was removed *in vacuo* and the crude product was purified by column chromatography (10:3 Hexane:EtOAc as eluent) to give the target compound **42** as a pale yellow oil (0.82 g, 1.63 mmol, 60% yield).

^{1}H NMR (400 MHz, CDCl$_3$) δ 7.98 (d, *J* = 8.5 Hz, 2H, Ar*H*), 7.55 (d, *J* = 8.5 Hz, 2H, Ar*H*), 4.21 (s, 2H, COOC*H$_2$*), 3.63 (t, J = 6.5 Hz, 4H, OC*H$_2$*CH$_2$), 3.37 (s, 4H, CC*H$_2$*O), 3.23 (s, 1H, CC*H*), 2.44 (t, J = 6.5 Hz, 4H, C*H$_2$*COO), 1.44 (s, 18H, 2 x C(C*H$_3$*)$_3$), 1.00 (s, 3H, CC*H$_3$*).

ESI-MS: m/z = 527.3 [M+Na]$^+$

43
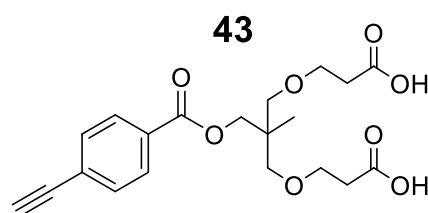
Compound **42** (0.76 g, 1.51 mmol) was dissolved in dry DCM (20 mL) and TFA (1 mL) was added. The reaction mixture was stirred at room temperature for 18 hours and then the solvent was removed *in vacuo*. Toluene (30 mL) was added and then removed *in vacuo* to give the target compound **43** as a cream solid (0.62 g, 1.58 mmol) which was used without further purification.

^{1}H NMR (400 MHz, DMSO-d$_6$) δ 7.97 (d, *J* = 8.5 Hz, 2H, Ar*H*), 7.64 (d, *J* = 8.5 Hz, 2H, Ar*H*), 4.10 (s, 2H, COOC*H$_2$*), 3.57 (t, *J* = 6.2 Hz, 4H, OC*H$_2$*CH$_2$), 3.33 (m, 5H, signals lost in residual water peak), 2.42 (t, *J* = 6.5 Hz, 4H, C*H$_2$*COO), 0.93 (s, 3H, CC*H$_3$*). Acid protons not observed.

44
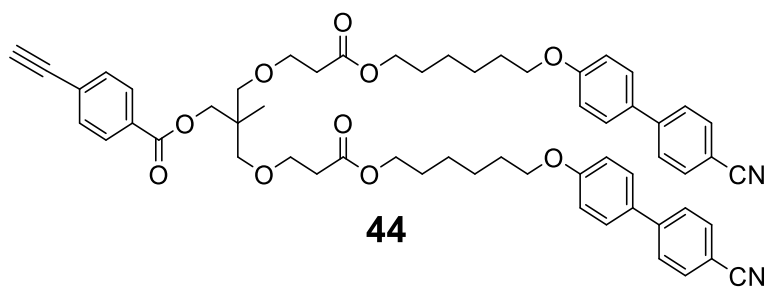
Compound **43** (0.31 g, 0.79 mmol), 4'-((6-hydroxyhexyl)oxy)-4-cyanobiphenyl (0.47 g, 1.59 mmol), EDC.HCl (0.26 g, 1.68 mmol) and DMAP (0.17 g, 1.39 mmol) were dissolved in THF (30 mL) and the mixture was stirred at room temperature for 18 hours. The solvent was removed *in vacuo* and the crude product was purified by column chromatography (10:1 DCM:EtOAc as eluent) to give the target compound **44** as a colourless oil (0.40 g, 0.53 mmol, 67% yield).

^{1}H NMR (400 MHz, CDCl$_3$) δ 7.96 (d, J = 8.5 Hz, 2H, Ar*H*), 7.68 (d, *J* = 9.0 Hz, 4H, Ar*H*), 7.63 (d, *J* = 8.5 Hz, 4H, Ar*H*), 7.56-7.49 (m, 6H, Ar*H*), 6.97 (d, *J* = 9.0 Hz, 4H, Ar*H*), 4.19 (s, 2H, COOC*H*$_2$), 4.07 (t, *J* = 6.5 Hz, 4H, COOC*H*$_2$), 3.98 (t, *J* = 6.5 Hz, 4H, C*H*$_2$OAr), 3.67 (t, *J* = 6.5 Hz, 4H, OC*H*$_2$CH$_2$), 3.37 (s, 4H, CC*H*$_2$O), 3.22 (s, 1H, CC*H*), 2.53 (t, *J* = 6.5 Hz, 4H, C*H*$_2$COO), 1.88 – 1.75 (m, 4H, COOCH$_2$C*H*$_2$), 1.73 – 1.62 (m, 4H, ArOCH$_2$C*H*$_2$), 1.55 – 1.35 (m, 8H, COOCH$_2$CH$_2$C*H*$_2$ and OCH$_2$CH$_2$C*H*$_2$), 1.00 (s, 3H CC*H*$_3$).

APCI-MS: m/z = 947.5 [M+H]$^+$

45
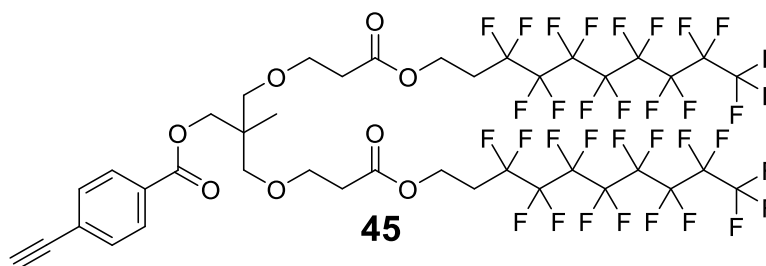
Diacid **43** (0.31 g, 0.79 mmol), 1H,1H,2H,2H-perfluorodecanol (0.73 g, 1.57 mmol), EDC.HCl (0.25 g, 1.61 mmol) and DMAP (0.16 g, 1.31 mmol) were dissolved in DCM (30 mL) and the reaction mixture was stirred at room temperature for 18 hours. The solvent was removed *in vacuo* and the crude product was purified by column chromatography (6:4 Petrol:EtOAc as eluent) to give the target compound **45** as a white powder (0.90 g, 0.70 mmol, 89% yield).

^{1}H NMR (400 MHz, CDCl$_3$) δ 7.97 (d, *J* = 8.5 Hz, 2H, Ar*H*), 7.55 (d, *J* = 8.5 Hz, 2H, Ar*H*), 4.38 (t, *J* = 6.5 Hz, 4H, OC*H$_2$*CH$_2$CF$_2$), 4.19 (s, 2H, COOC*H$_2$*), 3.68 (t, *J* = 6.5 Hz, 4H, OC*H$_2$*CH$_2$), 3.37 (s, 4H, CC*H$_2$*O), 2.56 (t, *J* = 6.5 Hz, 4H, C*H$_2$*COO), 2.47 (tt, *J* = 18.5, 6.5 Hz, 4H, C*H$_2$*CF$_2$), 1.00 (s, 3H, CC*H$_3$*).

APCI-MS: m/z = 1285.2 [M+H]$^+$

46
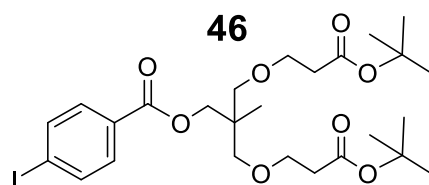
Dry DCM (20 mL) was added via syringe to 4-iodobenzoic acid (0.30 g, 1.21 mmol), DCC (0.34 g, 1.65 mmol), DMAP (0.02 g, 0.16 mmol) and compound **41** (0.48 g, 1.28 mmol) under nitrogen. The reaction mixture was stirred at room temperature for 18 hours then filtered through a pad of celite. The mixture was purified by column chromatography (1:1 diethyl ether:petrol as petrol) to give the target compound **46** as a colourless oil (0.27 g, 0.45 mmol, 37% yield).

^{1}H NMR (400 MHz, CDCl$_3$) δ 7.80 (d, *J* = 8.5 Hz, 2H, Ar*H*), 7.73 (d, *J* = 8.5 Hz, 2H, Ar*H*), 4.20 (s, 2H, COOC*H$_2$*), 3.63 (t, *J* = 6.5 Hz, 4H, OC*H$_2$*CH$_2$), 3.36 (s, 4H, CC*H$_2$*O), 2.44 (t, *J* = 6.5 Hz, 4H, C*H$_2$*COO), 1.43 (s, 18H, 2 x C(C*H$_3$)$_3$*), 1.00 (s, 3H, CC*H$_3$*).

ESI-MS: m/z = 629.2 [M+Na]$^+$

47
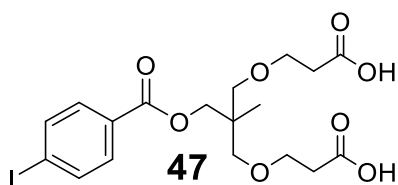
Compound **46** (0.77 g, 1.27 mmol) was dissolved in dry DCM (15 mL) and TFA (1.8 mL, 23.52 mmol) was added. The reaction mixture was stirred for 18 hours then the solvent removed *in vacuo*. Toluene (2 x 20 mL) was added and then removed *in vacuo* to give the target compound **47** as a colourless oil which was used without further purification (0.65 g, 1.32 mmol).

^{1}H NMR (400 MHz, CDCl$_3$) δ 7.81 (d, *J* = 8.5 Hz, 2H, Ar*H*), 7.72 (d, *J* = 8.5 Hz, 2H, Ar*H*), 4.18 (s, 2H, COOC*H$_2$*), 3.68 (t, *J* = 6.0 Hz, 4H, OC*H$_2$*CH$_2$), 3.40 (d, *J* = 8.5 Hz, 2H, CC*H$_2$*O), 3.37 (d, *J* = 8.5 Hz, 2H, CC*H$_2$*O), 2.59 (t, *J* = 6.0 Hz, 4H, C*H$_2$*COO), 0.99 (s, 3H, CC*H$_3$*). Acid protons not observed.

48
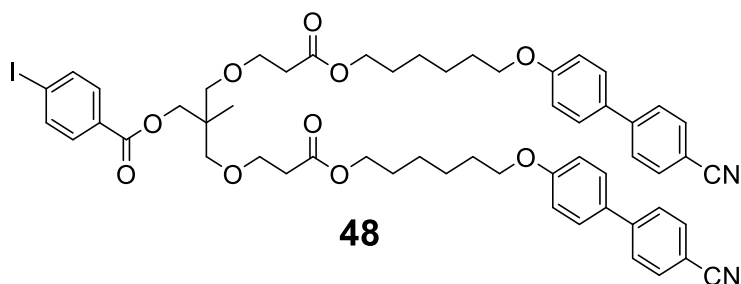
Compound **47** (0.35g, 0.71 mmol), 4'-((6-hydroxyhexyl)oxy)-4-cyanobiphenyl (0.49 g, 1.66 mmol), DCC (0.31 g, 1.50 mmol) and DMAP (0.03 g, 0.25 mmol) were dissolved in dry DCM (20 mL) under nitrogen. The mixture was stirred at room temperature for 6 days then the sample was filtered through a pad of celite and the solvent removed *in vacuo*. The crude product was purified by column chromatography (10:1 DCM:EtOAc as eluent) to give the target compound **48** as a colourless oil (0.47 g, 0.45 mmol, 63% yield).

^{1}H NMR (400 MHz, CDCl$_3$) δ 7.79 (d, *J* = 8.5 Hz, 2H, Ar*H*), 7.66-7.74 (m, 6H, Ar*H*), 7.63 (d, *J* = 8.5 Hz, 4H, Ar*H*), 7.52 (d, *J* = 8.5 Hz, 4H, Ar*H*), 6.97 (d, *J* = 9.0 Hz, 4H, Ar*H*), 4.18 (s, 2H, COOC*H$_2$*), 4.08 (t, *J* = 6.5 Hz, 4H, COOC*H$_2$*), 3.99 (t, *J* = 6.5 Hz, 4H, C*H$_2$*OAr), 3.67 (t, *J* = 6.3 Hz, 4H, OC*H$_2$*CH$_2$), 3.36 (s, 4H, CC*H$_2$*O), 2.58 (t, *J* = 6.5 Hz, 4H, C*H$_2$*COO), 1.88 − 1.75 (m, 4H, COOCH$_2$C*H$_2$*), 1.73 − 1.62 (m, 4H, ArOCH$_2$C*H$_2$*), 1.55 − 1.35 (m, 8H, COOCH$_2$CH$_2$C*H$_2$* and OCH$_2$CH$_2$C*H$_2$*), 0.99 (s, 3H, CC*H$_3$*).

APCI-MS: m/z = 1071.3 [M+Na]$^+$

137

49
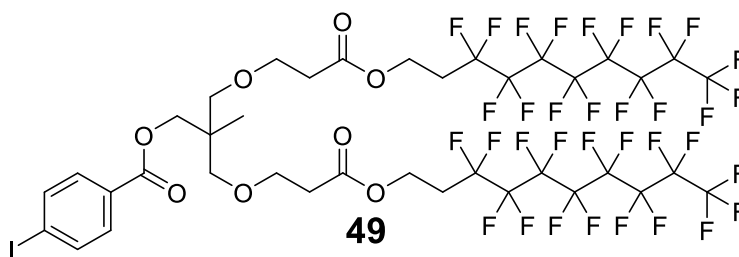
Compound **47** (0.31 g, 0.63 mmol), 1H,1H,2H,2H-perfluorodecanol (0.65 g, 1.40 mmol), DCC (0.29 g, 1.41 mmol) and DMAP (0.03 g, 0.25 mmol) were dissolved in dry DCM (20 mL) under nitrogen. The reaction mixture was stirred at room temperature for 8 days and then the reaction mixture was filtered through a pad of celite, the solvent removed *in vacuo* and the crude purified by column chromatography (DCM as eluent) to give the target compound **49** as a white crystalline solid (0.73 g, 0.35 mmol, 84% yield).

^{1}H NMR (400 MHz, CDCl$_3$) δ 7.81 (d, *J* = 8.5 Hz, 2H, Ar*H*), 7.72 (d, *J* = 8.5 Hz, 2H, Ar*H*), 4.46 (t, *J* = 6.5 Hz, 4H, OC*H$_2$*CH$_2$CF$_2$), 4.18 (s, 2H, COOC*H$_2$*), 3.67 (t, *J* = 6.0 Hz, 4H, OC*H$_2$*CH$_2$), 3.36 (s, 4H, CC*H$_2$*O), 2.56 (t, *J* = 6.0 Hz, 4H, C*H$_2$*COO), 2.45 (tt, *J* = 18.5, 6.5 Hz, 4H, C*H$_2$*CF$_2$), 0.99 (s, 3H, CC*H$_3$*).

APCI-MS: m/z = 1387.1 [M+Na]$^+$

61
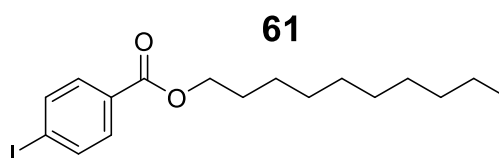
4-Iodobenzoic acid (0.50 g, 2.02 mmol), 1-decanol (0.32 g, 2.02 mmol), EDC.HCl (0.62 g, 3.23 mmol) and DPTS (0.06 g, 0.20 mmol) were dissolved in DCM (15 mL) and the reaction mixture was stirred at room temperature for 18 hrs. The solvent was removed *in vacuo* and the crude product was purified by column chromatography (DCM as eluent) to give the target compound **61** as a slightly yellow oil (0.54 g, 1.39 mmol, 69% yield).

^{1}H NMR (400 MHz, CDCl$_3$) δ 7.79 (d, *J* = 8.5 Hz, 2H, Ar*H*), 7.74 (d, *J* = 8.5 Hz, 2H, Ar*H*), 4.29 (t, *J* = 6.5 Hz, 2H, COOC*H$_2$*), 1.75 (dd, *J* = 6.5, 6.5 Hz, 2H, OCH$_2$C*H$_2$*), 1.45 – 1.22 (m, 14H), 0.87 (t, *J* = 7.0 Hz, 3H, CH$_2$C*H$_3$*).

APCI-MS: m/z = 389.1 [M+H]$^+$

3.4 References

1   E. Fischer and A. Speier, *Mittheilungen*, 1895, **28**, 3, 3252

2   P. Le Barny, J. C. Dubois, C. Friedrich and C. Noel, *Polym. Bull.*, 1986, 15, 341–348.

3   N. Bernhard and S. Wolfgang, *Angew. Chemie Int. Ed.*, 1978, **17**, 522–524.

4   V. Percec and M. Lee, *Macromolecules*, 1991, **24**, 1017–1024.

5   M. Tsakos, E. S. Schaffert, L. L. Clement, N. L. Villadsen and T. B. Poulsen, *Nat. Prod. Rep.*, 2015, **32**, 605–632.

6   B. Vanhaecht, M. N. Teerenstra, D. R. Suwier and C. E. Koning, *J. Macromol. Sci. - Pure Appl. Chem.*, 2000, **37**, 633–643.

7   C. J. Hawker and J. M. J. Fréchet, *J. Am. Chem. Soc.*, 1992, **114**, 8405–8413.

8   V. Percec, D. A. Wilson, P. Leowanawat, C. J. Wilson, A. D. Hughes, M. S. Kaucher, D. A. Hammer, D. H. Levine, A. J. Kim, F. S. Bates, K. P. Davis, T. P. Lodge, M. L. Klein, R. H. DeVane, E. Aqad, B. M. Rosen, A. O. Argintaru, M. J. Sienkowska, K. Rissanen, S. Nummelin and J. Ropponen, *Science.*, 2010, **328**, 1009–1014.

9   P. Guy and C. Dupuy, *Tetrahedron Lett.,* 1996, **37**, 1237–1240.

10   C. Dupuy, R. Viguier and A. Dupraz, *Synth. Commun.*, 2001, **31**, 1307–1313.

11   T. Ma, PhD Thesis, University of York, 2013.

12   A. M. Kasko, A. M. Heintz and C. Pugh, *Macromolecules*, 1998, **31**, 256–271.

13   B. Z. Tang, X. Kong, X. Wan and X. De Feng, *Macromolecules*, 1997, **30**, 5620–5628.

14   G. W. Gray, *Molecular Structure and Properties of Liquid Crystals. Academic Press, New York, 1962*

15   A. E. Blatch, I. D. Fletcher and G. R. Luckhurst, *J. Mater. Chem.*, 1997, **7**, 9–17.

16   A. Cook, S. Badriya, S. Greenfield and N. B. McKeown, *J. Mater. Chem.*, 2002, **12**, 2675–2683.

17   P. Taylor, R. Eidenschink, F. Kreuzer and W. H. De Jeu, *Liq. Cryst.*, 1990, **8** , 879

18   I. M. Saez and J. W. Goodby, *J. Mater. Chem.*, 2003, **13**, 2727–2739

19   a) J. Malthête, A. Collet and A.-M. Levelut, *Liq. Cryst*., 1989, 925. 123; (b) A. Pegenau, P. Goring and C. Tschierske, *New J. Chem*., 1999, 23, 465 c) X. H. Cheng, S. Diele and C. Tschierske, *Angew. Chem*. *Int. ed*., 2000, 39, 592; (d) A. Pegenau, T. Hegmann, C. Tschierske and S. Diele, *Chem. Eur. J.*, 1999, 5, 551, 1643.

Chapter 4. Symmetrical diphenyl acetylenes

The diphenyl acetylene unit is both weakly mesogenic – able to stabilise a liquid crystal mesophase, and able to undergo further reactions such as cyclotrimerisation. To this end a range of symmetrical diphenyl acetylenes were desired to enable an investigation into several aspects of the cyclotrimerisation reaction, which is used to convert three diphenyl acetylene molecules into a hexaphenyl benzene. While the diphenyl acetylene unit is weakly mesogenic, terminal chains are required to promote liquid crystallinity. As an extension to this, additional mesogenic groups may also be incorporated to produce liquid crystal oligomers featuring the diphenyl acetylene unit.

To put this work into context there are three classes of molecules to be discussed, firstly simple liquid crystal diphenyl acetylenes as reported by Malthête.[1] While these provide some information as to the role of the core, the focus of this work is instead on oligomers featuring the diphenyl acetylene unit (Chapters 4, 5 and 6). To this end several examples of liquid crystal oligomers will be discussed including some of the key areas of interest in this field, and finally some examples of liquid crystalline oligomers featuring the diphenyl unit will be introduced. As the materials discussed in this chapter were intended as intermediates only a brief review will be given. However, additional examples of chiral dimers featuring the diphenyl acetylene unit are given in chapter 6.

4.1 Introduction to liquid crystal oligomers

Liquid crystal oligomers were briefly described in the introduction (Section 1.4) and several different examples can be found within this thesis. For example, the materials described in Chapter 3 can be considered dendritic oligomers, which feature branching units such as pentaerythritol to link several mesogenic units to one dendritic core. These units also comprise the building blocks of the *Janus* materials which will be discussed in Chapter 5. While these dendritic oligomers represent the largest portion of the work reported here, linear oligomers such as dimers, trimers and so on consisting of mesogenic units linked by flexible spacers have been a key focus of liquid crystal research over the past twenty years.

While a comprehensive review of these materials is outside of the scope of this thesis three families of materials have been selected for discussion. This begins with the simplest cyanobiphenyl dimers which are discussed due to the emergence of the N$_{TB}$

phase[2], secondly the original asymmetric trimesogens reported by Yelammagad which feature a diphenyl acetylene unit[10] and finally main-chain liquid crystal dendrimers which share similarities with both dendritic and linear oligomers.[14] The design of liquid crystal oligomers can be used to drive novel liquid crystal behaviour as these examples show the interesting self-organisation arising from interplay between molecular interactions and molecular shape. This essentially leads to the formation of more exotic liquid crystal phases, such as the twist bend nematic phase which do not occur for the simple mesogenic units in isolation.

In the past ten years liquid crystal dimers and oligomers have been studied extensively due to the discovery and development of the twist-bend nematic phase (N_{TB}).[2] This interest is due to the spontaneous breaking of mirror symmetry induced by the formation of a helix from an achiral material, which is of importance across a range of scientific fields.[3,4] As the N_{TB} phase has been the focus of much of the research into liquid crystal dimers and oligomers it must be discussed although a full review is outside of the scope of this thesis.[5] The N_{TB} phase is formed when molecules with a bent molecular shape self-organise. This can either be achieved via odd-parity flexible spacers (Figure 76) between mesogenic units (rigid, cyclic rings)[6], or by oligomers featuring bent cores (Figure 77)[7]. Typically, the flexible spacer used is an alkyl chain, though linking groups such as ethers and esters are also known. An odd parity spacer will generate the bent molecular shape as another consequence of the trend seen as the odd-even effect. Even parity spacers give near-linear molecular shapes, while an odd number of atoms in the flexible spacer causes the molecular shape to be bent, though this effect is minimised by the rapidly increasing number of possible chain conformations as the length of the spacer increases. This series is typified by the cyanobiphenyl dimers shown below (Figure 76).

CBnCB
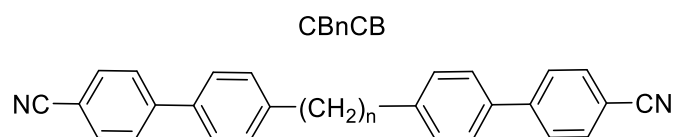
n	Compound name	Phase transition	Transition temperature /°C
6	CB6CB	Cr – N	183
		N – Iso	230
7	CB7CB	Cr – N_{TB}	102
		N_{TB} – N	104.5
		N – Iso	116
8	CB8CB	Cr – N	175.0
		N – Iso	193.9
9	CB9CB	Cr – N_{TB}	83.0
		N_{TB} – N	105
		N – Iso	119.8
10	CB10CB	Cr – N	-
		N – Iso	174.1
11	CB11CB	Cr – N_{TB}	99.9
		N_{TB} – N	108.6
		N – Iso	125.5

Figure 76. Structure and transition temperatures (°C) of the cyanobiphenyl dimers reported to exhibit the N_{TB} phase.[2,8-11]

As mentioned above, liquid crystal trimers showing the N_{TB} phase are often designed to feature a bent-core in order to encourage a bent molecular shape.[12] This can be achieved from supramolecular interactions such as the hydrogen bonded dimer shown in Figure 77 for which the carboxylic acid substituted units are linear.[13] It should be noted that the symmetrical diphenyl acetylenes reported in this chapter do not possess a bent-core, have long aliphatic spacers with even parity and many conformations. Therefore, it is not expected that the N_{TB} phase would be encountered in the compounds to be studied here.

62

Cr 160 (N_{TB} 159) N 197 Iso °C
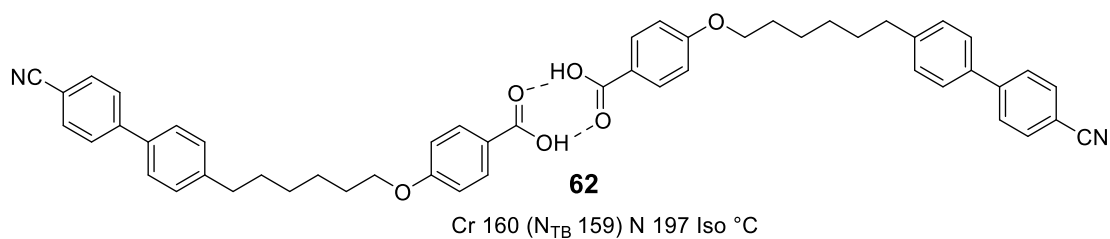
Figure 77. Structure of the hydrogen bonded liquid crystal trimer showing a bent molecular structure and the N_{TB} phase.[13]

The second class of oligomers to introduce were reported by Yelammagad. These di- and tri-mesogens incorporate units such as diphenyl acetylene and cholesteryl in the example given in Figure 78.[14,15] These oligomers reported by Yelammagad are notable as they were the first class of trimesogens reported where each mesogenic unit is different. The choice of mesogens in the asymmetric trimer (azobenzene, cholesteryl) is very different to the cyanobiphenyl mesogens used in the symmetrical materials reported here. For example, the different mesogenic units in the asymmetric trimers have different intermolecular interactions, while the symmetrical cyanobiphenyl oligomers have two units which will interact in a well-defined manner. The pair of cyanobiphenyl mesogens can show the classic antiparallel arrangement in order to maximise the quadrupolar interaction, while the cholesteryl unit is nonpolar and has little polarisability. Additionally, the asymmetric trimesogen contained short spacers (butyl, pentyl) which limits the flexibility between the mesogenic units, however gave a rich phase sequence. The enthalpy associated with the chiral nematic to isotropic transition is large (12.2 kJ mol^{-1}) likely due to the trimesogenic nature.

63

Cr 93.2 X 119.2 UTGB$_C$* 215 N* 247.7 Iso °C
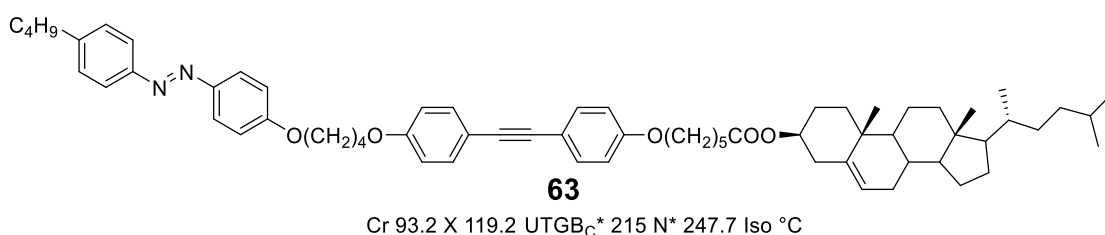
Figure 78. Asymmetric trimesogen 63 reported by Yelammagad.[14,15]

Following this asymmetric trimer Yelammagad reported a tetramer featuring four unique mesogenic units (Figure 79).[16] Again the diphenyl acetylene unit is present, though in this case it is substituted with three long alkyl chains as a 'half-disc', with some similarity to the branched materials reported in Chapter 5 with multiple chains.

Again, short spacers were used between the mesogenic units, and the three spacers which link the four mesogenic units were varied between even-odd-even parities and even-even-odd parity. It was found that when the middle spacer was odd (**64**, -O(CH$_2$)$_5$O-) the melting point and clearing point was reduced by around 50 °C compared to the even spacer **65**. This again is attributed to the odd-even effect altering the angle between the mesogenic units, which plays an even larger part considering the extended length of the molecule.

C$_{12}$H$_{25}$O— ... —O—(CH$_2$)$_6$-O— ... —O—(CH$_2$)$_n$-O— ... —O—(CH$_2$)$_5$COO—

C$_{12}$H$_{25}$O   OC$_{12}$H$_{25}$

64 n = 5, Cr 88.1 X 116.2 Iso °C
65 n = 4, Cr 123.1 X 172.3 Iso °C
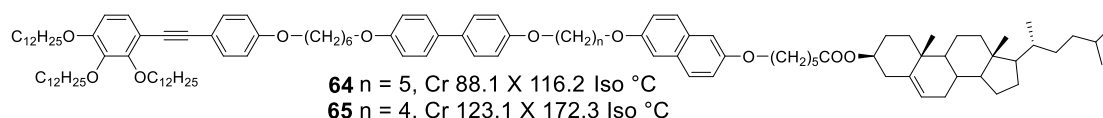
*Figure 79. Asymmetric tetramers **64** and **65** reported by Yelammagad.[16]*

The final class of compounds to be introduced are main-chain liquid crystal dendrimers as reported by Donnio and Serrano. The 'Octopus' dendrimers reported by Donnio[17-19] (Figure 80) share similarities to the liquid crystal oligomers already discussed in this chapter and to the dendritic oligomers discussed in Chapters 3 and 5. By following the path from the core to the periphery each arm can be considered a dimesogen comprising of diphenyl acetylene mesogenic units. In addition, the branching structure of a dendritic material is present. When the peripheral diphenyl acetylene unit features a single alkyl chain in compound **66** the liquid crystal behaviour is dominated by smectic behaviour, while an additional alkyl chain in compound **67** introduces curvature and provides a columnar mesophase.
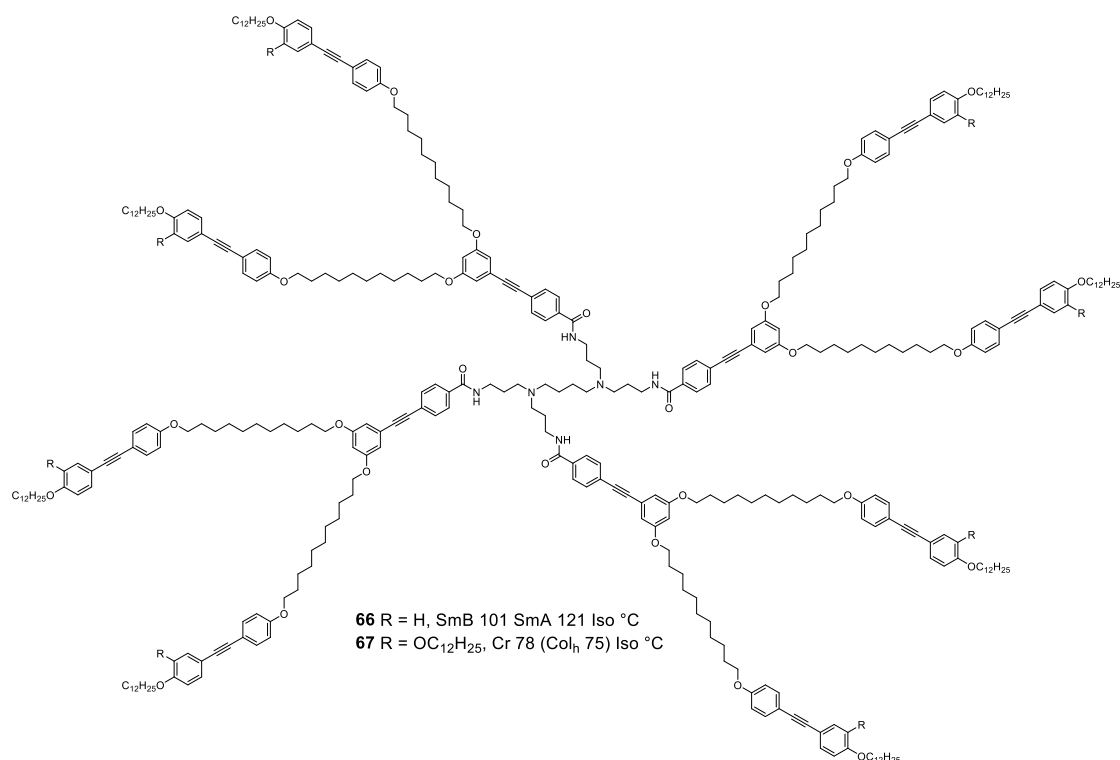
*Figure 80. Main chain 'Octopus' dendrimers **66** and **67** reported by Donnio.[18]*

The mesophase structures of both of these compounds are shown in Figure 81 and are intriguing. The columnar phases exhibited by **67** are described as being 'onion-like' due to the apparent microphase segregation of aliphatic and aromatic segments giving an aliphatic core surrounded by a segment of aromatic mesogens in order to maximise the π-π interactions. This segregation is then repeated for the aliphatic spacers, peripheral mesogens and finally terminal alkyl chains (Figure 81, right). In contrast, compound **66** bearing only a single terminal alkyl chain exhibits the smectic phase. When only one chain is present the dendrimer possesses a 'tube-like' shape therefore the molecules can pack to form a smectic phase. In this mesophase structure the terminal diphenyl acetylene units segregate, providing liquid crystallinity while the cores are buried between the layers (Figure 81, left).
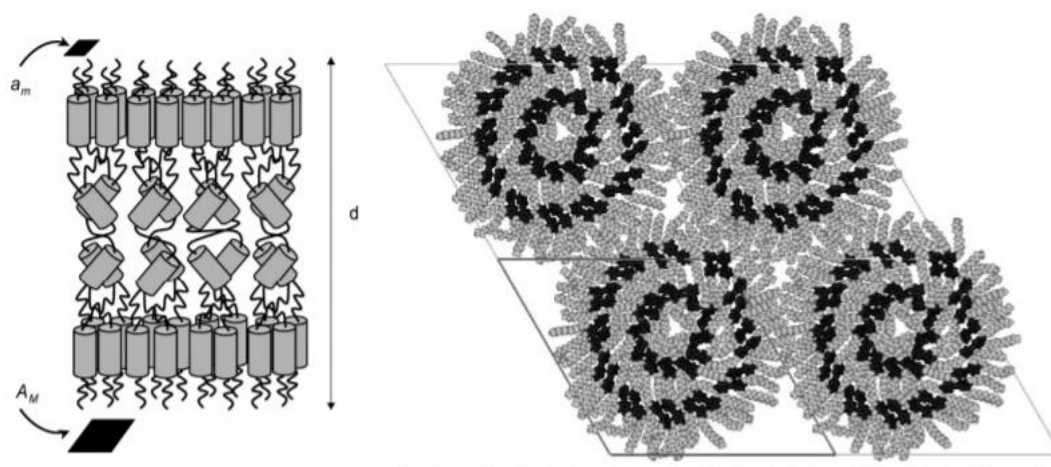
Figure 81. Mesophase structures of the smectic and columnar mesophases of the 'octopus' dendrimers reported by Donnio. (Figure reproduced from reference 18).

The materials reported by Donnio can be contrasted with the PAMAM and DAB dendrimers reported by Serrano[20], which similarly give smectic or columnar mesophases depending on the curvature provided by the number of terminal chains (**68** and **69**, Figure 82). The nature of these mesophases are similarly reliant upon microphase segregation between the aliphatic alkyl spacers and aromatic mesogenic units. This segregation increases the number of π-π interactions available and clearly the increased enthalpic contribution provided by these positive interactions outweighs the reduced entropy of the system providing more ordered phases.[21]

68 R =

g 27.7 SmA 191.6 Iso °C

69 R =

Cr 28.0 Col$_H$ 55.0 Iso °C
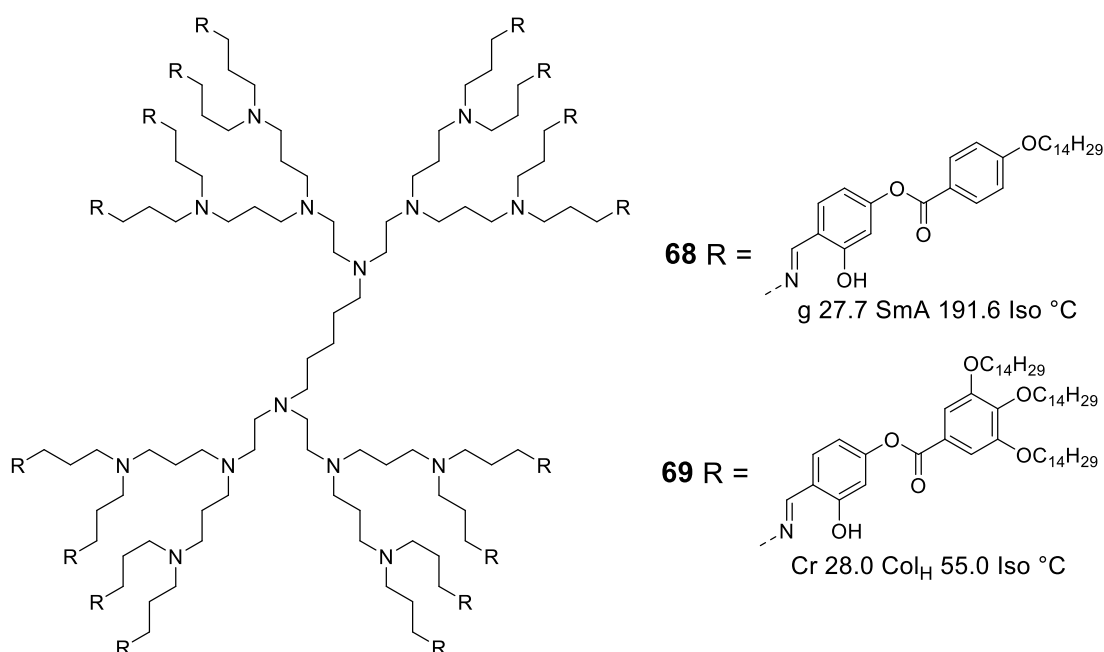
*Figure 82. Oligomeric dendrimers **68** and **69** reported by Serrano.[20]*

4.2 Synthesis

In addition to the compounds described in the previous chapter, several intermediates were required for the synthesis of symmetrical materials. These syntheses followed routes which are described previously[1,22] the details of which are given in schemes 10, and 11. In each case, as with the remainder of the project, the key step was the Sonogashira coupling reaction of an aryl halide and aryl ethynyl intermediate. The mechanism of the Sonogashira coupling reaction is shown in Figure 83.[23]
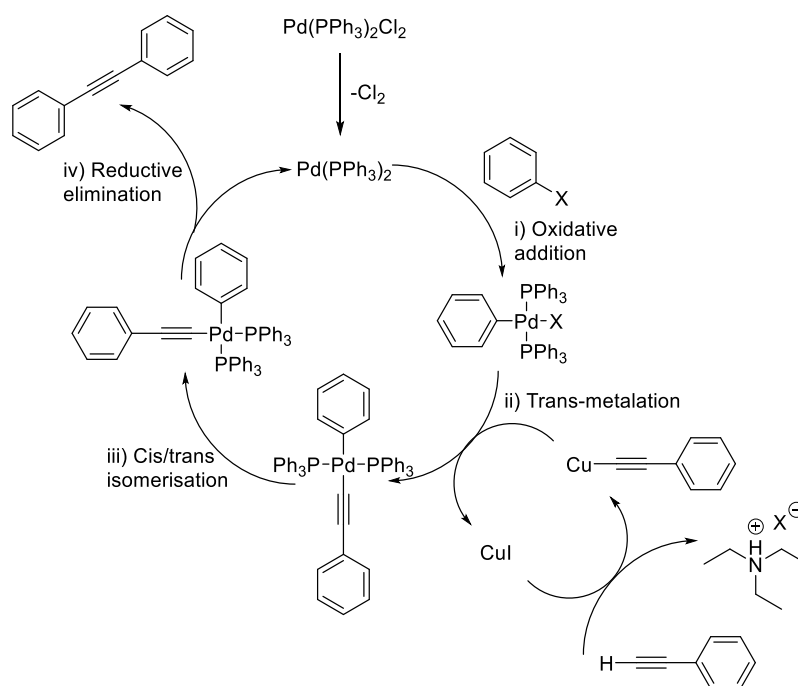
Figure 83. Mechanism of the Sonogashira coupling reaction.[23]

The mechanism begins with an oxidative addition of an aryl halide to the fourteen electron Pd[0] species (i).[24] In this step the electron density of the carbon-halogen bond is key in determining the rate of addition, and hence weaker C-I bonds are more active than C-Br bonds. The reactivity in this step can be enhanced by, electron withdrawing aryl substituents. Transmetallation using a copper co-catalyst delivers the ethynyl moiety to the palladium centre in what is typically the rate determining step (ii). Copper can complex to the alkynyl triple bond which may increase the acidity of the alkynic hydrogen allowing TEA to deprotonate it. A cis/trans isomerisation (iii) takes place at the reactive Pd centre to provide the correct geometry to allow reductive elimination of the diphenyl acetylene product (iv).

The catalytic cycle requires a base to deprotonate the alkyne and therefore triethylamine was used as the solvent. In the case of apolar or supermolecular compounds solubility in triethylamine was poor, and therefore toluene was used as a cosolvent to aid solubility. To avoid poisoning of the catalyst low-sulfur toluene was prepared via treatment with sulfuric acid to remove impurities such as thiophenes.[25] Sonogashira coupling reactions using aryl iodides could be performed at room temperature, however aryl bromides required heating for the reaction to progress.

The target compounds prepared in this thesis focused on para-substituted aryl iodides. Though the substituents on the aryl ring affect the reactivity[26] these compounds were typically sufficiently reactive and so alternative catalysts were not investigated.[27-29] In the span of this project acceptable yields were obtained using [PdCl$_2$(PPh$_3$)$_2$]with the largest challenge being reaction times and solubility. The linear oligomers reported in this chapter are sterically unhindered due to the para-substitution pattern, however in the case of dendritic materials such as reported in Chapter 5, it is more challenging to coordinate multiple highly branched structures around the palladium centre.

The symmetrical and linear diphenyl acetylenes shown in Schemes 10 and 11 were synthesised in this project discussed in this chapter were synthesised in order to investigate the trimerisation reactions, and not for their behaviour as diphenyl acetylene compounds. As such several have been reported previously and therefore these syntheses were used as guidelines. These materials were mainly of interest for further reactivity described in Chapter 7.

1-Bromo-4-dodecyl benzene **70** is commercially available and was converted to aryl ethynyl compound **72** in two steps using the Sonogashira coupling reaction in high yields (Scheme 10). Following this the aryl bromide and aryl ethynyl compounds were coupled together to provide the diphenyl acetylene compound **73**. The same procedure was used to provide dipentyldiphenyl acetylene **76** (Scheme 11). Compound **76** was known to be non-liquid crystalline and was desired for use as a model compound and for cotrimerisations described in chapter 7. In addition, **76** was found to give very large well defined crystals suitable for single crystal X-ray diffraction.
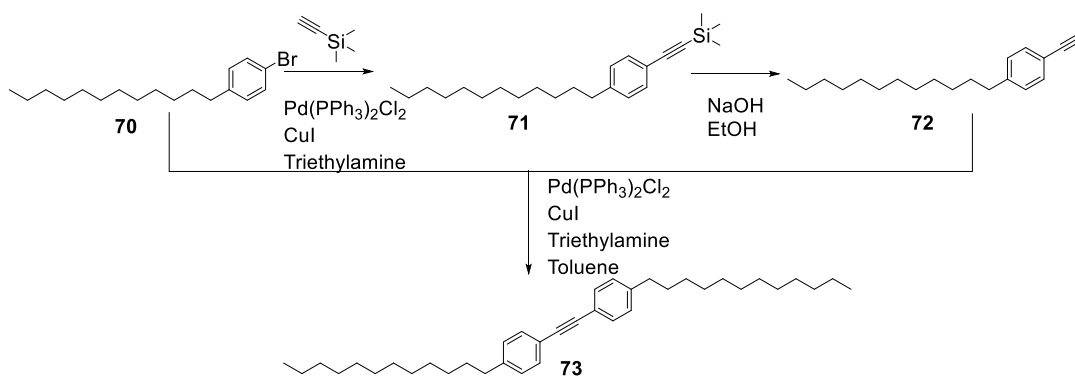
Scheme 10. Synthesis of compound 73 from commercially available 1-bromo-4-dodecyl benzene.
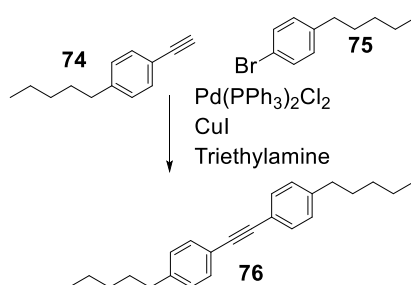
Scheme 11. Synthesis of dipentyldiphenyl acetylene 76 in one step from commercially available materials.

The para-substituted iodo- and ethynyl- aryl esters **77** and **33$_{iii}$**, produced as intermediates in Chapter 3 underwent the Sonogashira coupling reaction in good yields (71%) to provide a diphenyl acetylene bearing two cyanobiphenyl units **78** (Scheme 12).
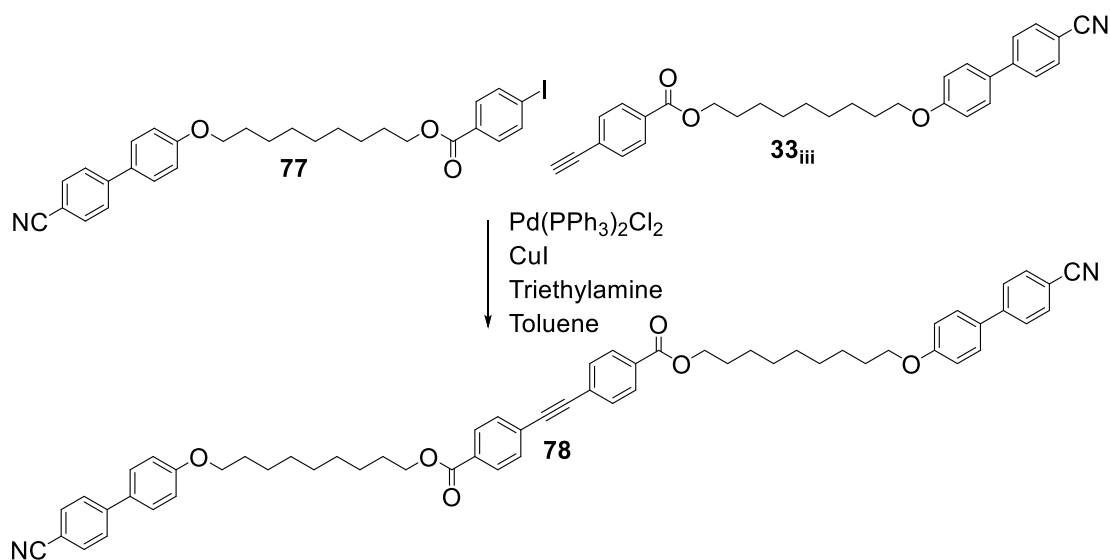
Scheme 12. Sonogashira coupling of aryl-iodide 77 and aryl-ethynyl 33$_{iii}$ to afford symmetrical diphenyl acetylene 78.

The chiral ethynyl- and iodo-aryl compounds **79** and **80** were prepared from the esterification of 4-iodobenzoic acid or 4-ethynyl benzoic acid with (S)-2-methyl butanol. These were coupled together using the Sonogashira coupling reaction in 73% yield to obtain the chiral diphenyl acetylene **81** (Scheme 13).
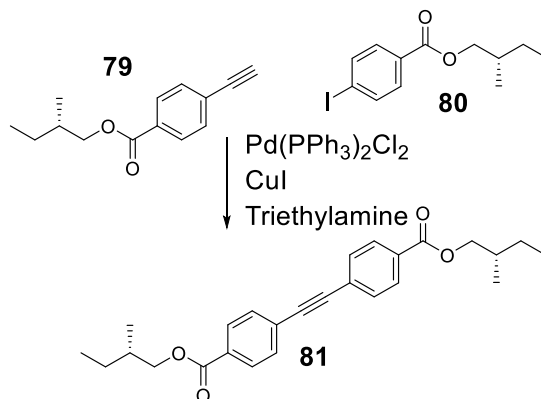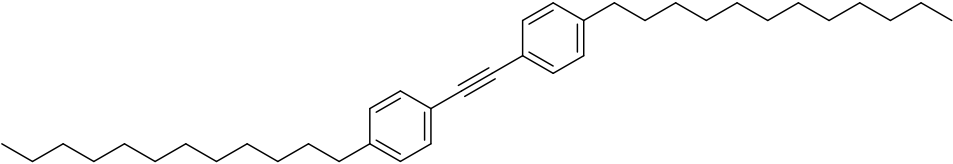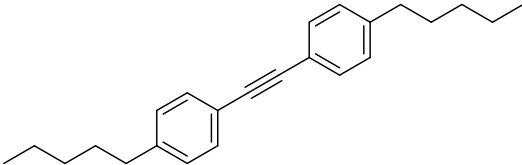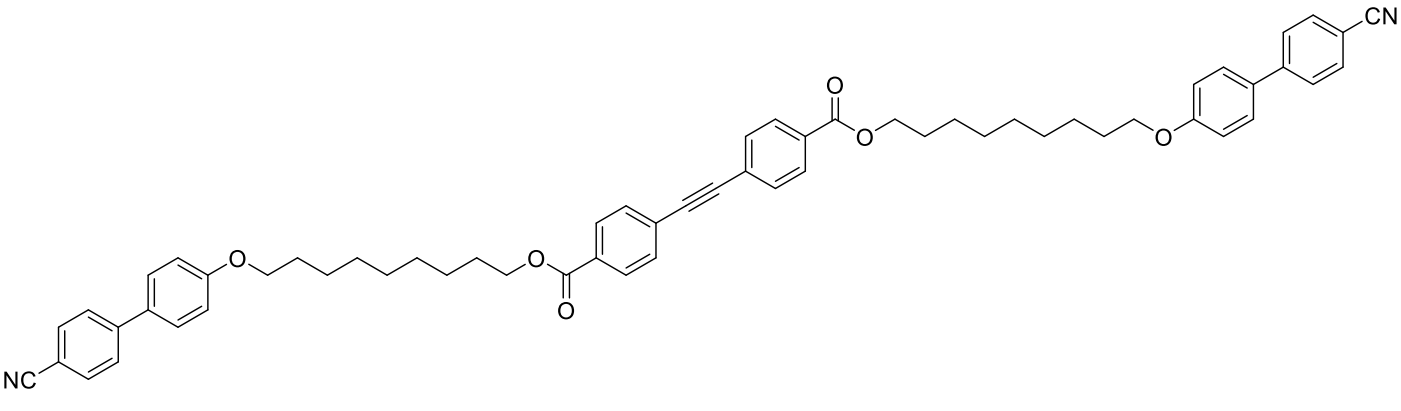
*Scheme 13. Synthesis of chiral diphenyl acetylene compound **81**.*

Scheme 14 shows the synthetic strategy to produce compound **88**. Methyl-10-undecynoate was coupled to 1-bromo-4-iodobenzene at room temperature to selectively react with the iodo-aryl bond giving compound **82**. This material was converted to the undecane using hydrogenation in the presence of palladium on carbon to provide the bromo-aryl compound **83**. Roughly half of the material produced was converted into the ethynyl-aryl compound **85** by coupling with trimethyl silyl acetylene followed by cleavage of the trimethyl silyl protecting group. The ethynyl-aryl and bromo-aryl compounds **85** and **83** could then be coupled to provide the alkyl linked diester **86**. Following this, two additional steps were required to deprotect the methyl ester using base hydrolysis giving **87** followed by esterification with 4-hydroxy cyanobiphenyl to give the target compound **88**.
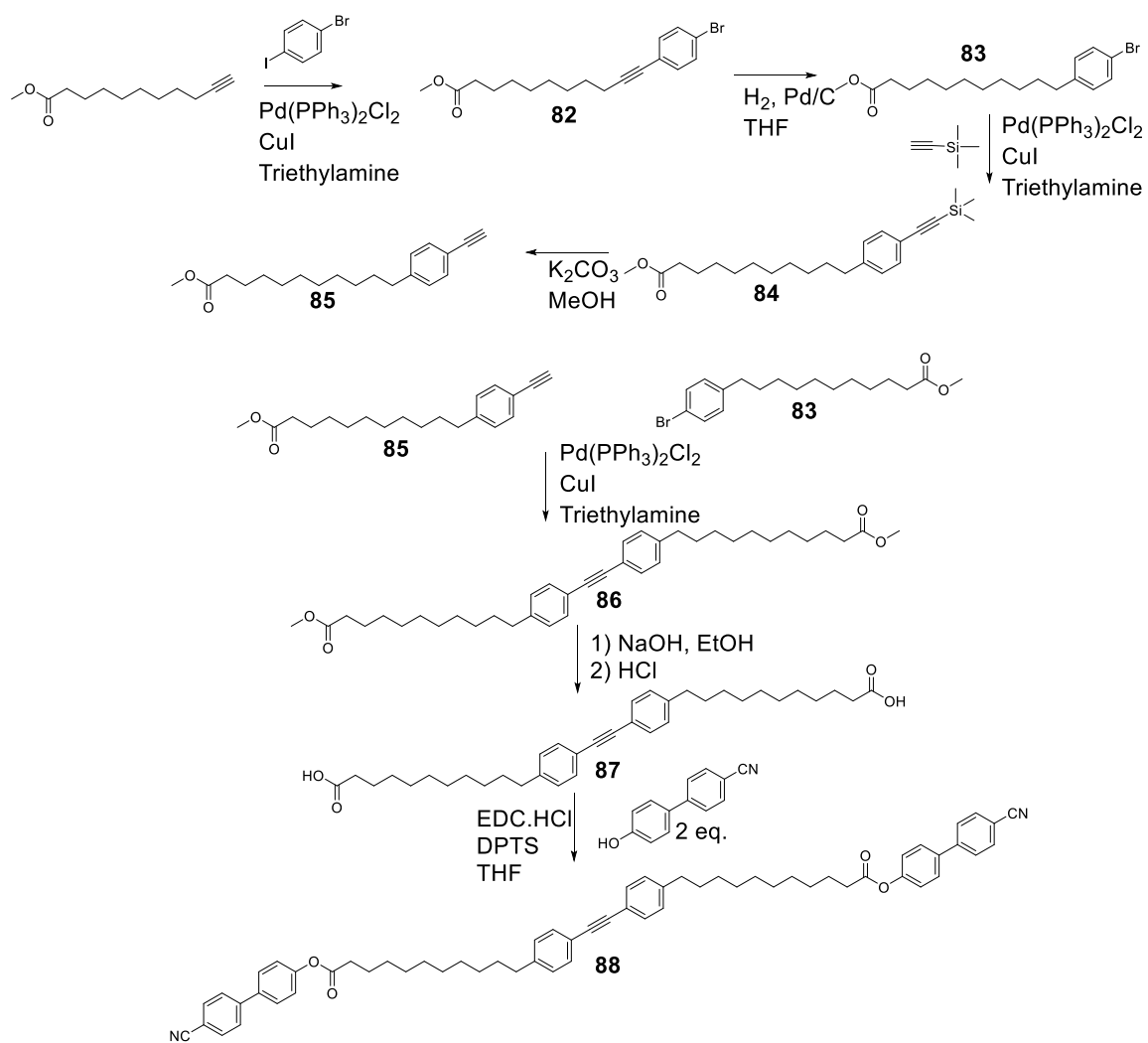
*Scheme 14. Strategy used to provide the alkyl linked cyanobiphenyl compound **88**.*

Table 8. Structure and transition temperatures of symmetrical diphenyl acetylene compounds.

Compound number	Chemical structure	Transition temperatures / °C
73		Cr 59.6 Iso °C
76		Cr 53.8 Iso °C
78		Cr 159 N 197 Iso °C
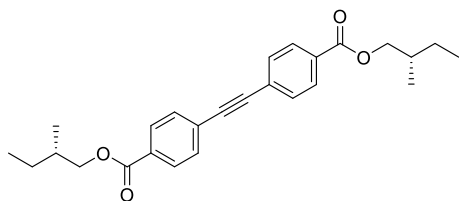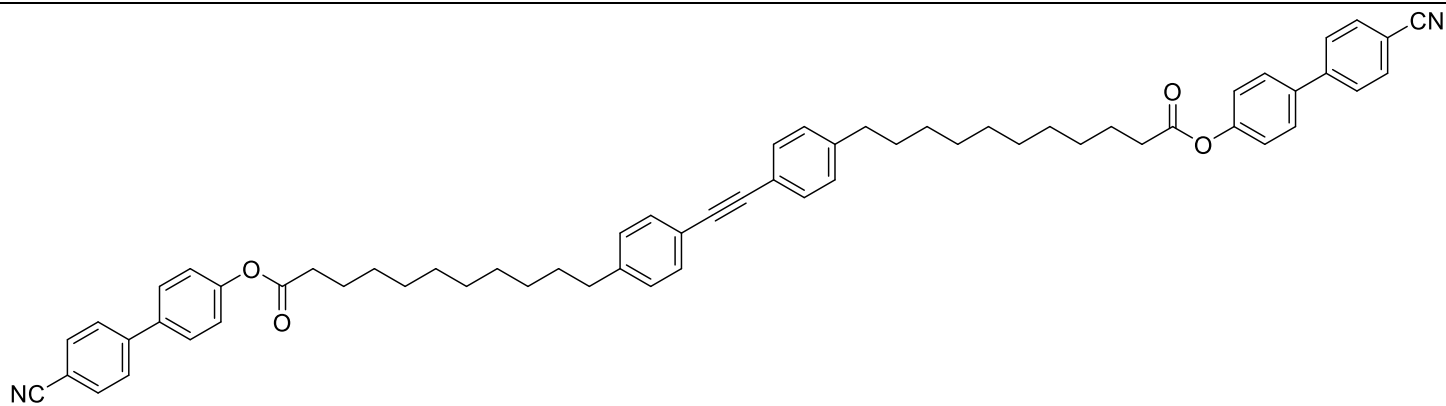
81		Cr 56.8 Iso °C
88		Cr 173.9 N 207.3 Iso °C

4.3 Liquid crystal properties

The symmetrical diphenyl acetylene compounds (**73**, **76**, **78**, **81** and **88**) were examined by POM and DSC to investigate their liquid crystal behaviour. The transition temperatures, enthalpies and entropies of transition of these materials are given in Table 9. Compounds **73**, **76** and **81** did not exhibit liquid crystallinity. Compounds **73** and **76** melted at 59.6 and 53.8 °C respectively which is in agreement with previous reports.[22,30] DSC experiments were not performed on the crystalline samples of **73** and **81**.

Single crystals of **76** which were of suitable quality for analysis were obtained and the crystal structure was found with help from the University of York crystallography service. The details of the crystal structure are provided below (Figure 84). The crystal structure and potential mesophase structure of materials are not easy to compare, however the crystal shows the same overlap of the aromatic cores that would be expected to stabilise a mesophase.
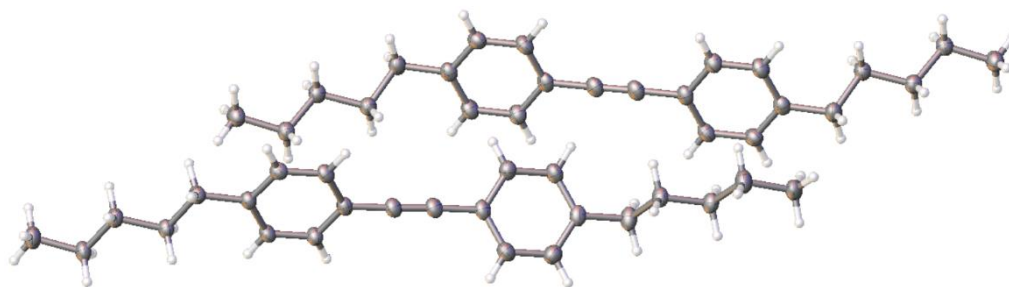
Empirical formula	$C_{24}H_{30}$
Formula weight	318.48
Temperature/K	110.05(10)
Crystal system	triclinic
Space group	P-1
a/Å	10.9746(6)
b/Å	11.9678(6)
c/Å	11.9732(6)
α/°	69.405(4)
β/°	85.067(4)
γ/°	86.718(4)
Volume/Å^3	1466.01(14)
Z	3
ρ_{calc}g/cm^3	1.082
μ/mm^{-1}	0.446
F(000)	522.0
Crystal size/mm^3	0.487 × 0.255 × 0.071
Radiation	CuKα (λ = 1.54184)
2Θ range for data collection/°	7.896 to 142.57
Index ranges	-13 ≤ h ≤ 13, -14 ≤ k ≤ 14, -14 ≤ l ≤ 14
Reflections collected	26546
Independent reflections	5628 [R_{int} = 0.0290, R_{sigma} = 0.0186]
Data/restraints/parameters	5628/0/328
Goodness-of-fit on F^2	1.026
Final R indexes [I>=2σ (I)]	R_1 = 0.0422, wR_2 = 0.1121
Final R indexes [all data]	R_1 = 0.0518, wR_2 = 0.1222
Largest diff. peak/hole / e Å^{-3}	0.17/-0.18

*Figure 84. Crystal structure and unit cell parameters of compound **76** as found by single crystal X-ray diffraction.*

Table 9. Transition temperatures, enthalpies and entropies of transition of symmetrical diphenyl acetylene compounds.

Compound number	Transition	T/ °C	ΔH / kJ mol^{-1}	ΔS / J K^{-1} mol^{-1}
73	Cr – Iso	59.6	-	-
76[30]	Cr – Iso	53.8	65.9	200
78	Cr – N	159	71.5	167
	N – Iso	197	11.0	24
81	Cr – Iso	56.8	-	-
88[22]	Cr – N	173.9	49.5	111
	N – Iso	207.3	23.8	40

In summary, including alkyl chains around a diphenyl acetylene unit does not effectively induce liquid crystalline behaviour with the exception of previously reported compound **89** (Figure 85). Compound **89** is liquid crystalline while the alkyl compounds reproduced for this work (**73** and **76**) and a similar structure with octyl alkyl chains are not.[30] This can be explained by comparing the transition temperatures of the compounds as the mesophase of **89** clears at 40.5 °C and is monotropic, 2 °C below the melting point. Meanwhile for compound **76** the shorter chains result in a more crystalline material as reflected in the higher melting point, and this material readily crystallised into large crystals which were suitable for single crystal X-ray diffraction. This more crystalline material will readily crystallise well above the clearing point of **89** and so there is no opportunity to see a monotropic mesophase. A similar observation can be made for **73** whereby the longer alkyl chains increase the melting point substantially from 43 °C (heptyl, **89**) to 59.6 °C (dodecyl, **73**). While the clearing point of a nematic mesophase would also be expected to be higher due to the increased aspect ratio and intermolecular interactions this monotropic transition is likely too far below the melting point and so is not seen.

89

Cr 43 (N 40.5) Iso °C
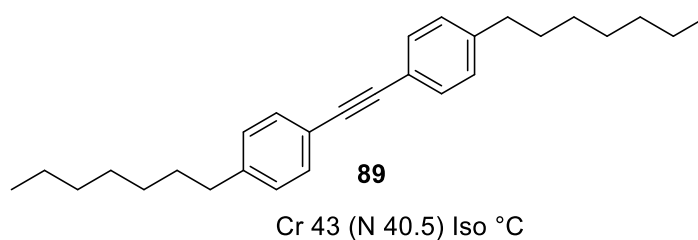
*Figure 85. Transition temperatures of compound **89**.[31]*

Likewise, adding branched methyl groups into the chains disrupts the packing of neighbouring molecules and ester linkages do not provide sufficient polarisability in the core to promote sufficient interactions to provide liquid crystalline behaviour as shown by **81**. As with the previous examples, the melting point of **81** is greater than that of **89**.

The introduction of mesogenic cyanobiphenyl groups at the end of the alkyl chains **78** and **88** promotes intermolecular interactions and therefore both exhibited nematic phases. Examples of the nematic textures given by these oligomers are given in Figure 86.
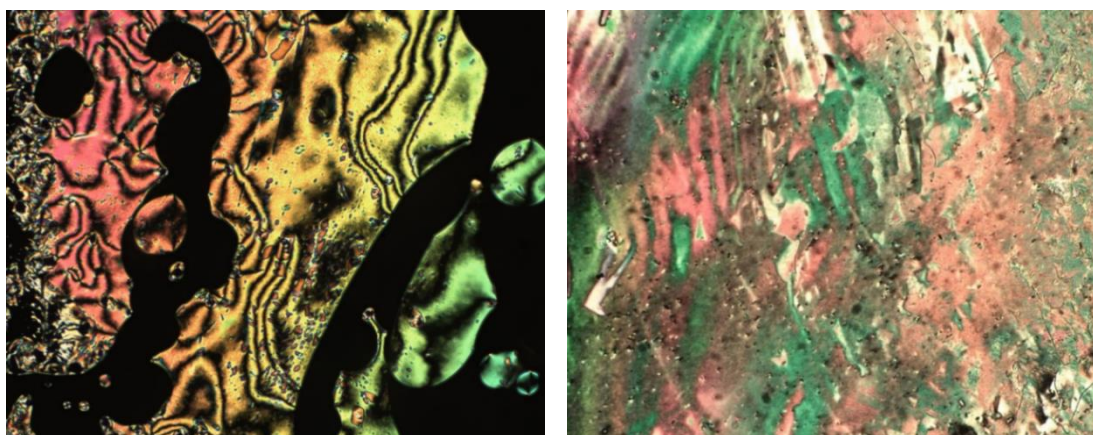
*Figure 86. Photomicrographs (x100 magnification) a) Left, Photomicrograph of **88** (206.1 °C) showing the schlieren texture. b) Right, Photomicrograph of **78** (159.9 °C) showing the planar texture of the nematic phase.*

The role of the cyanobiphenyl mesogen in stabilising the mesophase is clear as the trimesogens **78** and **88** have melting points roughly three times higher (159 and 173.9 °C respectively) than those of the alkyl substituted materials. Despite the higher melting points these trimesogens exhibit enantiotropic nematic phases with clearing points around 30 °C above the melting points. The direct comparison between **78** and

88 is complicated due to their being multiple effects linked to the method of attachment to the core.

Both compound **88** using an alkyl linkage features and compound **78** featuring an ester linkage include a total of twelve atoms separating the mesogenic unit from the diphenyl acetylene core. Due to similarity between these two compounds the clearing points are similar with around a 10 °C decrease in the melting and clearing points of the ester compound compared to the alkyl compound. However, in this case the constituent atoms are different with an additional oxygen atom in the ether linkage providing more flexibility. While this will play a role in the mesophase organisation it is expected to be smaller than the effect of the ester units on the diphenyl acetylene core. The ester linkages slightly extend the length of the core where π-electrons are delocalized, however the electronegativity and mesomeric effect result in these groups being electron withdrawing compared to the weak inductive effect of the alkyl spacers. Meanwhile the ester group is also considered more flexible than the alkyl linkage and this would destabilise the mesophase. The magnitude of these effects, is not clear however the combined result is seen in a roughly 10 °C decrease in the melting and clearing points of the ester analogue.

4.4 Experimental

Compounds **73**[30], **76**[24] and **88**[22] were synthesised following procedures which have been described previously. The characterisation data (^{1}H NMR spectra, mass spectrometry) of these compounds were in agreement with those reported previously.
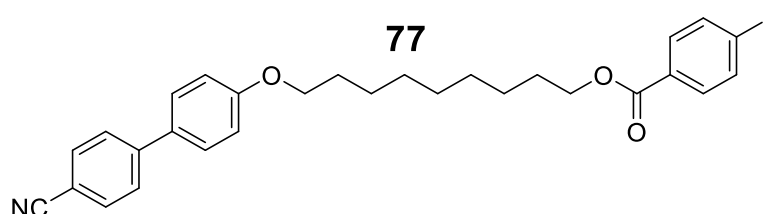
4-Iodobenzoic acid (1.50 g, 6.05 mmol), 4'-(9-(hydroxynonyl)oxy-4-cyanobiphenyl (2.0 g, 5.94 mmol), EDC.HCl (1.7 g, 8.90 mmol) and DMAP (0.3 g, 2.46 mmol) were dissolved in DCM (30 mL). The reaction mixture was stirred at room temperature for 18 hours. The solvent was removed *in vacuo* and the crude product purified by column chromatography (DCM/EtOAc as eluent) to give the target compound **77** as a white powdery solid (3.24 g, 5.71 mmol, 95% yield).

^{1}H NMR (400 MHz, CDCl$_3$) δ 8.13 (d, *J* = 8.5 Hz, 2H, Ar*H*), 8.08 (d, *J* = 8.5 Hz, 2H, Ar*H*), 8.03 (d, *J* = 8.5 Hz, 2H, Ar*H*), 7.97 (d, *J* = 8.5 Hz, 2H, Ar*H*), 7.86 (d, *J* = 8.5 Hz, 2H, Ar*H*), 7.32 (d, *J* = 8.5 Hz, 2H, Ar*H*), 4.64 (t, *J* = 6.5 Hz, 2H, COOC*H$_2$*), 4.34 (t, *J* = 6.5 Hz, 2H, OC*H$_2$*), 1.86 – 1.44 (m, 14H, OCH$_2$C*H$_2$* and CH$_2$CH$_2$C*H$_2$*).

78
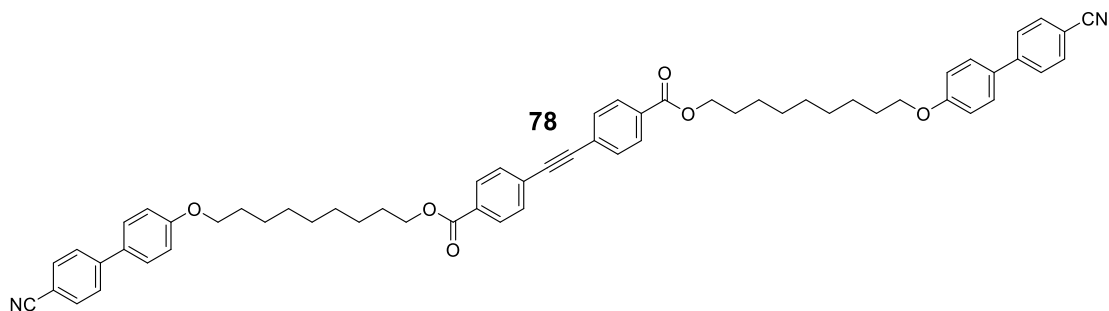
Compound **77** (2.77 g, 4.89 mmol) and Compound **33ᵢᵢᵢ** (2.27 g, 4.88 mmol) were charged to a Schlenk tube under argon. Triethylamine (20 mL) and toluene (20 mL) was added and the mixture degassed with argon gas for 20 minutes. [PdCl$_2$(PPh$_3$)$_2$](0.17 g, 0.24 mmol) and CuI (0.05 g, 0.26 mmol) were added under flow of argon and the reaction mixture stirred at room temperature for 18 hours. The solvent was evaporated to dryness and the crude product purified by column chromatography (DCM:EtOAc) then recrystallised from hot ethanol to give the target compound **78** as a white solid (3.13 g, 3.46 mmol, 71% yield).

^{1}H NMR (400 MHz, CDCl$_3$) δ 8.02 (d, *J* = 8.5 Hz, 4H, Ar*H*), 7.67 (d, *J* = 8.5 Hz, 4H, Ar*H*), 7.64 − 7.56 (m, 8H, Ar*H*), 7.51 (d, *J* = 8.5 Hz, 4H, Ar*H*), 6.97 (d, *J* = 8.5 Hz, 4H, Ar*H*), 4.32 (t, *J* = 6.5 Hz, 4H, COOC*H*$_2$), 3.99 (t, *J* = 6.5 Hz, 4H, OC*H*$_2$), 1.83 − 1.72 (m, 8H, OCH$_2$C*H*$_2$), 1.51 − 1.32 (m, 20H, CH$_2$CH$_2$C*H*$_2$)

APCI-MS: mz = 905.5 [M+H]$^+$

79
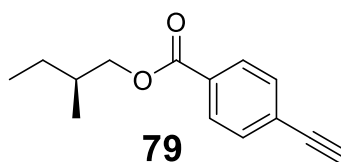
4-Ethynylbenzoic acid (0.54 g, 3.69 mmol), (S)-2-methyl butanol (0.38 g, 4.32 mmol), EDC.HCl (1.8 g, 9.39 mmol) and DMAP (0.3 g, 2.46 mmol) were dissolved in DCM (20 mL) and the reaction mixture was stirred at room temperature for 18 hours. The solvent was removed *in vacuo* and the crude product purified by column chromatography (DCM as eluent) to give the target compound **79** as a colourless oil (0.66 g, 3.05 mmol, 83% yield).

^{1}H NMR (400 MHz, CDCl$_3$) δ 8.00 (d, *J* = 8.0 Hz, 2H, Ar*H*), 7.55 (d, *J* = 8.0 Hz, 2H, Ar*H*), 4.21 (dd, *J* = 11.0, 6.0 Hz, 1H, OC*H*H), 4.13 (dd, *J* = 11.0, 6.5 Hz, 1H, OCH*H*), 3.23 (s, 1H, CC*H*), 1.92 − 1.80 (m, 1H, CH*H*CH$_3$), 1.56-1.46 (m, 1H, C*H*HCH$_3$), 1.35 − 1.22 (m, 1H, C*H*CH$_3$), 1.01(d, *J* = 7.0 Hz, 3H, CHC*H*$_3$), 0.96 (dd, *J* = 7.0, 7.0 Hz, 3H, CH$_2$C*H*$_3$).

80
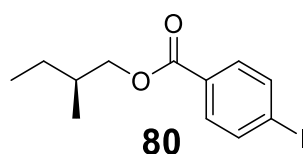
4-Iodobenzoic acid (2.5 g, 10.01 mmol), (S)-2-methyl butanol (0.9 g, 10.23 mmol), EDC.HCl (2.9 g, 15.13 mmol) and DMAP (0.6 g, 4.91 mmol) were dissolved in DCM (40 mL) added and the reaction mixture was stirred at room temperature for 18 hours. The solvent was removed *in vacuo* and the crude product purified by column chromatography (DCM as eluent) to give the target compound **80** as a colourless oil (3.18 g, 9.96 mmol, 99% yield).

^{1}H NMR (400 MHz, CDCl$_3$) δ 7.79 (dd, *J* = 8.5, 2.0 Hz, 2H, Ar*H*), 7.74 (dd, *J* = 8.5, 2.0 Hz, 2H, Ar*H*), 4.19 (dd, *J* = 10.5, 6.0 Hz, 1H, OC*H*H), 4.11 (dd, *J* = 10.5, 6.5 Hz, 1H, OCH*H*), 1.91 − 1.78 (m, 1H, CH*H*CH$_3$), 1.57 − 1.45 (m, 1H, C*H*HCH$_3$), 1.34 − 1.21 (m, 1H, C*H*CH$_3$), 1.00 (d, *J* = 7.0 Hz, 3H, CHC*H*$_3$), 0.94 (d, *J* = 7.0, 7.0 Hz, 3H, CH$_2$C*H*$_3$).

81
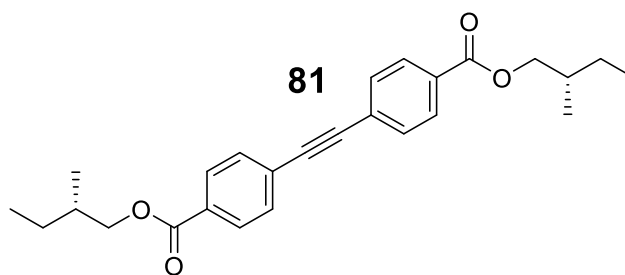
Compound **80** (0.97 g, 3.05 mmol), and compound **79** (0.66 g, 3.05 mmol), were charged to a Schlenk tube under argon. Triethylamine (20 mL) was added and the mixture degassed with argon gas for 20 minutes. [PdCl$_2$(PPh$_3$)$_2$](0.11 g, 0.15 mmol) and CuI (0.03 g, 0.16 mmol) were added under flow of argon and the reaction mixture stirred at room temperature for 18 hours. The solvent removed *in vacuo* and the crude product purified by column chromatography (Petrol:DCM as eluent) to give the target compound **81** as a white solid (0.90 g, 2.21 mmol, 73% yield).

^{1}H NMR (400 MHz, CDCl$_3$) δ 8.04 (d, *J* = 8.0 Hz, 4H, Ar*H*), 7.60 (d, *J* = 8.5 Hz, 4H, Ar*H*), 4.22 (dd, *J* = 10.5, 6.0 Hz, 2H, OC*H*H), 4.14 (dd, *J* = 10.5, 6.5 Hz, 2H, OC*H*H), 1.87 (dqd, *J* = 13.0, 6.5, 5.5 Hz, 2H, C*H*HCH$_3$), 1.54 (dqd, *J* = 13.0, 7.5, 5.5 Hz, 2H, C*H*HCH$_3$), 1.29 (m, 2H, C*H*CH$_3$), 1.02 (d, *J* = 6.5 Hz, 6H, CHC*H*$_3$), 0.96 (dd, *J* = 7.5, 7.5 Hz, 6H, CH$_2$C*H*$_3$).

APCI-MS: Mz = 407.2 [M+H]$^+$

4.5 References.

1   J. Malthête, M. Leclercq, M. Dvolaitzky, J. Gabard, J. Billard, V. Pontikis and J. Jacques, *Mol. Cryst. Liq. Cryst*., 1973, 23, 233–260.

2   M. Cestari, S. Diez-Berart, D. A. Dunmur, A. Ferrarini, M. R. De La Fuente, D. J. B. Jackson, D. O. Lopez, G. R. Luckhurst, M. A. Perez-Jubindo, R. M. Richardson, J. Salud, B. A. Timimi and H. Zimmermann, *Phys. Rev. E*., 2011, 84, 1–20.

3   J. Bailey, A. Chrysostomou, J. H. Hough, T. M. Gledhill, A. McCall, S. Clark, F. Ménard and M. Tamura, *Science*, 1998, 281, 672–674.

4   S. J. Sowerby, W. M. Heckl and G. B. Petersen, *J. Mol. Evol*., 1996, 43, 419–424.

5   R. J. Mandle, *Soft Matter*, 2016, 12, 7883–7901.

6   R. J. Mandle, M. P. Stevens and J. W. Goodby, *Liq. Cryst*., 2017, 44, 2046

7   D. Chen, M. Nakata, R. F. Shao, M. R. Tuchband, M. Shuai, U. Baumeister, W. Weissflog, D. M. Walba, M. A. Glaser, J. E. Maclennan and N. A. Clark, *Phys. Rev. E*., 2014, 89, 022506

8   P. J. Barnes, A. G. Douglass, S. K. Heeks and G. R. Luckhurst, *Liq. Cryst*., 1993, 13, 603–613.

9   J. W. Emsley, G. R. Luckhurst and G. N. Shilstone, *Mol. Phys*., 1984, 53, 1023–1028.

10   J. W. Emsley, G. R. Luckhurst, G. N. Shilstone and I. Sage, *Mol. Cryst. Liq. Cryst.,* 1984, 102, 223–233.

11   R. J. Mandle, E. J. Davis, C. T. Archbold, S. J. Cowling and J. W. Goodby, *J. Mater. Chem.*, 2014, 2, 556–566.

12   Y. Wang, G. Singh, D. M. Agra-Kooijman, M. Gao, H. K. Bisoyi, C. Xue, M. R. Fisch, S. Kumar and Q. Li, *CrystEngComm*, 2015, 17, 2778–2782.

13   S. M. Jansze, A. Martínez-Felipe, J. M. D. Storey, A. T. M. Marcelis and C. T. Imrie, *Angew. Chem. Int. Ed*., 2015, 54, 643–646.

14   C. V. Yelamaggad*, Mol. Cryst. Liq. Cryst*., 1998, 326, 149.

15   C. V. Yelamaggad, U. S. Hiremath, D. S. Shankar Rao and S. Krishna Prasad, *Chem. Commun.*, 2000, 57–58.

16   A. S. Achalkumar, U. S. Hiremath, D. S. S. Rao and C. V. Yelamaggad, *Liq. Cryst.*, 2011, 38, 1563–1589.

17   L. Gehringer, D. Guillon and B. Donnio, *Macromolecules*, 2003, 36, 5593–5601.

18   L. Gehringer, C. Bourgogne, D. Guillon and B. Donnio, *J. Am. Chem. Soc.*, 2004, 126, 3856–3867.

19   L. Gehringer, C. Bourgogne, D. Guillon and B. Donnio, *J. Mater. Chem.*, 2005, 15, 1696–1703.

20   J. Barberá, B. Donnio, R. Giménez, D. Guillon, M. Marcos, A. Omenat and J. L. Serrano, *J. Mater. Chem.*, 2001, 11, 2808–2813.

21   M. Marcos, R. Martín-Rapún, A. Omenat and J. L. Serrano, *Chem. Soc. Rev.*, 2007, 36, 1889–1901.

22   T. Ma, PhD Thesis, University of York, 2013.

23   K. J. Sonogashira, *Organomet. Chem.*, 2002, 46.

24   R. Chinchilla and C. Nájera, *Chem. Rev.*, 2007, 107, 874–922.

25   R. J. Mandle and J. W. Goodby, *React. Chem. Eng.*, 2018, 3, 515–519.

26   M. Schilz and H. Plenio, *J. Org. Chem.*, 2012, 77, 2798–2807.

27   A. E. Thompson, G. Hughes, A. S. Batsanov, M. R. Bryce, P. R. Parry and B. Tarbit, *J. Org. Chem.*, 2005, 70, 388–390.

28   A. S. Guram, A. O. King, J. G. Allen, X. Wang, L. B. Schenkel, J. Chan, E. E. Bunel, M. M. Faul, R. D. Larsen, M. J. Martinelli and P. J. Reider, *Org. Lett.*, 2006, 8, 1787–1789.

29   A. S. Guram, X. Wang, E. E. Bunel, M. M. Faul, R. D. Larsen and M. J. Martinelli, *J. Org. Chem.*, 2007, 72, 5104–5112.

30   S. Ito, M. Wehmeier, J. D. Brand, C. Kübel, R. Epsch, J. P. Rabe and K. Müllen, *Chem. Eur. J.*, 2000, 6, 4327–4342.

31   E. Kudo, Y. Shibata, M. Yamazaki, K. Masutomi, Y. Miyauchi, M. Fukui, H. Sugiyama, H. Uekusa, T. Satoh, M. Miura and K. Tanaka, *Chem. Eur.* J., 2016, 22, 14190–14194.

Chapter 5. Unsymmetrical diphenyl acetylene derivatives

Two structural blocks, each able to promote liquid crystalline behaviour, can be combined to synthesise cyanobiphenyl and perfluoroalkyl *Janus* liquid crystal supermolecules. This has the potential to enrich liquid-crystalline phase behaviour when compared to systems containing only one class of mesogen by introducing two competing intermolecular interactions, for example quadrupolar interactions observed between cyanobiphenyl units and the fluorophobic effect induced by perfluoroalkyl chains. Each of these effects can drive self-assembly of molecules into a liquid crystalline mesophase, and when combined, both are expressed in the liquid crystalline behaviour of the *Janus* supermolecule, via the mesophase type, structure and properties (Figure 87).[1]
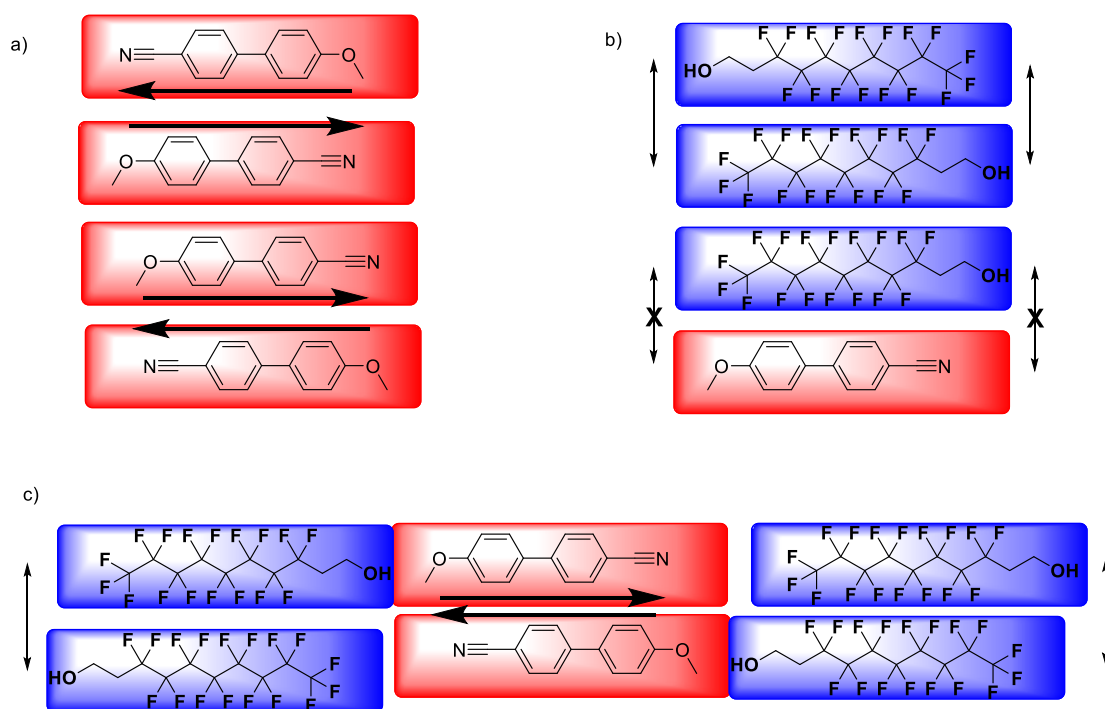
Figure 87. Effects driving self-assembly, a) cyanobiphenyls (red) share quadrupolar interactions when neighbouring cyanobiphenyl mesogens have an antiparallel arrangement. b) Perfluorinated units (blue) induce the fluorophobic effect, providing microphase segregation by excluding alkyl regions. c) When these units are combined both effects are present giving ordered liquid crystalline phases with well defined mesophase structures.

One way to modulate these competing effects is to control the volume of the two moieties, and in this way introduce interfacial curvature which must also be accommodated in the packing of the molecules and hence offer a route to control the mesophase structure (Figure 88). By probing this interplay of interfacial curvature and

Janus amphiphilic properties, rich mesomorphism may be encountered and by understanding this behaviour for diphenyl acetylene cores a similar approach could be used with any rigid core.
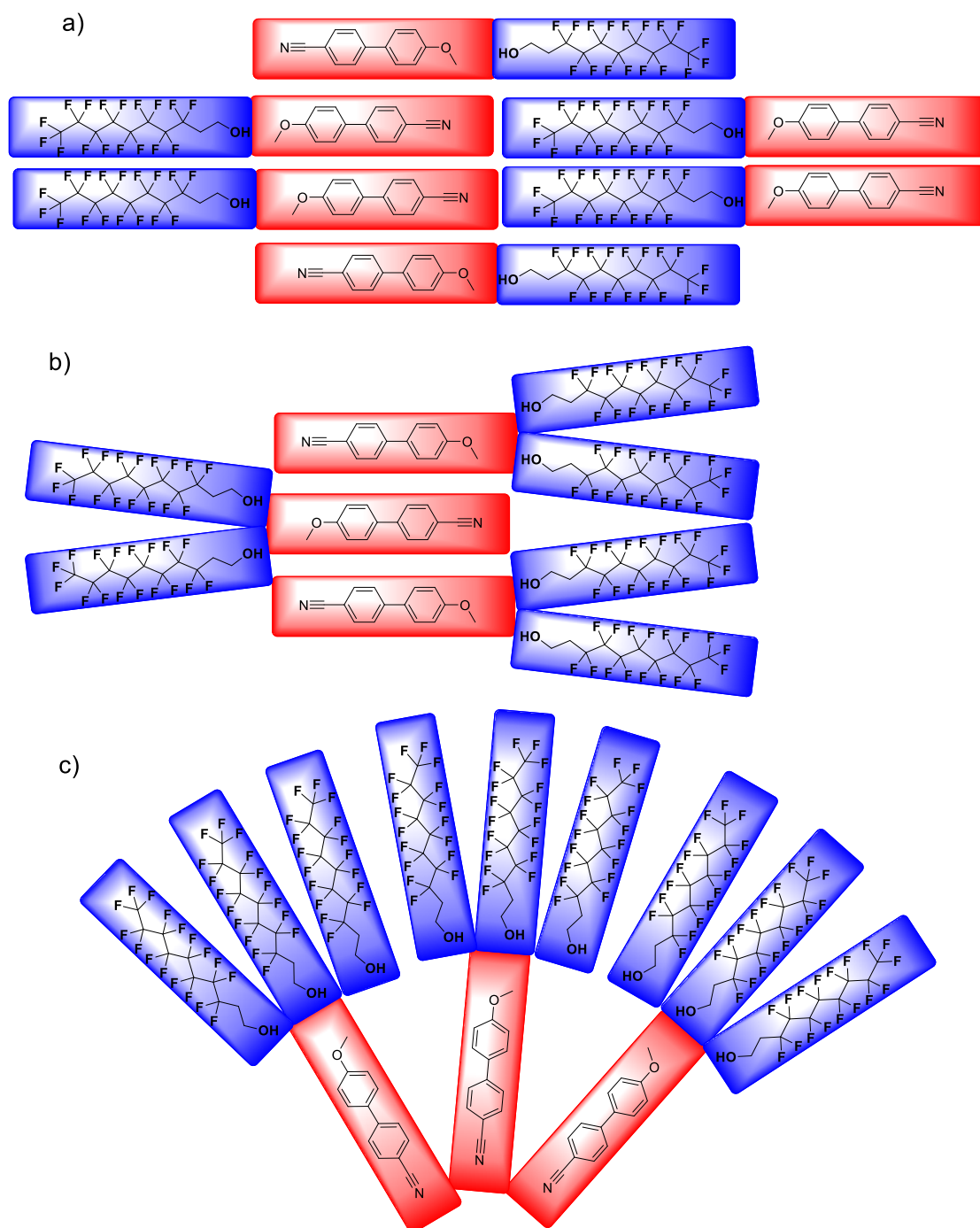
Figure 88. Changing the relative volumes of the two faces of a Janus molecule will reflect upon the mesophase structures formed. a) equal or near equal volumes tends to give well ordered lamellar phases, b) introducing curvature prevents these layers from packing as efficiently giving undulating layers, c) further increasing the curvature can produce columnar mesophases.

A convergent approach utilising a Sonogashira coupling reaction was used to join the aryl-iodo and phenyl acetylene units to form the diphenyl acetylene core, and concomitantly the unsymmetrical structure. This chapter describes a comprehensive range of *Janus* materials comprising of cyanobiphenyl-based units and fluoroalkyl chains in which the number of mesogenic units (cyanobiphenyl or perfluoroalkyl) can be varied from one to three chains per face through the multiplicity of the branching unit. Furthermore, the effect of the length of the flexible spacer connecting these units to the diphenylacetylene core is investigated. In this way the effect of the interfacial curvature on the mesophase structure can be explored.

The complexity of the molecular structures precludes the study of complete sets of materials where the length of each spacer unit is varied individually and systematically across the whole molecular structure. However, sufficient sets of materials are described to be able to conclude some general trends of behaviour.

Saez and Goodby utilised end-on smectogenic mesogens and side-on nematogenic mesogens tethered by a flexible spacer to form *Janus* supermolecules.[2] A number of examples using the same end-on and side-on mesogenic units were examined as *Janus* supermolecules using a rigid diphenyl acetylene core.[3]

5.1 Synthesis

The synthesis and any liquid crystalline behaviour of the intermediates required for the cross-coupling reactions for these materials were detailed previously in Chapter 3. For this final step a Sonogashira cross-coupling reaction was used since this convergent approach was the most efficient and provided access to the broadest range of materials in the least number of synthetic steps (Scheme 15). Additionally, due to the presence of multiple esters in the dendritic intermediates, this approach was expected to diminish the potential for any trans-esterification byproducts during the synthesis; both by reducing the number of steps whereby an ester was exposed to another alcohol, and by purification of the smaller dendritic moieties where separation of byproducts was expected to be easier. Alcohols were used routinely during the recrystallisation of materials described in this work however no evidence of trans-esterification was detected *via* MALDI-TOF MS (see Figure 90).
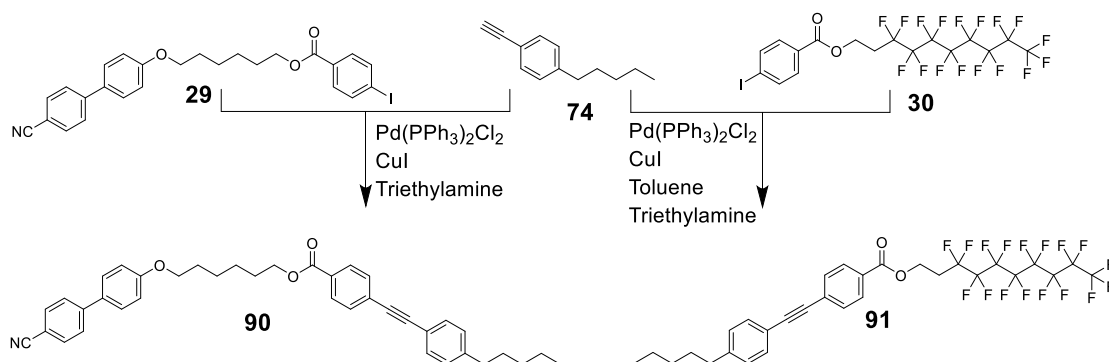
*Scheme 15. Synthesis of a pair of simple diphenyl acetylenes **90** and **91** from commercially available 1-ethynyl-4-pentylbenzene **74**.*

Scheme 15 shows the simplest class of materials produced in this study where an alkyl chain is attached on one side of the diphenyl acetylene core and either a cyanobiphenyl or perfluoroalkyl unit is attached opposite *via* an ester linkage to produce dimesogens **90** and **91**. The synthesis of the iodo-aryl intermediates was described in Chapter 3, and have been used commonly throughout the project. Commercially available 1-ethynyl-4-pentylbenzene **74** was used to enable the Sonogashira coupling approach, providing facile access to the target compounds. Following the Sonogashira coupling reaction the materials were purified by column chromatography followed by recrystallisation from hot ethanol to afford the target compounds in good purity as determined by elemental analysis. Following from these examples a family of *Janus* diphenyl acetylene compounds have been produced and will be introduced sequentially, beginning with a range of cyanobiphenyl compounds including linear materials **92** and **93** as shown in Scheme 16.
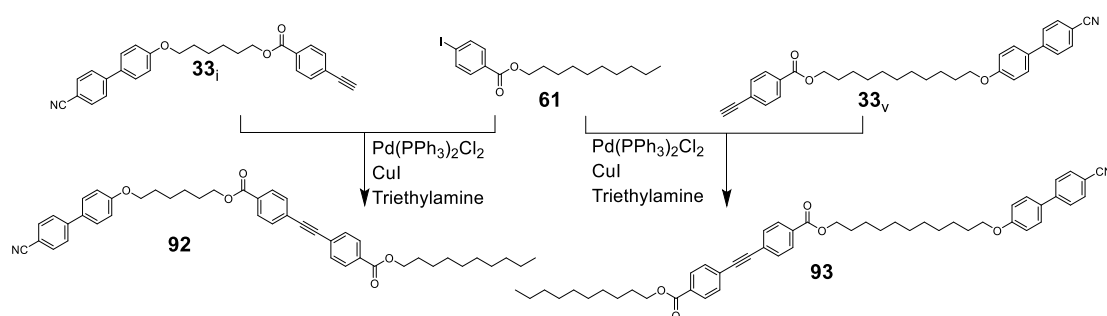
*Scheme 16. Synthesis of two alkyl/cyanobiphenyl diphenyl acetylene materials **92** and **93**.*

The materials shown in Scheme 15 and Scheme 16 may be considered dimesogens due to the nature of the diphenyl acetylene core which will be discussed later. Comparison of compounds **90** and **92** allows the effect of terminal chain length to be examined.

This is extended further where the role of the spacer length is compared in compounds **92** and **93**.

The decyl chain was chosen specifically to study the effect of chain length and to compare with the perfluorinated chain (1H,1H,2H,2H-perfluorodecanol) as featured in **91**. The synthesis and purification of the materials shown in Scheme 16 was identical to that described for the compounds in Scheme 15.

Schemes 17 and 18 shows the third class of linear diphenyl acetylenes which had increased complexity within their structures. In these compounds both the perfluoroalkyl and cyanobiphenyl units were introduced at either end of the diphenyl acetylene core unit to produce a trimesogen. These materials provide an example where the number of chains on each face of the diphenyl acetylene core are equal and as such the relative volumes are comparable. Compound **94** described in Scheme 17 contains short linkages from the mesogenic units to the diphenyl acetylene core whereas compound **95** shown in Scheme 18 contains branched units. These branching units represent the first examples of branching points being included in the diphenyl acetylene compounds, however the branching multiplicity is still considered to be zero as there is only a single extended chain an methyl units branching. Due to the use of the same mesogenic units being incorporated in these trimesogens it allows for comparisons to be made between their properties. Compound **94** was obtained in 70% yield following recrystallisation twice from ethanol, however a modest 32% yield was obtained for compound **95**. Compound **95** is less crystalline than **94** due to the disordered branching unit, additionally DCM, a better solvent for these materials was required to dissolve the sample to allow for recrystallisation. This resulted in poorer recovery during the two recrystallisation steps required for purity. The branched unit in compound **95** allows comparison with compounds that contain 2- or 3- mesogenic units attached to the diphenyl acetylene core in an investigation of curvature.

Scheme 17. Synthesis of linear diphenyl acetylene **94** bearing a perfluorinated chain and cyanobiphenyl mesogen.

Scheme 18. Synthesis of diphenyl acetylene **95** featuring a branched spacer, perfluorinated chain and cyanobiphenyl mesogen.

Although the compounds in this section were prepared via a convergent synthesis, in the case of the 4-pentyldiphenylacetylene bearing two cyanobiphenyl units compound **100** a divergent approach was used as shown in Scheme 19. Since 1-ethynyl-4-pentylbenzene was readily available, and not at risk of side reactions via transesterification in the final esterification step it was deemed a suitable material to explore a divergent synthesis to investigate whether the remaining purification steps were less demanding. The target compound **100** was isolated in a comparable yield with that achieved by convergent methods, and required additional synthetic steps which did not contribute to the synthesis of the remaining compounds. As a result the convergent approach was still favoured throughout the rest of the project.

*Scheme 19. Divergent approach used for the synthesis of compound **100** containing one alkyl chain and two cyanobiphenyl units.*

The convergent synthesis of the multiply branched compounds incorporating either two or more cyanobiphenyl units or perfluroalkyl chains are shown in Schemes 20 – 23 using intermediates described in Chapter 3. In summary, this convergent synthesis was similar to that used for other compounds in this chapter however the Sonogashira coupling reaction required the addition of toluene as a co-solvent alongside triethylamine to aid solubility of the perfluorinated intermediates. The recrystallisation of these multiply branched materials was generally more challenging than for the linear materials due to the disorder induced by branching which resulted in a lack of crystallinity. These branched materials were therefore purified by repeating the column chromatography until sufficient purity was obtained, and then the compound reprecipitated rather than recrystallised. Inclusion of multiple perfluorinated chains improved the crystallinity significantly when compared to cyanobiphenyl mesogenic units (see compounds **100** and **101**).

Scheme 20. Synthesis of Janus diphenyl acetylene compounds *101* - *103*.
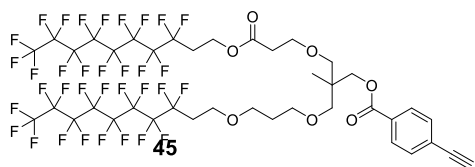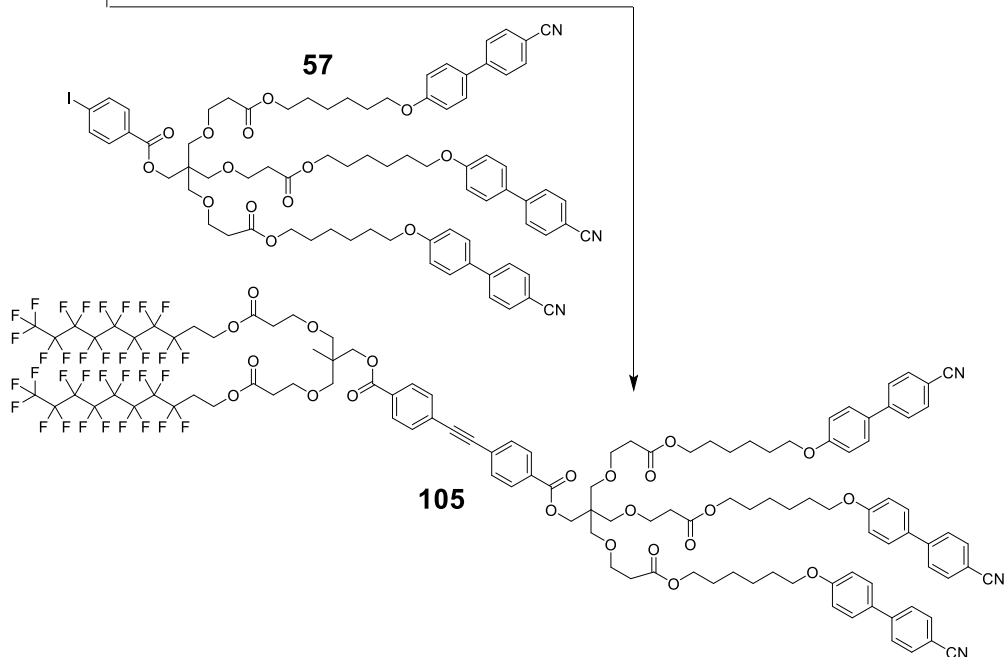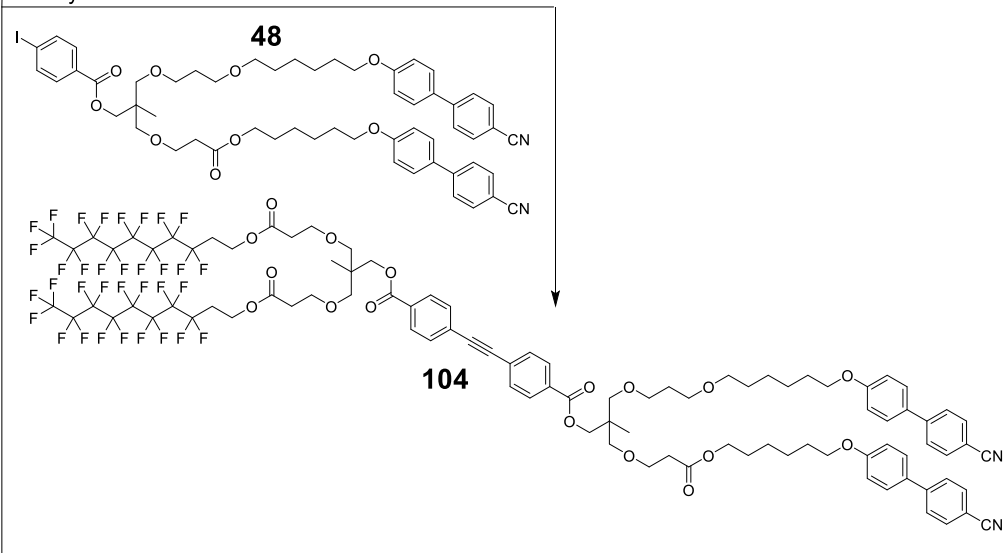
Scheme 21. Synthesis of Janus diphenyl acetylene compounds **104** and **105**.

44
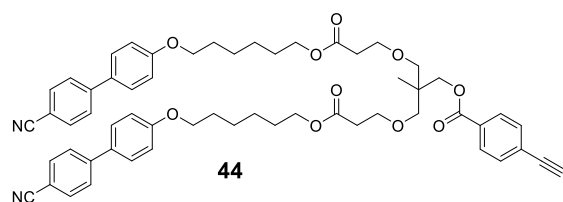
Pd(PPh₃)₂Cl₂
CuI
Toluene
Triethylamine

30

106

58

107
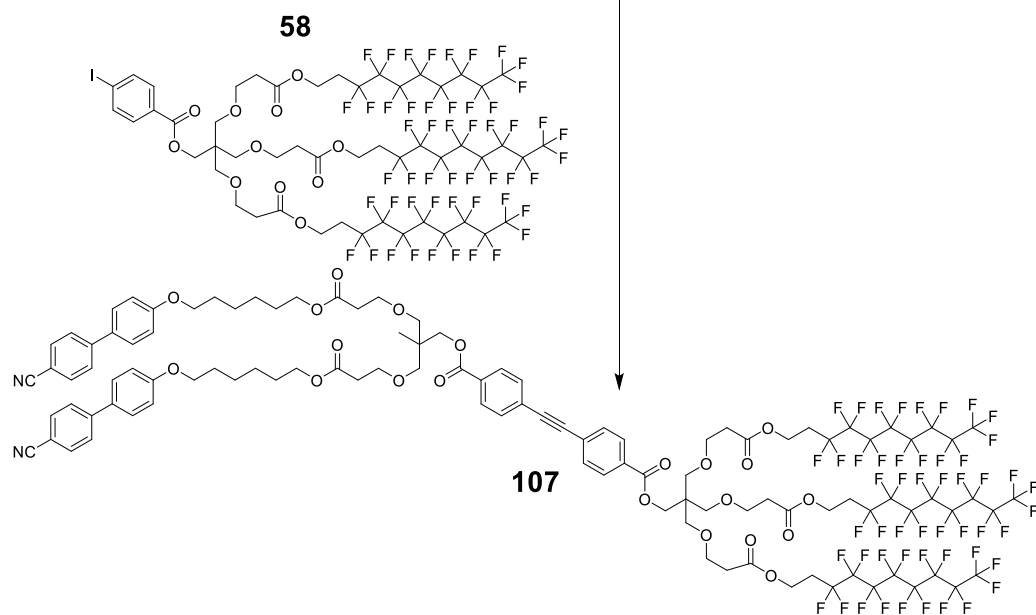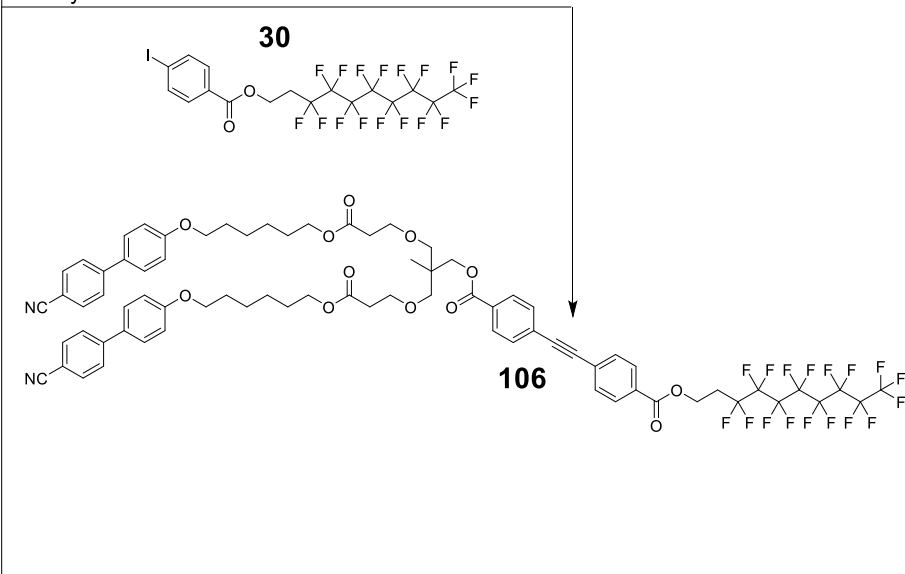
Scheme 22. Synthesis of Janus diphenyl acetylene compounds *106* and *107*.
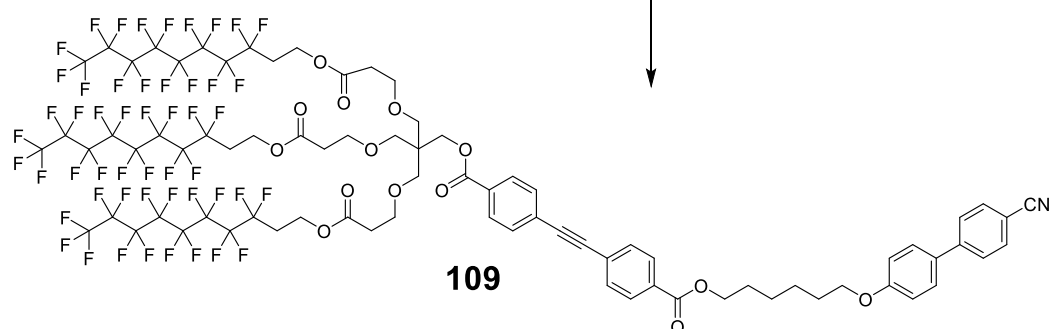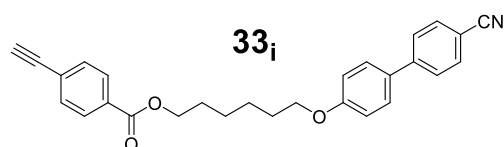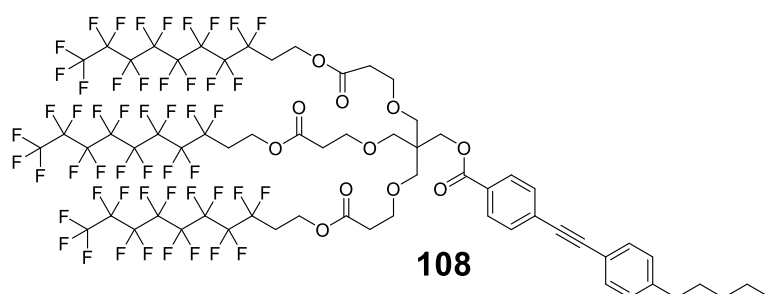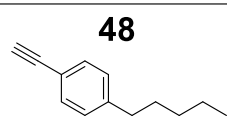
Scheme 23. *Synthesis of Janus diphenyl acetylene compounds **108** and **109**.*

In the case of several materials with a high number of perfluorinated chains (Compound **105**, **107** and **109**) the purification was more challenging as these materials proved to be organogelators in a wide range of common organic solvents

(DCM, THF, EtOH). This behaviour is known for many classes of polar/apolar amphiphiles including other compounds containing perfluorinated chains.[4,5] Due to this organogelation, recrystallisation of these compounds proved impossible and as such repeated column chromatography was used to obtain samples with acceptable purity.

5.2 Characterisation

Chemical characterisation of these materials was performed *via* multinuclear NMR (^{1}H, ^{13}C{^{1}H}, ^{19}F) spectroscopy. However, due to fact that these compounds are supermolecular and have a dendritic structure, the resulting NMR spectra are typically complex. An example for compound **104** is presented in Figure 89 and the full assignment is given in the experimental section at the end of this chapter. The chemical shift of the protons contained in the branching units tended to provide overlapping signals due to similar chemical environments. These signals are highlighted in blue in Figure 89. In this example these resonances include the identical branching units of the cyanobiphenyl and perfluoroalkyl faces as well as several downfield resonances associated with the mesogenic unit i.e. ester and ether linking units of the cyanobiphenyl spacer.

The resonances of the pentaerythritol derived branching unit the resonances typically shifted by less than 0.2 ppm when compared to the 1,1,1-tris(hydroxymethyl) ethane branching unit and thus remained poorly resolved. Due to the number of resonances within similar ranges assignment of these NMR spectra was most easily performed by following the introduction of each chemical moiety as the synthesis progressed. This is illustrated below showing how the aromatic resonances can be separated between the cyanobiphenyl units and diphenyl acetylene (highlighted in the red box). A second example shows the addition to the resonances of the branching and mesogenic units (highlighted in the blue box). A further issue due to the supermolecular structure is that some deviation was observed in the relative integrals of each peak typically due to relative relaxation rates in the aromatic environment.
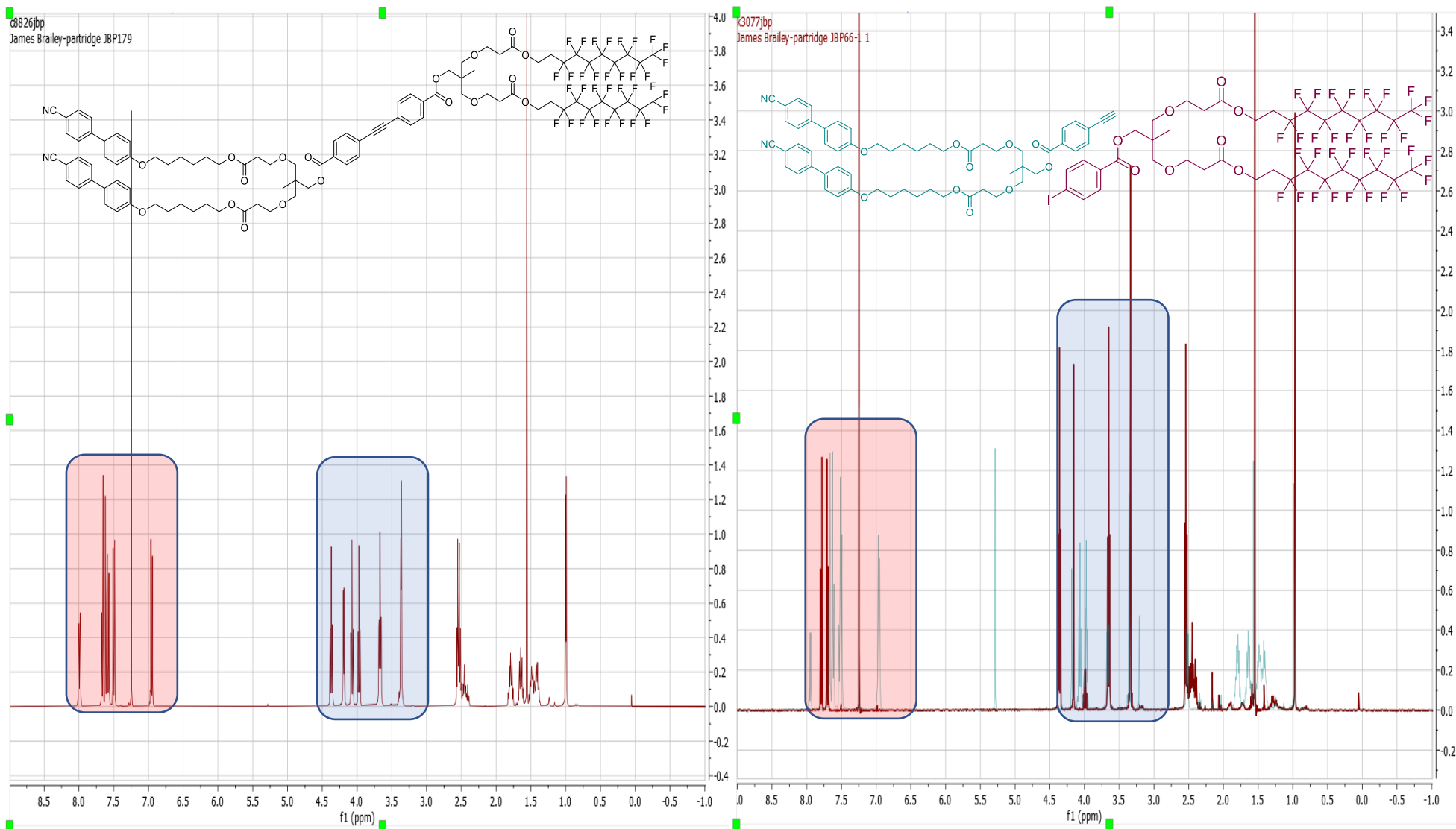
*Figure 89. ¹H NMR spectra of (**104**, left) and the intermediates (**44** right blue, **49** right black) used in its synthesis shown overlayed. The blue area highlights the similar chemical shifts of protons in the branching units and red area highlights how the chemical shifts of the aromatic region can be assigned.*

Elemental analysis was used to prove both the chemical composition and purity of the materials, effectively ruling out contamination. Due to the amphiphilic nature of these materials, it was desired to study the effect of changing the volume of the two 'faces' of the *Janus* materials. In this project this was achieved by synthesising a family of materials with a discrete increase in the number of chains on each side of the *Janus* supermolecule. Additionally, a brief investigation using binary mixtures of **101** and **108** is described in section 5.3.3. One additional method to change the relative volumes of one face of the *Janus* amphiphile would be *via* addition of solvent to swell one region preferentially. Changes in the mesophase behaviour of amphiphiles through the addition of solvent have been widely studied.[6] Organic solvents would be expected to associate with the hydrocarbon regions of the molecule preferentially to the perfluoroalkyl chains and thus serve to swell the hydrocarbon regions, and likewise perfluorinated solvents will swell the perfluorinated regions.[7] The compounds examined in this chapter are complex and their structures have been designed to investigate the effects of microphase segregation and curvature based on the ratio of fluorinated to non-fluorinated units. For this reason it was important to know that the liquid crystal behaviour observed was in the absence of any solvent effects, and rather was related to the assembly of the pure compounds.

It is commonly observed in the study of gelators that samples may trap residual solvent which is observed *via* elemental analysis. The percentage of carbon observed for compounds **105**, **107** and **109** was outside of the acceptable range of ±0.5% in their elemental analysis, for example **109** showed 0.59% more carbon than the theoretical result. Due to the size of these supermolecules and presence of perfluorinated chains it is unclear whether this discrepancy in the elemental analysis was due to the presence of an impurity such as solvent, or due to incomplete combustion of the perfluoroalkyl chains. V_2O_5 was utilised as a combustion aid which was procedurally added to the materials containing perfluorinated chains or otherwise possessing high molecular weights. In order to investigate this further the samples were purified by column chromatography using only dichloromethane as the eluent. Due to the low carbon content of dichloromethane any residual solvent would be expected to reduce the observed percentage of carbon when observed by elemental analysis however, no meaningful change was apparent.

This analysis effectively ruled out the presence of residual solvent to explain the results attained and as such HPLC was utilised to investigate the presence of other impurities. The three materials in question **105**, **107** and **109** were submitted to the University of York chromatography service using a normal phase column (Waters Spherisorb S3 CN 2.0 x 150 mm) and a gradient elution using dichloromethane/methanol. A pair of UV/vis detectors were used one operating at a fixed wavelength of 285 nm, and one operating in scanning mode to rule out impurities which may absorb at a different wavelength. The result of these experiments was that only a single peak was observed with no other clear contaminants in the sample. At this point the remaining factors to explain the discrepancies observed *via* elemental analysis (residual solvent and impurity) had been investigated and no evidence had been found and as such it has been tentatively attributed to issues with combustion.

Compounds were also characterised by mass spectrometry requiring different ionisation methods to provide the best results. The apolar nature of the diphenyl acetylene liquid crystals leads to poor ionisation *via* ESI which was exacerbated further by the presence of perfluorinated chains. Therefore, compounds including **90**, **91** and **94** were analyzed by APCI-ms. These materials had molecular weights near to or below 1000 mass units, and therefore the softer ionisation technique MALDI-ms was not suitable. MALDI-ms produces clusters of ions with m/z values up to around 1000 mass units due to fragmentation of the sample preparation matrix. This results in a large amount of noise in this area and thus information from signals below 1000 mass units is lost. For dendritic materials which have molecular weights far greater than 1000 mass units MALDI-TOF/ms was preferred. This soft ionisation method produces less fragmentation than ESI and APCI-ms, and thus can be used as proof that the dendritic structures are fully substituted. Figure 90 shows the MALDI-TOF-ms of compound **104** (Mass expected 2227.55), and the molecular envelope containing the isotope pattern is expanded. The theoretical isotope pattern (top) shows good agreement with the experimental isotope pattern (bottom). Due to the large number of atoms within the molecular structure the isotopic distribution of the $[M]^+$ and $[M+1]^+$ peaks are relatively equal.

This analysis provides evidence that the target compound is not contaminated with species where one or more mesogenic units is missing. As a soft ionisation technique

MALDI-ms provides very little fragmentation of the ester units used to construct the dendritic materials. Therefore, compounds where the dendritic branching units are not fully substituted would be plainly observed.
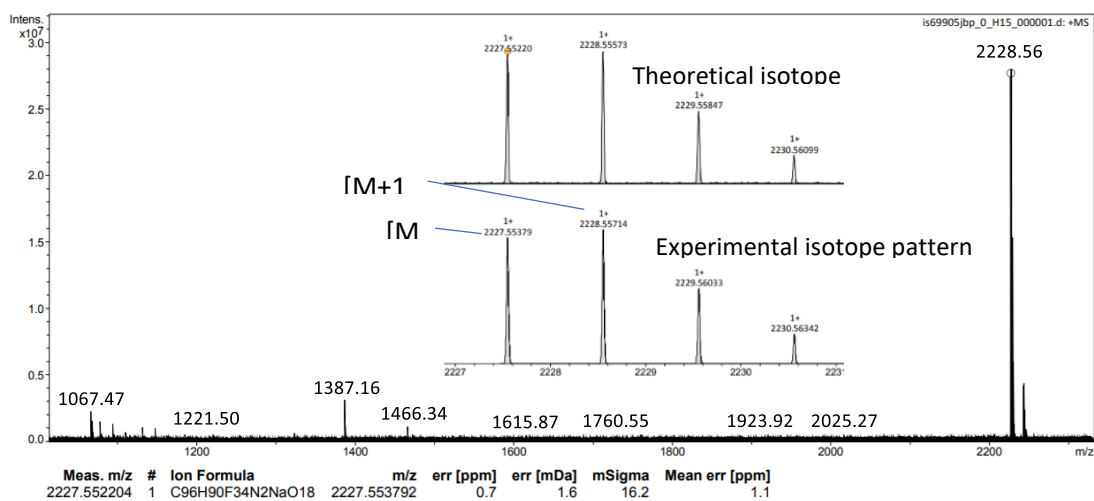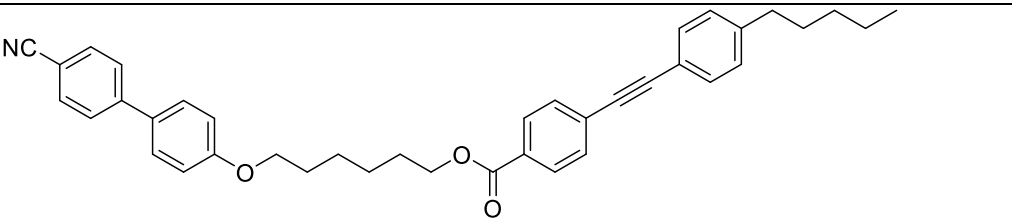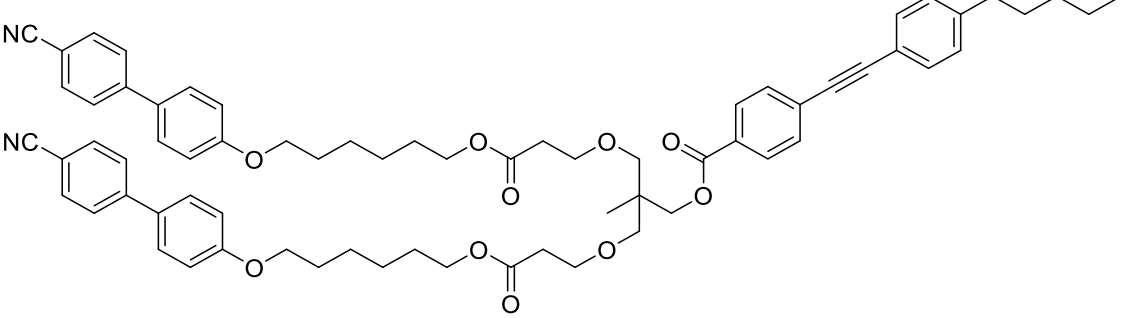
*Figure 90. MALDI-TOF/MS of compound **104** showing the full mass range, observed isotope pattern of the molecular envelope (top) and theoretical distribution (bottom).*

All the compounds prepared in this section of the thesis along with the related compounds prepared by Ma are summarised in Tables 10 – 13, including their phase transitions and other liquid crystalline properties. The compounds previously reported by Ma are shown in blue.[3]

Table 10. Family of Janus cyanobiphenyl:alkyl diphenyl acetylenes.

Compound number	Chemical structure	Transition temperatures /°C
90		Cr 75.0 N 79.6 Iso °C
100		g -8.2 N 49.5 Iso °C
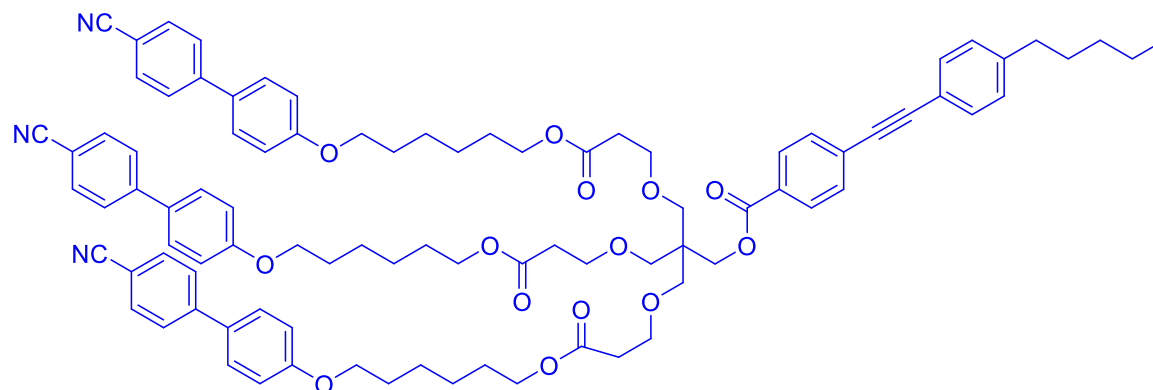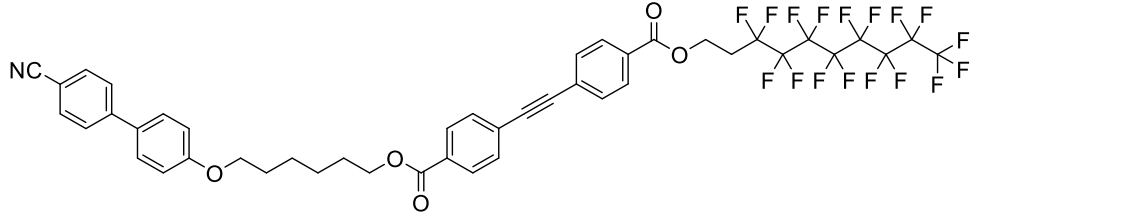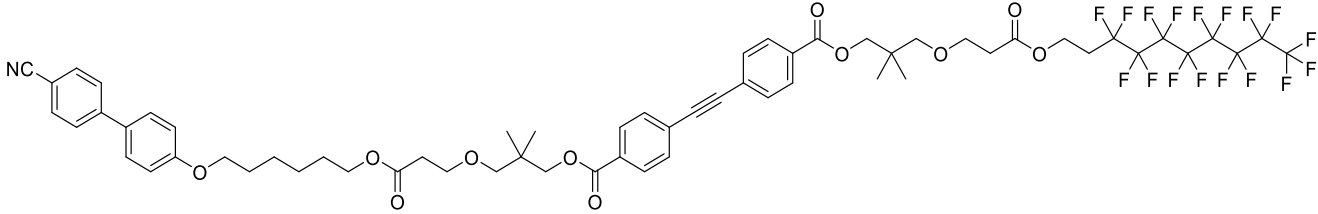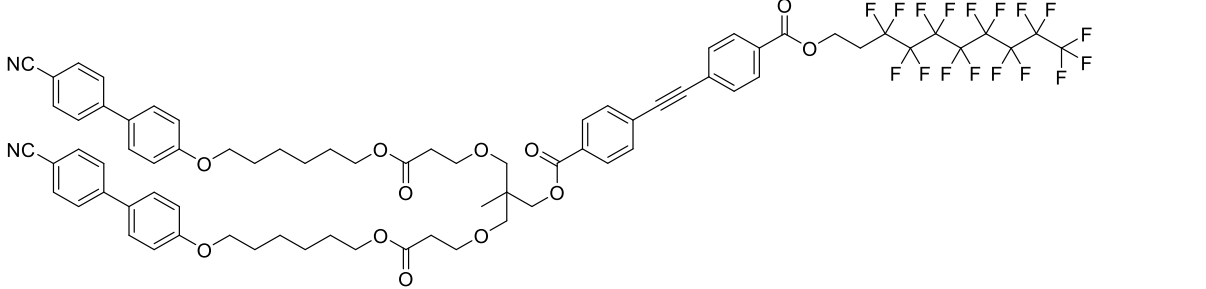
110		g -0.2 N 56.2 Iso °C
111		Cr 30.1 X 36.9 SmA 49.7 Iso °C
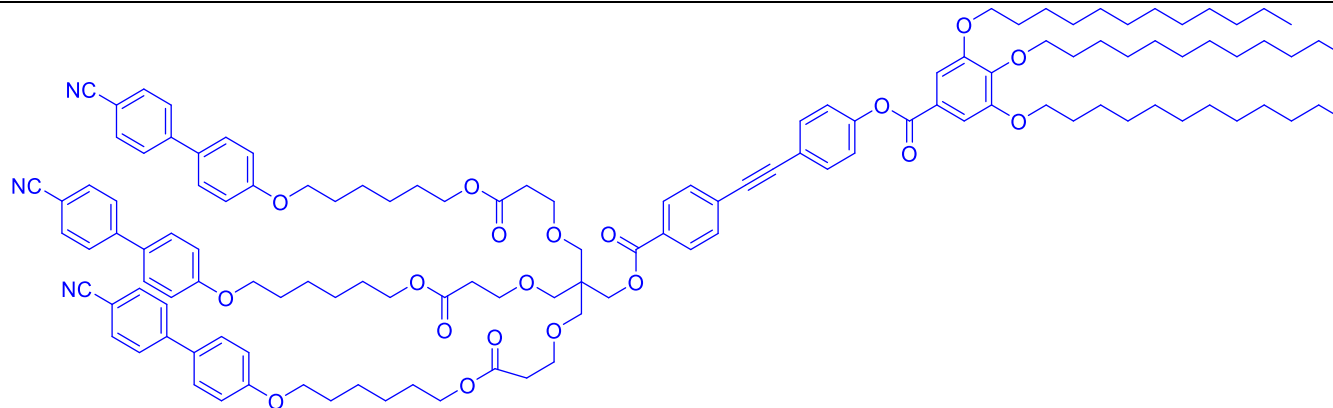
Table 11. Family of Janus cyanobiphenyl:perfluoroalky compounds, and alkyl references.

Compound number	Chemical structure	Transition temperatures /°C
94		Cr 150.1 SmA 151.3 Iso °C
95		Cr 90.3 (SmA 71.6) Iso °C
106		Cr 59.8 SmA 62.0 Iso °C
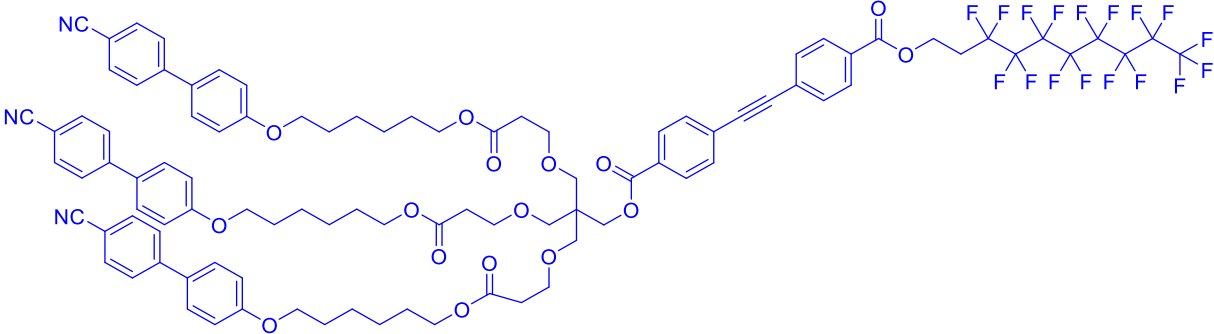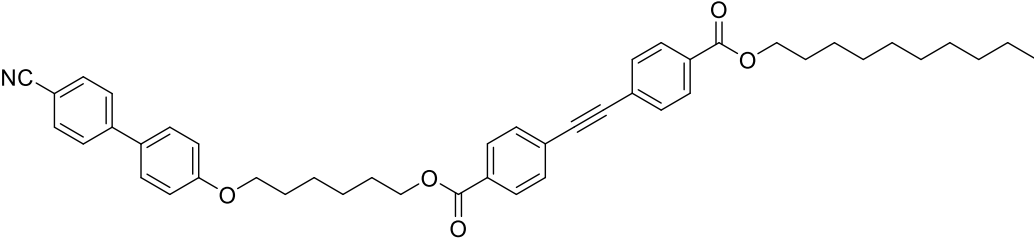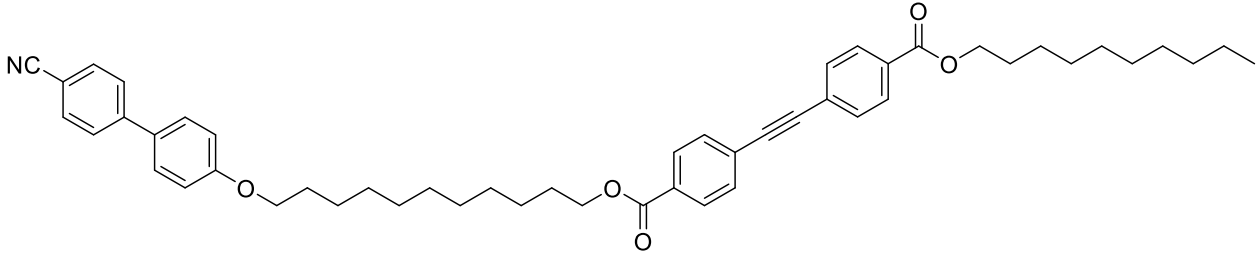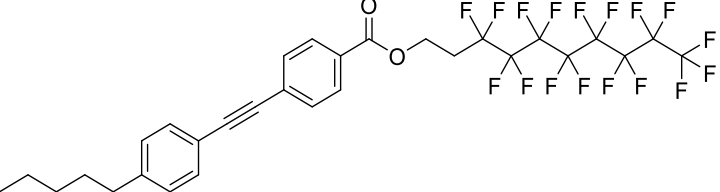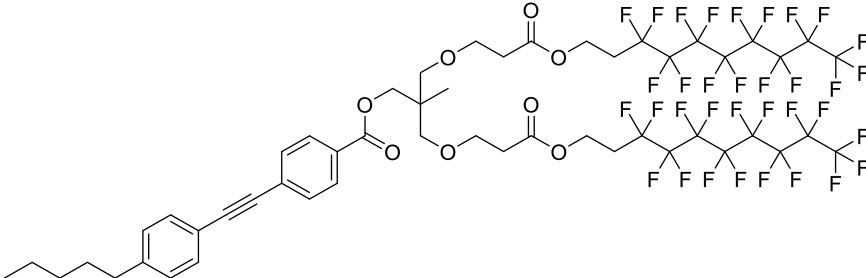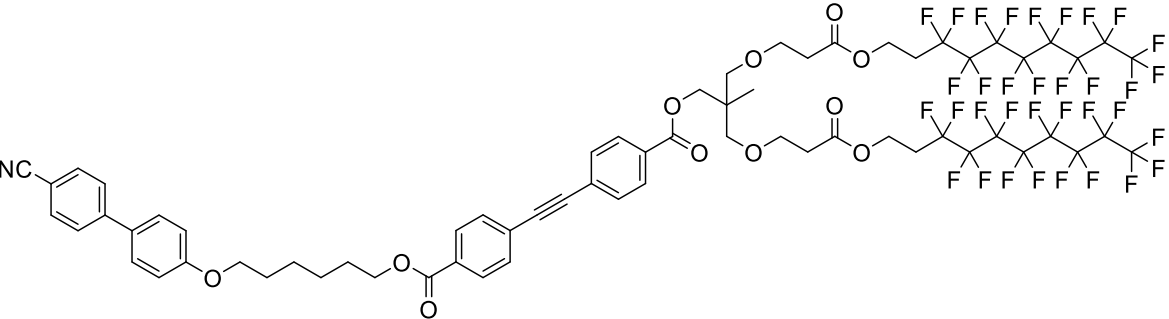
112		g 4.8 Col 59.5 SmA 60.7 Iso °C
92		Cr 77.9 (52.2 SmC 64.1 N) Iso °C
93		Cr 92.6 N 108.5 (SmA 84.7) Iso °C

Table 12. Family of Janus perfluoroalkyl:alkyl and perfluoroalkyl dominated compounds.

Compound number	Chemical structure	Transition temperatures /°C
91		Cr 111.9 SmA 124.2 Iso °C
101		Cr 77.4 Iso °C
102		Cr 106.4 Iso °C
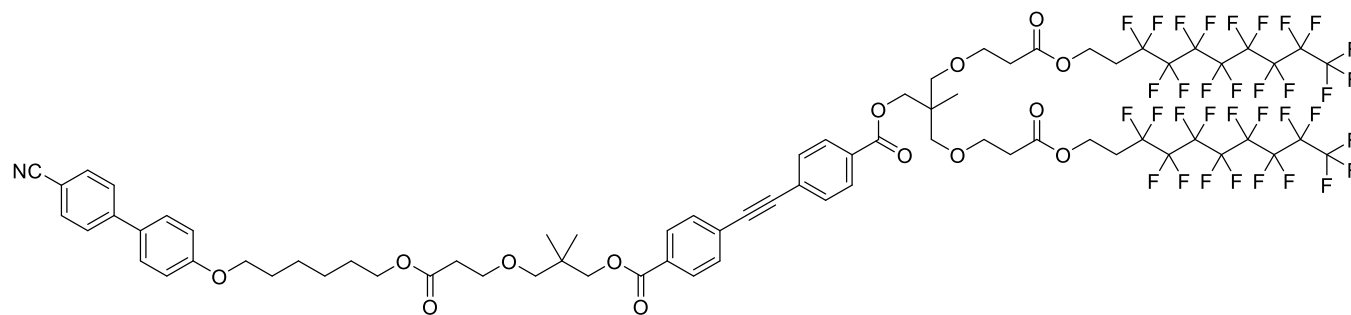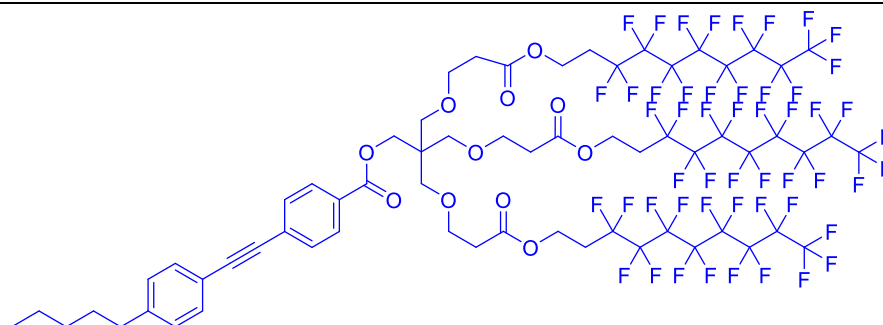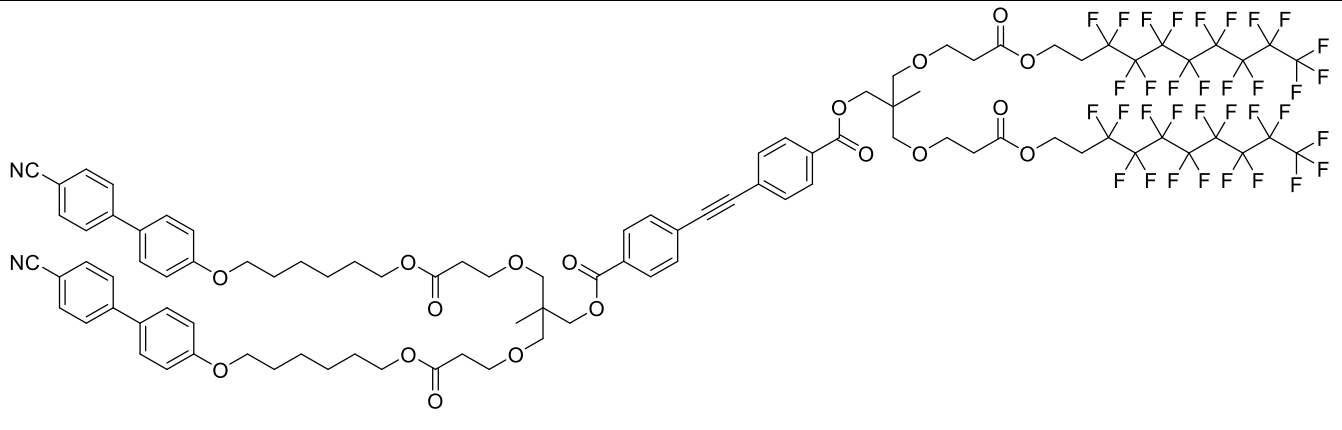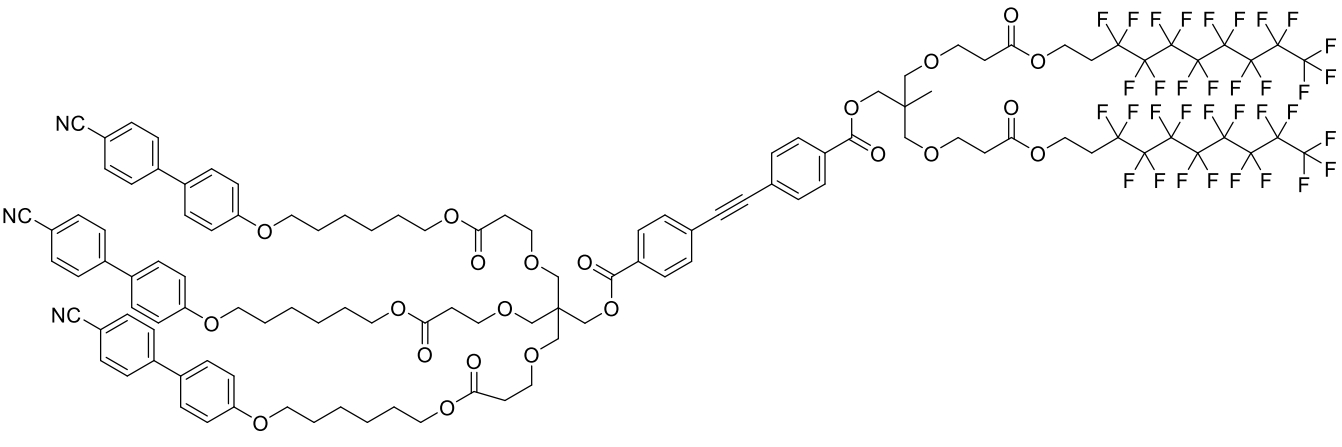
103		Cr 108.6 Iso °C
113		Cr 42.5 SmA 50.0 Iso °C
109		Cr 102.4 (Col$_X$ 75.1) Iso °C
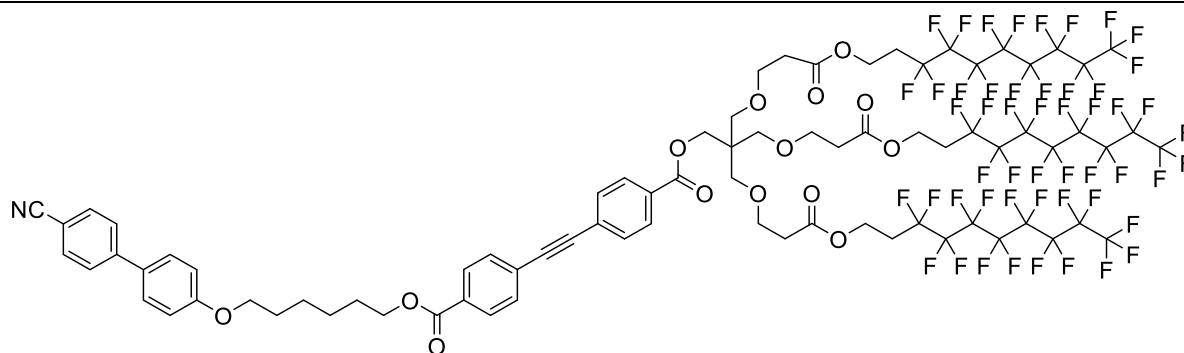
Table 13. Family of Janus cyanobiphenyl:perfluoroalkyl highly branched compounds.

Compound number	Chemical structure	Transition temperatures /°C
104		Cr 56.2 SmA 114.7 Iso °C
105		Cr 55.0 SmA' 80.1 SmA 110.6 Iso °C
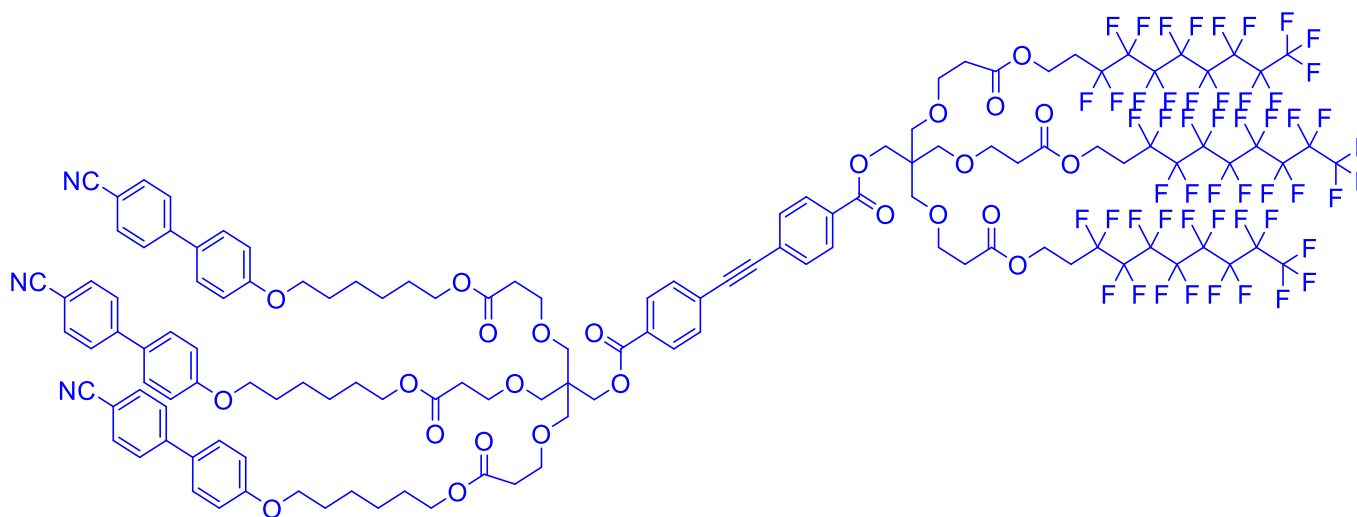
| 114 | | Cr 49.0 Colr 56.8 X 65 SmA 171 Iso °C |
| 107 | | Cr 91.2 SmA 130.6 Iso °C |
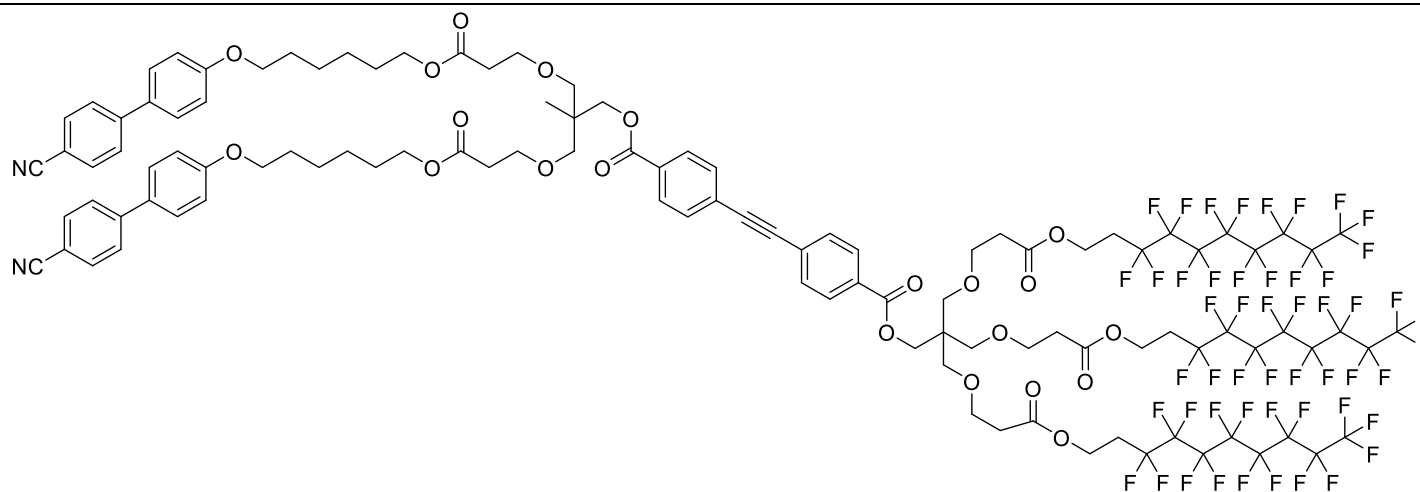
5.3 Liquid crystal properties

With the chemical characterisation of the *Janus* diphenyl acetylene materials having been detailed in section 5.2 the liquid crystal properties of these compounds will now be discussed in detail. The discussion in this chapter builds upon ideas introduced in the previous chapters for the intermediates and symmetrical bimesogens. Materials which were produced and characterised by Ma offer direct comparison with the materials presented in this chapter.[3] The compounds in this work and those produced by Ma comprise of many configurations of cyanobiphenyl and perfluoroalkyl chains affixed to the diphenyl acetylene core.

Figure 91 shows a simplified, visual representation of the distribution of materials discussed in this work. The X axis shows the total number of chains/mesogenic units attached to the diphenyl acetylene core, and the Y axis shows the mismatch in the number of chains attached to different sides of the core. The difference in number of chains has been given a value between two and minus two, whereby positive numbers represent an excess of cyanobiphenyl mesogens, and negative numbers representing an excess of alkyl or perfluorinated chains. Due to the number of materials discussed and the interrelationships between these materials families have been grouped and these groups are shown by colour coding. The distinction between groups can easily be blurred and this is intended solely as a tool to help convey the trends which have been identified.
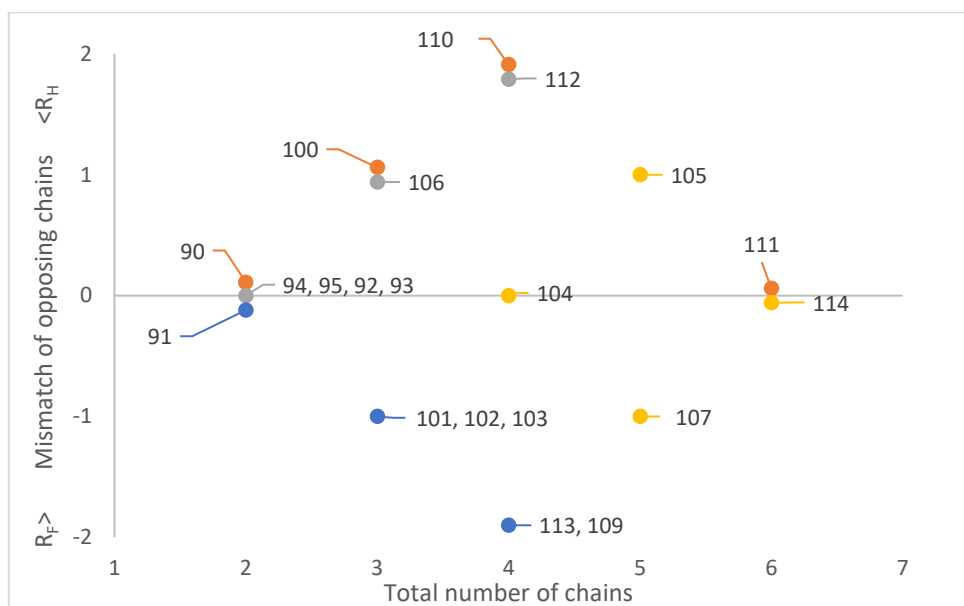
Compound number	Cartoon representation	Compound number	Cartoon representation
90		100	
111		111	
94		95	
92		93	
106		112	
91		101	
102		103	
109		113	
104		105	
107		114	

Figure 91. Simplified table and chart showing the structural factors of the Janus diphenyl acetylene families. **i) Orange**: *Janus cyanobiphenyl:alkyl compounds (section 5.3.1),* **ii) Grey**: *Janus cyanobiphenyl:perfluoroalkyl compounds (section 5.3.2),* **iii) Blue**: *Janus perfluoroalkyl:alkyl and perfluoroalkyl:cyanobiphenyl compounds (section 5.3.3),* **iv) Yellow**: *Janus cyanobiphenyl:perfluoroalkyl highly branched compounds (section 5.3.4).*

5.3.1 *Janus* cyanobiphenyl:alkyl diphenyl acetylenes.

Analysis of these compounds begins with examination of the simplest case, the alkyl *Janus* materials with an increasing number of cyanobiphenyl mesogens compounds **90**, **100**, **110** and **111**. In this case the behaviour of the diphenyl acetylenes can be discussed as dimers and oligomers, in comparison with the symmetrical diphenyl acetylene trimers described in Chapter 4. Transition temperatures and mesophase types were determined by polarised optical microscopy and DSC.

Table 14. Transition temperatures, enthalpies and entropies of transition of alkyl cyanobiphenyl compounds. $ = reported by Ma.[3]

Compound number	Transition	T /°C	ΔH / kJ mol^{-1}	ΔS / J K^{-1} mol^{-1}
90	Cr – N	75.0	25.0	70
	N – Iso	79.6	0.6	2
100	g – N	-8.2	-	
	N – Iso	49.5	1.5	5
110	g – N	-0.2	-	-
	N – Iso	56.2	1.4	4
111	Cr – X	30.1	28.4	94
	X – SmA	36.9	2.7	9
	SmA – Iso	49.7	5.1	16
48	g – N	-11.4	-	-
	N – Iso	9.1	0.9	3
44	g – N	-13.6	-	-
	N – Iso	13.9	0.8	3
57$	g – SmA	1.7	-	-
	SmA – N	33.7	0.7	2
	N – Iso	37.1	0.4	1
53$	g – SmA	2.0	-	-
	SmA – N	* Broad	-	-
	N – Iso	43.9	6.7	21

The mono and di-cyanobiphenyl compounds (**90** and **100**) attached to the pentyl diphenyl acetylene both exhibit nematic phases as shown in the photomicrographs in Figure 92. The nematic phase was confirmed by the streaky marbled texture for compound **90** and by the predominantly homeotropic texture shown for compound **100**. Upon shear stress a highly birefringent texture appeared before relaxing back to the homeotropic texture. As the number of cyanobiphenyl units increased branched

compound **100** did not recrystallise on cooling and instead it formed a nematic glass. The suppression of crystallisation for branched materials is common due to the increased disorder brought about by branched architectures. The two cyanobiphenyl units and the diphenyl acetylene core may be tethered together in many possible orientations both suppressing crystallisation and reducing the clearing point of the nematic phase. This behaviour was confirmed by DSC (Figure 93).
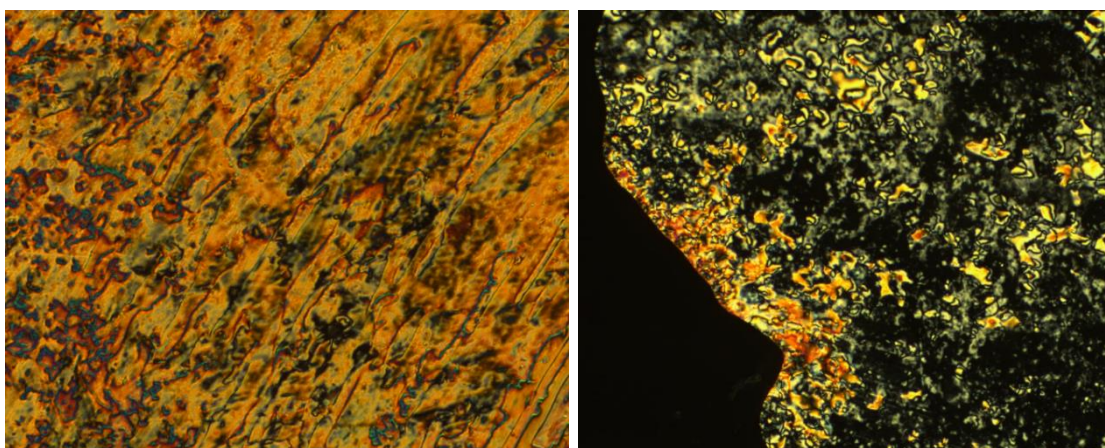
*Figure 92. Photomicrographs (x100 magnification) of the nematic phase of **90** (left, 73.5 °C) and the predominantly homeotropic nematic phase of **100** (right, 41.9 °C)*
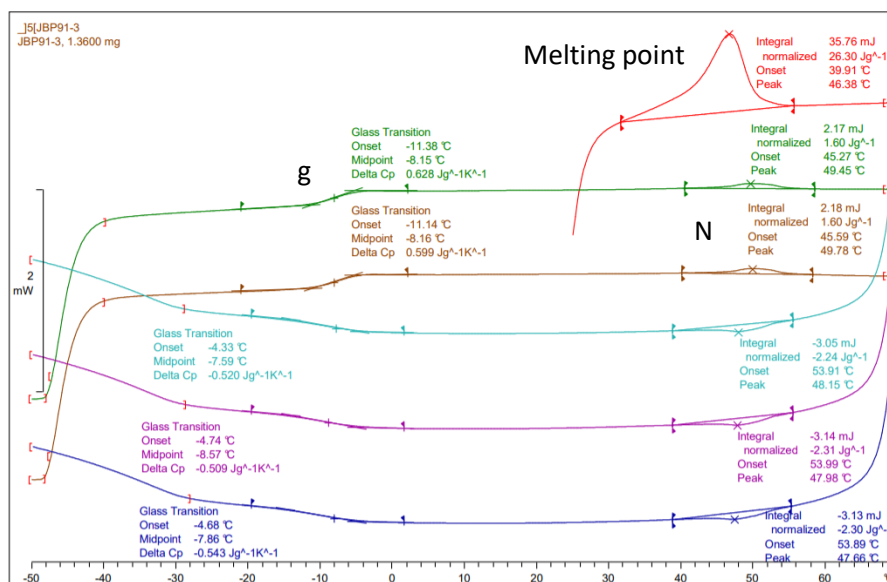
*Figure 93. DSC trace of compound **100** showing a second order transition to a nematic glass upon cooling.*

In trying to understand the role of each component unit in the molecules it is possible to look at the properties of the intermediates such as **33ᵢ** discussed in Chapter 3, and compare them to the resulting diphenyl acetylenes. Compound **33ᵢ** which is used for

the synthesis of **90** is not liquid crystalline while compound **90** possesses an enantiotropic nematic phase. This is clearly due to the extension of the phenyl acetylene of **33ᵢ** to a diphenyl acetylene core in **90**. This acts as a weak mesogen and due to this the material may be considered dimesogenic.

The diphenyl acetylene core possesses more polarisable electrons than the phenyl acetylene of **33ᵢ** and as such intermolecular interactions such as π-π interactions are stronger. In the case of compound **90** there is a weak +I effect introduced by the alkyl chain opposite a -M ester linking group giving a weak dipole which may be able to pair to provide quadrupolar interactions. The behaviour of this material alone is not of particular interest however as the material most closely resembling the classical rod-like liquid crystal design it does allow for the effect of several structural elements of the more complex materials to be explained.

The introduction of branching in these compounds sharply decreases transition temperatures with reduction in the clearing point. Examination of compound **100** reveals that recrystallisation is suppressed and this results in the formation of a glass ($\Delta Cp = 0.6$ J g^{-1} K^{-1}). Contrastingly, further increasing the number of cyanobiphenyl mesogens provides compound **110** for which additional stabilisation of the nematic phase increases the clearing point compared to compound **100**. Clearly increasing the number of mesogens via branching comes at the cost of moving away from the traditional rod-like structure and introducing a high degree of disorder (Figure 94). The flexibility around the 1,1,1-tris(hydroxymethyl) ethane branching unit means that the actual conformation of the material within the mesophase is unknown. For ease of visualisation these compounds have been drawn to place all the cyanobiphenyl units on one side of the diphenyl acetylene close to each other in space. However, in the mesophase they may easily splay outwards or more accurately be in equilibrium between the many possible orientations. Compounds of unusual shape have been observed to exhibit a nematic phase. Indeed, T-shaped liquid crystal dimers where one mesogen is attached side-on to the core of a second mesogenic unit have exhibited nematic phases.[8] Amphiphilic oligomers derived from a pentaerythritol core exhibiting more exotic phase sequences have been reported.[9] The amphiphilic nature provides different intermolecular interactions between the multiple branches, therefore a more ordered mesophase structure is required to maximise the positive interactions.

This is discussed in more detail in the discussion of perfluoroalkyl *Janus* diphenyl acetylenes (5.3.2).
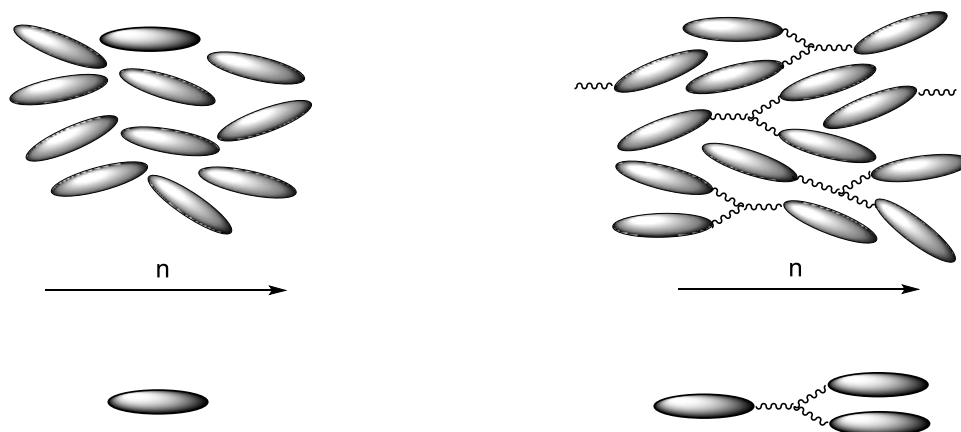
Figure 94. (Left) single rod-like mesogenic cores self-organise into a nematic mesophase by sharing orientational order. (Right) The three cores of a branched molecule may be orientated in many ways with regards to each other, and still share orientational order with other molecules to give a nematic phase.

The interplay between additional stabilisation and increased disorder is a recurring theme throughout these materials. With the addition of a third branched chain and cyanobiphenyl mesogen the glass transition temperature increases alongside the clearing point indicating the additional branching is more readily tolerated. A similar yet exaggerated trend is seen in the phenyl acetylene intermediates (Chapter 3), however while the phenyl acetylene **53** was reported to show both a columnar and smectic A phase, these mesophases are suppressed in favour of the nematic in **110**. This was rationalised by Ma as the longer diphenyl acetylene arm of the branched structure can disrupt the antiparallel arrangement that would be expected for the smectic phase of a tapered molecule, thereby forcing a more disordered mesophase organisation.[3]

A final compound introduced for comparison is the gallate derivative **111** reported by Ma.[3] The gallate structure allowed for a simple route to introduce multiple alkyl chains in addition to multiple cyanobiphenyl units for comparison with compounds **100** and **110**. Compound **111** possessed a smectic A phase unlike the nematic phases observed for the other branched cyanobiphenyl:alkyl diphenyl acetylenes **100** and **110**. The key theme investigated in this work is the effect of varying the volumes of chains on each side of the rigid core to vary the interfacial curvature. Therefore, this smectic

behaviour could be attributed to diminished curvature amongst the layers when equal numbers of chains are present on each side of the rigid core. However, although the number of chains has been balanced, the decreased structural flexibility of the gallate unit would also be expected to promote smectic layering with either interdigitated cyanobiphenyl units or alkyl chains at the interface. The alkyl chains extending from the gallate unit have less structural flexibility than chains branching from the pentaerythritol derived units. In addition, the diphenyl acetylene core is extended by an additional benzoate unit which further increases the intermolecular interactions experienced by the rigid core unit promoting smectic behaviour.

5.3.2 *Janus* cyanobiphenyl:perfluoroalkyl compounds.

The second group of compounds that will be discussed together begin to incorporate perfluoroalkyl chains into the structure. In this way two classes of intermolecular interactions are introduced (Figure 87) and both must be considered to accurately explain the liquid crystal properties of the materials. The transition temperatures, enthalpies and entropies of transition are presented in Table 15. These compounds include one or more cyanobiphenyl mesogens and only a single perfluorinated chain and as such the behaviour is still largely influenced by the cyanobiphenyl mesogenic units in a similar fashion as described for the alkyl equivalents in section 5.3.1. The monotropic smectic A to smectic C transition of **94** and smectic A to nematic transition of **93** were not observed by DSC. The enthalpy and entropy of transitions of compound **112** were broad and were not reported by Ma.

Compound number	Transition	T /°C	ΔH / kJ mol^{-1}	ΔS / J K^{-1} mol^{-1}
94	Cr – SmA	150.1	60.9	144
	SmA – Iso	151.3	5.1	12
	(SmC – SmA)	142.1	-	-
95	Cr – Iso	90.3	33.4	97
	(SmA – Iso)	71.6	1.2	3
106	Cr – SmA	59.8	11.1	51
	SmA – Iso	62.0	5.9	18
112$^\$$	g – Col	4.8	-	-
	Col – SmA	59.5	*	*
	SmA – Iso	60.7	*	*
90	Cr – N	75.0	25.0	70
	N – Iso	79.6	0.6	2
92	Cr – Iso	77.9	51.0	145
	(N – Iso)	64.1	0.1	0.3
	(SmC – N)	52.2	0.1	0.3
93	Cr – N	92.6	55.8	152
	N – Iso	108.5	5.7	15
	(SmA – N)	84.7	-	-

The introduction of a perfluorinated chain in the simple 1:1 linear dimesogen **94** gives rise to a smectic A phase and a monotropic smectic C phase, as shown in Figure 95.

*Figure 95. Photomicrographs (x100 magnification) of **94** showing the focal-conic texture of the smectic A phase (left, 150.8 °C) and tilt domains within the focal conic domains of the smectic C phase (right, 143.2 °C).*

The introduction of branching and an increase in the number of cyanobiphenyl units of **106** led to a reduction in the clearing point but the smectic A character was retained (Figure 96). This increase in the cyanobiphenyl content also led to the loss of the smectic C phase. The increased structural complexity due to the addition of a branching point for the attachment of the cyanobiphenyl units increased the viscosity of the smectic A mesophase of **106** compared to that of **94** and the compound required annealing to elucidate the focal conic texture of the smectic A mesophase which is shown in Figure 96. In contrast, the nematic mesophase of compound **100** did not become noticeably more viscous due to the presence of branching. The viscosity changes are explained by two factors, firstly in the more disorganised nematic phase of **100** reorganisation of a molecule is less disruptive than in the smectic mesophase of **106**. However, comparison of compounds **106** and **94** show that as more mesogenic units are linked by chemical bonds their freedom of movement is restricted and therefore the viscosity increases. This behaviour is seen through the branched *Janus* materials and is common for systems such as polymers.

Figure 96. Photomicrograph (x100 magnification) of the focal-conic texture of the smectic A phase of ***106*** *after annealing at 47 °C.*

In order to determine if the phase behaviour of compound **94** was driven by the presence of the fluorinated chain or simply due to the increased terminal chain length, alkyl compound **92** was prepared. Compound **92** showed a nematic phase with a clearing point almost 80 °C lower than compound **94**. An additional method to increase the order in the mesophase was to increase the length of the alkyl spacer between the

cyanobiphenyl and diphenyl acetylene units to give compound **93**. This allowed for the motions of the two cores to be decoupled and the transition temperatures increased. Compound **93** exhibited both a nematic and a smectic phase. In the nematic phase the molecules tended to orient parallel to the glass surface and gave rise to a planar nematic texture. Upon cooling it produced an unusual blocky smectic texture as though it were aligned planar to the surface (Figure 97, left). From this texture it was not possible to conclude whether this was a smectic A or smectic C phase. However, in areas of the sample which were not constrained by the slide and coverslip it was clear that a smectic A phase was evident as confirmed by the presence of a focal conic texture containing elipse and hyperbola defects alongside homeotropic domains (Figure 97, right).

*Figure 97. Photomicrographs (x100 magnification) of **93** showing the blocky smectic texture upon cooling from the nematic phase, (left, 82.8 °C) and the smectic A focal conic texture in uncovered droplets (right, 82.2 °C).*

Comparing alkyl compound **90** to compound **94** reveals that the perfluoroalkyl chain has increased the order within the mesophase to promote a smectic organisation. The origins of the fluorophobic effect are described in section 1.5.2 and a short summary given.[10] Individual C-F bonds in perfluoroalkyl chains are highly polarised due to the high electronegativity of the fluorine atom. However, as the perfluoroalkyl chain is saturated the dipoles of the individual C-F bonds are effectively cancelled out, resulting in no overall dipole. In contrast to alkyl chains, the highly polarised C-F bonds ensure that the perfluoroalkyl chain are not polarisable and therefore the Van der Waals forces are minimal. This results in microphase segregation of perfluorinated and alkyl units in order to maintain the Van der Waals interactionsof the alkyl chains.

Since the length of the alkyl and perfluoroalkyl chains of **94** and **90** are unequal compound **92** featuring a decyl alkyl chain allows for a more complete comparison between the two. The first set of comparisons to be made is between **90** and **92**. Upon increasing the terminal chain from pentyl to decyl the clearing point drops by 15.5 °C. In addition, the longer terminal chain introduces a monotropic smectic C phase.

Since the length of the alkyl and perfluoroalkyl chains are equal in compounds **94** and **92** respectively, it allows the effect of the interactions of the perfluoroalkyl chain to be isolated. In addition to the change in polarity, perfluorinated chains are known to be more rigid than alkyl chains due to the larger size of fluorine atoms. These factors combine to favour the formation of smectic phases in order to allow the perfluorinated chains to microphase segregate. The increase in the number and strength of interlayer interactions sees a smectic phase in the perfluorinated compound versus a nematic phase in the alkyl analogue. Both compounds exhibit monotropic smectic C phases.

Compound **93** was produced to compare with compound **92** using an extended undecyl spacer to stabilise the mesophase rather than including a perfluorinated chain. Increasing the length of the spacer allows for effective decoupling of the two mesogenic units which stabilises the nematic phase to be enantiotropic. Both materials also show monotropic smectic phases with the longer alkyl spacer promoting smectic A behaviour, while the shorter spacer provides a smectic C phase. This can be tentatively attributed to the relative freedom of the two halves to organise themselves within the mesophase. In the more constrained **92** featuring a shorter spacer the smectic phase shows additional order due to tilting while this is not required in the smectic A phase of **93**. As these phases are monotropic and occur far below the melting point additional studies *via* the synthesis of additional compounds is not appealing.

Comparison between **93** and **78** (Chapter 4), has several small disparities however the ~100 °C difference in clearing points is still instructive. The additional mesogen of **78** will provide additional interactions to help stabilise the mesophase when compared to the alkyl chain in **93**, however the symmetry of the molecules also changes. In a second example both **78** and **100** possess the diphenyl acetylene core and two cyanobiphenyl mesogens however show nearly 150 °C difference between the clearing points. Therefore, it is clear that the molecular architecture, as well as the number of

mesogens is key to the liquid crystal properties. The symmetrical linear oligomers have much higher transition temperatures as the increased symmetry allows them to pack more easily while maximising the intermolecular interactions.

The extended spacer incorporated in **95** was designed to mimic the branching unit used to vary the number of mesogens in compounds such as **104**. Instead of having branching units attached by alkyl chains the spacer contains two lateral methyl groups. These groups would be expected to reduce the stability, and transition temperatures of the mesophase as lateral chains are known to disrupt the packing and intermolecular interactions. Comparison of **95** and **94** show that this is observed, and the transition temperatures are decreased substantially with the mesophase becoming monotropic. Due to the presence of the perfluorinated chain the smectic A phase is preserved despite the presence of branched methyl units and the lengthened, flexible spacer.

Compounds **94, 95**, **106** and **112** in Table 15 can be used to examine the role of branching. Compounds **94** and **106** differ by the introduction of the branching unit and an additional cyanobiphenyl mesogen. In this case the introduction of branching reduces the transition temperatures by around 90 °C, however the smectogenic perfluorinated unit maintains a periodic structure. As discussed in section 5.3.1 the two-dimensional drawings of these materials may not accurately reflect the structure within the mesophase. However, due to the lower cohesive energy density of the perfluoroalkyl chains, tapered conformations are encouraged, as these conformations more easily realise microphase segregation of the perfluorinated units within the mesophase structure.[11,12] Structural inspection of **106** and **95** shows that in **106** the spacer to the perfluoroalkyl chain is reduced, and one methyl unit is replaced by a cyanobiphenyl substituted chain. The transition temperatures of **95** are higher than **106** indicating the disorder induced by the branched cyanobiphenyl unit is greater than the additional stabilisation it provides. In addition, this suggests that the negative effects of the branched methyl unit found in 1,1,1-tris(hydroxymethyl) ethane unit can be overlooked as minimal in comparison with mesogenic chains. In the case of **112** previous POM studies observed textures of both the smectic A and hexagonal columnar phases.[3] This was rationalised by the microphase segregation of the perfluorinated chain giving a pronounced tapered shape. At higher temperatures, the

chains have enough flexibility to pack in a rod-like fashion, however when cooled the chains stiffen and the shape becomes more wedge like giving a columnar mesophase. Increasing the branching multiplicity of the cyanobiphenyl mesogens from 2 in compound **106** to 3 for compound **112** has little effect upon the clearing point, however, does suppress crystallisation. The glass obtained reflect both the disordered nature of the branching unit and expected viscosity of the columnar mesophase both inhibiting crystallisation. The smectic A mesophase is consistently observed, despite the changes in interfacial curvature expected. This shows that different mesophase structures are tolerated within the smectic A phase as investigated by X-ray diffraction studies in section 5.4.

5.3.3 *Janus* perfluoroalkyl:alkyl compounds.

A second group of perfluoroalkyl containing compounds have been selected in which the perfluoroalkyl unit(s) are expected to dominate the phase behaviour. These compounds were characterised by POM and DSC and the transition temperatures, enthalpies and entropies of transition are presented in Table 16.

Table 16. Transition temperatures, enthalpies and entropies of transition of perfluoroalkyl:hydrocarbon materials. $ = reported by Ma.[3]

Compound number	Transition	T /°C	ΔH / kJ mol^{-1}	ΔS / J K^{-1} mol^{-1}
91	Cr – SmA	111.9	42.4	110
	SmA – Iso	124.2	2.7	7
101	Cr – Iso	77.4	53.9	154
102	Cr – Iso	106.4	17.1	45
103	Cr – Iso	108.6	23.6	61
113$^\$$	Cr – SmA	42.5	28.1	89
	SmA – Iso	50.0	12.0	37
109	Cr – Iso	102.4	143.0	381
	(Col – Iso)	75.1	1.0	3

The simplest of these partially perfluorinated materials **91** featured a perfluoroalkyl chain and a pentyl chain attached either side of the diphenyl acetylene core. This compound exhibited an enantiotropic smectic A mesophase (Figure 98) as characterised by the focal conic texture featuring ellipse and hyperbolae defects and domains of homeotropic alignment
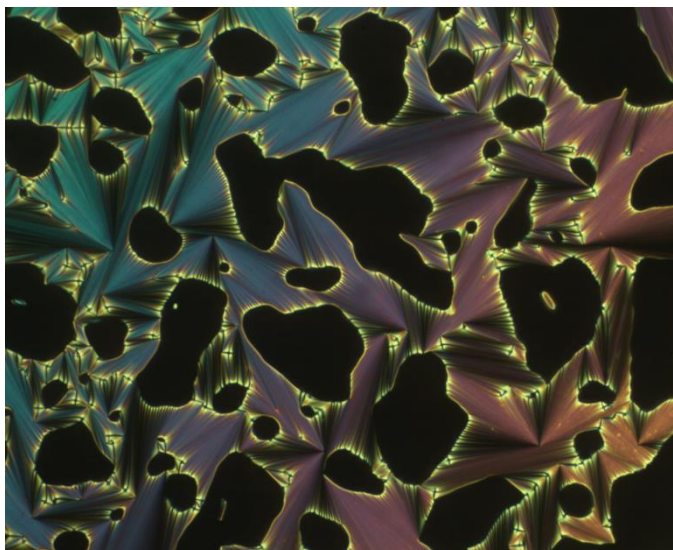
*Figure 98. Photomicrograph of **91** (x100 magnification) after annealing at the clearing point showing the focal-conic texture of the smectic A phase and regions of isotropic material (112.5 °C).*

Interestingly when two perfluroalkyl chains were attached opposite a single chain (**101** – **103**) no liquid crystalline mesophases were observed. Liquid crystallinity was recovered for the compounds with three perfluoroalkyl chains and a single alkyl or cyanobiphenyl unit such as **113** reported by Ma[3] and **109** with three perfluoroalkyl chains and a single cyanobiphenyl unit which gave a fan-like texture indicative of an unidentified columnar mesophase (Figure 99).
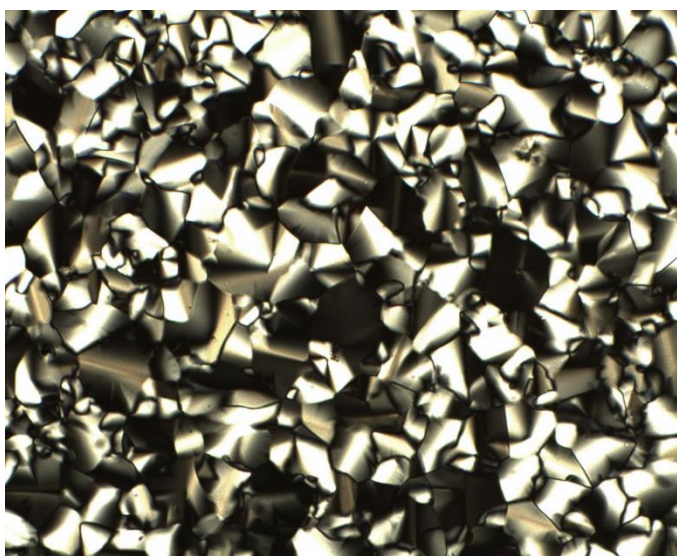
*Figure 99. Photomicrograph (x100 magnification) of **109** showing the texture of the columnar phase (73.6 °C).*

The smectic A mesophase of **91** is relatively narrow, however the clearing point is higher than that of the cyanobiphenyl analogue **90**. This reflects the smectogenic nature of the perfluoroalkyl chain requiring periodic structures to maximise intermolecular interactions. The mesophase structure of the smectic A phase has been analysed by X-ray diffraction (section 5.4) and is reliant on two complementary effects. The traditional calamitic shape of the diphenyl acetylene core contains many polarisable electrons providing π-π interactions with neighbouring molecules. This is sufficient to stabilise liquid crystallinity in some alkyl diphenyl acetylene materials.[13] In addition, the perfluoroalkyl chains must be segregated from the remaining alkyl units – this provides liquid crystallinity and increases overlap between the diphenyl acetylene cores.

Compound **115** (Figure 100) has a similar structure to **91** albeit with a shorter perfluoroalkyl chain and a terminal chlorine atom. The authors claim the chlorine increases the stability of smectic C phases by increasing polarisability.[14] It is also noted that the ether linkage of the alkyl chain to the diphenyl acetylene unit provides a greater electron donating effect (+M effect), increasing polarisability when compared to **91**. The transition temperature of **115** is slightly reduced which can be attributed to the shorter perfluoroalkyl chain. The same perfluoroalkyl chain (1H,1H,2H,2H-perfluoro-1-decanol) featured in compound **91** has been used throughout this project, comparison of compound **115** and **91** can be used to suggest shortening the perfluoroalkyl chain would reduce the stability of the liquid crystal phases obtained.

115
Cr 95.4 SmC 103.0 SmA 115.5 Iso °C
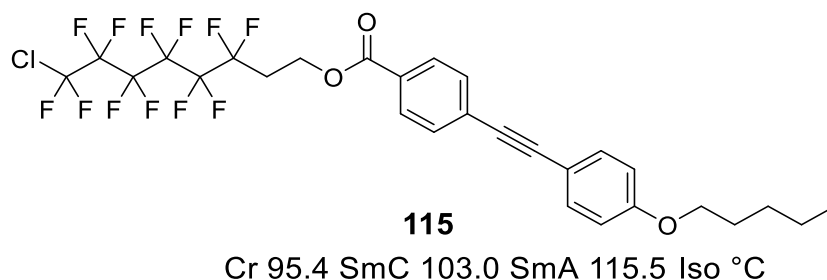
*Figure 100. Compound **115** featuring a perfluoroalkyl chain with terminal Cl atom reported by Yang.[14]*

In a bid to understand how microphase segregation drives self-assembly it is possible to consider compounds **116a** – **116c** which were described by Percec (Figure 101).[15] Compound **116a** featuring a nitrile group exhibited a narrow smectic A phase. Due to the use of a single phenyl rather than diphenyl acetylene ring system there are less

polarisable electrons and so the presence of a nitrile group is less effective at stabilising a mesophase. Nonetheless considering the quadrupolar interactions available compound **116$_a$** can pack in an antiparallel arrangement analagous to that suggested for compounds **94** and **91** (X-ray section 5.4). The use of shorter perfluorinated chains was investigated and again found to be less effective at stabilising a mesophase as observed for compound **115** in Figure 100. The presence of a benzyl alcohol lacked sufficient interactions to provide an enantiotropic mesophase, however the use of a carboxylic acid in **116$_b$** provided a highly stable mesophase. **116$_c$** possesses far higher transition temperatures due to its ability to form a hydrogen bonded dimer. The hydrogen bonded benzoic acid cores can be considered a tricyclic ring system with perfluoroalkyl terminal chains on each side. Symmetrical cyanobiphenyl substituted diphenyl acetylenes were reported in Chapter 4, however no symmetrical perfluoroalkyl materials were produced in this work. Compound **116$_c$** indicates a similar trend would be expected giving a considerable increase in the transition temperatures when compared to compound **91**.
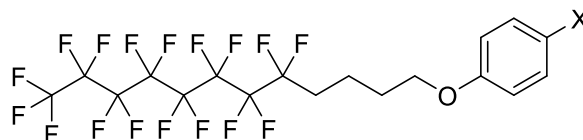
116$_a$ = CN, Cr 72 SmA 73 Iso °C
116$_b$ = CH$_2$OH, Cr 91 (SmA 81) Iso °C
116$_c$ = CO$_2$H, Cr 165 SmX 178 SmC 190 SmA 193 Iso °C

Figure 101. Perfluorinated/hydrocarbon diblock compounds reported by Percec.[15]

Upon increasing the number of perfluorinated chains it was expected that this would enhance the smectic self-assembly. Instead compounds **101**, **102** and **103** were not liquid crystalline. The previously described trend whereby introducing a branching and additional mesogenic unit decreased the transition temperatures was also apparent by comparison of compounds **91** and **101** as well as **95** and **102**. Due to the crystalline nature of the perfluorinated chains compound **101** did not form a glass as observed for the cyanobiphenyl analogue compound **100**. This crystalline character prevents the observation of monotropic mesophases as the samples crystallised before a mesophase could occur. Due to this compound **103** was synthesised using the 2,2,-dimethyl-1,3-propanediol derived branching analogue in an attempt to suppress

crystallisation. However the melting point was largely unchanged and in fact increased slightly and therefore no liquid crystalline behaviour could be observed. A possible explanation for the lack of liquid crystallinity for these materials is shown in Figure 75. This suggests that the two fluorinated chains emerging from the tetrahedral centre may be planar to each other which results in the remaining chain projecting above or below this chain and disrupting the packing.

Interestingly increasing the number of perfluoroalkyl chains to three, as for compound **113**, recovers liquid crystallinity. Compared to the simple 1:1 diphenyl acetylene **91** the melting point and clearing point are both significantly lower in temperature. Indeed, the melting and clearing points of **113** are lower than that of **103** with fewer perfluoroalkyl chains. A similar trend was observed for the intermediates **53** and **58** described in chapter 3, whereby three mesogenic units are required to stabilise a smectic A phase. In order for these compounds to exhibit a smectic A phase an antiparallel arrangement of molecules within the mesophase structure would be essential in order to both efficiently fill space and allow for microphase segregation. The proposed mesophase structure of compound **113** is shown in section 5.4.

Since **101** was found to be non-liquid crystalline while **113** exhibits a smectic A mesophase, miscibility studies were used to determine a virtual clearing point for **101**. **101** and **113** were mixed together at different concentrations and the proportions of each compound in the mixture is given in Table 17. Transition temperatures were determined by POM and the results are plotted in Figure 102. In mixtures comprising of 60 wt% or more of **113** the smectic A phase was observed while mixtures below 60 wt% of **113** were non-liquid crystalline. Ideal mixing was demonstrated and a linear extrapolation of the clearing point revealed a virtual smectic A to isotropic transition for **101** at 41.4 °C, however this is limited by the accuracy with which the broad transitions could be measured.

Mixture	**101** used / mg	**113** used / mg	Weight fraction **113**	Melting point / °C	Clearing point / °C
1	1.0	0.0	0.00	77.4	-
2	6.1	3.9	0.32	49.6	-
3	4.0	3.9	0.42	47.4	-
4	4.3	6.3	0.52	46.1	46
5	2.9	6.8	0.63	41.2	48
6	2.2	8.1	0.73	46.1	49
7	0.0	1.0	1.00	42.5	50
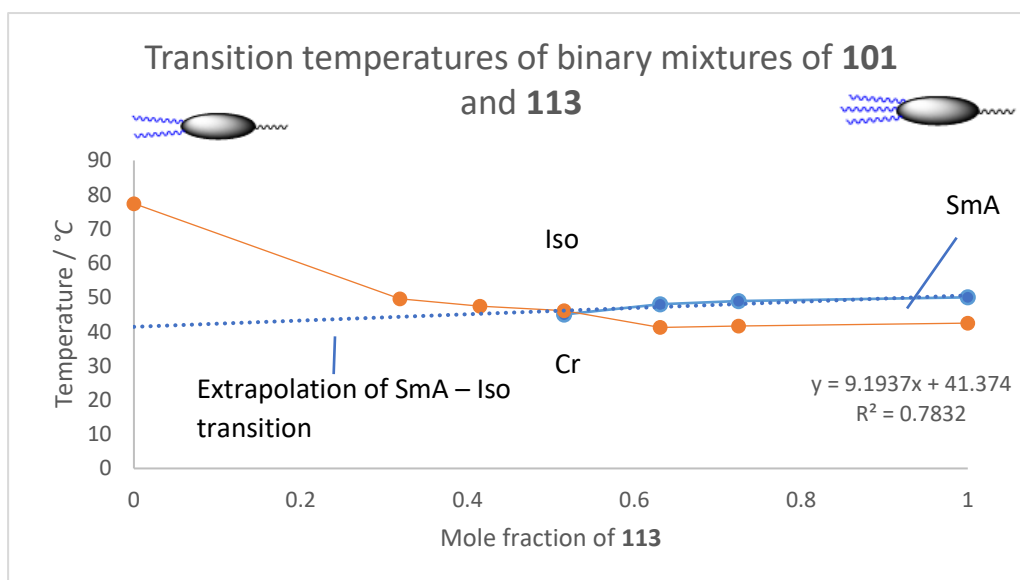
Figure 102. Plot of the transition temperatures of a range of mixtures of compounds 101 and 113.

Exchanging the short alkyl chain of **113** for a cyanobiphenyl mesogen gives rise to a columnar mesophase for compound **109**. The columnar phase indicates that molecule **109** assumes a tapered shape being driven by microphase segregation of the perfluorinated chains. This is similar to that seen in other tapered molecules[16,17] The structural factors which result in a columnar phase when a cyanobiphenyl mesogen is placed opposite the three perfluorinated chains, and a smectic phase when a pentyl chain is used are complex. It is likely that the longer chain and cyanobiphenyl mesogen is not able to efficiently pack into an antiparallel bilayer as found for **113**. In contrast, the pentyl chain of **113** would produce a greater tapered angle and so be expected to give a columnar mesophase. Therefore, the formation of a smectic phase rather than

columnar phase in **113** indicates that the antiparallel smectic arrangement is favoured when possible, and a disruption to this, such as the longer chain of the cyanobiphenyl unit in **109** is required to form columnar mesophases in these materials.

Interestingly both **109** and **112** give columnar phases while **113** and **110** do not. In both cases it is believed that the shape of the molecule does not efficiently pack within a lamellar organisation which drives the formation of the columnar phase alongside, the incompatibility of each face of the molecules. A lamellar phase formed from **109** or **112** would require chemically incompatible moieties to pack together to efficiently fill space.

The columnar mesophases of similar dendritic compounds were commonly reported by Percec featuring gallic acid derivatives related to compound **117** (Figure 103).[18] These compounds feature a similar perfluorinated chain albeit with a longer alkyl spacer than found in the perfluorinated compounds produced in this project. The largest difference between the Percec materials and those with multiple chains in this project is the shape induced by the gallate or pentaerythritol branching unit chosen. In the case of pentaerythritol the tetrahedral centre produces a three-dimensional tetrahedral shape, which is presumably enforced due to the microphase segregation of the terminal chains. Contrastingly, the aromatic gallate branching unit is initially two-dimensional, although the chains will orient themselves to fill space efficiently. This two-dimensional slice is more easily assigned to a columnar mesophase than the more three-dimensional structure reported here, however both may be seen.[12]

$F(CF_2)_8(CH_2)_4O$ ... $O(CH_2CH_2O)_4H$

$F(CF_2)_8(CH_2)_4O$

$O(CH_2)_4(CF_2)_8F$

117

Cr 35 Col$_h$ 68 Iso
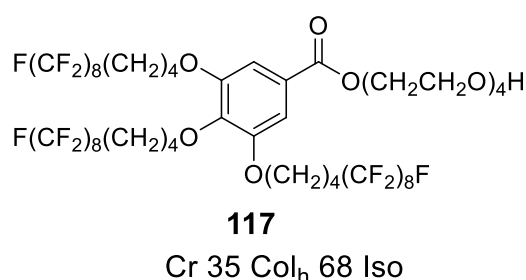
*Figure 103. Perfluoroalkyl substituted gallate derivative **117** reported by Percec.[18]*

This gallate architecture can be considered an inverted version of the cyanobiphenyl:perfluoroalkyl gallate compounds reported by Yoshizawa and discussed in the introduction (1.5.3.1). In the materials reported by Yoshizawa

cyanobiphenyl and biphenyl units stabilise liquid crystal phases opposite of the perfluoroalkyl chain however alkyl chains are not sufficient to provide liquid crystallinity (Figure 104). The closest analogue in the compounds reported here is compound **112**, for which a similar phase sequence is observed. Considering the differences in the three-dimensional structures achieved by the pentaerythritol and gallate branching units the similarity in phase sequence is interesting. The increased structural flexibility of the pentaerythritol is still expressed in the transition temperatures, as the clearing point of **112** is 100 °C lower than **21**. Interestingly substituting the cyanobiphenyl units of **21** for biphenyls in **118** gave vastly different mesophase structures. The cyanobiphenyl units provide additional quadrupolar interactions which stabilise a smectic A and cubic bicontinuous phase. Contrastingly the biphenyl units which lack a dipole provides a columnar mesophase. This indicates that the interfacial curvature and π-π interactions are sufficient to stabilise the formation of supermolecular columns, however stronger interactions result in a smectic A or Cub$_v$ mesophase. When considering the possible mesophase structures of **112**, compounds **21** and **118** must be considered. This shows that while the cyanobiphenyl interactions are not required for liquid crystallinity, or for the tapered molecular shape to be expressed upon the mesophase, the quadrupolar interactions both raise the clearing point dramatically and change the nature of the mesophase. Therefore, the cyanobiphenyl interactions should be maximised in the proposed mesophase structures. In addition, replacing the biphenyl mesogenic units with alkyl chains in **119** results in a complete loss of liquid crystallinity.

21	R =	-O(H$_2$C)$_6$O— [biphenyl] —CN	g 9.3 Cub$_v$ 135.9 SmA 155.0 Iso °C
118	R =	-O(H$_2$C)$_6$O— [biphenyl]	CrX 73.3 Col 87.9 Iso °C
119	R =	-OC$_{12}$H$_{25}$	Cr 20.1 Iso °C
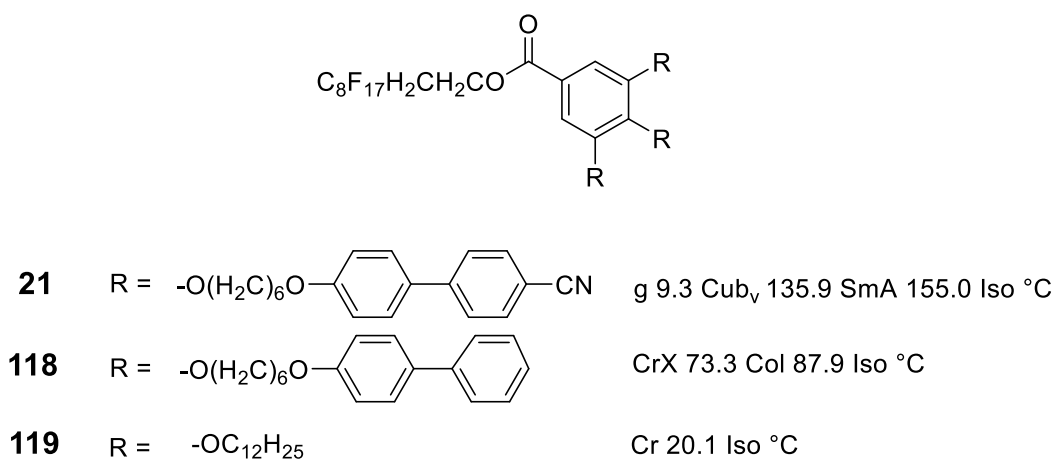
Figure 104. Perfluoroalkyl:cyanobiphenyl substituted gallate derivatives reported by Yoshizawa.

5.3.4 *Janus* cyanobiphenyl:perfluoroalkyl highly branched compounds.

The structural complexity of the materials discussed has been gradually increased by increasing the number of chains attached to each side of the diphenyl acetylene core. The family of materials described here are examples of dendritic supermolecular liquid crystals which share some physical properties with polymers such as highly viscous phases which require long periods of annealing to provide clear texture for phase identification. In many cases this is exacerbated by unexpectedly low birefringence being observed. The multiply branched compounds **104**, **105**, **114** and **107** were examined by POM and DSC. The transition temperatures, enthalpies and entropies of transition are presented in Table 18. The transition of compound **105** noted as SmA – SmA' consisted of an overlap of two transitions (see Figure 107) and so the enthalpy could not be accurately calculated.

Table 18. Transition temperatures, enthalpies and entropies of transition highly branched Janus perfluoroalkyl/cyanobiphenyl materials. $ = reported by Ma.[3]

Compound number	Transition	T /°C	ΔH / kJ mol^{-1}	ΔS / J K^{-1} mol^{-1}
104	Cr – SmA	56.2	24.9	76
	SmA - Iso	114.7	1.0	2
105	Cr – SmA'	55.0	22.4	68
	SmA' – SmA	80.1	-	-
	SmA – Iso	110.6	0.8	2
114$^{\$}$	Cr – Col$_r$	49.0	27.8	86
	Col$_r$ – X	56.8	23.2	70
	X – SmA	65	-	-
	SmA – Iso	171	1.2	3
107	Cr – SmA	91.2	58.6	161
	SmA – Iso	130.6	0.6	1

Compound **104** was annealed overnight in order to develop a texture suitable for phase identification as the domains formed were typically too small for characteristic defects to be observed. Nevertheless, the texture of **104** shown below remained poorly developed. Small regions of focal conic domains indicative of a smectic phase can be seen in the largely homeotropic texture (Figure 105). For these reasons the phase was assigned as a Smectic A phase.
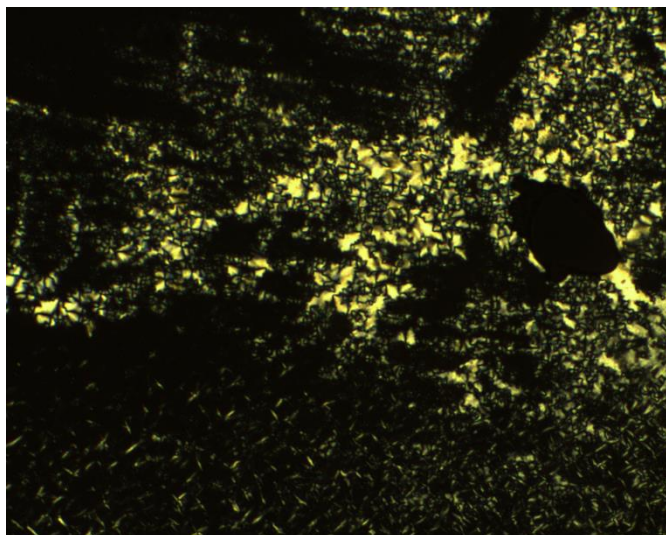
*Figure 105. Photomicrograph (x100 magnification) showing the poorly developed texture of **104** with small regions of focal-conic domains (60.0 °C).*

Compound **104** possesses roughly equal volumes of the two faces with two cyanobiphenyl units on one side of the diphenyl acetylene core and two perfluorinated chains on the opposing side. Given the equal number of chains on either side of the diphenyl acetylene unit it is unsurprising that the molecule can assume a rod-like conformation and a broad smectic A phase is evident. The cyanobiphenyl units provide a great deal of stabilisation to the mesophase due to the quadrupolar interactions enabled by an antiparallel arrangement. In addition, an antiparallel arrangement enables the perfluorinated chains to be segregated away from the alkyl regions of the molecule more easily.

Compound **105** was found to have a low birefringence phase at higher temperatures, which underwent a phase transition corresponding to a large change in birefringence upon cooling to 80 °C. Throughout the transition the texture and structure of domains remained largely similar with ellipse and hyperbola defects characteristic of smectic phases (Figure 106). The transition was reversible upon heating or cooling across the transition and relatively little deterioration of the fan-like focal conic domains were observed, however a transition into a smectic B phase cannot be ruled out. This change in birefringence is mirrored by a large reorganisation detected *via* X-ray diffraction, and the nature of the structural changes are discussed in section 5.4. The change in birefringence indicates that one or more component of the molecule which contains polarisable electrons is reorienting itself relative to the alignment of the optical axis.

214

Therefore, it is likely one or more cyanobiphenyl or diphenyl acetylene units reorienting to provide the change in birefringence. This transition is observed by DSC as a peak alongside a broad shoulder (see Figure 107) which suggests more than one transition may be simultaneously occurring, however this has not been deconvoluted to treat each transition separately.
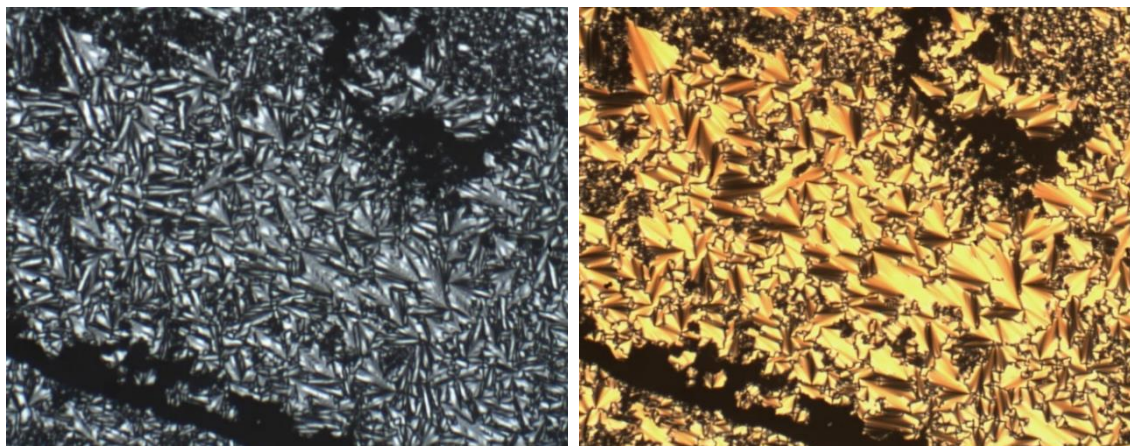
*Figure 106. Photomicrographs (x100 magnification) of **105** on either side of the smectic A (left, 91.0 °C) to smectic A' (right, 60.3 °C) transition.*
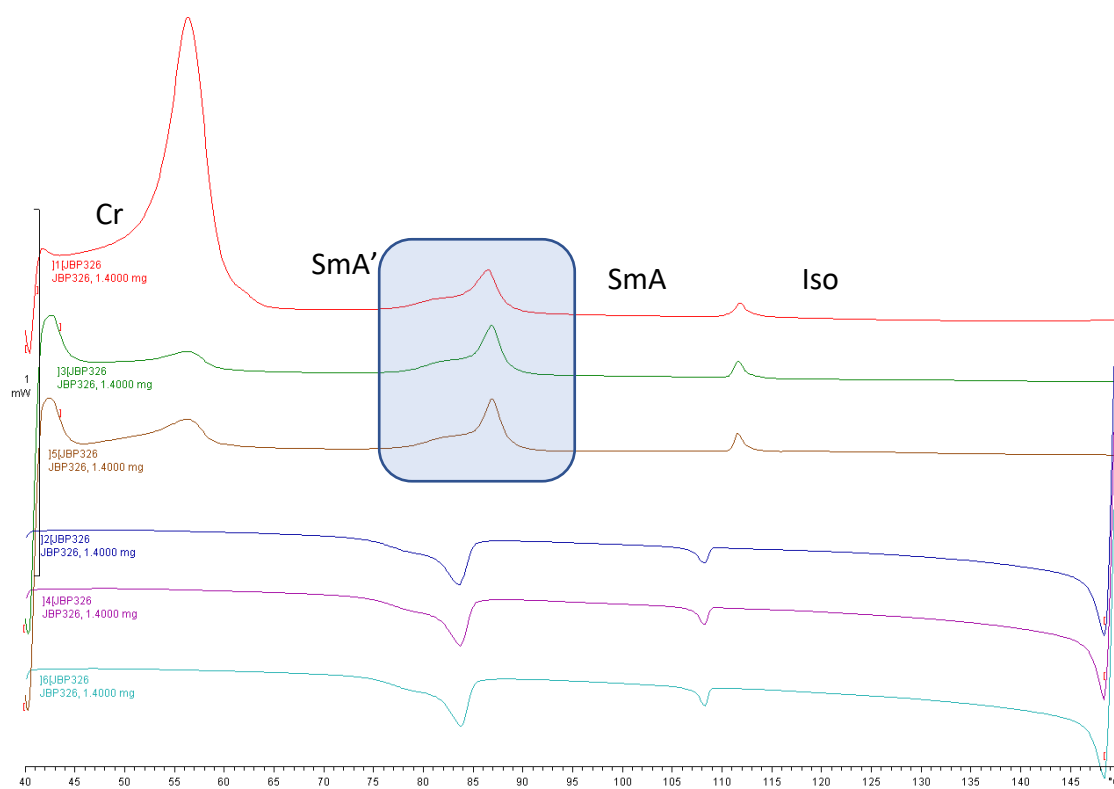
*Figure 107. DSC trace of **105**, highlighted is an area with a single clear peak and broad signal which is likely multiple transitions.*

Compound **105** has three cyanobiphenyl units on one side of the diphenyl acetylene unit and two perfluoroalkyl chains on the other opposite side. The introduction of a third cyanobiphenyl mesogen has little effect on transition temperatures relative to compound **104**, and the nature of the mesophase appears to remain somewhat similar. However, compound **105** exhibits a transition from the smectic A phase into another phase which is similar in appearance via microscopy however there is a large increase in the birefringence. By optical microscopy the nature of this lower temperature phase could not be proven and other mesophases such as smectic B phases are possible. However, X-ray diffraction studies described in section 5.4 do not show any evidence of hexagonal packing. The phase transition is first order as shown by DSC with an enthalpy change of 2.6 kJ mol^{-1}. Therefore, while the introduction of a third cyanobiphenyl unit has little effect upon the transition temperatures of **105** relative to **104** there is a significant impact upon the mesophase organisation to incorporate this additional unit. This can again be related to the equal number of chains in **104** giving a rod-like calamitic structure whereas, the wedge shape of **105** has more constraints when packing into a mesophase.

Swallow-tail like compound **120** with a pair of alkyl chains opposite a perfluoroalkyl unit has been reported and does not show microphase segregation in the smectic A mesophase structure (Figure 108).[19] These materials undergo a phase transition from smectic A layers where microphase segregation cannot be stabilised due to steric restraints, into a columnar rectangular mesophase for which the expected antiparallel arrangement is achieved. While this example shows that perfluoroalkyl units do not guarantee an antiparallel layered structure, the presence of cyanobiphenyl units in **105** provides another structural factor which favours an antiparallel arrangement.

120
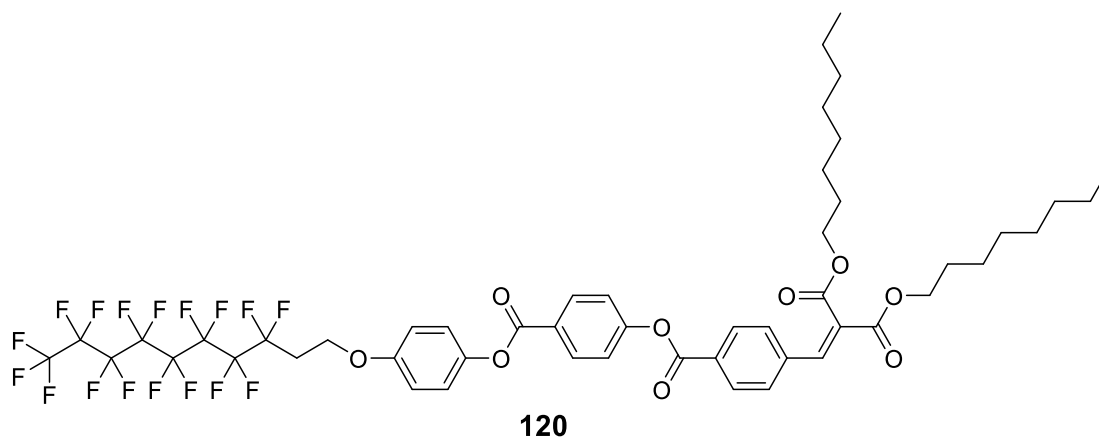
Cr 98 Col$_R$ 99 SmA 175 Iso °C

Figure 108. Swallow tail compound 120 reported by Diele.[19]

A similar core was used by Nishikawa to provide a polycatenary material **121** where microphase segregation was again not observed in the smectic A phase and more ordered mesophases are required for the perfluorinated chain to segregate (Figure 109).[20] Again this example is given to show that while chemical incompatibility can drive liquid crystalline behaviour, steric effects must also be considered and in some circumstances can overcome the fluorophobic effect. In contrast to these materials, the combination of a second perfluorinated chain and stronger intermolecular interactions between cyanobiphenyl units when compared to alkyl chains ensures that compound **105** is expected to maintain segregation in both mesophase structures. However, these materials further highlight the effects that changing the shape of each domain may have on the mesophase structure.

121
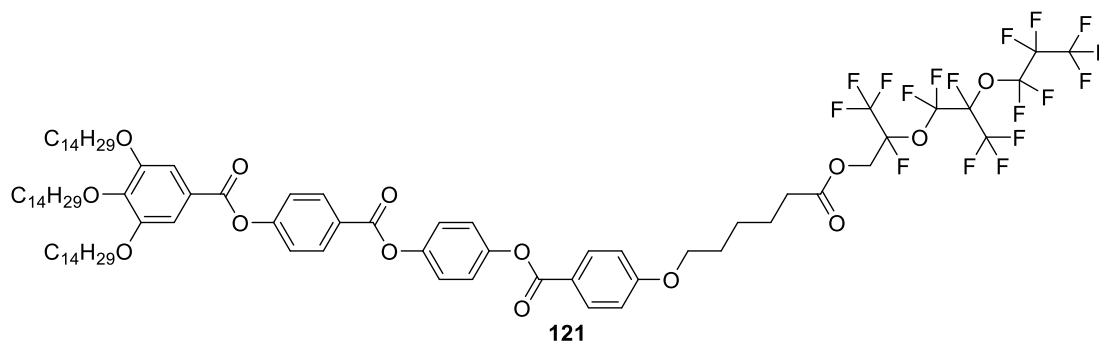
Cr 52.6 Cub 56.3 Col 94.2 SmA 115 Iso °C

Figure 109. Example alkyl:perfluoroalkyl compound 121 reported by Nishikawa.[20]

In addition to the phase transition observed between the smectic phases of **105** a similar reorganisation was reported for compound **114**.[3] A phase transition was

observed by POM and DSC which was accompanied by a drastic change in birefringence, however in the case of **114** this passed through an optically extinct mesophase structure. Subsequent X-ray diffraction experiments showed the transition to be between a higher temperature smectic A phase and lower temperature phase which was assigned as a rectangular columnar mesophase. Within the rectangular columnar phase, the molecules packed into a highly interdigitated structure which allows for the perfluorinated chains to be segregated within the structure, and accounts for the greater volume of perfluorinated alkyl chains. The greatest difference in size across the molecule is between the diphenyl acetylene core and mesogenic units on each side. Due to this difference it can be expected that the cyanobiphenyl units may overlap with the diphenyl acetylene core to more easily account for the difference in volume. Finally, it is worth noting that the melting point of **114** is again close to both **104** and **105**, however the clearing point is increased significantly as the additional mesogen stabilises the mesophase.

The final compound to be discussed is compound **107** which exhibited a low birefringence smectic A phase which was very viscous and did not spread across the slide significantly after melting. Small birefringent domains were observed around the edges of the sample where the sample underwent some stress upon cooling from the isotropic into the phase or melting from the crystal (Figure 110). Visual inspection indicated very small focal conic domains which were corroborated as evidence of a smectic A phase by X-ray diffraction (see Figure 125).
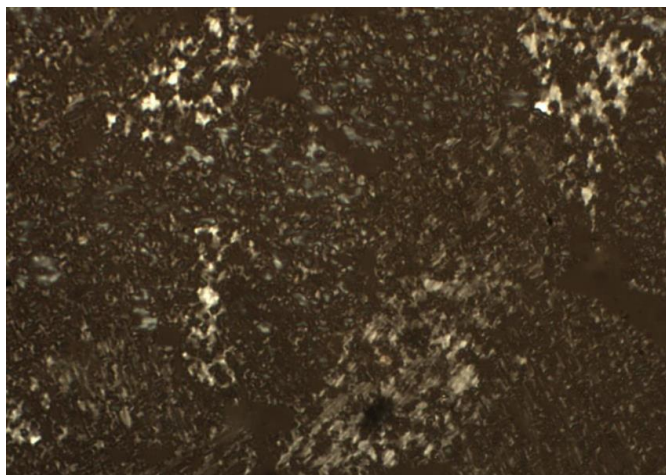
*Figure 110. Photomicrograph (x100 magnification) of **107** showing the low birefringence texture of the smectic A phase (69.9 °C).*

The transition temperatures for this compound are higher than for **104** or **105** while the role of the cyanobiphenyl mesogens is decreased, and the role of the fluorophobic effect and microphase segregation within the mesophase structure increased. While **109** gave a columnar mesophase due to the greater interfacial curvature, the addition of a second cyanobiphenyl unit reduced the tapering of the overall molecular shape and thus resulted in a smectic phase. This behaviour is paralleled within the compounds **112** and **105** and other amphiphiles where a smaller interfacial curvature or mismatch between the volume of the two faces of the material results in lamellar structures like the smectic A phase. While **105** undergoes a smectic A to smectic A' transition to more efficiently pack at lower temperatures no such transition is seen in **107**. Interestingly, the enthalpy and entropy changes upon clearing are low for compound **107** which is indicative of a fairly disordered mesophase, in some disagreement with the more ordered mesophase structure expected to achieve microphase segregation.

5.4 X-ray diffraction and mesophase structure

Selected compounds were investigated using X-ray diffraction in order to provide some insight into their mesophase structures and how the molecules self-assemble within their phases. Lamellar structures were the most prevalent within this family of compounds. However, much can be learnt about the molecular self-organisation based upon the layer spacings in the smectic A mesophase. Owing to the complex nature of the structure of these compounds the molecular length was estimated by modelling the fully extended conformation of discrete fragments and measuring their individual length, then combining the results to give the overall molecular length. The molecular length of each material was roughly estimated using Gaussian[21] via a molecular mechanics calculation with the universal force field (UFF).[22] This approach was used to find the length of the fully extended conformation of selected whole compounds and of several fragments. The lengths of the fragments are given in Table 19. The lengths of these constituent parts could be added together to approximate their contribution to the molecular length, however no attempt was made at this point to account for the three dimensional shape of the molecule.

The limitations of this approach were demonstrated *via* optimising the fully extended structures of two of the simplest compounds (**94** and **104**) using the same UFF

approach. Predictably the molecular lengths of the three-dimensional structures were shorter than the sum of the fragments. This is expected given the primitive approach used which does not accurately account for the three-dimensional structure and tetrahedral shape of the branching units. This variation was deemed acceptable as while clearly limited the approach does allow for an estimate of molecular length, and thus some identification of mesophase structure. The molecular lengths found by modelling the three-dimensional structure and sum of fragments were around 5% shorter as shown in Table 20.

Table 19. Lengths of selected fragments calculated from van der Waals radii via molecular mechanics using UFF in Gaussian.
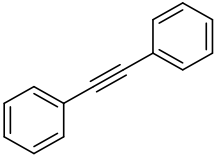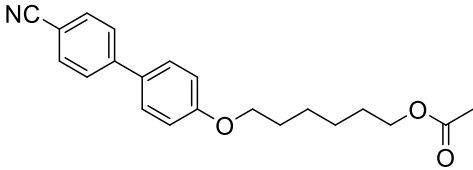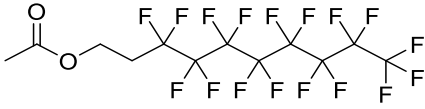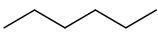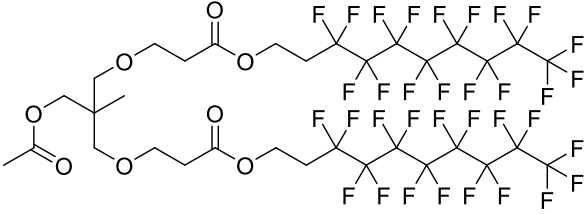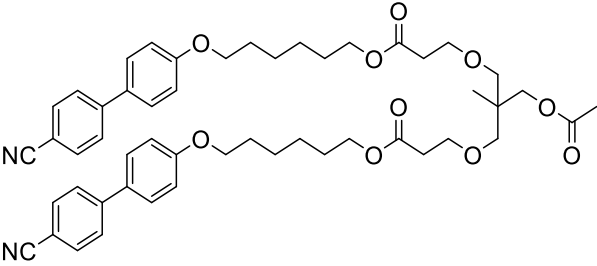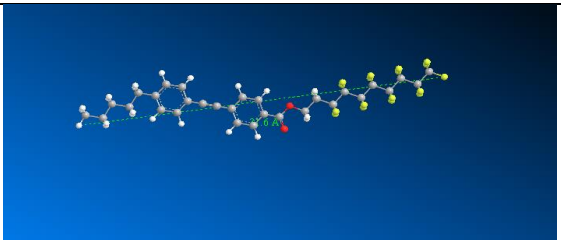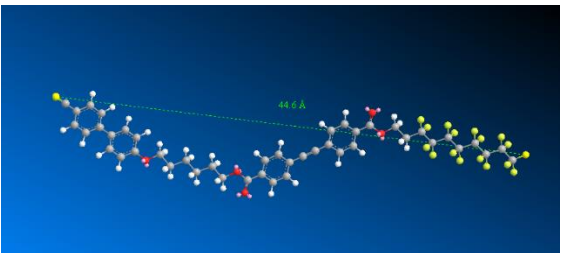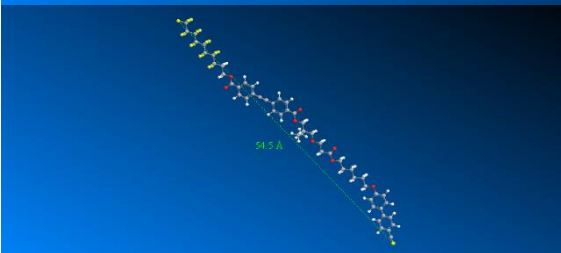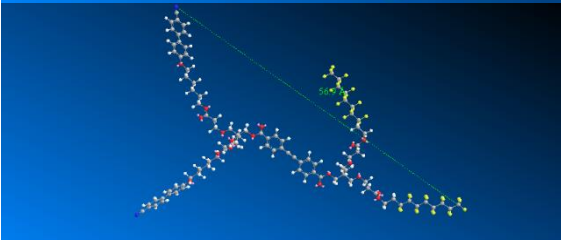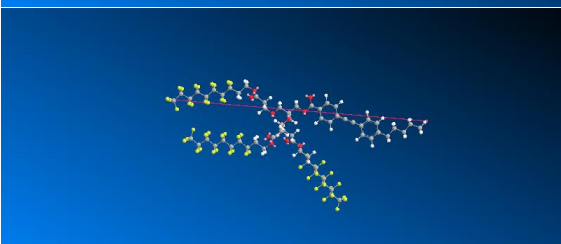
Chemical fragment	Fragment length / Å
	10
	21
	16
	7
	26
	29

Table 20. Calculated fragment lengths and lengths of extended conformations.

Compound	Molecular length / Å
94 sum of fragments	47
94 3D structure	44.3
104 sum of fragments	65
104 3D structure	61.2

Although less powerful than Gaussian modelling, Chem3D was used to provide an alternative measure of molecular lengths. This approach revealed that the three-dimensional nature of the complex structures examined provided molecular lengths that varied by ± 10 Å. For simplicity, the fully extended conformation was used to approximate the molecular length. In the case of the branched materials an axis running through the core of the dendrimers was used to determine the most extended molecular length. Additional mesogenic units splayed away from this axis according to their conformational freedom, however this does not increase the length of the axis measured. Therefore, simpler structures with less branched chains could be used to give results for branched compounds **105** and **107**. The values from Chem3D were in good agreement with the values from Gaussian considering the limitations and degree of confidence in the results (Table 21).

Table 21. Molecular lengths calculated with molecular mechanics using Chem3D.

Compound number	Chemical structure	Molecular length / Å	Sum of fragments/Å
90		31.6	33
94		44.6	47
95		63.9	65
106		54.5	55
104		56.9 / 63.9	65
113		38.8	42

5.4.1 X-ray diffraction of linear materials

The linear molecules were examined by X-ray diffraction (Table 22, Figures 111 – 113) and each compound will be discussed in turn. The layer spacing of each molecule was measured from the diffraction pattern at several temperatures.

*Table 22. Layer spacing and calculated molecular lengths of linear Janus diphenyl acetylenes **90**, **94** and **95**. Full structures are shown on pages 184 – 191.*

Compound number	Temperature / °C	Layer spacing / Å	Molecular length / Å
91	123	35.5	31.6
94	144	68.5	44.6
95	65.9	53.9	63.9

d WL = λ 1.54060
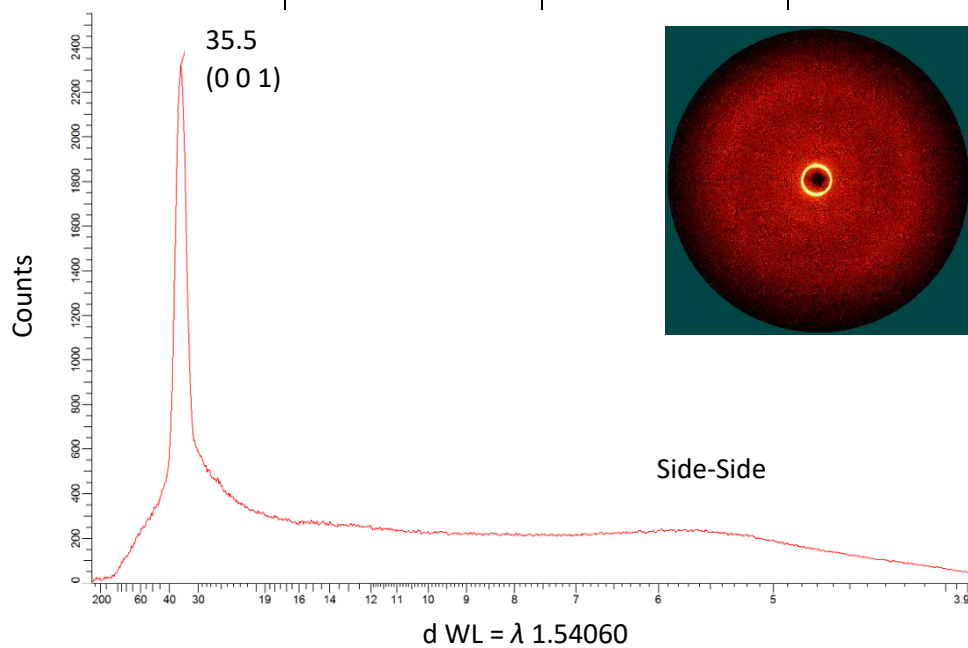
*Figure 111. Diffraction pattern of **91** recorded at 123 °C. The proposed mesophase structure is shown in Figure 114.*

d WL = λ 1.54060
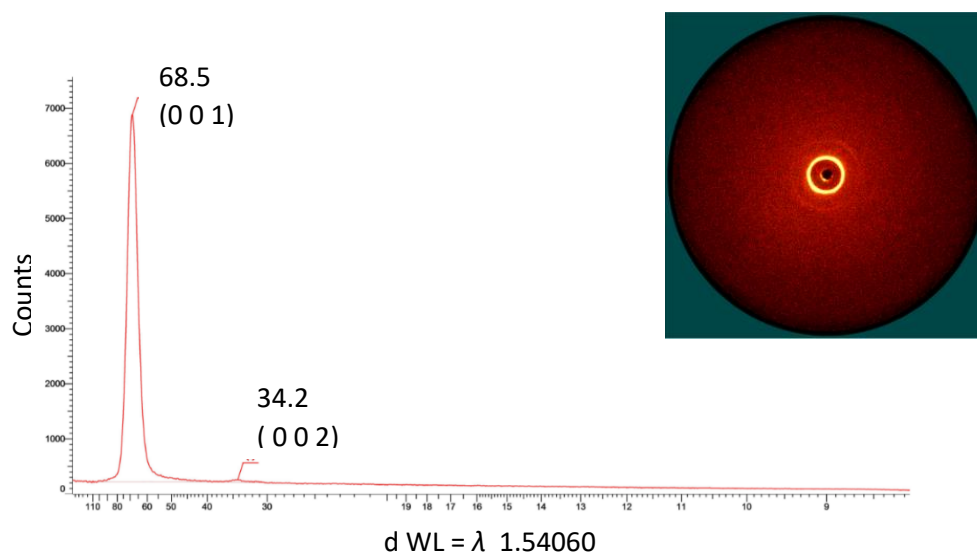
*Figure 112. Diffraction pattern of **94** recorded at 144 °C. The proposed mesophase structure is shown in Figure 115.*

d WL = λ *1.54060*
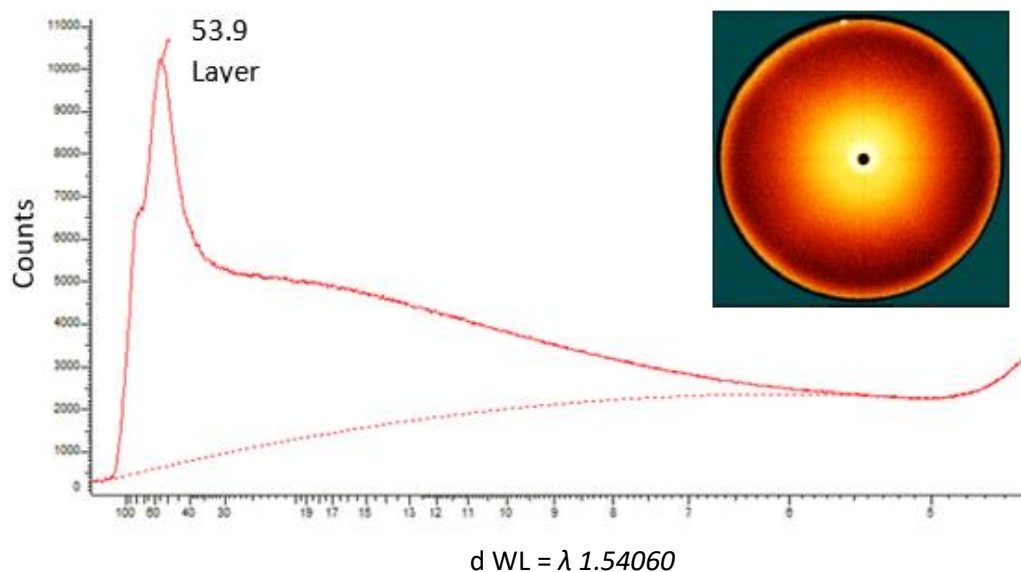
*Figure 113. Diffraction pattern of **95** recorded at 65.9 °C. the proposed mesophase structure is shown in Figure 116.*

The diffraction patterns of these compounds are typical of smectic A phases and therefore can be discussed together. Compound 1was found to have a layer spacing of 35.5 Å observed as a peak due to scattering from the (0 0 1) plane. This is slightly larger than the estimated molecular length of 31.6 Å. In contrast to the *Janus* perfluoroalkyl:alkyl compound **91**, when a cyanobiphenyl mesogen is incorporated in **94** a second order peak relating to the (0 0 2) plane is observed indicating a more well defined layering in the smectic phase. This can be attributed to the additional quadrupolar interactions between cyanobiphenyl units which increases the order at the interface.

For compound **91** the layer spacing is longer than the estimated molecular length indicating an interdigitated structure. An antiparallel arrangement of molecules within the layer fulfils the expected microphase segregation and provides a layer spacing similar to that observed indicating that the model shown in Figure 114 of the mesophase structure is suitable. The layer was measured while cooling over an 18 °C range and showed only a small expansion of 0.3 Å. This is typical as the fully extended conformation of individual molecules becomes more favourable as the temperature

225

decreases, in addition as the motion within layers decreases less interdigitation between neighbouring layers is expected.
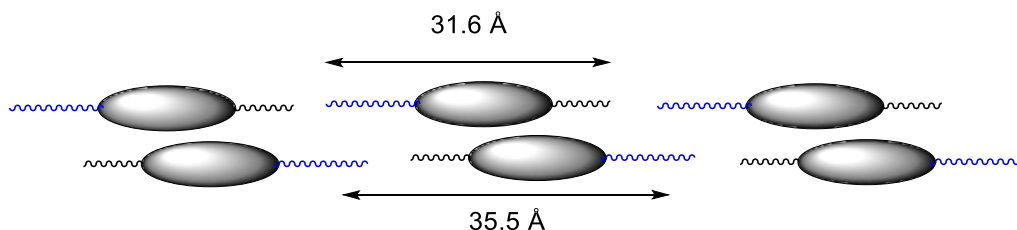
*Figure 114. Proposed structure of the smectic phase of **91** showing the layer spacing and molecular length. Perfluorinated units are represented in blue.*

Compound **94** was estimated to have a molecular length around 44.6 Å while X-ray diffraction revealed the layer spacing to be 68.5 Å. As stated above a low intensity peak can be seen at d = 34.1 Å, which relates to $1/\sqrt{4}$ of the primary peak indicating a second order relationship and that the scattering originates from the (0 0 2) plane. This is a sign of a more ordered mesophase than that of **91** which can be explained by a model of the mesophase structure. The layer spacing of 68.5 Å clearly relates to an interdigitated structure as the layer spacing is greater than the molecular length. The fragments shown in Table 19 can be used to estimate the degree of interdigitation. Using these values shows good agreement with a mesophase structure incorporating the fluorophobic effect and quadrupolar interactions of cyanobiphenyl mesogens (Figure 115). This reorganisation of the smectic phase of **94** relative to **91** is clearly due to the additional interactions provided by the cyanobiphenyl mesogen and the cooperation of the two mesogenic units results in high transition temperatures for this compound. The enantiotropic range of the mesophase is narrow, and little change in the layer spacing with temperature could be observed. This was further hindered as the sample readily crystalised upon cooling and as such X-ray diffraction data from the monotropic smectic C phase could not be recorded.
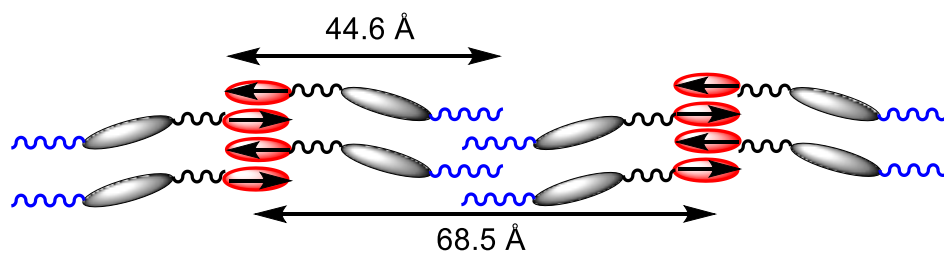
*Figure 115. Proposed interdigitated structure of **94** showing the measured layer spacing and estimated molecular length. Cyanobiphenyl units are represented by red ovals showing the quadrupolar interaction.*

The X-ray diffraction pattern of **95** was recorded at 65.9 °C several degrees beneath the clearing point of the monotropic smectic A phase. The diffraction pattern is clearly less ordered than the previous results shown both by the wide diffuse scattering and increased peak width of the (0 0 1) phase. The layer spacing is far below the expected molecular length and the layer spacing of **94** shown above. Considering the high flexibility of the elongated spacer units it is likely that this is due to folding of the spacer units in some way (Figure 116). Despite the wide peak indicating a poorly defined interface it is expected that the perfluorinated chains can still segregate in the mesophase structure. Insufficient data is provided by the diffraction patterns obtained to conclusively assign a structure to the mesophase.
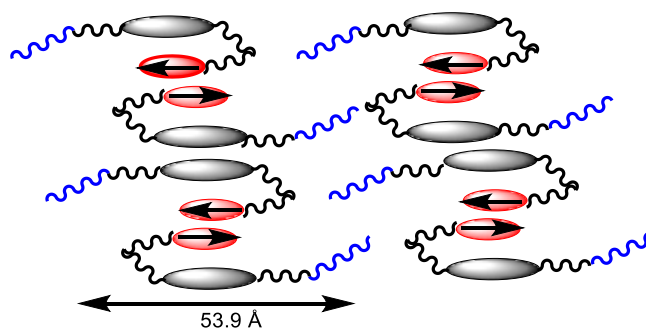
*Figure 116. A cartoon representation of the folding of chains responsible for the shortened layer spacing observed for **95**.*

5.4.2 *Janus* dendritic liquid crystals

Following on from the linear materials discussed in section 5.4.1, dendritic materials featuring multiple mesogenic units on one or both faces of the diphenyl acetylene have been studied by X-ray diffraction. The results are summarised in Table 23.

Table 23. Observed layer spacing and molecular length of Janus dendritic diphenyl acetylenes. Full structures are shown on pages 184 – 191.

Compound number	Temperature / °C	Layer spacing / Å	Molecular length / Å
106	69	80.1	54.5
104	112	60.9	63.9
104	53	69.6	63.9
105	109	61.1	63.9
105	64	87.3	63.9
107	127	61.4	63.9
107	72	64.1	63.9

d WL = λ 1.54060
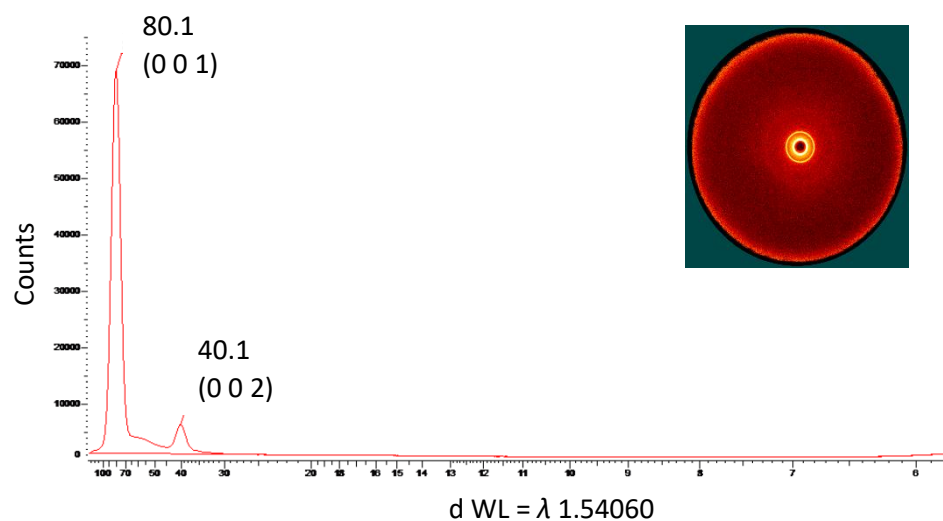
*Figure 117. Diffraction pattern of **106** recorded at 69 °C. The proposed mesophase structure is shown in Figure 118.*

The presence of branching in this family of compounds complicates the mesophase structure due to the tapered molecular shape. Due to the tapered shapes, the interfaces must undulate or the cores begin to tilt in order to efficiently pack into a three-dimensional shape.[23] **106** displayed a smectic A phase with a layer spacing of 80.1 Å while the molecular length was estimated at 55 Å (Figure 117). This suggests an interdigitated bilayered structure with a layer spacing around 1.5 times molecular

length, which is similar to that proposed for **94**. The diffraction pattern shows a first order and a second order diffraction peak with a slight diffuse halo. This indicates that the interface is not as clearly defined as **94**. A second order peak due to diffraction from the (0 0 2) is observed at d = 1/√4 of the primary peak (40.1 Å) suggesting the repeating layer unit is well defined. Comparison of the nematic mesophase of **100** and smectic phase of **106** shows the strong smectogenic influence of the perfluorinated chain. The diffraction pattern indicates that the lack of intermolecular interactions between the perfluorinated chain and alkyl units is sufficient to provide segregation as shown by the well-defined layer intervals.

Due to the tapered molecular shape the interdigitated structure is unlikely to feature full overlap of the cyanobiphenyl units. Consequently, the two proposed mesophase structures shown in Figure 118 show cyanobiphenyl units at the interface with overlap between the perfluorinated units to account for the measured layer spacing. Despite the overlap of the perfluorinated units, the layer spacing observed is slightly shorter than expected using the results in Tables 19-21. This could be due to an inaccurate model in those tables, or otherwise be accounted for by slight tilting of the alkyl chains or diphenyl acetylene core (Figure 118, left) or slight interpenetration of the perfluoroalkyl chains (Figure 118, right). While the tapered shape likely rules out full overlap of the cyanobiphenyl units as proposed for compound **94**, partial overlap of the cyano-groups at the interface will enable the quadrupolar interactions to be maintained while reducing the steric burden. This proposed structure may explain the less well-defined interface as seen in the diffraction pattern.

The layer spacing estimated for this arrangement using the values in Table 19 is slightly larger than observed. This can either be attributed to the simplistic calculations; or can be accounted for by the partial overlap of cyanobiphenyl units, undulation of the layers or tilting of the cores which will serve to reduce the average layer spacing. No evidence of tilted phases such as smectic C were observed by POM and as such it is expected that the layer boundaries undulate to account for the tapered shape.
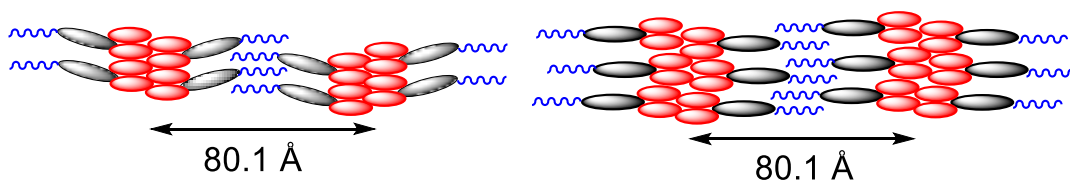
*Figure 118. Proposed mesophase structure of **106**.*
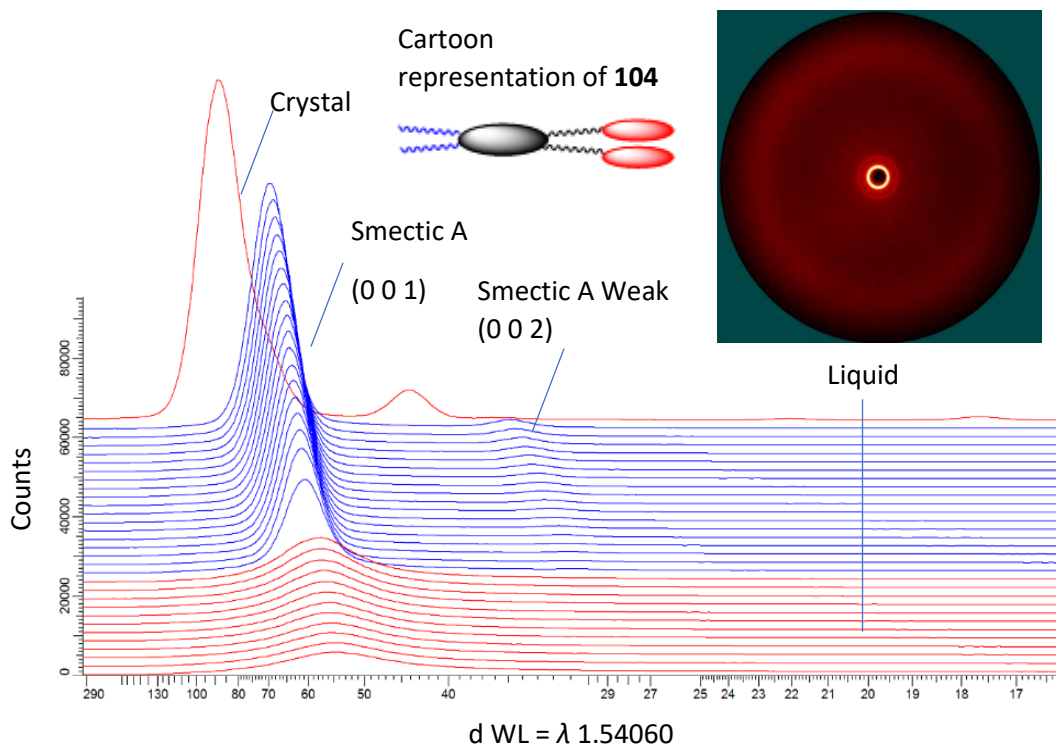
*Figure 119. X-ray diffraction pattern and integration of **104** at different temperatures shown as a waterfall plot.*

The waterfall plot shown in Figure 119 shows the integrated diffraction patterns of compound **104** between 53 and 112 °C recorded at intervals of 2 °C. From back to front the diffraction patterns show heating from the crystal in red, smectic A phase in blue and finally liquid in red. Compound **104** shows a typical diffraction pattern for a smectic A phase with a weak 2nd order diffraction peak (Figure 119, blue). This showed a continuous expansion of the layer spacing during cooling which ranged from 60.9 to 69.6 Å (Figure 120). An inverse relationship between temperature and layer spacing is common because the fully extended conformations of the molecules are more common at lower temperatures, and the mesophase structure tends to be more organised with less interpenetration of chains at the interfaces.
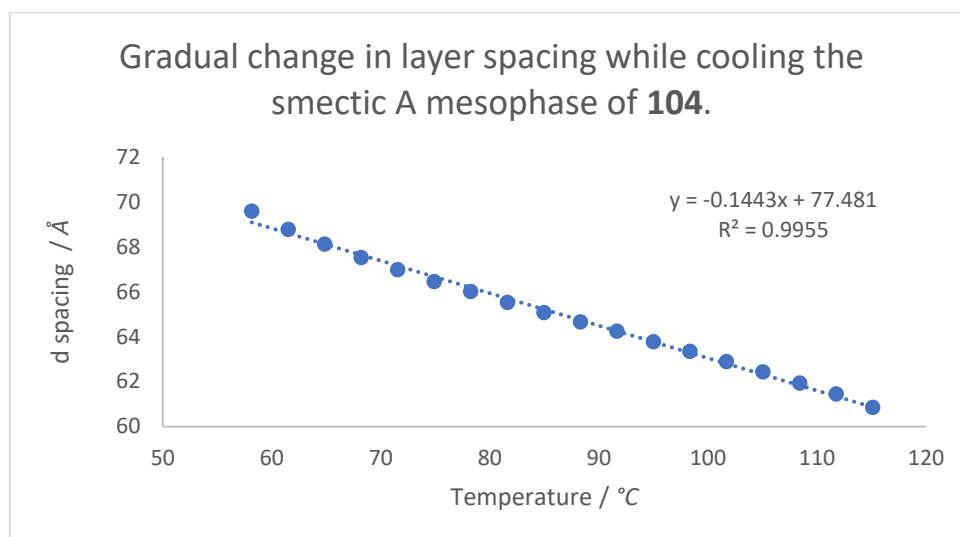
*Figure 120. Plot showing the change in the layer spacing of **104** with cooling of the mesophase.*

Nonetheless the scale of this change being 8.7 Å or 14% of the upper phase is remarkably large for a continuous trend indicating no discrete transition or reorganisation has taken place. Comparison of **104** and **106** shows that addition of the second perfluorinated chain causes the mesophase structure to differ greatly as the layer spacing becomes roughly equal to the molecular length. Interdigitation of the perfluorinated chains in **104** will necessitate the diphenyl acetylene core and cyanobiphenyls to be outside of this overlap due to the fluorophobic effect giving a longer layer spacing. Upon addition of a second perfluorinated chain in **106** it appears that the overlap of the perfluorinated units is disfavoured in favour of a much greater overlap of the cyanobiphenyl and diphenyl acetylene units. This lends some more support to the theory that it is the perfluorinated chain of **106** which is interdigitated, as an additional chain cannot be accommodated, resulting in the change in mesophase structure. The expansion of the layer spacing of **104** is continuous with temperature (Figure 120) and no transition of first or second order is seen via DSC therefore the expansion is unlikely to be due to a reorganisation of the mesophase. Further information as to the nature of this expansion can be found by studying compound **105**.

Compound **105** shows a clear transition at 80.1 °C *via* microscopy and DSC which is accompanied by a reorganisation as seen by a change in the layer spacing albeit with a slight temperature discrepancy between instruments (Figure 121). Between 110 and

85 °C a similar gradual increase in layer spacing is observed as for **104** above as the layer spacing expands from 61.1 to 69.3 Å (Figure 122).
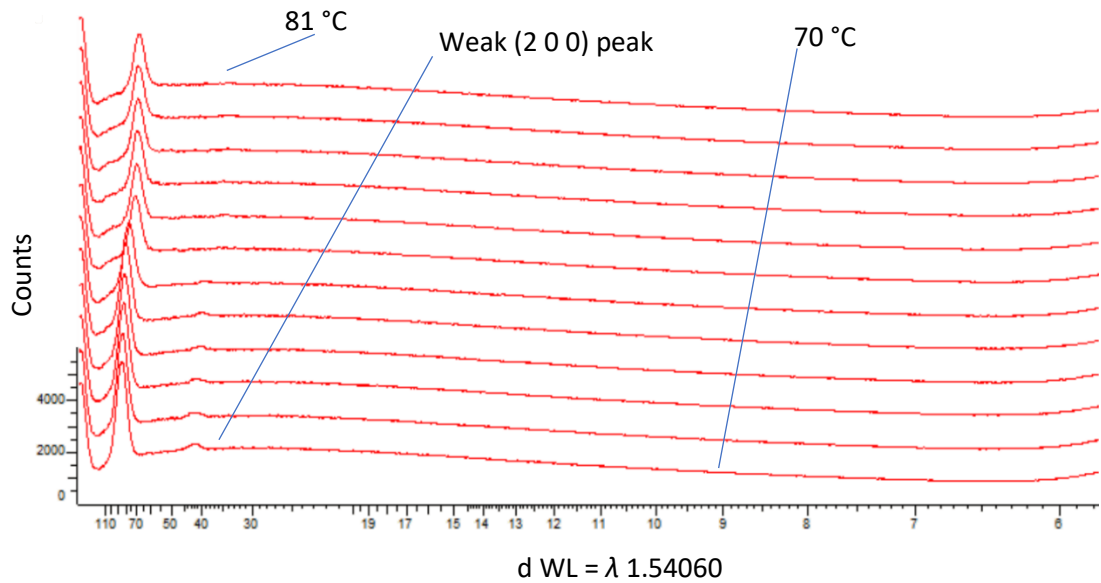
*Figure 121. Waterfall plot of **105** at 1 °C intervals from 81 °C to 70 °C. The proposed mesophase structures are shown in Figures 123 and 124.*
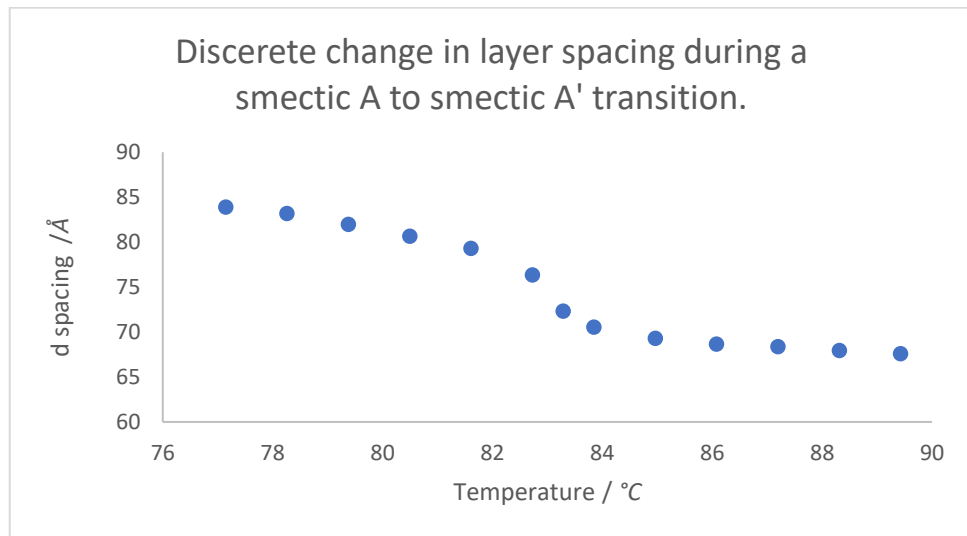
*Figure 122. Plot showing a discontinuous change in layer spacing of **105** due to a smectic A to smectic A transition.*

A clear reorganisation is seen as a discontinuation of this gradual increase as the mesophase structure is reorganised before again gradually increasing (Figure 122), this time ranging from 79.3 Å at 81 °C to 87.3 Å at 64 °C. Models for the mesophase structure of **105** in the upper and lower temperature phases have been proposed following a detailed investigation (Figure 123, 124). The results are not entirely

conclusive and as such, these structures are provided to illustrate and support the discussion, rather than as conclusive models. The three notable features of the transition are a change in birefringence observed by POM, an increase in layer spacing, and the presence of a broad transition by DSC overlapping with a sharp peak (Figure 107). The increase in birefringence indicates a greater difference between n_e and n_o which is likely due to a better alignment of the polarisable aromatic cores. That is when the cores are fully aligned the contributions of each are maximised, whereas when one core is tilted that contributes to the birefringence less, or may even detract from the overall birefringence of the molecule. In addition, a change in birefringence is indicative of a reorganisation of the aromatic cores, rather than that of the perfluorinated chains which are not polarisable and therefore not birefringent. There are two apparent transitions observed by DSC, however the temperature of the transitions by DSC do not align perfectly with either the POM or X-ray diffraction transitions. These two transitions overlap and so accurate values for the enthalpy and entropy of transitions cannot be found.

The fluorophobic effect induced by the perfluorinated chains would require an antiparallel arrangement so as to enable segregation of the perfluorinated and alkyl domains. This antiparallel arrangement requires a bilayered mesophase structure. As the higher temperature mesophase structure is close to that of the molecular length this suggests a highly interdigitated structure or considerable tilting. Similarly, as evoked in the case of **106** POM does not show textures characteristic of a tilted smectic phase. However, it could be that the low birefringence aspects of the molecule (alkyl and perfluroalkyl chains) tilt without being observed. Alternatively, it is unclear if one core were to tilt, however the layer normal remain smectic A with respect to the remaining cores that the change would be visible as a schlieren or smectic C texture. It is notable that a change in tilt may also contribute to the observed change in birefringence and as such the first proposed mesophase structures invoked tilting of one component in the higher temperature phase to account for the decreased layer spacing. The change in layer spacing resulting from the tilting of each of the individual components was calculated by trigonometry and found to be too short to explain the observed difference as either a monolayer or bilayer. The mesophase structure that would provide the shortest layer spacing was found to be that given by the model

below, which is estimated to be around 61 – 65 Å. An additional observation was made that the tapered molecular shape likely results in an uneven interface between layers which then undulates rather than being flat. This has the effect of reducing the average layer spacing observed slightly, however this structure cannot be accurately modelled to quantify the effect. A similar difficulty arises when accounting for non-fully extended chain conformations.
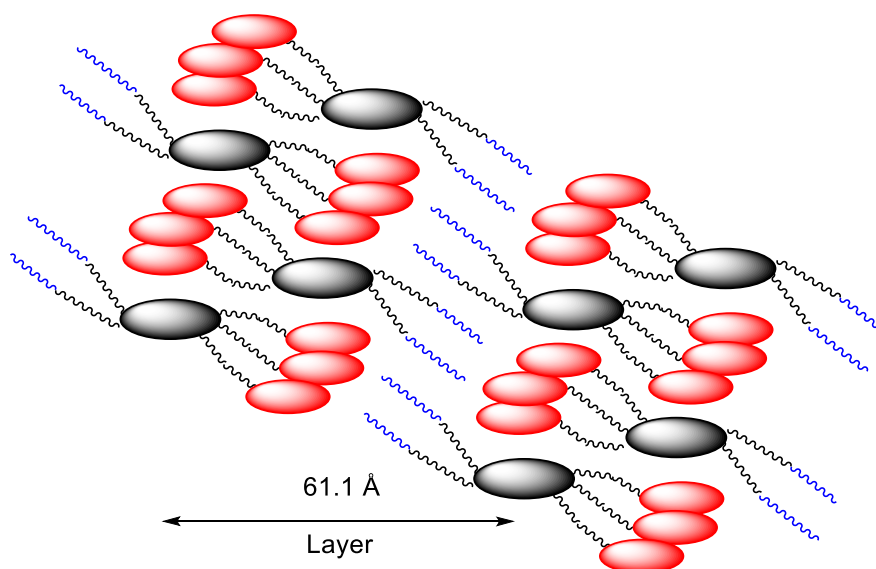
*Figure 123. Proposed mesophase structure of the higher temperature phase of **105** with full interdigitation of perfluorinated chains and diphenyl acetylene/cyanobiphenyl overlap. Perfluorinated chains are represented in blue, cyanobiphenyl units in red, and the diphenyl acetylene core in black.*

While the branching unit introduces flexibility into the system the remainder of the molecule i.e. the rigid aromatic cores and perfluorinated chains are not flexible. Shorter hexymethylene spacers are used in this work however can be considered extended by the branching unit. Highly twisted conformations of alkyl spacers to allow for greater overlap of cyanobiphenyls have been proposed by Deschenaux for cyanobiphenyl: alkyl *Janus* dendrimers.[24] However, in the case of **105** the nature of the core and branching units, and their positions relative to the spacer and mesogens are different, this results in a different molecular shape and different packing considerations including the presence of perfluoroalkyl chains. Therefore, highly twisted conformations are not considered possible. Nevertheless, the proposed structure cannot be confirmed and is only put forth as a suggestion.

This compound then undergoes an expansion of the layer spacing when cooled from around 69.3 Å in the higher temperature phase to a range between 82.7 to 87.3 Å in the lower temperature phase. In addition, this transition is combined with an increase in birefringence as observed by POM. It is thought that this is likely due to a decrease in the interdigitation observed when the material is cooled, with the transitions in the DSC showing this to be a gradual process containing a clear peak (Figure 107). There are two regions of overlap in the model suggested for the lower temperature phase, that is the perfluorinated region and the overlap of the cyanobiphenyl:diphenyl acetylene. Due to the change in birefringence it is expected that the aromatic cores must undergo a change in alignment, suggesting that it is these units that are displaced. The model suggested for the higher temperature mesophase requires overlap of the cyanobiphenyl with the far side of the diphenyl acetylene core in order to minimise the layer spacing, while maintaining the segregation of perfluoralkyl chains. Should this overlap slip to the near end of the opposing diphenyl acetylene the resulting change in the layer spacing would be roughly twice the length of the diphenyl acetylene core (2 x 10 Å). While it is possible that the perfluorinated chains are reorganised this is not supported by evidence such as the change in birefringence.
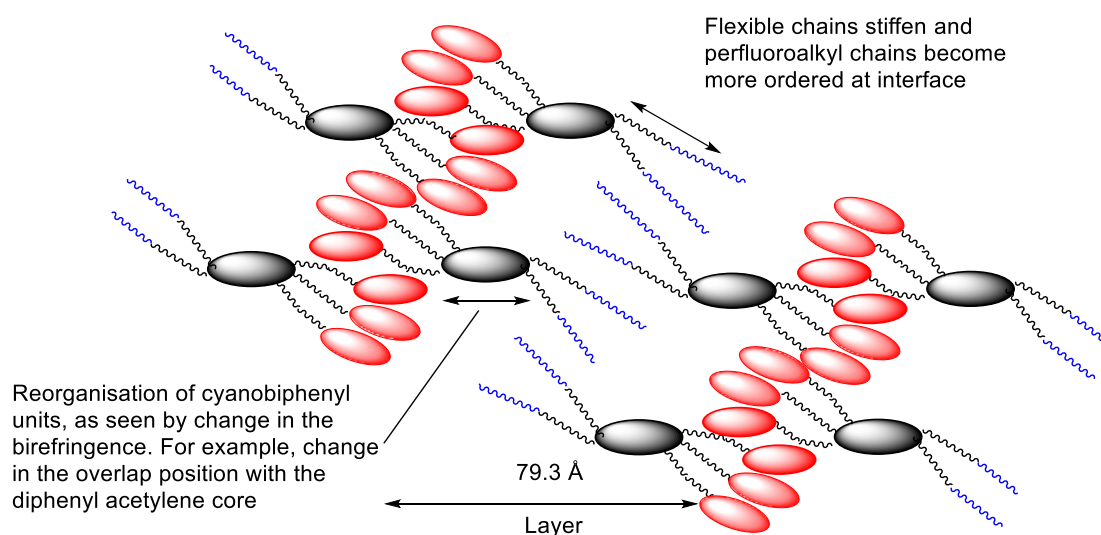
*Figure 124. Lower temperature mesophase structure of **105** with decreased interdigitation. Perfluorinated chains are represented in blue, cyanobiphenyl units in red, and the diphenyl acetylene core in black.*

Compound **107** did not appear to show a similar trend with temperature as the layer spacing changed by only 2.7 Å from 61.4 to 64.1 Å upon cooling by 55 °C from the clearing point (Figure 125) to the point of crystallisation. This shows that the mesophase structure of **107** is much more rigid than that of **104** or either phase of **105**. This may be due to the additional perfluorinated chain which ensures the tapered shape is wider on the perfluorinated face, this appears to result in more ordered interfaces which are less variable with temperature.
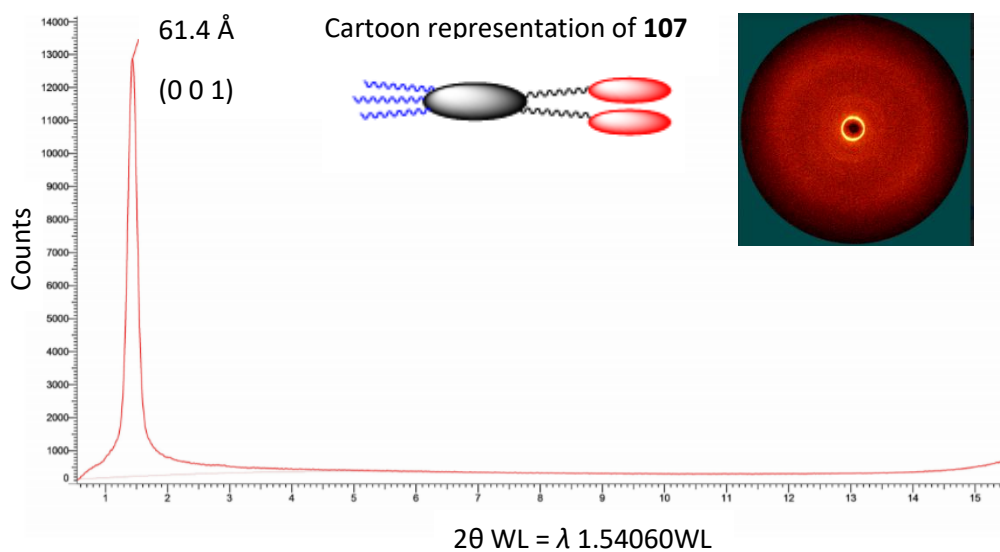
*Figure 125. Diffraction pattern of **107** recorded at 127 °C*

5.4.3 X-ray diffraction studies of highly tapered *Janus* perfluoroalkyl compounds.

The final *Janus* diphenyl acetylenes to be analysed by X-ray diffraction were the highly tapered compounds **113** and **109**. Compound **113** was first reported by Ma[3] however this is the first report of the mesophase structure as revealed by X-ray diffraction.

*Table 24. Observed layer spacing and calculated molecular length of **113**. Full structures is shown on page 189.*

Compound number	Temperature / °C	Layer spacing / Å	Molecular length / Å
113	42	36.6	38.8
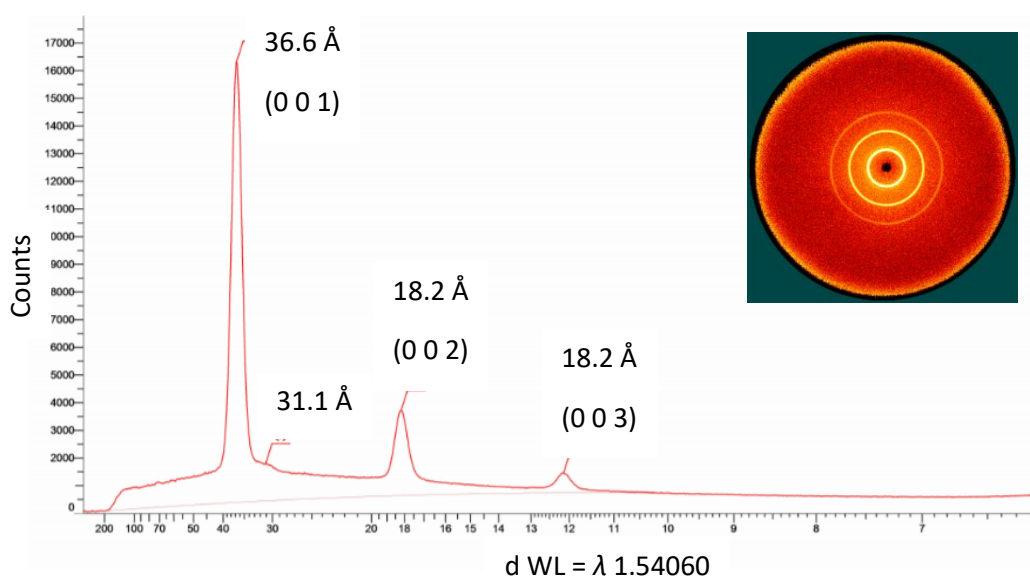
*Figure 126. Diffraction pattern of compound **113** recorded at 42 °C. The proposed mesophase structure is shown in Figure 127.*

Compound **113** is interesting in that the observed layer spacing is lower than the expected molecular length (Figure 126). In addition to difficulties modelling a three-dimensional structure, this may be rationalised by the highly tapered shape resulting in the core and alkyl chain likely having to tilt in order to more effectively fill the remaining volume (Figure 127). Similarly to the compounds discussed above an undulating or rippled interface between layers may also serve to reduce the average layer spacing observed. The result of this is packing is a highly ordered mesophase as shown by the diffraction pattern which shows both a second order peak at d = 1/√4 and third order d = 1/√9. This sample did not appear to show much variation of layer

spacing with temperature, however this was measured over a far smaller range than that of the larger supermolecules.
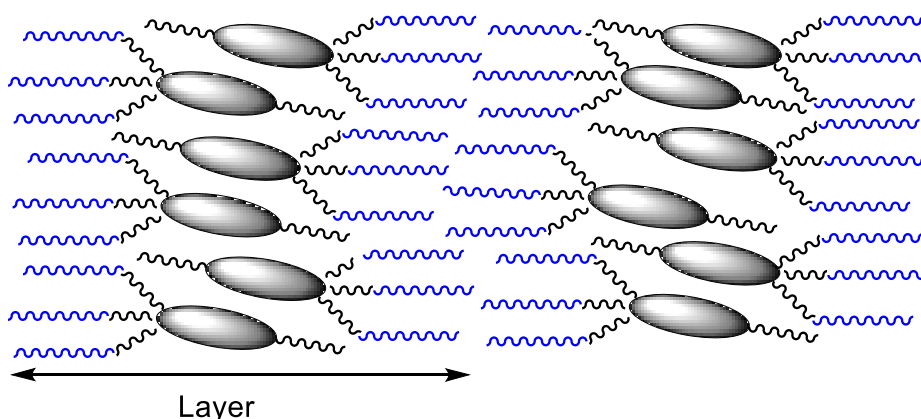
*Figure 127. Highly ordered mesophase structure possible for **113**.*

Compound **109** showed a texture clearly indicative of a columnar mesophase and the diffraction pattern showed a high number of reflections present (Figure 128). The relationship between the reflections can easily rule out a hexagonal columnar mesophase as the characteristic ratio of 1:1/√3:1/√4 between the reflections is not seen. Attempts to index this mesophase to a rectangular columnar phase also showed difficulty as there was no clear (0 0 2) or (0 1 1) reflections.[25] In addition there are no second order peaks observed relative to the intense reflections. Peaks were observed corresponding to distances of 57.7, 40.1, 30.7, 22.5, 16.8, 13.3, 11.2, 5.8 and 5.0 Å.

d WL = λ 1.54060
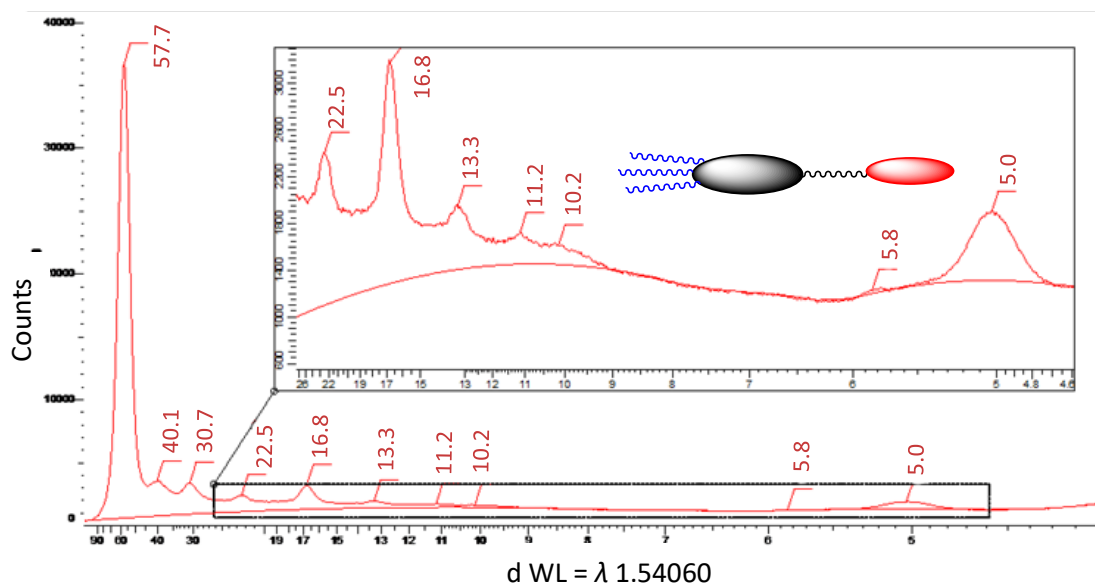
*Figure 128. Diffraction pattern and d values of reflections from the columnar phase of **109**, full structure of **109** is given on page 181.*

These diffraction peaks could not be indexed to a specific columnar lattice, however the intensity and frequency of the peaks is clearly related to an organised mesophase structure. Complex molecular structures may give rise to columnar phases with complicated or mixed lattices.[26-28] In this case the complex structure could not be assigned owing to its complex structure, however POM confirmed a texture indicative of a hexagonal columnar mesophase.

5.5 Summary

The self-organisation of diphenyl acetylene based supermolecular liquid crystals, oligomers and dimers has been investigated. Due to the number of comparisons available across this family of compounds, the liquid crystalline behaviour is understood in terms of increasing molecular complexity. Three linear cyanobiphenyl – diphenyl acetylene dimers **90**, **92** and **93** exhibiting nematic phases and monotropic smectic phases were synthesised. The introduction of dendritic branching gives cyanobiphenyl oligomers **100** and **110** for which only the nematic phase was observed. In both these linear and branched materials, the introduction of a self-segregating perfluoroalkyl chain promoted smectic A phases over nematic phases (Table 15). X-ray diffraction revealed the mesophase structures may vary in terms of the degree of overlap between cyanobiphenyl units however the microphase segregation of the perfluoroalkyl unit was maintained. This is instructive in terms of the competing factors driving the self-organisation of these materials. The prevalence of the smectic A phase was maintained for diphenyl acetylene **91** featuring the perfluoroalkyl unit and no cyanobiphenyl.

By further increasing the number of mesogens or self-segregating chains on each side of the diphenyl acetylene core, the complexity was further increased. Compounds **112** and **109** had the largest interfacial curvature as a result of different volumes either side of the diphenyl acetylene core with a 3:1 substitution ratio of cyanobiphenyl and perfluoroalkyl units respectively and both compounds exhibited columnar phases. However, in each case this was dependent upon the nature of the single chain, as the same three mesogenic units opposite of a pentyl chain provided different mesophase types (**110** nematic or **113** smectic). This indicates the fine balance that is achieved between the competing factors of chemical incompatibility and molecular shape which control the packing of the mesophase.

In contrast, having a similar number of cyanobiphenyl and perfluorinated chains respectively on each side of the diphenyl acetylene core lead predominantly to smectic phases (Table 18). However, due to the competing intermolecular interactions the self-organisation remains highly complex. For example, compounds **105** and **114** show large rearrangements of the mesophase structure observed by changes in birefringence, first order transitions in DSC measurements and large changes in the X-ray diffraction pattern of the mesophase. The mesophase structures of compound **105** has been discussed and suggestions for the molecular arrangements giving rise to the two smectic A phases are provided. This drastic rearrangement of the mesophase structure is reliant upon the supermolecular molecular structure, and competing effects of the quadrupolar interactions and fluorophobic effect. Compound **104** appears to share a similar mesophase structure of the higher temperature phase of **105**. Despite **104** sharing a large expansion of up to 14% of the layer spacing upon cooling as was observed for the higher temperature phase of **105**, the discontinuous shift to a second mesophase structure is not observed. This is evidence of the finely balanced interplay between the molecular shape and intermolecular interactions. Finally, compound **107** which shares a wide-ranging smectic phase with comparable layer spacing with **104** also behaves differently. The layer spacing of compound **107** is largely unchanged with temperature indicating that the mesophase structure of the smectic A phase is different and unable to change. This may agree with observations during polarised optical microscopy studies that the phase was very viscous and difficult to shear, instead giving largely homeotropic alignment with small areas of low birefringence textures. Interestingly, in contrast to this evidence of a fixed and possibly highly organised mesophase structure DSC results show that the entropy of isotropisation of this of transition is in fact lower than that of **104**, **105** and **114**.

5.6 Experimental

90
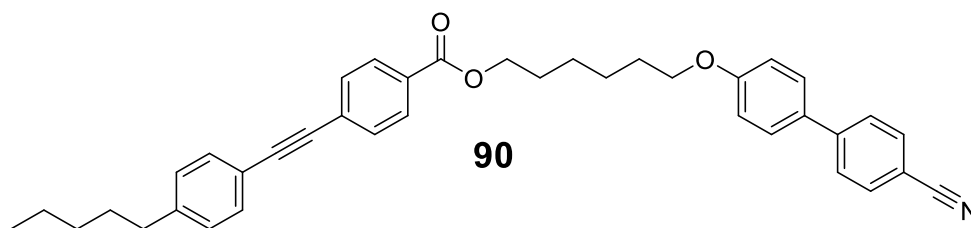
Compound **29** (0.31 g, 0.59 mmol), [PdCl$_2$(PPh$_3$)$_2$](0.014 g, 0.02 mmol) and CuI (0.004 g, 0.02 mmol) were charged to a Schlenk tube which under argon. Triethylamine (10 mL), low-sulfur toluene (5 mL) and 1-ethynyl-4-pentylbenzene (0.12 mL, 0.11 g, 0.62 mmol) were charged to a second Schlenk tube and degassed with argon gas for 20 minutes. The degassed solvent was transferred to the reaction mixture which was then stirred at room temperature for 18 hours. The solvent was removed *in vacuo* and the crude product purified by column chromatography (DCM:EtOAc as eluent) then recrystallised twice from ethanol to give the target compound **90** as an off-white solid (0.17 g, 0.29 mmol, 49% yield).

^{1}H NMR (400 MHz, CDCl$_3$) δ 8.01 (d, *J* = 8.5 Hz, 2H, Ar*H*), 7.70 – 7.60 (m, 4H, Ar*H*), 7.57-7.49 (m, 4H, Ar*H*), 7.45 (d, *J* = 8.0 Hz, 2H, Ar*H*), 7.18 (d, *J* = 8.0 Hz, 2H, Ar*H*), 6.98 (d, *J* = 8.5, Hz, 2H, Ar*H*), 4.35 (t, *J* = 6.5 Hz, 2H, COOC*H$_2$*), 4.02 (t, J = 6.5 Hz, 2H, OC*H$_2$*), 2.62 (t, *J* = 8.0 Hz, 2H, ArC*H$_2$*), 1.94 – 1.75 (m, 4H, OCH$_2$C*H$_2$*), 1.72 – 1.50 (m, 6H, OCH$_2$CH$_2$C*H$_2$* and ArCH$_2$C*H$_2$*), 1.42 – 1.25 (m, 4H, CH$_3$C*H$_2$*CH$_2$ and CH$_3$CH$_2$C*H$_2$*), 0.89 (t, *J* = 7.0 Hz, 3H, C*H$_3$*CH$_2$).

^{13}C{^{1}H} NMR (101 MHz, CDCl$_3$) δ 166.3, 159.8, 145.4, 144.3, 132.7, 131.8, 131.6, 131.5, 129.6, 129.6, 128.7, 128.5, 128.3, 127.2, 119.9, 119.3, 115.2, 110.1, 92.8, 88.2, 68.0, 65.2, 36.1, 31.6, 31.1, 29.2, 28.8, 26.0, 25.9, 22.7, 14.2.

APCI-MS: m/z = 570.36 [M+H]$^+$

Anal. Calcd for C$_{39}$H$_{39}$NO$_3$: C, 82.22, H, 6.90, N, 2.46; found C, 82.27, H, 7.34, N, 2.33

91
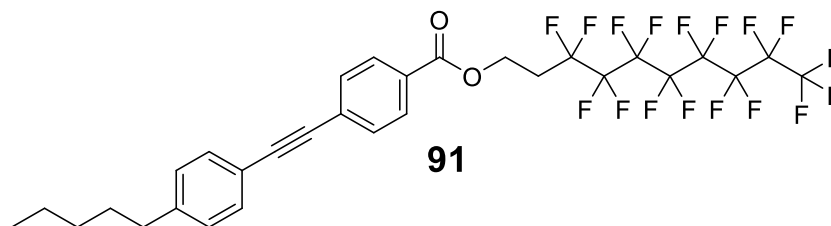
Compound **30** (0.18 g, 0.26 mmol), [PdCl$_2$(PPh$_3$)$_2$](0.03 g, 0.04 mmol) and CuI (0.01 g, 0.05 mmol) were charged to a Schlenk tube under argon. Triethylamine (5 mL), toluene (5 mL) and 1-ethynyl-4-pentylbenzene (0.06 mL, 0.05 g, 0.31 mmol) were charged to a second Schlenk tube and degassed with argon gas for 20 minutes. The degassed solvent was transferred to the reaction mixture which was then stirred at room temperature for 18 hours. The solvent was removed *in vacuo* and the crude product was purified by column chromatography (DCM as eluent) then recrystallised from DCM:methanol to give the target compound **91** as an off-white solid (0.11 g, 0.15 mmol, 58% yield)

^{1}H NMR (400 MHz, CDCl$_3$) δ 8.01 (d, *J* = 8.5 Hz, 2H, Ar*H*), 7.58 (d, J = 8.5 Hz, 2H, Ar*H*), 7.46 (d, J = 8.0 Hz, 2H, Ar*H*), 7.18 (d, J = 8.0 Hz, 2H, Ar*H*), 4.64 (t, J = 6.5 Hz, 2H, OC*H$_2$*CH$_2$CF$_2$), 2.62 (t, *J* = 7.5 Hz, 2H, ArC*H$_2$*) 2.45 (tt, J = 18.5, 6.5 Hz, 2H, C*H$_2$*CF$_2$), 1.63 (d, 7.5 Hz, 2H, ArCH$_2$C*H$_2$*), 1.40 – 1.24 (m, 4H, C*H2* CH$_2$CH$_2$CH$_3$ and C*H$_2$*CH$_3$), 0.89 (t, J = 7.0 Hz, 3H, CH$_2$C*H$_3$*).

^{19}F NMR (376 MHz, CDCl$_3$) δ -80.62, -112.96, -113.98, -121.55, -121.81, - 122.61, -123.38, -126.00.

^{13}C{^{1}H} NMR (101 MHz, CDCl$_3$) δ 165.8, 144.3, 131.8, 131.7, 129.7, 128.9, 128.7, 128.6, 119.8, 93.2, 88.1, 76.8, 57.1, 36.1, 31.6, 31.1, 30.8, 22.7, 14.2.

APCI-MS: m/z = 739.1 [M+H]$^+$

Anal. Calcd for C$_{30}$H$_{23}$F$_{17}$O$_2$: C, 48.79, H, 3.14, N, -; found C, 48.61, H, 3.02, N, -.

92
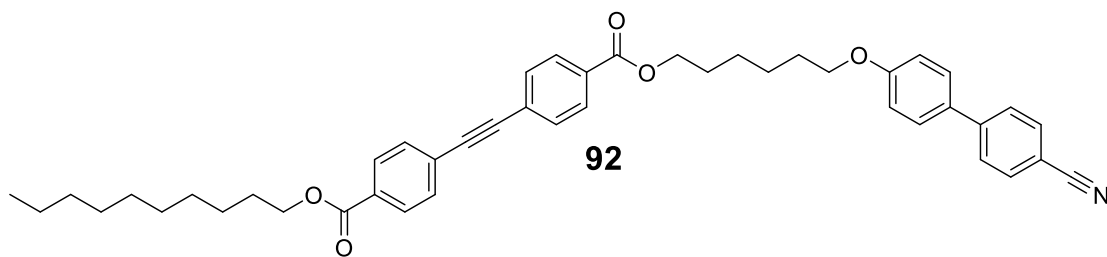
Compound **33**ᵢ (0.20 g, 0.47 mmol), [PdCl$_2$(PPh$_3$)$_2$](0.06 g, 0.09 mmol) and CuI (0.03 g, 0.16 mmol) were charged to a Schlenk tube under argon. Triethylamine (5 mL), toluene (5 mL) and compound **61** (0.21 g, 0.54 mmol) were charged to a second Schlenk tube and degassed with argon gas for 20 minutes. The degassed solvent was transferred to the reaction mixture which was then stirred at room temperature for 18 hours. The solvent was removed *in vacuo* and the crude product purified by column chromatography (DCM:EtOAc as eluent) followed by recrystallisation from hot ethanol to give the target compound **92** as a crystalline white solid (0.19 g, 0.28 mmol, 60% yield).

^{1}H NMR (400 MHz, CDCl$_3$) δ 8.02 (d, *J* = 8.5 Hz, 4H, Ar*H*), 7.68 (d, *J* = 8.5 Hz, 2H, Ar*H*), 7.63 (d, *J* = 8.5 Hz, 2H, Ar*H*), 7.59 (d, *J* = 8.5 Hz, 4H, Ar*H*), 7.52 (d, *J* = 8.5 Hz, 2H, Ar*H*), 6.98 (d, *J* = 9.0 Hz, 2H, Ar*H*), 4.32 – 4.28 (m, 4H, COOC*H$_2$*), 4.03 (t, *J* = 6.5 Hz, 2H, OC*H$_2$*), 1.91 – 1.72 (m, 6H, OCH$_2$C*H$_2$*), 1.47 – 1.20 (m, 18H, CH$_2$C*H$_2$*), 0.88 (t, *J* = 7.0 Hz, 3H, C*H$_3$*CH$_2$).

^{13}C{^{1}H} NMR (101 MHz, CDCl$_3$) δ 166.2, 163.9, 163.7, 159.8, 145.4, 132.7, 131.8, 131.8, 131.5, 130.5, 130.3, 129.7, 128.5, 127.5, 127.3, 127.2, 119.3, 115.2, 111.5, 110.2, 91.6, 68.1, 65.6, 65.3, 32.0, 29.7, 29.5, 29.4, 29.3, 28.8, 28.8, 26.2, 25.9, 22.8, 14.3.

APCI-MS: 706.4 [M+Na]$^+$

Anal. Calcd for C$_{45}$H$_{49}$NO$_5$ C, 79.03, H, 7.22, N, 2.05; found C, 79.21, H, 6.62, N, 2.32

93
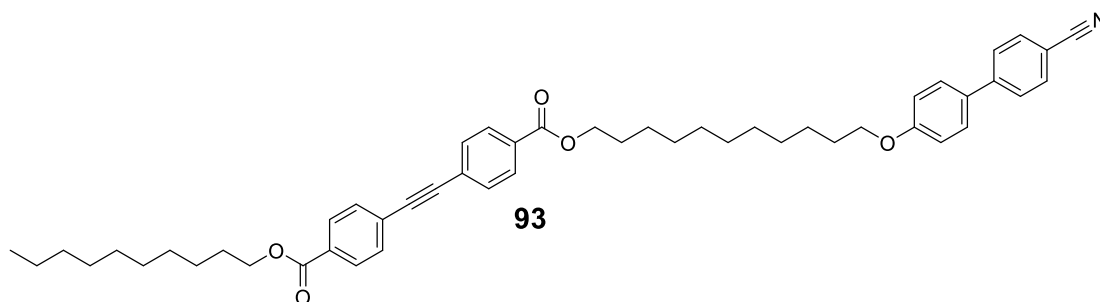
Compound **33$_v$** (0.21 g, 0.28 mmol), [PdCl$_2$(PPh$_3$)$_2$](0.01 g, 0.014 mmol) and CuI (0.003 g, 0.016 mmol) were charged to a Schlenk tube under argon. Triethylamine (10 mL), toluene (10 mL) and compound **61** (0.11 g, 0.42 mmol) were charged to a second Schlenk tube and degassed with argon gas for 20 minutes. The degassed solvent was transferred to the reaction mixture which was then stirred at room temperature for 18 hours. The solvent was removed *in vacuo* and the crude product was purified by column chromatography (DCM:EtOAc as eluent) followed by recrystallisation from hot ethanol to give the target compound **93** as a crystalline white solid (0.17 g, 0.23 mmol, 80% yield).

^{1}H NMR (400 MHz, CDCl$_3$) δ 8.02 (d, *J* = 8.0 Hz, 4H, Ar*H*), 7.69 (d, *J* = 8.5 Hz, 2H, Ar*H*), 7.64 – 7.55 (m, 6H, Ar*H*), 7.51 (d, *J* = 8.5 Hz, 2H, Ar*H*), 6.98 (d, *J* = 9.0 Hz, 2H, Ar*H*), 4.31 (t, *J* = 6.5 Hz, 4H, COOC*H$_2$*), 3.99 (t, *J* = 6.5 Hz, 2H, OC*H$_2$*), 1.91 – 1.66 (m, 6H, OCH$_2$C*H$_2$*), 1.49 – 1.19 (m, 28H), 0.86 (t, *J* = 7.0 Hz, 3H, C*H$_3$*CH$_2$).

^{13}C{^{1}H} NMR (101 MHz, CDCl$_3$) δ 166.3, 164.0, 163.5, 159.7, 145.4, 132.6, 131.8, 131.7, 131.4, 130.6, 130.3, 129.7, 128.4, 127.4, 127.2, 127.2, 119.5, 115.4, 111.6, 110.3, 91.6, 68.0, 65.5, 65.4, 31.9, 29.9, 29.6, 29.2, 29.3, 28.8, 28.8, 26.2, 25.9, 22.8, 14.3.

APCI-MS: 754.44 [M+H]$^+$

Anal. Calcd for C$_{50}$H$_{59}$NO$_5$: C, 79.65, H, 7.89, N, 1.86; found C, 79.52, H, 8.01, N, 1.85

94
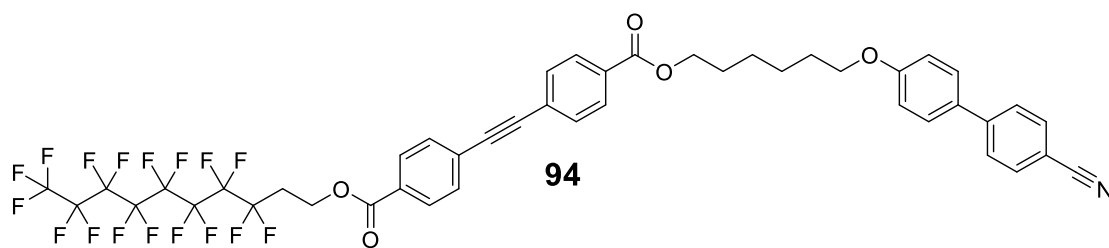
Compound **30** (0.21 g, 0.30 mmol), compound **33ᵢ** (0.08 g, 0.19 mmol), [PdCl₂(PPh₃)₂](0.02 g, 0.03 mmol) and CuI (0.006 g, 0.03 mmol) were charged to a Schlenk tube under argon. Triethylamine (5 mL) and toluene (5 mL) were charged to a second Schlenk tube and degassed with argon gas for 20 minutes. The degassed solvent was transferred to the reaction mixture which was then stirred for 18 hours. The solvent was removed *in vacuo* and the crude product was purified by column chromatography (DCM:EtOAc as eluent) then recrystallised twice from ethanol to give the target compound **94** as a white solid (0.14 g, 0.14 mmol, 70% yield).

^{1}H NMR (400 MHz, CDCl₃) δ 8.04 (d, *J* = 8.5 Hz, 4H, Ar*H*), 7.69 (d, *J* = 8.5 Hz, 2H, Ar*H*), 7.62 – 7.56 (m, 6H), 7.52 (d, *J* = 9.0 Hz, 2H, Ar*H*), 6.98 (d, *J* = 9.0, Hz, 2H, Ar*H*), 4.65 (t, J = 6.5 Hz, 2H, OC*H₂*CH₂CF₂), 4.36 (t, *J* = 6.5 Hz, 2H, COOC*H₂*), 4.02 (t, J = 6.5 Hz, 2H, OC*H₂*), 2.63 (tt, *J* = 18.5, 6.5 Hz, 2H, C*H₂*CF₂), 1.94 – 1.74 (m, 4H, OCH₂C*H₂*), 1.67 – 1.46 (m, 4H, COOCH₂CH₂C*H₂* and OCH₂CH₂C*H₂*).

^{19}F NMR (376 MHz, CDCl₃) δ -80.60, -111.84, -114.7, -121.52, -121.79, -122.59, -123.35, -125.99.

^{13}C{^{1}H} NMR (101 MHz, CDCl₃) δ 166.2, 165.6, 159.8, 145.4, 132.7, 132.7, 131.9, 131.8, 131.5, 130.4, 129.8, 129.7, 129.4, 128.5, 127.9, 127.3, 127.2, 119.3, 115.2, 115.2, 110.2, 91.8, 91.4, 68.1, 65.3, 57.2, 29.2, 28.8, 26.0, 25.9. 14.3

MALDI-TOF-MS: m/z = 1012.2 [M+Na]$^+$

Anal. Calcd for C₄₅H₃₂F₁₇NO₅: C, 54.61, H, 3.26, N, 1.42; found C, 54.22, H, 3.20, N, 1.31
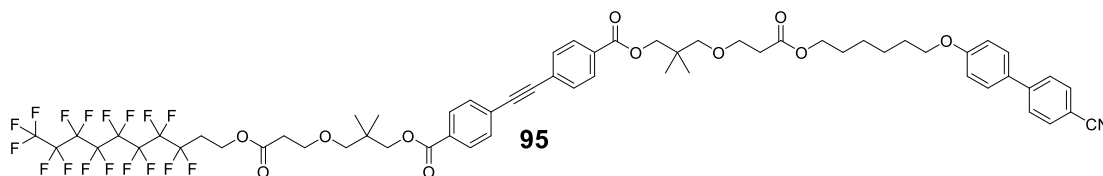
Compound **40** (0.29 g, 0.50 mmol), Compound **37** (0.44 g, 0.52 mmol), [PdCl$_2$(PPh$_3$)$_2$](0.03 g, 0.04 mmol) and CuI (0.01 g, 0.05 mmol) were charged to a Schlenk tube under argon. Triethylamine (10 mL) and toluene (10 mL) were charged to a second Schlenk tube and degassed with argon gas for 20 minutes. The degassed solvent was transferred to the reaction mixture which was stirred at room temperature for 18 hours. The solvent was removed *in vacuo* and the crude product was purified by column chromatography (DCM:EtOAc as eluent) then recrystallised twice from DCM:ethanol to give the target compound **95** as a white solid (0.21 g, 0.16 mmol, 32% yield).

^{1}H NMR (400 MHz, CDCl$_3$) δ 8.01 (d, *J* = 8.5, 4H, Ar*H*), 7.67 (d, *J* = 8.5 Hz, 2H, Ar*H*), 7.64 – 7.55 (m, 6H, Ar*H*), 7.50 (d, *J* = 8.5 Hz, 2H, Ar*H*), 6.96 (d, *J* = 8.5 Hz, 2H, Ar*H*), 4.37 (t, *J* = 6.5 Hz, 2H, OC*H$_2$*CH$_2$CF$_2$), 4.18 – 4.03 (m, 6H, COOC*H$_2$*), 3.98 (t, *J* = 6.5 Hz, 2H, OC*H$_2$*), 3.38 (t, *J* = 6.5 Hz, 4H, OC*H$_2$*CH$_2$), 3.29 (s, 2H, CC*H$_2$*O), 3.28 (s, 2H, CC*H$_2$*O), 2.55 (t, *J* = 6.0 Hz, 4H, C*H$_2$*COO), 2.43 (tt, *J* = 18.5, 6.5 Hz, 2H, C*H$_2$*CF$_2$), 1.83 – 1.63 (m, 4H, OCH$_2$C*H$_2$*), 1.65 (m, 4H, OCH$_2$CH$_2$C*H$_2$*), 1.00 (s, 12H, C(C*H$_3$*)$_2$).

^{13}C{^{1}H} NMR (101 MHz, CDCl$_3$) δ 172.0, 166.3, 165.8, 165.5, 159.9, 145.4, 132.3, 131.8, 131.5, 130.7, 129.8, 127.5, 127.2, 119.4, 115.2, 110.3, 91.8, 91.4, 68.1, 67.7, 67.2, 57.0, 35.2, 29.5, 28.4, 25.9, 14.4 14.3.

MALDI-TOF-MS: m/z = 1328.4 [M+Na]$^+$

Anal. Calcd for C$_{45}$H$_{32}$F$_{17}$NO$_5$: C, 56.10, H, 4.63, N, 1.07; found C, 56.48, H, 4.65, N, 0.89.

96
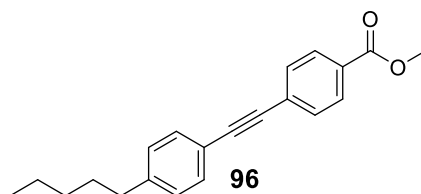
Methyl 4-iodobenzoate (1.01 g, 3.85 mmol), [PdCl$_2$(PPh$_3$)$_2$](0.03 g, 0.04 mmol) and CuI (0.02 g, 0.08 mmol) were charged to a Schlenk tube under argon. Triethylamine (20 mL) and 1-ethynyl-4-pentylbenzene (0.81 mL, 0.72 g, 4.16 mmol) were charged to a second Schlenk tube and degassed with argon gas for 20 minutes. The degassed solvent was transferred to the reaction mixture which was then stirred overnight. The solvent was removed *in vacuo* and the crude product was twice purified *via* a short silica plug (toluene as eluent) to give the target compound **96** as a dark solid (1.07 g, 3.49 mmol, 91% yield).

^{1}H NMR (400 MHz, CDCl$_3$) δ 8.01 (d, *J* = 8.0 Hz, 2H, Ar*H*), 7.57 (d, *J* = 8.0 Hz, 2H, Ar*H*), 7.45 (d, *J* = 8.0 Hz, 2H, Ar*H*), 7.18 (d, *J* = 8.0 Hz, 2H, Ar*H*), 3.93 (s, 3H, COOC*H$_3$*), 2.61 (t, *J* = 7.0 Hz, 2H, ArC*H$_2$*), 1.62 (tt, *J* = 7.5, 7.5 Hz, 2H, ArCH$_2$C*H$_2$*), 1.40 − 1.26 (m, 4H, CH$_3$C*H$_2$*CH$_2$ and CH$_3$CH$_2$C*H$_2$*), 0.89 (t, *J* = 7.0 Hz, 3H, C*H$_3$*CH$_2$).

^{13}C{^{1}H} NMR (101 MHz, CDCl$_3$) δ 166.9, 144.3, 131.9, 131.7, 129.7, 129.5, 128.8, 128.5, 120.0, 92.9, 88.3, 52.5, 36.2, 31.7, 31.2, 22.8, 14.3.

97
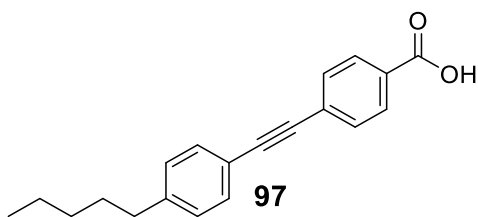
Compound **96** (1.07 g, 3.49 mmol) was charged to a flask then acetone (30 mL) and 1M NaOH solution (8 mL) was added. The reaction mixture was stirred at room temperature for three days then additional acetone (30 mL) added. The reaction mixture was acidified with 1 M HCl solution (10 mL) and extracted with DCM (3 x 15 mL). The combined organic extracts were washed with brine (15 mL) and dried over magnesium sulfate. The solvent was removed *in vacuo* and the product passed through a short silica plug with ethyl acetate as eluent to give the target compound **97** as a tacky white solid (0.58 g, 1.99 mmol, 57% yield).

^{1}H NMR (400 MHz, CDCl$_3$) δ 8.05 (d, *J* = 8.0 Hz, 2H, Ar*H*), 7.57 (d, *J* = 8.0 Hz, 2H, Ar*H*), 7.45 (d, *J* = 8.0 Hz, 2H, Ar*H*), 7.18 (d, *J* = 8.0 Hz, 2H, Ar*H*), 2.61 (t, *J* = 7.0 Hz, 2H, ArC*H*$_2$), 1.62 (tt, *J* = 7.5, 7.5 Hz, 2H, ArCH$_2$C*H*$_2$), 1.40 – 1.26 (m, 4H, CH$_3$C*H*$_2$CH$_2$ and CH$_3$CH$_2$C*H*$_2$), 0.89 (t, *J* = 7.0 Hz, 3H, C*H*$_3$CH$_2$). Acid proton not observed.

98
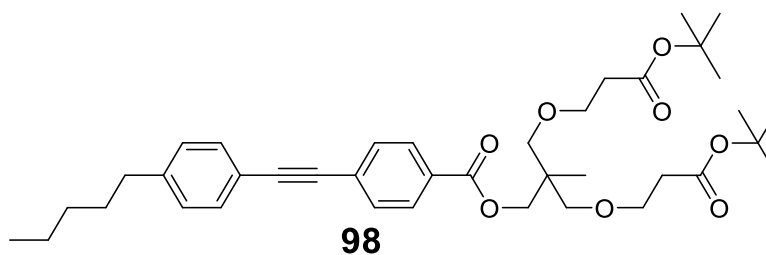
Compound **97** (0.58 g, 1.99 mmol), Compound **41** (0.75 g, 1.99 mmol), DCC (0.46 g, 2.23 mmol) and DMAP (0.06 g, 0.49 mmol) were dissolved in dry DCM (40 mL). The reaction mixture was stirred at room temperature for 18 hours then the solvent removed *in vacuo*. The crude product was purified by column chromatography (petrol:diethyl ether as eluent) to give the target compound 98 as a colourless oil (0.69 g, 1.06 mmol, 53% yield).

^{1}H NMR (400 MHz, CDCl$_3$) δ 7.98 (d, *J* = 8.0 Hz, 2H, Ar*H*), 7.56 (d, *J* = 8.0 Hz, 2H, Ar*H*), 7.45 (d, *J* = 8.0 Hz, 2H, Ar*H*), 7.16 (d, *J* = 8.0 Hz, 2H, Ar*H*), 4.20 (s, 2H, COOC*H*$_2$), 3.63 (t, *J* = 6.5 Hz, 4H, OC*H*$_2$CH$_2$), 3.37 (s, 4H, CC*H*$_2$O), 2.65 (t, *J* = 7.0 Hz, 2H, ArC*H*$_2$), 2.43 (t, *J* = 6.5 Hz, 4H, C*H*$_2$COO), 1.61 (tt, *J* = 7.5, 7.5 Hz, 2H, ArCH$_2$C*H*$_2$), 1.43 (s, 18H, C(C*H*$_3$)$_3$), 1.40 – 1.26 (m, 4H, CH$_3$C*H*$_2$CH$_2$ and CH$_3$CH$_2$C*H*$_2$),1.01 (s, 3H, CC*H*$_3$), 0.88 (t, *J* = 7.0 Hz, 3H, C*H*$_3$CH$_2$).

99
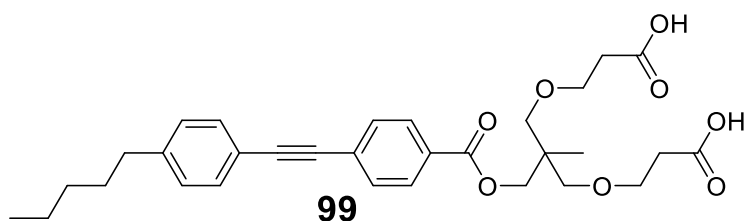
Compound **98** (0.46 g, 0.71 mmol mmol) was dissolved in dry DCM (20 mL) and TFA (1.2 mL) was slowly added. The reaction mixture was stirred at room temperature for 18 hours then the solvent removed *in vacuo* to give the crude product as an oil. Sequential (2 x) addition of toluene (20 mL) and removal of the solvent *in vacuo* gave the target compound **99** as a tacky cream solid (0.43 g, 0.79 mmol) which was used without further purification.

^{1}H NMR (400 MHz, CDCl$_3$) δ 7.99 (d, *J* = 8.5 Hz, 2H, Ar*H*), 7.57 (d, *J* = 8.5 Hz, 2H, Ar*H*), 7.46 (d, *J* = 8.0 Hz, 2H, Ar*H*), 7.18 (d, *J* = 8.0 Hz, 2H, Ar*H*), 4.20 (s, 2H, COOC*H*$_2$), 3.69 (t, *J* = 6.5 Hz, 4H, OC*H*$_2$CH$_2$), 3.41 (apparent quartet, *J* = 8.5 Hz, 4H, CC*H*$_2$O), 2.61-2.39 (m, 6H, ArC*H*$_2$ and C*H*$_2$COO), 1.62 (t, *J* = 7.5 Hz, 2H, ArCH$_2$C*H*$_2$), 1.41 − 1.24 (m, 4H, CH$_3$C*H*$_2$CH$_2$ and CH$_3$CH$_2$C*H*$_2$), 1.02 (s, 3H, CC*H*$_3$), 0.89 (t, *J* = 7.0 Hz, 3H, C*H*$_3$CH$_2$). Acid protons not observed.

ESI-MS: m/z = 561.3 [M+Na]$^+$

100
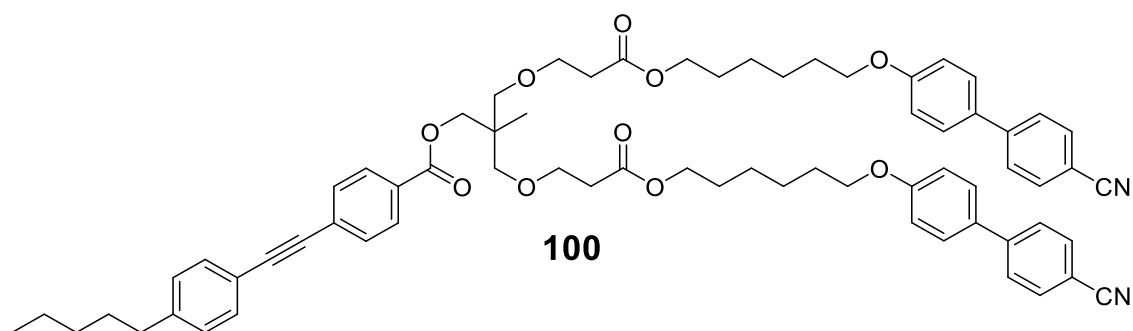
Compound **99** (0.10 g, 0.19 mmol), compound **32ᵢ** (0.12 g, 0.41 mmol), DCC (0.12 g, 0.58 mmol) and DMAP (0.03 g, 0.25 mmol) were charged to a flask and dry DCM (40 mL) added. The reaction mixture was stirred at room temperature for seven days and then the solvent removed *in vacuo*. The crude product was purified by column chromatography (DCM:MeOH as eluent) to give the target compound **100** as a colourless oil (0.095 g, 0.09 mmol, 45% yield).

^{1}H NMR (400 MHz, CDCl$_3$) δ 7.97 (d, *J* = 8.0 Hz, 2H, Ar*H*), 7.66 (d, *J* = 8.0 Hz, 4H, Ar*H*), 7.62 (d, *J* = 8.0 Hz, 4H, Ar*H*), 7.55 (d, *J* = 8.0 Hz, 2H, Ar*H*), 7.50 (d, *J* = 8.5 Hz, 4H, Ar*H*), 7.43 (d, *J* = 8.0 Hz, 2H, Ar*H*), 7.16 (d, *J* = 7.5 Hz, 2H, Ar*H*), 6.96 (d, *J* = 8.5 Hz, 4H, Ar*H*), 4.20 (s, 2H, COOC*H₂*), 4.08 (t, *J* = 6.5 Hz, 4H, COOC*H₂*), 3.99 (t, *J* = 6.5 Hz, 4H, ArOC*H₂*), 3.68 (t, *J* = 6.0 Hz, 4H, OC*H₂*CH₂), 3.38 (s, 4H, CC*H₂*O), 2.62(t, *J* = 8.0 Hz, 2H, ArC*H₂*), 2.56 (t, *J* = 6.0 Hz, 4H, C*H₂*COO), 1.84-1.74 (m, 4H, COOCH₂C*H₂*), 1.73 − 1.62 (m, 4H, ArOCH₂C*H₂*), 1.61 (t, *J* = 7.5 Hz, 2H, ArCH₂C*H₂*), 1.53-1.38 (m, 8H, COOCH₂CH₂C*H₂* and OCH₂CH₂C*H₂*), 1.35-1.27 (m, 4H, CH₃C*H₂*CH₂ and CH₃CH₂C*H₂*), 1.01 (s, 3H, CC*H₃,*), 0.89 (t, *J* = 6.5 Hz, 3H, C*H₃*CH₂).

^{13}C{^{1}H} NMR (101 MHz, CDCl$_3$) δ 171.8, 166.0, 159.8, 145.4, 144.3, 132.7, 131.8, 131.8, 131.6, 129.6, 128.7, 128.5, 127.2, 119.3, 115.2, 110.2, 92.9, 88.2, 73.6, 68.1, 67.6, 67.1, 64.6, 40.4, 36.1, 35.3, 31.6, 31.1, 29.3, 28.7, 25.9, 22.7, 17.4, 14.2.

MALDI-TOF-MS: m/z = 1115.5 [M+Na]$^+$

Anal. Calcd for C$_{69}$H$_{76}$N$_2$O$_{10}$: C, 75.80, H, 7.01, N, 2.56; found C, 75.36, H, 7.04, N, 2.52

101
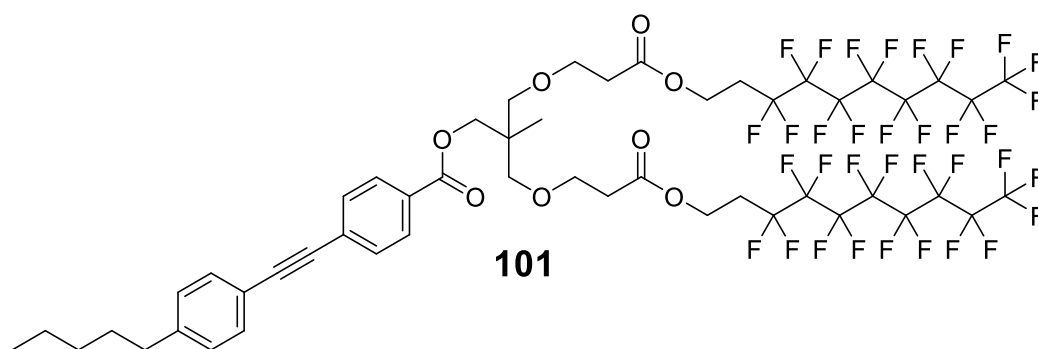
Compound **49** (0.65 g, 0.26 mmol), [PdCl$_2$(PPh$_3$)$_2$](0.02 g, 0.03 mmol) and CuI (0.004 g, 0.02 mmol) were charged to a Schlenk tube under argon. Triethylamine (5 mL), toluene (5 mL) and 1-ethynyl-4-pentylbenzene (0.06 mL, 0.05 g, 0.31 mmol) were charged to a second Schlenk tube and degassed with argon gas for 20 minutes. The degassed solvent was transferred to the reaction mixture which was then stirred for 18 hours. The solvent was removed *in vacuo* and the crude product was purified by column chromatography (DCM:EtOAc as eluent) then recrystallised from DCM:ethanol to give the target compound **101** as a white solid (0.11 g, 0.15 mmol, 58% yield).

^{1}H NMR (400 MHz,) δ 7.97 (d, *J* = 8.0 Hz, 2H, Ar*H*), 7.55 (d, *J* = 8.0 Hz, 2H, Ar*H*), 7.44 (d, *J* = 8.0 Hz, 2H, Ar*H*), 7.16 (d, *J* = 8.0 Hz, 2H, Ar*H*), 4.37 (t, *J* = 6.5 Hz, 4H, OC*H$_2$*CH$_2$CF$_2$), 4.18 (s, 2H, COOC*H$_2$*C(CH$_2$O)$_2$), 3.67 (t, *J* = 6.0 Hz, 4H, OC*H$_2$*CH$_2$), 3.36 (s, 4H, CC*H$_2$*O), 2.61 (t, *J* = 7.5 Hz, 2H, ArC*H$_2$*), 2.55 (t, *J* = 6.0 Hz, 4H, C*H$_2$*COO), 2.44 (tt, J = 18.5, 6.5 Hz, 4H, C*H$_2$*CF$_2$), 1.61 (d, 7.5 Hz, 2H, ArCH$_2$C*H$_2$*), 1.39 – 1.22 (m, 4H, C*H2* CH$_2$CH$_2$CH$_3$ and C*H$_2$*CH$_3$), 0.99 (s, 3H, CC*H$_3$*), 0.88 (t, *J* = 6.5 Hz, 3H, CH$_2$C*H$_3$*).

^{13}C{^{1}H} NMR (101 MHz, CDCl$_3$) δ 171.0, 165.9, 144.3, 131.6, 131.4, 129.6, 129.4, 128.5, 120.0, 92.6, 88.0, 70.1, 66.5, 56.3, 44.2, 35.4, 34.9, 31.3, 31.0, 30.6, 30.3, 29.5, 22.6, 14.2.

MALDI-TOF-MS: 1453.24 [M+Na]$^+$

Anal. Calcd for C$_{51}$H$_{44}$F$_{34}$O$_8$: C, 42.81, H, 3.10, N, -; found C, 42.61, H, 3.07, N, -.

102
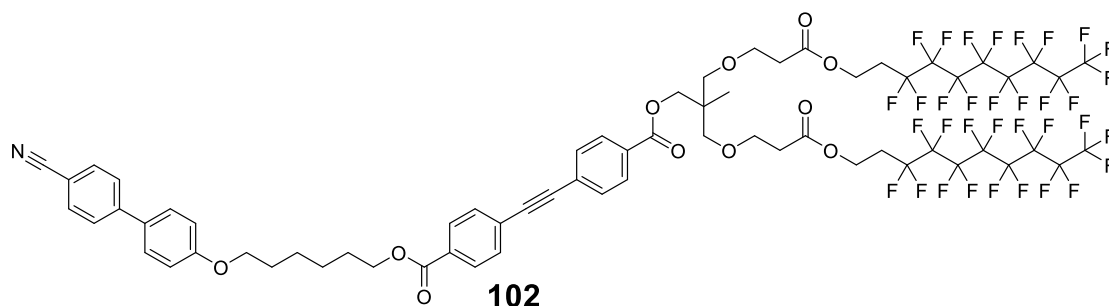
Compound **49** (0.39 g, 0.28 mmol), Compound **33**ᵢ (0.21 g, 0.50 mmol), [PdCl₂(PPh₃)₂](0.03 g, 0.04 mmol) and CuI (0.01 g, 0.05 mmol) were charged to a Schlenk tube under argon. Triethylamine (12 mL) and toluene (12 mL) were charged to a second Schlenk tube and degassed with argon gas for 20 minutes. The degassed solvent was transferred to the reaction mixture which was then stirred at room temperature for 18 hours. The solvent was removed *in vacuo* and the crude product was purified by column chromatography (DCM:EtOAc as eluent) then recrystallised from DCM:ethanol to give the target compound **102** as a white solid (0.22 g, 0.13 mmol, 47% yield).

^{1}H NMR (400 MHz, CDCl₃) δ 8.02 (d, *J* = 8.5 Hz, 4H, Ar*H*), 7.68 (d, J = 8.0 Hz, 2H, Ar*H*), 7.63-7.57 (m, 6H, Ar*H*), 7.52 (d, *J* = 8.0 Hz, 2H, Ar*H*), 6.98 (d, *J* = 8.0 Hz, 2H, Ar*H*), 4.37 (t, *J* = 6.5 Hz, 4H, OC*H₂*CH₂CF₂), 4.20 (s, 2H, COOC*H₂*C(CH₂O)₂), 4.07 (t, *J* = 6.5 Hz, 2H, COOC*H₂*CH₂), 3.68 (t, *J* = 6.0 Hz, 4H, OC*H₂*CH₂), 3.38 (s, 4H, CC*H₂*O), 2.58-2.41 (m, 6H, C*H₂*COO), 2.48 (tt, *J* = 18.5, 6.5 Hz, 4H, C*H₂*CF₂), 1.90 – 1.79 (m, 4H, OCH₂C*H₂*), 1.61-1.43 (m, 4H, OCH₂CH₂C*H₂*), 1.01 (s, 3H, CC*H₃*).

^{13}C{^{1}H} NMR (101 MHz, CDCl₃) δ 171.3, 159.8, 146.3, 132.7, 131.8, 129.7, 128.5, 127.2, 115.2, 73.5, 68.1, 66.8, 65.3, 56.5, 40.4, 35.0, 30.6, 29.2, 28.8, 26.0, 17.3.

MALDI-TOF-MS: m/z = 1704.3 [M+Na]$^+$

Anal. Calcd for C₆₆H₅₃F₃₄NO₁₁: C, 59.52, H, 4.60, N, 1.85; found C, 59.39, H, 4.57, N, 2.05.

103
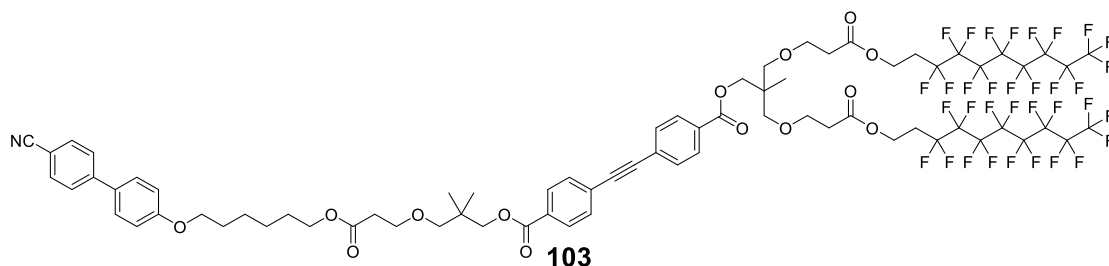
Compound **49** (0.66 g, 0.48 mmol), compound **37** (0.21 g, 0.36 mmol), [PdCl$_2$(PPh$_3$)$_2$](0.05 g, 0.07 mmol) and CuI (0.02 g, 0.01 mmol) were charged to a Schlenk tube under argon. Triethylamine (10 mL) and toluene (10 mL) were charged to a second Schlenk tube and degassed with argon gas for 20 minutes. The degassed solvent was transferred to the reaction mixture which was then stirred for 18 hours. The solvent was removed *in vacuo* and the crude product was purified by column chromatography (DCM:EtOAc as eluent) then recrystallised twice from ethanol to give the target compound **103** as a white solid (0.19 g, 0.10 mmol, 29% yield).

^{1}H NMR (400 MHz, CDCl$_3$) δ 8.00 (d, *J* = 8.5 Hz, 4H, Ar*H*), 7.67 (d, *J* = 8.5 Hz, 2H, Ar*H*), 7.64 – 7.55 (m, 6H, Ar*H*), 7.50 (d, *J* = 8.5 Hz, 2H, Ar*H*), 6.96 (d, *J* = 8.5 Hz, 2H, Ar*H*), 4.37 (t, *J* = 6.5 Hz, 4H, OC*H$_2$*CH$_2$CF$_2$), 4.19 (s, 2H, COOC*H$_2$*C(CH$_2$O)$_2$), 4.09 (s, 2H, COOC*H$_2$*), 3.98 (t, *J* = 6.5 Hz, 2H, COOC*H$_2$*CH$_2$), 3.68 (t, *J* = 6.0 Hz, 2H, OC*H$_2$*CH$_2$), 3.42 (t, *J* = 6.5 Hz, 4H, OC*H$_2$*CH$_2$), 3.36 (s, 4H, CC*H$_2$*O), 3.29 (s, 2H, CC*H$_2$*O), 2.68 – 2.48 (m, 8H, C*H$_2$*COO), 2.45 (tt, *J* = 18.5, 6.5 Hz, 4H, C*H$_2$*CF$_2$), 1.89 – 1.73 (m, 4H, OCH$_2$C*H$_2$*), 1.60 – 1.39 (m, 4H, OCH$_2$CH$_2$C*H$_2$*), 1.00 (s, 9H, C(C*H$_3$*)$_2$).

^{13}C{^{1}H} NMR (101 MHz, CDCl$_3$) δ 169.9, 166.1, 165.7, 165.6, 159.9, 145.6, 132.2, 131.9, 131.4, 130.8, 129.8, 127.4, 127.3, 119.6, 115.2, 110.5, 91.8, 91.2, 68.3, 67.7, 67.4, 57.1, 35.4, 29.7, 28.3, 26.0, 14.3 14.2.

MALDI-TOF-MS: m/z = 1862.4 [M+Na]$^+$

Anal. Calcd for C$_{74}$H$_{67}$F$_{34}$NO$_{14}$: C, 48.30, H, 3.67, N, 0.76; found C, 48.66, H, 3.68, N, 0.69.

104
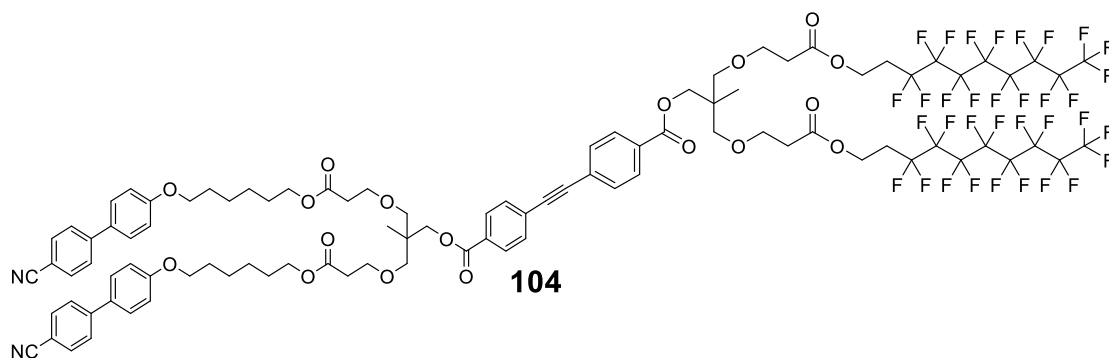
Compound **45** (0.24 g, 0.22 mmol), [PdCl$_2$(PPh$_3$)$_2$](0.03 g, 0.04 mmol) and CuI (0.01 g, 0.05 mmol) were charged to a Schlenk tube under argon. Triethylamine (8 mL), toluene (8 mL) and compound **48** (0.29 g, 0.23 mmol) were charged to a second Schlenk tube and degassed with argon gas for 20 minutes. The degassed solvent was transferred to the reaction mixture which was then stirred at room temperature for 18 hours. The solvent was removed *in vacuo* and the crude product was purified by column chromatography (DCM:EtOAc as eluent) then recrystallised from DCM:ethanol to give the target compound **104** as an off-white solid (0.10 g, 0.05 mmol, 20% yield).

^{1}H NMR (400 MHz, CDCl$_3$) δ 8.01 (d, *J* = 8.5 Hz, 4H, Ar*H*), 7.68 (d, *J* = 8.5 Hz, 4H, Ar*H*), 7.65 – 7.57 (m, 8H, Ar*H*), 7.51 (d, *J* = 9.0 Hz, 4H, Ar*H*), 6.97 (d, *J* = 9.0 Hz, 4H, Ar*H*), 4.38 (t, *J* = 6.5 Hz, 4H, OC*H$_2$*CH$_2$CF$_2$), 4.23 (s, 2H, COOC*H$_2$*C(CH$_2$O)$_2$), 4.21 (s, 2H, COOC*H$_2$*C(CH$_2$O)$_2$), 4.09 (t, *J* = 6.5 Hz, 4H, COOC*H$_2$*CH$_2$), 3.98 (t, *J* = 6.5 Hz, 8H, OC*H$_2$*CH$_2$COO), 3.74 – 3.61 (m, 8H, OC*H$_2$*CH$_2$), 3.45 – 3.31 (m, 8H, CC*H$_2$*O), 2.58-2.41 (m, 8H, C*H$_2$*COO), 2.45 (tt, *J* = 18.5, 6.5 Hz, 4H, C*H$_2$*CF$_2$), 1.88 – 1.73 (m, 4H, OCH$_2$C*H$_2$*), 1.72 – 1.60 (m, 4H, OCH$_2$C*H$_2$*), 1.57 – 1.35 (m, 8H, OCH$_2$CH$_2$C*H$_2$*), 1.01 (m, 6H, CC*H$_3$*).

^{19}F NMR (376 MHz, CDCl$_3$) δ -80.69, -113.09, -114.10, -121.61, -121.77,- 122.68, -123.49, -126.07.

^{13}C{^{1}H} NMR (101 MHz, CDCl$_3$) δ 171.8, 171.3, 165.8, 159.8, 145.3, 132.7, 131.8, 131.4, 130.3, 129.6, 128.5, 127.5, 127.2, 119.2, 115.1, 110.1, 91.4, 73.5, 73.4, 68.0, 67.7, 67.1, 66.8, 64.60, 56.46, 40.41, 40.4, 35.2, 35.0, 30.5, 29.2, 28.7, 25.9, 17.4, 17.3.

MALDI-TOF-MS: 2227.6 [M+Na]$^+$

Anal. Calcd for C$_{96}$H$_{90}$F$_{34}$N$_2$O$_{18}$: C, 52.28, H, 4.11, N, 1.72; found C, 52.09, H, 3.99, N, 1.05.

105
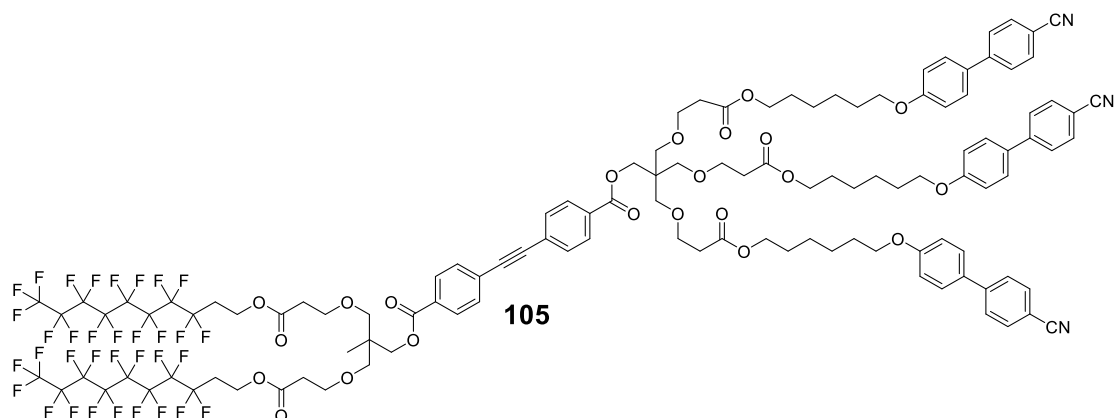
Compound **45** (0.05 g, 0.04 mmol), [PdCl$_2$(PPh$_3$)$_2$](0.003 g, 0.004 mmol) and CuI (0.001 g, 0.005 mmol) were charged to a Schlenk tube under argon. Triethylamine (4 mL), toluene (4 mL) and compound **53** (0.04 g, 0.03 mmol) were charged to a second Schlenk tube and degassed with argon gas for 20 minutes. The degassed solvent was transferred to the reaction mixture which was then stirred at room temperature for 18 hours. The solvent was removed *in vacuo* and the crude product was purified multiple times by column chromatography (DCM:EtOAc as eluent, followed by DCM as eluent) to give the target compound **105** as an off-white solid (0.06 g, 0.02 mmol, 75% yield).

^{1}H NMR (400 MHz, CDCl$_3$) δ 8.00 (d, *J* = 8.5 Hz, 4H, Ar*H*), 7.67 (d, *J* = 8.0 Hz, 6H, Ar*H*), 7.65 − 7.56 (m, 10H, Ar*H*), 7.51 (d, *J* = 8.0 Hz, 6H, Ar*H*), 6.96 (d, *J* = 8.0 Hz, 6H), 4.38 (t, *J* = 6.5 Hz, 4H, OC*H$_2$*CH$_2$CF$_2$), 4.31 (s, 2H, COOC*H$_2$*C(CH$_2$O)$_3$), 4.20 (s, 2H, COOC*H$_2$*C(CH$_2$O)$_2$), 4.07 (t, *J* = 6.5 Hz, 6H, COOC*H$_2$*CH$_2$), 3.98 (t, *J* = 6.5 Hz, 6H, OC*H$_2$*CH$_2$COO), 3.70 − 3.64 (m, 10H, OC*H$_2$*CH$_2$), 3.49 (s, 6H, CC*H$_2$*O), 3.37 (s, 4H, CC*H$_2$*O), 2.60-2.38 (m, 10H, C*H$_2$*COO), 2.44 (tt, *J* = 18.5, 6.5 Hz, 4H, C*H$_2$*CF$_2$), 1.86 − 1.74 (m, 6H, OCH$_2$C*H$_2$*), 1.72 − 1.60 (m, 6H, OCH$_2$C*H$_2$*), 1.55 − 1.36 (m, 12H, OCH$_2$CH$_2$C*H$_2$*), 1.00 (s, 3H, CC*H$_3$*).

^{13}C{^{1}H} NMR (101 MHz, CDCl$_3$) δ 171.8, 171.3, 159.8, 145.3, 132.7, 131.8, 131.5, 129.6, 128.5, 127.2, 115.2, 110.2, 73.4, 69.9, 68.5, 68.0, 67.1, 66.8, 64.6, 56.5, 40.4, 35.2, 35.0, 29.3, 28.69, 25.88, 17.3.

MALDI-TOF-MS: 2592.7 [M+Na]$^+$

Anal. Calcd for C$_{118}$H$_{113}$F$_{34}$N$_3$O$_{22}$: C, 55.12, H, 4.60, N, 1.85; found C, 56.12, H, 4.57, N, 1.36.

106

Compound **30** (0.09 g, 0.15 mmol), [PdCl$_2$(PPh$_3$)$_2$](0.02 g, 0.03 mmol) and CuI (0.005 g, 0.03 mmol) were charged to a Schlenk tube under argon. Triethylamine (6 mL), toluene (6 mL) and compound **44** (0.15 g, 0.14 mmol) were charged to a second Schlenk tube and degassed with argon gas for 20 minutes. The degassed solvent was transferred to the reaction mixture which was stirred at room temperature for 18 hours. The solvent was evaporated to dryness and the crude purified by column chromatography (DCM:EtOAc as eluent) then recrystallised from DCM:ethanol to give the target compound **106** as an off-white solid (0.12 g, 0.08 mmol, 56% yield).

^{1}H NMR (400 MHz, CDCl$_3$) δ 8.01 (d, J = 8.5 Hz, 4H, ArH), 7.67 (d, J = 8.0 Hz, 4H, ArH), 7.65 − 7.57 (m, 8H, ArH), 7.51 (d, J = 8.0, Hz, 4H, ArH), 6.96 (d, J = 8.0, Hz, 4H, ArH), 4.64 (t, J = 6.5 Hz, 2H, OCH_2CH$_2$CF$_2$), 4.21 (s, 2H, COOCH_2C(CH$_2$O)$_2$), 4.09 (t, J = 6.5 Hz, 4H, COOCH_2CH$_2$), 3.99 (t, J = 6.5 Hz, 4H, OCH_2CH$_2$), 3.69 (t, J = 6.5 Hz, 4H, OCH_2CH$_2$), 3.39 (s, 4H, CCH_2O), 2.58-2.41 (m, 4H, CH_2COO), 2.45 (tt, J = 18.5, 6.5 Hz, 2H, CH_2CF$_2$), 1.86 − 1.75 (m, 4H, OCH$_2$CH_2), 1.73 − 1.61 (m, 4H, OCH$_2$CH_2), 1.56 − 1.37 (m, 8H, OCH$_2$CH$_2$CH_2), 1.02 (s, 3H, CCH_3).

^{13}C{^{1}H} NMR (101 MHz, CDCl$_3$) δ 171.8, 165.8, 165.6, 159.8, 145.3, 132.7, 131.9, 131.8, 131.4, 130.4, 129.8, 129.7, 129.4, 128.5, 127.9, 127.4, 127.2, 119.2, 115.2, 110.2, 91.8, 91.4, 76.8, 73.5, 68.0, 67.7, 67.1, 64.6, 57.0, 40.4, 35.2, 30.7, 29.3, 28.7, 28.2, 25.9, 17.4.

MALDI-TOF MS: 1535.45 [M+Na]$^+$

Anal. Calcd for C$_{75}$H$_{69}$F$_{17}$N$_2$O$_{12}$: C, 59.52, H, 4.60, N, 1.85; found C, 59.39, H, 4.57, N, 2.05.

107

Compound **58** (0.26 g, 0.14 mmol), [PdCl$_2$(PPh$_3$)$_2$](0.01 g, 0.014 mmol) and CuI (0.003 g, 0.016 mmol) were charged to a Schlenk tube which was backfilled with argon. Triethylamine (6 mL), toluene (6 mL) and compound **44** (0.12 g, 0.13 mmol) were charged to a second Schlenk tube and degassed with argon gas for 20 minutes. The degassed solvent was transferred to the reaction mixture which was then stirred at room temperature for 18 hours. The solvent was evaporated to dryness and the crude purified multiple times by column chromatography (DCM:EtOAc as eluent, followed by DCM as eluent) to obtain **107** as an off-white solid (0.12 g, 0.08 mmol, 56% yield).

^{1}H NMR (400 MHz, CDCl$_3$) δ 8.00 (d, J = 8.5 Hz, 4H, ArH), 7.68 (d, J = 8.5 Hz, 4H, ArH), 7.65 – 7.56 (m, 8H, ArH), 7.50 (d, J = 9.0 Hz, 4H, ArH), 6.96 (t, J = 9.0 Hz, 4H, ArH), 4.37 (t, J = 6.5 Hz, 6H, OCH_2CH$_2$CF$_2$), 4.29 (s, 2H, COOCH_2C(CH$_2$O)$_3$), 4.21 (s, 2H, COOCH_2C(CH$_2$O)$_2$), 4.09 (t, J = 6.5 Hz, 4H, COOCH_2CH$_2$), 4.02 (t, J = 6.5 Hz, 6H, COOCH_2CH$_2$), 3.99 (t, J = 6.5 Hz, 4H, OCH_2CH$_2$COO), 3.68 (t, J = 6.5 Hz, 4H, OCH_2CH$_2$), 3.47 (s, 6H, CCH_2O), 3.38– 3.34 (m, 4H, CCH_2O), 2.58-2.41 (m, 10H, CH_2COO), 2.45 (tt, J = 18.5, 6.5 Hz, 6H, CH_2CF$_2$), 1.86 – 1.75 (m, 4H, OCH$_2$CH_2), 1.73 – 1.61 (m, 4H, OCH$_2$CH_2), 1.56 – 1.36 (m, 8H, OCH$_2$CH$_2$CH_2), 1.01 (s, 3H, CCH_3).

^{19}F NMR (376 MHz, CDCl$_3$) δ -80.70, -112.29, -114.35, -121.66, -121.91, -122.70, -123.51, -126.09.

^{13}C{^{1}H} NMR (101 MHz, CDCl$_3$) δ 171.8, 171.3, 165.8, 159.8, 145.3, 132.7, 131.8, 131.4, 130.3, 129.6, 128.5, 127.5, 127.2, 119.2, 115.1, 110.1, 91.4, 73.5, 73.4, 68.0, 67.7, 67.1, 66.8, 64.6, 56.5, 40.4, 40.4, 35.2, 35.0, 30.5, 29.2, 28.7, 25.9, 17.4, 17.3.

MALDI-TOF-MS: 2761.6 [M+Na]$^+$

Anal. Calcd for C$_{109}$H$_{97}$F$_{51}$N2O$_{21}$: C, 47.78, H, 3.57, N, 1.02; found C, 48.36, H, 3.64, N, 1.00.

109
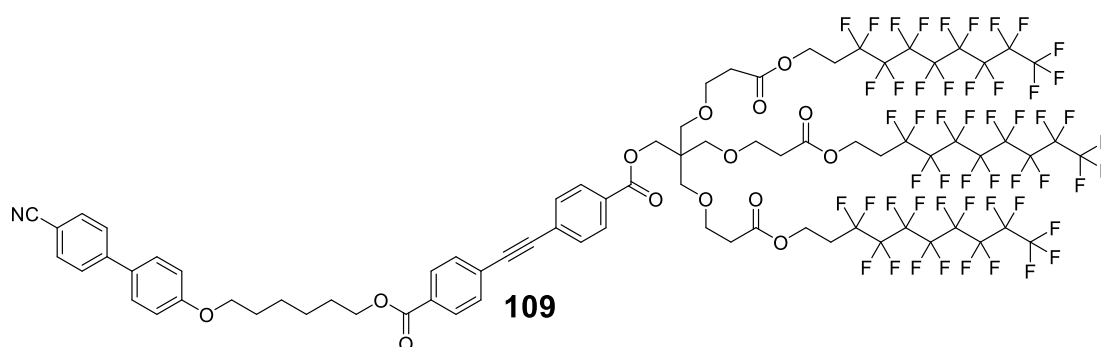
Compound **58** (0.25 g, 0.08 mmol), ethynyl cyanobiphenyl compound (0.03 g, 0.07 mmol), [PdCl$_2$(PPh$_3$)$_2$](0.01 g, 0.04 mmol) and CuI (0.03 g, 0.05 mmol) were charged to a Schlenk tube under argon. Triethylamine (5 mL) and toluene (7 mL) were charged to a second Schlenk tube and degassed with argon gas for 20 minutes. The degassed solvent was transferred to the reaction mixture which was then stirred at room temperature for 18 hours. The solvent was removed *in vacuo* and the crude product was purified multiple times by column chromatography (DCM:EtOAc as eluent, followed by DCM as eluent) to give the target compound **109** as a white solid (0.11 g, 0.05 mmol, 64% yield).

^{1}H NMR (400 MHz, CDCl$_3$) δ 8.02 (d, *J* = 8.5 Hz, 4H, Ar*H*), 7.68 (d, J = 8.0 Hz, 2H, Ar*H*), 7.62-7.55 (m, 6H, Ar*H*), 7.52 (d, *J* = 8.0 Hz, 2H, Ar*H*), 6.98 (d, *J* = 8.0 Hz, 2H, Ar*H*), 4.39 (t, *J* = 6.5 Hz, 6H, OC*H$_2$*CH$_2$CF$_2$), 4.31 (s, 2H, COOC*H$_2$*C(CH$_2$O)$_3$), 4.06 (t, *J* = 6.5 Hz, 6H, COOC*H$_2$*CH$_2$), 3.98 (t, *J* = 7.0 Hz, 2H, OC*H$_2$*CH$_2$), *3.69* (t, *J* = 6.0 Hz, 2H, OC*H$_2$*CH$_2$), 3.38 (s, 6H, CC*H$_2$*O), 2.58-2.40 (m, 6H, C*H$_2$*COO), 2.47 (tt, *J* = 18.5, 6.5 Hz, 6H, C*H$_2$*CF$_2$), 1.89 – 1.78 (m, 4H, OCH$_2$C*H$_2$*), 1.62-1.40 (m, 4H, OCH$_2$CH$_2$C*H$_2$*).

^{13}C{^{1}H} NMR (101 MHz, CDCl$_3$) δ 166.1, 165.6, 159.8, 145.3, 132.7, 131.8, 131.8, 131.5, 130.4, 129.8, 129.7, 129.3, 128.4, 127.9, 127.3, 127.2, 119.2, 115.2, 110.1, 91.8, 91.3, 76.8, 68.0, 65.3, 57.2, 30.7, 29.2, 28.7, 25.9, 25.9.

MALDI-TOF MS: 2238.3 [M+Na]$^+$

Anal. Calcd for C$_{79}$H$_{60}$F$_{51}$NO$_{14}$: C, 42.81, H, 2.73, N, 0.63; found C, 43.40, H, 2.74, N, 0.67.

5.7 References

1   C. Tschierske, *Isr. J. Chem*., 2012, 52, 935–959.

2   I. M. Saez and J. W. Goodby, *Chem. Eur. J*., 2003, 9, 4869–4877.

3   T. Ma, PhD Thesis, University of York, 2013.

4   H. Sato, T. Yajima and A. Yamagishi, *Chirality*, 2016, 28, 361–364.

5   M. Yamanaka, Y. Miyake, S. Akita and K. Nakano, *Chem. Mater*., 2008, 20, 2072–2074.

6   J. A. Schröter, C. Tschierske, M. Wittenberg and J. H. Wendorff, *J. Am. Chem. Soc.*, 1998, 120, 10669–10675.

7   M. Murase, Y. Takanishi, I. Nishiyama, A. Yoshizawa and J. Yamamoto, *RSC Adv.,* 2015, 5, 215–220.

8   J. W. Lee, X. L. Piao, Y. K. Yun, J. Il Jin, Y. S. Kang and W. C. Zin, *Liq. Cryst*., 1999, 26, 1671–1685.

9   F. Dumoulin, D. Lafont, T. L. Huynh, P. Boullanger, G. Mackenzie, J. J. West and J. W. Goodby, *Chem. Eur. J.*, 2007, 13, 5585–5600.

10   C. Tschierske, Topics in Current Chemistry, 2012, Springer-Verlag Berlin, Heidelberg, vol 318, pp 1-101 .

11   V. Percec, G. Johansson, G. Ungar and J. Zhou*, J. Am. Chem. Soc*., 1996, 118, 9855–9866.

12   B. M. Rosen, D. A. Wilson, C. J. Wilson, M. Peterca, B. C. Won, C. Huang, L. R. Lipski, X. Zeng, G. Ungar, P. A. Heiney and V. Percec, J. *Am. Chem. Soc*., 2009, 131, 17500–17521.

13   J. Malthête, M. Leclercq, M. Dvolaitzky, J. Gabard, J. Billard, V. Pontikis and J. Jacques, *Mol. Cryst. Liq. Cryst.,* 1973, 23, 233–260.

14   H. Li, J. Wen and Y. Yang, *Mol. Cryst. Liq. Cryst*., 2007, 473, 15–22.

15   G. Johansson, V. Percec, G. Ungar and K. Smith, *Chem. Mater*., 1997, 9, 164–175.

16   I. Bury, B. Heinrich, C. Bourgogne, D. Guillon and B. Donnio, *Chem. Eur. J*., 2006, 12, 8396–8413.

17   K. C. Elbert, D. Jishkariani, Y. Wu, J. D. Lee, B. Donnio and C. B. Murray, *Chem. Mater.*, 2017, 29, 8737–8746.

18   G. Johansson, V. Percec, G. Ungar and J. P. Zhou, *Macromolecules*, 1996, 29, 646–660.

19   D. Lose, S. Diele, G. Pelzl, E. Dietzmann and W. Weissflog, *Liq. Cryst.,* 1998, 24, 707–717.

20   E. Nishikawa, J. Yamamoto and H. Yokoyama, *J. Mater. Chem*., 2003, 13, 1887–1893.

21   GaussView, Version 6.1, Roy Dennington, Todd A. Keith, John M. Millam, Semichem Inc., Shawnee Mission. KS, 2016.

22   A. K. Rappé, C. J. Casewit, K. S. Colwell, W. A. Goddard and W. M. Skiff, *J. Am. Chem. Soc*., 1992, 114, 10024–10035.

23   A. Kohlmeier and D. Janietz, *Liq. Cryst*., 2007, 34, 65–71.

24   S. Guerra, T. L. A. Nguyen, J. Furrer, J. F. Nierengarten, J. Barberá and R. Deschenaux, *Macromolecules*, 2016, 49, 3222–3231.

25   S. Laschat, A. Baro, N. Steinke, F. Giesselmann, C. Hägele, G. Scalia, R. Judele, E. Kapatsina, S. Sauer, A. Schreivogel and M. Tosoni, *Angew. Chem. Int. Ed*., 2007, 46, 4832–4887.

26   C. Tschierske, C. Nürnberger, H. Ebert, B. Glettner, M. Prehm, F. Liu, X. B. Zeng and G. Ungar, *Interface Focus,* 2012, 2, 669–680.

27   M. Poppe, C. Chen, S. Poppe, F. Liu and C. Tschierske, *Chem. Commun.,* 2020, 3, 1–8.

28   X. Zeng, R. Kieffer, B. Glettner, C. Nürnberger, F. Liu, K. Pelz, M. Prehm, U. Baumeister, H. Hahn, H. Lang, G. A. Gehring, C. H. M. Weber, J. K. Hobbs, C. Tschierske, G. Ungar, *Science*, 2011, 4206, 1302–1306.

Chapter 6. Chiral diphenyl acetylene derivatives

A family of diphenyl acetylene derivatives featuring a chiral group were synthesised in an attempt to begin to establish a structure-activity relationship (Figure 129). The chiral chain (S)-2-methylbutyl was attached to the diphenyl acetylene core using either an ether or ester linkage to investigate the role of parity and electronic effects on mesomorphic behaviour. The parity and length of the methylene spacer was varied to investigate odd/even effects and the effects of coupling/decoupling of the aromatic units on the liquid crystalline behaviour.
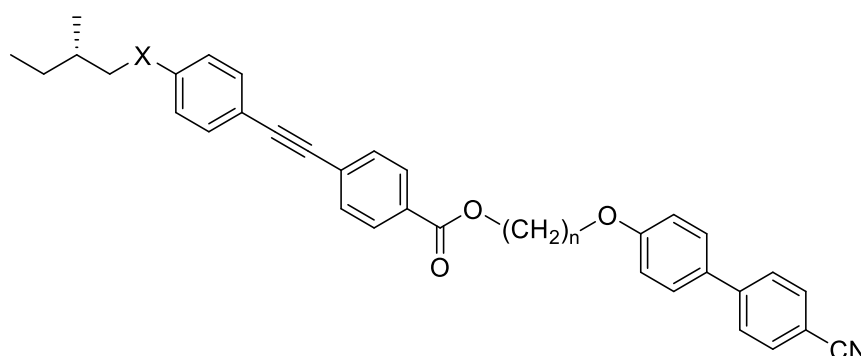
Figure 129. Generic structure of the chiral materials described in this work. X = ester or ether linkage.

Five spacer lengths were utilised, with even (hexyl, octyl, dodecyl) or odd (nonyl, undecyl) numbers of methylene units. In order to provide comparisons to understand and contextualise the results, analogues using (S)-1-methylheptyl as the chiral group were also investigated using an undecyl methylene spacer. Additionally, one compound was produced for which the diphenyl acetylene core was replaced with a biphenyl unit and secondly a chiral diphenyl acetylene monomer was also prepared to determine the mesomorphic behaviour of this half of the compounds investigated. For each material produced in addition to the bulk liquid crystalline properties the helical twisting power of the materials when used as a chiral dopant in the nematic host E7 was determined.

6.1. Introduction to chiral liquid crystal materials.

Many chiral units have been used in the development of chiral liquid crystals including sugars[1] and chiral alkyl chains.[2] Depending on where and how these chiral units are incorporated can have a profound effect on the liquid crystal properties.[3] In this work the chiral unit is incorporated close to a rigid core which will provide a shorter pitch or

higher helical twisting power than if the chiral unit were at the periphery such as the end of an alkyl chain.

6.1.1 Design of chiral liquid crystal materials

In this project the chiral units used are chiral alkyl chains and as such several factors are of importance when designing the material including the distance separating the chiral unit to the core and parity of any spacer between them.

In studying chiral nematic materials Gray and McDonnell established a set of empirical rules which may be used to predict the handedness of a chiral nematic helix.[4] This uses three letters each of which describe a different property of the chiral nematic material – absolute configuration, parity and twist sense (Table 25). The first letter (S or R) describes the absolute configuration at the chiral centre, the second (E or O) describes the parity or number of atoms between the chiral unit and ring system as an even or odd value and the third letter predicts the sense of the helical rotation in the chiral nematic phase as D-(*dextro*) or L-(*levo*).

Table 25. Gray and McDonnel rules to predict the handedness of a chiral nematic helix.

Right-handed helices	Left-handed helices
SED	SOL
ROD	REL

These rules indicate that either switching the absolute configuration at the chiral centre (S or R) or altering the parity of the spacer to include an even or odd number of atoms (E or O) will give the opposite twist sense of the chiral nematic helix. Notably the parity in this case is concerned only by the number of atoms and not their nature as carbon, oxygen etc. These rules were developed empirically to describe a series of calamitic compounds and are proven to work well to predict this behaviour, thus giving confidence that should the absolute configuration of the chiral centre used throughout the work be kept constant, altering the parity of a spacer should allow the helical twist sense to be switched. For this reason, an ester linkage would be expected to give a different parity and thus helical sense than an ether linkage.

As will be discussed chiral units closer to the ring system or that can be considered less flexible are expected to provide a shorter pitch related to a greater magnitude of the twisting power. The Gray and McDonnell rules can be used to predict the behaviour of

compounds with multiple chiral centres. In the case that the rules predict a different sense of the helix for two centres, a cancelling out approach correctly predicts that the chiral centre with a greater twisting power is expressed in the twist sense of the mesophase.[4]

While cholesteryl esters were the first chiral nematic (or cholesteric) materials discovered they possess several undesirable properties such as high melting points, low birefringence and low polarisability which have led to the need for new materials in devices. Three classes of chiral liquid crystal can be described depending on the nature of the chiral group and its location with respect to the core. Examples of these three classes are described in this section with increasing complexity of structures. The first class of compounds to be discussed feature a chiral unit attached to the mesogenic core such as compounds **122** and **123** (Figure 130). Materials of this first class may be varied in several ways including the chiral unit, core unit and the length of any alkyl chains attached to the core. This modular design has allowed many materials of this type to be produced and the structure to be modified to attain the desired properties for a given application. Compounds **122**[5] and **123**[6] incorporate the diphenyl acetylene core which is used throughout the project for relevance, however the most common linking units between aromatic rings include azobenzenes, Schiff's bases or esters. Of these, azobenzene and Schiff's base units bring their own issues with chemical stability and colouration.

$C_{10}H_{21}O$—

122

Cr 53 Cr' 55 SmA* 59 Iso °C[5]

$C_9H_{19}O$—

123

Cr 59 N* 70 Iso °C[6]
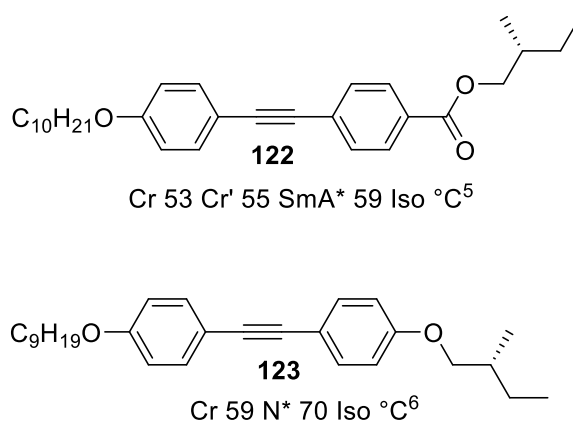
Figure 130. Examples of the simplest form of chiral liquid crystal featuring a chiral unit attached to a calamitic core.[5,6]

The presence of the chiral unit, for example (S)-2-methyl butyl is expressed on the liquid crystal properties depending on the method of attachment to the core. There

are two properties related to the expression of chirality that can be quantified and so different linking units can be described as more or less effective at transmitting chiral information. Firstly, the pitch of the chiral helix, and secondly the helical twisting power (HTP). The HTP is measured by using the chiral molecule as a dopant, to induce a chiral nematic mesophase into an achiral host.

A shorter pitch length or greater HTP indicates the chirality from a chiral centre is transmitted to a liquid crystal mesophase more effectively. The key factor influencing the pitch length and HTP is the flexibility around the chiral unit. This is demonstrated well by the cyanobiphenyl compounds **124** and **125** given below (Figure 131).[4] The 2-methyl butyl chiral unit has been commonly used in liquid crystals for over forty years due to its chemical stability. Therefore, a good understanding of these materials has been established and it is understood that the 2-methylbutyl chiral unit tends to give chiral nematic materials with a short pitch.[3] Comparison of **124** and **125** shows the pitch is much shorter for the alkyl compound **124** (P = 0.2 µm) than ether compound **125** (P = 1.5 µm).

Cr 4 (N* -30 SmA* -54) Iso °C

P = 0.2 µm

124

Cr 53.5 (N* 9) Iso °C

P = 1.5 µm

125
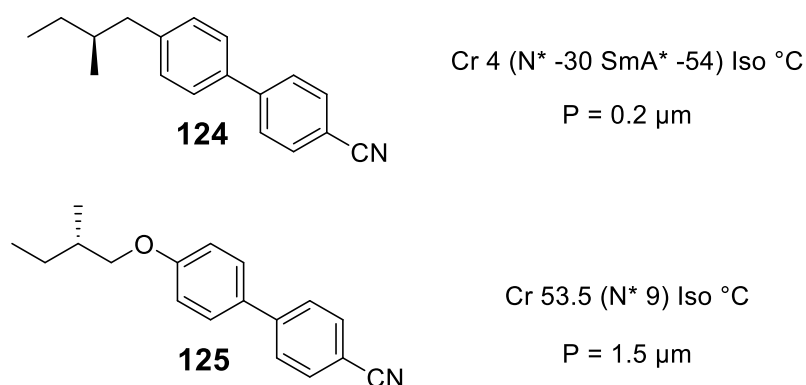
Figure 131. Simple chiral cyanobiphenyl mesogens which demonstrate a shorter pitch length for the alkyl than ether linked chiral unit.[4]

The proximity of the chiral unit to the rigid core leads to an increase in rotary power. This is observed through a shorter pitch length in the N* phase. Comparing compounds **124** and **125** the alkyl compound places the chiral centre one atom closer to the core, and as such more restricted rotation of the chain leads to a shorter helical pitch. Note that the flexibility of the alkyl and ether linkages vary significantly with ether linkages known to be far more flexible. This increased freedom of the chiral unit leads to a weaker influence and therefore it exhibits a longer pitch.

The second class of chiral liquid crystalline compounds encompasses a wide range of dimesogens (two mesogenic core units separated by a spacer, Figure 132). This dimesogenic template can be varied to include many different possible arrangements of units or blocks (see Chapter 4). The chiral unit may be incorporated into either the flexbile spacer (**126**), one – or more – of the mesogenic cores (**127**) or as a terminal chain attached to either core (**128**). Within these structural motifs the spacer lengths, chiral unit and linking group may be altered to target specific self-organising behaviours or specific properties i.e. helical pitch. The dimesogenic nature of these materials has a mixture of benefits and drawbacks since the two mesogenic cores may behave as a single molecule at low spacer lengths or behave independently of each other whereby they are decoupled from each other at longer spacer lengths.

126
Cr 159.2 N* 208.1 Iso °C[7]

127
Cr 113 TGB$_{q3}$ 120 N* 205 Iso °C[8]

128
Cr 137 (SmA 104) N* 176 Iso °C[9]
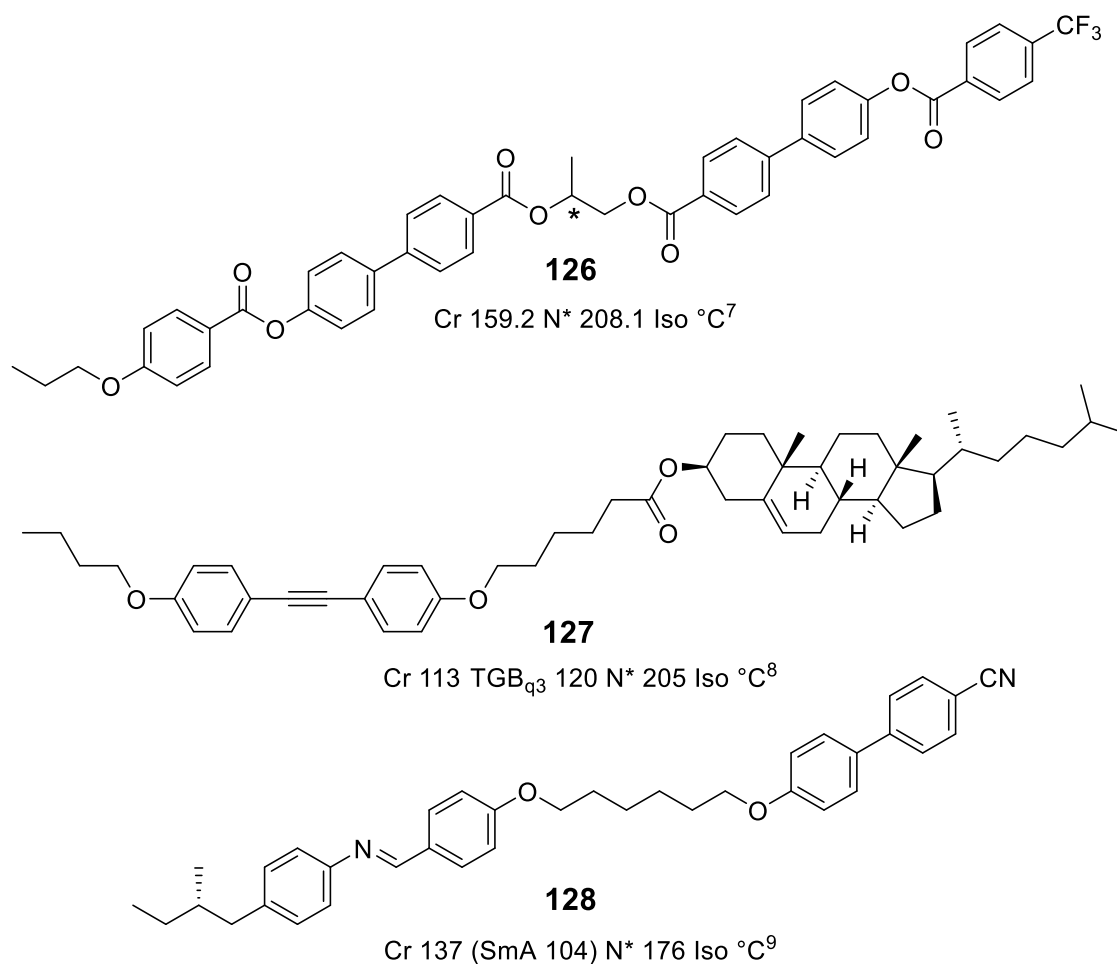
*Figure 132. Examples of a second class of chiral materials which are dimesogenic in nature. These can contain a chiral spacer between two cores (**126**)[7], a chiral mesogenic core (**127**)[8], or a chiral terminal chain (**128**)[9].*

The third and final overall class of chiral liquid crystal involve a point of asymmetry within the liquid crystalline core or *via* structural effects. For example, binaphthyl compounds such as **129** are commonly studied for use as chiral dopants due to their high helical twisting powers (Figure 133). In this case the high helical twisting power arises from the twisted structure as it forces the mesogenic units to twist which is spread through intermolecular interactions in the liquid crystal phase.[10]

Cr 76 SmX* (67.5) N* 82.2 Iso °C[10]
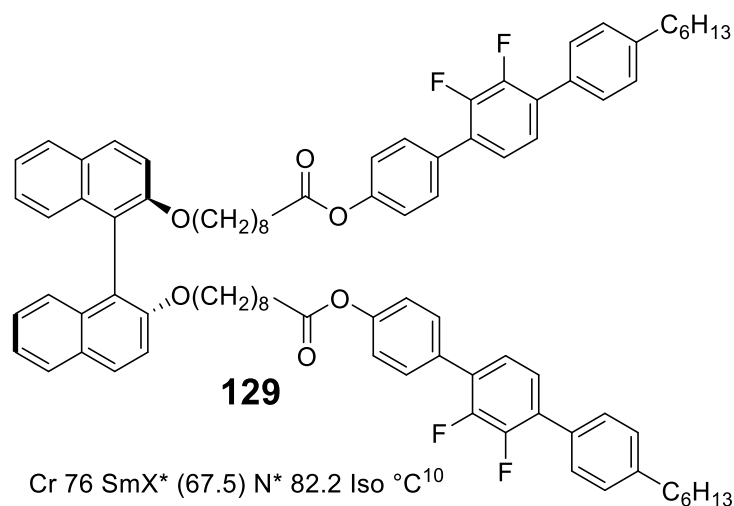
Figure 133. A third class of chiral liquid crystal utilises structural effects such as the axial chirality of BINOL materials such as 129.[10]

The helical twisting power (HTP) of chiral dopant relates to the ability of a chiral substrate to transmit chirality into an achiral nematic host. A dopant possessing a higher HTP will result in a shorter pitch length at a given weight fraction of dopant than a less effective dopant. This helical twisting power is dependent upon the chemical structure of the dopant. Since helical twisting power is related to interactions of the dopant with the host, the resultant pitch will vary based on the structure or composition of the host. Pitch length and weight fraction of dopant are inversely proportional and so the miscibility and liquid crystal properties of the dopant are also important factors in the design of chiral dopants. If the liquid crystal properties of the dopant are such that it depresses the clearing point too much, then liquid crystal behaviour may be suppressed by adding additional dopant. In addition to the binaphthyl dopants, other examples of materials with high helical twisting powers include the TADDOL dopants[11] (Figure 134, left) while additional advances have given more effectively twisting dopants with responsive properties (Figure 134, right).[12]

TADDOL dopant

Reponsive binaphthyl dopant

HTP in E7[12]: 60 µm^{-1} wt %$^{-1}$

HTP in 5CB[11]: 31 µm^{-1} wt %$^{-1}$
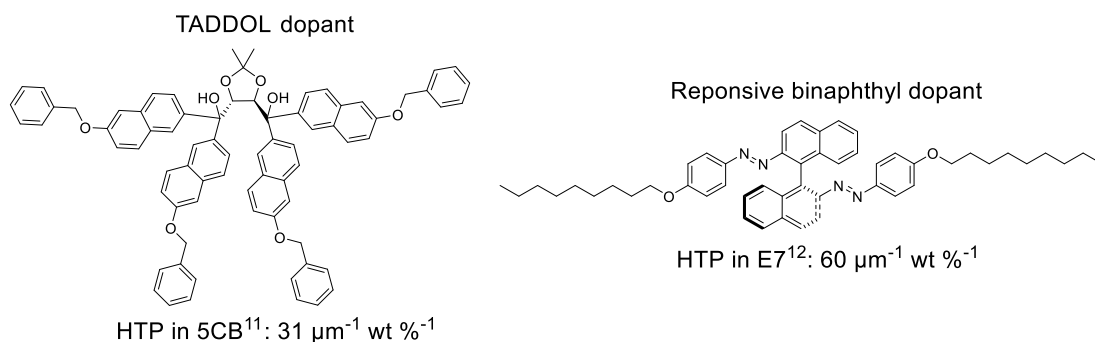
Figure 134. Chemical structures of two example chiral dopants with high helical twisting powers.[11,12]

6.1.2 Measurements of chiral liquid crystal materials

As stated before there are two measurable parameters for which the magnitude reflects upon the ability of the material to transmit chiral information into the system, that is: the pitch, and helical twisting power. The pitch of a chiral liquid crystal is defined as the distance in which the director precesses through 360° in a helix. This is shown below (Figure 135) as imaginary slices through the helix though in reality this is not a layered system as depicted below.

Pitch length
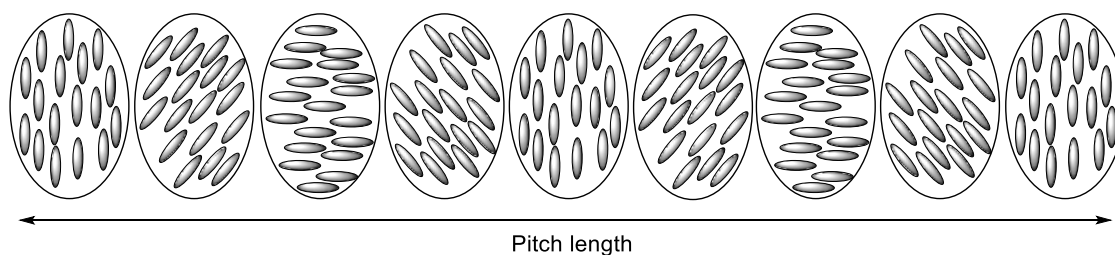
Figure 135. Representation of the chiral nematic helix via imaginary slices.

One of the most common techniques to measure the pitch of a chiral nematic mesophase is the use of a Grandjean-Cano wedge.[13] Each surface of the Cano-wedge cell is coated with an alignment agent to promote planar alignment of the liquid crystal. The boundary conditions only allow for domains whereby half or full rotations of the helix are possible so as to maintain planar alignment at the cell surfaces. In the cell, disclination lines form at the boundary between the domains of half or full rotations of the helix. This occurs at regular intervals and represent P/4, 3P/4 and so on (Figure 136).
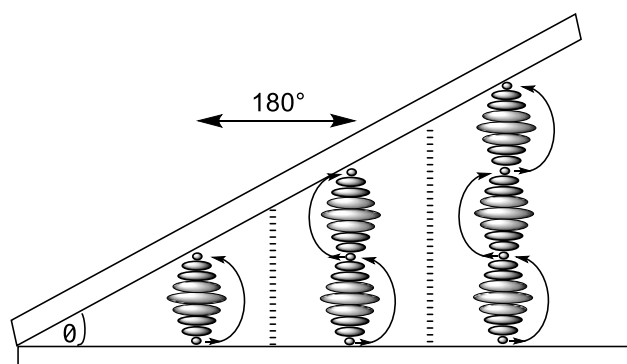
Figure 136. Grandjean-Cano wedge used for measuring the pitch of a chiral nematic liquid crystal. The hashed marks represent the defects that form to allow an additional half-twist of the helix granting a rotation of the director through 180°.

The distance between the disclination lines can be measured and the pitch of the chiral nematic helix may be calculated using Equation 10. P is the pitch, s the distance between disclination lines of the cell and θ the angle formed by the walls of the wedge cell. Alternatively, the pitch may be found *via* x-ray diffraction measurements (i.e. resonant X-ray scattering), though this is typically of more interest in more complicated mesophase structures than the chiral nematic.[14]

$$P = 2s\,(\tan\theta)$$

Equation 10. Calculation of the pitch of a chiral nematic helix (P) from a Cano-wedge cell.

Helical twisting power (HTP) relates to the ability of a chiral dopant to propagate chirality through the nematic mesophase of an achiral host. Importantly at low concentrations of the chiral dopant there exists an inversely proportional relationship between the dopant concentration and the pitch of the induced chiral nematic helix. Therefore, a mixture of a known concentration of chiral dopant may be measured and the helical twisting power found *via* Equation 11. β is the helical twisting power, P_0 the pitch induced and w the mass fraction of the chiral dopant.

$$\beta = \frac{1}{P_0 w}$$

Equation 11. Equation for the helical twisting power of a chiral dopant, where β is the helical twisting power, P_0 the pitch induced and w the mass fraction of the chiral dopant.

Measurements of the helical twisting power are most accurately performed by making a series of mixtures as performed in section 6.4. The pitch can be calculated for each concentration of dopant and plotted to give the helical twisting power.

6.2 Synthesis

The chiral target compounds were prepared using a similar synthetic strategy as was previously detailed for the synthesis of the *Janus* liquid crystal materials (See section 5.1). A convergent strategy using an iodo-aryl and an ethynyl-aryl intermediate which could be coupled via a palladium-mediated Sonogashira coupling to afford a diphenyl acetylene compound. The intermediates in the syntheses were characterised by ^{1}H NMR spectroscopy and mass spectrometry as required. All the final chiral diphenyl acetylene compounds were characterised by ^{1}H and ^{13}C{^{1}H} NMR spectroscopy, mass spectrometry and elemental analysis.

The target compounds contained the chiral unit (S)-2-methylbutyl attached to the diphenyl acetylene core *via* either an ether or ester linking group. Scheme 24 shows the synthesis of 4-(2-methylbutyloxy) iodobenzene using a Mitsunobu reaction and the Sonogashira coupling with **33**$_i$ - **33**$_{iii}$ to produce a series of 2-methyl-butyloxy diphenyl acetylenes **131** - **133**.

Although the reported yield of the Mitsunobu reaction was lower than typical for such reactions (55%) this was variable upon repeated synthesis and not troubling due to the commercial availability of the starting materials.
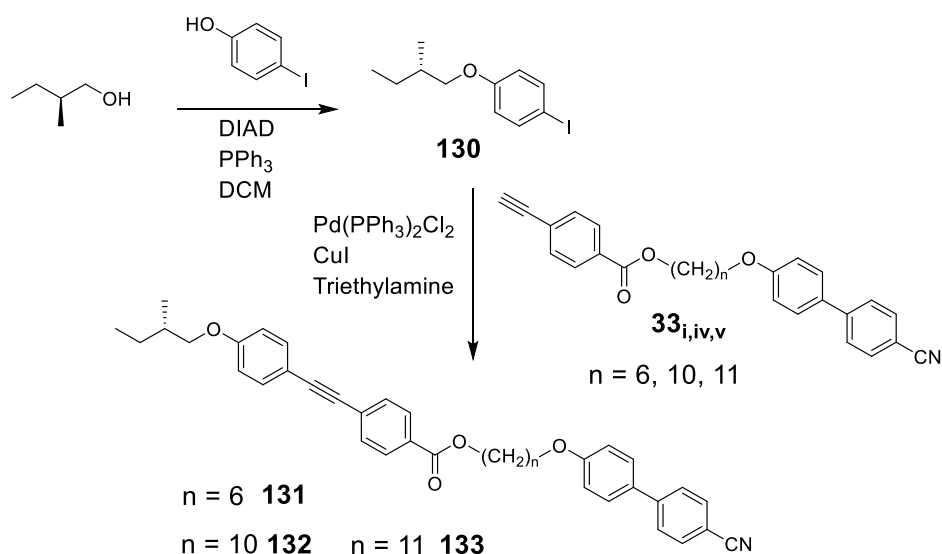
*Scheme 24. Synthesis of ether linked diphenyl acetylene derivatives of (S)-2-methyl butanol **131 – 133**.*

The synthesis of the ester linked compound **134** - **138** were performed in a similar manner utilising Steglich esterification in good yield to form the chiral ester followed by Sonogashira coupling with the ethynyl aryl intermediates as shown in scheme 25. The ethynyl-aryl coupling partners (**33**$_{i-v}$ n = 6, 8, 9, 10 and 11) were afforded *via* esterification of the appropriate alcohol with 4-ethynyl benzoic acid (See section 3.2).
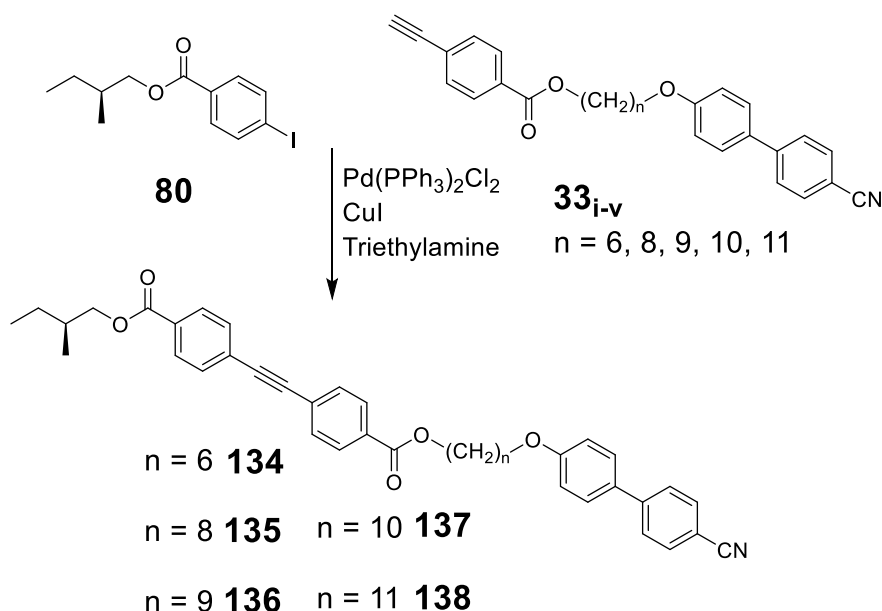
Scheme 25. Synthesis of ester linked diphenyl acetylene derivatives of (S)-2-methyl butanol 134 – 138.

This allowed for Sonogashira cross coupling between the iodo-(**130, 80**) and ethynyl-(**33**$_{i-v}$) intermediates to yield the desired diphenyl acetylene target compounds (**131 – 133, 134 – 138**). The esterification reaction to afford the chiral coupling partner proceeded with 99% yield. However, the yields of the Sonogashira cross coupling reactions varied from 36 to 85%. There was no clear trend observed as to the effect of the ether or ester linking group on the Sonogashira coupling step with the yields for both ether and ester compounds varying. This is attributed to repeated crystallisation to provide pure compounds for liquid crystalline analysis. The poor yield for the Sonogashira coupling was due repeated purification steps to remove trace metal impurities from the palladium catalyzed coupling. Recrystallisation from either hot ethanol or a dichloromethane:methanol solvent:antisolvent mixture provided each material with high purity as shown by elemental analysis.

The Mitsunobu reaction does not invert the stereochemistry of (S)-2-methyl butanol due to the reaction taking place at the primary alcohol. An alteration to the synthetic

scheme was required in the case of the (S)-1-methyl heptyloxy derivative **140**. The mechanism of the Mitsunobu reaction is shown in (Scheme 26) and proceeds *via* activation of the alcohol into an effective leaving group and electrophile in the presence of DIAD.
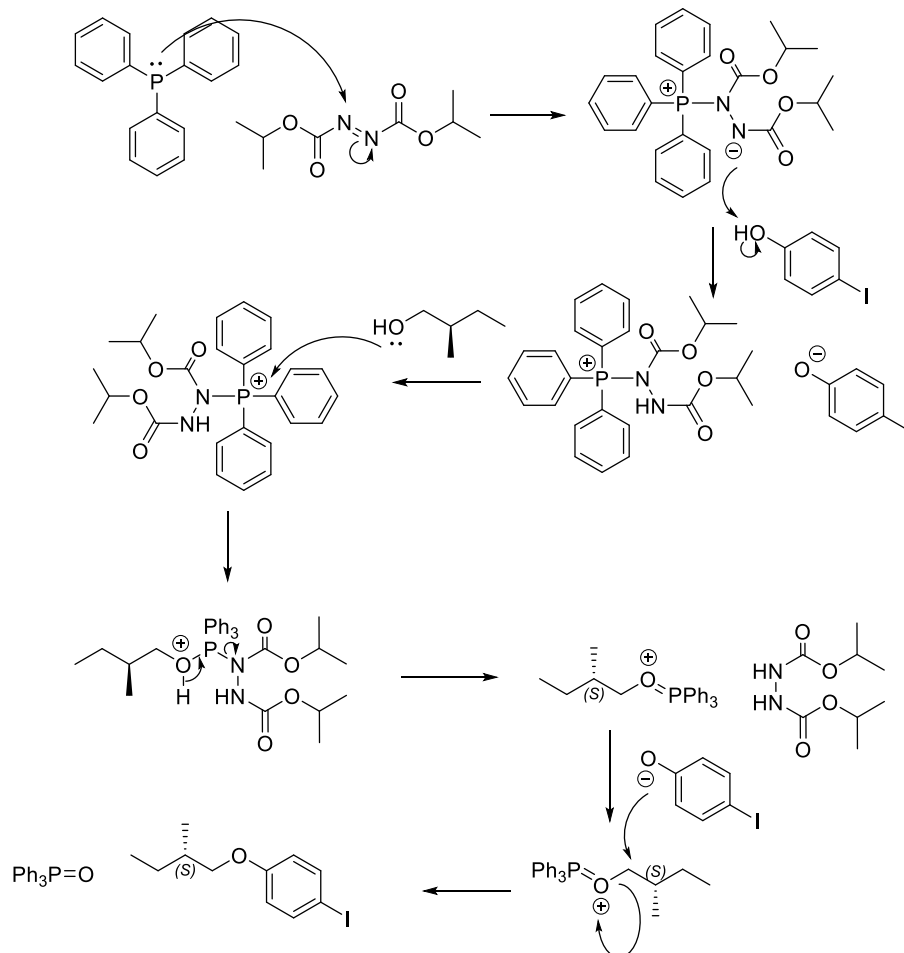
Scheme 26. Mechanism of the Mitsunobu reaction utilising PPh₃ and DIAD. In the case of 2-methyl butanol the chiral centre is not affected by the inversion of stereochemistry due to the location of the electrophilic carbon.

Synthesis of (S)-2-methylheptyloxy compound **140** required (R)-1-methyl heptanol to be used as the starting material (Scheme 27) because the nucleophilic attack occurs at the chiral centre of the secondary alcohol with inversion of stereochemistry. Neither the primary or secondary alcohols used in the Mitsunobu reaction produce intermediates for which a S_N1 pathway would occur and the chiral unit racemised. The synthesis of **142** used the same strategy as described for the ester compounds above. Steglich esterification using the secondary alcohol was low yielding (30%) due to the

sterically hindered secondary alcohol. The remaining synthesis proceeded without difficulty.
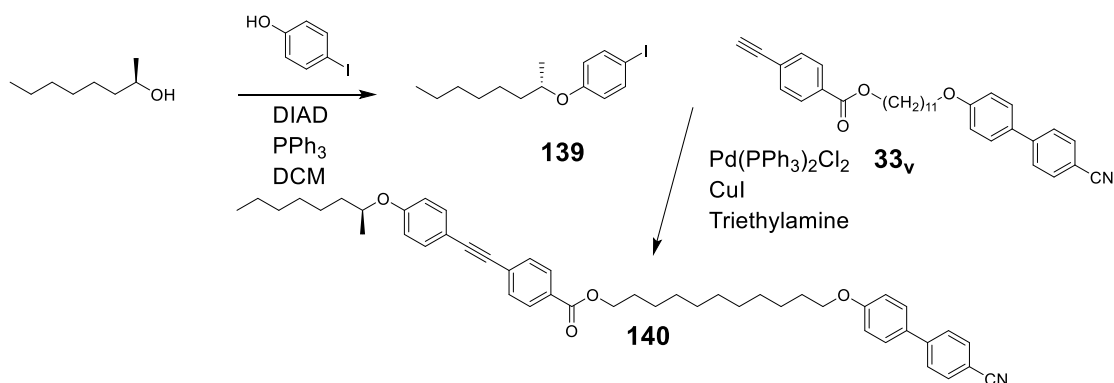
*Scheme 27. Synthesis of ether diphenyl acetylene derivative of (S)-1-methyl heptanol **140** featuring an inversion of stereochemistry.*

Compound **142** which is the ester analogue of **140** was synthesised using (S)-1-methylheptanol as the esterification reaction does not invert stereochemistry (Scheme 28). Therefore, this route followed that shown in Scheme 25.
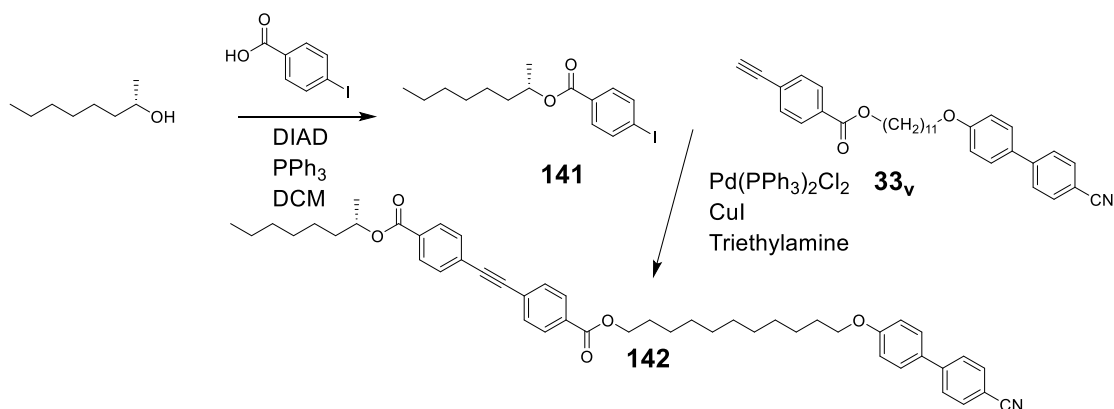
*Scheme 28. Synthesis of ester diphenyl acetylene derivative of (S)-1-methyl heptanol **142**.*

In addition to the target compounds above two comparative compounds **143** and **147** were synthesised. (S)-1-iodo-4-ether-2-methylbutoxybenzene **130** underwent Sonogashira cross-coupling with commercially available 1-ethynyl-4-pentylbenzene to prepare the simple diphenyl-acetylene compound **143** (Scheme 29). This compound

was prepared to investigate the liquid crystal properties of the diphenyl acetylene unit in isolation, rather than in the dimesogen.
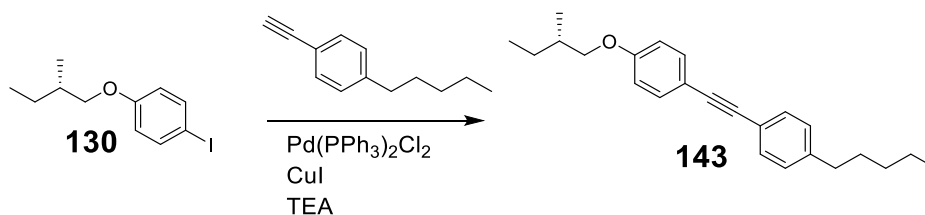
*Scheme 29. Synthesis of diphenyl acetylene compound **143** which can be considered an example of a class one chiral liquid crystal.*

In order to determine the effect of the acetylene bridge a biphenyl analogue **147** was prepared. An alternative synthetic strategy was required as the Sonogashira coupling approach was not feasible. A similar convergent approach could be attempted *via* a Suzuki cross coupling reaction however only one comparative compound was desired and the starting material 4-(4-hydroxyphenyl) benzoic acid was available therefore a divergent synthesis was used (Scheme 30). The 4-hydroxylbiphenyl carboxylic acid of the starting material was protected as the methyl ester **144** in quantitative yield. The 2-methylbutyloxy unit was attached using a Mitsunobu reaction to provide **145** and subsequent hydrolysis of the methyl ester to give the biphenyl carboxylic acid **146** in good yield. Finally, esterification of **146** with alcohol **33ᵥ** gave target compound **147** in 59% yield.
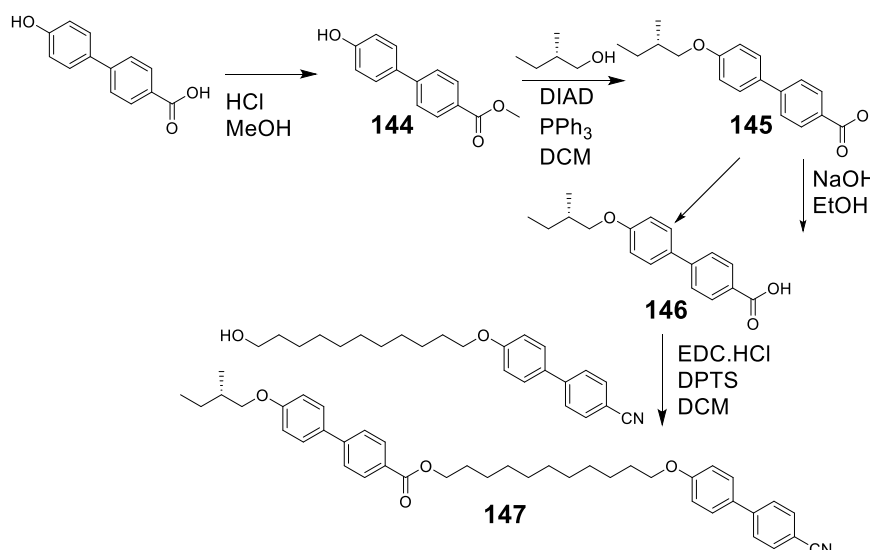
*Scheme 30. Synthesis of **147** via a divergent synthetic route.*

Each of the intermediates were characterised primarily *via* ^{1}H NMR spectroscopy. The target compounds were characterised *via* ^{1}H NMR spectroscopy, ^{13}C{^{1}H} NMR

spectroscopy, mass spectrometry, and elemental analysis. The incorporation of the chiral units is easily visualised *via* the presence of diasetereotopic protons (*-CH₂O*) of the ester in the ^{1}H NMR spectrum of each compound which are well resolved from the remaining signals (Figure 137). The diastereotopic protons couple to the proton labelled H_x on the chiral carbon giving a characteristic ABX pattern with the two AB doublets colour coded below. The characteristic peaks related to the cyanobiphenyl aromatic rings show the successful incorporation of the mesogenic unit, alongside the formation of the diphenyl acetylene core.
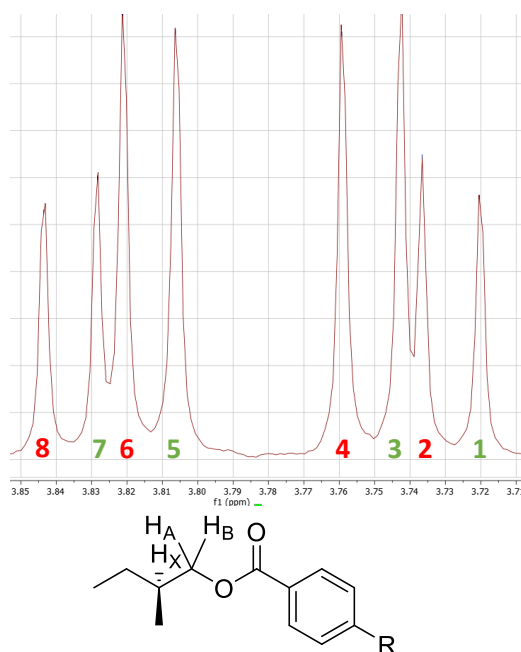
Figure 137. Characteristic ABX pattern of the diastereotopic (CH₂O-) protons within the ^{1}H NMR spectrum of the ester (S)-2-methyl butanol derivatives. Protons H_A and H_B are coupled to each other, and H_x. δ H_A 3.82 ppm, 1H, dd (J_{A-B} = 8.8, J_{A-X} = 6.1 Hz), H_B 3.74 ppm, 1H, dd (J_{A-B} = 8.8, J_{B-X} = 6.7 Hz).

APCI-MS was required to effectively ionise the target compounds due to their apolar nature. The mass spectrometry serves as evidence of the varying methylene spacer lengths which were key in the explanation of the liquid crystal properties.

Elemental analysis was used to prove the purity of each target compound. This was achieved following several recrystallisations from hot ethanol to provide materials for analysis. Due to the lower molecular weight and absence of perfluorinated alkyl chains no difficulties were encountered for these materials.

The optical rotation in solution for both the chiral alcohol and each of the target compounds was measured in chloroform at 20 °C (Table 26). Note that throughout the synthesis of the target compounds the same source of (S)-2-methyl butanol starting material was used to ensure that the enantiopurity is consistent throughout. Compound **142** was found to have a far higher optical rotation which is in line with common results using the 1-methyl heptanol chiral unit.[15]

Table 26. Chemical structure and optical rotation of the chiral materials produced (S)-2MB = (S)-2-methyl butyl, (S)-1MH = (S)-1-methylheptyl.

Compound number	Spacer length	Linking unit	Chiral unit	Optical rotation / $[\alpha]^{20}_D$ (c = 1.0, CHCl$_3$)
(S)-2-methyl butanol	N/A	N/A	(S)-2MB	5.8
131	Hexyl	Ether	(S)-2MB	6.0
132	Decyl	Ether	(S)-2MB	5.8
133	Undecyl	Ether	(S)-2MB	3.0
134	Hexyl	Ester	(S)-2MB	1.2
135	Octyl	Ester	(S)-2MB	3.2
136	Nonyl	Ester	(S)-2MB	2.9
137	Decyl	Ester	(S)-2MB	0.5
138	Undecyl	Ester	(S)-2MB	3.2
140	Undecyl	Ether	(S)-1MH	0.3
142	Undecyl	Ester	(S)-1MH	20.5
143	N/A	Ether	(S)-2MB	9.2
147	Undecyl	Ether	(S)-2MB	4.7

In summation a family of twelve chiral materials were produced and characterised for this work, focusing on dimesogenic compounds with a terminal chiral (S)-2-methyl butyl unit. This was joined to the core either *via* an ester or ether linking group and the chain length of the methylene spacer between core and mesogen varied.

Table 27. Family of ether linked (S)-2-methyl butyl compounds.
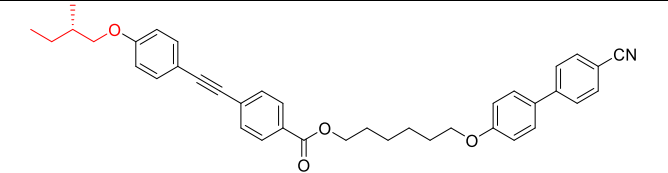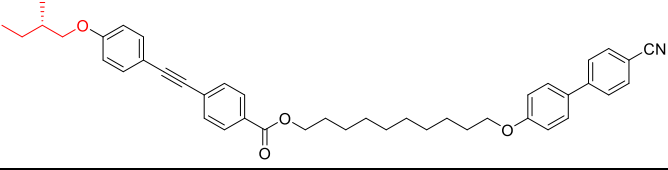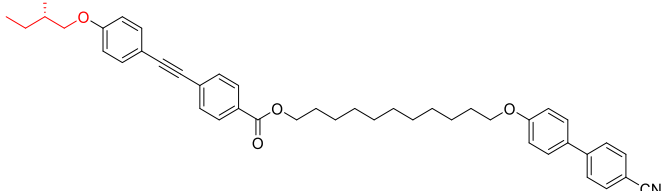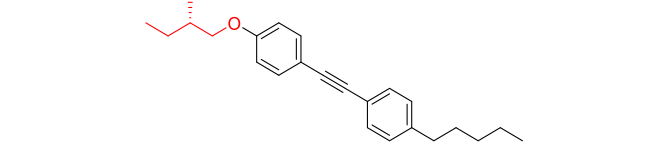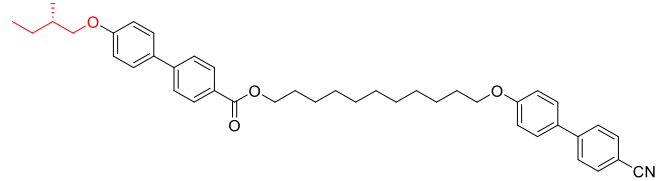
Compound number	Chemical structure	Transition temperatures /°C
131		Cr 126.9 (113.4 SmC$_A$*) Iso °C
132		Cr 93.0 X 93.7 SmC* 119.6 Iso °C
133		Cr 87.9 SmE 106.4 SmB 109.0 SmA* 141.7 Iso °C
143		Cr 30.5 (N* 20.7) Iso °C
147		Cr 124.1 X 130.4 SmA* 144.2 Iso °C

Table 28. Family of ester linked (S)-2-methyl butyl compounds.
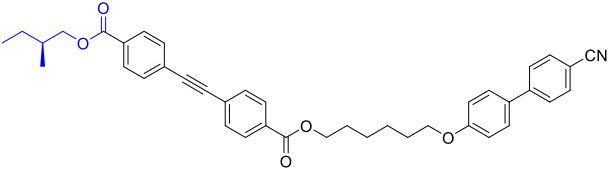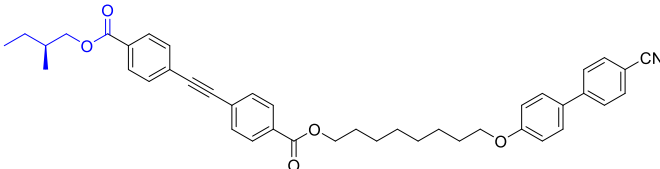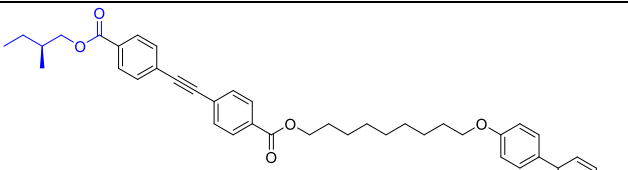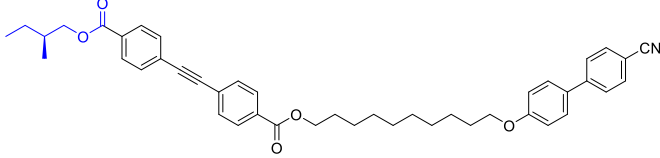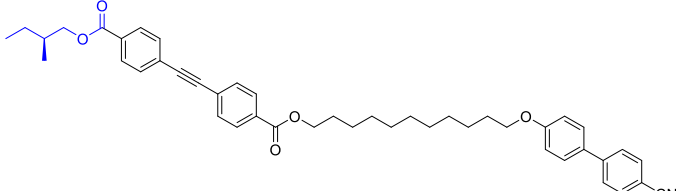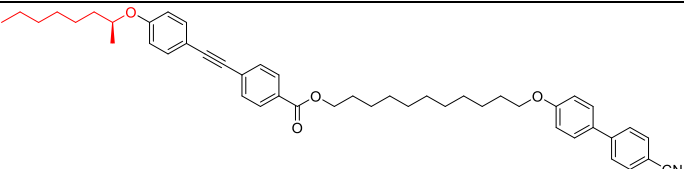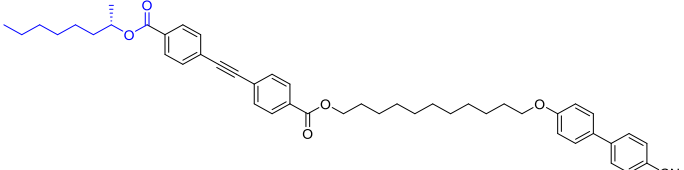
Compound number	Chemical structure	Transition temperatures /°C
134		Cr 77.9 (N* 54.5) Iso °C
135		Cr 65.6 SmA* 74.3 N* 78.6 Iso °C
136		Cr 85.1 SmA* 92.0 N* 125.3 Iso °C
137		Cr 81.1 N* 84.8 BPI, BPIII 87.0 Iso °C
138		Cr 89.8 SmA* 102.0 N* 115.9 Iso °C

Table 29. Structures of (S)-1-methylheptyl compounds.

Compound number	Chemical structure	Transition temperatures /°C
140		Cr 110 (SmA* 93.0) Iso °C
142		Cr 97.1 (BPIII 76.3 N* 76.1 TGB 75.0 SmA* 75.0) Iso °C

6.3 Liquid crystal properties

All compounds were characterised using polarised optical microscopy (POM) to identify the mesophase behaviour and differential scanning calorimetry to determine transition temperatures and enthalpies of transition.

6.3.1 Liquid crystal properties of ether compounds

The transition temperatures from polarised optical microscopy and enthalpies and entropies of transition taken differential scanning calorimetry for the 2-methyl butyl ethers **131** - **133** are given in Table 30.

*Table 30. Transition temperatures, enthalpies and entropies of transition of the ether linked compounds (**131** - **133**).*

Compound number	Transition	T /°C	ΔH / kJ mol^{-1}	ΔS / J K^{-1} mol^{-1}
131	Cr - Iso	126.9	35.1	88
	(Iso – SmC$_A$*)	113.4	9.1	24
132	Cr - X	93.0	26.3	72
	X – SmC*	93.7	9.3	26
	SmC* - Iso	119.6	12.3	31
133	Cr – SmE	87.9	16.9	41
	SmE – SmB	106.4	3.9	10
	SmB – SmA*	109.0	3.1	8
	SmA* - Iso	141.7	28.8	80

DSC revealed that compound **133** exhibited a rich mesomorphism with a number of transitions arising. From microscopy it was observed that upon cooling from the isotropic liquid a Smectic A* phase was observed with a characteristic focal conic texture. Upon further cooling transient bars formed on the backs of the focal conic fans (Figure 138), characteristic of the transition from a SmA phase to a SmB phase, and corresponded with a first order transition by DSC.
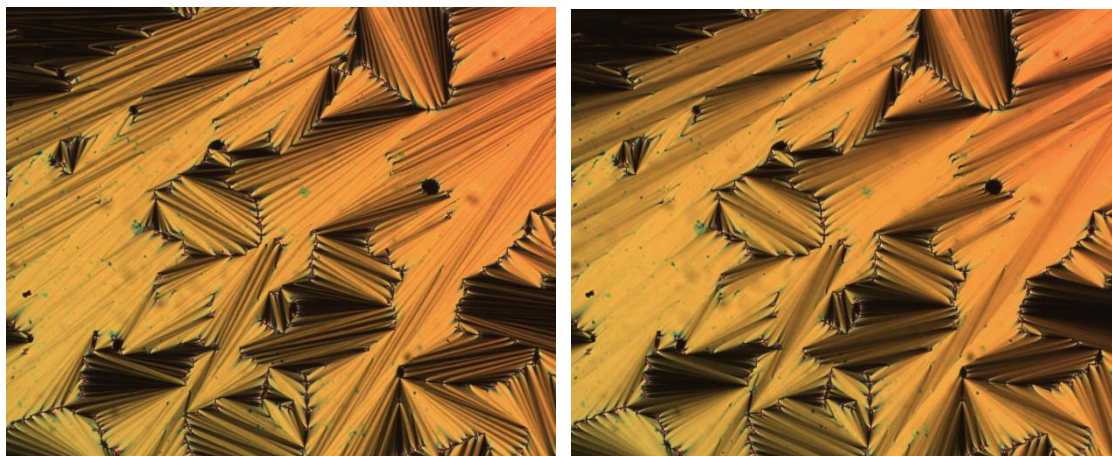
*Figure 138. Photomicrographs (x100 magnification) of compound **133**. Transient bands formed in the focal conic texture (left, 109.0 °C) The bands fade again over time without changing the temperature of the system (right, 109.0 °C).*

Upon further cooling a transition was observed at 106.4 °C from the SmB phase to a higher ordered smectic phase. Bands formed across the backs of the focal conics as seen in Figure 139 and these bands were retained upon further cooling. This transition is consistent with the assignment of the smectic E phase.
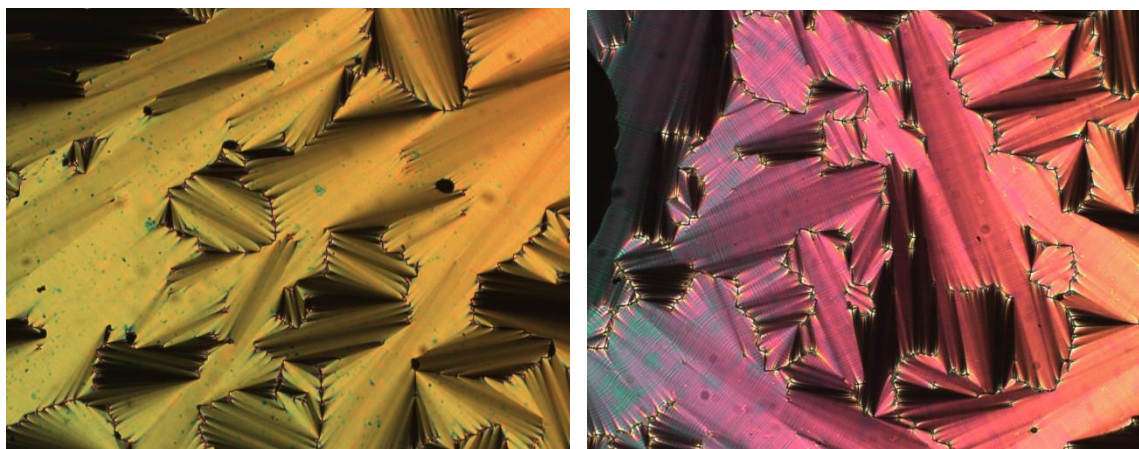
*Figure 139 Photomicrographs (x 100 magnification) of the lower temperature phase of **133** showing banding across the backs of the focal conic fans. (left, 106.6 °C, right, 105.3 °C).*

Upon cooling from the isotropic liquid compound **132** possessed a striated focal conic texture which is consistent with the SmC* phase. The spacing of the striations is directly related to the pitch of the SmC* phase. For compound **132** the pitch was measured to be 4 µm (Figure 140, left). Upon shearing the sample a schlieren texture was obtained and rotation of the polarisers revealed the twist sense of the chiral smectic C helix as right-handed (Figure 140, right).
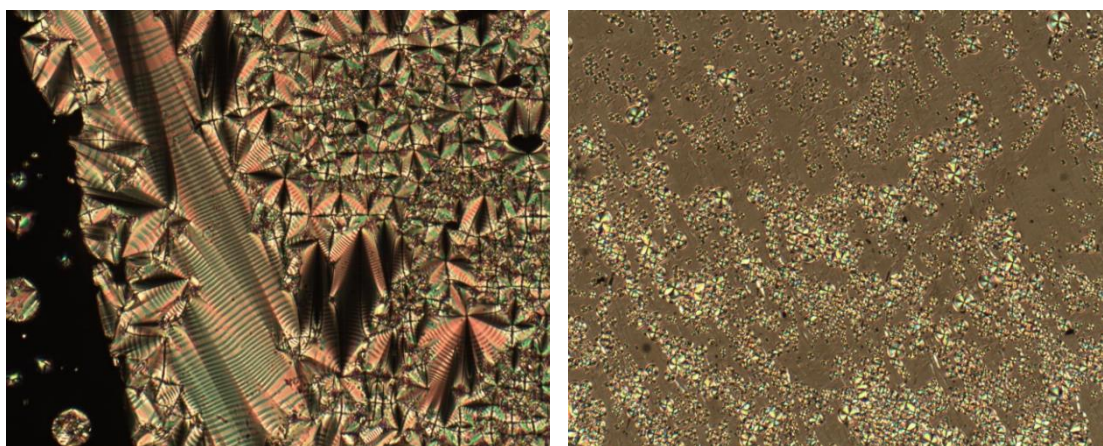
*Figure 140. Photomicrographs (x 100 magnification) showing the regularly banded texture of **132** (left, 107.0 °C), and schlieren texture with the polarisers rotated to 60° showing a right-handed helix (right, 94.5 °C).*

Cooling the sample further led to the formation of a higher ordered phase for which additional bands formed across the focal conics and the schlieren regions formed a mosaic texture as shown in Figure 141. This phase is likely a smectic G or J phase. It was not possible to shear the phase indicating the crystal-like order.
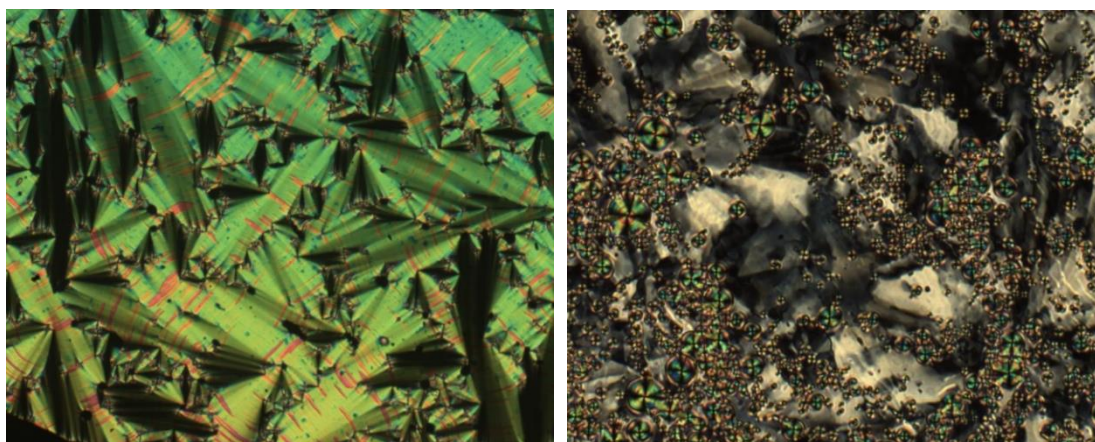
*Figure 141. Photomicrographs (x 100 magnification) of 1**32** showing the banding of the higher ordered phase (left, 90.5 °C), and mosaic texture found in place of the schlieren texture (right, 91.3 °C).*

In contrast to the above, compound **131** bearing a shorter alkyl spacer possessed an anticlinic chiral smectic C phase (SmC$_A$*) as shown by the presence of both 2-brush and 4-brush defects in the schlieren texture (Figure 142). Compound **131** has a melting point roughly 35 °C higher than the equivalent compounds with a longer spacer which leads to a monotropic mesophase.

*Figure 142. Photomicrograph (x100 magnification) of the Schlieren texture of **131** showing the presence of both 2-brush and 4-brush defects, the presence of 2-brush defects allows the mesophase to be assigned as SmC$_A$* (113.5 °C).*

The ether linking unit favours the formation of well-organised mesophases as seen by the stability of smectic phases for the ether compounds while the ester analogues tend to possess both smectic and nematic mesophases. Notably the smectic phases observed for the ether compounds are typically more ordered (SmB, SmC*, SmC$_A$*) than the smectic A* phase most commonly found in the ester analogues. Structurally this effect is rationalised *via* increased polarisability within the diphenyl acetylene core due to the push-pull electronic effects induced by the ether group leading to stronger intermolecular interactions.

An alternative way to demonstrate this increased organisation is the presence of achiral smectic C phases in several of the linear achiral materials **94** and **95** discussed in chapter 5. The materials discussed in chapter 5 vary significantly in the structure to the materials discussed here however the structural factors can be discussed in terms of the expected effect upon the mesophase organisation. Compound **131** and **92** are the most closely related, with an equal length spacer to the cyanobiphenyl unit however **92** has a longer, unbranched terminal alkyl chain which will therefore increase the organisation of the mesophase. The stabilisation offered by the longer unbranched chain appears equal to the presence of the ether linkage and subsequent increase in polarisability of the diphenyl acetylene core.

The mesophase stabilisation induced *via* the ether unit can be seen in many examples ranging from very similar cores such as compound **122** (Figure 130) to very different

structures such as compound **125** (Figure 131). For this reason, diphenyl acetylene material **143** was produced to screen out the phase stabilisation of the cyanobiphenyl unit and provide a simple case where the diphenyl acetylene serves as the only mesogen (Figure 143). In this case the diphenyl acetylene core is sufficient to stabilise a mesophase due to the presence of the ether. Previously the presence of the ether group on the diphenyl acetylene core has been shown to provide narrow monotropic mesophases while wholly alkyl chains may be substantially longer and provide non-liquid crystalline behaviour.[16] Additionally the ester analogue of **143** is non-liquid crystalline showing the reliance of the mesomeric effect from the ether linkage.[17] Removal of the cyanobiphenyl mesogen had the expected effect of drastically reducing the clearing point however a narrow monotropic mesophase remained in spite of the disruptive branching introduced by the chiral chain.

143

Cr 30.5 (N* 20.7) Iso °C
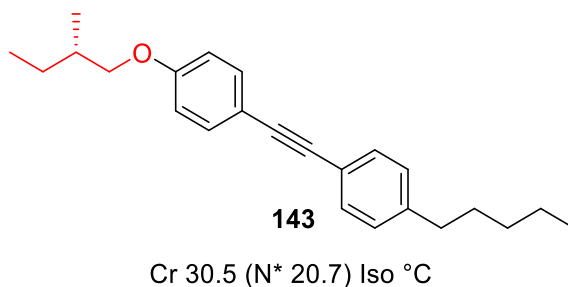
*Figure 143. Structure of compound **143** featuring no cyanobiphenyl unit.*

Additionally, a biphenyl analogue was desired to serve as a contrast with the diphenyl acetylene derivatives which served to change the profile of the electronic effects and shorten the core (Figure 144). Comparison of **133** and **147** which differ only by the acetylene linker show little effect on the phase behaviour or clearing point, however the melting point of **147** is higher reflecting a stronger crystalline lattice of the biphenyl compound. Additionally, a transition to a second higher order phase was observed by DSC however the nature of this phase was not characterised. The poor solubility of the biphenyl derivative **147** in miscibility studies (Section 6.4). is likely linked to this increased crystallinity.

147

Cr 124.1 X 130.4 SmA 144.2 Iso °C
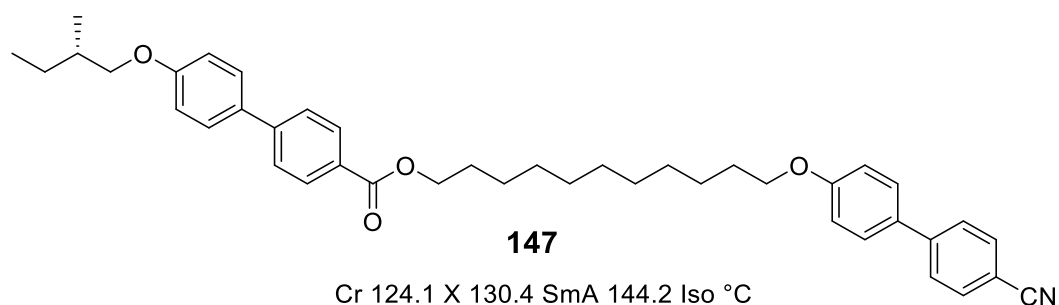
*Figure 144.Structure of **147** with an alternative shortened biphenyl core.*

The Gray and McDonnell rules described previously can be used to predict the handedness of chiral liquid crystalline compounds. These empirical rules predict that whether the chiral helix is right or left-handed will depend on the parity between the chiral unit and mesogenic core. In the case of these compounds the ether linked compound **132** was found to have a right-handed helix *via* rotation of the polarisers. Repeating this procedure with the chiral nematic phases of ester linked compounds showed that these to form a right-handed helix despite the change in parity between the ether and ester linked units, in apparent contravention of the Gray and McDonnell rules.

6.3.2. Liquid crystal properties of ester compounds.

A total of five ester linked compounds featuring the 2-methyl butyl chiral unit were synthesised and their liquid crystalline behaviour identified by polarised optical microscopy and differential scanning calorimetry. The transition temperatures, enthalpies and entropies of transition liquid crystalline behaviour is summarised in Table 31.

*Table 31.Transition temperatures, enthalpies and entropies of transition of ester linked compounds (**134**-**138**). *The blue phases of compound **137** were not observed by DSC.*

Compound number	Transition	T /°C	ΔH / kJ mol⁻¹	ΔS / J K⁻¹ mol⁻¹
134	Cr – Iso	77.9	44.7	118
	(Iso – N*)	54.5	2.07	7
135	Cr – SmA*	65.6	30.3	87
	SmA* – N*	74.3	2.8	9
	N* - Iso	78.6	0.3	1
136	Cr – SmA*	85.1	23.6	86
	SmA* – N*	92.0	0.3	1
	N* - Iso	125.3	1.7	4
137	Cr – N*	81.1	56.1	158
	N* Iso	87.0	0.3	1
	Iso – BPI, BPIII	87.0	*	*
	BPIII – N*	84.8	*	*
138	Cr – SmA*	89.8	43.7	121
	SmA* – N*	102.0	0.5	1
	N* - Iso	115.9	4.3	11

The behaviour of the ester compounds is a little more consistent with the change in chain length of the spacer than was observed for the ether compounds reported in section 6.3.1. The liquid crystal behaviour of this family of compounds is dominated by the chiral nematic and smectic A* phase and as such photomicrographs are not provided for each material. Compound **138** provided a planar texture with the characteristic 'oily streaks' of the chiral nematic mesophase (Figure 145).
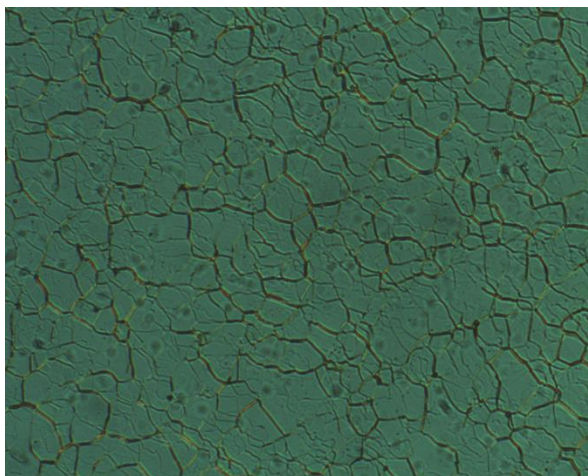
*Figure 145. Photomicrograph (x100 magnification) of **138** showing the oily streaks texture of the chiral nematic mesophase (113.3 °C).*

Compound **137** exhibited a BPIII and BPI texture on cooling from the isotropic liquid. Slowly cooling and then annealing compound **137** just beneath the clearing point allowed for the platelet texture of the BPI phase to develop from the blue fog of the BPIII (Figure 146).
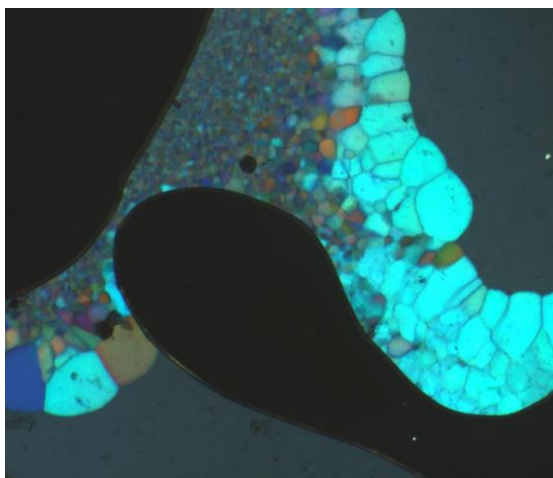
Figure 146. Photomicrograph (x100 magnification) of the platelet texture formed via annealing the blue fog texture of BPIII, the texture has been assigned as BPI (87.0 °C).

Compound **136** showed the broadest mesophase range overall, and the highest clearing point of the ester family of compounds. This was characterised by a planar chiral nematic texture featuring oily streaks and the focal conic texture of the smectic A* phase. The colour of the planar texture is related to the selective reflection of light and corresponds to the pitch length of the chiral nematic helix. There was little difference in the colour of the planar textures among many of the ester compounds with the largest difference being between **136** (Figure 147) and **138** (Figure 145). The

colour of the planar phase of **136** is shifted towards the blue end of the spectrum indicating a shorter wavelength of light is reflected and therefore there is a shorter pitch length when compared to **138**. The colour of the remaining planar textures is more closely related and so a trend cannot be clearly assigned.
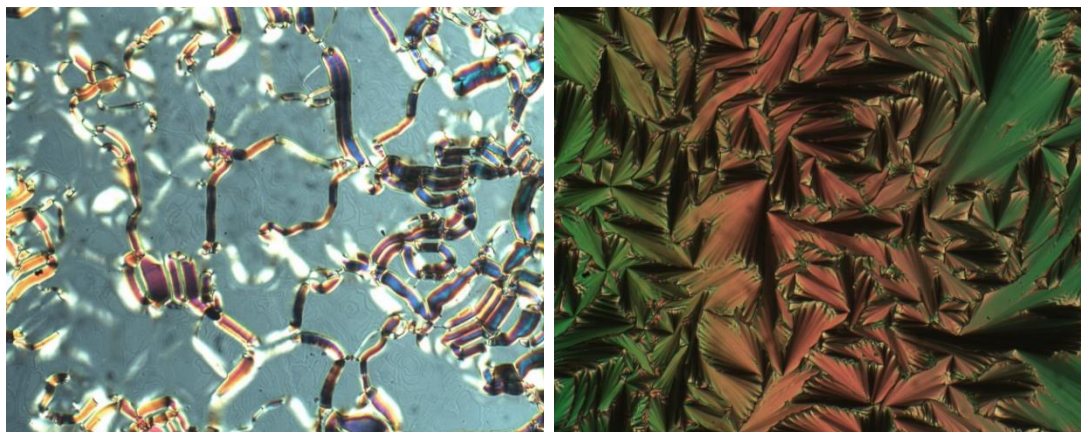
*Figure 147. Photomicrograph (x100 magnification) of the planar chiral nematic texture of **136** (left, 125.2 °C), and focal conic texture of the smectic A phase (right, 83.1 °C).*

Compound **148** reported by Seto can be used to discern some of the effect of the dimeric structure (Figure 148).[15] This provides a similar structure to **134** whereby the cyanobiphenyl mesogen has been removed and one ester replaced with an ether link to the core and thus increasing the stabilisation offered by the diphenyl acetylene. The addition of the cyanobiphenyl unit increases the melting point by 30 °C as to be expected for the larger molecule however there is only a small change in the clearing point. Due to the dimesogenic nature of **134** a nematic phase is favoured as the cyanobiphenyl is not effectively decoupled. Removing this cyanobiphenyl and increasing the polarisability of the core enables a smectic A* phase to be stabilised with similarity to compound **122** (see Figure 130). In comparison with compound **143** this shows a notable stabilisation as the opposing +M effects of the ether and -M effect of the ester linkages further increase the dipole across the diphenyl acetylene core.

148

Cr 40 SmA 52 Iso °C
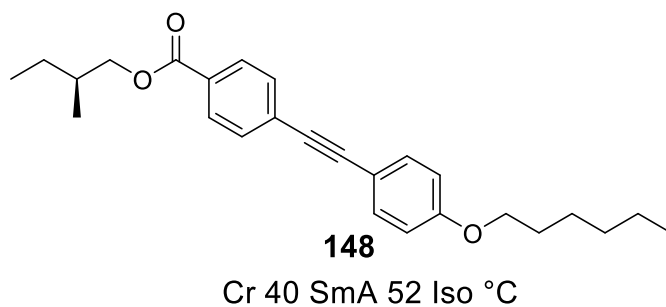
Figure 148. Diphenyl acetylene featuring an ester linking group with mesomorphism enabled by an ether.[15]

The family of five ester compounds **134 – 138** show an odd-even effect. Within the ester compound series the spacer chain lengths between C_{11}-C_8 are represented. Figure 149 shows a plot of the transition temperatures as a function of spacer length for the (S)-2-methylbutyl esters. From the data presented there is a clear odd/even effect where the odd parity spacers lengths exhibit higher clearing points than the even parity spacers.
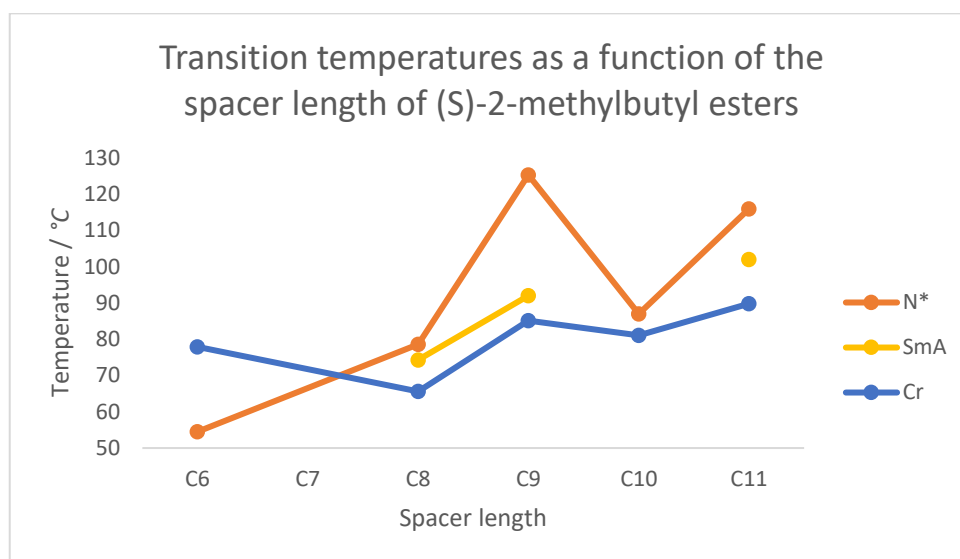
Figure 149. Plot of the transition temperatures of the ester linked compounds against the length of alkyl spacer.

The ester compound **136** incorporating the nonyl alkyl spacer exhibits the highest clearing point. This may indicate that extending the chain length beyond nonyl has diminishing effects on phase stability. While insufficient data points are present for a similar plot of the ether linked materials, the C_{11} methylene spacer again provides higher transition temperatures than the C_{10}. This is rationalised based upon the overall shape of the dimers as the rod-like shape formed by the odd parity alkyl spacer is

significantly easier to pack within the mesophase than the bent structure given by the even parity alkyl spacer (Figure 150). The ester and ether linkages between the diphenyl acetylene and cyanobiphenyl units introduce a further three atoms to the chain and so effectively invert the parity of the alkyl spacer.
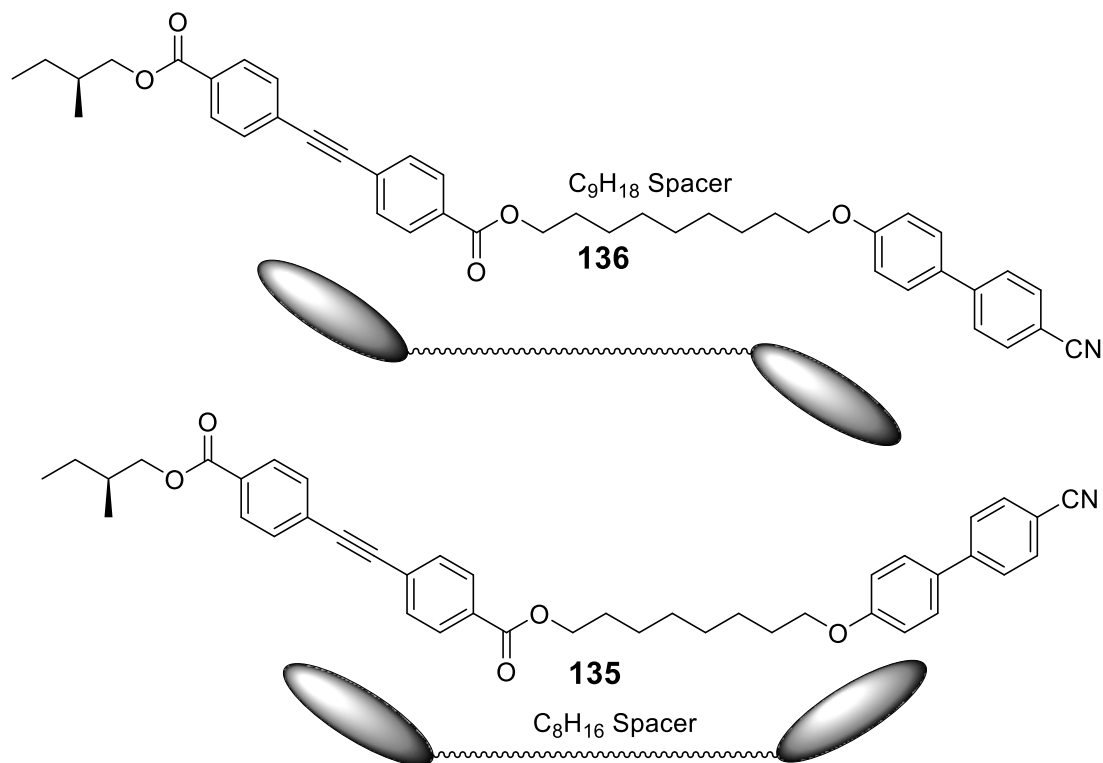
Figure 150. The angle between mesogenic units changes based upon the parity of the spacer.

The same effect is seen with either the ether or ester linking unit as the terminal chain has no effect on the angle between of the two mesogenic units. For both the ether and ester linking units the hexyl chain appears too short to effectively decouple the core and cyanobiphenyl mesogen. In both cases the melting point occurs at a higher temperature and so monotropic mesophases are observed.

The presence of an odd-even effect in the spacer length is also seen in the family of bimesogens where one of the mesogens is a Schiff's base for example **128** and **149** shown in (Figure 151).[9] A range of spacer lengths were produced between six and nine methylene units long with the clearing points of the even spacer lengths over 30 °C higher than the odd spacer counterparts. This appears the inverse of the trend seen in the diphenyl acetylene compounds reported here. However, this is simply due to the differing design of the two families of compounds, in the diphenyl acetylene materials the ester and ether linkages between the cores add an odd number of atoms to the

alkyl spacer and so invert the parity. In the imine materials such as **149** the two ether linkages provide an even number of atoms and so the parity of the alkyl spacer is maintained. Therefore, both effectively show an overall even parity of spacer provides greater stabilisation of the mesophase. Of more interest is the notably higher transitions observed for the C6 spacer imine (Compound **128**) found in this family while in the diphenyl acetylenes the shortened spacer length is less effective at stabilising the mesophase. This may be due to the increased flexibility of the ether linking unit when compared to the ester used in the diphenyl acetylenes.

128

Cr 137 (SmA 104) N* 176 Iso °C[9]

149

Cr 97 (SmA 74) N* 131.9 Iso °C[9]
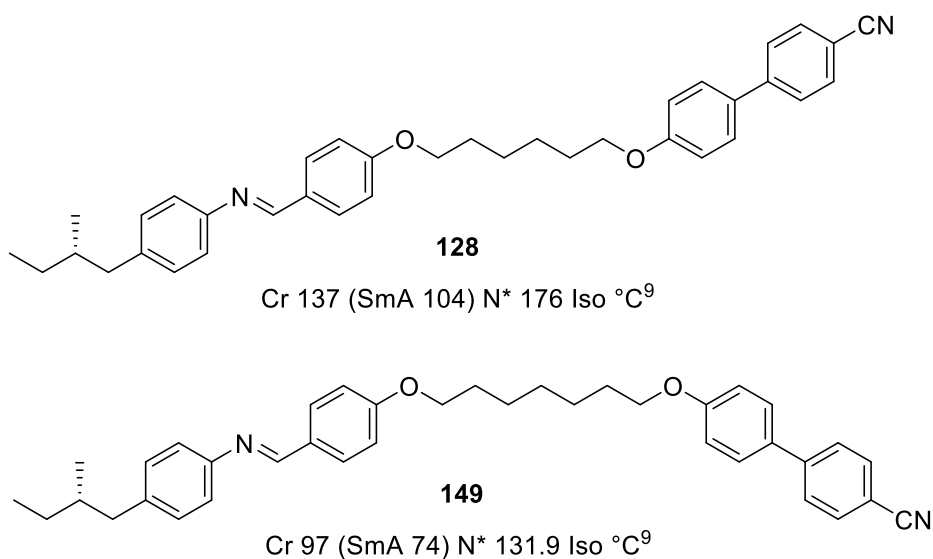
*Figure 151. Compound **128** and **149** show an apparently inverted odd-even effect as the diphenyl acetylenes.*

Both the transition enthalpies of the diphenyl acetylenes given in Table 31 and the transition enthalpies of the imine compounds given in Table 32 show a clear trend with the more stable mesophases possessing higher enthalpy values associated with the transition.

Table 32. Transition temperatures, enthalpies and entropies of the N – Iso transition for the family of dimesogenic compounds containing **128**.[9]*

Spacer length / n (C_nH_{2n+1})	Melting point T /°C	Clearing point T /°C	ΔH / kJ mol^{-1}	ΔS / J K^{-1} mol^{-1}
6	137	176	4.5	1
7	97	131.9	0.7	0.2
8	128	165	5.1	2
9	110	132.8	1.3	0.4

6.3.3 Liquid crystal properties of 1-methylheptyl analogues.

A pair of compounds featuring the 1-methylheptyl chiral unit were synthesised with one each featuring the ether and ester linking units. The liquid crystal phases were identified by polarised optical microscopy and the enthalpies of fusion taken from DSC (Table 33). The samples crystallised when cooled during DSC experiments and therefore no enthalpies or entropies can be reported for the monotropic transitions.

*Table 33. Transition temperatures, enthalpies and entropies of transition of the (S)-1-methylheptyl derivatives **140** and **142**.*

Compound number	Transition	T /°C	ΔH / kJ mol^{-1}	ΔS / J K^{-1} mol^{-1}
140	Cr – Iso	110.0	79.3	207
	(Iso – SmA*)	93.0	-	-
142	Cr - Iso	97.1	75.5	204
	(Iso – BPIII)	76.3	-	-
	(Iso – N*)	76.1	-	-
	(N* – TGB)	75.0	-	-
	(TGB – SmA*)	75.0	-	-

Compounds **140** and **142** were synthesised featuring the (S)-1-methyl-2-heptanol chiral unit in place of the (S)-2-methyl butanol unit used previously. The ether compound **140** exhibits a monotropic smectic A* phase that exists over a narrow temperature range. The ester analogue **142** exhibits a rich mesomorphism albeit all monotropic in nature. Upon cooling from the isotropic liquid the blue fog texture of BPIII is observed (Figure 152) which undergoes a transition into a narrow chiral nematic phase. Cooling the chiral nematic phase leads to the formation of a smectic A* mesophase. Shearing the sample while in the smectic A* phase gives a homeotropic texture with no birefringence, and upon slowly heating the material towards the chiral

nematic phase a filament texture which is characteristic of the TGB phase was observed (Figure 153).

*Figure 152. Photomicrograph (x100 magnification) of the blue fog texture of the BPIII of compound **142** (76.3 °C).*
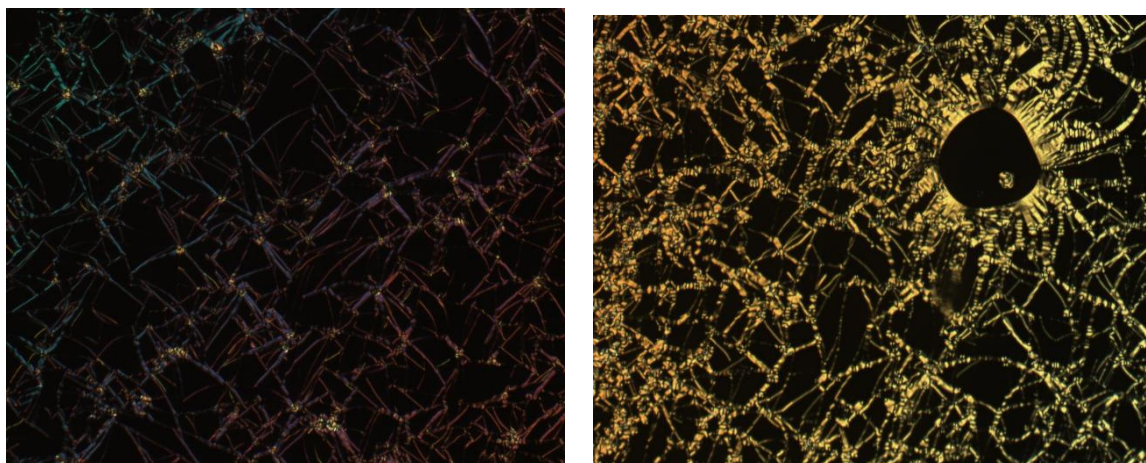
*Figure 153. Photomicrograph (x100 magnification) showing filament growth in the TGB phase of **142** (left, 75.0 °C), and growth of the filaments into domains of the chiral nematic phase (right, 75.0 °C).*

Compound **142** exhibited the richest mesomorphism possessing both BPIII and the TGB phase - both of which are indicative of a highly twisted organisation within the mesophase. This is apparently reflected in the optical rotation of **147** which was notably higher than the remaining compounds. Compound **150** (Figure 154) was previously reported featuring only a single mesogenic core and showed no liquid crystalline behaviour.[15] Therefore the effect of the dimeric structure can only be

observed by stabilisation of the mesophase by the cyanobiphenyl mesogen, and no comparison can be made in terms of the nature of the mesophase.

150
Cr 78 Iso °C
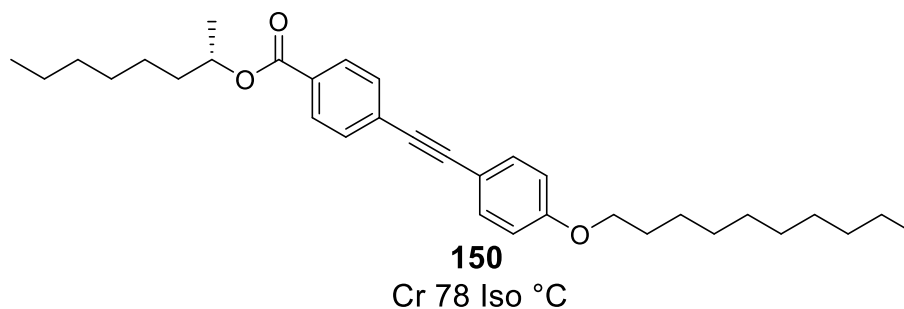
*Figure 154. Compound **150** was reported to be non-liquid crystalline.[15]*

This is contrasted with the 2-methyl butyl derivative **148** shown in Figure 148, which exhibited a smectic A* phase. The lateral group of the 1-methyl heptyl derivative is likely too close to the diphenyl acetylene core, thus disrupting the formation of any mesophases unless the core is extended by an additional benzyl ester (see Figure 155). In the dimesogenic compounds produced in this work this disruption is overcome by the presence of the undisrupted cyanobiphenyl and thus allowing for the rich phase behaviour observed. This disruption of the mesophase is nonetheless revealed *via* comparison of compound **138** containing the 2-methyl butyl chiral unit and **142** featuring the 1-methyl heptyl unit (Table 34). The disruption induced *via* placing the lateral branch of the chiral unit closer to the diphenyl acetylene core is responsible for a decrease of nearly 30 °C in the clearing point regardless of the lengthened alkyl chain. Furthermore, as the melting point of the two compounds remains similar the enantiotropic behaviour of **138** is replaced by monotropic behaviour in **142**. An enhanced effect is seen in the ether derivatives as would be expected as the branching methyl group is placed closer still to the diphenyl acetylene core.

*Table 34. Comparison of 2-methylbutyl analogues **133** and **138**.with their 1-methylheptyl equivalents **140** and **142**.*

Compound number	Transition	T /°C	ΔH / kJ mol^{-1}	ΔS / J K^{-1} mol^{-1}
133	Cr – SmE	87.9	16.9	41
	SmE – SmB	106.4	3.9	10
	SmB – SmA*	109.0	3.1	8
	SmA* - Iso	141.7	28.8	80
138	Cr – SmA*	89.8	43.7	121
	SmA* – N*	102.0	0.5	1
	N* - Iso	115.9	4.3	11
140	Cr – Iso	110.0	79.3	207
	(Iso – SmA*)	93.0	-	-
142	Cr - Iso	97.1	75.5	204
	(Iso – BPIII)	76.3	-	-
	(Iso – N*)	76.1	-	-
	(N* – TGB)	75.0	-	-
	(TGB – SmA*)	75.0	-	-

A similar family of compounds featuring the 1-methylheptyl chiral unit and a benzoate extended diphenyl acetylene core such as compound **151** have previously been shown to possess the TGB phase. This effect was deemed to be reliant on the lateral fluorine substituents as the hydrogen-analogues did not display the TGB phase (Figure 155).[18-21] This family rely upon the extended core to stabilise the mesophase as seen above. The persisting smectic order within the blue phase as an example of additional positional order is intriguing however while **142** shares the BPIII and TGB phase the presence of the nematic phase in between shows clearly different behaviour.

151
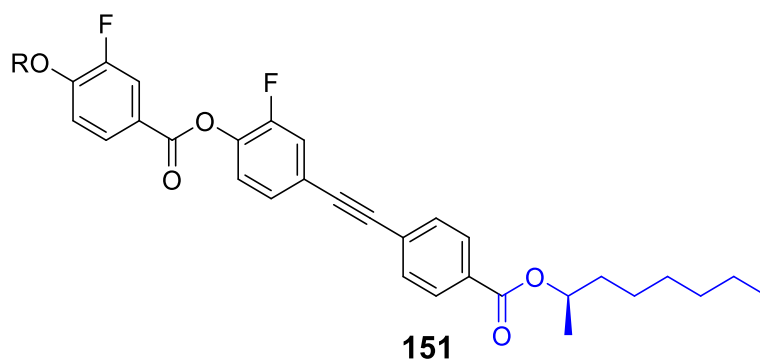
Figure 155. The same linking unit, chiral group and an extended core have previously been found to give the TGB phase, at longer terminal chain lengths (R = C$_{16}$H$_{33}$, a BP$_{Sm}$ phase was also observed).[18-21]

Additional evidence of the highly twisting phase organisation of **142** was found *via* miscibility studies of these compounds (Tables 35, 36) as **142** possesses a far greater helical twisting power. Interestingly the highly twisted blue phase was also found for compound **137** which instead bears the more commonly represented (S)-2-methylbutyl chiral unit. Other spacer lengths of 8, 9 and 11 methylene units (**135**, **136** and **138**) using the same chiral group and linking unit did not reproduce this behaviour. Compound **128** described earlier was synthesised as part of a series of Schiff's bases which bear several structural similarities to the materials produced here. The greater prevalence of BPI in the case of the Schiff's base compounds may be related to the shorter pitch attributed to the alkyl linking group over that of the ester linking group used in this work.

6.4 Miscibility Studies

As described previously the addition of a chiral dopant into a nematic mesophase will propagate chirality into the system. The pitch of the chiral helix is inversely proportional to the concentration as described in equation 10. This pitch may be measured using a Grandjean-Cano wedge cell as described in section 6.1.2. This measurement was performed once for each target compound for a concentration of between two and six weight% of chiral dopant in the nematic host E7. This allowed an estimate of the helical twisting power to be made for each material and while the values were not precise, helped to identify the trends associated with the various structural factors (Table 35).

*Table 35. Helical twisting powers as found via initial measurements using the Cano-wedge method. *Compounds 140 and 142 differ in that they bear the 1-methyl-2-heptanol chiral unit while the remaining compounds feature the 2-methyl-1-butanol unit.*

Compound number	Chiral linking group	Alkyl spacer length	Helical twisting power/ μm^{-1} $wt\%^{-1}$	Helical twisting power/ μm^{-1} $mol\%^{-1}$
131	Ether	Hexyl, C_6	0.1	0.2
132	Ether	Decyl, C_{10}	0.2	0.4
133	Ether	Undecyl, C_{11}	0.3	0.7
134	Ester	Hexyl, C_6	1.0	2.3
135	Ester	Octyl, C_8	1.4	3.4
136	Ester	Nonyl, C_9	1.7	4.0
137	Ester	Decyl, C_{10}	1.1	2.7
138	Ester	Undecyl, C_{11}	1.5	3.7
140*	Ether	Undecyl, C_{11}	0.7	1.7
142*	Ester	Undecyl, C_{11}	4.2	10.7
143	Ether	N/A	0.5	0.6
147	Ether	Undecyl, C_{11}	0.5	1.1

The error associated with these values is large as only one measurement has been used in the estimate. Additionally, solubility issues arose for the ether compounds as they proved to share low helical twisting powers, and therefore higher concentrations (6 wt.%) were required to measure accurately *via* the Cano-wedge method. In particular the solubility of **147** in E7 was very poor with the dopant crystallising from the mixture at a concentration of 6 wt.% before measurements could be made. As such the measurement was taken at a concentration of 2 wt.% where only two defect lines were resolved in the wedge cell. Although higher, the helical twisting powers of the ester series was also low in comparison to many chiral materials and as such at the concentrations measured the defect lines were measured as an average of multiple defects on millimeter scale.

In spite of the error associated with these values it is clear that the ester linker provides a far higher helical twisting power than the ether equivalent. The higher helical

twisting power of the ester compounds may be explained firstly with regards to the increased flexibility of the ether over ester linkers.

It is noteworthy that **143** with no cyanobiphenyl has a higher helical twisting power when measuring concentration in units of weight% of the mixture, relative to fellow ether compounds **131**, **132**, and **133** with the addition of a cyanobiphenyl mesogen. This effect is reduced when considering the molar helical twisting power (μm^{-1} mol%$^{-1}$) which brings the value in line with the remaining ether compounds. Clearly the incorporation of additional (S)-2-methylbutyl substituted diphenyl acetylene units is more effective at imparting helical twisting than the achiral cyanobiphenyl unit. Similarly, the non-liquid crystalline ester analogue of **268** has been reported to be an effective chiral dopant.[17]

The helical twisting power associated with these compounds is far below that of materials designed for the purpose of chiral dopants (Figure 134). The family of Schiff's base dimers reported by Luckhurst (see Figure 151) show notably higher molar helical twisting powers – between 5.6 and 6.7 – which may be attributed to the greater induction of chirality *via* the alkyl linking group as discussed previously. While these estimated values indicate the possibility of an odd-even effect in the ester series this notion was discarded in the case of the Schiff's base compounds. Many examples of chiral dimesogenic materials utilise cholesterol as one of the mesogenic units and to incorporate chirality into the material.[22] These materials can show a large variation in helical twisting power in spite of the use of the same chiral mesogen indicating the impact of both the mesogen close to the chiral centre and attached *via* spacer.

Following this initial data set more accurate values were attained *via* a series of mixtures at different concentrations using compounds **133**, **136**, **138**, and **142** (Figure 156). This selection of compounds was chosen to allow direct comparison of several parameters such as; the ether vs ester linking unit between **133** and **138**, the effect of the chain length between **138** and **136**, and finally the 2-methyl-1-butanol and 1-methyl-2-heptanol chiral units between **138** and **142**. The pitch was measured for each of these mixtures and the results are given in a plot of chiral dopant concentration against inverse pitch.
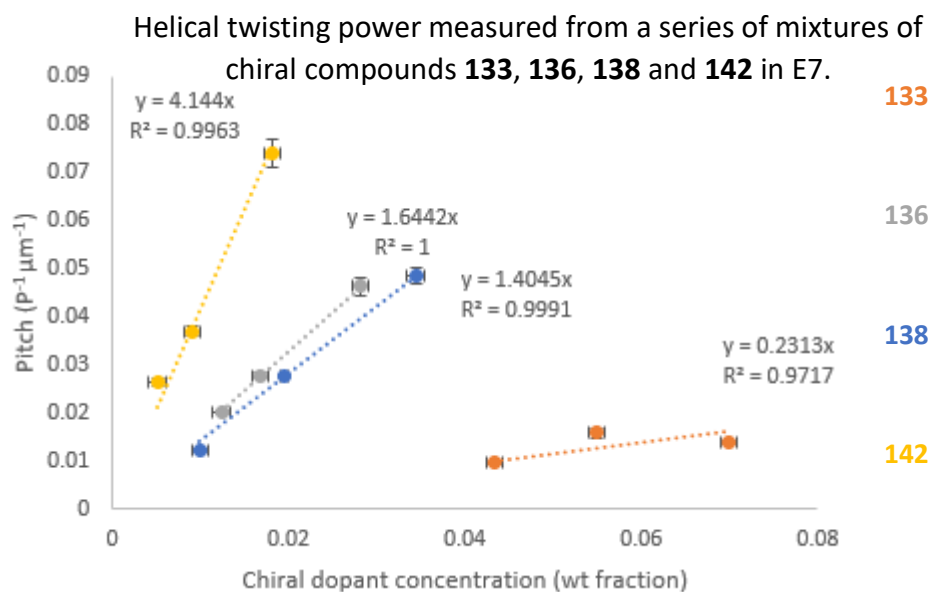
Figure 156. Plot of mass fraction of chiral dopant in E7 against inverse of the mixtures pitch as measured for compounds *133, 136, 138,* and *142* recorded for mixtures at a series of concentrations between 0.2 – 3 mol % dopant (0.02 wt fraction ≈ 0.8 mol %).

As described previously the relationship between chiral dopant concentration and pitch is linear at low concentrations and in the absence of a dopant the pitch is zero as the mesophase is achiral. The gradient of each series gives the helical twisting power with a greater degree of confidence than those reached by a single measurement above, however the agreement between these values and the previous estimates appears to be acceptable (Table 36). The measurements recorded for **133** however do not give a good linear plot due to the greater errors associated with measuring the longer pitch and issues arising from the solubility at higher dopant concentrations.

Table 36. Helical twisting power of selected compounds as measured from a series of mixtures.* 1-methyl-2-heptanol chiral unit

Compound number	Chiral linking group	Alkyl spacer length	Helical twisting power / μm^{-1} $wt\%^{-1}$	Helical twisting power estimate/ μm^{-1} $wt\%^{-1}$
133	Ether	Undecyl, C_{11}	0.2	0.3
136	Ester	Nonyl, C_9	1.6	1.7
138	Ester	Undecyl, C_{11}	1.4	1.5
142*	Ester	Undecyl, C_{11}	4.1	4.2

The previously established trends are upheld with the ether compound **133** having a far lower helical twisting power than the ester compounds produced. In the bulk liquid crystal mesophases described earlier there appeared to be an odd-even effect for the mesophase stability with the greatest stability belonging to compound **136**. This appears to be reflected in the helical twisting power associated with each compound as **136** again has the highest HTP, while the estimated values show an odd-even effect for this series. Finally, it has previously been established that **142** featuring the (S)-1-methyl-2-heptanol chiral unit gives a highly twisting mesophase structure as observed by the presence of blue phases and the TGB phase. This is also seen in the far greater helical twisting power measured for **142** than the (S)-2-methyl-1-butanol analogue **138**.

6.5 Summary

The liquid crystalline properties of this family of materials have been evaluated using several analytical techniques and their effectiveness as chiral dopants was measured. This has formed the start of a structure activity relationship which may help with the design of further materials in this class. The chiral linking unit was varied between ether and ester linkages across multiple chain lengths showing the greater impact of the diphenyl acetylene unit upon the mesophase structure when the intermolecular forces were increased *via* the introduction of the ether unit and thus increased polarisability. This linking unit stabilised the mesophase increasing both transition temperatures and the mesophase organisation as shown by the presence of more ordered smectic phases. However, the ester linking unit appeared to be more effective at transmitting the chirality into other liquid crystalline systems as found by miscibility studies and gave evidence of highly twisted mesophase structures as shown by the presence of blue phases and the TGB phase. The effect of varying the spacer chain length was investigated by the synthesis of five ester linked compounds for which the four successive spacer chain lengths (**134** – **138**) showed the emergence of an odd-even effect. The behavior of the C_{11} and C_{10} spacer chain lengths was mirrored between the ester and ether units implying the trend may be extended to the ether analogues too. Importantly in the case of the C_6 spacer length which is used commonly throughout this project the trends observed do not apply as cleanly and the phase behavior differs from the other compounds in the series. This is thought to be due to

the short spacer not allowing decoupling of the cyanobiphenyl and diphenyl acetylene units showing that the diphenyl acetylene unit plays an important part in the liquid crystalline behavior of the compounds described elsewhere in this work.

6.6 Experimental

130
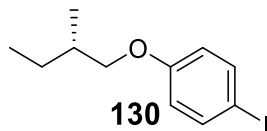
4-Iodophenol (1.02 g, 4.64 mmol), (S)-2-methyl butanol (0.35 g, 3.98 mmol) and PPh$_3$ (1.10 g, 4.19 mmol) were charged to a flask under argon. Dry THF (30 mL) was added and the mixture cooled in an ice bath then DIAD (0.80 mL, 0.82 g, 4.06 mmol) was slowly added. The mixture was warmed to room temperature and stirred for 18 hours. The solvent was removed *in vacuo* and the crude product was purified by column chromatography (DCM as eluent) to give the target compound **130** as a colourless oil (0.66 g, 2.17 mmol, 55% yield).

^{1}H NMR (400 MHz, CDCl$_3$) δ 7.53 (dd, *J* = 9.0, 2.0, 2H, Ar*H*), 6.69 (dd, *J* = 9.0, 2.0, 2H, Ar*H*), 3.77 (dd, *J* = 9.0, 6.0 Hz, 1H, OC*H*H), 3.69 (dd, *J* = 9.0, 6.6 Hz, 1H, OCH*H*), 1.90 – 1.77 (m, 1H, C*H*CH$_3$), 1.62-1.57 (m, 1H, C*H*HCH$_3$), 1.29 – 1.19 (m, 1H, CH*H*CH$_3$), 1.00 (d, *J* = 6.5 Hz, 3H, CHC*H*$_3$), 0.94 (dd, *J* = 7.5, 7.5 Hz, 3H, CH$_2$C*H*$_3$).

^{13}C{^{1}H} NMR (101 MHz, 400 MHz) δ 166.3, 137.8, 131.1, 130.1, 100.7, 69.9, 34.4, 26.9, 26.2, 16.6, 11.4.
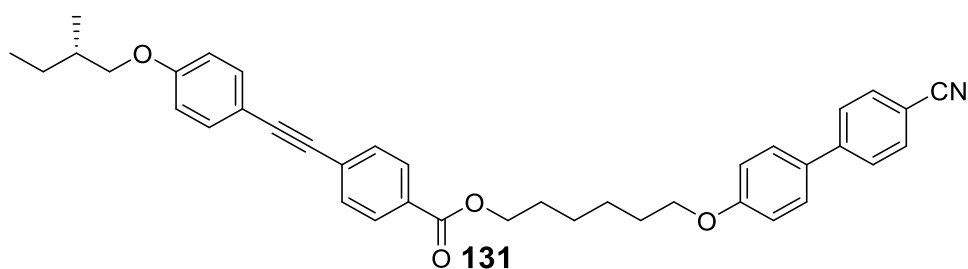
Compound **130** (0.17 g, 0.56 mmol) and **33**$_i$ (0.21 g, 0.49 mmol), were charged to a Schlenk tube under argon. Triethylamine (5 mL) and toluene (5 mL) was added and the mixture degassed with argon gas for 20 minutes. [PdCl$_2$(PPh$_3$)$_2$](0.17 g, 0.24 mmol) and CuI (0.05 g, 0.26 mmol) were added under flow of argon and the reaction mixture stirred at room temperature for 18 hours. The solvent was removed *in vacuo* and the crude product was purified by column chromatography (DCM:EtOAc as eluent) followed by recrystallisation from hot ethanol to give the target compound **131** as a powdery white solid (0.11 g, 0.19 mmol, 39% yield).

^{1}H NMR (400 MHz, CDCl$_3$) δ 7.99 (d, *J = 8.5* Hz, 2H, Ar*H*), 7.67 (d, *J = 8.5* Hz, 2H, Ar*H*), 7.63 (d, *J = 8.5* Hz, 2H, Ar*H*), 7.54 (d, *J = 8.5* Hz, 2H, Ar*H)*, 7.52 (d, *J = 8.5* Hz, 2H, Ar*H)* 7.46 (dd, *J = 8.5, 2.5* Hz, 2H, Ar*H*), 6.98 (dd, *J = 8.5, 2.5* Hz, 2H, Ar*H*), 6.88 (dd, *J = 8.5, 2.5* Hz, 2H, Ar*H*), 4.35 (t, *J = 6.5* Hz, 2H, COOC*H$_2$*), 4.02 (t, *J = 6.5* Hz, 2H, OC*H$_2$*), 3.84 (dd, *J = 9.0, 6.0* Hz, 1H, OC*H*H), 3.76 (dd, *J = 9.0, 6.5* Hz, 1H, OC*H*H), 1.90-1.79 (m, 5H, 2 x OCH$_2$C*H$_2$,* and C*H*CH$_3$), 1.62 – 1.52 (m, 5H, OCH$_2$CH$_2$C*H$_2$* and CH*H*CH$_3$), 1.31-1.23 (m, 1H, CH*H*CH$_3$), 1.03 (d, *J = 6.5* Hz, 3H, CHC*H$_3$*), 0.96 (t, *J = 7.5* Hz, 3H, CH$_2$C*H$_3$*).

^{13}C{^{1}H} NMR (101 MHz, CDCl$_3$) δ 166.4, 160.0, 145.4, 133.4, 132.7, 131.4, 129.6, 128.5, 127.2, 119.3, 115.2, 114.8, 110.2, 100.5, 92.9, 87.6, 73.1, 68.1, 65.2, 39.5, 34.8, 30.6, 29.2, 28.8, 26.3, 26.0, 24.9, 16.7, 12.7, 11.5.

APCI-MS: m/z = 614.29 [M+H]$^+$

Elemental analysis: calc'd (%) for C$_{39}$H$_{39}$NO$_4$: C 79.97, H 6.71, N 2.39; found: C 79.68, H 6.85, N 2.45.

132

Compound **130** (0.04 g, 0.13 mmol) and **33**iv (0.07 g, 0.15 mmol), were charged to a Schlenk tube under argon. Triethylamine (4 mL) and toluene (2 mL) were added and the mixture degassed with argon gas for 20 minutes. [PdCl$_2$(PPh$_3$)$_2$](0.01 g, 0.02 mmol) and CuI (0.001 g, 0.01 mmol) were added under flow of argon and the reaction mixture stirred at room temperature for 18 hours. The solvent was removed *in vacuo* and the crude product was purified by column chromatography (DCM:EtOAc as eluent) followed by recrystallisation from hot ethanol to obtain **132** as a crystalline white solid (0.07 g, 0.11 mmol, 85% yield).

^{1}H NMR (400 MHz, CDCl$_3$) δ 8.00 (d, *J* = 8.0 Hz, 2H, Ar*H*), 7.68 (d, *J* = 8.0 Hz, 2H, Ar*H*), 7.63 (d, *J* = 8.0 Hz, 2H, Ar*H*), 7.59 – 7.49 (m, 4H, Ar*H*), 7.46 (d, *J* = 8.0 Hz, 2H, Ar*H*), 6.99 (d, *J* = 8.0 Hz, 2H, Ar*H*), 6.87 (d, *J* = 8.0 Hz, 2H, Ar*H*), 4.32 (t, *J* = 6.5 Hz, 2H, COOC*H$_2$*), 4.00 (t, *J* = 6.5 Hz, 2H, OC*H$_2$*), 3.84 (dd, *J* = 8.5, 6.0 Hz, 1H, OC*H*H), 3.75 (dd, *J* = 8.5, 7.0 Hz, 1H, OCH*H*), 1.93 – 1.73 (m, 5H, OCH$_2$C*H$_2$,* and C*H*CH$_3$), 1.51 – 1.20 (m, 14H), 1.02 (d, *J* = 6.5 Hz, 3H, CHC*H$_3$*), 0.96 (t, *J* = 7.5 Hz, 3H, CH$_2$C*H$_3$*).

^{13}C{^{1}H} NMR (101 MHz, CDCl$_3$) δ 166.4, 159.9, 145.4, 133.3, 132.7, 131.4, 129.6, 128.5, 127.2, 119.3, 115.2, 114.8, 114.5, 110.1, 92.8, 73.1, 68.3, 65.4, 34.8, 29.6, 29.5, 29.5, 29.3, 28.8, 26.2, 26.2, 16.7, 11.5.

APCI-MS: m/z = 642.36 [M+H]$^+$

Elemental analysis: calc'd (%) for C$_{43}$H$_{47}$NO$_4$: C 80.47, H 7.38, N 2.18; found: C 80.09, H 7.41, N 2.16.

133

Compound **130** (0.11 g, 0.36 mmol) and compound **33ᵥ** (0.20 g, 0.41 mmol), were charged to a Schlenk tube under argon. Triethylamine (5 mL) and toluene (4 mL) were added and the mixture degassed with argon gas for 20 minutes. [PdCl₂(PPh₃)₂](0.01 g, 0.01 mmol) and CuI (0.003 g, 0.02 mmol) were added under flow of argon and the reaction mixture stirred at room temperature for 18 hours. The solvent was removed *in vacuo* and the crude product was purified by column chromatography (DCM as eluent) followed by recrystallisation from hot ethanol to give the target compound **133** as a powdery white solid (0.18 g, 0.28 mmol, 76% yield).

^{1}H NMR (400 MHz, CDCl₃) δ 8.01 (dd, *J* = 8.0, 2.0 Hz, 2H, Ar*H*), 7.68 (dd, *J* = 8.5, 2.0 Hz, 2H, Ar*H*), 7.63 (dd, *J* = 8.5, 2.0 Hz, 2H, Ar*H*), 7.55 (dd, *J* = 8.5, 2.0 Hz, 2H, Ar*H*), 7.52 (dd, *J* = 9.0, 3.0 Hz, 2H, Ar*H*), 7.46 (dd, *J* = 9.0, 2.0 Hz, 2H, Ar*H*), 6.99 (dd, *J* = 9.0, 2.5 Hz, 2H, Ar*H*), 6.88 (dd, *J* = 9.0, 2.5 Hz, 2H, Ar*H*), 4.32 (t, *J* = 6.5 Hz, 2H, OC*H₂*), 4.00 (t, *J* = 6.5 Hz, 2H, OC*H₂*), 3.84 (dd, *J* = 9.0, 6.0 Hz, 1H, OC*H*H), 3.75 (dd, *J* = 9.0, 6.5 Hz, 1H, OCH*H*), 1.83-1.73 (m, 5H, OCH₂C*H₂,* and C*H*CH₃), 1.50 – 1.23 (m, 17H), 1.02 (d, *J* = 6.5 Hz, 3H, CHC*H₃*), 0.95 (t, *J* = 7.5 Hz, 3H, CH₂C*H₃*).

^{13}C{^{1}H} NMR (101 MHz, CDCl₃) δ 166.4, 159.9, 145.4, 133.4, 132.7, 131.4, 129.6, 128.5, 127.2, 119.3, 115.2, 114.8, 110.1, 87.6, 68.3, 65.4, 34.8, 29.7, 29.6, 29.5, 29.4, 29.4, 28.8, 26.2, 26.2, 16.7, 11.5.

APCI-MS: m/z = 656.4 [M+H]⁺

Elemental analysis: calc'd (%) for C₄₄H₄₉NO₄: C 80.58, H 7.53, N 2.14; found: C 80.46, H 7.75, N 2.06.
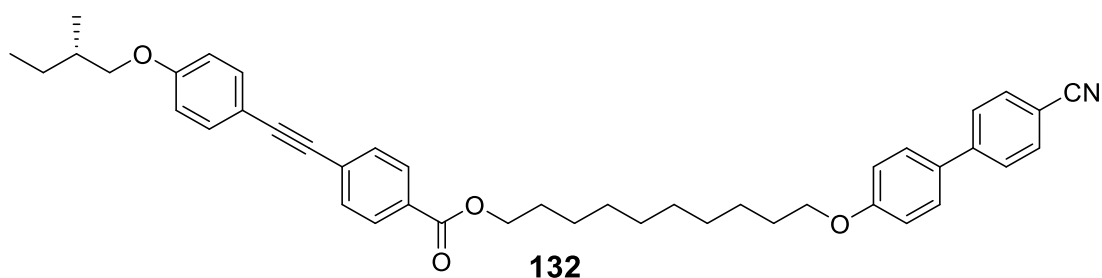
Compound **80** (0.15 g, 0.47 mmol) and **33ᵢ** (0.19 g, 0.45 mmol), were charged to a Schlenk tube under argon. Triethylamine (5 mL) and toluene (5 mL) was added and the mixture degassed with argon gas for 20 minutes. [PdCl$_2$(PPh$_3$)$_2$](0.17 g, 0.24 mmol) and CuI (0.06 g, 0.32 mmol) were added under flow of argon and the reaction mixture stirred at room temperature for 18 hours. The solvent was removed *in vacuo* and the crude product was purified by column chromatography (DCM:EtOAc as eluent) followed by recrystallisation from hot ethanol to give the target compound **134** as a white powdery solid (0.17 g, 0.27 mmol, 60% yield).

^{1}H NMR (400 MHz, CDCl$_3$) δ 8.04 (dd, *J* = 8.5, 2.5 Hz, 4H, COOArAr*H*), 7.68 (d, *J* = 8.5 Hz, 2H, Ar*H*), 7.63 (d, *J* = 8.5 Hz, 2H, Ar*H*), 7.59 (d, *J* = 8.5 Hz, 4H, CCAr*H*), 7.52 (d, *J* = 8.5 Hz, 2H, Ar*H*), 7.02 − 6.95 (dd, *J* = 8.5, 2.5 Hz, 2H, Ar*H*), 4.36 (t, *J* = 6.5 Hz, 2H, COOC*H$_2$*), 4.23 (dd, *J* = 11.0, 6.0 Hz, 1H, OC*H*H), 4.14 (dd, *J* = 11.0, 6.5 Hz, 1H, OCH*H*), 4.03 (t, *J* = 6.5 Hz, 2H, OC*H$_2$*), 1.92-1.80 (m, 5H, OCH$_2$C*H$_2$,* and C*H*CH$_3$), 1.64 − 1.48 (m, 5H, OCH$_2$CH$_2$C*H$_2$* and CH*H*CH$_3$), 1.36 − 1.23 (m, 1H, CH*H*CH$_3$), 1.03 (d, *J* = 7.0 Hz, 3H, CHC*H$_3$*), 0.97 (t, *J* = 7.5 Hz, 3H, CH$_2$C*H$_3$*).

^{13}C{^{1}H} NMR (101 MHz, CDCl$_3$) δ 166.2, 159.8, 145.4, 132.7, 131.8, 131.5, 130.5, 130.3, 129.7, 128.5, 127.5, 127.3, 127.2, 119.3, 115.2, 110.2, 91.6, 91.4, 70.0, 68.1, 65.3, 34.4, 29.3, 28.8, 26.3, 26.0, 25.9, 16.7, 11.5.

APCI-MS: m/z = 586.29 [M+H]$^+$

Elemental analysis: calc'd (%) for C$_{40}$H$_{39}$NO$_5$: C 78.28, H 6.40, N 2.28; found: C 77.89, H 6.39, N 2.28.
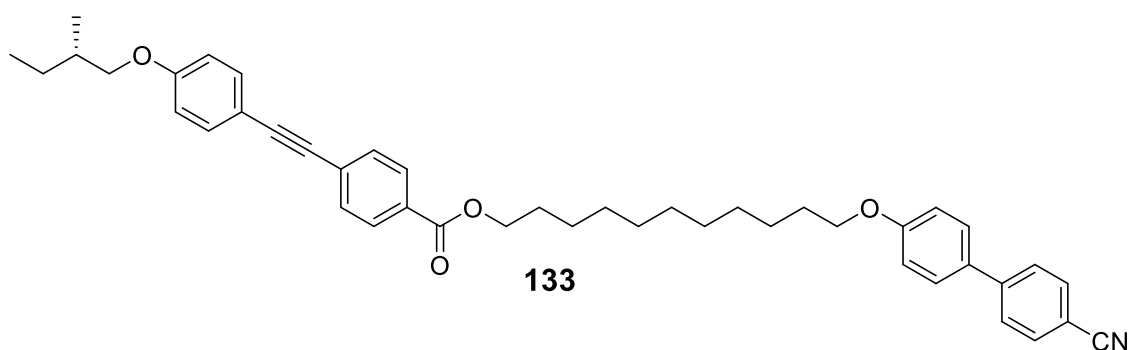
Compound **80** (0.21 g, 0.67 mmol) and **33$_{ii}$** (0.30 g, 0.69 mmol), were charged to a Schlenk tube under argon. Triethylamine (5 mL) and toluene (3 mL) were added and the mixture degassed with argon gas for 20 minutes. [PdCl$_2$(PPh$_3$)$_2$](0.03 g, 0.04 mmol) and CuI (0.01 g, 0.05 mmol) were added under flow of argon and the reaction mixture stirred at room temperature for 18 hours. The solvent was removed *in vacuo* and the crude product was purified by column chromatography (DCM:EtOAc as eluent) followed by recrystallisation from hot ethanol to give the target compound **135** as a crystalline white solid (0.21 g, 0.32 mmol, 48% yield).

^{1}H NMR (400 MHz, CDCl$_3$) δ 8.04 (d, *J* = 8.5 Hz, 4H, Ar*H*), 7.68 (d, *J* = 8.5 Hz, 2H, Ar*H*), 7.65 − 7.57 (m, 6H, Ar*H*), 7.52 (d, *J* = 8.5 Hz, 2H, Ar*H*), 6.98 (d, *J* = 8.5 Hz, 2H, Ar*H*), 4.33 (t, *J* = 6.5 Hz, 2H, COOC*H$_2$*), 4.22 (dd, *J* = 11.0, 6.0 Hz, 1H, OC*H*H), 4.14 (dd, *J* = 11.0, 6.5 Hz, 1H, OCH*H*), 4.00 (t, *J* = 6.5 Hz, 2H, OC*H$_2$*), 1.92 − 1.75 (m, 5H, OCH$_2$C*H$_2$,* and C*H*CH$_3$), 1.62 − 1.37 (m, 9H), 1.36 − 1.21 (m, 1H, CH*H*CH$_3$), 1.02 (d, *J* = 6.5 Hz, 3H, CHC*H$_3$*), 0.97 (t, *J* = 7.5 Hz, 3H, CH$_2$C*H$_3$*).

^{13}C{^{1}H} NMR (101 MHz, CDCl$_3$) δ 166.2, 159.9, 145.4, 132.7, 131.8, 131.4, 130.5, 130.4, 129.7, 128.5, 127.4, 127.3, 127.2, 119.3, 115.2, 110.1, 91.5, 91.4, 70.0, 68.2, 65.5, 34.4, 29.4, 29.3, 28.8, 26.3, 26.1, 16.7, 11.5.

APCI-MS: m/z = 642.32 [M+H]$^+$

Elemental analysis: calc'd (%) for C$_{42}$H$_{43}$NO$_5$: C 78.60, H 6.75, N 2.18; found: C 78.58, H 6.66, N 2.09.
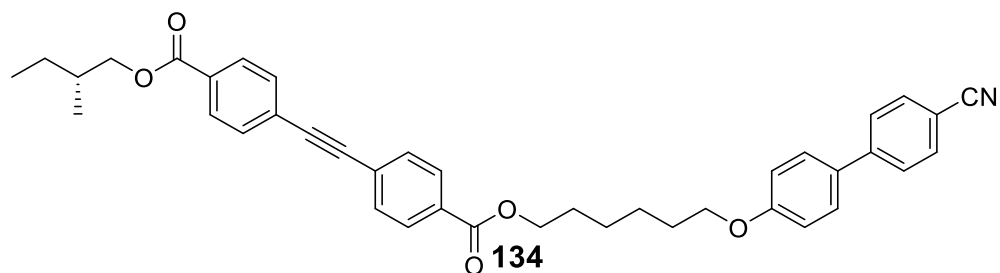
136

Compound **130** (0.21 g, 0.67 mmol) and **33ᵢᵢᵢ** (0.30 g, 0.66 mmol), were charged to a Schlenk tube under argon. Triethylamine (5 mL) and toluene (3 mL) were added and the mixture degassed with argon gas for 20 minutes. [PdCl$_2$(PPh$_3$)$_2$](0.03 g, 0.04 mmol) and CuI (0.01 g, 0.05 mmol) were added under flow of argon and the reaction mixture stirred at room temperature for 18 hours. The solvent was removed *in vacuo* and the crude product was purified by column chromatography (DCM:EtOAc as eluent) followed by recrystallisation from hot ethanol to give the target compound **136** as a powdery white solid (0.25 g, 0.38 mmol, 58% yield).

^{1}H NMR (400 MHz, CDCl$_3$) δ 8.04 (d, *J* = 8.0 Hz, 4H, Ar*H*), 7.68 (d, *J* = 8.0 Hz, 2H, Ar*H*), 7.66 – 7.57 (m, 6H, Ar*H*), 7.52 (d, *J* = 8.0 Hz, 2H, Ar*H*), 6.99 (d, *J* = 8.5 Hz, 2H, Ar*H*), 4.33 (t, *J* = 6.5 Hz, 2H, COOC*H$_2$*), 4.22 (dd, *J* = 10.5, 6.0 Hz, 1H, OC*H*H), 4.14 (dd, *J* = 10.5, 6.5 Hz, 1H, OCH*H*), 4.00 (t, *J* = 6.5 Hz, 2H, OC*H$_2$*), 1.93 – 1.73 (m, 5H, OCH$_2$C*H$_2$,* and C*H*CH$_3$), 1.61 – 1.34 (m, 11H), 1.28 (m, 1H, C*H*HCH$_3$), 1.02 (d, *J* = 6.5 Hz, 3H, CHC*H$_3$*), 0.97 (t, *J* = 7.5 Hz, 3H, CH$_2$C*H$_3$*).

^{13}C{^{1}H} NMR (101 MHz, CDCl$_3$) δ 166.2, 159.9, 145.4, 132.7, 131.8, 131.4, 130.5, 129.7, 128.5, 127.4, 127.4, 127.2, 119.3, 115.2, 110.1, 91.5, 70.0, 68.2, 65.5, 34.4, 29.6, 29.4, 29.3, 28.8, 26.3, 26.1, 16.7, 11.5.

APCI-MS: m/z = 656.34 [M+H]$^+$

Elemental analysis: calc'd (%) for C$_{43}$H$_{45}$NO$_5$: C 78.75, H 6.92, N 2.14; found: C 78.69, H 6.70, N 2.38.
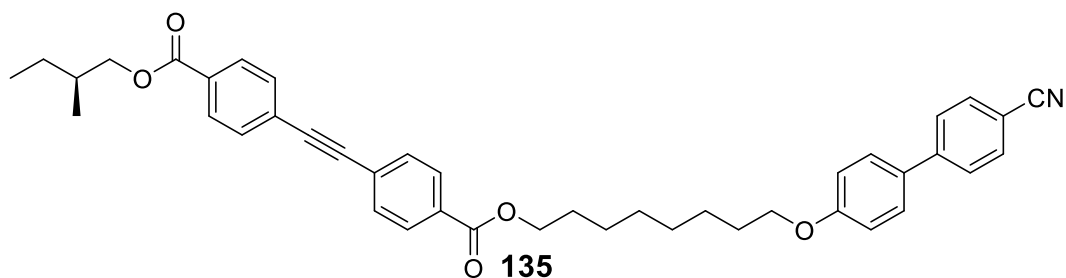
137

Compound **80** (0.048 g, 0.15 mmol) and **33ᵢᵥ** (0.07 g, 0.15 mmol), were charged to a Schlenk tube under argon. Triethylamine (4 mL) and toluene (2 mL) were added and the mixture degassed with argon gas for 20 minutes. [PdCl$_2$(PPh$_3$)$_2$](0.01 g, 0.02 mmol) and CuI (0.001 g, 0.01 mmol) were added under flow of argon and the reaction mixture stirred at room temperature for 18 hours. The solvent was removed *in vacuo* and the crude product was purified by column chromatography (DCM:EtOAc as eluent) followed by recrystallisation from hot ethanol to give the target compound **137** as a powdery white solid (0.080 g, 0.12 mmol, 78% yield).

^{1}H NMR (400 MHz, CDCl$_3$) δ 8.04 (d, *J* = 8.5 Hz, 4H, Ar*H*), 7.69 (d, *J* = 8.5 Hz, 2H, Ar*H*), 7.65 – 7.56 (m, 6H, Ar*H*), 7.50 (d, *J* = 8.5 Hz, 2H, Ar*H*), 7.00 (d, *J* = 8.5 Hz, 2H, Ar*H*), 4.33 (t, *J* = 6.5 Hz, 2H, COOC*H*$_2$), 4.22 (dd, *J* = 11.0, 6.0 Hz, 1H, OC*H*H), 4.14 (dd, *J* = 10.5, 6.5 Hz, 1H, OCH*H*), 4.00 (t, *J* = 6.5 Hz, 2H, OC*H*$_2$), 1.93 – 1.70 (m, 5H, OCH$_2$C*H*$_2$, and C*H*CH$_3$), 1.59 – 1.22 (m, 14H), 1.02 (d, *J* = 7.0 Hz, 3H, CHC*H*$_3$), 0.97 (t, *J* = 7.5 Hz, 3H, CH$_2$C*H*$_3$).

^{13}C{^{1}H} NMR (101 MHz, CDCl$_3$) δ 166.2, 159.9, 145.4, 132.7, 131.8, 131.4, 130.5, 130.4, 129.7, 128.4, 127.4, 127.4, 127.2, 119.3, 115.2, 110.1, 91.5, 70.0, 68.3, 65.5, 34.4, 29.6, 29.6, 29.5, 29.4, 28.8, 26.3, 26.2, 26.1, 16.7, 11.5.

APCI-MS: m/z = 670.36 [M+H]$^+$

Elemental analysis: calc'd (%) for C$_{44}$H$_{47}$NO$_5$: C 78.89, H 7.07, N 2.09; found: C 78.40, H 7.08, N 1.98.
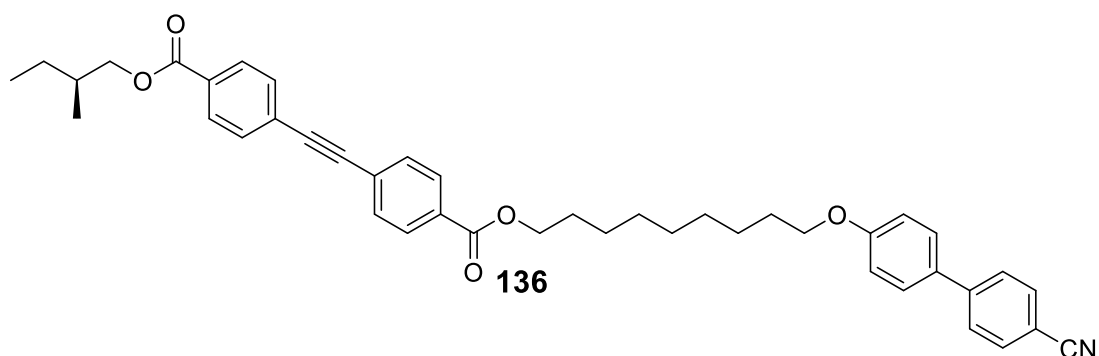
Compound **130** (0.11 g, 0.35 mmol) and **33ᵢᵥ** (0.20 g, 0.41 mmol), were charged to a Schlenk tube under argon. Triethylamine (5 mL) and toluene (4 mL) were added and the mixture degassed with argon gas for 20 minutes. [PdCl$_2$(PPh$_3$)$_2$](0.01 g, 0.01 mmol) and CuI (0.003 g, 0.02 mmol) were added under flow of argon and the reaction mixture stirred at room temperature for 18 hours. The solvent was removed *in vacuo* and the crude product was purified by column chromatography (DCM:EtOAc as eluent) followed by recrystallisation from hot ethanol to give the target compound **138** as a white solid (0.14 g, 0.21 mmol, 59% yield).

^{1}H NMR (400 MHz, CDCl$_3$) δ 8.03 (d, *J* = 8.5 Hz, 4H, Ar*H*), 7.69 (d, *J* = 8.5 Hz, 2H, Ar*H*), 7.66 − 7.57 (m, 6H), 7.53 (d, *J* = 8.5 Hz, 2H, Ar*H*), 6.99 (d, *J* = 8.5 Hz, 2H, Ar*H*), 4.33 (t, *J* = 6.5 Hz, 2H, COOC*H$_2$*), 4.22 (dd, *J* = 11.0, 6.0 Hz, 1H, OC*H*H), 4.14 (dd, *J* = 11.0, 6.5 Hz, 1H, OCH*H*), 4.00 (t, *J* = 6.5 Hz, 2H, OC*H$_2$*), 1.93 − 1.84 (m, 1H, C*H*CH$_3$), 1.84 − 1.73 (m, 5H, OCH$_2$C*H$_2$,* and C*H*CH$_3$), 1.58 − 1.21 (m, 14H), 1.02 (d, *J* = 6.5 Hz, 3H, CHC*H$_3$*), 0.97 (t, *J* = 7.5 Hz, 3H, CH$_2$C*H$_3$*).

^{13}C{^{1}H} NMR (101 MHz, CDCl$_3$) δ 166.2, 159.9, 145.4, 132.7, 131.8, 131.4, 130.4, 129.7, 128.5, 127.4, 127.2, 119.3, 115.2, 110.1, 91.5, 70.0, 68.3, 65.5, 34.4, 29.7, 29.6, 29.5, 29.4, 29.4, 28.8, 26.3, 26.2, 16.7, 11.5.

APCI-MS: m/z = 684.4 [M+H]$^+$

Elemental analysis: calc'd (%) for C$_{45}$H$_{49}$NO$_5$: C 79.03, H 7.22, N 2.05; found: C 79.15, H 7.39, N 2.05.

139
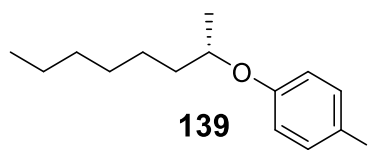
1,4-Iodophenol (0.34 g, 1.55 mmol), (R)-1-methyl-heptanol (0.20 g, 1.54 mmol) and PPh$_3$ (0.40 g, 1.52 mmol) were charged to a flask under nitrogen. Dry THF (30 mL) was added and the mixture cooled in an ice bath then DIAD (0.30 mL, 0.31 g, 1.52 mmol) was slowly added. The mixture was warmed to room temperature and stirred for 18 hours. The solvent was removed *in vacuo* and the crude product was purified by column chromatography (petrol:DCM as eluent) to give the target compound **139** as a colourless oil (0.23 g, 0.69 mmol, 45% yield).

^{1}H NMR (400 MHz, CDCl$_3$) δ 7.53 (dd, *J* = 8.5, 2.0 Hz, 2H, Ar*H*), 6.66 (dd, *J* = 8.5, 2.0 Hz, 2H, Ar*H*), 4.29 (tq, *J* = 6.0, 6.0 Hz, 1H, OC*H*CH$_3$), 1.75 – 1.65 (m, 1H, OCHC*H*H), 1.59 – 1.49 (m, 1H, OCHCH*H*), 1.46 – 1.23 (m, 11H, C*H$_2$*C*H$_2$*), 0.87 (t, *J* = 7.0 Hz, 3H CH$_2$C*H$_3$*).
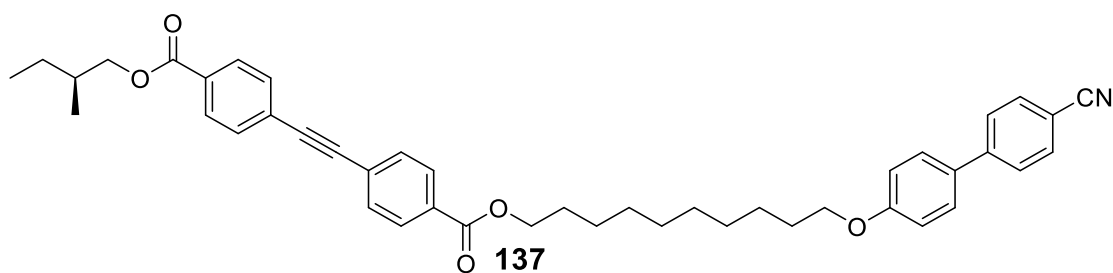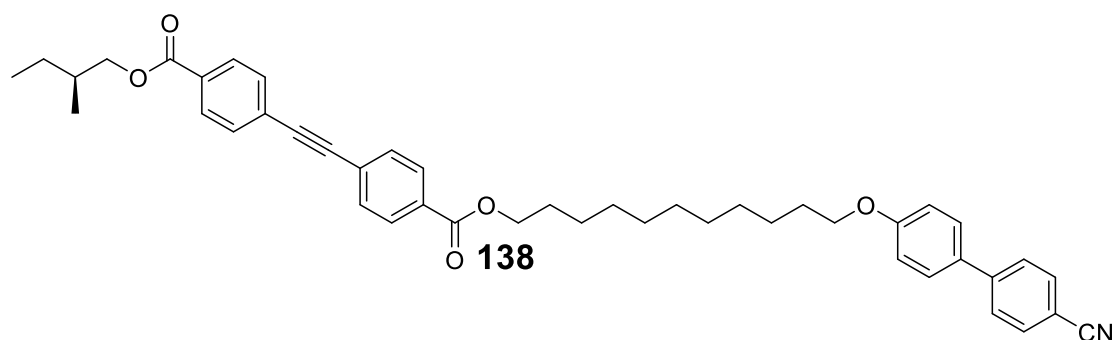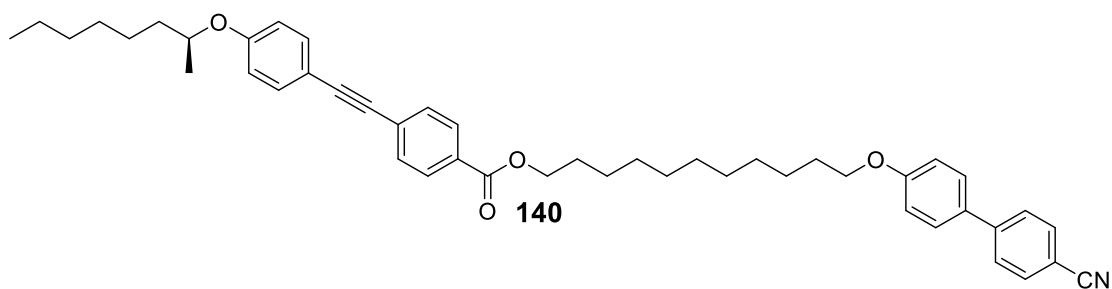
Compound **139** (0.15 g, 0.30 mmol) and **33**ᵥ (0.12 g, 0.36 mmol), were charged to a Schlenk tube under argon. Triethylamine (4 mL) and toluene (2 mL) were added and the mixture degassed with argon gas for 20 minutes. [PdCl$_2$(PPh$_3$)$_2$](0.01 g, 0.02 mmol) and CuI (0.003 g, 0.02 mmol) were added under flow of argon and the reaction mixture stirred at room temperature for 18 hours. The solvent was removed *in vacuo* and the crude product was purified by column chromatography (DCM:EtOAc as eluent) followed by recrystallisation from DCM:MeOH to give the target compound **140** as a crystalline white solid (0.12 g, 0.18 mmol, 60% yield).

^{1}H NMR (400 MHz, CDCl$_3$) δ 8.00 (dd, *J* = 8.5, 2.0 Hz, 2H, Ar*H*), 7.69 (dd, *J* = 8.0, 2.0 Hz, 2H, Ar*H*), 7.63, (dd, *J* = 8.5, 2.0 Hz, 2H, Ar*H*), 7.58 – 7.49 (m, 4H, Ar*H*), 7.46 (dd, *J* = 8.5, 2.0 Hz, 2H, Ar*H*), 6.99 (dd, *J* = 8.5, 2.0 Hz, 2H, Ar*H*), 6.86 (dd, *J* = 8.5, 2.0 Hz, 2H, Ar*H*), 4.43 – 4.34 (tq, *J* = 6.5, 6.5 Hz, 1H, OC*H*CH$_3$), 4.31 (t, *J* = 6.7 Hz, 2H, COOC*H$_2$*), 4.00 (t, *J* = 6.6 Hz, 2H, OC*H$_2$*), 1.86 – 1.67 (m, 5H, OCH$_2$C*H$_2$*, and OCHC*H*H), 1.52 – 1.21 (m, 26H), 0.88 (t, *J* = 7.5 Hz, 3H, CH$_2$C*H$_3$*).

^{13}C{^{1}H} NMR (101 MHz, CDCl$_3$) δ 166.4, 159.9, 158.9, 145.4, 133.4, 132.7, 131.4, 129.6, 128.5, 127.2, 119.3, 115.9, 115.2, 114.4, 110.1, 92.8, 87.5, 74.1, 68.3, 65.4, 36.5, 31.9, 29.7, 29.6, 29.5, 29.4, 28.8, 26.2, 25.6, 22.7, 19.8, 14.2.

APCI-MS: m/z = 698.42 [M+H]$^+$

Elemental analysis: calc'd (%) for C$_{47}$H$_{55}$NO$_4$: C 80.88, H 7.94, N 2.01; found: C 80.46, H 7.14, N 2.62.

141
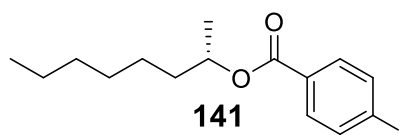
4-Iodobenzoic acid (0.39 g, 1.57 mmol), (S)-1-methyl heptanol (0.21 g, 1.61 mmol), EDC.HCl (0.51 g, 2.66 mmol) and DMAP (0.16 g, 1.31 mmol) were charged to a flask and DCM (20 mL) added. The reaction mixture was stirred at room temperature for 18 hours then the solvent removed *in vacuo* and the crude product was purified by column chromatography (petrol:DCM as eluent) to give the target compound **141** as a colourless oil (0.17 g, 0.47 mmol, 30% yield).

^{1}H NMR (400 MHz, CDCl$_3$) δ 7.79 (dd, *J* = 8.5, 2.0 Hz, 2H, Ar*H*), 7.74 (dd, *J* = 8.5, 2.0 Hz, 2H, Ar*H*), 5.11 (tq, *J* = 6.5, 6.5 Hz, 1H, OC*H*CH$_3$), 1.77-1.67 (m, 1H, OCHC*H*H), 1.66-1.56 (m, 1H, OCHCH*H*), 1.41 – 1.20 (m, 11H), 0.87 (t, *J* = 7.0 Hz, 3H).
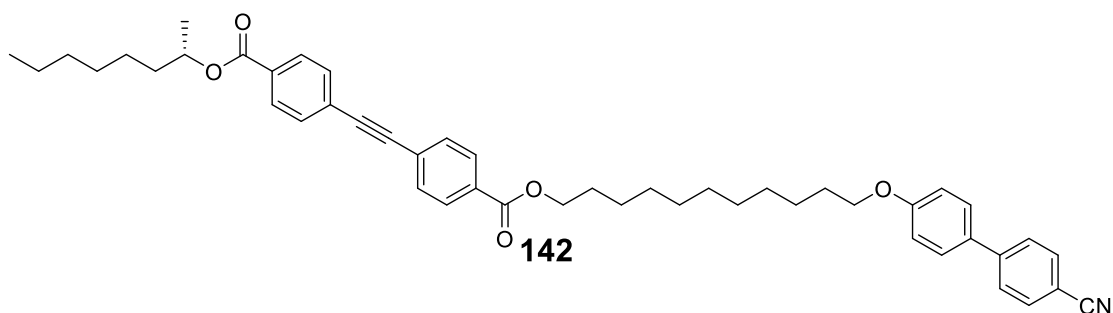
Compound **141** (0.08 g, 0.22 mmol) and **33ᵥ** (0.11 g, 0.22 mmol), were charged to a Schlenk tube under argon. Triethylamine (4 mL) and toluene (2 mL) were added and the mixture degassed with argon gas for 20 minutes. [PdCl$_2$(PPh$_3$)$_2$](0.01 g, 0.02 mmol) and CuI (0.003 g, 0.02 mmol) were added under flow of argon and the reaction mixture stirred at room temperature for 18 hours. The solvent was removed *in vacuo* and the crude product was purified by column chromatography (DCM:EtOAc as eluent) followed by recrystallisation from DCM:MeOH to give the target compound **142** as a crystalline white solid (0.06 g, 0.08 mmol, 36% yield).

^{1}H NMR (400 MHz, CDCl$_3$) δ 8.03 (dd, *J* = 8.5, 2.5 Hz, 4H, Ar*H*), 7.69 (dd, *J* = 8.5, 2.5 Hz, 2H, Ar*H*), 7.66 − 7.56 (m, 6H, Ar*H*), 7.53 (dd, *J* = 8.5, 2.5 Hz, 2H, Ar*H*), 6.99 (dd, *J* = 9.5, 2.5 Hz, 2H, Ar*H*), 5.16 (tq, *J* = 6.5, 6.5 Hz, 1H, OC*H*CH$_3$), 4.33 (t, *J* = 6.5 Hz, 2H, COOC*H$_2$*), 4.00 (t, *J* = 6.5 Hz, 2H, OC*H$_2$*), 1.85 − 1.69 (m, 5H, OCH$_2$C*H$_2$,* and OCHC*H*H), 1.67 − 1.58 (m, 1H, OCHCH*H*), 1.51 − 1.23 (m, 27H), 0.88 (t, *J* = 7.0 Hz, 3H, CH$_2$C*H$_3$*).

^{13}C{^{1}H} NMR (101 MHz, CDCl$_3$) δ 169.4, 159.9, 145.4, 132.7, 131.7, 129.7, 128.5, 127.2, 119.3, 115.2, 91.6, 91.4, 72.3, 68.3, 36.2, 31.9, 29.7, 29.6, 29.5, 29.4, 29.4, 28.8, 26.2, 25.6, 22.7, 20.2, 17.7, 14.2.

APCI-MS: m/z = 726.42 [M+H]$^+$

Elemental analysis: calc'd (%) for C$_{48}$H$_{55}$NO$_5$: C 79.41, H 7.64, N 1.93; found: C 78.98, H 7.62, N 1.86.

143
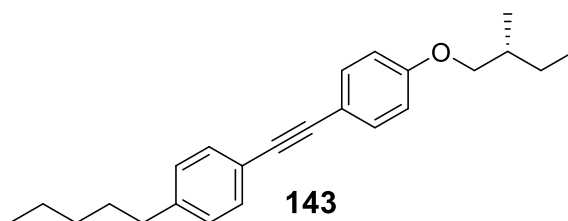
Compound **130** (0.15 g, 0.52 mmol) and 1-pentyl-4-ethynylbenzene (0.09 g, 0.52 mmol) were charged to a Schlenk tube under argon. Triethylamine (4 mL) was added and the mixture degassed with argon gas for 20 minutes. [PdCl$_2$(PPh$_3$)$_2$](0.03 g, 0.02 mmol) and CuI (0.02 g, 0.02 mmol) were added under flow of argon and the reaction mixture stirred at room temperature for 18 hours. The solvent was removed *in vacuo* and the crude product was purified by column chromatography (DCM:Petrol as eluent) followed by recrystallisation from hexane to give the target compound **143** as a crystalline white solid (0.09 g, 0.27 mmol, 69% yield).

^{1}H NMR (400 MHz, CDCl$_3$) δ 7.44 – 7.40 (m, 4H, Ar*H*), 7.15 (d, *J* = 8.0 Hz, 2H, Ar*H*), 6.87 (d, *J* = 8.0 Hz, 2H, Ar*H*), 3.83 (dd, *J* = 9.0, 6.0 Hz, 1H, OC*H*H), 3.74 (dd, *J* = 9.0, 6.5 Hz, 1H, OCH*H*), 2.60 (t, *J* = 7.5 Hz, 2H, ArC*H$_2$*), 1.93 – 1.80 (m, 1H, OCHHC*H*), 1.67 – 1.51 (m, 4H, ArCH$_2$C*H$_2$*, CHC*H$_2$*), 1.40 – 1.20 (m, 4H, C*H$_2$*C*H$_2$*), 1.02 (d, *J* = 6.5 Hz, 3H), 0.96 (t, *J* = 7.5 Hz, 3H), 0.88 (t, *J* = 7.0 Hz, 3H).

^{13}C{^{1}H} NMR (101 MHz, CDCl$_3$) δ 159.4, 143.2, 133.1, 131.5, 128.6, 120.9, 115.4, 114.6, 88.9, 88.2, 73.0, 36.0, 34.8, 31.6, 31.1, 26.3, 22.7, 16.7, 14.2, 11.5.

APCI-MS: m/z = 335.24 [M+H]$^+$

Elemental analysis: calc'd (%) for C$_{24}$H$_{30}$O: C 86.18, H 9.04; found: C 86.31, H 9.06.

144
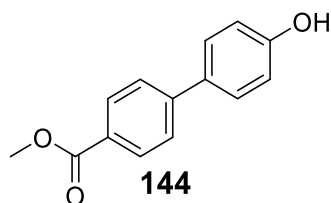
4-(4-Hydroxyphenyl) benzoic acid (0.98 g, 4.58 mmol) was dissolved in 10 mL MeOH and 12M HCl (0.03 mL) was added slowly. The mixture was heated to reflux for 18 hours then cooled to room temperature. The desired product crystallised from solution and was collected by vacuum filtration then the liquors were cooled in an ice bath and a second crop of crystals were collected to give the target compound **144** as a white crystalline solid (0.93 g, 4.07 mmol, 89% yield).

^{1}H NMR (400 MHz, CDCl$_3$) δ 7.95 (d, J = 8.0 Hz, ArH), 7.73 (d, 2H, J = 8.0 Hz, ArH), 7.60 (d, J = 8.5 Hz, ArH), 6.91 (d, J = 8.0 Hz, 2H, ArH), 3.85 (s, 3H, COOCH_3).

145
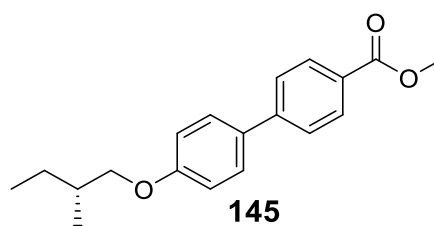
Methyl 4-(4-hydroxyphenyl) benzoate **144** (0.60 g, 2.63 mmol), (S)-2-methylbutanol (0.23 g, 2.61 mmol) and PPh$_3$ (0.80 g, 3.05 mmol) were charged to a flask under nitrogen. Dry THF (20 mL) was added and the mixture cooled in an ice bath then DIAD (0.60 mL, 0.62 g, 3.04 mmol) was slowly added. The mixture was warmed to room temperature and stirred for 18 hours. The solvent was removed *in vacuo* and the crude product was purified by column chromatography (DCM as eluent) to give the target compound **145** as a colourless oil (0.59 g, 1.98 mmol, 76% yield).

^{1}H NMR (400 MHz, CDCl$_3$) δ 8.12 (d, J = 8.5 Hz, 2H, ArH), 7.64 (d, J = 8.5 Hz, 2H, , ArH), 7.56 (d, J = 8.5 Hz, 2H, ArH), 6.99 (d, J = 8.5 Hz, 2H, ArH), 3.90-3.80 (m, 4H, OCHHCH and COOCH_3), 3.78 (dd, J = 9.0, 6.5 Hz, 1H, OCHHCH), 1.88 – 1.79 (m, 1H, CHCH$_3$), 1.63-1.56 (m, 1H, CHHCH$_3$), 1.30 – 1.20 (m, 1H, CHHCH$_3$), 1.01 (d, J = 6.5 Hz, 3H, CHCH$_3$), 0.93 (dd, J = 7.5, 7.0 Hz, 3H, CH$_2$CH$_3$).

146
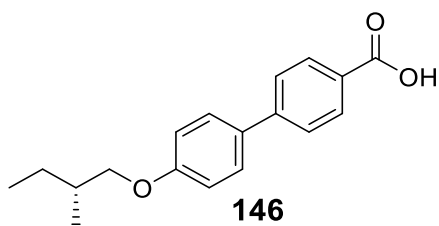
Compound **145** (0.59 g, 1.98 mmol) was dissolved in ethanol (10 mL) and 1M NaOH (3 mL) added. The mixture was heated to reflux for 3 hours then cooled to room temperature and acidified with 1M HCl. The mixture was extracted with ethyl acetate (3 x 10 mL) and the organic extracts were combined, washed with saturated brine solution (10 mL) and dried over magnesium sulfate. The solvent was removed *in vacuo* to give the target compound **146** as a tacky white solid (0.50 g, 1.76 mmol, 89% yield) which was used without further purification.

^{1}H NMR (400 MHz, CDCl$_3$) δ 8.12 (d, *J* = 8.5 Hz, 2H, Ar*H*), 7.65 (d, *J* = 8.5 Hz, 2H, Ar*H*), 7.56 (d, *J* = 8.0 Hz, 2H, Ar*H*), 6.99 (d, *J* = 8.5 Hz, 2H, Ar*H*), 3.85 (dd, *J* = 8.5, 6.5 Hz, 1H, OC*H*HCH), 3.77 (dd, *J* = 8.5, 6.5 Hz, 1H, OC*H*HCH), 1.92 – 1.83 (m, 1H, C*H*CH$_3$), 1.62 – 1.52 (m, 1H, C*H*HCH$_3$), 1.29 – 1.23 (m, 1H, C*H*HCH$_3$) 1.03 (d, *J* = 7.0 Hz, 3H, CHC*H*$_3$), 0.96 (t, *J* = 7.5 Hz, 3H, CH$_2$C*H*$_3$).

147
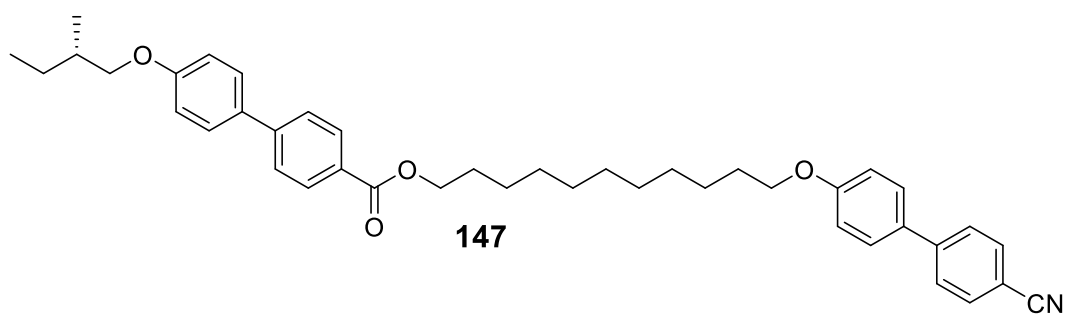
Compound **146** (0.20 g, 0.70 mmol), 4'-((11-hydroxyundecyl)oxy)-4-cyanobiphenyl (0.38 g, 1.04 mmol) EDC.HCl (0.32 g, 1.67 mmol) and DMAP (0.10 g, 0.82 mmol) were dissolved in DCM (30 mL) and the reaction mixture was stirred at room temperature for 18 hours. The solvent was removed *in vacuo* and the crude product was purified by column chromatography (DCM:EtOAc as eluent) followed by recrystallisation from hot ethanol to give the target compound **147** as a white crystalline solid (0.26 g, 0.41 mmol, 59% yield).

^{1}H NMR (400 MHz, CDCl$_3$) δ 8.06 (dd, *J* = 8.5, 2.5 Hz, 2H, Ar*H*), 7.69 (dd, *J* = 8.5, 2.5 Hz, 2H, Ar*H*), 7.66 – 7.59 (m, 4H, Ar*H*), 7.57 – 7.49 (m, 4H, Ar*H*), 6.98 (dd, *J* = 8.0, 2.5 Hz, 4H, Ar*H*), 4.33 (t, *J* = 6.5 Hz, 2H, COOC*H$_2$*), 4.00 (t, *J* = 6.5 Hz, 2H, OC*H$_2$*), 3.86 (dd, *J* = 9.0, 6.0 Hz, 1H, OC*H*H), 3.78 (dd, *J* = 9.0, 6.5 Hz, 1H, OCH*H*), 1.93 - 1.85 (m, 1H, C*H*CH$_3$), 1.84 – 1.73 (m, 4H, OCH$_2$C*H$_2$*), 1.50 – 1.23 (m, 16H), 1.03 (d, *J* = 7.0 Hz, 3H, CHC*H$_3$*), 0.96 (t, *J* = 7.0 Hz, 3H, CH$_2$C*H$_3$*).

^{13}C{^{1}H} NMR (101 MHz, CDCl$_3$) δ 166.8, 159.9, 145.4, 132.7, 132.3, 131.4, 130.2, 128.7, 128.5, 128.4, 127.2, 126.5, 119.3, 115.2, 115.1, 73.12, 68.3, 65.2, 34.9, 29.6, 29.5, 29.4, 29.4, 28.9, 26.3, 26.2, 16.7, 11.5.

APCI-MS: m/z = 632.37 [M+H]$^+$

Elemental analysis: calc'd (%) for C$_{42}$H$_{49}$NO$_4$: C 79.84, H 7.82, N 2.22; found: C 79.75, H 7.65, N 2.08.

6.7 References

1   H. A. Van Doren, E. Smits, J. M. Pestman, J. B. F. N. Engberts and R. M. Kellogg, *Chem. Soc. Rev*., 2000, 29, 183–199.

2   R. Eelkema and B. L. Feringa*, Org. Biomol. Chem*., 2006, 4, 3729–3745.

3   A. Taugerbeck and C. J. Booth, in Handbook of Liquid Crystals, eds. J. W. Goodby, P. J. Collings, T. Kato, C. Tschierske, H. F. Gleeson, P. Raynes, Wiley-VCH Verlag GmbH & Co. KGaA, 2nd., 2014, Vol 8, Ch 14, pp 1.

4   D. G. McDonnell and G. W. Gray, *Mol. Cryst. Liq. Cryst*., 1977, 34, 211.

5   U. B. Vasconcelos, A. Schrader, G. D. Vilela, C.A. Borges and A. A. Merlo, *Tetrahedon*, 2008, 64, 4619.

6   C. Pugh and V. Percec, *Chem. Mater*., 1991, 3, 107–115.

7   L. Dong, Z. Xu, H. Tao, X. Chen, J. Hu, D. Yao and M. Tian, *Liq. Cryst*., 2018, 45, 1734–1745.

8   D. S. S. Rao, S. K. Prasad, V. N. Raja, C. V. Yelamaggad and S. A. Nagamani, *Phys. Rev. Lett*., 2001, 87, 085504.

9   A. E. Blatch, I. D. Fletcher and G. R. Luckhurst, *J. Mater. Chem*., 1997, 7, 9–17.

10   Y. Kogawa and A. Yoshizawa, *Liq. Cryst.*, 2011, 38, 303–307.

11   A. J. Seed, M. E. Walsh, J. W. Doane and A. Khan*, Mol. Cryst. Liq. Cryst*., 2004, 410, 201.

12   Q. Li, L. Green, N. Venkataraman, I. Shiyanovskaya, A. Khan, A. Urbas and J. W. Doane, *J. Am. Chem. Soc*., 2007, 129, 12908–12909.

13   I. Smalyukh and O. D. Lavrentovich*, Phys. Rev. E*, 2002, 66, 16.

14   M. Salamończyk, N. Vaupotič, D. Pociecha, C. Wang, C. Zhu and E. Gorecka, *Soft Matter*, 2017, 13, 6694–6699.

15   H. M. and S. T. K. Seto, H. Shimojitosho, H. Imazaki*, Bull. Chem. Soc. Jpn*., 1990, 63, 1020.

16   J. Malthête, M. Leclercq, M. Dvolaitzky, J. Gabard, J. Billard, V. Pontikis and J. Jacques, *Mol. Cryst. Liq. Cryst*., 1973, 23, 233–260.

17   EU. Pat., 0217354B1, 1986

18   B. Pansu, E. Grelet, M. H. Li and H. T. Nguyen, *Phys. Rev. E.*, 2000, 62, 658–665.

19   B. Pansu, M. H. Li and H. T. Nguyen*, J. Phys. I.,* 1997, 7, 751–763.

20   C. Da Cruz, J. C. Rouillon, J. P. Marcerou, N. Isaert and H. T. Nguyen, *Liq. Cryst*., 2001, 28, 125–137.

21   J. W. Goodby*, Curr. Opin. Colloid Interface Sci*., 2002, 7, 326–332.

22   Y. Kim and N. Tamaoki, *ACS Appl. Mater. Interfaces*, 2016, 8, 4918–4926.

Chapter 7. Cyclotrimerisation

7.1 Introduction to cyclotrimerisations

The use of molecular complexity as a tool to control the mesophase structure is vital in the study of supermolecular liquid crystals. Molecular complexity can be achieved by making judicious step-wise changes in the molecular structure in order to achieve the desired mesophase structure. This approach to molecular engineering can be slow if a number of structures are to be screened. Another route to increased molecular complexity consists of the manipulation of a certain functional group already present in a family of liquid crystal materials. Furthermore, by choosing the correct functionality such manipulation can be attained in a single reaction making this approach particularly attractive in order to explore different materials and mesophase structures.

In addition to the structural features of the diphenylacetylene core justifying its use as the dendritic core in the materials described in earlier chapters, one further advantage of utilising this structural element is the ease of further functionalisation of these materials via transition metal-catalysed cyclotrimerisation reactions. The transition metal-catalysed cyclotrimerisation of alkynes is an elegant and well-established transformation of the C≡C triple bond in a *single* synthetic step to afford a benzene ring. This transition metal-catalysed reaction enables the formation of aryl rings from three alkynyl units, such as those found at the core of the diphenyl acetylene. This enables a rapid increase in molecular complexity and an interesting disc-like core to enable alternative mesophase structures to form.

This chapter describes the cobalt-catalysed cyclotrimerisation of some of the materials described in Chapters 4 and 6, to afford the relevant cyclotrimerised products in one single reaction. In addition, as a proof of principle, it describes the cyclotrimerisation of two different diphenylacetylene precursors to obtain novel hexaphenylbenzene materials with defined substitution patterns depending on the choice of acetylene precursors and their relative ratio used in the cyclotrimerisation.

This approach avoids the need for challenging multistep organic synthesis and provides monodisperse materials with molecular weight three times that of the starting diphenylacetylene precursors. One added advantage of this methodology is that it avoids the serious deleterious effect of partial substitution encountered when

319

using dendritic materials due to steric congestion around the reactants focal point and/or dendritic surface.

In the case of symmetrical diphenylacetylene precursors, the isolated cyclotrimerisation products are not only monodisperse but also monomolecular species. This required careful column chromatography from a mixture of reaction products, or the reaction stoichiometry to be varied to limit the number of products obtained from the reaction. For example, an a chiral diphenyl acetylene may undergo a cyclotrimerisation reaction in the presence of an excess of an achiral diphenyl acetylene to provide a chiral hexaphenyl benzene material in one synthetic step. In the case of an unsymmetrically substituted diphenylacetylene precursor being used, the two resulting hexaphenylbenzenes isomers cannot be separated and the resulting mixture is analysed as such.

7.2 Methodology

A wide range of both acetylenes and transition metal catalysts have previously been investigated. This classical organometallic reaction has been repeatedly surveyed since its discovery.[1] A recent comprehensive review by Malacria details much of the work.[2] Select examples will be discussed in detail including the cyclotrimerisation of relevant alkynes, routes to desirable substitution patterns and cyclotrimerisation of mixtures of alkynes.

Thus, some of the novel diphenyl acetylene materials discussed in previous chapters were used in a range of trimerisation and cotrimerisation reactions. These can be grouped into two general categories: 1) trimerisation reactions of single diphenylacetylene precursors, and 2) trimerisation reactions of a mixture of diphenylacetylene precursors. Notably the symmetry of the reaction products obtained from both categories was the main factor controlling the physical properties. In the case of high symmetry hexaphenyl benzenes high melting solids were obtained, however lower symmetry or mixed products tended to provide oils or glasses.

7.2.1 Single diphenylacetylene precursors

The cyclotrimerisation of symmetrically substituted diphenylacetylenes affords the relevant hexaphenylbenzenes, where the six peripheral phenyl rings are uniformly substituted (Scheme 31a), whereas the cyclotrimerisation of unsymmetrically substituted diphenylacetylenes affords a mixture of the 1,2,4- and 1,3,5-substituted

hexaphenylbenzene derivative (Scheme 31b). The cyclotrimerisation of phenylacetylenes yields the relevant triphenylbenzene derivatives with a 1,3,5-substitution pattern (Scheme 31c).
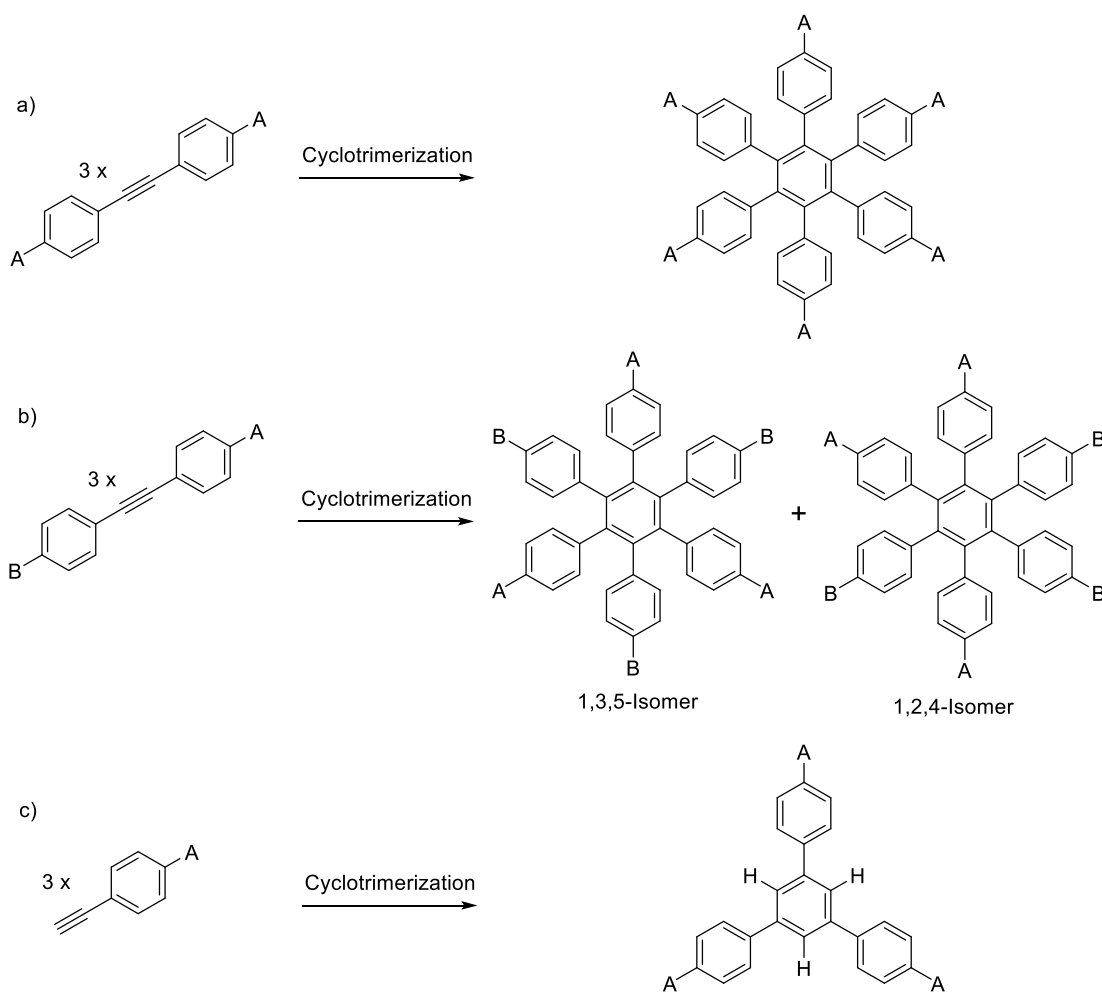
Scheme 31. Reaction products of cyclotrimerisations varies depending upon the substitution pattern of the reactant either a) symmetrical, b) unsymmetrical or c) phenyl acetylenes.

The widely proposed mechanism for low oxidation state cobalt carbonyl catalysed cyclotrimerisation of alkynes involves the sequential loss of two ligands from the metal catalyst which are each replaced by η^2 alkynes to give **151** which rearranges and coordinates a third alkyne to give complex **153**. Following coordination of the third alkyne, three routes are proposed, and the key intermediates are shown below (Scheme 32). Firstly, the upper route shows insertion of the alkyne into a metal-carbon bond to give a metallacycloheptadiene complex **154**. The middle and bottom routes both follow [4+2] additions. While the middle route is a direct addition with no

intermediate, the bottom proceeds through the 7-metallanorbornadiene intermediate **155**.
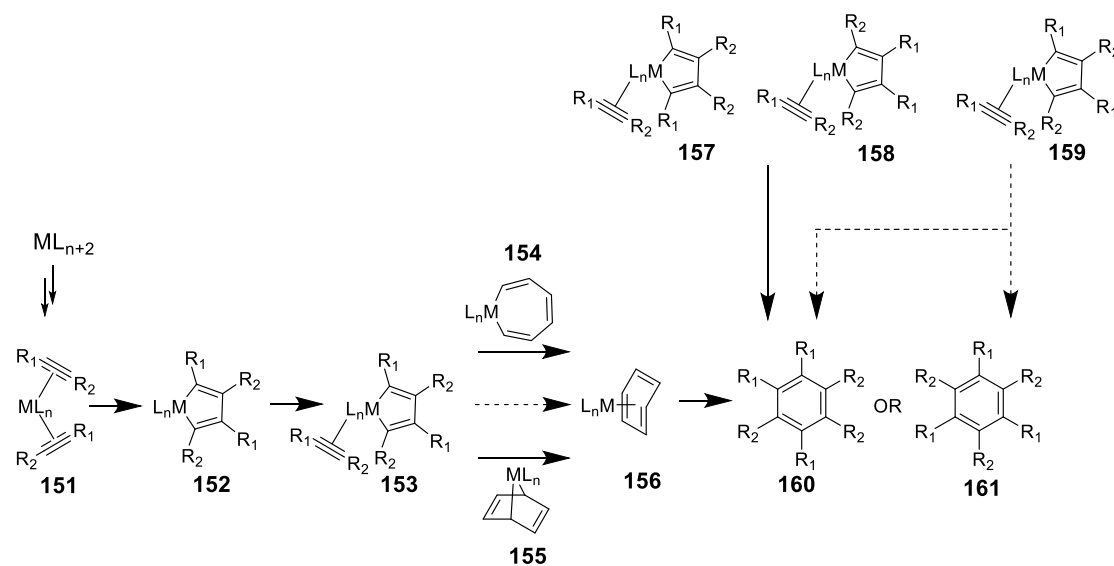
Scheme 32. The metallacyclopentadiene route for cyclotrimerisation of alkynes.

The regioselectivity of the reaction depends both on the formation of the metallacyclopentadiene and addition of the third alkyne. The two possible metallacyclopentadienes with adjacent identical groups **157** and **158** can give only the 1,2,4 substitution pattern **160**, meanwhile the complex **159** with alternating substitution patterns may give either the 1,2,4 or 1,3,5 substitution pattern (**160** and **161** respectively) depending on the orientation of the third alkyne.

The final possible substitution pattern bearing identical substituents in the 1,2,3 positions has been reported by Maitlis *et al. via* bis(benzonitrile) palladium (II) chloride-catalysed cyclotrimerisation of methylphenylacetylene.[3] This was obtained in 3% yield following fractional crystallisations to separate the major 1,2,4-and 1,3,5-substituted isomers.

7.2.2 Mixed diphenylacetylene precursors

A different strategy to generate *Janus* materials is the use of two different alkynes in the cyclotrimerisation reaction. Although in principle the cotrimerisation of diphenyl acetylenes can yield a complex mixture of the homo- and co-trimerised hexaphenylbenzenes, Nierengarten[4] and co-workers have shown that by choosing alkynes of similar reactivity (**162** and **163**) and in the appropriate ratio, the desired co-trimerised hexaphenylbenzene **164** is the main product of the reaction (Scheme 33).

This was reported to require similar levels of reactivity between the two diphenyl acetylene reactants to avoid homotrimerisations.
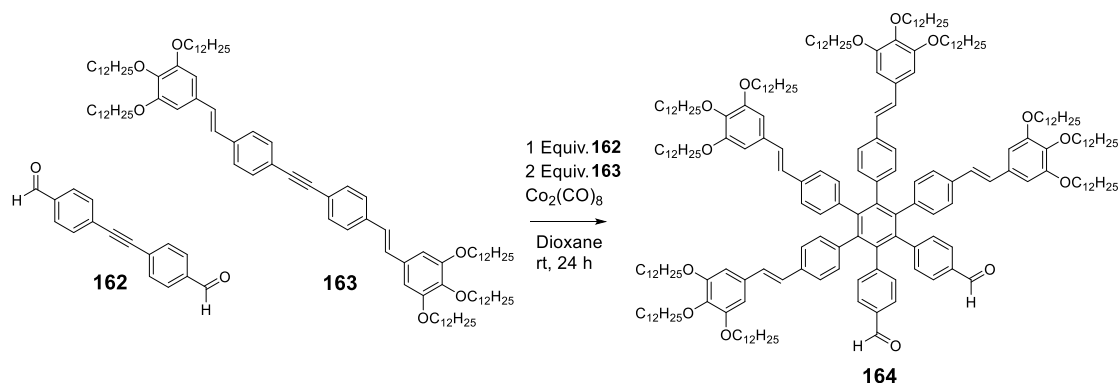
Scheme 33. Cotrimerisation of two diphenyl acetylenes can be used to provide Janus materials provided the two materials have similar reactivities.

More recently Jux *et al*. have reported hexaphenyl benzene:porphyrin conjugates **167 – 170** which were synthesised from a mixed cyclotrimerisation reaction (Scheme 34).[5] A range of products with different ratios of porphyrin and tert-butyl units were isolated from the reaction mixture and the reaction stoichiometry was used to control the statistical mixture provided.
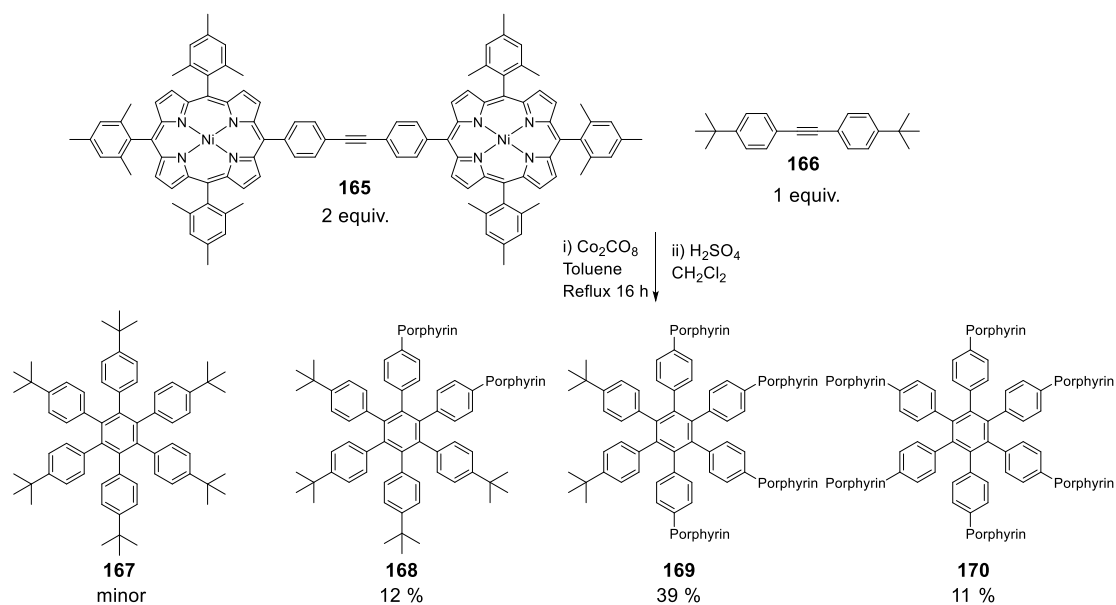
Scheme 34. Mixed cyclotrimerisation using stoichiometry to control the statistical outcome of the reaction.

This strategy provides hexaphenyl benzenes with specific substitution patterns which can be isolated provided that appropriate control of the relative ration of the precursors is used and their reactivity is matched.

Cotrimerisation reactions of diphenyl acetylenes A and B with equal stoichiometry therefore produce a statistical 1:3:3:1 ratio of products featuring either 3, 2, 1 or 0 molecules of reactant A as shown below (Scheme 35). Depending on the nature of the substituents A and B the different compounds may be separable by column chromatography as shown by the examples above.
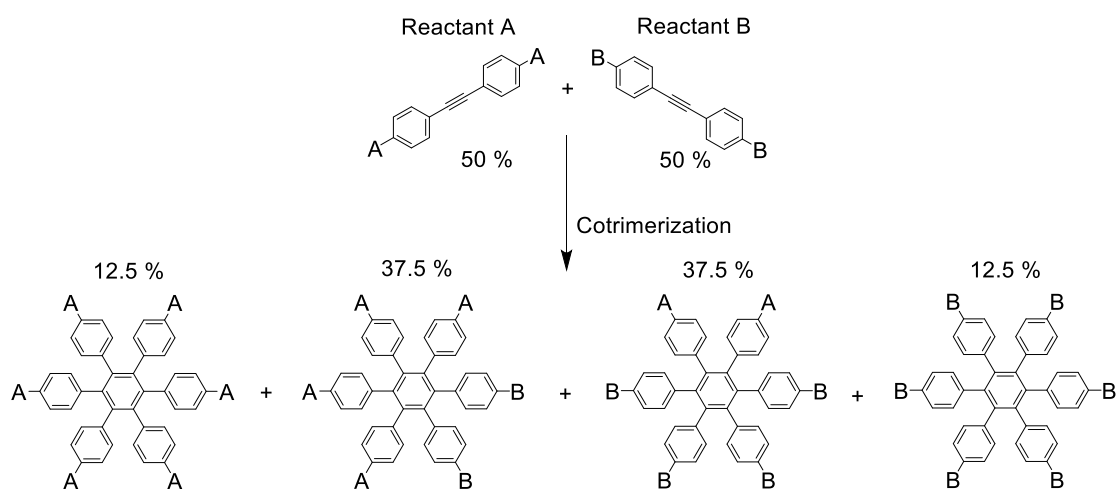
Scheme 35. Expected products and regiochemistry of a cotrimerisation of reactant A and B in equal stoichiometry.

One area of investigation was whether the ratio of these products can be skewed such as in the examples above, by controlling the starting stoichiometry of reactants A and B to favour or disfavour one side of the products. As established previously, unsymmetrical materials cyclotrimerise to form isomeric mixtures due to the different regiochemistry of the substituents A and B as shown in Scheme 31 above. Therefore, cotrimerisation of these unsymmetrical materials is less useful as a complex mixture of isomers above will be given. However, by utilising stoichiometric control to input a smaller ratio of reactant A into an excess of reactant B, some of the possible trimerisation products may be suppressed (Scheme 36). The likelihood of two molecules of reactant A colliding to react are diminished and so the two products to the left are very minor, while both products shown to the right are formed the majority is the symmetrical hexaphenyl benzene compound however depending upon the nature of the polarity of A and B the mixture may be separable. As there is only a single

molecule of reactant A incorporated into the structure and reactant B is symmetrical the relative orientation of the substituents A_1 and A_2 is of no consequence due to the symmetry of the molecule.
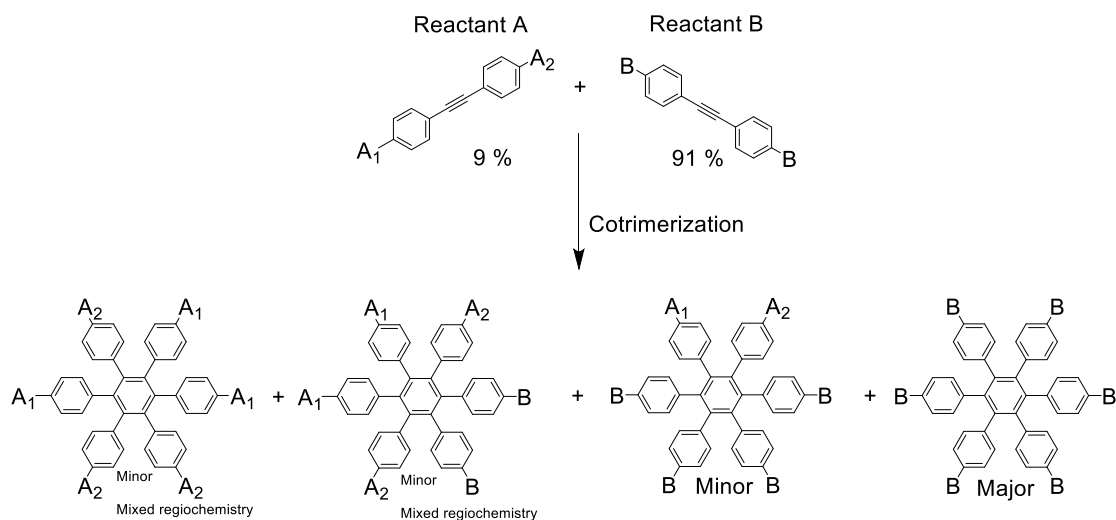
Scheme 36. Expected products from the cotrimerisation of a mixture of A and B with different stoichiometry.

7.3. Synthesis

As detailed in the review by Malacria[2] many cobalt complexes show catalytic behaviour for the trimerisation reaction. Dicobalt (0) octacarbonyl was used as the catalyst with variable loading between 5 and 55 mol%, in dry, distilled and thoroughly degassed 1,4-dioxane, heating to reflux for 18 h under Ar. The reaction crude was subjected to careful column chromatography in order to eliminate traces of metallic species and to separate the products. The relevant hexaphenylbenzene obtained has lower Rf than the starting diphenyl acetylene, thus facilitating its purification by column chromatography. When traces of coloured metallic impurities were present, a further separation by column chromatography was carried out. The relevant product was recrystallised when possible and submitted to analysis. In the proof of principle co-cyclotrimerisation reactions, the identity of the products was confirmed by ^{1}H NMR spectra and their molecular mass was ascertained by MALDI-MS to show that the two different precursors had been incorporated into a single molecule rather than being a physical mixture of the homo-trimerised materials.

7.3.1 Trimerisation of single acetylene precursors.

The exact reaction conditions were optimised by performing the cyclotrimerisation of alkynes **33$_i$**, **73** and **88**, described in Chapters 3 and 4. Thus, reaction of **33$_i$** with

$Co_2(CO)_8$ as described above yields **171** in 90% yield (Scheme 37), whereas cyclotrimerisation of **73** yields hexadodecyl-hexaphenyl benzene **172** in 70% yield (Scheme 38). Characterisation data of **172** agree with those reported by Müllen.[6]
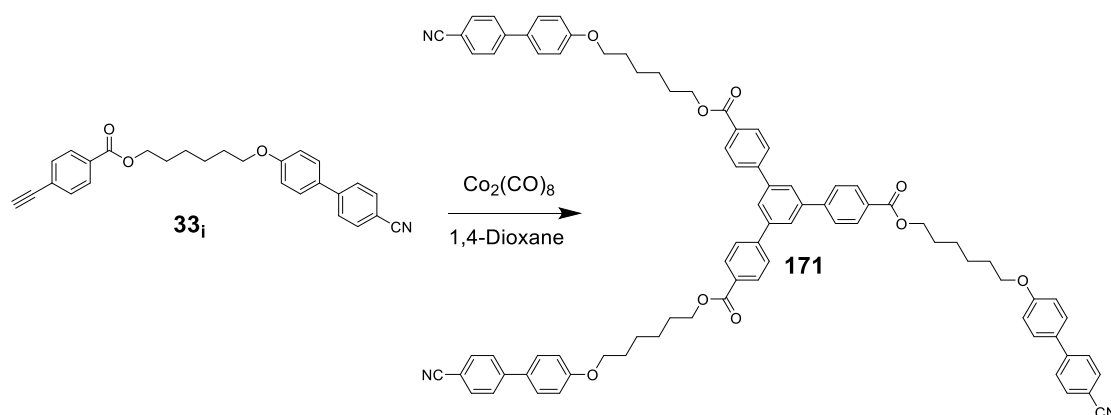
Scheme 37. Cobalt catalysed trimerisation of terminal alkynes proceeds well giving a 1,3,5-trisubstituted benzene.
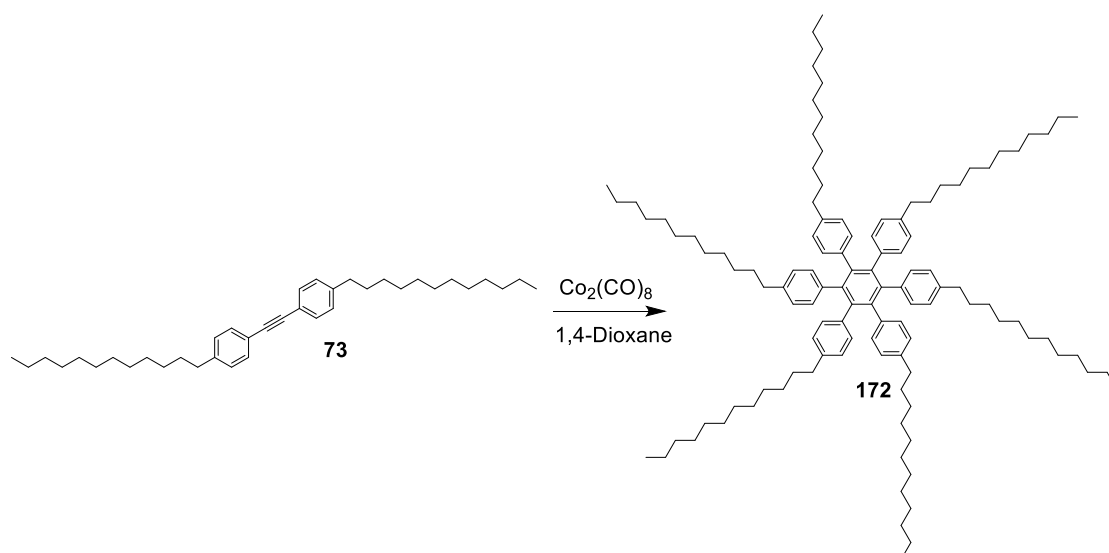
*Scheme 38. Homotrimerisation of alkyl diphenyl acetylene **73** proceeded in good yield as reported by Müllen.*

Similarly, cyclotrimerisation of **88** affords hexa(cyanobiphenyl)-hexaphenylbenzene **173** in 60% yield, whose characterisation data agree with those reported previously (Scheme 39).[7]

Due to the higher polarity of the cyanobiphenyl units a more polar solvent system was required for reaction monitoring and column chromatography. The hexaphenyl benzene product again had a lower Rf that the reactants allowing simple separation. However, some colouration was observed in the sample and therefore a second

purification step via column chromatography was required, following this desired product was obtained as a white solid in 60% yield.
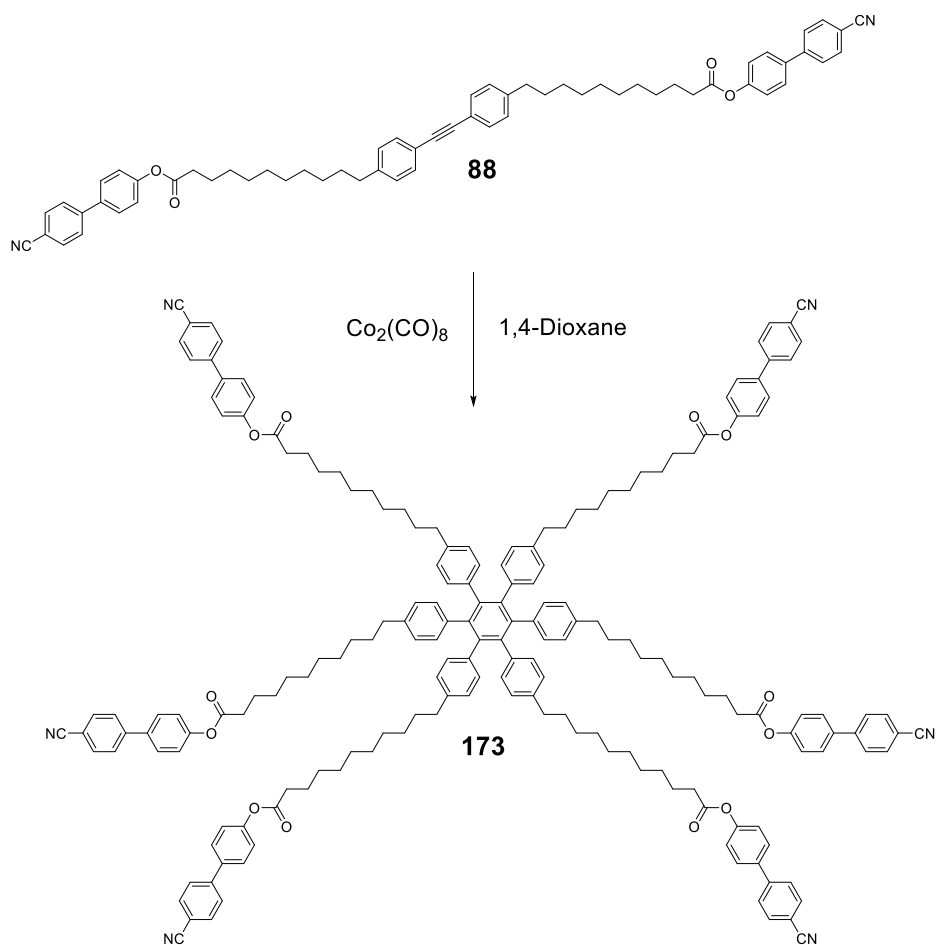
*Scheme 39. The cyclotrimerisation of cyanobiphenyl substituted hexaphenyl benzene **88** was repeated using the same methodology.*

Following the same procedure, homotrimerisation of the chiral diphenyl acetylene **81** affords the novel chiral hexaphenylbenzene **174** in 62% yield isolated as a white powder following purification by column chromatography (Scheme 40). The reaction progress could be followed by TLC and reaction completion was clear by ^{1}H NMR spectra and MALDI-MS.
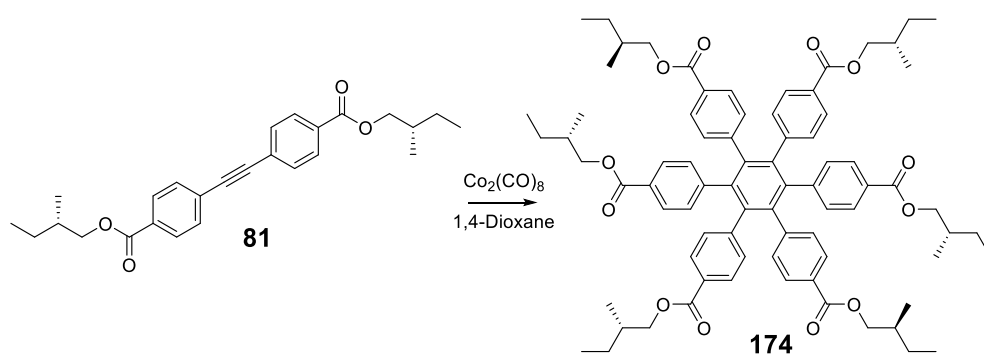
*Scheme 40. Homotrimerisation of chiral symmetrical diphenyl acetylene **81** to provide the symmetrical chiral hexaphenyl benzene **174**.*

The second group of reactions involved homotrimerisation of asymmetrical materials with similar reaction conditions being used as above. In this case a mixture of regioisomers result as shown in Scheme 31. The behaviour of chiral hexaphenyl benzenes were of particular interest due to their potential liquid crystalline behavior therefore several of the materials reported in chapter 6 were cyclotrimerised.

Thus, cyclotrimerisation reactions of **131** and **135** both afford mixtures of 1,2,4- and 1,3,5- substituted regioisomers **175** and **176** respectively (Scheme 41, Scheme 42). The mixture of products obtained from the cyclotrimerisation of asymmetrical materials appeared as a single spot via TLC during reaction monitoring. Due to the similar polarity of the two regioisomers produced they could not be separated via column chromatography and so the products are analysed as a mixture. Reaction monitoring showed that the starting material was consumed during the reaction, and the mass balance following column chromatography gave between 84 – 89% yield. However, the initial product obtained from column chromatography showed colouration indicating the presence of traces of cobalt-containing impurities[8] and so this purification step was repeated depleting the yield. Nonetheless this mixture could be recovered in an acceptable yield of 60 – 67%.
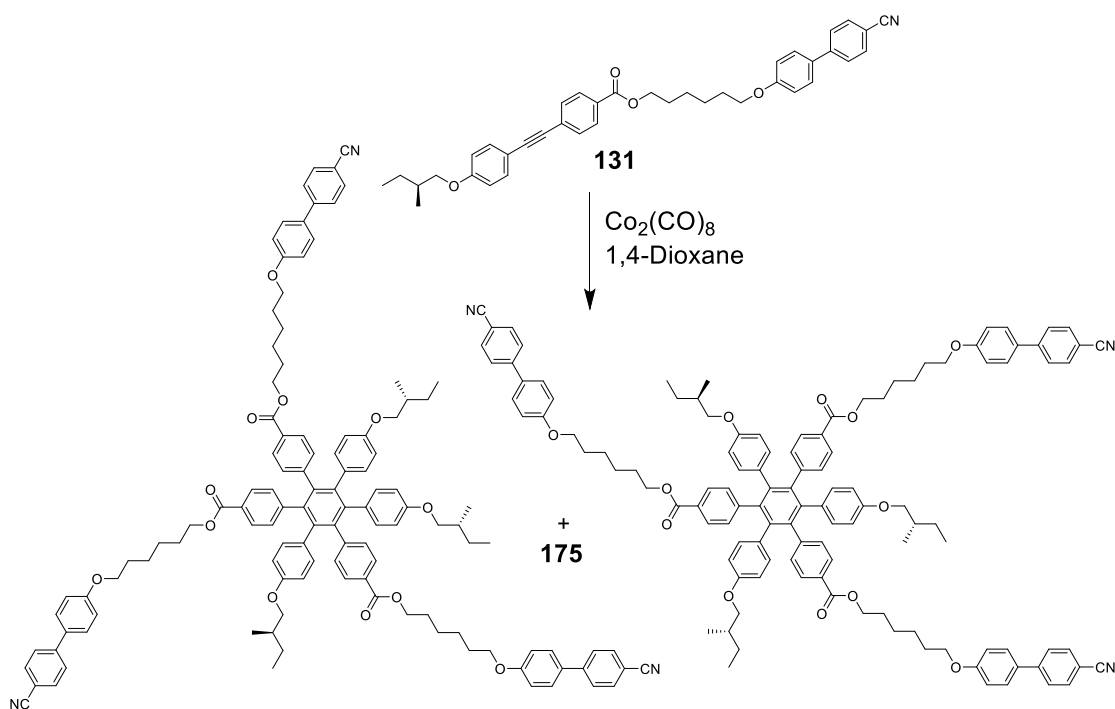
*Scheme 41. Homotrimerisation of chiral asymmetrical diphenyl acetylene **131** provides an inseparable mixture of two compounds **175**.*
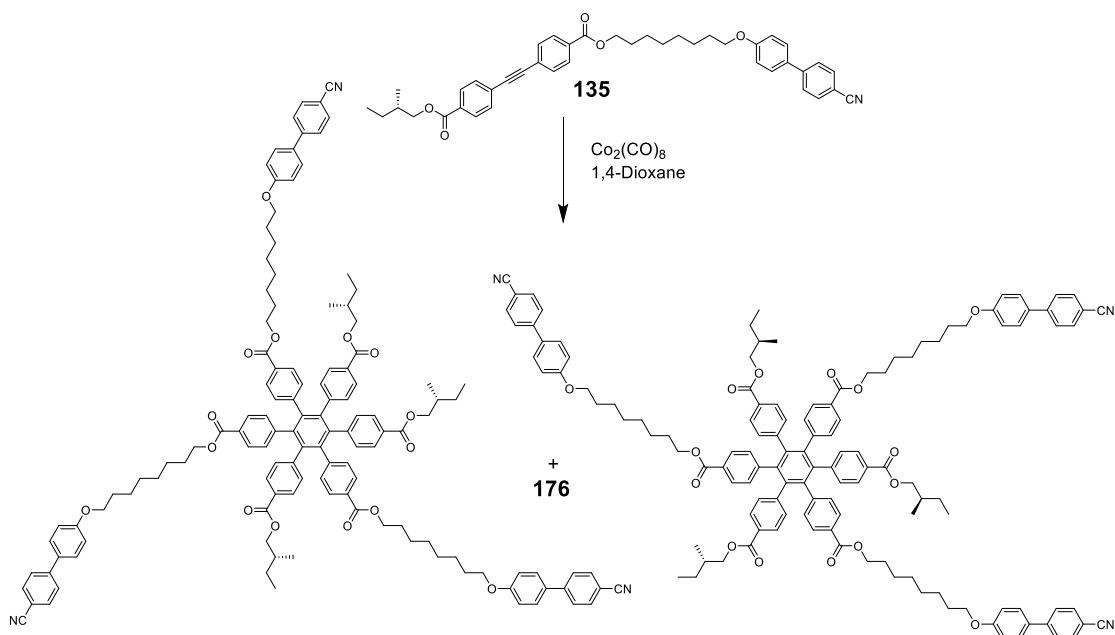
*Scheme 42. Homotrimerisation of chiral asymmetrical diphenyl acetylene **135** provides an inseparable mixture of two compounds **176**.*

For example, the ^{1}H NMR spectrum of the cyclotrimerisation product **175** shows a considerable shift of the resonances of the aromatic protons with respect to those observed for the parent diphenyl acetylene **131** (Figure 157), showing the absence of the starting material (Blue, bottom). There is a large change in the chemical shifts of

the aromatic diphenyl acetylene protons (Blue, top) and a smaller change in the chemical shifts of some of the aliphatic protons (Red) such as the diastereomeric protons of the (S)-2-methyl butyl unit and protons alpha to the ester linkage of the cyanobiphenyl spacer close to the core. Notably the ether linkage of the cyanobiphenyl spacer is unchanged due to its distance from the trimerised core.
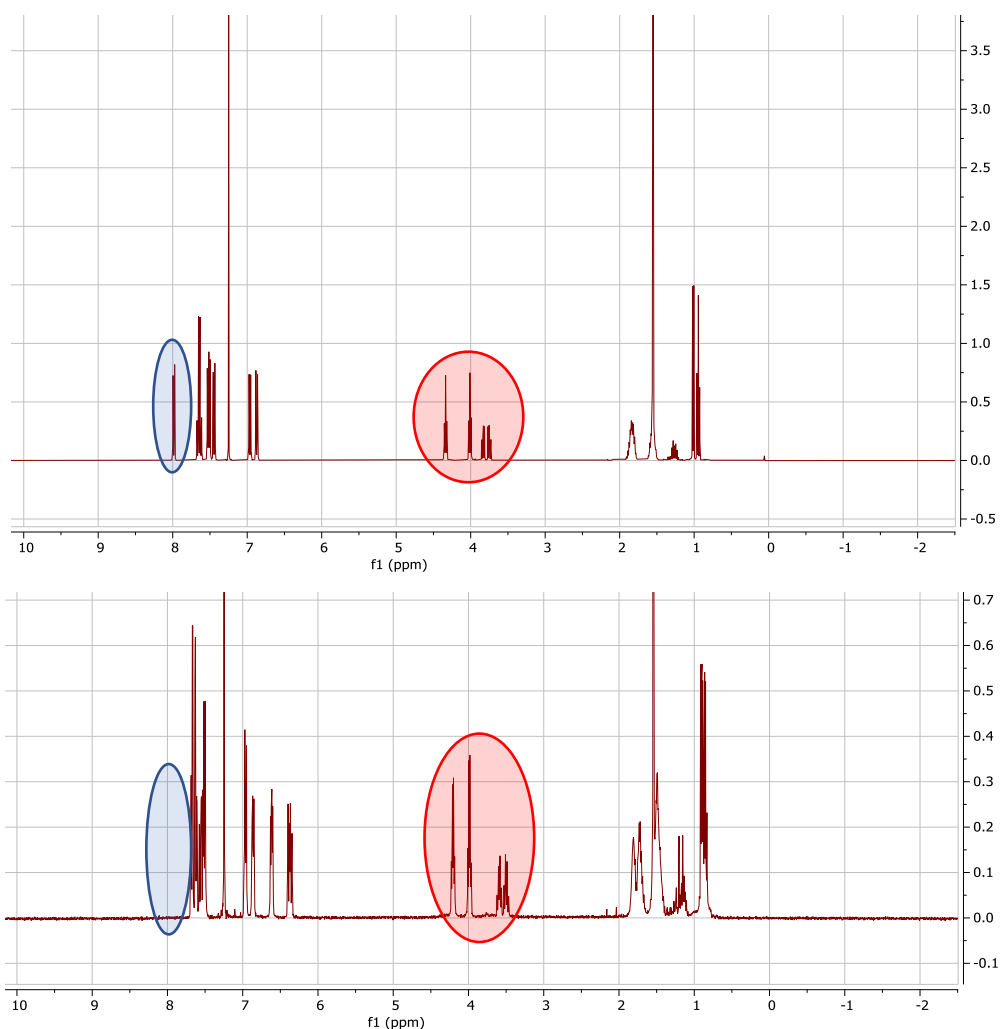
Figure 157. ^{1}H NMR spectrum of the chiral diphenyl acetylene 131 (top) and cyclotrimerisation product 175 a mixture of hexaphenyl benzene isomers (bottom). Assignments and integrals are given in the experimental, the blue area highlights the shift in resonance of aromatic protons, the red area shows a small shift in aliphatic protons close to the core.

Due to the similarity of chemical environments in both regioisomers of the product and the complexity of the spectrum, the ^{1}H NMR spectrum did not show different resonances for the two products in the mixture obtained from the reaction, rendering impossible to ascertain their relative ratio in the mixture. $^{13}C\{^1H\}$ NMR spectra showed low intensity resonances as expected for the quaternary carbons, which could have

otherwise given more information as to the nature of the mixture. MALDI-TOF-MS proved to be crucial in ascertaining the identity of the cyclotrimerised product, with three times the molecular weight of that of the parent. The ratio of isotopes in the molecular envelope matched that of the theoretical distribution, accompanied by the absence of the parent diphenyl acetylene. However, in some cases the diphenyl acetylene starting materials had a molecular weight below 1000 mass units, and therefore their signals were lost within the peaks relating to the fragmentation of the MALDI matrix.

With the aim of establishing the effect on the regioselectivity of the reaction depending on the relative orientation of the reactants during the reaction sequence, a pair of experiments were performed in parallel attempting the cyclotrimerisation reaction of **177** in its smectic A phase (a) and in solution (b) as comparison (Scheme 43). The aim of these experiments was to establish if the order within the mesophase could be translated to the reaction intermediates and therefore a change in the ratio of isomers would be detected. To investigate the reaction in the smectic A phase – reaction (a) – the cobalt catalyst was added to the neat reactant the mixture heated to 115 °C.

177

Cr 97 CrE 98 SmA 132 N 135 Iso °C

a) Co₂(CO)₈
neat, 115 °C

b) Co₂(CO)₈
1,4-Dioxane, 115 °C

+

178
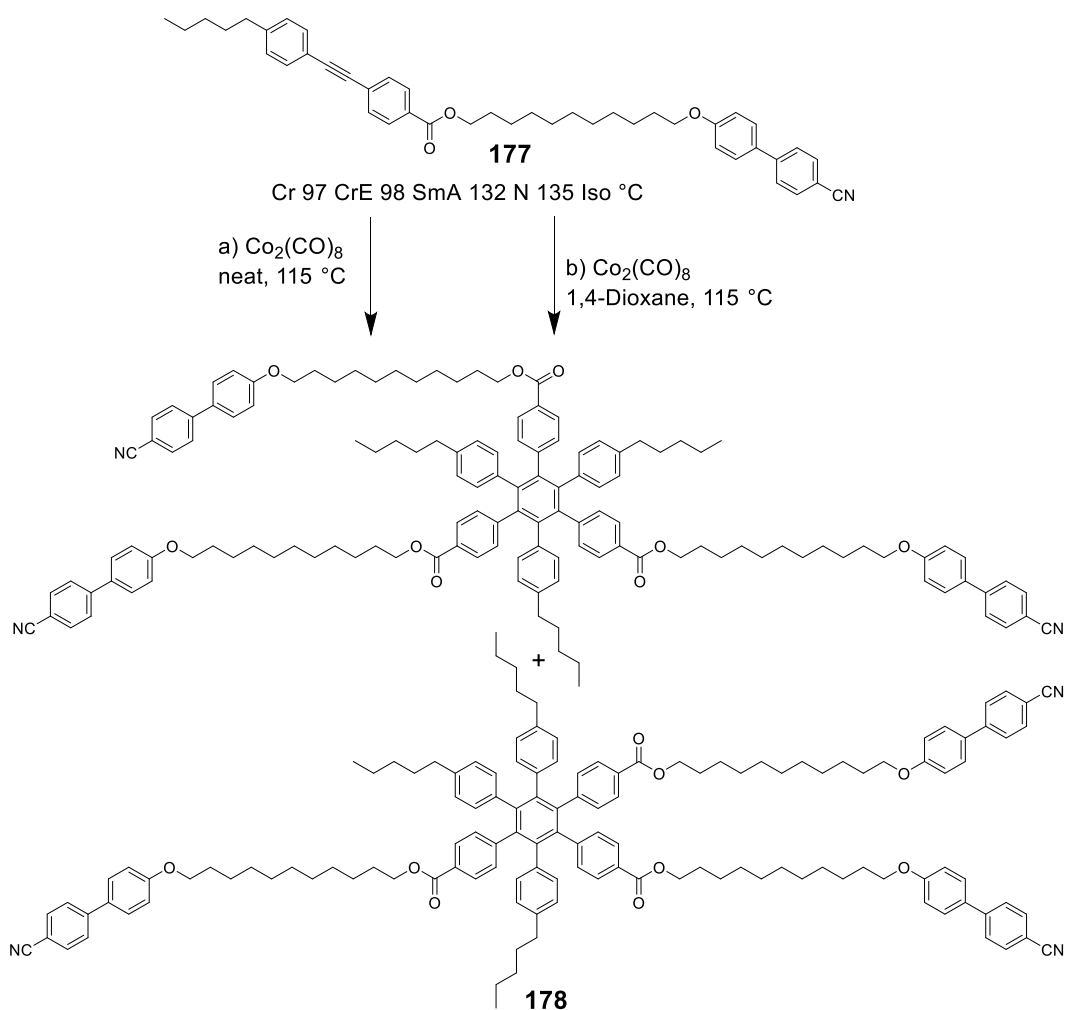
Scheme 43. Two reactions, a) and b) were performed in parallel to investigate whether the trimerisation reaction could be altered by the organisation of the smectic A mesophase of the reactant.

The impact of the cobalt catalyst on the phase stability was not investigated due to the toxicity of transition metal carbonyl complexes and so a temperature comfortably below the smectic A – nematic transition was chosen. In parallel the reaction was performed in solution using 1,4-dioxane – reaction (b). Aliquots of the crude reaction mixtures were analysed by HPLC *via* the university chromatography service and no significant differences in the chromatography traces were observed. This indicates that the structural organisation of the smectic A phase does not affect the reaction coordinate or distribution of products within mixture **178**. These samples were purified by column chromatography providing a mixture of isomers in each case.

7.3.2 Cotrimerisation of acetylene precursors

The cotrimerisation of two symmetrical diphenyl acetylenes, **76** and **88**, was investigated to allow for a rapid increase in complexity to provide a *Janus* like structure (Scheme 44). These mixed reactions would be expected to form a mixture containing two homotrimerisation products and the two mixed-trimerised products as shown in Scheme 35 and as such the key challenge in this type of reactions is separation of the individual compounds from the crude reaction mixture. As discussed before, the requirement for a successful cotrimerisation is that both diphenylacetylenes should have similar reactivity. Thus, **76** and **88** in a 1:1 ratio were co-trimerised to yield a mixture of **173** and compounds **179 – 181** (Scheme 44). **76** and **88** were chosen for cotrimerisation since they both present alkylene chains as the substituents on the phenyl group of the diphenyl acetylene moiety. Furthermore, to enable the desired separation by column chromatography a significant difference in the polarity of the hexaphenyl benzene products was required. In this case polar nitrile and apolar alkyl groups were used and therefore the hexaphenyl benzene products could be separated based upon the ratio of polar to apolar units and therefore both products could be obtained from two intermediates in a single synthetic step. The two homotrimers (**173**, **179**) were present in the crude reaction mixture but not isolated as these materials could easily be synthesised separately (See 7.3.1). The expected ratio between products **173**, **179**, **180** and **181** is 1:3:3:1, and therefore the theoretical yield of the two *Janus* materials **180** and **181** isolated from the mixture is 37.5%. In practice, **180** and **181** were each recovered in 25% yield. In both cases the ratio of methyl protons to aromatic cyanobiphenyl protons was in good agreement with the structural assignment. The MALDI-MS is shown to prove that the compounds were successfully isolated from the mixture of products without contamination (Figure 158 and 159).
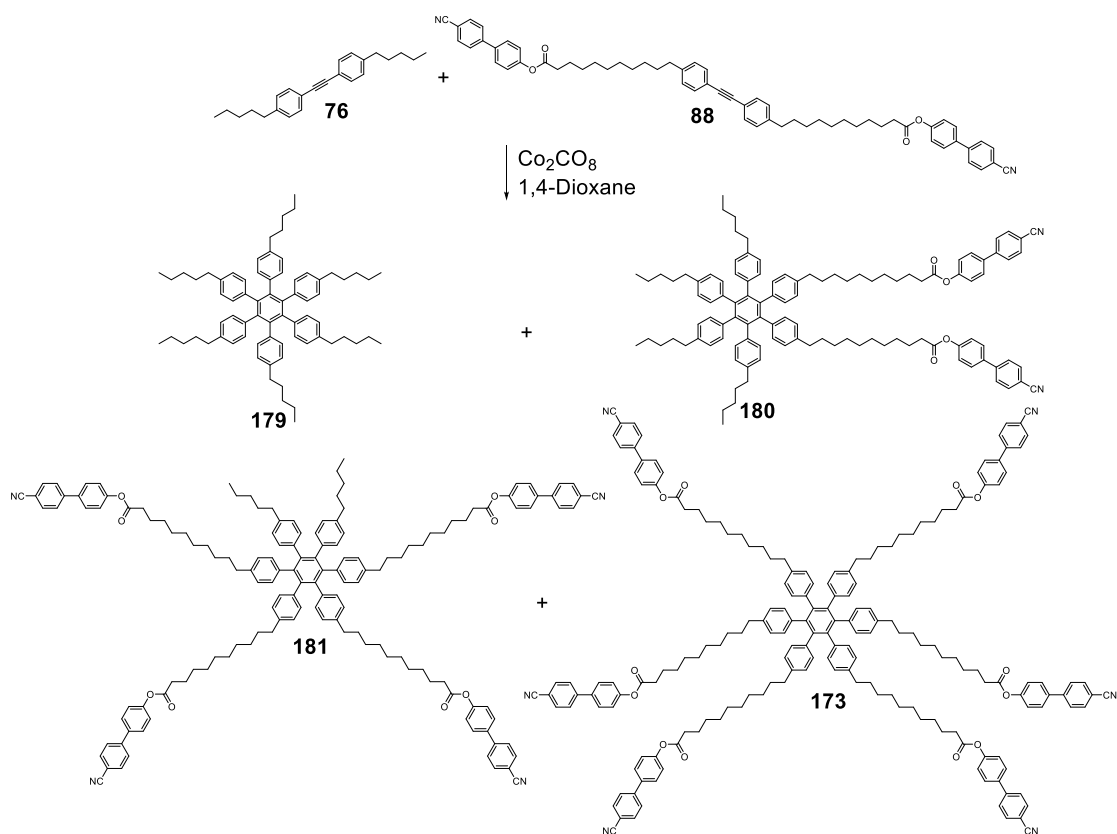
*Scheme 44. Cotrimerisation of two symmetrical diphenyl acetylenes **76** and **88** to afford a separable mixture of hexaphenyl benzenes comprising of **173** and **179** - **181**.*

Meas. m/z	#	Ion Formula	m/z	err [ppm]	err [mDa]	mSigma	Mean err [ppm]
1536.955743	1	C110H124N2O4	1536.955562	-0.1	-0.2	30.5	-0.9
1559.945650	1	C110H124N2NaO4	1559.945331	-0.2	-0.3	13.7	-0.6
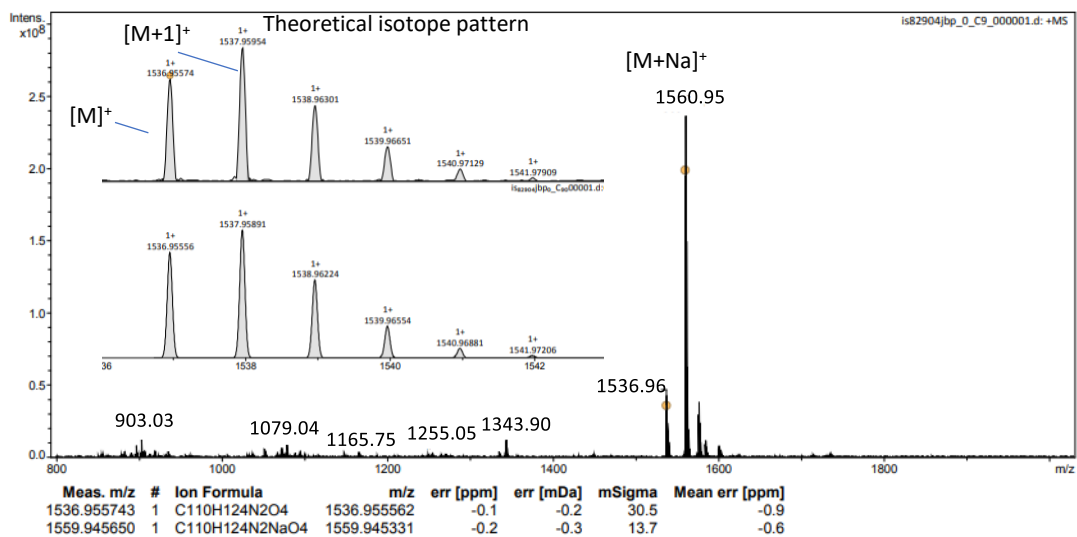
*Figure 158. MALDI-TOF/MS of compound **180**: expected 1527.0, Mass observed 1561.0 [M+Na]+*
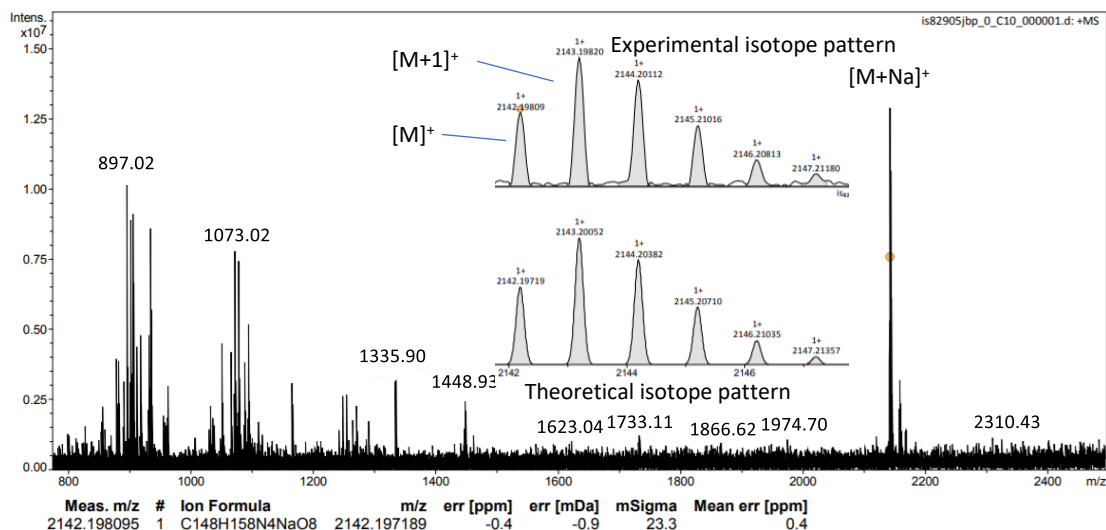
*Figure 159. MALDI-TOF/MS of compound **181**: Mass expected 2119.2, Mass observed 2143.2 [M+Na]⁺.*

In order to further the investigation into the impact of chirality on the hexaphenyl benzene materials a cotrimerisation reaction between the symmetrical chiral diphenyl acetylene **81** and symmetrical cyanobiphenyl substituted diphenyl acetylene **78** was performed. To match the C≡C triple bond reactivity, the ester linked chiral diphenyl acetylene **81** was paired with ester linked cyanobiphenyl diphenyl acetylene **78** in this case. Regardless of the orientation or order in which the reaction intermediates form the products with the same ratio of substituents are equivalent. Thus, a mixture of cyanobiphenyl diphenyl acetylene **78** and chiral diphenyl acetylene **81** in a 1:1 ratio were co-trimerised (Scheme 45). In this case, although four products **174** and **182** – **184** are present in the crude reaction mixture, only the product with four cyanobiphenyl units and two chiral units **183** was isolated cleanly from the reaction mixture and so the other products are shown in red. As above, **183** would be expected to make up 37.5% of the statistical mixture of reaction products in a 1:3:3:1 ratio, in practice, it was recovered in 26% yield. The ratio of methyl protons to aromatic cyanobiphenyl protons can be clearly distinguished in the NMR spectra and are in agreement with the structural assignment of compound **183**. The MALDI-MS of this product (Figure 160) proves the structural assignment and shows the successful isolation of this product from the crude product mixture.
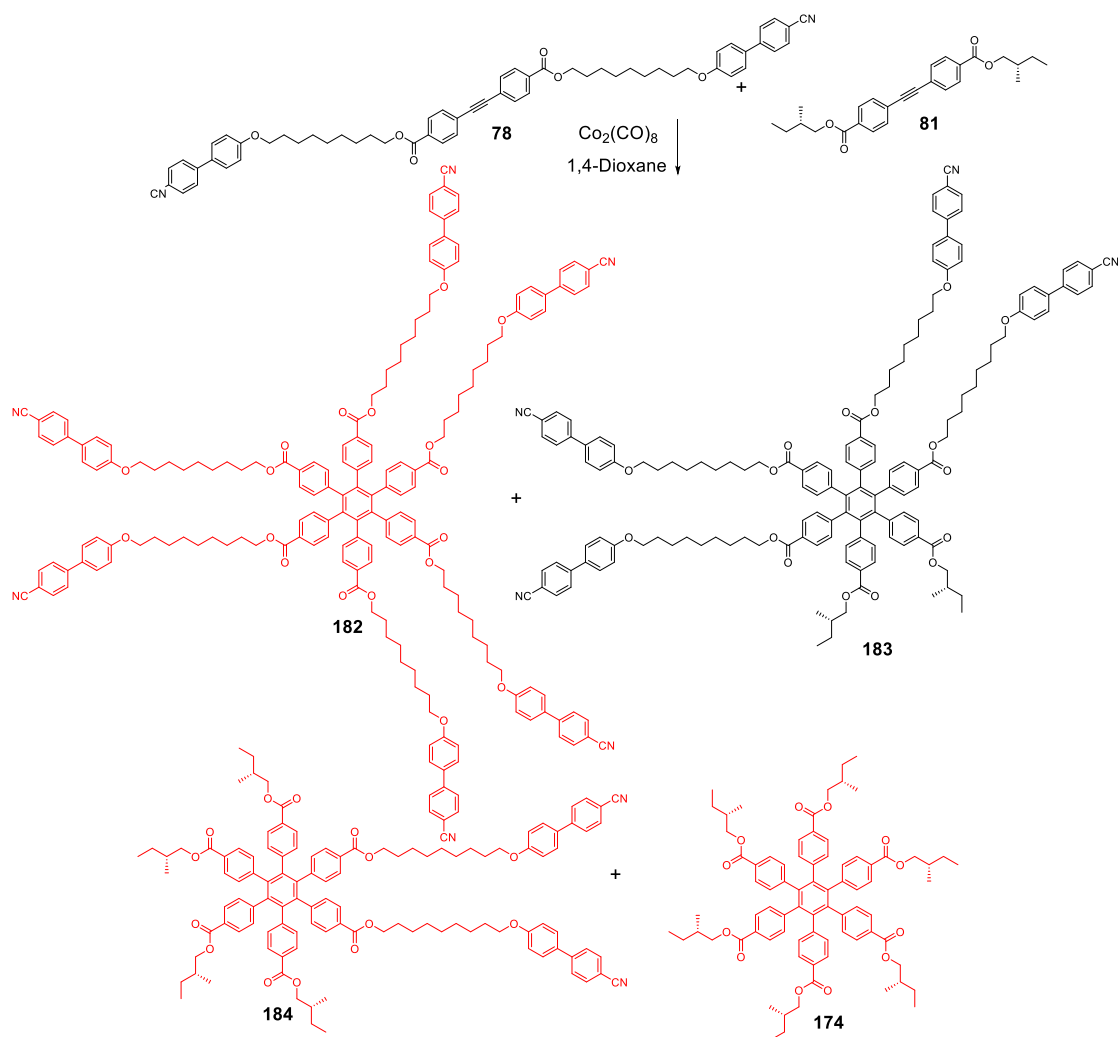
*Scheme 45. Cotrimerisation of equal ratios of chiral diphenyl acetylene **81** and achiral diphenyl acetylene **78** affords a statistical mixture of products **174, 181, 182** and **183** in a 1:3:3:1 ratio, however only **183** (shown in black) was successfully isolated from the mixture.*

Meas. m/z	#	Ion Formula	m/z	err [ppm]	err [mDa]	mSigma	Mean err [ppm]
2238.095648	1	C146H150N4NaO16	2238.093905	-0.8	-1.7	194.4	0.8
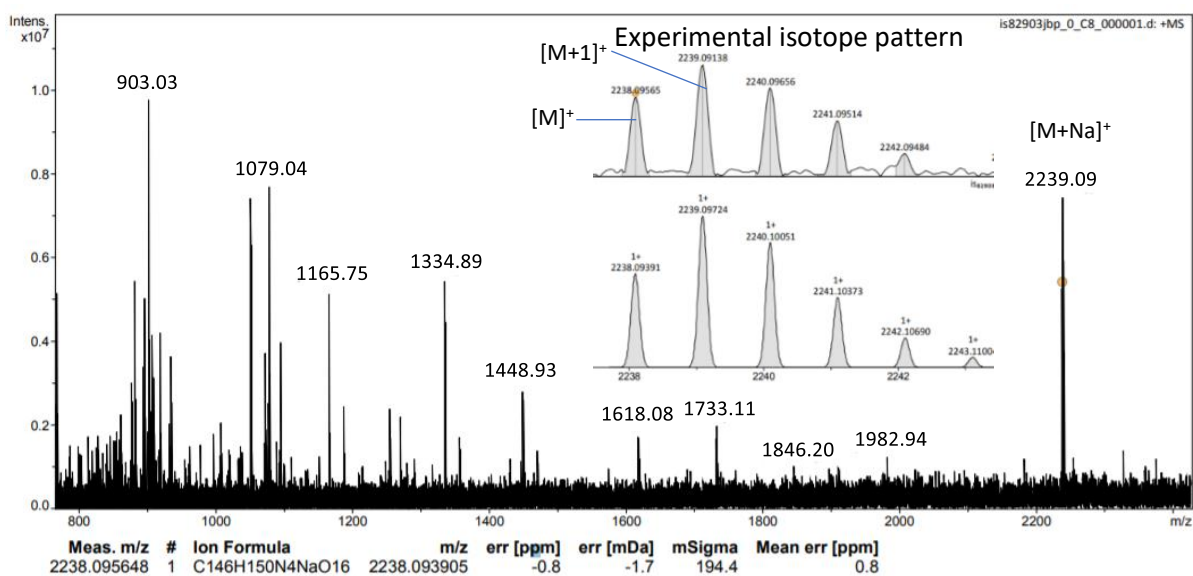
*Figure 160. MALDI-TOF-MS of compound **183**: mass expected 2215.1, mass observed 2239.1 [M+Na]+, no other products are detected such as compound **184**: mass expected 1716.9.*

336

In addition, the cotrimerisation of non-stoichiometric mixtures of diphenyl acetylenes was investigated to allow for control over the incorporation of asymmetrical materials within the cotrimerisation reaction. By using a large excess of a symmetrical diphenyl acetylene the statistical mixture of reaction products would be expected to contain very few compounds featuring two or more of the asymmetric reactants. Using this strategy for example a hexaphenylbenzene carrying one single chiral unit could be synthesised, avoiding long reaction schemes or complicated substitution reactions. As described above, to ease the separation of the homotrimers and the co-trimerised products, diphenyl acetylene with contrasting functionalities to include a polar unit such as cyanobiphenyl and apolar units such as alkyl chains were chosen. As only one asymmetric diphenyl acetylene was added to two symmetrical materials no isomerism is present. This avoided the formation of mixtures due to the incorporation of two chiral units whereby their location on the ring would be expected to show an effect.[10,11]

Unsymmetrical chiral diphenyl acetylene **131** and symmetrical diphenyl acetylene **73** were chosen for cotrimerisation with the aim of isolating the hexaphenylbenzene derivative **185** featuring a single chiral group (Scheme 46). In this case the precursors contain different linking groups between the diphenyl acetylene core and the chains attached to it, which induce different electronic effects therefore imparting different reactivity on the C≡C bond.

The possible influence of the differing reactivity of the two cores was minimised by heating the solvent at 110 °C before adding the reagents. Thus, cotrimerisation of **131** and **73** in a 1:10 ratio under these conditions successfully yields the hexaphenylbenzene **185** featuring one single chiral group and one single cyanobiphenyl group as a single regioisomer (Scheme 46). The reaction was proven to be successful by MALDI-MS as the desired co-trimerised product **185**, was detected and no molecular ions were detected showing the presence of two or more of the chiral diphenyl acetylene units in the hexaphenyl benzene. In addition, the ^{1}H NMR spectrum showed good agreement with this structure with the assignment given in the experimental. The desired product was obtained in 20% yield with respect to the sum of diphenyl acetylene reactants. However, considering the sacrificial nature of the

excess symmetrical diphenyl acetylene used, it may be more useful to note that the reaction provides around 80% yield with respect to the lower stoichiometry reactant.
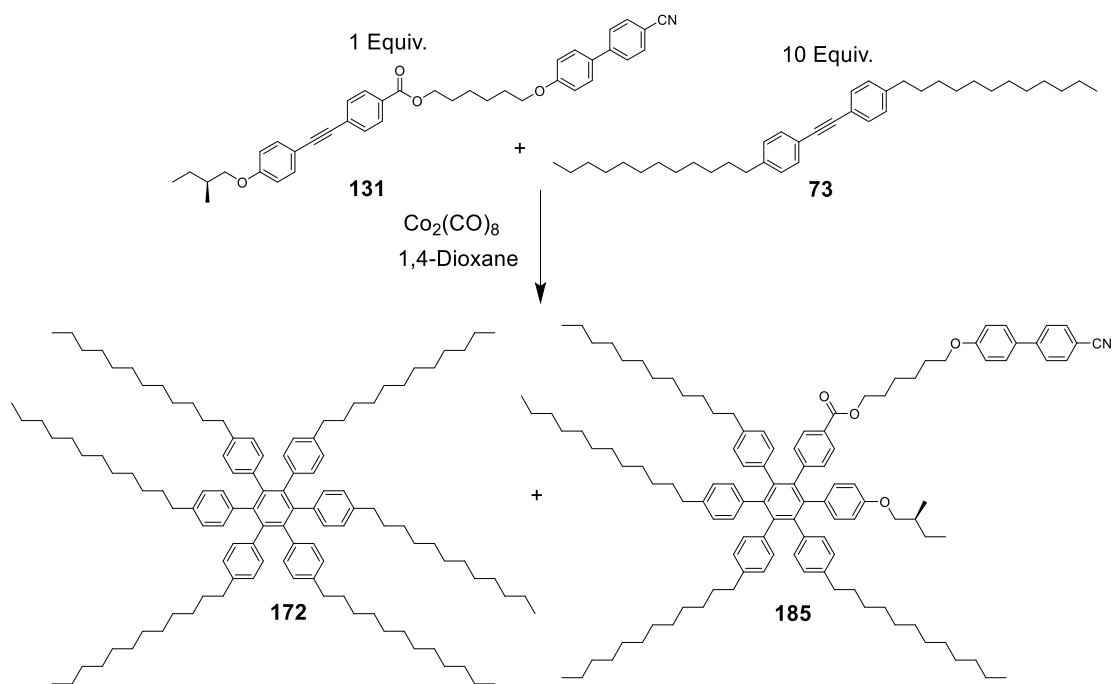
*Scheme 46. Cotrimerisation of **131** a chiral cyanobiphenyl and **73** a dialkyl diphenyl acetylene in unequal stoichiometry providing **185**.*

Pleasingly, following a similar procedure the cotrimerisation of **136** and **73** in 1:10 ratio affords **186**, corroborating the robustness of the strategy (Scheme 47). In this case the yields obtained were higher with around 30% of the total reactants being converted to the desired product and near quantitative yield with respect to the lower stoichiometry reactant. As above the ^{1}H NMR spectrum showed agreement with the proposed structure due to agreement of the cyanobiphenyl protons and methyl units of the (S)-2-methyl butyl unit and dodecyl chains. MALDI-MS confirms the presence of only one product with the correct molecular mass.
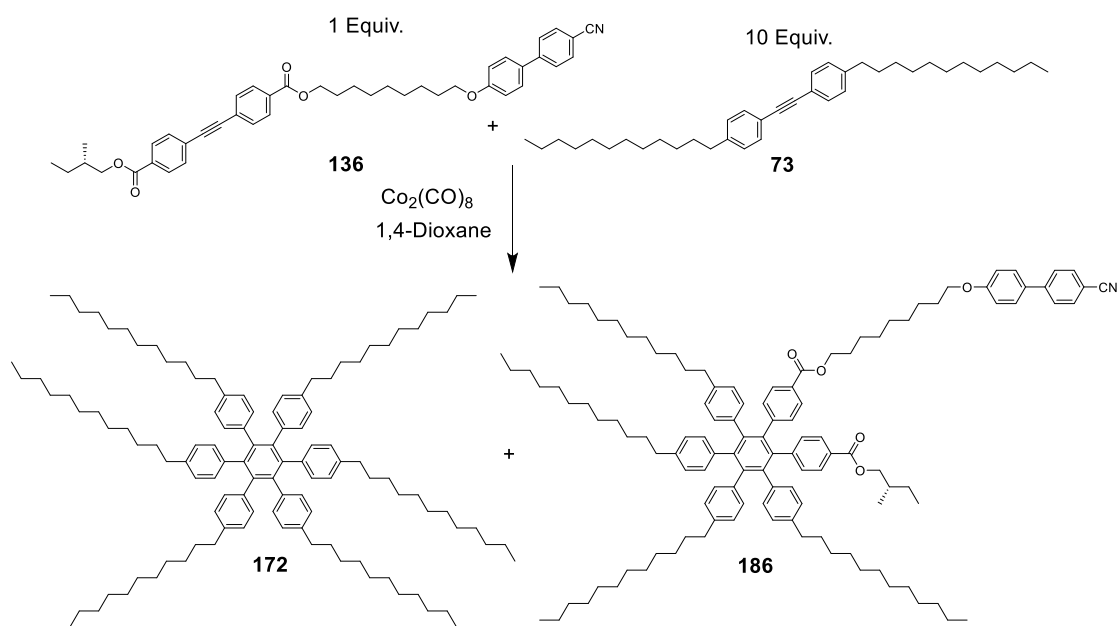
*Scheme 47. Repeated cotrimerisation using unequal reactant stoichiometry of **136** and **73** to provide*

***186**.*

In both cases the desired hexaphenyl benzene compounds were isolated and MALDI-TOF/ms used to show that only one compound was present in the mass range of any combinations of three of the reactant diphenyl acetylenes (Figure 161 and 162).

Meas. m/z	#	Ion Formula	m/z	err [ppm]	err [mDa]	mSigma	Mean err [ppm]
1638.188316	1	C115H156NNaO4	1638.192658	2.7	4.3	261.6	3.4
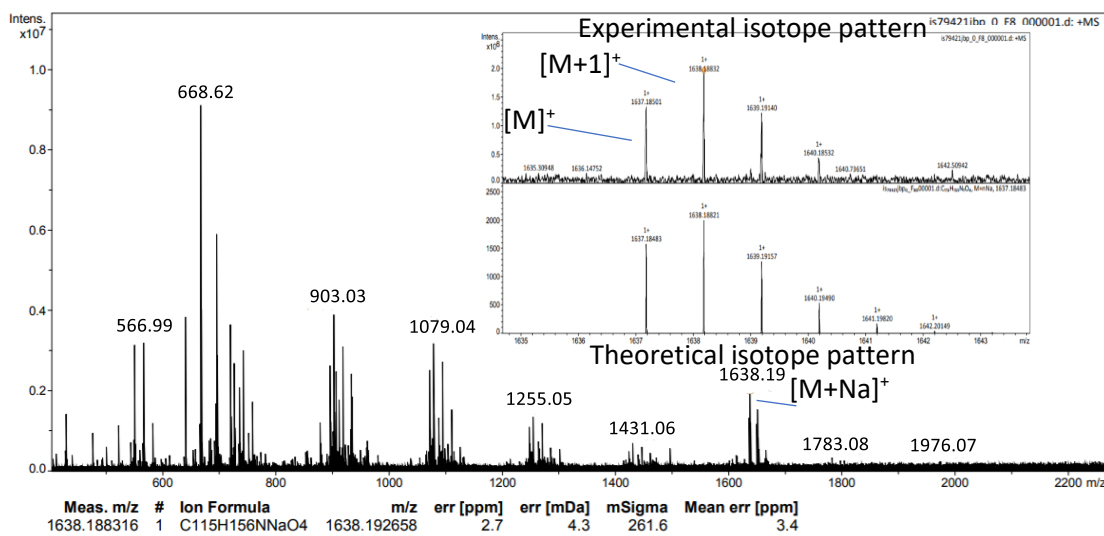
*Figure 161. MALDI-TOF-MS spectrum of **185**. Mass expected 1614.2, mass observed 1638.2 [M+Na]⁺.*

Hexaphenyl benzene with two chiral units would have expected mass 1685.0
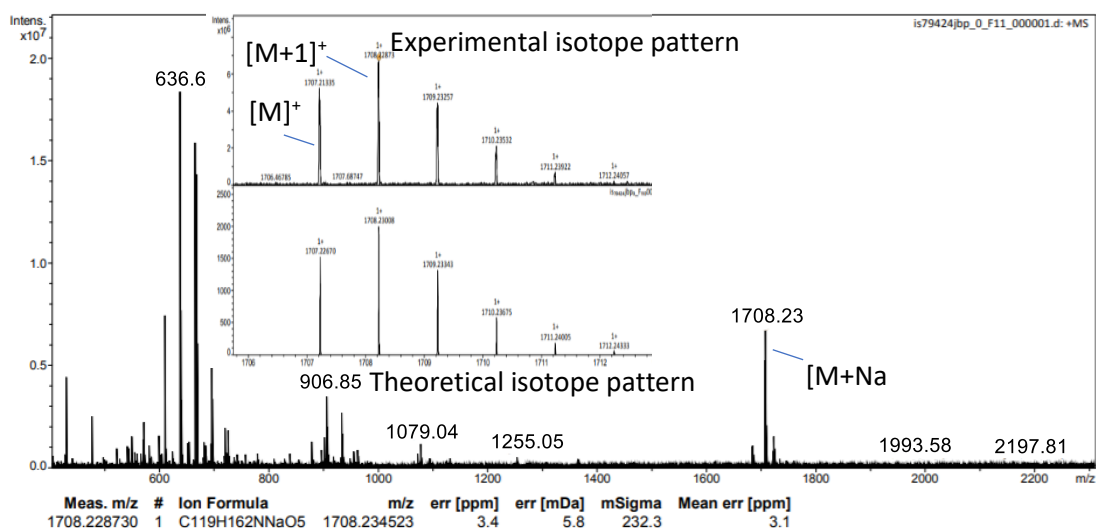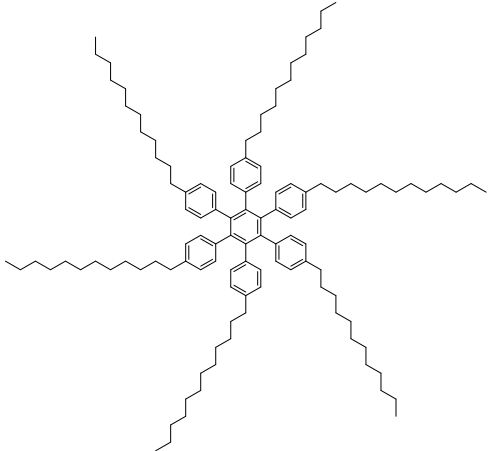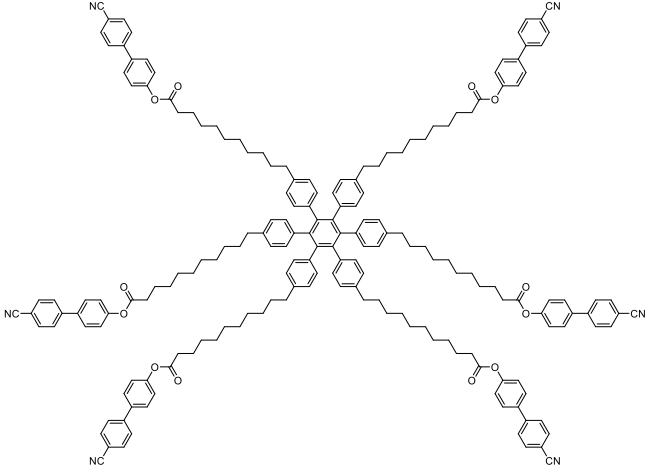
*Figure 162. MALDI-TOF-MS spectrum of **186**. Mass expected 1684.2, mass observed 1708.2 [M+Na]⁺. Hexaphenyl benzene with two chiral units would have expected mass 1825.1.*

Overall, the methodology is deemed successful as a multistep synthesis has been avoided and the desired products were separable from the reaction mixture. However, due to the nature of the materials synthesised in this way many of the compounds obtained were oils which could not be recrystallised to give suitable purity for elemental analysis. It is likely that a multistep synthesis to obtain these materials would face similar challenges, however a likely source of contamination is thought to be residual cobalt or cobalt complexes considering the presence of nitriles as possible ligands.[8] The details of the materials produced for this work are summarised in Tables 37 and 38.

Table 37. Achiral hexaphenyl benzene materials

Compound Number	Chemical structure	Transition temperatures / °C
172		Cr 56.5 Col 66.6 Iso °C[6]
173		Cr 142.1 SmA 159.3 Iso °C[7]

180
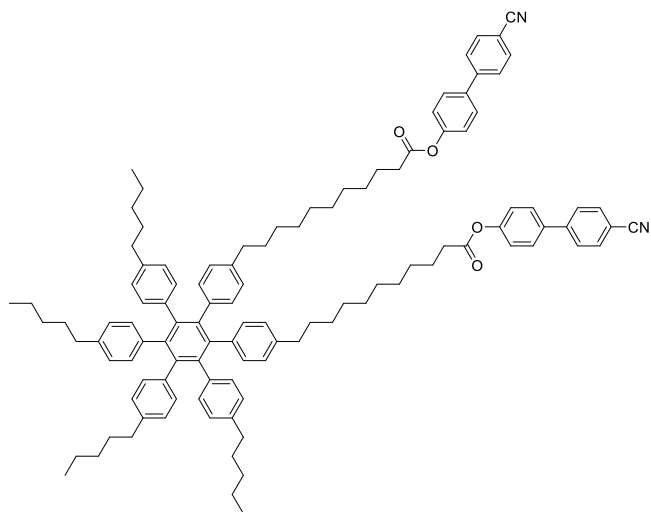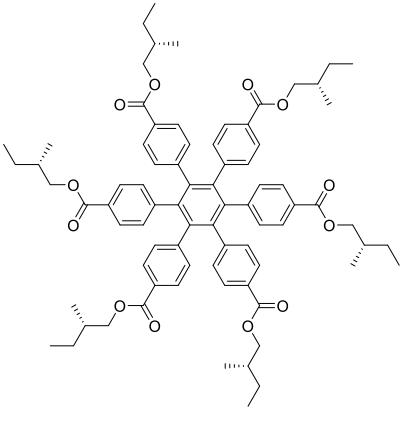
Cr 80.5 (SmA 76.8) Iso °C

181
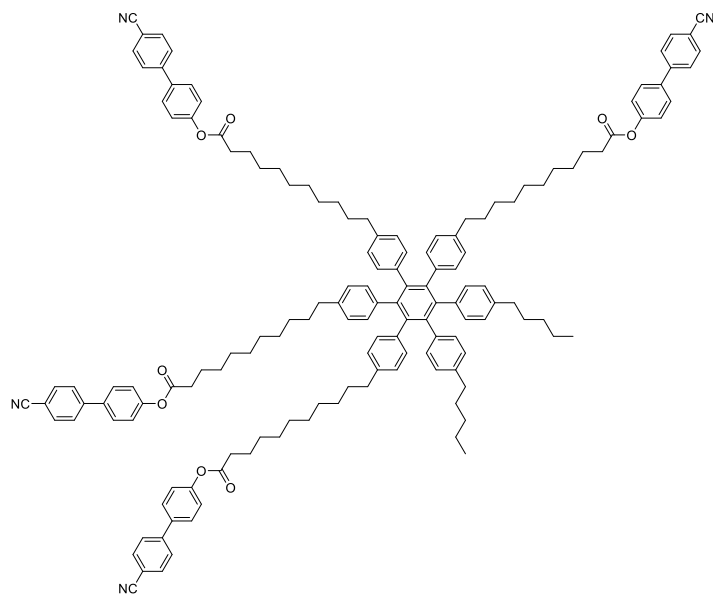
Cr 98.2 SmA 121.4 Iso °C

Table 38. Chiral hexaphenyl benzene materials.

Compound Number	Chemical structure	Transition temperatures / °C
174		Cr 174.8 Iso °C

175
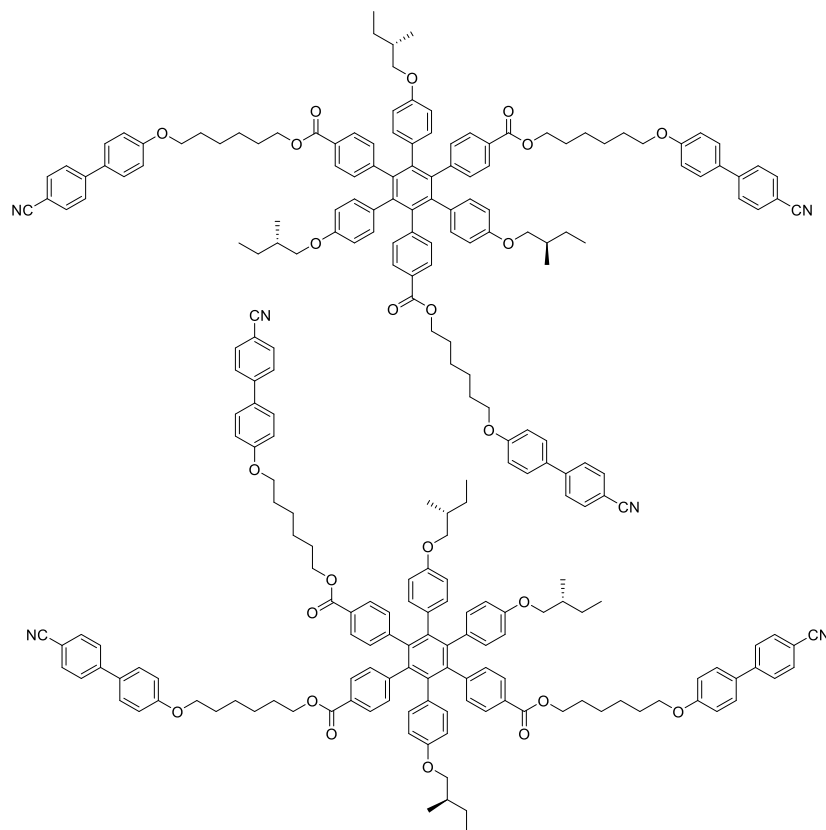
Cr 58.9 (g 49.3) Iso °C

176
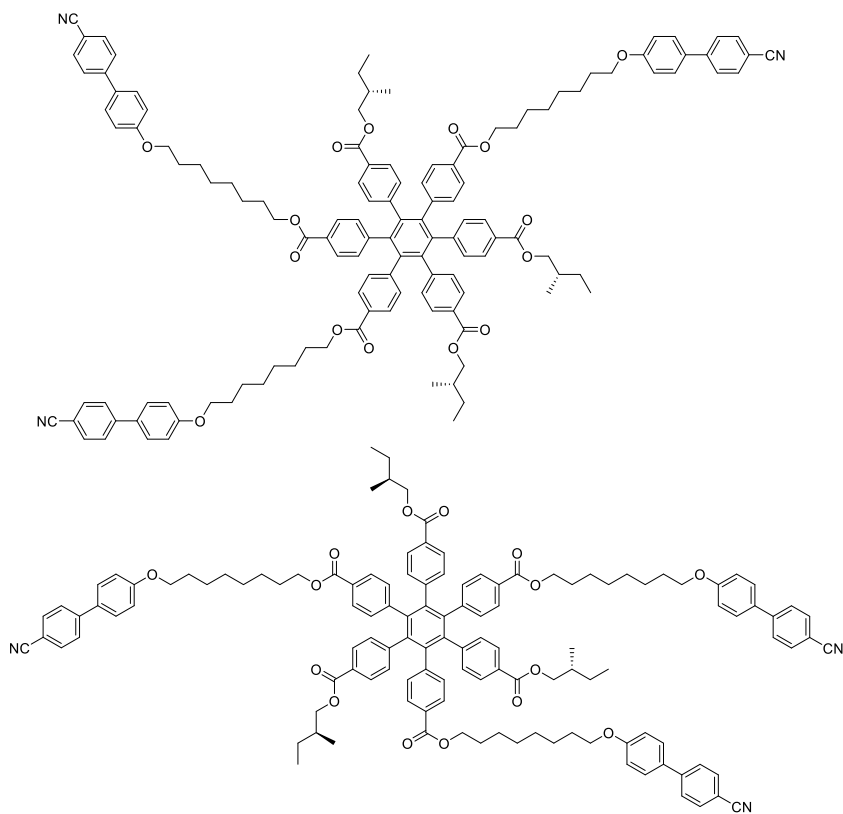
Cr 55.1 (g 45.5) Iso °C

183
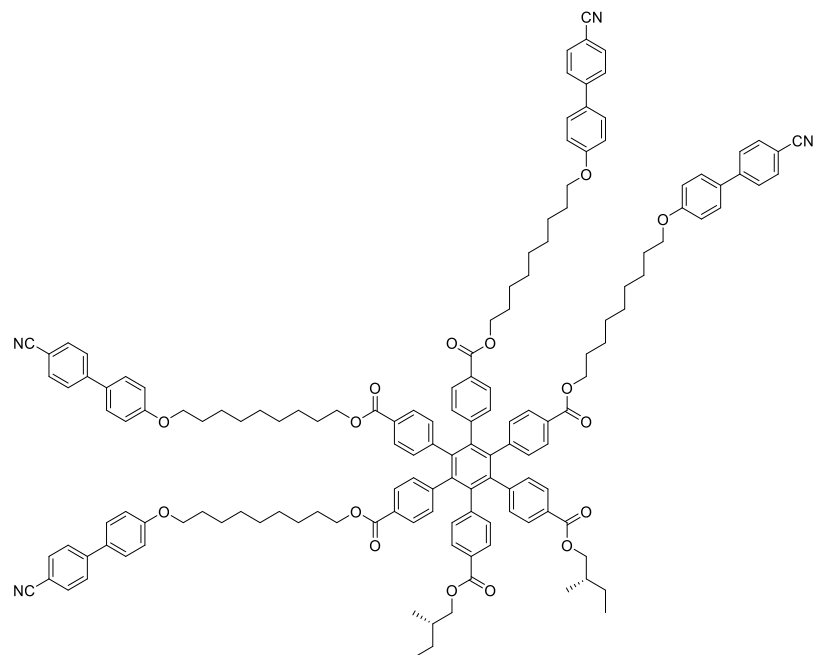
Cr 50.7 (g 47.2) Iso °C
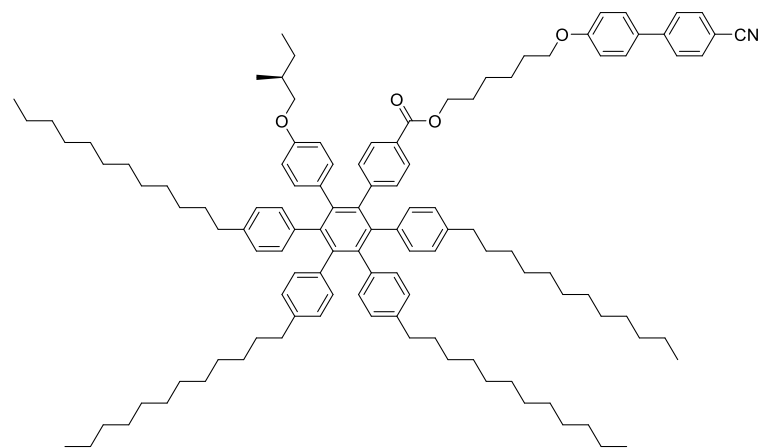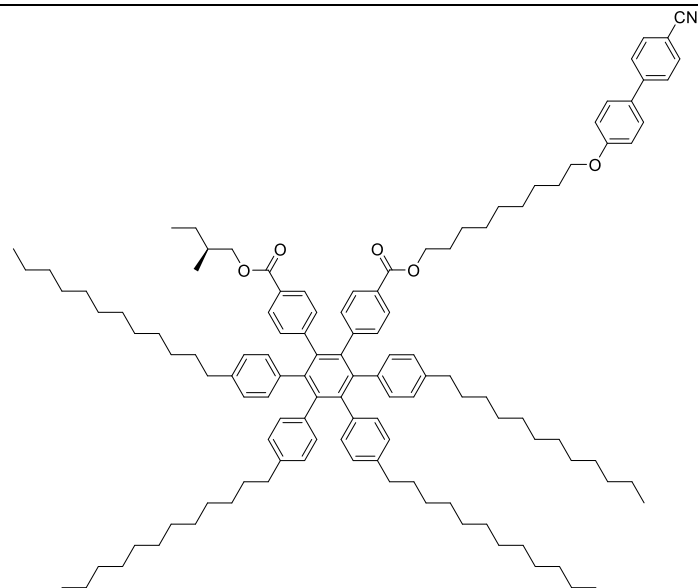
| 185 | | g -9 Iso °C |
| 186 | | g -2 Iso °C |

7.4 Liquid crystal properties and phase transitions of hexaphenyl benzenes.

Once synthesised the phase transitions and any liquid crystal properties were characterised using POM and DSC. The nature of the mesophase can be understood by comparison with previously reported compounds and the interplay between calamitic and columnar mesophases.

7.4.1 Liquid crystal properties of achiral hexaphenyl benzenes

Compounds **172**, **173**, **180** and **181** were characterised using polarised optical microscopy (POM) to identify the liquid crystal polymorphism and differential scanning calorimetry to determine the transition temperatures, enthalpies and entropies of transition (Table 39). Due to the large size of these molecules the textures developed slowly and required annealing for over 18 hours with some textures remaining poorly resolved.

*Table 39. Transition temperatures, enthalpies and entropies of transition of achiral hexaphenyl benzene compounds. **172** - Data reproduced from reference[6]. **173** - Data reproduced from reference[7].*

Compound number	Transition	T /°C	ΔH / kJ mol^{-1}	ΔS / J K^{-1} mol^{-1}
172[6]	Cr – Cr'	47.2	-	-
	Cr' – Col	56.5	-	-
	Col – Iso	66.6	92.5	272
173[7]	Cr – SmA	142.1	89.6	216
	SmA – Iso	159.3	4.3	10
180	Cr – Iso	80.5	32.0	91
	(SmA – Iso)	76.8	8.5	24
181	Cr – SmA	98.2	25.0	67
	SmA – Iso	121.4	10.5	27

Compound **172** exhibited a columnar phase which required annealing in order to develop a texture suitable for phase identification. The texture had low birefringence fan-like domains showing the characteristic offset spherulitic defects of the columnar phase and areas of high birefringence which were poorly resolved (Figure 163).
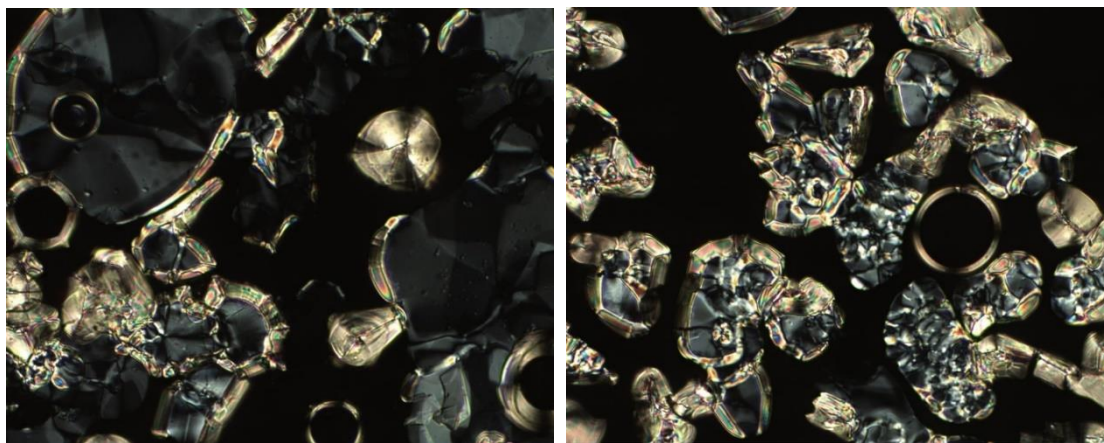
*Figure 163. Photomicrographs (x100 magnification) of **172** after annealing (60.2 °C).*

Compound **173** exhibited the characteristic focal-conic pair of ellipse and hyperbolae of the smectic A phase (Figure 164, left) including homeotropic areas. Droplets of the material developed the texture more quickly and clearly than in the bulk mesophase (Figure 164, right).
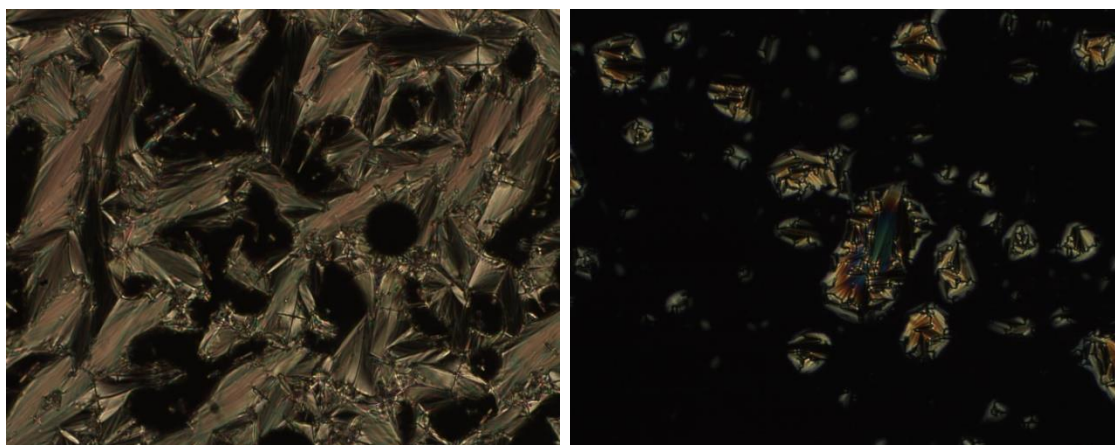
*Figure 164. Photomicrographs (x100 magnification) of the smectic A phase of **173** (160.1 °C) in the bulk, and droplets.*

Compound **180** exhibited a similar smectic A texture to the cyanobiphenyl compound **173** with the characteristic ellipse and hyperbolae focal-conic lines of optical discontinuity (Figure 165, left). Despite annealing for an extended period of time a clear texture was not obtained, rather the texture persisted with fine defects (Figure 165, right).
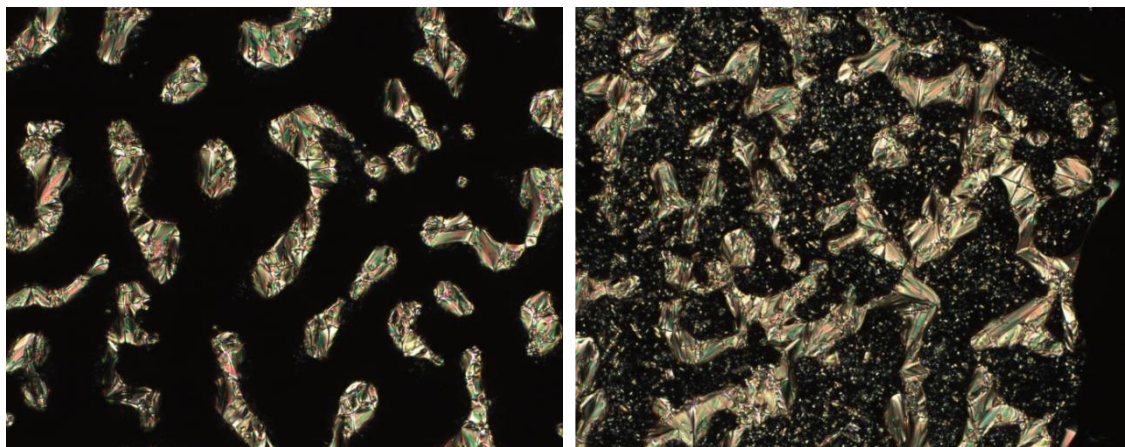
*Figure 165. Photomicrographs (x100 magnification) of the smectic A phase of **180** (120.6 °C) taken before (left) and after annealing (right).*

Contrastingly compound **181** more quickly developed into clearer textures with large domains of the focal-conic texture of the smectic A phase (Figure 166). This is notable as the number of calamitic cyanobiphenyls of **181** is increased relative to compound **180** and this fits a trend described below (Table 40).
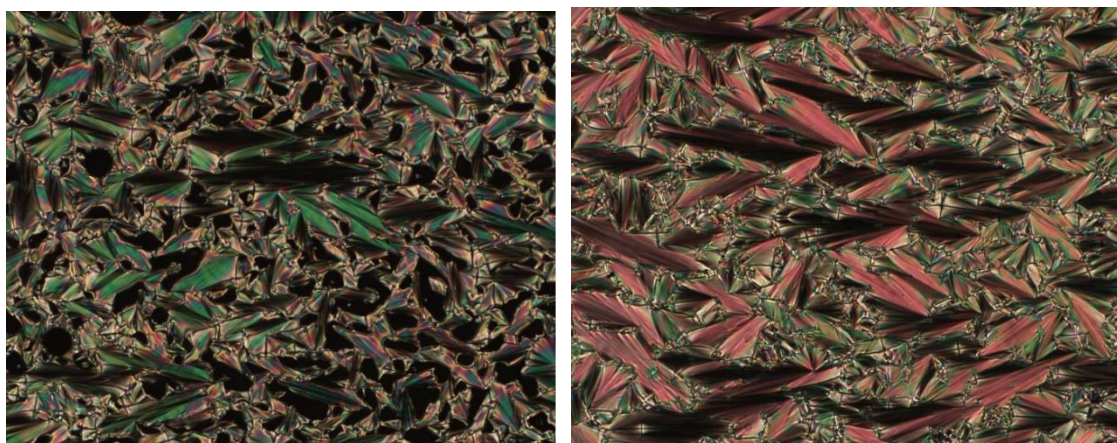
*Figure 166. Photomicrographs (x100 magnification) of the smectic A phase of **181** (left 77.2 °C, right 76.0 °C).*

Compound **172** has previously been reported by Müllen as possessing a disordered hexagonal columnar phase and the same transitions were observed here by POM.[6] The thermal properties of the symmetrical hexaphenyl hexacyanobiphenyl **173** agree with those reported previously by Ma.[7]

Both compounds **180** and **181** showed calamitic mesomorphism despite their discoidal molecular shape and displayed the defect textures typical of the smectic A phase. The calamitic mesophase structure is evidence that it is the cyanobiphenyls units which

drive the mesomorphism. While **180** showed monotropic mesomorphism, the exchange of two short alkyl chains to cyanobiphenyl units in **181** increased the clearing point by around 35 °C which resulted in enantiotropic behaviour. Comparison of **180**, **181** and **173** shows a smooth increase in the mesophase temperature range and mesophase stability with an increase in the number of cyanobiphenyl units in the molecule.

The columnar mesophase of compound **172** has a very high entropy of isotropisation due to the well-ordered mesophase required to maximise interactions between the propeller-shaped hexaphenyl benzene units. However, introduction of the cyanobiphenyl units clearly disrupts this in favour of a calamitic smectic A mesophase. This is accompanied by a large drop in the entropy of isotropisation as the smectic A phase is less well ordered than the columnar phase. In the case of supermolecular liquid crystals the entropy per mesogen of a transition can be considered to describe the degree of order of the mesogens. By comparing the entropy of isotropisation per mesogen of these compounds (Table 40) a trend emerges as increasing the number of calamitic mesogens in turn decreases the entropy per mesogen. This reflects a greater shift away from the influence of the hexaphenyl benzene cores which provide a more ordered mesophase in favour of the calamitic behaviour of the cyanobiphenyl units. Interestingly this could not apply in the case of the *Janus* materials reported in chapter 5 due to the flexibility of the branching units used, and so this trend is only observed where the alkyl units may crystallise as the exterior of these supramolecular columns.

Table 40. Entropy change of calamitic mesophases of cyanobiphenyl hexaphenyl benzene compounds.

Compound number	Clearing point / °C	Enthalpy of isotropisation / kJ mol^{-1}	Entropy of isotropisation / J mol^{-1}	Entropy of isotropisation per mesogen / J mol^{-1} mesogen^{-1}
172[6]	66.6	92.5	272.2	-
180	76.8	8.5	24.2	12.1
181	121.4	10.5	26.7	6.7
173[7]	159.3	4.3	10.0	1.7

SWAXS studies of **180** showed a primary diffraction peak at 66.4 Å, and a diffuse peak around 17.3 Å (Figure 167) with a fully extended conformation having a molecular length estimated around 42 Å. The hexaphenyl benzene core and pentyl chains have a diameter around 22 Å suggesting the diffuse peak relates to interactions around the hexaphenyl core. A similar broad peak in this range is observed in the X-ray diffraction of **172**.[6]
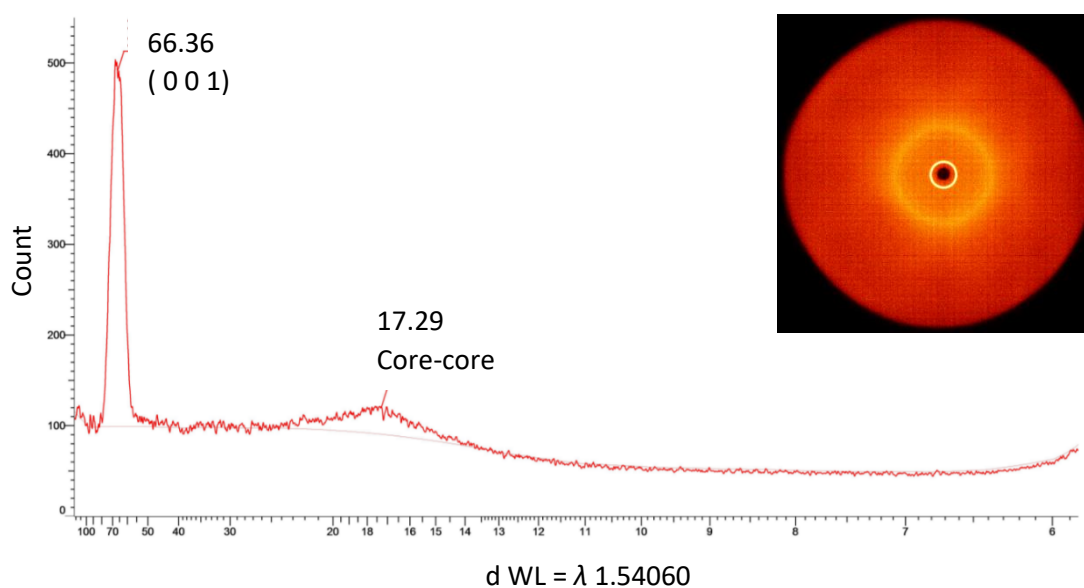
*Figure 167. SWAXS diffraction pattern from compound **180** showing an intense peak around 66.4 Å and a diffuse peak around 17.3 Å.*

The mesophase structure of the disc-rod oligomers and other supermolecular liquid crystals have been discussed previously[7,9-12]. In each case it is suggested that the cyanobiphenyl units (shown in red) extend above or below the supermolecular core so as to allow for the quadrupolar interactions of these mesogenic units to occur (Figure 168).
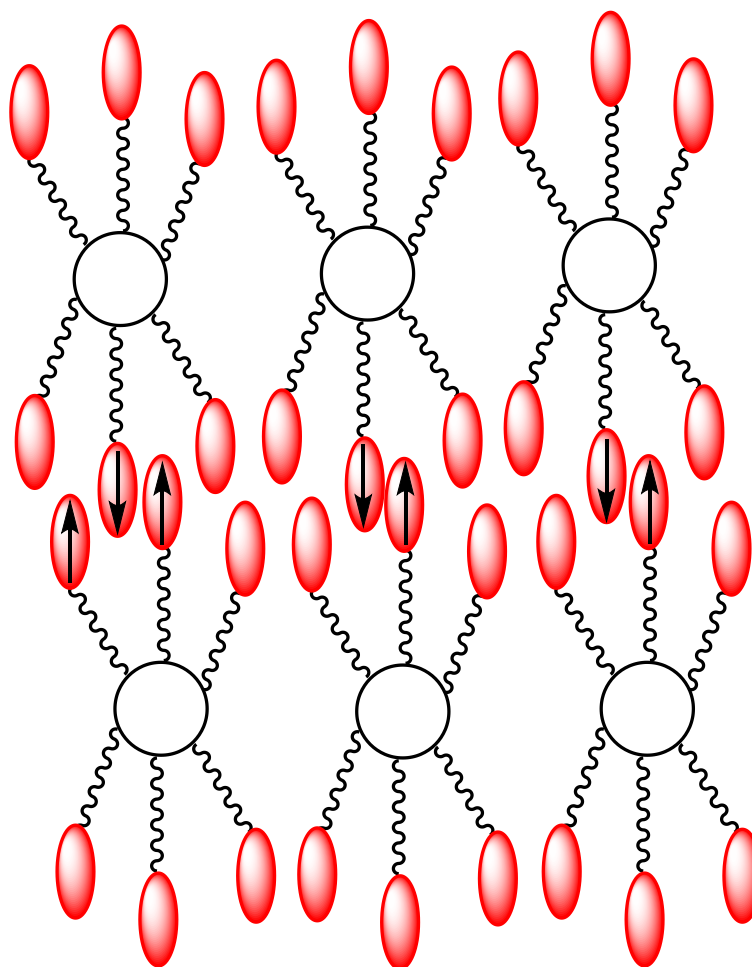
Figure 168. Commonly proposed mesophase structure of disc-rod oligomers and other supermolecular liquid crystals with incompatible units.

In this case it is interesting that a calamitic mesophase was stable considering the relatively low number of mesogenic units. This would destabilise a mesophase structure as shown in Figure 168 as the fewer mesogenic units would struggle to fill the space effectively. Instead, a modified structure is proposed whereby the cyanobiphenyl units may only extend from one side of the core providing an interface of calamitic materials as above. However, the opposite face of the hexaphenyl benzene core must therefore comprise of the short alkyl chains (Figure 169). A similar mesophase structure is tentatively proposed for compound **181** however as additional cyanobiphenyl units are introduced the mesophase will more closely resemble that shown in Figure 168.
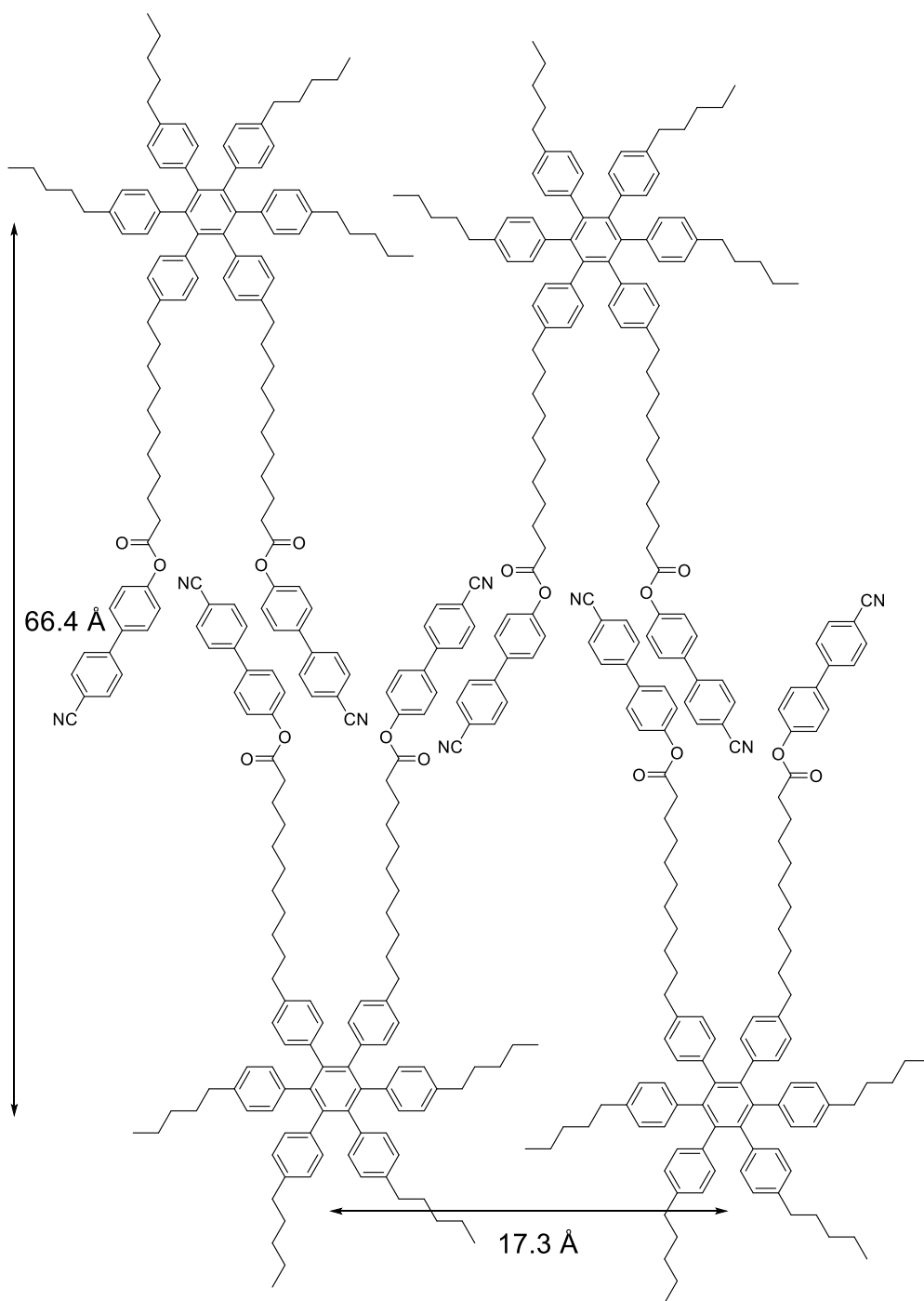
*Figure 169. Proposed mesophase structure of **179**.*

7.4.2 Transition temperatures of chiral hexaphenyl benzenes

The chiral materials produced were of lower symmetry than the achiral materials and therefore did not show liquid crystalline behaviour (Table 41). The transition temperatures were recorded by DSC and samples observed by polarised optical microscopy to check for birefringence. Typically, the chiral materials formed glasses due to their low symmetry. Some samples showed first order melting transitions during the first heating cycle however the magnitude of the enthalpy of these

transitions were low and likely did not represent the entire sample undergoing the transition. As the mass of the sample undergoing the transition is unknown the molar enthalpy and entropy values of the transition cannot be calculated.

Table 41. Transition temperatures, enthalpies and entropies of transition of chiral hexaphenyl benzene materials.

Compound number	Transition	T /°C	ΔH / kJ mol^{-1}	ΔS / J K^{-1} mol^{-1}
174	Cr – Iso	174.8	41.6	93
175	Cr – Iso	58.9	-	-
	g – Iso	49.3	-	-
176	Cr – Iso	55.1	-	-
	g – Iso	45.5	-	-
183	Cr – Iso	50.7	-	-
	g – Iso	47.2	-	-
185	g – Iso	-9	-	-
186	g – Iso	-2	-	-

Although no first order transitions were observed by DSC and no-liquid crystal texture was visible, **183** shows areas of birefringence were observed around air bubbles present in the sample (Figure 170).
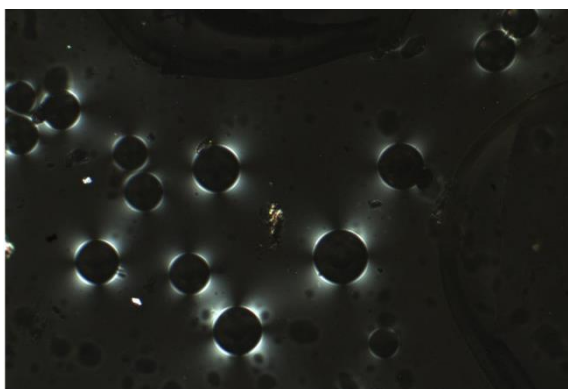
Figure 170. Photomicrograph (x100 magnification) of **183** showing birefringent beachfronts around air bubbles (49 °C).

Compound **174** was non-mesogenic and notably more crystalline than **172** as shown by the higher melting point. This is attributed to the shorter alkyl chains doing less to disrupt the packing of the hexaphenyl benzene cores.

Compounds **175** and **176** showed no liquid crystallinity and formed glasses as shown by DSC. The samples analysed by DSC had small first order transitions during the first heating cycle however the enthalpy and entropy values have not been calculated as it is unknown what fraction of the material had crystallised and as such contributed to the transition.

Compound **183** is of interest when compared with **181** due to the widely different properties. The introduction of the branched alkyl chains carrying the chiral methyl group is expected to disrupt the packing of low molecular weight calamitic materials. In addition, the presence of ester and not alkyl linking groups reduced the transition temperatures of the parent diphenyl acetylenes as reported in chapter 4. It is still notable that these factors accumulate to give a roughly 40 °C decrease in the clearing point and suppress the formation of the smectic phase. While **183** did not show a liquid crystal phase some evidence of anisotropy was observed *via* the presence of birefringence around air bubbles as shown in Figure 170.

Compounds **185** and **186** showed no evidence of liquid crystallinity and due to the highly disordered structure were liquids at room temperature forming glasses when cooled at lower temperatures. This is instructive as to the powerful role that the symmetry of these structures plays on their thermal behaviour. Comparison of **185** and **186** with **172** shows that the introduction of the chiral unit and single cyanobiphenyl disrupt the symmetry of the core. The single cyanobiphenyl mesogen would not be expected to stabilise a calamitic mesophase alone considering the large bulk of these materials, and typically multiple mesogenic units are used to stabilise liquid crystal phases of supermolecular molecules. The dodecyl chains used in **185** and **186**, were chosen as they stabilise the columnar mesophase in the highly symmetrical compound 1**72**.

7.5 Mixture studies

Many of the hexaphenyl benzene materials produced were designed to feature a chiral (S)-2-methyl butyl unit, with the same source being used throughout the project. Mori has investigated the effect of the propeller-like shape of the hexaphenyl benzene core when chirality is introduced into the system, and additionally the effect of sequentially adding multiple cores and their regiochemistry.[13,14] The chiral materials produced were designed to feature a symmetrical material with chiral units, molecules designed to feature only a single chiral unit in the mesophase structure and isomeric mixtures of materials with multiple chiral units. The helical twisting power of these materials was measured at a single concentration *via* the Cano-wedge cell method in the nematic host E7 (Table 42). As only one measurement was performed any trends derived should be treated with considerable caution. These values were compared with those of the parent diphenyl acetylenes detailed in Chapter 6.

Table 42. Helical twisting power of hexaphenyl benzenes and example diphenyl acetylenes. *Compounds 175 and 186 did not show the presence of any defect lines in the Cano-wedge cell at concentrations of 2.6 and 1.5 wt% respectively. [†] Compound was unstable in the host and readily crystallised.

Compound number	Dopant wt%	Helical twisting power/ μm^{-1} wt%$^{-1}$	Helical twisting power/ μm^{-1} mol%$^{-1}$
174	2.5	$0.3^{\dagger}$	$1.4^{\dagger}$
175	2.6	-*	-*
176	2.5	0.1	0.9
183	1.5	-*	-*
185	3.0	0.1	0.8
186	2.3	0.3	1.6
81	1.1	11	16
131	1.8	1.4	3.4
135	5.8	0.1	0.2

Preliminary values taken from a single measurement were sufficient to draw conclusions as to the effect of the hexaphenyl benzene core, when compared to the diphenyl acetylenes. Several experimental factors have been noted and introduce

further error into the measurements beyond that of the single measurement, however the effect is dramatic enough to allow for qualitative discussion.

Firstly, the diphenyl acetylene **81** featuring two (S)-2-methyl butyl groups linked by esters provided a very high helical twisting power, at least twice as large as the highest asymmetrical diphenyl acetylene described in chapter 6 which featured the (S)-1-methyl-2-heptanol chiral unit. This high helical twisting power was lost when the material was trimerised as the discotic hexaphenyl benzene **174** had a far lower helical twisting power. This is unsurprising as this material would be expected to be far less efficient at integrating itself within the calamitic nematic mesophase of the host. This resulted in the hexaphenyl benzene core crystallising from solution, with the helical twisting power noted being that of a saturated mixture as crystallisation began. Clearly the crystallisation served to effectively remove some of the dopant from solution and as such the value given is effectively for an unknown wt% of dopant, however due to the magnitude of the decrease in helical twisting power it is clear that the overall effect of the trimerisation is catastrophic.

Compound **175** was found to be a very poor dopant to the extent that no defect lines formed in the wedge cell. The mixture of isomers in **175** was better stabilised in the nematic mixture as shown by an increased solubility compared to **174**. This is due to the presence of multiple cyanobiphenyl units enabling better compatibility of the hexaphenyl benzene dopant and nematic host. Although the presence of the cyanobiphenyl units enabled the material to remain miscible in the mixture, as seen in the diphenyl acetylene precursor **131** the ether linking group was inefficient at imparting a helical twist within the nematic mesophase. Although the effect of having two regioisomers in the mixtures of **175** and **176** is not known, for each dopant the absolute configuration of the chiral unit is the same, and so the chiral groups may act cooperatively, additionally once dispersed into the mesophase the two chiral groups will act independently. It is likely however, that the helical twisting power of each isomer may differ, and in this way the mixture may be less effective than a sample of a single isomer.

Compound **176** is similarly the result of trimerisation of compound **135**, and a similar large decrease is seen in the helical twisting power as observed for **175**. While the

helical twisting power of **176** still decreased relative to the parent diphenyl acetylene **135**, this decrease was relatively smaller when compared to the symmetrical diphenyl acetylene **81** and hexaphenyl benzene **174**. This is attributed to the greater compatibility imparted by the cyanobiphenyl mesogens.

Interestingly the helical twisting powers of compounds **185** featuring only a single chiral unit appears to be higher than that of the homo-trimerised material **175** containing three chiral centres and the same ether linkage. Similarly, the helical twisting power of **186** featuring a single ester linked chiral unit is greater than that of the ester linked homo-trimer **176**. Both of these results rely on comparison with different weight% of dopants and so should be treated as caution, however the emergence of a trend may be a result of increased in symmetry in **185** and **186** compared to the chiral homo-trimers. Both **185** and **186** are isotropic liquids at room temperature indicating they share less intermolecular interactions than the homotrimerised materials, and so the interactions between the dopant and host would be expected to differ.

Compound **183** featuring two chiral units alongside four cyanobiphenyl chains did not show the presence of a defect line in the wedge cell as was described above for **175**. This is attributed to the lower weight percentage of dopant which is soluble in the host. Due to this a value of the helical twisting power cannot be calculated, however, a range can be estimated as the helical twisting power must be lower than 0.25 μm^{-1} $wt\%^{-1}$ to avoid the formation of a pair of defect line in the length of the cell. Without an accurate value this cannot be compared to the remaining hexaphenyl benzene materials however it is clearly far lower than the chiral diphenyl acetylene **81** which is incorporated into the structure. The structure of **81 is** clearly more 'rod-like' and will be better incorporated into the nematic mesophase than **183**. Compound **176** was notably more miscible in E7 than compound **183** while possessing fewer calamitic cyanobiphenyl units. This is likely related to the longer alkyl chains of **176** which disrupts aggregation of the hexaphenyl benzene cores. While a measurement was recorded for compound **174** at a greater dopant concentration (2.5 wt%) the mixture quickly began to crystallise and so the miscibility of this compound cannot be compared to other results.

The results from this initial study showed significantly large decreases in the helical twisting power for the hexaphenyl benzene materials that alternative nematic hosts were not investigated.

7.6 Summary

The cobalt catalysed [2+2+2] cyclotrimerisation reaction was used to afford a series of materials featuring the hexaphenyl benzene core. This was achieved *via* symmetrical and asymmetrical homotrimerisations and cotrimerisations of two species either in stoichiometric ratios or with one reactant in excess. The success of these reactions were proven by MALDI-TOF-ms, and multistep syntheses of each compound was avoided.

Homotrimerisation reactions of asymmetrical diphenyl acetylenes was known to give mixtures and result in alternating substitution patterns between the different substituents. This can be avoided by using cotrimerisations of symmetrical materials as demonstrated previously by Nierengarten[4] and Jux[5]. The observed behaviour **180** and **181** highlighted in Table 40 appear to show a transition between discotic and calamitic mesomorphism, which may not be possible with less defined regiochemistry. In addition, although the chiral hexaphenyl benzenes produced in this work were not liquid crystalline the principle of heavily skewing the reaction stoichiometry to control the outcome of the reaction was successful. In addition, this approach appeared to allow for the incorporation of diphenyl acetylenes where the reactivity of the core was not equal.

It was shown that while multiple cyanobiphenyl units may stabilise a mesophase in some materials, the lack of symmetry in these materials results in far lower transition temperatures than those of previously reported symmetrical materials. The chiral materials produced were added as chiral dopants to the nematic host E7 to induce the chiral nematic phase. They were found to be relatively poor dopants, exhibiting lower helical twisting power than their parent diphenyl acetylene compounds in the same host. Due to the high degree of error involved in these measurements only qualitative discussion of the results was possible. Repeated experiments with higher weight percentages of dopant may be used to generate more accurate data however their miscibility in the host may result in further difficulties. It is clear that the overall effect of the trimerisations was to hinder the incorporation of the hexaphenyl benzene core

into the calamitic nematic mesophase. One interesting avenue to explore in future work is their miscibility in a discotic nematogen to induce the rare chiral nematic discotic phase.[15]

172
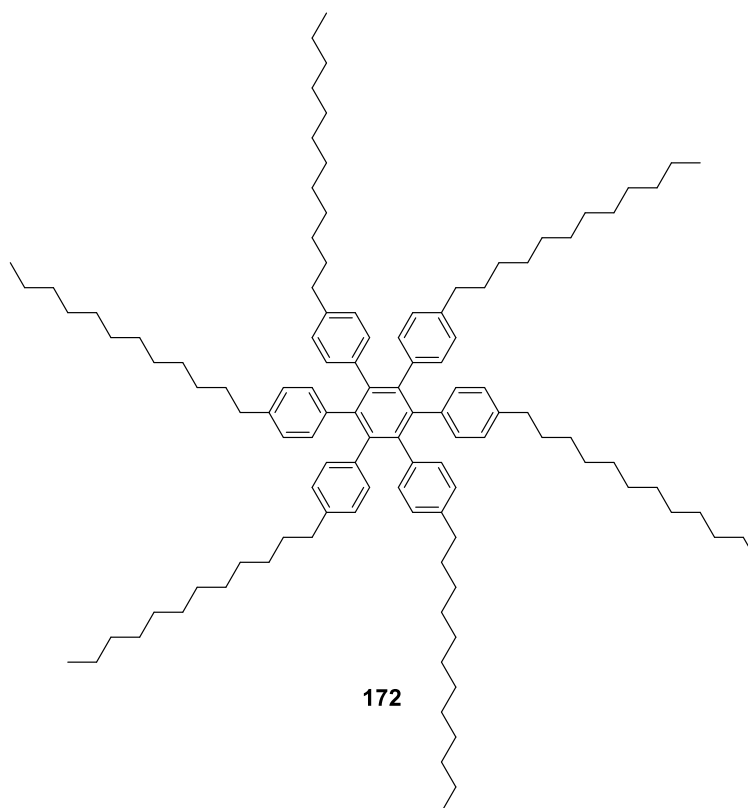
Compound **73** (0.10 g, 0.19 mmol) was charged to a dry Schlenk tube, then Co_2CO_8 (0.02 g, 0.06 mmol) added in a glovebox under nitrogen. Dry 1,4-dioxane (8 mL) was charged to a second dry Schlenk tube under argon and degassed with argon for 20 minutes. The degassed solvent was transferred to the reagents and the mixture heated to reflux for 18 hours. The mixture was cooled to room temperature, the solvent removed in vacuo and the crude product was purified by column chromatography (SiO_2, DCM as eluent, Rf = 0.29) to give the target compound **172** as a white solid (0.07 g, 0.05 mmol, 70% yield).

^{1}H NMR (400 MHz, CDCl$_3$) δ 7.43 (d, *J* = 8.0 Hz, 12H, Ar*H*), 7.15 (d, *J* = 8.0 Hz, 12H, Ar*H*), 2.60 (t, *J* = 8.5 Hz, 12H, ArC*H$_2$*), 1.60 (tt, *J* = 8.5 Hz, 7.5 Hz, 12H, ArCH$_2$C*H$_2$*), 1.37 – 1.18 (m, 120H, -CH$_2$C*H$_2$*), 0.92 – 0.83 (t, *J* = 7.0 Hz, 18H, C*H$_3$*).

MALDI-TOF/ms: mz = 1566.4 [M+Na]$^+$

Compound **88** (0.10 g, 0.11 mmol) was charged to a dry Schlenk tube, then Co_2CO_8 (0.02 g, 0.06 mmol) added in a glovebox under nitrogen. Dry 1,4-dioxane (6 mL) was charged to a second dry Schlenk tube under argon and degassed with argon for 20 minutes. The degassed solvent was transferred to the reagents and the mixture heated to reflux for 18 hours. The mixture was cooled to room temperature, the solvent removed in vacuo and the crude product was purified by column chromatography (SiO$_2$, 10:1 DCM:Ethyl acetate as eluent, Rf = 0.18) followed by recrystallisation from DCM:Ethanol to give the target compound **173** as a white powdery solid (0.06 g, 0.02 mmol, 60% yield).

^{1}H NMR (400 MHz, CDCl$_3$) δ 7.70 (d, J = 8.5 Hz, 12H, ArH), 7.62 (d, J = 8.5 Hz, 12H, ArH), 7.55 (d, J = 8.5 Hz, 12H, ArH), 7.20 (d, J = 8.5 Hz, 12H, ArH), 6.62 (m, 24H, ArH), 2.58 (t, J = 7.5 Hz, 12H, ArCH_2), 2.34 (t, J = 7.0 Hz, 12H, OCOCH_2), 1.76 − 1.53 (m, 24H, (CH_2CH$_2$COO and ArCH$_2$CH_2), 1.33 (m, 72H, CH$_2$CH$_2$CH_2), 1.10 (m, 12H, CH$_2$CH$_2$CH_2).

MALDI-TOF/ms: mz = 2724.5 [M+Na]$^+$

174

Compound **81** (0.50 g, 1.23 mmol) was charged to a dry Schlenk tube, then Co_2CO_8 (0.02 g, 0.06 mmol) added in a glovebox under nitrogen. Dry 1,4-dioxane (15 mL) was charged to a second dry Schlenk tube under argon and degassed with argon for 20 minutes. The degassed solvent was transferred to the reagents and the mixture heated to reflux for 18 hours. The mixture was cooled to room temperature, the solvent removed in vacuo and the crude product was purified by column chromatography (SiO_2, DCM as eluent, Rf = 0.38) to give the target compound **174** as a crystalline white solid (0.31 g, 0.25 mmol, 62% yield).

^{1}H NMR (400 MHz, CDCl$_3$) δ 7.56 (d, *J* = 8.5 Hz, 12H, Ar*H*), 6.89 (d, *J* = 8.0 Hz, 12H, Ar*H*), 4.09 (dd, *J* = 10.5, 6.0 Hz, 6H, OC*H*H), 3.99 (dd, *J* = 11.0, 6.5 Hz, 6H, OC*H*H), 1.78 (dqd, *J* = 13.0, 6.5, 6.0 Hz, 6H, C*H*HCH$_3$), 1.47 (dqd, *J* = 13.5, 7.5, 6.0 Hz, 6H, C*H*HCH$_3$), 1.23 (m, 6H, C*H*CH$_3$), 0.95 (d, *J* = 7.0 Hz, 18H, CHC*H$_3$*), 0.91 (t, *J* = 7.5 Hz, 18H, CH$_2$C*H$_3$*).
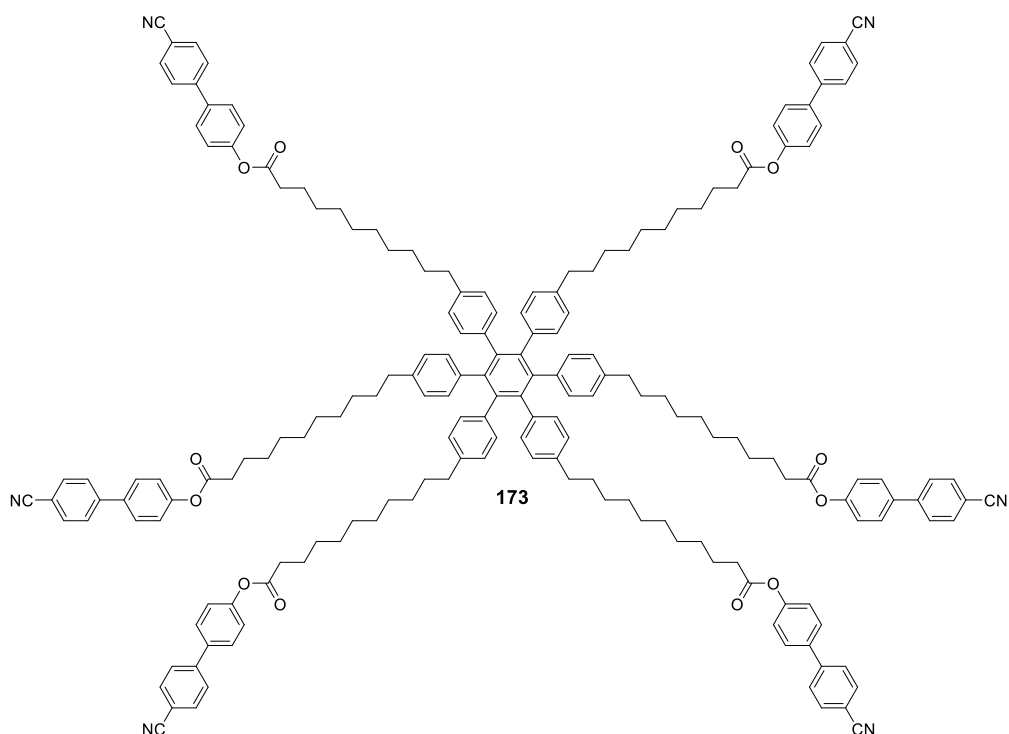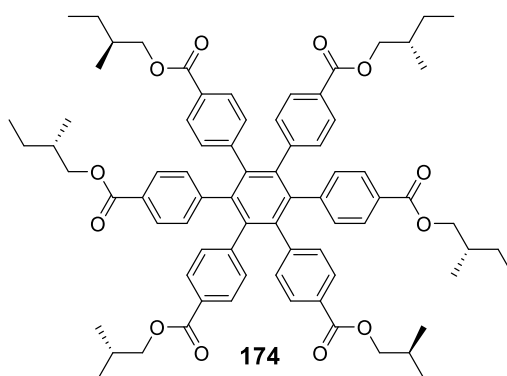
MALDI-TOF-MS: mz = 1231.6 [M+Na]$^+$

Compound **131** (0.12 g, 0.21 mmol) was charged to a dry Schlenk tube, then Co_2CO_8 (0.02 g, 0.06 mmol) added in a glovebox under nitrogen. Dry 1,4-dioxane (6 mL) was charged to a second dry Schlenk tube under argon and degassed with argon for 20 minutes. The degassed solvent was transferred to the reagents and the mixture heated to reflux for 18 hours. The mixture was cooled to room temperature, the solvent was removed in vacuo and the crude product was purified by column chromatography (SiO$_2$, 10:1 DCM:EtOAc as eluent, Rf = 0.22) to give the target compound **175** as a yellow oil (0.08 g, 0.05 mmol, 67% yield).

^{1}H NMR (400 MHz, CDCl$_3$) δ 7.68 (d, J = 7.5 Hz, 6H, ArH), 7.63 (d, J = 7.5 Hz, 6H, ArH), 7.60 – 7.50 (m, 12H, ArH), 6.98 (d, J = 6.0 Hz, 6H, ArH), 6.88 (dt, J = 8.5, 3.0 Hz, 6H, ArH), 6.64 (d, J = 8.5, Hz, 6H, ArH), 6.44 – 6.34 (m, 6H, ArH), 4.22 (t, J = 6.5 Hz, 6H, COOCH_2), 4.00 (td, J = 6.5 Hz, 6H, OCH_2), 3.61 (dd, J = 11.0, 6.5 Hz, 3H, OCHH), 3.52 (dd, J = 11.0, 6.5 Hz, 3H, OCHH), 1.89 – 1.77 (m, 6H, OCH$_2$CH_2), 1.78 – 1.67 (m, 9H, CHHCH$_3$ and OCH$_2$CH_2), 1.57 – 1.42 (m, 18H), 0.93 (d, J = 7.0 Hz, 9H, CHCH_3), 0.89 (t, J = 7.5 Hz, 9H, CH$_2$CH_3).
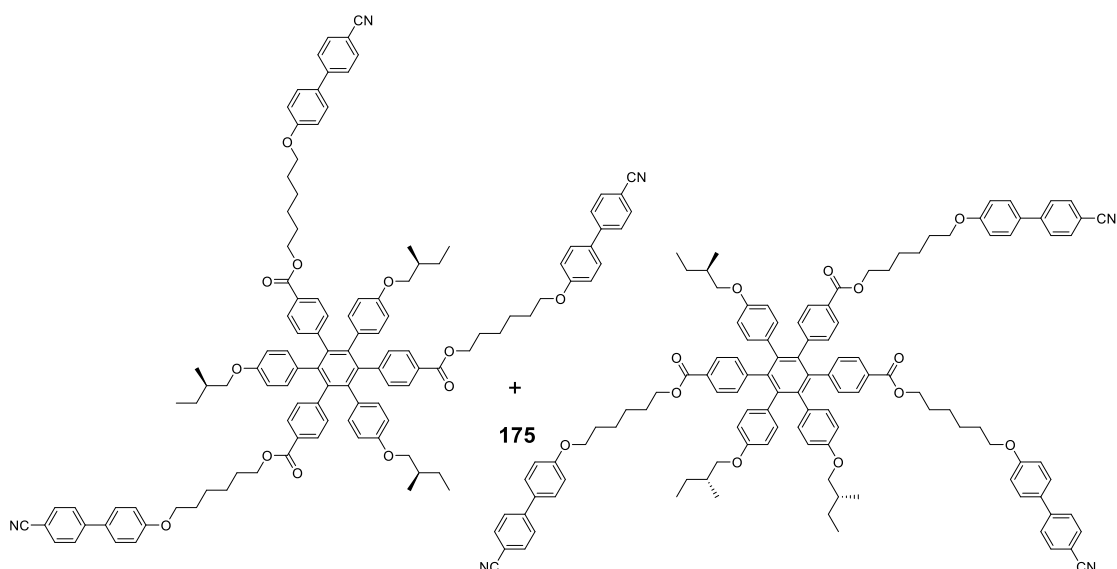
MALDI-TOF/MS: mz = 1778.9 [M+Na]$^+$
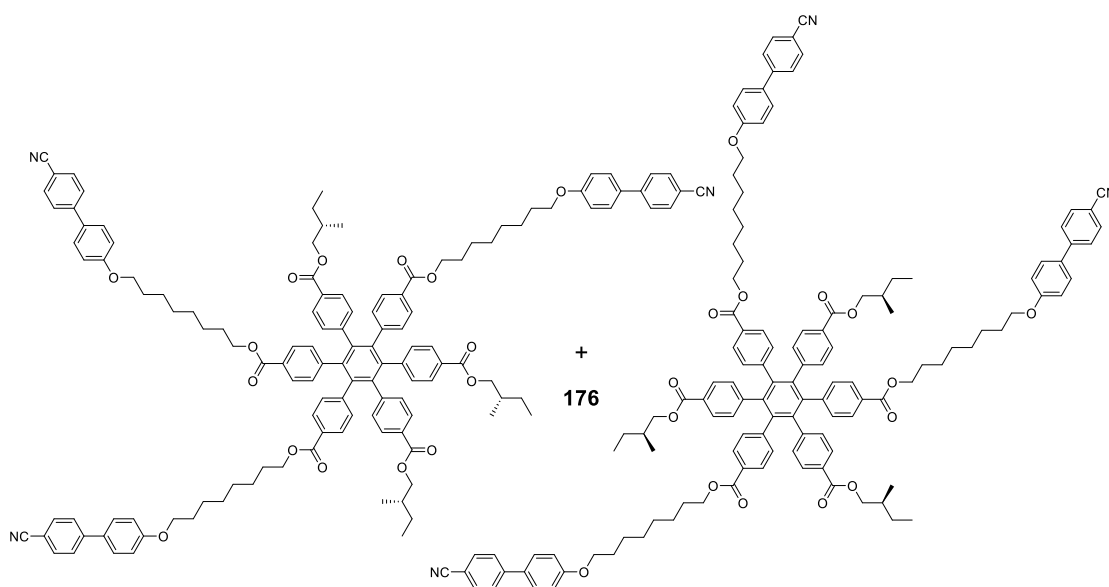
Compound **135** (0.10 g, 0.16 mmol) was charged to a dry Schlenk tube, then Co$_2$CO$_8$ (0.02 g, 0.06 mmol) added in a glovebox under nitrogen. Dry 1,4-dioxane (7 mL) was charged to a second dry Schlenk tube under argon and degassed with argon for 20 minutes. The degassed solvent was transferred to the reagents and the mixture heated to reflux for 18 hours. The mixture was cooled to room temperature, the solvent removed in vacuo and the crude product was purified by column chromatography (SiO$_2$, 10:1 DCM:EtOAc as eluent, Rf = 0.24) to give the target compound **176** as a yellow oil (0.06 g, 0.03 mmol, 60% yield).

^{1}H NMR (400 MHz, CDCl$_3$) δ 7.68 (d, J = 8.5 Hz, 6H, ArH), 7.62 (d, J = 8.5 Hz, 6H, ArH), 7.59 – 7.46 (m, 18H, ArH), 6.97 (d, J = 8.5 Hz, 6H, ArH), 6.88 (d, J = 8.5 Hz, 12H, ArH), 4.18 (t, J = 7.0 Hz, 6H, COOCH_2), 4.08 (dd, J = 11.0, 6.0, 3H, OCHH), 4.00 – 3.94 (m, 9H, OCH_2 and OCHH), 1.83 – 1.73 (m, 9H, CHHCH$_3$ and OCH$_2$CH_2), 1.68 (m, 6H, OCH$_2$CH_2), 1.51 – 1.32 (m, 30H), 0.93 (d, J = 7.0 Hz, 9H, CHCH_3), 0.89 (t, J = 7.5 Hz, 9H, CH$_2$CH_3).

MALDI-TOF/MS: mz = 1946.9 [M+Na]$^+$
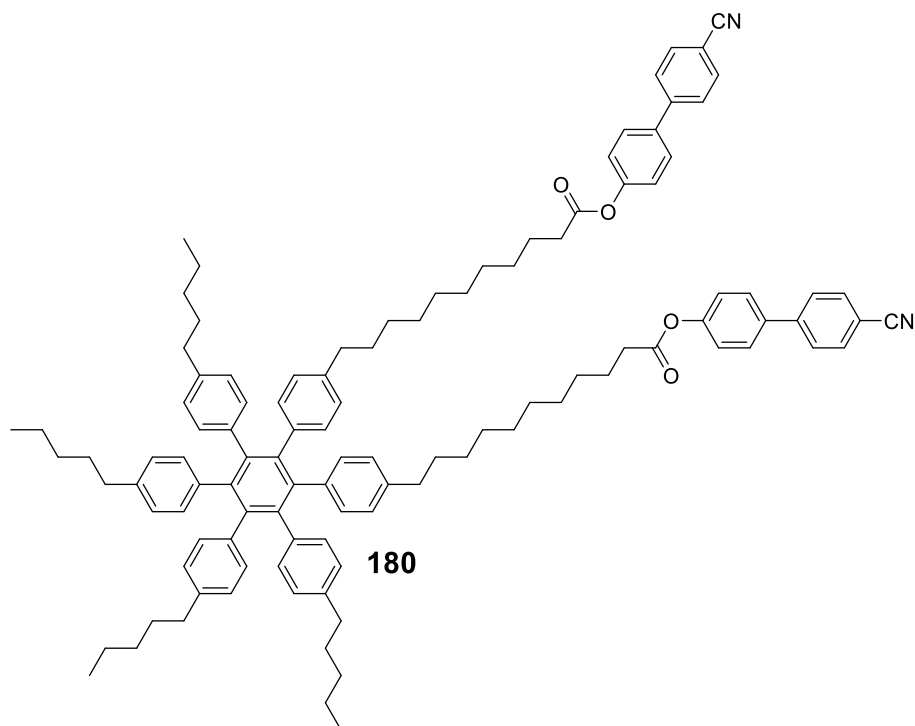
180

Compound **76** (0.16 g, 0.50 mmol) and **88** (0.48 g, 0.53 mmol) were charged to a dry Schlenk tube, then Co_2CO_8 (0.02 g, 0.06 mmol) was added in a glovebox under nitrogen. Dry 1,4-dioxane (12 mL) was charged to a second dry Schlenk tube under argon and degassed with argon for 20 minutes. A heating oil bath was heated to 115 °C and equilibrated for 1 hour, then the solvent transferred to the reagents and the mixture heated to reflux for 18 hours. The mixture was cooled to room temperature, the solvent was removed in vacuo and the crude product was purified by column chromatography (SiO$_2$, 10:1 DCM:EtOAc as eluent, Rf = 0.25) to give the target compound **180** as an off-white solid (0.13 g, 0.09 mmol, 25% yield).

^{1}H NMR (400 MHz, CDCl$_3$) δ 7.70 (d, *J* = 8.5 Hz, 4H, Ar*H*), 7.63 (d, *J* = 8.5 Hz, 4H, Ar*H*), 7.56 (d, *J* = 8.5 Hz, 4H, Ar*H*), 7.21 − 7.15 (m, 4H, Ar*H*), 6.65 (d, *J* = 8.0 Hz, 12H, Ar*H*), 6.60 (d, *J* = 8.0 Hz, 12H, Ar*H*), 2.57 (m, 12H, ArC*H*$_2$), 2.33 (t, *J* = 7.5 Hz, 4H, C*H*$_2$COO), 1.78 − 1.70 (m, 4H, C*H*$_2$CH$_2$COO), 1.42 − 1.17 (m, 44H), 1.14 − 1.04 (m, 8H), 0.83 (t, *J* = 7.5 Hz, 12H).

MALDI-TOF/MS: mz = 1561.0 [M+Na]$^+$
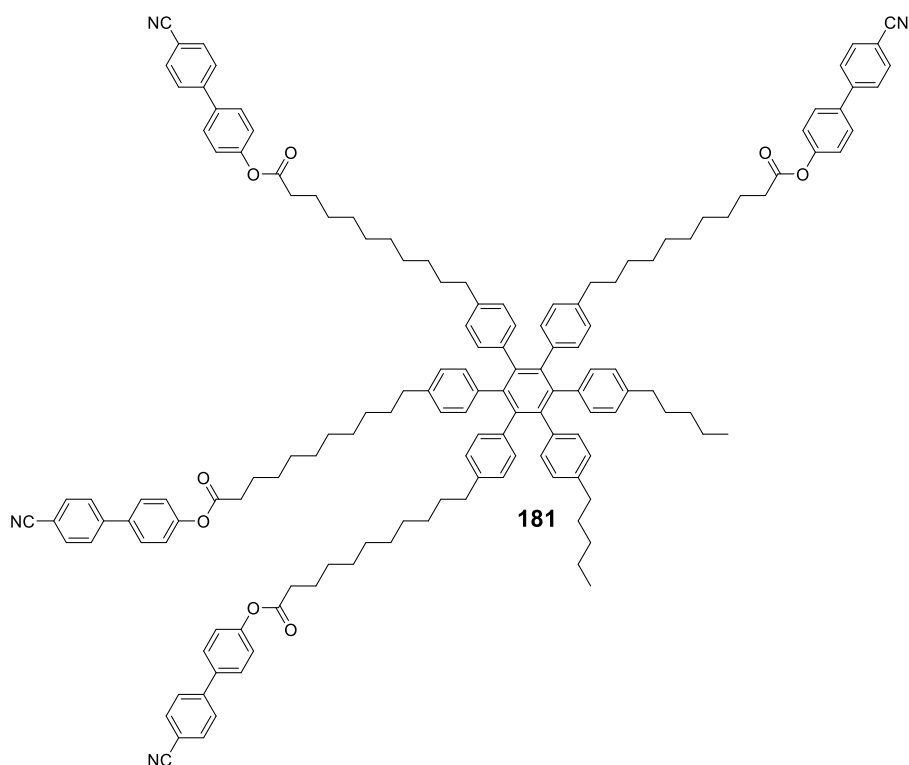
Compound **76** (0.16 g, 0.50 mmol) and **88** (0.48 g, 0.53 mmol) were charged to a dry Schlenk tube, then Co_2CO_8 (0.02 g, 0.06 mmol) was added in a glovebox under nitrogen. Dry 1,4-dioxane (12 mL) was charged to a second dry Schlenk tube under argon and degassed with argon for 20 minutes. A heating oil bath was heated to 115 °C and equilibrated for 1 hour, then the solvent transferred to the reagents and the mixture heated to reflux for 18 hours. The mixture was cooled to room temperature, the solvent was removed in vacuo and the crude product was purified by column chromatography (SiO$_2$, 10:1 DCM:EtOAc as eluent, Rf = 0.18) to give the target compound **181** as a powdery cream solid (0.18 g, 0.09 mmol, 25% yield).

^{1}H NMR (400 MHz, CDCl$_3$) δ 7.70 (d, *J* = 8.5 Hz, 8H, Ar*H*), 7.63 (d, *J* = 8.5 Hz, 8H, Ar*H*), 7.56 (d, *J* = 8.5 Hz, 8H, Ar*H*), 7.20 − 7.15 (m, 8H, Ar*H*), 6.65 (d, *J* = 8.0 Hz, 12H, Ar*H*), 6.60 (d, *J* = 8.0 Hz, 12H, Ar*H*), 2.57 (m, 12H, ArC*H$_2$*), 2.33 (t, *J* = 7.5 Hz, 8H, C*H$_2$*COO), 1.78 − 1.70 (m, 8H, C*H$_2$*CH$_2$COO), 1.42 − 1.17 (m, 52H), 1.14 − 1.04 (m, 16H), 0.83 (t, *J* = 7.5 Hz, 6H).

MALDI-TOF-MS: m/z = 2143.2 [M+Na]$^+$
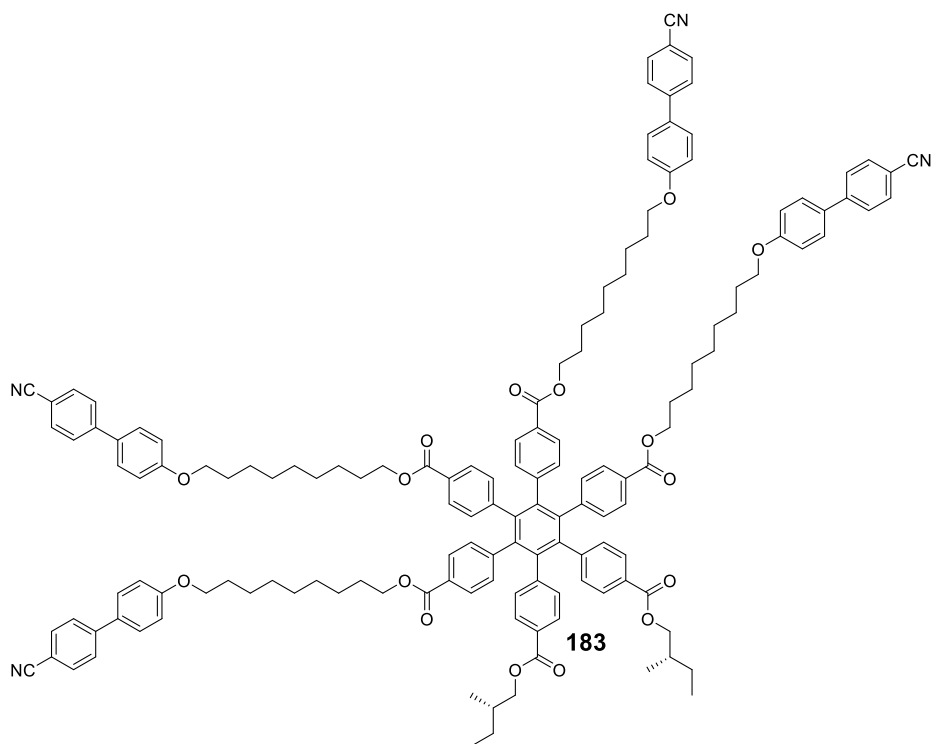
Compound **81** (0.20 g, 0.49 mmol) and **78** (0.45 g, 0.50 mmol) were charged to a dry Schlenk tube, then Co_2CO_8 (0.04 g, 0.12 mmol) was added in a glovebox under nitrogen. Dry 1,4-dioxane (25 mL) was charged to a second dry Schlenk tube under argon and degassed with argon for 20 minutes. The degass solvent was transferred to the reagents and the mixture heated to reflux for 18 hours. The mixture was cooled to room temperature, the solvent removed in vacuo and the crude product was purified by column chromatography (SiO_2, 10:1 DCM:EtOAc as eluent, Rf = 0.20) to give the target compound **183** as an off-white solid (0.19 g, 0.09 mmol, 26% yield).

^{1}H NMR (400 MHz, CDCl$_3$) δ 7.66 (d, *J* = 8.5 Hz, 8H, Ar*H*), 7.62 (d, *J* = 8.5 Hz, 8H, Ar*H*), 7.53 (d, *J* = 8.5 Hz, 12H, Ar*H*), 7.50 (d, *J* = 8.5 Hz, 8H, Ar*H*), 6.96 (d, *J* = 8.5 Hz, 8H), 6.88 (dd, *J* = 8.5, 2.0 Hz, 12H), 4.17 (t, *J = 7.5* Hz, 8H, COOC*H$_2$*), 4.08 (dd, *J* = 10.5, 6.0 Hz, 2H, OC*H*H), 3.98 (m, 10H, COOC*H$_2$* and OC*H*H), 1.81 – 1.72 (m, 16H), 1.49 – 1.40 (m, 40H), 1.40 – 1.28 (m, 6H), 0.93 (d, *J* = 7.5 Hz, 6H, CHC*H$_3$*), 0.89 (t, *J* = 7.5 Hz, 6H, CH$_2$C*H$_3$*).

MALDI-TOF-MS: m/z = 2239.1 [M+Na]$^+$

185
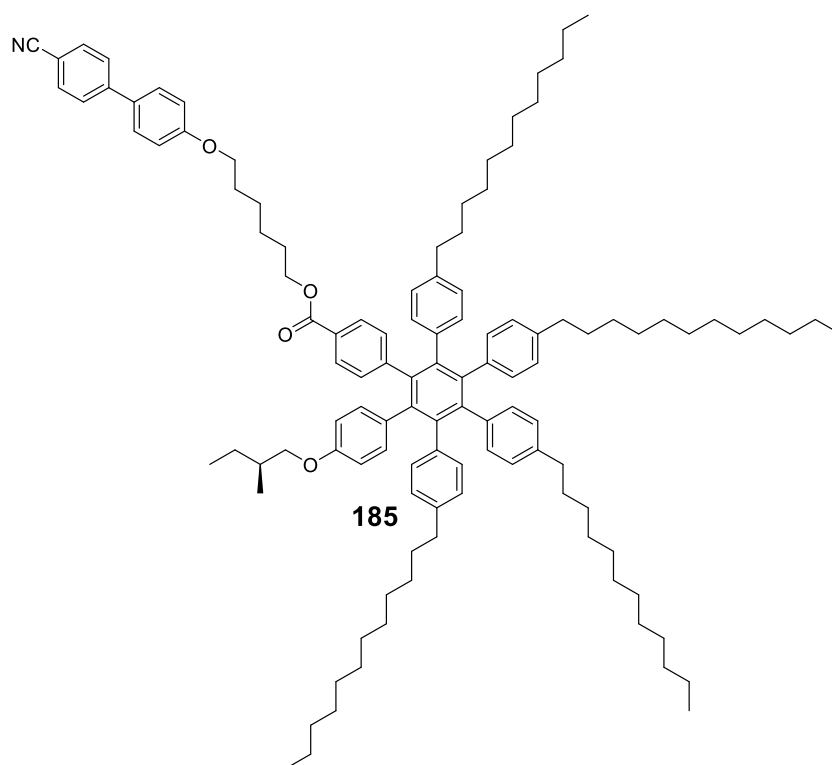
Compound **73** (0.29 g, 0.56 mmol) and **131** (0.03 g, 0.05 mmol) were charged to a dry Schlenk tube, then Co_2CO_8 (0.02 g, 0.06 mmol) added in a glovebox under nitrogen. Dry 1,4-dioxane (25 mL) was charged to a second dry Schlenk tube under argon and degassed with argon for 20 minutes. A heating oil bath was heated to 115 °C and equilibrated for 1 hour, then the solvent transferred to the reagents and the mixture heated to reflux for 18 hours. The mixture was cooled to room temperature, the solvent removed in vacuo and the crude product was purified by column chromatography (SiO$_2$, 10:1 DCM:EtOAc as eluent, Rf = 0.29) to give the target compound **185** as an orange oil (0.07 g, 0.04 mmol, 77% yield).

^{1}H NMR (400 MHz, CDCl$_3$) δ 7.68 (d, *J* = 8.5 Hz, 2H, Ar*H*), 7.62 (d, *J* = 8.5 Hz, 2H, Ar*H*), 7.58 – 7.41 (m, 4H, Ar*H*), 6.97 (d, *J* = 9.0 Hz, 2H, Ar*H*), 6.89 (d, *J* = 8.5 Hz, 2H, Ar*H*), 6.67 – 6.57 (m, 18H, Ar*H*), 6.36 (d, *J* = 9.0 Hz, 2H, Ar*H*), 4.20 (t, *J* = 6.5 Hz, 2H, COOC*H*$_2$), 3.99 (t, *J* = 6.4 Hz, 2H, OC*H*$_2$), 3.58 (dd, *J* = 9.0, 6. Hz, 1H, OC*H*H), 3.49 (dd, *J* = 9.0, 6.5 Hz, 1H, OC*H*H), 2.32 (t, *J* = 7.5 Hz, 8H, ArC*H*$_2$), 1.89 – 1.79 (m, 2H), 1.74 – 1.63 (m, 3H), 1.46 – 1.16 (m, 86H), 1.11 (t, *J* = 7.5 Hz, 12H), 0.93 (d, *J* = 7.5 Hz, 3H, CHC*H*$_3$), 0.89 (t, *J* = 7.5 Hz, 3H, CH$_2$C*H*$_3$).

MALDI-TOF-MS: m/z = 1627.2 [M+Na]$^+$

186
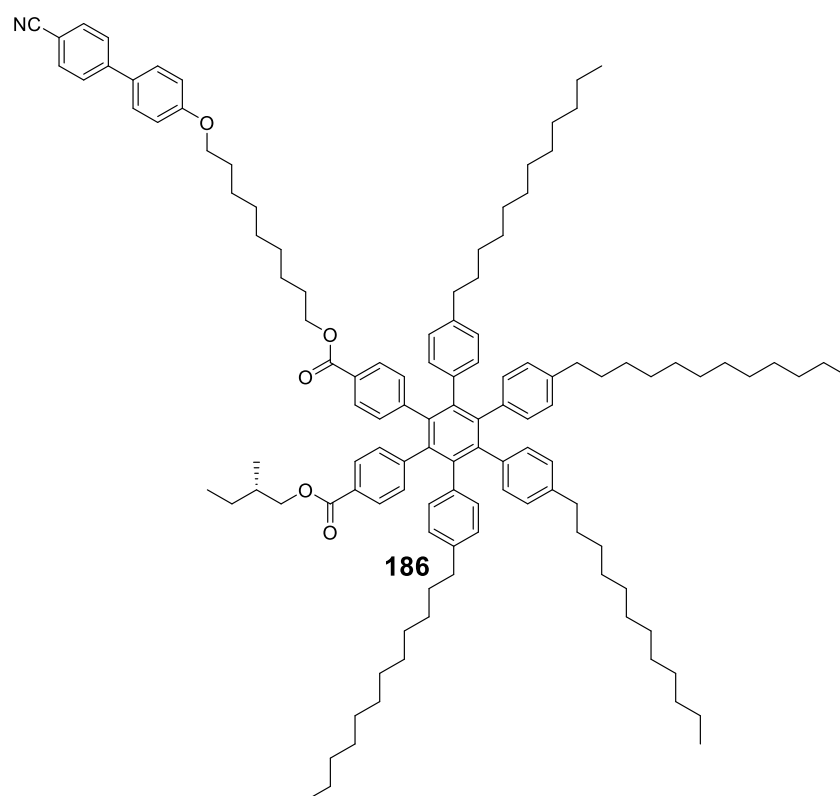
Compound **135** (0.05 g, 0.08 mmol) and **73** (0.48 g, 0.76 mmol) were charged to a dry Schlenk tube, then Co_2CO_8 (0.02 g, 0.06 mmol) added in a glovebox under nitrogen. Dry 1,4-dioxane (25 mL) was charged to a second dry Schlenk tube under argon and degassed with argon for 20 minutes. A heating oil bath was heated to 115 °C and equilibrated for 1 hour, then the solvent transferred to the reagents and the mixture heated to reflux for 18 hours. The mixture was cooled to room temperature, the solvent was removed in vacuo and the crude product was purified by column chromatography (SiO$_2$, 10:1 DCM:EtOAc as eluent, Rf = 0.31) to give the target compound **186** as a yellow oil (0.14 g, 0.08 mmol, 30% yield).

^{1}H NMR (400 MHz, CDCl$_3$) δ 7.67 (d, J = 8.5 Hz, 2H, ArH), 7.62 (d, J = 8.5 Hz, 2H, ArH), 7.53 – 7.49 (m, 4H, ArH), 6.97 (d, J = 8.5 Hz, 2H, ArH), 6.88 (d, J = 8.5 Hz, 2H, ArH), 6.70 – 6.52 (m, 20H, ArH), 4.16 (t, J = 7.0 Hz, 2H, OOCH_2), 4.07 (dd, J = 10.5, 6.0 Hz, 1H, OCHH), 3.99 (m, 3H, OCHH and OCH_2), 2.32 (t, J = 7.5 Hz, 8H, ArCH$_2$), 1.87 – 1.76 (m, 3H), 1.74 – 1.62 (m, 2H), 1.49 – 1.32 (m, 25H), 1.28 – 1.17 (m, 67H), 1.14 – 1.05 (m, 12H), 0.93 (d, J = 7.5 Hz, 3H, CHCH_3), 0.89 (t, J = 7.5 Hz, 3H, CH$_2$CH_3).

MALDI-TOF-MS: m/z = 1707.2 [M+Na]$^+$

7.8 References

1   D. B. Grotjahn, in Comprehensive Organometallic Chemistry II, 1995, vol 12, Ch 7, pp 741.

2   N. Agenet, O. Buisine, F. Slowinski, V. Gandon, C. Aubert and M. Malacria In Organic Reactions, Wiley; Hoboken, 2007. Vol 68, Ch 1, pp 1.

3   H. Dietl, H. Reinheimer, J. Moffat and P. M. Maitlis, *J. Am. Chem. Soc.*, 1970, 92, 2276.

4   T. M. Figueira-Duarte, A. Gégout, J. Olivier, F. Cardinali and J. F. Nierengarten*, European J. Org. Chem*., 2009, 3879–3884.

5   M. M. Martin, M. Dill, J. Langer and N. Jux*, J. Org. Chem*., 2019, 84, 1489–1499.

6   Y. Geng, A. Fechtenkötter and K. Müllen, *J. Mater. Chem*., 2001, 11, 1634–1641.

7   T. Ma, PhD Thesis, University of York, 2013.

8   P. Nockemann, M. Pellens, K. Van Hecke, L. Van Meervelt, J. Wouters, B. Thijs, E. Vanecht, T. N. Parac-Vogt, H. Mehdi, S. Schaltin, J. Fransaer, S. Zahn, B. Kirchner and K. Binnemans, *Chem. Eur. J.*, 2010, 16, 1849–1858.

9   H. K. Bisoyi, V. A. Raghunathan and S. Kumar, *Chem. Commun*., 2009, 7003–7005.

10   I. Bala and S. K. Pal, *Liq. Cryst*., 2016, 43, 963–971.

11   R. K. Gupta, V. Manjuladevi, C. Karthik and S. Kumar, J*. Phys. Conf. Ser*., 2013, **417**, 012068.

12   P. H. J. Kouwer and G. H. Mehl, *J. Am. Chem. Soc.,* 2003, 125, 11172–11173.

13   T. Kosaka, S. Iwai, Y. Inoue, T. Moriuchi and T. Mori, *J. Phys. Chem. A*, 2018, 122, 7455–7463.

14   T. Kosaka, S. Iwai, G. Fukuhara, Y. Imai and T. Mori, *Chem. Eur. J.,* 2019, 25, 2011–2018.

15   H. Taing, J. G. Rothera, J. F. Binder, C. L. B. Macdonald and S. H. Eichhorn, *Liq. Cryst*., 2018, 45, 1147–1154.

Chapter 8. Conclusions

The diphenyl acetylene core has been incorporated into dimeric, trimeric and supermolecular liquid crystals. The strategy of linking multiple mesogenic units in a single molecule to drive novel self-organisation is widespread, for example in the field of liquid crystal dendrimers the self-assembly may be tuned by altering the number of mesogenic units or peripheral chains. In this work, the self-organisation of the diphenyl acetylene liquid crystals was investigated alongside other structural factors such as chirality, and chemically incompatible units which show microphase segregation. In this way, multiple factors affecting the self-organisation are placed into competition, and therefore the materials produced show rich mesomorphism. In addition, this allows for the different liquid crystal properties and mesophase structures of these diphenyl acetylene materials to be studied in order to learn more about the interplay of the competing intermolecular interactions.

In this work, a dendritic structure derived from either pentaerythritol or 1,1,1-tris(hydroxymethyl) ethane with branching multiplicity of two or three respectively was used to tether two or three mesogenic- (cyanobiphenyl) or self-segregating (perfluoroalkyl) units together. The dendritic branching units derived from pentaerythritol or 1,1,1-tris(hydroxymethyl) ethane were alkylated under phase transfer conditions and deprotected to give tri- and di-acids respectively. These compounds could be esterified with the desired mesogenic units providing dendritic iodo-aryl and ethynyl-aryl intermediates. In the final synthetic step, these intermediates were coupled together via the Sonogashira coupling reaction to provide diphenyl acetylenes completing the convergent synthetic strategy. This strategy was found to be easier than utilising a divergent approach, and the yields obtained for the two strategies were comparable. One challenging aspect of this synthesis was the purification of the final compounds following the transition metal catalysed reaction, and complicated by the formation of organogels. However, this was overcome by repeated column chromatography.

By introducing branching as found in some of the materials reported in Chapters 3 and 5 the molecular shape could be altered from linear rod-like molecules to give highly tapered shapes. The introduction of the first dendritic branched chain via 1,1,1-tris(hydroxymethyl) ethane sharply decreased the transition temperatures. This

observation is consistent with that found within other materials reported in the literature. The decrease of the transition temperatures is attributed to a large increase in the number of conformations available to the mesogenic units when compared to a linear chain. In the case of the cyanobiphenyl compounds discussed in Chapter 3, and the cyanobiphenyl:alkyl compounds discussed in Chapter 5, branching led to the formation of nematic mesophases with the exception of compounds **53** and **57**. Although compounds **53** and **57,** with three cyanobiphenyl units, exhibited smectic phases, either reducing the number of cyanobiphenyl units to two, or increasing the length of the fourth arm from ethynyl-aryl or iodo-aryl units (**44**, **48**) to a diphenyl acetylene (**110**) provided nematic materials. This effect demonstrates the balance between the intermolecular interactions – which are increased with the number of cyanobiphenyl mesogens – and molecular shape. A further example of the balance between the intermolecular interactions and molecular shape can be seen by the inability to pack the longer arm of the diphenyl acetylene unit of **110** within the smectic A phase of **53** and **57**. Alternatively, reducing the number of mesogens from three in **53** and **57** to two in **44** and **48** both reduces the strength of the intermolecular interactions and changes the molecular shape via the projection of the mesogenic arms from the branching unit. Upon introducing a self-segregating perfluoroalkyl chain alongside two cyanobiphenyl mesogens, the smectic A phase is again observed with similarities to previous reports by Yoshizawa.

In the case of materials featuring self-segregating perfluoroalkyl chains, compounds with two perfluorinated chains did not exhibit liquid crystallinity unless multiple cyanobiphenyl mesogens were attached on the opposite face of the diphenyl acetylene core. In contrast, three perfluoroalkyl chains were found to promote smectic phases irrespective of the group that was attached on the opposite end of the molecule. As with the cyanobiphenyl compounds, this can be attributed either to the increased intermolecular interactions when a third chain is present, or to the effect on the molecular shape. The effect is likely a combination of both factors, however the strength of the intermolecular interactions can be increased by the addition of cyanobiphenyl mesogens without promoting liquid crystallinity. Therefore, it is likely that the tetrahedral nature of the branching units used results in greater packing efficiency when three self-segregating arms are present. In the case of materials with

two cyanobiphenyl mesogens on the opposite face of the *Janus* diphenyl acetylene core **104** and **107** appeared to possess similar phase behaviour, both exhibiting wide ranging smectic phases. However, X-ray diffraction studies showed that the layer spacing of compound **104** with two perfluoroalkyl units and two cyanobiphenyl units changed by around 14% across a 60 °C temperature range. In contrast, the layer spacing of compound **107** with three perfluoroalkyl chains and two cyanobiphenyl units changed by less than 4% over a range of 55 °C. This indicates a different mesophase structure, which may relate to the difference in self-organisation of the smaller perfluoroalkyl substituted aryl molecules.

A further contrast can be drawn between compounds **113**, **54**, **58** and **109,** all of which feature three perfluorinated arms. Each of **113**, **54** and **58** exhibit smectic A phases, however, extending the alkyl diphenyl acetylene arm of **113** to a cyanobiphenyl in compound **109** changes the mesophase structure to a columnar phase which had an unidentified structure owing to the complex x-ray diffraction pattern. This again shows that the molecules must pack into a different structure as the longer cyanobiphenyl arm prevents the molecules from efficiently packing in a similar manner to the other compounds. The presence of a columnar phase for a highly tapered structure is in agreement with previous results, for example many materials using the Percec-style dendron to alter the shape of a molecule are known to exhibit columnar mesophases. However, in this case the additional flexibility of the pentaerythritol derived branching unit appears to allow smectic phases to form unless otherwise disrupted.

As noted above, compound **104**, featuring two cyanobiphenyl units and two perfluoroalkyl units, exhibited a large continuous change in layer spacing across the temperature range of the mesophase. However, when the number of cyanobiphenyl units was increased from two to three (compound **105**) a reorganisation of the mesophase structure occurred approximately halfway through the mesophase temperature range. This reorganisation was observed as a change in the birefringence by POM and a discontinuous increase in the layer spacing by around 10 Å in x-ray diffraction studies. The mesophase structures of these materials are only tentatively assigned, and a similar change in structure was observed for compound **114** previously. This reorganisation is dependent upon the supermolecular structure and

could not be achieved from low molecular weight mesogenic units demonstrating the benefits of using dendritic and supermolecular liquid crystals.

As may be expected linear materials with less complex molecular structures tended to give simpler mesophase structures. The linear cyanobiphenyl – diphenyl acetylene dimers predominantly gave nematic phases. Substituting the alkyl chain for an additional cyanobiphenyl unit stabilised the nematic phase with an increase in clearing point of roughly 150 °C. In contrast, exchanging the alkyl chain for a perfluoroalkyl chain lead to the domination of the smectic phase as the cyanobiphenyl and perfluoroalkyl units provide two competing sets of intermolecular interactions. Despite sharing the same mesogenic units, the packing of the molecules into the mesophase structures of compound **94** with a single cyanobiphenyl unit and **106** with two cyanobiphenyls are different to each other. Due to the change in molecular shape the cyanobiphenyl units of **106** cannot fully overlap as predicted for compound **94**. Therefore, while the interdigitation of the cyanobiphenyl mesogens is preserved, the interactions must be weakened to accommodate the change in molecular shape.

In addition to the use of mutually incompatible units, the impact of chirality upon the self-assembly was studied. The same convergent strategy used in the synthesis of the *Janus* supermolecular liquid crystals was altered for the synthesis of the chiral dimers. Following the Sonogashira coupling reaction in the final step, purification of the chiral dimers was notably easier than that of the supermolecular liquid crystals. Recrystallisation from hot ethanol or dichloromethane and methanol provided materials with high purity. (S)-2-methylbutyl and (S)-1-methylheptyl chiral units were used to promote chiral phases with short helical pitches. The nature of the chiral liquid crystalline mesophases obtained were reliant on the linking group between the chiral unit and diphenyl acetylene core. The ether linking unit at the opposite end of the diphenyl acetylene core to an ester linkage provided a push-pull electronic effect and so increased the intermolecular interactions of the diphenyl acetylene core giving smectic phases. In contrast, materials with an ester linkage between the chiral chain and the diphenyl acetylene gave two materials which exhibited frustrated phases. Of these ester linked compounds, (S)-2-methylbutyl compound **137** exhibited the blue fog texture of BPIII and platelet texture of BPI when annealed, while compound **142** with an (S)-1-methylheptyl chiral unit exhibited both BPIII and the TGB phase. The

incorporation of chirality into the diphenyl acetylene – cyanobiphenyl dimers was also investigated by measuring the helical twisting power of the chiral liquid crystals when used as a dopant in E7. The ester linked materials were found to be far more effective at imparting a chiral twist into the mesophase due to the reduced flexibility around the chiral centre. Because the ether linked compounds primarily exhibited the smectic A phase it is difficult to comment on the impact of chirality in their self-organisation. However, by changing the length of the alkyl spacer from hexyl in compound **131** to decyl in compound **132** the structure of the chiral smectic C phase appeared to change from ferroelectric to antiferroelectric. The results from the miscibility studies were in line with previous reports whereby ether linking units tend to provide low helical twisting powers due to the increased flexibility around the chiral unit. The formation of frustrated phases for diphenyl acetylene dimers was previously observed for asymmetric dimers featuring diphenyl acetylene and cholesterol units where it was attributed to the different packing periodicities of each segment.

Finally, the diphenyl acetylene core was investigated as a reactive moiety enabling cyclotrimerisation reactions to provide a route to hexaphenyl benzene molecules. Of particular interest was the controlled regiochemistry of mixed or cotrimerisation reactions and strategies with which to control the outcome of the reaction. On the theme of competing structural factors, the disc-like hexaphenyl benzene core encourages the formation of columnar phases, especially when long alkyl chains are used. However, the materials produced in this work feature cyanobiphenyl units attached to the hexaphenyl benzene core by flexible alkyl spacers, which provide an additional self-organisation force . The materials produced by the cotrimerisation of an alkyl and cyanobiphenyl substituted diphenyl acetylene appear to show an incremental transition between these two mesophase structures. As the number of cyanobiphenyl mesogens increases the quadrupolar interactions at the interface dominate giving rise to a smectic phase. As the number of cyanobiphenyl units decreases from six in compound **173** to four in compound **181** and further to two (**180**) the entropy of isotropisation per mesogen increases showing that the mesophase structure becomes more organised.

Hexaphenyl benzenes featuring between one to three chiral centres were isolated following one synthetic step from the diphenyl acetylene constituents. By using

cotrimerisation reactions the regiochemistry could be altered and in some cases only a single chiral centre was incorporated selectively. Hexaphenyl benzene compounds with chiral units were contrasted with the parent diphenyl acetylene compounds and found to greatly diminish the helical twisting power, with little correlation between the helical twisting power and the number of chiral units used. Previous work by Mori featuring chiral 1-methylpropyl units on a diphenyl acetylene core observed large solvent effects and therefore interest in the behaviour of these materials in liquid crystalline environments is due.

In summary, the diphenyl acetylene core has been incorporated as the supporting core into a range of supermolecular liquid crystalline materials where multiple structural factors contribute to the self-organisation. In this way, complex mesophase structures and rich mesomorphism were obtained. Controlling the molecular shape by altering the branching multiplicity of a tetrahedral carbon lead to fine balances in the self-organisation for example while three identical mesogenic units appeared to drive the liquid crystal behaviour the fourth arm exhibited control of the mesophase structure switching between smectic and columnar mesophases. The diphenyl acetylene unit was incorporated into chiral dimers for which frustrated phases were obtained indicating competing structural effects. Finally, the cyclotrimerisation reaction was investigated to allow for a rapid increase in molecular complexity, while methods to maintain control over the regiochemistry were identified. The mesophase structure of some of the hexaphenyl benzenes produced in this way appeared to show an incremental change between calamitic and columnar character.